

Application of Nitrene Transfer Reactions for Streamlining Amine Synthesis

Part One: Development of C–H Amination via Metal-Catalyzed Nitrene Transfer

Part Two: Stereocontrolled 4π -Electrocyclization via Eneallene Aziridination

By

Joshua Robert Corbin

A dissertation submitted in partial fulfillment of
the requirements for the degree of

Doctor of Philosophy
(Chemistry)

at the

UNIVERSITY OF WISCONSIN-MADISON

2020

Date of final oral examination: June 10, 2020

The dissertation is approved by the following members of the Final Oral Committee:

Jennifer M. Schomaker, Professor, Chemistry

Steven D. Burke, Professor, Chemistry

John F. Berry, Professor, Chemistry

Clark R. Landis, Professor, Chemistry

Abstract

Metal-catalyzed nitrene transfer is a versatile strategy for the direct incorporation of C–N bonds into organic compounds through direct C–H insertion to form amines or C=C insertion to form aziridines. The identity of the metal catalyst plays a crucial role in controlling the fate of the hyperelectrophilic nitrene when multiple reaction outcomes are possible.

Part One of this thesis details the development of a catalytic system based on Ag(I) supported by diverse pyridyl *N*-donor ligands to achieve unprecedented and tunable site-selectivity in the amination of sterically and electronically similar tertiary C(*sp*³)–H bonds. When ligand-control in Ag(I) catalysis failed, exchanging the metal/ligand identity to Rh₂L_n frequently provided selectivity for the orthogonal site. Further work demonstrated water could be employed as the solvent in these C–H amination reactions using Ag(I) or Rh₂(II,II) catalysts and sulfamate nitrene precursors.

Intramolecular chemo- and regioselective aziridination of allenes using Rh₂(II,II)-catalyzed nitrene transfer provides access to bicyclic methyleneaziridine intermediates that can be rapidly diversified into complex amine-containing products by forming up to four new bonds across the cumulated π -bonds. An underexploited strategy for accessing amidoallyl cations is treating these methyleneaziridines with a mild Lewis acid to heterolytically open the strained ring. This strategy is applied in Part Two to overcome the challenges that are associated with 3-amidopentadienyl cation imino-Nazarov electrocyclizations and the method provides access to densely functionalized aminocyclopentanes with flexible substitution patterns and control over the stereochemical outcome. This thesis in its entirety demonstrates the utility of metal-nitrenes as useful oxidants in the context of the diversity-oriented synthesis of both simple and complex amines.

Acknowledgements

I could not have gotten through these last 5 years without the help and encouragement of so many people! There were multiple times I tried so hard to shoulder everything myself and become independent, but everyone mentioned below (and sorry if I forget you) helped remind me how valuable a support network can be, especially in science!

First, I would like to thank the remarkable coworkers I have had the pleasure of working directly with over the years. When I was getting started in lab, Drs. Juliet Alderson and Minxue Huang were tremendously helpful mentors and enjoyable office mates to be around. I learned a lot from you both during my time in the Ag-subgroup and I am so proud of the work we accomplished together! Both Minxue and Julie's work ethic was consistent and focused in their own way and the atmosphere you both set with Dr. Steve Schmid was motivating and conducive to concentrating. Devin Ketelboeter was a lot of fun to work with on the 2-imino-Nazarov project and tremendous help; I wish him all the best during his graduate studies. I learned a ton about working with others with you and you helped motivate me when I needed it. You picked up on techniques so easily I was afraid you would outperform me! Minxue always knew a sweet snack could go a long way to cheer up a mood when things were tough, and I'll miss our office talks. I am so glad to have met all of you and I hope our friendships are long-lasting! Hopefully, I will be able to keep surrounding myself with such positive and high-quality coworkers like you all going forward, so I can just bask in awe at how much we can accomplish together.

Along those lines, I consider myself extremely lucky to have been placed in the supportive (and clean) North lab! Dr. Steve Schmid always played such cool music to the extent I was way too embarrassed to play any of my avant-garde electronic, so along those lines, thanks to whoever invented headphones! I'll miss our conversations about news or just whatever. I need to thank Dr.

Steve Schmid more seriously for encouraging me to explore the reactivity of eneallenes when I was between projects and having difficulty finding hits shooting metal-carbenes at X-H bonds. Mahzad Dehghany could always make me laugh and I hope to stay friends with you as well. Good luck finishing, you can do it. Thanks so much, all of you (including Robert Ward and Medena Noikham), for respecting each other's space and chemicals- lab can certainly become a very toxic place without trust and respect for each other! Additionally, being part of the cleanest lab was awesome when I was CHO. I hope the old saying that a clean hood is an unproductive hood goes away soon!

Other Schomaker group members old and present have also been a great deal of help to me. Amirah Mat Lani became an amazing friend and colleague! I miss working with you so much, you were always down to listen to me talk about my science and vice versa...when you weren't asking "What's the G?!". The South lab's struggles were a constant reprieve for me and I hope to always remember how hilarious you all could be. Dr. Josephine Eshon went through this entire experience with me and we certainly experienced a lot and had a ton of fun travelling to conferences together! Soon-to-be Dr. Ryan Reeves could give me both the biggest headache and the heartiest laugh simultaneously and I hope we'll stay good friends so I can hear about your wonky hobbies and antics. I hope I picked up a bit of your sense for sniffing out BS. I also appreciate how good of a friend Hillary Dequina has become and I hope the rest of your PhD goes successfully and that your working relationships are healthy and productive. I hope you experience that grad school can be really amazing when you find the right coworkers...and thanks for all the quarantine entertainment! Dr. Jon Paretsky was always a solid rock and has continued to offer me advice when I asked for it since he's left. Dr. Lu Liu became a good friend who offered good advice in the allene subgroup as well. Ethan Licht, thanks for carrying the torch, so to speak. Dr. Nels

Gerstner gave a lot of helpful advice early on and certainly has a unique sense of humor and stubbornness that I'll remember for a long time.

I also need to thank the department staff and especially Dr. Martha Vestling for being an amazing TA boss and showing me the ropes of mass spectrometry. I enjoyed going down to work with you for the two years I helped run samples (you're always doing something interesting!) and I learned a great deal while gaining a deep appreciation for your instruments. Thanks so much for that opportunity!

Thanks to my committee, Profs. Steve Burke and John Berry for taking the time and having the patience to go through so many program requirements with me and additionally Prof Clark Landis for serving on my defense committee. Also thanks to my undergrad mentors, Prof. Lin Pu and graduate student Shifeng Nian, for giving me an opportunity to get into organic chemistry at UVa.

Of course, none of this would be possible without the guidance and support of my advisor, Prof. Jen Schomaker. I've enjoyed learning from you these recent years and you certainly made an impression on me as a scientist (and person) that will certainly last the rest of my career (and life)! I'm always astounded by how hard you work and how dedicated you are to science. I will forever have an appreciation for interesting and creative organic reactions from my time studying small strained rings and other reactive intermediates here. I hope I gained a fraction of your confidence and resilience in the face of a struggling project; your positivity and excitement for chemistry are infectious and motivating! Hopefully, we'll see each other again in the future!

Lastly, I'd like to thank friends and family. BJ Lee, best of luck in the future, I'm glad I met you and I hope to keep discussing chemistry with you for years to come. My undergraduate friends, especially Ray Ramirez, Mary-Rolfe Zeller, and the UNLIMITED-WIFI Discord crew (JB Reiter, Arisa Koyama, Brian Denten, Siddharth Hariharan) were extremely supportive over the internet

even when I was losing it- thanks for being a non-chemistry outlet. Thanks especially to the Discord crew for calling to play games online with me to help unwind when I needed it! Additionally, I must thank my family- especially my sister Amy, my Dad and Mom, and my grandparents- for having the patience and love to support me throughout this long PhD education. I've been forever touched by everyone's support and I hope a ton of happiness is in everyone's future!

Table of Contents

Abstract.....	i
Acknowledgements.....	ii
Table of Contents.....	vi
List of Figures.....	x
List of Schemes.....	xi
List of Tables.....	xiv
Abbreviations and Acronyms.....	xvi
Chapter 1. Introduction to Transition Metal-Catalyzed Nitrene Transfer and Selected Discussion on Application to C(sp³)-H Amination Reactions.....	1
1.1 Introduction.....	2
1.2 Background.....	3
1.3 Chemodivergent Amination via Changes in the Silver:Ligand Ratio.....	6
1.4 Chemoselective, Asymmetric Intramolecular Aziridination.....	11
1.5 Chemoselective, Intermolecular Ag-catalyzed Amination.....	11
1.6 Catalysts for Tuning the Site-Selectivity of C-H Bond Amination.....	14
1.6.1 Catalysts Favoring Amination of 3° Alkyl C(sp ³) -H Bonds.....	15
1.6.2 Catalysts for Amination of Benzylic C-H Over 3° Alkyl C-H Bonds.....	16
1.7 Selective C-H Oxidation of C-H Bonds in Similar Chemical Environments.....	20
1.7.1 Representative Stoichiometric Methods.....	21
1.7.2 Representative Catalytic Methods.....	22
1.8 Conclusions.....	25
1.9 References.....	26

Chapter 2. Tunable Differentiation of Tertiary C–H Bonds in Intramolecular Transition Metal-Catalyzed Nitrene Transfer Reactions.....33

2.1. Introduction.....	35
2.2. Background.....	35
2.3. Catalyst Screen and Substrate Scope.....	37
2.4. Conclusions.....	46
2.5. References.....	47
2.6. Experimental Details and Characterization.....	49
2.6.1. Synthesis of Alcohol Precursors.....	49
2.6.2. Synthesis of Sulfamate Esters.....	55
2.6.3. Nitrene Transfer Procedures and Characterization of C-H Amination Products.....	59
2.6.4. Procedures for the Synthesis of [Ag(Me ₄ phen)]OTf and [Ag(Me ₄ phen) ₂]OTf Crystals.....	70

Chapter 3. Investigation of Transition Metal-Catalyzed Nitrene Transfer Reactions in Water...72

3.1 Introduction.....	74
3.2 Reaction Optimization.....	76
3.3 Scope of C-H Amination Reactions in Water Compared to Halogenated Solvents.....	80
3.4 Concluding Remarks.....	82
3.5 References.....	83
3.6 Experimental Details and Characterization.....	85
3.6.1 Synthesis of homoallylic carbamates.....	85

3.6.2 Synthesis of homoallylic sulfamates.....	85
3.6.3 Synthesis of C-H insertion products.....	86
Chapter 4. <i>Amine-Substituted Allyl Cations: Brief Overview and Use in 4π-Electrocyclizations.</i>	89
4.1 Introduction.....	90
4.2 [4+3]-Cycloaddition Reactions of Allyl Cations.....	91
4.2.1 [4+3]-Cycloaddition of 1-Amidoallyl Cations.....	91
4.2.2 [4+3]-Cycloaddition of 2-Amidoallyl Cations.....	92
4.3 Other Methods Utilizing Amidoallyl Cations.....	94
4.4 Brief Introduction to Nazarov Electrocyclization Reactions.....	96
4.4.1 Aza-Nazarov Reactions and Aza-Piancatelli Reactions.....	98
4.4.2 Imino-Nazarov Reactions.....	99
4.5 Allene Oxide Cyclization and Oxidation-Initiated Nazarov Reactions.....	102
4.6 Conclusions.....	104
4.7 References.....	105
Chapter 5. <i>Biomimetic 2-Imino-Nazarov Cyclizations via Eneallene Aziridination.</i>	110
5.1 Introduction.....	112
5.2 Background.....	113
5.3 Reaction Optimization.....	115
5.4 Reaction Scope.....	116
5.5 Experimental and Computational Mechanistic Investigation.....	119
5.6 Product Utility.....	121
5.7 Conclusion.....	122
5.8 References.....	122

5.9 Experimental Details and Characterization.....	126
5.9.1 General procedure for eneallene synthesis.....	126
5.9.2 Procedures for alcohol deprotection.....	135
5.9.3 Procedure for (<i>Z</i>)-eneallene substrate.....	144
5.9.4 General procedure for the synthesis of homoallenic sulfamates.....	145
5.9.5 Procedure for eneallene aziridination/electrocyclization.....	154
5.9.6 Representative nOe studies.....	164
5.9.7 Axial-to-point chirality transfer and asymmetric catalysis experiments....	166
5.9.8 Tether length/ <i>N</i> -source optimization and reaction monitoring.....	178
5.9.9 Procedures for functionalization of iminocyclopentene 5.6a	186
Appendix. Selected ¹H- and ¹³C-NMR Data, X-Ray Data, and Computational Data.....	192
Chapter 2 ¹ H- and ¹³ C-NMR Data.....	193
Chapter 2 X-Ray Data.....	255
Chapter 3 ¹ H and ¹³ C-NMR Data.....	278
Chapter 5 ¹ H and ¹³ C-NMR Data.....	284
Chapter 5 Computational Details.....	450

List of Figures

Figure 1.1. Chemo-, site- and stereoselective C–N bond formation via silver catalysis.....	6
Figure 1.2. A) X-ray crystal structure of [<i>t</i> Bu ₃ tpy)AgOTf] ₂ . B) Optimized computed structure of [(tpy)Ag] ₂ (DfsN)(OTf). C) Optimized computed structure of (tpa)Ag(OTf)(NSO ₃ R).....	13
Figure 1.3. KIE values for catalysts promoting nitrene transfer.....	16
Figure 1.4. Dynamic behavior of (tpa)AgOTf.....	17
Figure 2.1. Approaches to chemo- and site-selectivity in nitrene group transfer reactions.....	36
Figure 2.2A. X-ray single crystal structure of a dimer of [Ag(Me ₄ phen)(OTf)] _n shown with 50% probability ellipsoids. 2.2B. Molecular drawing of [Ag(Me ₄ phen)(OTf)] _n , showing the metal- π interactions between the Ag center and the phenanthroline ligands of neighboring molecules above and below. 2.2C. Molecular structure of Ag(Me ₄ phen) ₂ (OTf) shown with 50% probability ellipsoid.....	39
Figure 2.3. Traditional substrate control explanations of site-selectivity fail when similar logic is applied to tertiary C(sp ³)–H differentiation.....	43
Figure 4.1. Heteroatom positioning impacts allyl cation stability <i>via</i> lone-pair conjugation.....	90
Figure 4.2. Heteroatom placement on pentadienyl cation and resonance effects.....	96
Figure 5.1. 2-Imino-Nazarov Electrocyclization described in this work.....	112
Figure 5.2. Computed reaction profile for the 2-imino-Nazarov of aziridine 5.22	120

List of Schemes

Scheme 1.1. General features and complexes employed for metal-catalyzed nitrene transfer.....	4
Scheme 1.2. Early efforts in chemo- and site-selective nitrene transfer.....	5
Scheme 1.3. Early examples of Ag-catalyzed nitrene transfer.....	6
Scheme 1.4. Mechanistic probes of chemoselective, Ag-catalyzed nitrene transfer.....	9
Scheme 1.5. Proposed mechanisms of chemodivergent aziridination and C–H amination.....	10
Scheme 1.6. Computed Ag-nitrene intermediate of (tpa)AgOTf supports non-covalent interactions between catalyst and substrate.....	21
Scheme 1.7. Selective C-H oxidation at most sterically accessible and electron-rich sites.....	22
Scheme 1.8. Strain-release as a selectivity determining feature and hyperconjugation effects....	23
Scheme 1.9. Electronic differentiation of similar C-H bonds for selective catalytic oxidation....	24
Scheme 1.10. Directing group approaches to selective tertiary C-H amination.....	24
Scheme 1.11. Metal-controlled site-divergent amination of sterically and electronically similar C-H bonds.....	25
Scheme 3.1. Ag-catalyzed nitrene transfer.....	76
Scheme 3.2. Intermolecular C-H amination in water.....	82
Scheme 4.1. Generic [4+3]-cycloaddition between an oxyallyl cation and butadiene and oxyallyl cation generation.....	91
Scheme 4.2. Generation and utility of 1-amido-2-oxyallyl cation intermediates.....	92

Scheme 4.3. Ag(I)-promoted chloride abstraction to form 2-amidoallyl cation intermediates.....	92
Scheme 4.4. Methyleneaziridines as intermediates towards 2-amidoallyl cations.....	93
Scheme 4.5. Allene aziridination/[4+3]-reaction: strategy to obtain complete stereodivergence..	94
Scheme 4.6. <i>Umpolung</i> reactivity of enamine α -carbons by nucleophilic trapping of 2-amidoallyl cations.....	95
Scheme 4.7. Oxidative allene amination to generated 2-amidoallyl cations from 1,1-disubstituted allenes.....	95
Scheme 4.8. The classic Nazarov reaction of 3-oxypentadienyl cations.....	97
Scheme 4.9. 2-oxy-3-amidopentadienyl cation electrocyclization.....	98
Scheme 4.10. Chiral diamine-promoted electrocyclization of diketones.....	98
Scheme 4.11. Tandem condensation/electrocyclization of 1-amino-4-oxypentadienyl cations....	99
Scheme 4.12. Electrocyclization of arylallenamides via Au(I) catalysis.....	100
Scheme 4.13. Cyclization of 2-chloro-3-aminopentadienyl cations.....	100
Scheme 4.14. 3-imino-Nazarov electrocyclization of divinyl imines.....	101
Scheme 4.15. Mechanism of the Piancatelli and aza-Piancatelli rearrangement.....	102
Scheme 4.16. Example aza-Piancatelli rearrangement from aniline trapping a 2-furylcarbinol dehydration intermediate.....	102
Scheme 4.17. Allene oxide cyclization in plant biosynthesis of jasmonates.....	103
Scheme 4.18. Oxidation-initiated 2-oxy-Nazarov electrocyclization of eneallenes.....	103
Scheme 4.19. Utility of eneallene oxidation-initiated oxy-Nazarov electrocyclization.....	104
Scheme 5.1. Background and proposed 2-Imino-Nazarov reaction.....	113

Scheme 5.2. Flexible transformations of 5.6a	122
--	-----

List of Tables

Table 1.1. Influence of ligand and silver:ligand ratio on chemoselectivity.....	7
Table 1.2. Influence of catalyst identity and Ag:ligand ratio on chemoselectivity in reactions of homoallylic carbamates.....	8
Table 1.3. Selected examples of asymmetric, silver-catalyzed nitrene transfer.....	11
Table 1.4. Catalyst control of the chemoselectivity of intermolecular nitrene transfer.....	13
Table 1.5. Site-selective amination of 3° alkyl C(sp ³)–H over benzylic C–H bonds.....	15
Table 1.6. Comparison of benzylic amination selectivity with known and new Ag(I) catalysts...	18
Table 1.7. Impact of ligand identity on preference for benzylic C–H amination.....	19
Table 1.8. Testing the possibility of π - π interactions through catalyst design.....	20
Table 2.1. Initial efforts to differentiate between similar tertiary C(sp ³)–H bonds.....	37
Table 2.2. Selectivity in the amination of carbocyclic <i>vs.</i> acyclic C–H bonds.....	42
Table 2.3. Competitive amination of activated C–H <i>vs.</i> tertiary C(sp ³)–H bonds.....	45
Table 3.1. Effect of water on carbamate nitrene transfer reagents.....	77
Table 3.2. Water tolerance of sulfamate nitrene transfer reagents.....	78
Table 3.3. Catalyst activity in aqueous solvent.....	79
Table 3.4. Reaction optimization.....	80
Table 3.5. Examples of intramolecular amination in water.....	81
Table 4.1. Thermodynamic/kinetic barriers to 3-amidopentadienyl cation electrocyclization....	97

Table 5.1. N-Group transfer tether optimization.....	115
Table 5.2. Selected optimization studies.....	116
Table 5.3. Scope of the tandem allene aziridination/2-imino-Nazarov reaction.....	118

Abbreviations and Acronyms

Å	angstrom(s)
Ac	acetyl
acac	acetylacetate
Ad	1-admantyl
Ar	aryl
Bathophen	bathophenanthroline
BHT	4-methyl-2,6-di-tert-butyl phenol (bis-hydroxylated toluene)
Boc	<i>tert</i> -butoxycarbonyl
BOX	bis(oxazole)
Bn	benzyl
CS	closed-shell
DCC	N,N'-dicyclohexylcarbodiimide
Dfs	2,6-difluorophenoxysulfonyl
DFT	density functional theory
DHA	9,10-dihydroanthracene
DMAP	4-(dimethylamino)pyridine
DMSO	dimethylsulfoxide
DOSY	diffusion-ordered spectroscopy
DPPA	diphenylphosphorylazide
<i>ee</i>	enantiomeric excess
esp	$\alpha,\alpha,\alpha',\alpha'$ -tetramethyl-1,3-benzenedipropionic acid
Et	ethyl

HAA	hydrogen atom abstraction
HAT/HT	hydrogen atom transfer
Hfs	1,1,1,3,3,3-hexafluoroisopropoxysulfonyl
hp	tetrakis(2-oxypyridinato)
IMes	1,3-(2,4,6-trimethylphenyl)imidazolidene
<i>i</i> Pr	isopropyl
IPr	1,3-(2,6-diisopropylphenyl)imidazolidene
KIE	kinetic isotope effect
Mbs	<i>p</i> -methoxybenzenesulfonyl
Me	methyl
Me3tpy	4,4',4''-trimethyl-2,2':6',2''-terpyridine
MECP	minimum-energy crossing point
(MeO)2bipy	4,4'-dimethoxy-2,2'-bipyridine
MS	molecular sieves
Ms	2,4,6-mesityl
NHC	N-heterocyclic carbene
NMR	nuclear magnetic resonance
<i>n</i> Pent	<i>n</i> -pentyl
<i>n</i> Pr	<i>n</i> -propyl
Ns	<i>p</i> -nitrobenzenesulfonyl
NT	nitrene transfer
Oct	cyclooctene
OEP	2,3,7,8,12,13,17,18-octaethyl-21 <i>H</i> ,23 <i>H</i> -porphine

OS	open-shell
<i>p</i> -CITPP	5,10,15,20- tetra(<i>p</i> -chlorophenyl)porphyrin
Pc	phthalocyanine
PDP	(2 <i>R</i> ,2' <i>R</i> -(+)-[N,N'-bis(2-pyridylmethyl)]-2,2'-bipyrrolidine
PES	potential energy surface
Ph	phenyl
phen	1,10-phenanthroline
PhthN	phthalamido
Piv	pivaloyl
PMB	<i>p</i> -methoxybenzenesulfonyl
Por	porphyrin (generalized)
<i>R</i> -PTAD	[(<i>R</i>)-(-)-(1-adamantyl)-(N-phthalimido)acetato]
Py	pyridyl
Py ₅ Me ₂	2,6-bis(1,1-bis(2-pyridyl)ethyl)pyridine
<i>S</i> (Br)nttl	(2 <i>S</i>)-2-(1,3-dioxo-7-bromo-1 <i>H</i> -benzo[<i>de</i>]isoquinolin-2(3 <i>H</i>)-yl) propanoic acid
<i>S</i> -MEOX	(4 <i>S</i>)-2-oxo-4oxazolidinecarboxylic acid methyl ester
<i>S</i> -nta	(2 <i>S</i>)-2-(1,3-dioxo-1 <i>H</i> -benzo[<i>de</i>]isoquinolin-2(3 <i>H</i>)-yl) propanoic acid
<i>S</i> -nttl	N-1,8-naphthaloyl-(<i>S</i>)-tert-leucine
<i>S</i> -TBSP	(<i>S</i>)-N-(4- <i>tert</i> -butylbenzenesulfonyl)proline
<i>t</i> Bu	<i>tert</i> -butyl
<i>t</i> Bubipy	4,4'- <i>tert</i> -butyl-2,2'-bipyridine
<i>t</i> BuPc	<i>tert</i> -butylphthalocyanine
<i>t</i> Bu3tpy	4,4',4''-tri- <i>tert</i> -butyl-2,2':6',2''-terpyridine

Tces	2,2,2-trichloroethanoxysulfonyl
TDCITPP	5,10,15,20- tetra(2,6-dichlorophenyl)porphyrin
TEMPO	(2,2,6,6-tetramethylpiperidin-1-yl)oxyl
terpy	2,2':6',2''-terpyridine
Tf	trifluoromethanesulfonyl (triflyl)
THF	tetrahydrofuran
Tp	tris(pyrazolyl)borate
TPA	tetraphenylacetate
tpa	tris(picoly)amine
TPP	tetraphenylpophyrin
Ts	<i>p</i> -toluenesulfonyl
TTN	total turnover number
VT-NMR	variable-temperature nuclear magnetic resonance

Chapter 1:

Introduction to Transition Metal-Catalyzed Nitrene Transfer and Selected Discussion on Application to C(sp^3)-H Amination Reactions

This chapter is reprinted (adapted) with permission from work published in:

Alderson, J. M.; Corbin, J. R.; Schomaker, J. M. *Acc. Chem. Res.*, **2017**, *50*, 2147-2158.

Chapter 1

Introduction to Transition Metal-Catalyzed Nitrene Transfer and Selected Applications to C(sp³)-H and C=C Amination Reactions

1.1 Introduction

Carbon–nitrogen (C–N) bonds are ubiquitous in pharmaceuticals, agrochemicals, diverse bioactive natural products, and ligands for transition metal catalysts. An effective strategy for introducing a new C–N bond into a molecule is through transition metal-catalyzed nitrene transfer chemistry. In these reactions, a metal–supported nitrene can either add across a C=C bond to form an aziridine or insert into a C–H bond to furnish the corresponding amine. Typical catalysts for nitrene transfer include Rh₂L_n and Ru₂L_n complexes supported by bridging carboxylate and related ligands, as well as complexes based on Cu, Co, Ir, Fe, and Mn supported by porphyrins and related ligands. A limitation of metal-catalyzed nitrene transfer is the ability to predictably select which specific site will undergo amination in the presence of multiple reactive groups; thus, many reactions rely primarily on substrate control. Achieving true catalyst-control over nitrene transfer would open up exciting possibilities for flexible installation of new C–N bonds into hydrocarbons, natural product-inspired scaffolds, existing pharmaceuticals or biorenewable building blocks. Silver-catalyzed nitrene transfer enables flexible control over the position at which a new C–N bond is introduced. Ag(I) supported by simple N-donor ligands accommodates a diverse range of coordination geometries, from linear to tetrahedral to seesaw, enabling the electronic and steric parameters of the catalyst to be tuned independently. In addition, the ligand, Ag salt counteranion,

Ag/ligand ratio and the solvent all influence the fluxional and dynamic behavior of Ag(I) complexes in solution. Understanding the interplay of these parameters to manipulate the behavior of Ag-nitrenes in a predictable manner is a key design feature and advantage of Ag(I)-catalyzed nitrene transfer.

1.2 Background

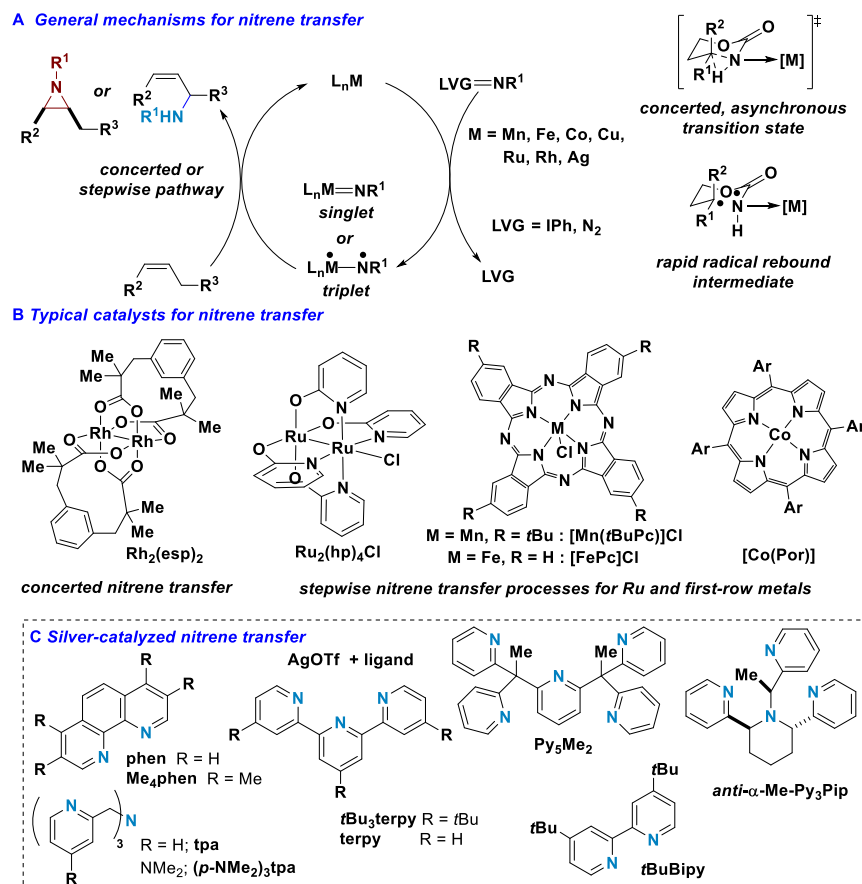
A contemporary challenge in catalysis is to achieve non-directed oxidation reactions, where the catalyst bears primary responsibility for dictating the specific site of functionalization. While the prevalence of C–H bonds in organic compounds render them useful functional handles, controlling the site of reaction in a predictable manner is difficult without relying on directing groups or inherent steric, electronic and stereoelectronic features of the substrate. 'Holy grail' C–H functionalizations that are selective for single reactive sites, controlled by catalyst rather than substrate, and tunable for different reactive sites within a single substrate are highly desirable.

Metal-catalyzed nitrene transfer reactions^{1–8} transform C=C and C–H bonds into new C–N bonds, streamlining syntheses of amines present in pharmaceuticals, agrochemicals, natural products, polymers and ligands. Nitrene transfer is promoted by diverse metals, including Rh,² Ru,³ Cu,⁴ Fe,⁵ Co,⁶ Mn,⁷ and Ag.⁸ The general mechanism (Scheme 1.1A) involves reaction of a nitrogen transfer reagent with an oxidant to generate an imidoiodinane (LVG=NR¹), which eventually forms a metal-supported singlet or triplet nitrene species. Whether addition or insertion of the metal nitrene into a C=C or C–H bond occurs in a concerted or stepwise fashion can impact the chemo-, site- and stereoselectivity of the reaction. For example, Rh₂L_n complexes supported by carboxylate and related ligands, such as Du Bois' Rh₂(esp)₂ catalyst (Scheme 1.1B),^{2g} promote concerted nitrene transfer and preserve the substrate's stereochemical information. In contrast,

Ru_2L_n and Co, Fe- and Mn-based catalysts reported by Zhang, Betley, White and others exhibit features of stepwise nitrene transfer and are thought to proceed via radical intermediates.³⁻⁷

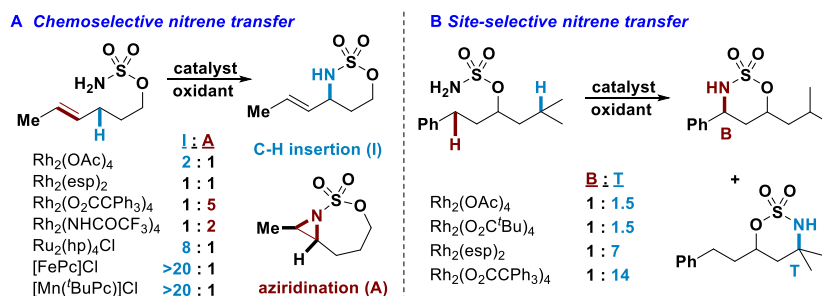
Rh_2L_n and Ru_2L_n complexes exhibit 'paddlewheel'-type coordination environments around the metal center,^{2,3b} while Co, Mn and Fe complexes employ porphyrin- and phthalocyanine-type ligands leading to similar coordination environments for first-row metals.⁵⁻⁷ In contrast, the diversity of ligands supporting Ag-catalyzed nitrene transfer⁸⁻¹⁹ (Scheme 1.1C) results in a broad range of steric environments around the metal.¹⁹ Our work highlights how differences in the coordination geometry and the fluxional behavior of Ag complexes in solution enables flexible, catalyst-controlled chemo- and site-selective nitrene transfer reactions.

Scheme 1.1. General features and complexes employed for metal-catalyzed nitrene transfer.



Catalyst control of reactive metal nitrene intermediates is challenging; however, some solutions have been developed. For example, substrates containing both C=C and allylic C–H bonds favor aziridination using Rh_2L_n with sulfamates (Scheme 1.2A).² Switching to a different metal, such as Ru_2L_n supported by a bridging 2-hydroxypyridine ligand, favors allylic amination instead.^{3b} Co, Fe- and Mn-based catalysts supported by modified porphyrin and phthalocyanine-type ligands also lead to chemoselective allylic C–H amination over aziridination.⁵⁻⁷ A more difficult problem occurs when two reactive C–H bonds are in competition (Scheme 1.2B). Rh_2L_n prefers amination of 3° alkyl C(sp³)–H (**T**) over benzylic C–H bonds (**B**); although **T**:**B** varies with the ligand identity, preference for **B** was not observed.^{2d} While **B** could be favored by switching to a different metal, changes to the substrate in Scheme 1.2B resulted in altered selectivity that could not be controlled through the catalyst.^{2d,7} We posit that the establishment of reliable design principles with predictive power is best served by limiting reaction variables and carefully studying nitrene transfer behaviors catalyzed by scaffolds based on a single metal.

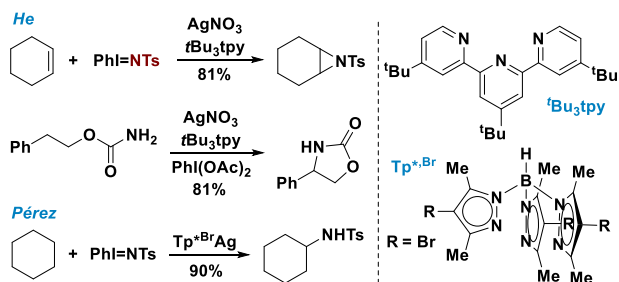
Scheme 1.2. Early efforts in chemo- and site-selective nitrene transfer.



He and co-workers reported the first examples of Ag-catalyzed nitrene transfer using terpyridine (tpy)-based ligands (Scheme 1.3).^{8a-c} Reactions were chemoselective for aziridination, although C–H insertion was possible in the absence of alkenes. In related work, Pérez described anionic trispyrazolylborate (Tp) ligands for Ag-catalyzed nitrene transfer.^{8d,e} While electronic

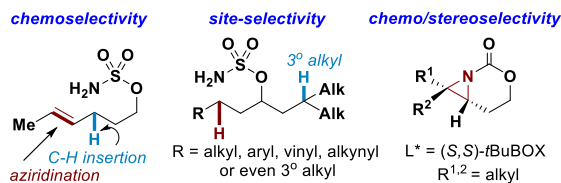
modifications to Tp ligands impact catalyst reactivity, the similar coordination geometries and lack of reported dynamic behavior precluded our further investigations of these scaffolds.

Scheme 1.3. Early examples of Ag-catalyzed nitrene transfer.



In the course of the work described in this chapter, four major design principles were identified to enable the Schomaker group to achieve chemo-, site- and stereoselective nitrene transfer reactions (Figure 1.1) catalyzed by Ag(I) complexes supported by simple N-donor ligands.⁹⁻¹⁹ 1) changing Ag:ligand ratios to influence chemoselectivity,^{9-11,15,17,18} 2) manipulating the steric environment of the catalyst to achieve site-selective C–H bond amination,^{12-14,16,19} 3) promoting non-covalent interactions between Ag/substrate or substrate/ligand to direct C–H functionalization¹⁹ and 4) dictating the trajectory of approach of substrate to Ag-nitrene.^{14,18}

Figure 1.1. Chemo-, site- and stereoselective C–N bond formation via silver catalysis.

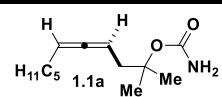
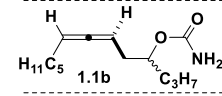
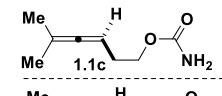
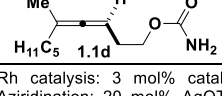


1.3 Chemodivergent Amination via Changes in the Silver:Ligand Ratio

The ability of Ag(I) to accommodate diverse coordination geometries stimulated our curiosity as to whether changes in the Ag:ligand ratio could control chemoselectivity in nitrene transfer.^{10,11}

Table 1.1 compares the behavior of Rh_2L_n with Ag(I) complexes supported by 1,10-phenanthroline (phen) in reactions of homoallylic carbamates **1.1a-d** to furnish bicyclic methyleneaziridines **1.2a-d** and allenic amines **1.3a-d**, respectively.¹⁰ $\text{Rh}_2(\text{esp})_2$ (entries 1, 8, 11, 14) yielded mixtures of **1.2:1.3**, indicating significant substrate control; however, a 1:1.25 $\text{AgOTf}:\text{phen}$ stoichiometry with **1.1a-d** (entries 4, 9, 12 and 15) gave a good balance between yield and selectivity for **1.2a-d**. Increasing the phen: AgOTf ratio to 3:1 (entries 7, 10, 13 and 16) favored C–H insertion to deliver **1.3a-d** as the major product, irrespective of the substrate.

Table 1.1. Influence of ligand and silver:ligand ratio on chemoselectivity.

substrate	entry	catalyst ^{a-c}	1.2 : 1.3	yield
 1.1a	1	$\text{Rh}_2(\text{esp})_2$	1 : 16	85%
	2	0.2 : 0.1 equiv $\text{AgOTf}:\text{phen}$	5.6 : 1	72%
	3	0.2 : 0.2	5.8 : 1	88%
	4	0.2 : 0.25	5.9 : 1	93%
	5	0.2 : 0.3	5.6 : 1	82%
	6	0.2 : 0.4	1 : 4.0	90%
	7	0.2 : 0.6	1 : >19	78%
 1.1b	8	$\text{Rh}_2(\text{esp})_2$	1 : 1	68%
	9	(phen) AgOTf	8.9 : 1	89%
	10	(phen) $_2\text{AgOTf}$	1 : >19	78%
 1.1c	11	$\text{Rh}_2(\text{esp})_2$	2 : 1	52%
	12	(phen) AgOTf	>19 : 1	83%
	13	(phen) $_2\text{AgOTf}$	1 : >19	81%
 1.1d	14	$\text{Rh}_2(\text{esp})_2$	1 : 1.3	78%
	15	(phen) AgOTf	12.4 : 1	94%
	16	(phen) $_2\text{AgOTf}$	1 : >19	88%

^aRh catalysis: 3 mol% catalyst, 2 equiv PhIO, 4 Å MS, CH_2Cl_2 , rt.
^bAziridination: 20 mol% AgOTf , 25 mol% phen, 2 equiv PhIO, 4 Å MS, CH_2Cl_2 , rt. ^cC–H insertion: 10 mol% AgOTf , 30 mol% phen, 3.5 equiv PhIO, 4 Å MS, CH_2Cl_2 , rt.

Varying Ag:ligand ratios in the amination of homoallylic carbamates (Table 1.2) showed similar levels of chemodivergence.¹⁰ For example, *trans*-disubstituted **1.4a** gave increased selectivity for aziridine **1.5a** when switching from $\text{Rh}_2(\text{OAc})_4$ to (phen) AgOTf (entries 1-2), while increasing the Ag:ligand ratio (entry 3) favored C–H insertion to furnish **1.6a**. This trend held for **1.4b** (entries 4-6) and **1.4c** (entries 7-9); olefin stereochemistry was transferred to products with no isomerization.

The 1,1'-disubstituted **1.4d** gave better results for aziridination (entry 11) compared to $\text{Rh}_2(\text{OAc})_4$ (entry 10), but moderate selectivity for C–H insertion (entry 12). The multiple activated C–H and C=C bonds in **1.4e** (entries 13-15) presented the opportunity for competing aziridination in addition to amination at the allylic C-H_a and benzylic C-H_b bonds. $\text{Rh}_2(\text{esp})_2$ (entry 13) gave poor chemoselectivity, but good site-selectivity for C–H_a amination. (Phen)AgOTf (entry 14) favored aziridination, while (phen)₂AgOTf showed a 2:1 preference for allylic over benzylic C–H amination in **1.6e** (entry 15).

Table 1.2. Influence of catalyst identity and Ag:ligand ratio on chemoselectivity in reactions of homoallylic carbamates.

substrate	entry	catalyst ^{a-c}	1.5 : 1.6	yield	dr	substrate	entry	catalyst ^{a-c}	1.5 : 1.6	yield	dr
	1	$\text{Rh}_2(\text{OAc})_4$	4.9 : 1	82%	trans		10	$\text{Rh}_2(\text{OAc})_4$	7 : 1	40%	---
	2	(phen)AgOTf	11.6 : 1	97%	trans		11	(phen)AgOTf	>19 : 1	85%	---
	3	(phen) ₂ AgOTf	1 : 6.6	84%	trans		12	(phen) ₂ AgOTf	1 : 2.9	89%	---
	4	$\text{Rh}_2(\text{OAc})_4$	3.2 : 1	76%	cis		13	$\text{Rh}_2(\text{esp})_2$	1 : 1.1 H _a : 0 H _b	79%	---
	5	(phen)AgOTf	16 : 1	71%	cis		14	(phen)AgOTf	9.4 : 1 (H _a +H _b)	94%	6.2:1
	6	(phen) ₂ AgOTf	1 : >19	93%	cis		15	(phen) ₂ AgOTf	0 : 2 H _a : 1 H _b	95%	H _a 2.5:1 H _b 2.9:1
	7	$\text{Rh}_2(\text{esp})_2$	1.8 : 1	70% ^d	---						
	8	(phen)AgOTf	9.9 : 1	98%	3.2:1						
	9	(phen) ₂ AgOTf	1 : >19	91%	3:1						

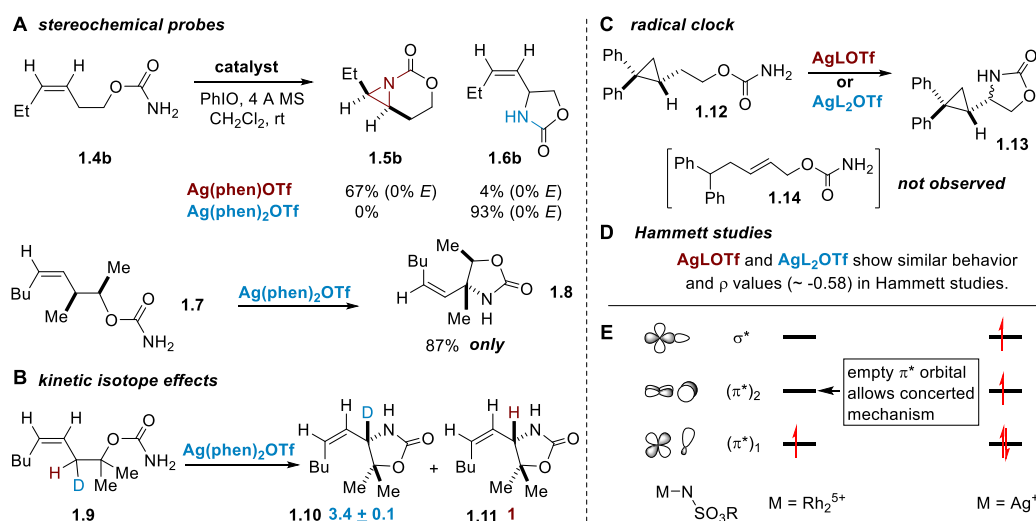
^a Rh: 3 mol% Rh cat, 2 equiv PhIO, 4 Å MS, CH_2Cl_2 , rt. ^b Aziridination: 20 mol% AgOTf, 25 mol% **Lig**, 2 equiv PhIO, 4 Å MS, CH_2Cl_2 , rt. ^c C–H insertion: 10 mol% AgOTf, 30 mol% **Lig**, 3.5 equiv PhIO, 4 Å MS, CH_2Cl_2 , rt. ^d NMR yields, mesitylene as internal standard.

The mechanisms of nitrene transfer catalyzed by AgLOTf and AgL₂OTf (L=phen or *t*BuBipy) were explored using stereochemical probe, kinetic isotope effect (KIE), radical clock and Hammett studies (Scheme 1.4).^{10,15} Lack of isomerization in the aziridination of **1.4b** or C–H amination of **1.7** (Scheme 1.4A) supported either a concerted or rapid radical rebound pathway, corroborated by the similarity of the KIE value of 3.4 (Scheme 1.4B) to values reported for Rh_2L_n catalysts² and the absence of cyclopropane **1.12** ring-opening (Scheme 1.4C) with (*t*BuBipy)AgOTf or

(*t*BuBipy)₂AgOTf. Hammett studies (Scheme 1.4D) gave ρ values of ca. -0.58 for both (*t*BuBipy)AgOTf and (*t*BuBipy)₂AgOTf, indicating positive charge build-up in the transition state. While aziridination and C–H amination initially appeared to occur *via* similar concerted mechanistic pathways, computational studies showed concerted nitrene transfer in Rh₂L_n catalysis requires an empty N-centered orbital in the metal-nitrene intermediate, necessitating a low-spin state (Scheme 1.4E).²⁰ Interestingly, the electronic structures of Ag-nitrenes are high-spin and do not contain empty N-centered orbitals; thus, these reactions must be stepwise.

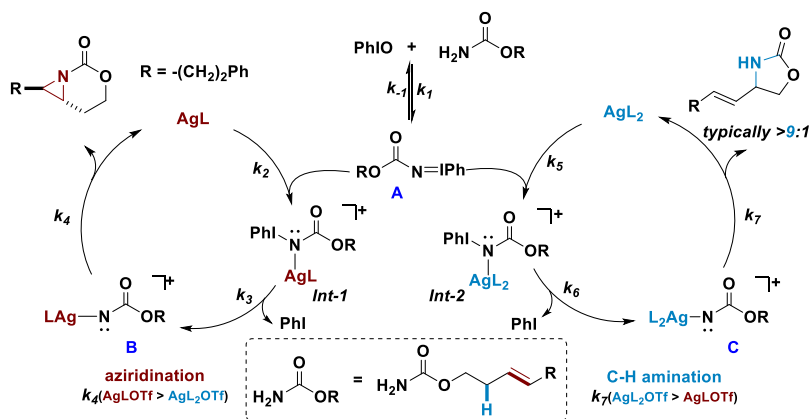
These contradictory results were studied computationally, inspired by a Pérez report describing TpAg-catalyzed aziridination.²¹ These studies suggested that Ag-nitrenes engage C=C or C–H bonds in a stepwise fashion, but discrete radical species representing stationary points on the potential energy surface are never formed. The Schomaker group termed this 'elementary hydrogen transfer/radical recombination' (EHT-RR), which occurs via a single hydrogen-transfer transition state, followed by a 'barrierless' radical recombination step to form the new C–N bond, resulting in retention of the substrate's stereochemical information.¹⁵

Scheme 1.4. Mechanistic probes of chemoselective, Ag-catalyzed nitrene transfer.



Since experimental and computational studies indicated that AgLOTf and AgL₂OTf catalyze nitrene transfer through similar mechanisms, chemodivergence likely arises from the differing steric environment around the Ag-nitrene, furnishing different rates of aziridination *vs.* C–H amination.¹⁵ Kinetic profiling of the entire reaction course with AgLOTf and AgL₂OTf showed similar steady-state kinetics for aziridination and C–H insertion, with the overall reaction rate primarily controlled by imidoiodinane **A** formation (Scheme 1.5). The active metal-nitrene species **B** or **C** carries out aziridination or C–H insertion, depending on the Ag coordination number. Reaction rates using varied ligand loadings and initial substrate concentrations suggest aziridination is intrinsically faster than C–H amination.

Scheme 1.5. Proposed mechanisms of chemodivergent aziridination and C–H amination.



However, Ag catalysis displays a complex dependence on both the stability and population of reactive intermediates dictated by the steric environment at Ag; the aziridination rate was suppressed as steric congestion increased in AgL₂OTf, while the C–H insertion rate decreased slightly using AgLOTf *vs.* AgL₂OTf. Overall, the steric environment of the putative nitrene exerts the primary influence on chemoselectivity and leads to differences in the rate constants for the key oxidative steps (k_4 for aziridination and k_7 for C–H amination) in each cycle (Scheme 1.5).

1.4. Chemoselective, Asymmetric Intramolecular Aziridination

Asymmetric aziridination reactions are powerful tools for synthesizing enantioenriched amine building blocks, but the scope is limited to mono- and disubstituted alkenes.²² Our ability to control the chemoselectivity of Ag-catalyzed nitrene transfer prompted us to explore bis(oxazoline) (BOX) ligands to transform di- and trisubstituted homoallylic carbamates into enantioenriched [4.1.0]-carbamate-tethered aziridines.¹⁷ Optimal *ee* values (Table 1.3) were obtained using AgClO₄ and a (*S,S*)-*t*BuBOX ligand in CH₂Cl₂ at -20 °C. Carbamates were required for good chemoselectivity and *ee*. Both *E*- and *Z*- di- and trialkylsubstituted homoallylic carbamates **1.15a-g** (Table 1.3) delivered aziridines **1.16a-g** in good yields and *ee* >90%. Aziridine ring-opening occurred smoothly at the distal aziridine carbon with halides, azide, cuprates, sulphides and carboxylates, to furnish amines with no erosion in the *ee*.¹⁷ Efforts to identify chiral ligands for the corresponding asymmetric C-H bond amination reactions are ongoing.

Table 1.3. Selected examples of asymmetric, silver-catalyzed nitrene transfer.

Reaction scheme showing the conversion of homoallylic carbamate **1.15a-g** to aziridine **1.16a-g** using 20 mol% AgClO_4 , 10 mol% ligand, 2 equiv PhIO , 4 Å MS, CH_2Cl_2 , -20°C . The product **1.16a-g** is shown with a (S,S) -tBuBOX ligand.

entry	R^1, R^2	yield	<i>ee</i>	entry	R^1, R^2	yield	<i>ee</i>
1	Et, H	83% 1.16a	91% <i>ee</i> ^a	5	H, PhCH_2	80% 1.16e	91% <i>ee</i>
2	H, Et	87% 1.16b	92% <i>ee</i> ^a				>99% <i>ee</i> ^b
3	H, <i>i</i> Pr	63% 1.16c	92% <i>ee</i> ^a	6	Me, Et	81% 1.16f	92% <i>ee</i> ^a
4	H, $(\text{CH}_2)_2\text{OTBS}$	87% 1.16d	92% <i>ee</i> ^a	7	Me, <i>c</i> -Hex	84% 1.16g	90% <i>ee</i>

^a *ee* determined after ring-opening of aziridine with NaI . ^b *ee* after recrystallization.

^a *ee* determined after ring-opening of aziridine with NaI. ^b *ee* after recrystallization.

1.5. Chemoselective, Intermolecular Ag-catalyzed Amination

Control over intermolecular chemoselectivity in the presence of multiple reactive sites was the next goal. A dimeric silver complex supported by 4,4',4''-tri-*tert*-butyl-2,2':6',2''-terpyridine (*t*Bu₃tpy), [(*t*Bu₃tpy)AgOTf]₂, favored intermolecular aziridination of cyclic alkenes when paired

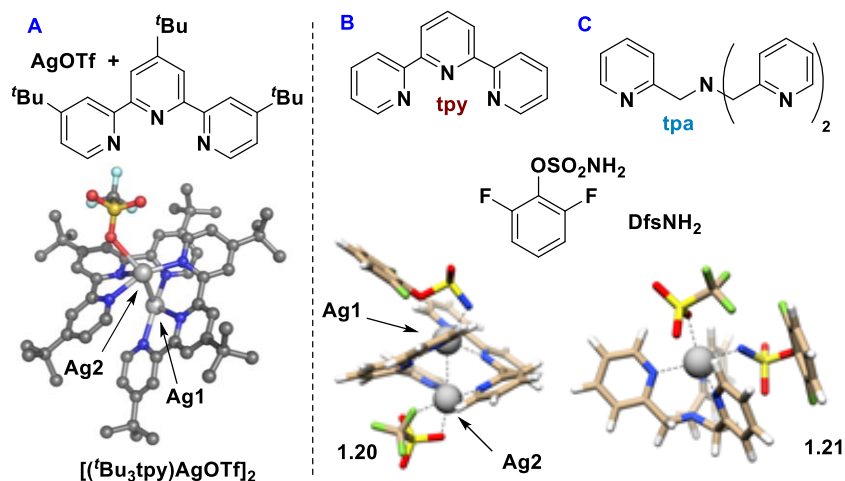
with HfsNH₂.¹⁴ Selectivity increased with ring size (Table 1.4, compare entries 1, 3, 5), with **1.17c** giving mainly aziridine **1.18c**. Trisubstituted cyclohexenes **1.17d-g** gave similarly high levels of chemoselectivity (entries 7, 9, 11) when R=Me or Ph, but exhibited a decreased preference for aziridination in the enyne **1.17g** (entry 13). In contrast, employing tris(2-pyridylmethyl)amine (tpa) as the ligand with DfsNH₂ favored allylic C-H bond amination. Selectivity depended on ring size; cyclohexene (entry 4) proved superior to either 5- or 7-membered rings (entries 2, 6). Preference for C-H amination in trisubstituted cyclohexenes **1.17d-g** gave good-to-excellent chemoselectivities ranging from 3.2:1 to 17:1 (entries 8, 10, 12, 14). In addition, site-selectivity between C-H_a and the hindered C-H_b (H_a:H_b) ranged from 3.0:1 when R=Me in **1.17d** (entry 8) to ~5.5:1 for R=Ar in **1.17e** and **1.17f** (entries 10, 12). Interestingly, the highest H_a:H_b ratio of 11:1 was noted in enyne **1.17g** (entry 14). These examples showcase the sensitivity of intermolecular metal-nitrene transfer to the steric environment at the reactive site.

Experimental probes of chemoselective, intermolecular amination using [(^tBu₃tpy)AgOTf]₂ and (tpa)AgOTf presented a puzzling mechanistic picture.¹⁴ [(^tBu₃tpy)AgOTf]₂ exists as a dimer in both the solid and solution states as determined by X-ray crystallography (Figure 1.2A) and NMR diffusion spectroscopy (DOSY).^{10,18} The crystal structure contained a single bound triflate anion, resulting in two inequivalent Ag atoms, Ag1 and Ag2. This complex was employed as the starting point for computational studies, except ^tBu₃tpy was replaced with Bu₃tpy to simplify the calculations. As the Ag counteranion has minimal effect on the chemoselectivity, the nitrene complex formed from DfsNH₂ was optimized bound to Ag1 (Figure 1.2B) to yield the computed structure **1.20** [(tpy)Ag]₂(DfsN)(OTf).

Table 1.4. Catalyst control of the chemoselectivity of intermolecular nitrene transfer.

substrate	entry	ligand	A ^a (1.18) I	(H _a + H _b) ^a (1.19) A : I
	n = 0 1.17a 1	^t Bu ₃ tpy	61%	11% 5.5 : 1
	2	tpa	13%	35% 1 : 2.7
	n = 1 1.17b 3	^t Bu ₃ tpy	84%	13% 6.5 : 1
	4	tpa	8%	46% 1 : 5.8
	n = 2 1.17c 5	^t Bu ₃ tpy	59%	2% 30 : 1
	6	tpa	20%	24% 1 : 1.2
	7	^t Bu ₃ tpy	73%	7% 10 : 1
	8	tpa	7%	61% 1 : 8.7
	9	^t Bu ₃ tpy	73% ^b	16% 4.6 : 1
	10	tpa	20%	60% 1 : 3.2
	11	^t Bu ₃ tpy	57% ^b	6% 9.5 : 1
	12	tpa	3%	51% 1 : 17
	13	^t Bu ₃ tpy	51%	17% 3.0 : 1
	14	tpa	8%	62% 1 : 7.8
	15	^t Bu ₃ tpy	65% 1:11 <i>syn:anti</i>	10% 6.5 : 1
	16	tpa	12%	49% 1 : 4.1

A: 10 mol% AgOTf, 12 mol% ^tBu₃tpy, **HfsNH₂**, 3.5 equiv PhIO, CH₂Cl₂, 4 A MS, 4 h, rt. **I:** 10 mol% AgOTf, 12 mol% tpa, **DfsNH₂**, 1.2 equiv PhIO, CH₂Cl₂, 4 A MS, 1 h, rt. ^b Aziridine was opened with MeOH.

Figure 1.2. A) X-ray crystal structure of [(^tBu₃tpy)AgOTf]₂. B) Optimized computed structure of [(tpy)Ag]₂(DfsN)(OTf) **1.20**. C) Optimized computed structure of (tpa)Ag(OTf)(NSO₃R) **1.21**.

Chemoselectivity is impacted by the Ag counteranion when a tpa ligand is utilized, suggesting it is bound to the Ag-nitrene.¹⁴ Optimization of (tpa)Ag(OTf)(NSO₃R) **1.21** (Figure 2C) showed the nitrene prefers equatorial binding *cis* to the tertiary amine, while the triflate anion binds at the axial site. This contrasts with axial binding of the nitrene ligand in **1.20** (Figure 2B), implying that changes in the trajectory of approach of substrate to the Ag-nitrene influence chemoselectivity in intermolecular reactions. More importantly, computations revealed two distinct nitrene-transfer mechanisms for the two different catalysts:¹⁴ 1) a late transition-state from **1.20**, followed by barrierless recombination to preserve stereochemical information present in the substrate and 2) an early transition state from **1.21**, proceeding through H-atom transfer to yield radical intermediates. The major difference between these mechanisms is the extent to which the Ag–N bond breaks during the HAT transition state, with the stronger Ag-nitrene bond in **1.21** resulting in longer-lived radicals. The strength of the Ag–N bond in the Ag-nitrene complex determines whether reaction proceeds via 'barrierless' radical recombination or generates radicals that respond to experimental probes. Both supporting ligand and counteranion binding influence the mechanism and the trajectory of approach of substrate to the Ag-nitrene, with the ligand displaying an unusual ability to influence the lifetime of the Ag-nitrene.¹⁴

1.6. Catalysts for Tuning the Site-Selectivity of C-H Bond Amination. Moving from chemoselective to site-selective C-H amination required an expanded ligand scope (Scheme 1.1C). Depending on counteranion, ligand, Ag:ligand ratio, solvent and concentration, Ag(I) can be 3-, 4-, 5- or even 6-coordinate, giving rise to different steric and electronic environments that can be leveraged to choose a specific C–H bond for amination.¹⁸ The following discussion is sub-divided into different classes of competing C–H bonds.

1.6.1. Catalysts Favoring Amination of 3° Alkyl C(sp³)–H Bonds.

Rh₂L_n catalysts prefer amination of 3° C(sp³)–H over benzylic C–H bonds (Scheme 1.1B), particularly as the size of the ligand on Rh is increased.^{3c} Achieving similar selectivity using silver catalysis could be advantageous, as Ag is ~50 times less expensive than Rh on a molar basis. Bipyridine-based ligands showed some success (Table 1.5) and were relatively insensitive to sterics; moving from Me to isopropyl had minimal impact on selectivity (entries 1, 4).¹² However, electronic effects were still important, as selectivity for **1.23g** over **1.24g** was improved when the benzylic C–H bond was electron-poor as opposed to electron-rich (entries 6-7). Nonetheless, the ability of (*t*Bubipy)₂AgOTf to select for 3° alkyl C–H over benzylic C–H bonds, irrespective of substrate, was a promising step towards achieving catalyst-controlled C–H amination.

Table 1.5. Site-selective amination of 3° alkyl C(sp³)–H over benzylic C–H bonds.

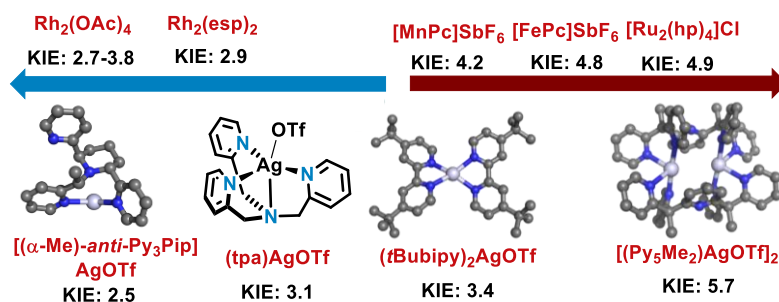
entry	R ¹ /R ²	Ar	1.23: 1.24	yield
1		Ph	1.22a	2.9 : 1 75%
2		Ph	1.22b	5.2 : 1 81%
3		Ph	1.22c	4.8 : 1 81%
4		Ph	1.22d	2.6 : 1 75%
5		Ph	1.22e	8.0 : 1 81%
6		1.22f Me	2.0 : 1	77%
7		1.22g CF ₃	6.3 : 1	80%

1.6.2. Catalysts for Amination of Benzylic C–H Over 3° Alkyl C(sp³)–H Bonds.

We reasoned the design of Ag catalysts for reaction of benzylic C–H over 3° C(sp³)–H bonds could be approached in three ways: 1) identify Ag catalysts for stepwise H-atom abstraction to target the weakest C–H bond, 2) leverage the steric accessibility of the 2° benzylic site using bulky ligands and/or dimeric catalysts or 3) identify catalysts that engage non-covalent Ag- π interactions between metal/substrate or π - π interactions between substrate/ligand to drive selectivity.

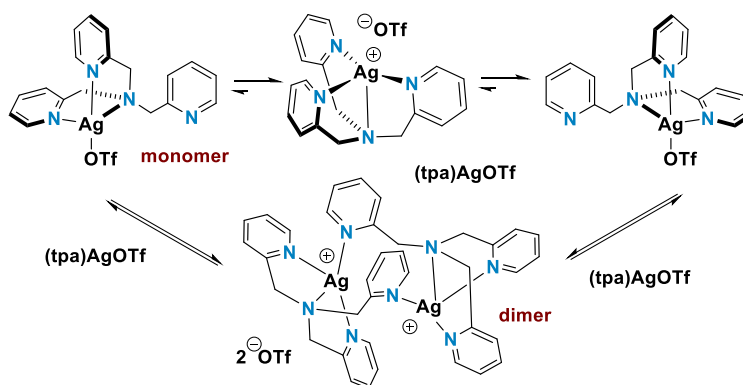
To aid in the choice of catalysts for further studies, KIE values for several nitrene transfer catalysts were obtained (Figure 1.3).^{10,12,15,24} KIE values reflect a spectrum of reaction mechanisms, with lower values associated with concerted processes and higher values indicating the potential for long-lived radical intermediates. Stepwise nitrene transfer for [(Py₅Me₂Ag)OTf]₂, a sterically congested dimeric complex in both the solid and solution state, is suggested by its high KIE of 5.7 and response to radical inhibitors.¹³ Tris(2-pyridylmethyl)amine-supported (tpa)AgOTf has a KIE similar to Rh₂L_n catalysts, but mechanistic studies show it engages in what we have termed 'elementary hydrogen transfer/radical recombination'. A single hydrogen-transfer transition state is followed by a radical recombination step with no energy barrier (the radical species are not stationary points on the potential energy surface).

Figure 1.3. KIE values for catalysts promoting nitrene transfer.



While (tpa)AgOTf prefers a monomeric solution-state structure, the picture is complicated by monomer:dimer equilibria and fluxional behavior of the pyridine arms of the ligand (Figure 1.4).¹⁸ We were curious how this unusual mechanism and dynamic behavior might influence the site-selectivity of the reaction. Finally, we designed the catalyst [α -Me-(*anti*)-Py₃Pip]AgOTf (KIE 2.5), which displays minimal dynamic behavior and contains open coordination sites to facilitate non-covalent interactions between catalyst and substrate.²³

Figure 1.4. Dynamic behavior of (tpa)AgOTf.



Several catalysts in Figure 3 were investigated with **1.22a** (Table 1.6).^{19,23} Rh₂(esp)₂ favored **1.24a** (entry 1), but surprisingly, Ru₂(hp)₄Cl, [(Py₅Me₂)AgOTf]₂ and (tpa)AgOTf showed only a modest preference for **1.23a** (entries 2-4).^{2d} [FePc]Cl/AgSbF₆ (entry 3) gave mainly **1.23a**, although its KIE was similar to that of Ru₂(hp)₄Cl. Interesting, the selectivity for **1.23a** using (tpa)AgOTf (entries 5-6)¹⁸ or [α -Me-(*anti*)-Py₃Pip]AgOTf (entries 7-10) were further improved by decreasing the temperature or switching the solvent. The preference for benzylic amination, despite the low KIEs of (tpa)AgOTf and [α -Me-(*anti*)-Py₃Pip]AgOTf, stimulated our curiosity as to whether there might be other factors at play in dictating the site-selectivity, including potential non-covalent interactions (*vide infra*).

Table 1.6. Comparison of selectivity for benzylic amination with known and new Ag(I) catalysts.

entry	catalyst	solvent	temp (°C)	1.23a : 1.24a	yield
1	[Rh ₂ (esp) ₂] ^{ref}	CH ₂ Cl ₂	40	1 : 7	---
2	[Ru ₂ (hp) ₄ Cl] ^{ref}	CH ₂ Cl ₂	40	1.5 : 1	---
3	[FePc]Cl/AgSbF ₆ ^{ref}	4:1 PhMe:MeCN	rt	14 : 1	51%
4	[(Py ₅ Me ₂)AgOTf] ₂	CH ₂ Cl ₂	rt	2.6 : 1	80%
5	(tpa)AgOTf	CH ₂ Cl ₂	rt	2.6 : 1	84%
6	(tpa)AgOTf	CH ₂ Cl ₂	-20	3.5 : 1	94%
7	(tpa)AgOTf	CHCl ₃	-20	4.3 : 1	92%
8	[α-Me-(<i>anti</i>)-Py ₃ Pip]AgOTf	CH ₂ Cl ₂	rt	3.6 : 1	96%
9	[α-Me-(<i>anti</i>)-Py ₃ Pip]AgOTf	CH ₂ Cl ₂	-20	4.5 : 1	91%
10	[α-Me-(<i>anti</i>)-Py ₃ Pip]AgOTf	CHCl ₃	-20	5.7 : 1	87%
11	[α-Me-(<i>anti</i>)-Py ₃ Pip]AgOTf	F ₃ CPh	-20	8.5 : 1	95%

^a General conditions for Ag-catalyzed reactions: 10 mol % Ag catalyst, 3.5 equiv PhIO, 4 Å molecular sieves.

Substrate scope studies (Table 1.7) showed selectivity for benzylic amination increased as steric hindrance at the 3° C–H bond increased (entries 1-9). Altering the electronics of the benzylic C–H bond in **25c-d** had a drastic effect on selectivity (entries 10-13). An electron-donating OMe in **25c** favored **26c** with both tpa and α-Me-(*anti*)-Py₃Pip ligands (entries 10-11); however, an electron-withdrawing CF₃ decreased selectivity to 1.4-1.8:1 **26d:27d** (entries 12-13). A 3° benzylic C–H bond in **25e-g** required [(Py₅Me₂)AgOTf]₂ to favor **26e-g** (entries 16, 18, 20), although the overall selectivity was lower compared to substrates with 2° benzylic C–H bonds.

The KIE (Figure 1.3) and Hammett ρ values (not shown) for various nitrene transfer catalysts showed similarities between (tpa)AgOTf/[(Py₅Me₂)AgOTf]₂ and Rh₂L_n catalysts, yet the selectivity displayed by (tpa)AgOTf was reminiscent of Fe and Ru complexes. While Ag, Fe and Ru complexes all promote stepwise nitrene transfer, the differing KIEs and behaviors in standard mechanistic probes led us to consider if additional factors might be contributing to the observed selectivity. Attractive, non-covalent π⋯π interactions between aromatic rings, as well as metal-π interactions, are well-known and play important structural roles in molecular recognition, template-directed synthesis and protein folding.²¹ We wanted to explore if similar π-π or Ag-π

interactions could explain the unexpected selectivities observed in our Ag-catalyzed nitrene transfer reactions.^{19,23}

Table 1.7. Impact of ligand identity on preference for benzylic C–H amination.

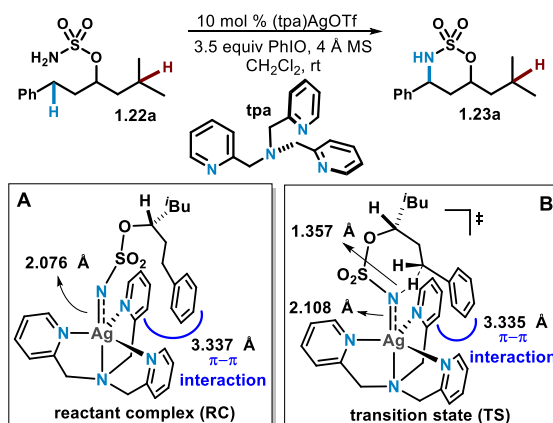
substrate	entry	catalyst/ligand ^a	solvent	temp	29 : 30	yield
	1	[(Py ₅ Me ₂)AgOTf] ₂	CH ₂ Cl ₂	rt	2.6 : 1	80%
	2	(tpa)AgOTf	CHCl ₃	-20	4.3 : 1	92%
	3	α -Me-(<i>anti</i>)-Py ₃ Pip	CHCl ₃	-20	5.7 : 1	87%
	4	[(Py ₅ Me ₂)AgOTf] ₂	CH ₂ Cl ₂	rt	7.6 : 1	95%
	5	(tpa)AgOTf	CHCl ₃	-20	8.6 : 1	94%
	6	α -Me-(<i>anti</i>)-Py ₃ Pip	CHCl ₃	-20	12.8 : 1	87%
	7	[(Py ₅ Me ₂)AgOTf] ₂	CH ₂ Cl ₂	rt	>19 : 1	77%
	8	(tpa)AgOTf	CH ₂ Cl ₂	rt	>19 : 1	63%
	9	α -Me-(<i>anti</i>)-Py ₃ Pip	CHCl ₃	-20	>19 : 1	63%
	10	(tpa)AgOTf	CHCl ₃	-20	>19 : 1	84%
	11	α -Me-(<i>anti</i>)-Py ₃ Pip	CHCl ₃	-20	>19 : 1	81%
	12	(tpa)AgOTf	CHCl ₃	-20	1.4 : 1	92%
	13	α -Me-(<i>anti</i>)-Py ₃ Pip	CHCl ₃	-20	1.8 : 1	88%
	14	[Rh ₂ (tpa) ₄]	CH ₂ Cl ₂	rt	1.1 : 1	93%
	15	(Me ₄ phen) ₂ AgOTf	CH ₂ Cl ₂	rt	1 : 3.8	95%
	16	[(Py ₅ Me ₂)AgOTf] ₂	CH ₂ Cl ₂	rt	2.3 : 1	84%
	17	[Rh ₂ (tpa) ₄]	CH ₂ Cl ₂	rt	1 : >19	70%
	18	[(Py ₅ Me ₂)AgOTf] ₂	CH ₂ Cl ₂	rt	8.4 : 1	81%
	19	[Rh ₂ (tpa) ₄]	CH ₂ Cl ₂	rt	1 : >19	93%
	20	[(Py ₅ Me ₂)AgOTf] ₂	CH ₂ Cl ₂	rt	2.7 : 1	83%

^a10 mol% AgOTf, 12 mol% **ligand**, 3.5 equiv PhIO, 0.05 M solvent, 4 Å MS

Experimental support for non-covalent interactions between Ag catalysts and substrates bearing π bonds was provided by pairing an electron-rich ligand (*p*-Me₂N)₃tpa ligand with substrates **1.28a** and **1.25d**, containing electron-poor benzylic C–H bonds (Table 1.8).¹⁹ The selectivity for **1.29a** and **1.26d** was essentially doubled (entries 3, 6) compared to the parent (tpa)AgOTf catalyst.

and catalytic methods for selective C-H oxidations that meet this criterion are outlined in the following subsections.

Scheme 1.6. Computed Ag-nitrene intermediate of (tpa)AgOTf supports non-covalent interactions between catalyst and substrate.



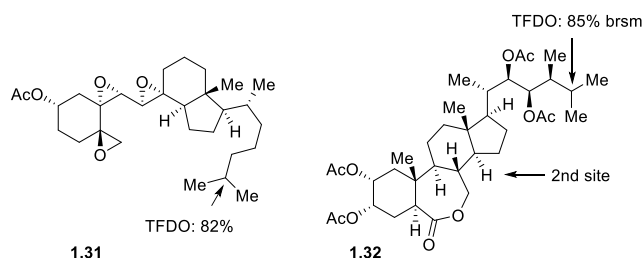
1.7.1 Representative Stoichiometric Methods

Interestingly, in the context of stoichiometric C-H oxidations in the absence of a transition metal catalyst, most examples involve structurally complex small molecules to highlight the utility of the method in late stage modification of molecules with multiple reactive sites and oxidizable functionality. These methods can be highly selective for a single C-H bond in good yields and are extremely impressive looking. However, in the absence of the development of a new reagent or transition metal-catalyzed variations, the inherent substrate-controlled selectivity cannot be overcome, and predicting which site will be oxidized prior to running the reaction can be difficult to predict.

A few general lines of thinking can be used to rationalize the substrate-controlled outcomes in complex molecule C-H oxidation reactions.^{25a} Scheme 1.7 shows the selective tertiary C-H

hydroxylation of **1.31** and **1.32** by TFDO in the presence of other similar C-H bond sites. While the selectivity is impressive, this substrate-controlled outcome can be rationalized by oxidizing the most sterically accessible C-H bond that is simultaneously farthest from electron-withdrawing groups; ethers in the case **1.31** or acetoxy groups in the case of **1.32**.^{25b-e}

Scheme 1.7. Selective C-H oxidation at most sterically accessible and electron-rich sites.

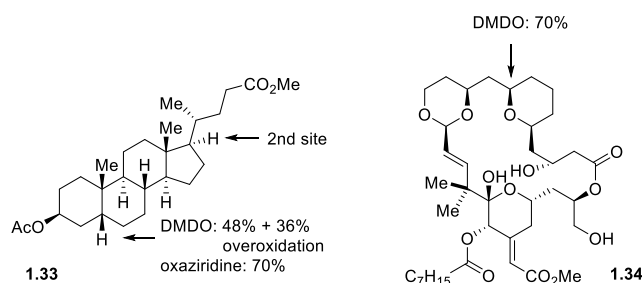


More striking is the selective oxidation of **1.33** by DMDO or oxaziridine (Scheme 1.8). While multiple sterically similar and more electron-rich C-H bonds are present in the molecule, the lone equatorial C-H bond undergoes hydroxylation despite being closest to the electron-withdrawing acetoxy group. Strain-release in the transition state is thought to be the reason that equatorial C-H bonds generally undergo oxidation at a faster rate than axial C-H bonds.^{25f-g} Unfortunately, the underlying reason for a given selectivity is not readily apparent, as in **1.34**, in which an ethereal C-H bond undergoes selective hydroxylation. While this is certainly in part due to increased electron-density in this C-H bond by hyperconjugation with the vicinal oxygen lone-pair, without a better understanding of the substrate conformation in solution no definitive reason can be stated.^{25h}

1.7.2. Representative Catalytic Methods

A more powerful approach would be to develop catalyst-controlled C-H oxidation methods that are highly chemo- and site-selective in a predictable and modular way. Catalyst-controlled C-H bond oxidations have the potential to overcome inherent substrate-controlled outcomes by tuning the steric and electronic environment around the transition metal to override substrate preferences. This area has been largely underexplored, especially in the context of transition metal-catalyzed nitrene transfer but some strategies have surfaced.

Scheme 1.8. Strain-release as a selectivity determining feature and hyperconjugation effects.

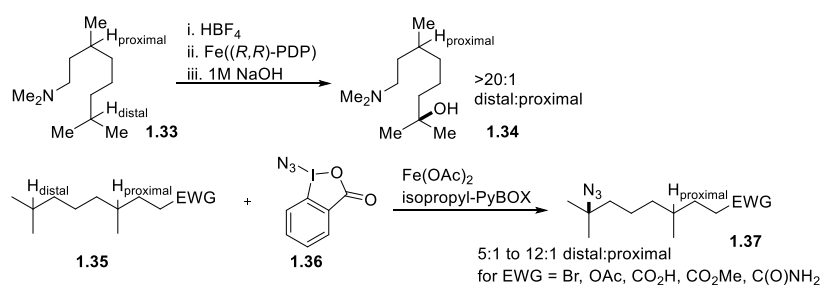


The simplest strategy to catalytically achieve site-selective oxidation of similar C-H bonds is to electronically differentiate the C-H bonds (Scheme 1.9). For example, protonation of the tertiary amine in **1.33** makes the C-H bond closest to the cationic ammonium group electronically deactivated for electrophilic hydroxylation by Fe((*R,R*)-PDP) resulting in the selective formation of **1.34** by oxidation of the most electron-rich C-H bond.^{26a} Similarly, Hartwig used this approach to differentiate tertiary C-H bonds in an Fe-catalyzed C-H azidation reaction.^{26b}

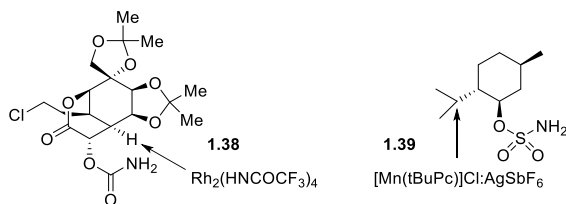
Another approach is to utilize directing groups; in the context of transition metal-catalyzed nitrene transfer, tethering the nitrene precursor to the substrate can afford some impressive site selectivity as shown in Scheme 1.10. Despite multiple tertiary C-H bonds and activated ethereal C-H bonds in **1.38**, selective amination takes place at the C-H vicinal to the carbamate tether due

to the preference of carbamate-derived nitrene precursors to form five-membered oxazolidinone rings and the difficulty of the tether reaching any other C-H bond on the substrate.^{27a} Another example of this is directing strategy is shown in **1.39** in which the acyclic tertiary C-H undergoes selective amination due to the sulfamate tether being unable to conformationally reach the cyclic tertiary C-H bond.⁷

Scheme 1.9. Electronic differentiation of similar C-H bonds for selective catalytic oxidation.



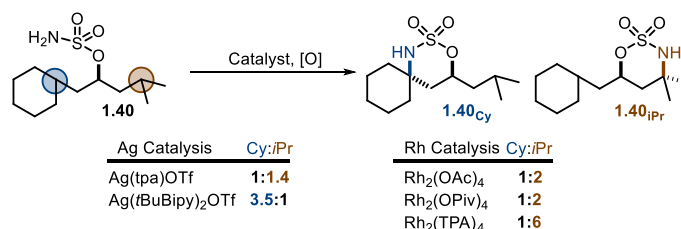
Scheme 1.10. Directing group approaches to selective tertiary C-H amination.



The DuBois and Schomaker groups both performed preliminary unbiased intramolecular studies using substrate **1.40** to measure the ability of their Rh_2L_n and AgL_n catalysts to control selectivity during an amination event (Scheme 1.11).^{12,27} Rh_2 -nitrene transfer catalysis favored amination of the acyclic C-H bond while $\text{Ag}(\text{tBuBipy})_2\text{OTf}$ favored amination of the cyclic C-H bond. While

this level of catalyst control was interesting, the underlying reasons for this swap in selectivity were unclear.

Scheme 1.11. Metal-controlled site-divergent amination of sterically and electronically similar C-H bonds.



1.8. Conclusions

The development of transition metal-catalyzed nitrene transfer has expedited the synthesis of amine-containing organic compounds through both direct C-H amination to form relatively unfunctionalized amines or C=C bond aziridination en route to more complex amine-containing scaffolds. Catalysts that can promote chemo- and site-selective nitrene transfer need to be developed to make these reactions useful; a particularly tough challenge is developing catalysts that can select for a C-H bond in the presence of multiple sterically and electronically similar C-H bonds. The next chapter describes investigating the selectivity provided by a series of transition metals in catalyzing the amination of sterically and electronically similar tertiary C-H bonds. Chapter 3 that follows will describe efforts in exploring the robustness of C-H amination reactions in polar media, finding that may expand the utility of nitrene transfer reactions to polar substrates.

1.9. References

(1) For highlights, see: (a) Zalatan, D. N.; Du Bois, J. Metal-catalyzed oxidations of C-H to C-N bonds. *Top. Curr. Chem.* **2009**, *292*, 347–78. (b) Muller, P.; Fruit, C. Enantioselective Catalytic Aziridinations and Asymmetric Nitrene Insertions into CH Bonds. *Chem. Rev.* **2003**, *103*, 2905–20. (c) Halfen, J. A. Recent advances in metal-mediated carbonnitrogen bond formation reactions: Aziridination and amidation. *Curr. Org. Chem.* **2005**, *9*, 657–69. (d) Dequierez, G.; Pons, V.; Dauban, P. Nitrene chemistry in organic synthesis: Still in its infancy? *Angew. Chem., Int. Ed.* **2012**, *51*, 7384–95. (e) Collet, F.; Dodd, R. H.; Dauban, P. Catalytic CH amination: recent progress and future directions. *Chem. Commun.* **2009**, *34*, 5061–74. (f) Collet, F.; Lescot, C.; Dauban, P. Catalytic C-H amination: the stereoselectivity issue. *Chem. Soc. Rev.* **2011**, *40*, 1926–36.

(2) For highlights, see: (a) Roizen, J. L.; Harvey, M. E.; Du Bois, J. Metal-catalyzed nitrogen-atom transfer methods for the oxidation of aliphatic C-H bonds. *Acc. Chem. Res.* **2012**, *45*, 911–22. (b) Collet, F.; Lescot, C.; Liang, C. G.; Dauban, P. Studies in catalytic C-H amination involving nitrene C-H insertion. *Dalton Trans.* **2010**, *39*, 10401–13. (c) Fiori, K. W.; Du Bois, J. Catalytic intermolecular amination of C-H bonds: method development and mechanistic insight. *J. Am. Chem. Soc.* **2007**, *129*, 562–68. (d) Fiori, K. W.; Espino, C. G.; Brodsky, B. H.; Du Bois, J. A mechanistic analysis of the Rh-catalyzed intramolecular C-H amination reaction. *Tetrahedron* **2009**, *65*, 3042–51. (e) Espino, C. G.; Du Bois, J. A Rh-catalyzed C-H insertion reaction for the oxidative conversion of carbamates to oxazolidinones. *Angew. Chem., Int. Ed.* **2001**, *40*, 598. (f) Padwa, A.; Flick, A. C.; Leverett, C. A.; Stengel, T. Rhodium(II)-catalyzed aziridination of allyl-substituted sulfonamides and carbamates. *J. Org. Chem.* **2004**, *69*, 6377. (g) Espino, C. G.; Fiori, K. W.; Kim, M.; Du Bois, J. Expanding the scope of C-H amination through catalyst design. *J. Am. Chem. Soc.* **2004**, *126*, 15378. (h) Davies, H. M. L.; Morton, D. Guiding principles for site

selective and stereoselective intermolecular C-H functionalization by donor/acceptor rhodium carbenes. *Chem. Soc. Rev.* **2011**, *40*, 1857. (i) Lescot, C.; Darses, B.; Collet, F.; Retailleau, P.; Dauban, P. Intermolecular C-H Amination of Complex Molecules: Insights into the Factors Governing the Selectivity. *J. Org. Chem.* **2012**, *77*, 7232. (j) Dauban, P.; Dodd, R. Iminoiodanes and C-N bond formation in organic synthesis. *Synlett* **2003**, *11*, 1571–1586. (k) Espino, C. G.; Wehn, P. M.; Chow, J.; Du Bois, J. Synthesis of 1,3-difunctionalized amine derivatives through selective C-H bond oxidation. *J. Am. Chem. Soc.* **2001**, *123*, 6935–36.

(3) (a) Au, S.-M.; Fung, W.-H.; Cheng, M.-C.; Che, C.-M.; Peng, S.- M. Aziridination of alkenes and amidation of alkanes by bis- (tosylimido)ruthenium(VI) porphyrins. *Chem. Commun.* **1997**, 1655–58. (b) Harvey, M. E.; Musaev, D. G.; Du Bois, J. A diruthenium catalyst for selective, intramolecular allylic C–H amination: reaction development and mechanistic insight gained through experiment and theory. *J. Am. Chem. Soc.* **2011**, *133*, 17207– 16.

(4) (a) Evans, D. A.; Faul, M. M.; Bilodeau, M. T. Copper-catalyzed aziridination of olefins by (N-(p-toluenesulfonyl) imino) phenyliodinane. *J. Org. Chem.* **1991**, *56*, 6744–46. (b) Evans, D. A.; Faul, M. M.; Bilodeau, M. T. Development of the copper-catalyzed olefin aziridination reaction. *J. Am. Chem. Soc.* **1994**, *116*, 2742–53. (c) Dielmann, F.; Andrada, D. M.; Frenking, G.; Bertrand, G. Isolation of bridging and terminal coinage metal-nitrene complexes. *J. Am. Chem. Soc.* **2014**, *136*, 3800–02.

(5) (a) Kuppuswamy, S.; Powers, T. M.; Johnson, B. M.; Bezpalko, M. W.; Brozek, C. K.; Foxman, B. M.; Berben, L. A.; Thomas, C. M. Metal–Metal Interactions in C 3-Symmetric Diiron Imido Complexes Linked by Phosphinoamide Ligands. *Inorg. Chem.* **2013**, *52*, 4802–11. (b) King, E. R.;

Hennessy, E. T.; Betley, T. A. Catalytic C-H bond amination from high-spin iron imido complexes. *J. Am. Chem. Soc.* **2011**, *133*, 4917–23.

(6) For highlights: (a) Lu, H. J.; Subbarayan, V.; Tao, J. R.; Zhang, X. P. Cobalt (II)-Catalyzed Intermolecular Benzylic C–H Amination with 2, 2, 2-Trichloroethoxycarbonyl Azide (TrocN₃). *Organometallics* **2010**, *29*, 389–393. (b) Lu, H.-J.; Jiang, H.-L.; Hu, Y.; Wojtas, L.; Zhang, X. P. Chemoselective Intramolecular Allylic C-H Amination versus C=C Aziridination Through Co (II)-Based Metalloradical Catalysis. *Chem. Sci.* **2011**, *2*, 2361–2366.

(7) Paradine, S. M.; Griffin, J. R.; Zhao, J.; Petronico, A. L.; Miller, S. M.; White, M. C. A manganese catalyst for highly reactive yet chemoselective intramolecular C(sp³)-H amination. *Nat. Chem.* **2015**, *7*, 987–94.

(8) (a) Cui, Y.; He, C. Efficient aziridination of olefins catalyzed by a unique disilver (I) compound. *J. Am. Chem. Soc.* **2003**, *125*, 16202–03. (b) Cui, Y.; He, C. A Silver-Catalyzed Intramolecular Amidation of Saturated C-H Bonds. *Angew. Chem., Int. Ed.* **2004**, *43*, 4210–12. (c) Li, Z.; Capretto, D. A.; Rahaman, R. H.; He, C. Silver-Catalyzed Intermolecular Amination of C-H Groups. *Angew. Chem., Int. Ed.* **2007**, *46*, 5184–86. (d) Llaveria, J.; Beltran, A.; Diaz-Requejo, M. M.; Matheu, M. I.; Castillon, S.; Perez, P. J. Efficient Silver-Catalyzed Regio- and Stereospecific Aziridination of Dienes. *Angew. Chem., Int. Ed.* **2010**, *49*, 7092–95. (e) Fructos, M. R.; Trofimenko, S.; Diaz-Requejo, M. M.; Perez, P. J. Facile Amine Formation by Intermolecular Catalytic Amidation of Carbon–Hydrogen Bonds. *J. Am. Chem. Soc.* **2006**, *128*, 11784–91.

(9) Rigoli, J. W.; Weatherly, C. D.; Vo, V. T.; Neale, S.; Meis, A. R.; Schomaker, J. M. Chemoselective Allene Aziridination via Ag (I) Catalysis. *Org. Lett.* **2013**, *15*, 290–3.

- (10) Rigoli, J. W.; Weatherly, C. D.; Alderson, J. M.; Vo, B. T.; Schomaker, J. M. Tunable, chemoselective amination via silver catalysis. *J. Am. Chem. Soc.* **2013**, *135*, 17238–41.
- (11) Scamp, R. J.; Rigoli, J. W.; Schomaker, J. M. Chemoselective silver-catalyzed nitrene insertion reactions. *Pure Appl. Chem.* **2014**, *86*, 381–93.
- (12) Alderson, J. A.; Phelps, A. M.; Scamp, R. J.; Dolan, N. S.; Schomaker, J. M. Ligand-controlled, tunable silver-catalyzed C-H amination. *J. Am. Chem. Soc.* **2014**, *136*, 16720–3.
- (13) Scamp, R. J.; Jirak, J. G.; Dolan, N. S.; Guzei, I. A.; Schomaker, J. M. A General Catalyst for Site-Selective C (sp³)–H Bond Amination of Activated Secondary over Tertiary Alkyl C (sp³)–H Bonds. *Org. Lett.* **2016**, *18*, 3014–17.
- (14) Dolan, N. S.; Scamp, R. J.; Yang, T.; Berry, J. F.; Schomaker, J. M. Catalyst-Controlled and Tunable, Chemoselective Silver-Catalyzed Intermolecular Nitrene Transfer: Experimental and Computational Studies. *J. Am. Chem. Soc.* **2016**, *138*, 14658–67.
- (15) Weatherly, C. D.; Alderson, J. M.; Berry, J. F.; Hein, J.; Schomaker, J. M. Catalyst-Controlled Nitrene Transfer by Tuning Metal:Ligand Ratios: Insight into the Mechanisms of Chemoselectivity. *Organometallics* **2017**, *36*, 1649–61.
- (16) Corbin, J. R.; Schomaker, J. M. Tunable differentiation of tertiary C–H bonds in intramolecular transition metal-catalyzed nitrene transfer reactions. *Chem. Commun.* **2017**, *53*, 4346–49.
- (17) Ju, M.; Weatherly, C. D.; Guzei, I. A.; Schomaker, J. M. Chemoand Enantioselective Silver-catalyzed Aziridinations. *Angew. Chem., Int. Ed.* **2017**, *56*, 9944–48.

(18) Huang, M.; Corbin, J. R.; Dolan, N. S.; Fry, C. G.; Vinokur, A. I.; Guzei, I. A.; Schomaker, J. M. Synthesis, characterization and VT-NMR studies of silver(I) complexes for selective nitrene transfer. *Inorg. Chem.* **2017**, *56*, 6725–33.

(19) Huang, M.; Yang, T.; Paretsky, J.; Berry, J. F.; Schomaker, J. M. Inverting steric effects: Using “attractive” non-covalent interactions to direct silver-catalyzed nitrene transfer. *J. Am. Chem. Soc.* **2017**, *139*, 17376–86.

(20) (a) Hung-Low, F.; Renz, A.; Klausmeyer, K. K. An X-ray diffraction study of anion and ratio dependence in the formation of discrete molecules versus polymeric arrays involving silver salts and bipyridine ligands. *Polyhedron* **2009**, *28*, 407. (b) Hung-Low, F.; Renz, A.; Klausmeyer, K. K. X-ray Crystal Structures of Silver Based Molecules Containing 5,5'-Dimethyl-2,2'-bipyridine and 2,2'-bipyridine. *J. Chem. Crystallogr.* **2011**, *41*, 1174. (c) Du, J.; Hu, T.; Zhang, S.; Zeng, Y.; Bu, X. Tuning silver(I) coordination architectures by ligands design: from dinuclear, trinuclear, to 1D and 3D frameworks. *CrystEngComm* **2008**, *10*, 1866. (d) Zhang, H.; Chen, L.; Song, H.; Zi, G. Synthesis, structure, and catalytic activity of chiral silver(I) and copper(II) complexes with biaryl-based nitrogen-containing ligands. *Inorg. Chim. Acta* **2011**, *366*, 320. (e) Hung-Low, F.; Renz, A.; Klausmeyer, K. K. X-ray Crystal Structures of Discrete and Polymeric Silver Based Molecules Containing 4,4'-Dimethyl-2,2'-Bipyridine and 2,2'-Bipyridine. *J. Chem. Crystallogr.* **2009**, *39*, 438.

(21) (a) Liu, K. E.; Johnson, C. C.; Newcomb, M.; Lippard, S. J. Radical Clock Reactions. *J. Am. Chem. Soc.* **1993**, *115*, 939–947. (b) Simmons, E. M.; Hartwig, J. F. On the Interpretation of Deuterium Kinetic Isotope Effects in C-H Bond Functionalizations by Transition-Metal Complexes. *Angew. Chem., Int. Ed.* **2012**, *51*, 3066–3072.

- (22) Varela-Álvarez, A.; Yang, T.; Jennings, H.; Kornecki, K. P.; Macmillan, S. N.; Lancaster, K. M.; Mack, J. B. C.; Du Bois, J.; Berry, J. F.; Musaev, D. G. Rh₂(II,III) Catalysts with Chelating Carboxylate and Carboxamidate Supports: Electronic Structure and Nitrene Transfer Reactivity. *J. Am. Chem. Soc.* **2016**, *138*, 2327–2341.
- (23) Maestre, L.; Sameera, W. M. C.; Diaz-Requejo, M. M.; Maseras, F.; Perez, P. J. A general mechanism for the copper- and silver-catalyzed olefin aziridination reactions: Concomitant involvement of the singlet and triplet pathways. *J. Am. Chem. Soc.* **2013**, *135*, 1338–48.
- (24) (a) Liang, J.-L.; Yuan, S.-X.; Chan, P. W. H.; Che, C.-M. Chiral rhodium (II, II) dimers catalyzed enantioselective intramolecular aziridination of sulfonamides and carbamates. *Tetrahedron Lett.* **2003**, *44*, 5917–20. (b) Esteoule, A.; Duran, F.; Retailleau, P.; Dodd, R. H.; Dauban, P. Enantioselective intramolecular copper-catalyzed aziridination of sulfamates. *Synthesis* **2007**, *2007*, 1251–54.
- (25) For select references on reagent-controlled C-H oxidation, see: (a) Newhouse, T.; Baran, P. S. *Angew. Chem. Int. Ed.* **2011**, *50*, 3362–3374. (b) B. Voigt, A. Porzel, D. Golsch, W. Adam, G. Adam, *Tetrahedron* **1996**, *52*, 10653 – 10658; (c) H. Seto, S. Fujioka, H. Koshino, S. Yoshida, M. Tsubuki, T. Honda, *Tetrahedron* **1999**, *55*, 8341 – 8352.; (d) R. Curci, A. Detomaso, T. Prencipe, G. B. Carpenter, *J. Am. Chem. Soc.* **1994**, *116*, 8112 – 8115. (e) P. Bovicelli, A. Gambacorta, P. Lupattelli, E. Mincione, *Tetrahedron Lett.* **1992**, *33*, 7411 – 7412; (f) A. Arnone, M. Cavicchioli, V. Montanari, G. Resnati, *J. Org. Chem.* **1994**, *59*, 5511 – 5513; (g) T. Iida, T. Yamaguchi, R. Nakamori, M. Hikosaka, N. Mano, J. Goto, T. Nambara, *J. Chem. Soc. Perkin Trans. I* **2001**, 2229 – 2236. (h) P. A. Wender, M. K. Hilinski, A. V. W. Mayweg, *Org. Lett.* **2005**, *7*, 79 – 82.

- (26) (a) Howell, J. M.; Feng, K.; Clark, J. R.; Trzepkowski, L. J.; White, M. C. *J. Am. Chem. Soc.* **2015**, *137*, 14590-14593. (b) Sharma, A.; Hartwig, J. F. *Nature*, **2015**, *517*, 600-604.
- (27) (a) Hinman, A.; Du Bois, J. *J. Am. Chem. Soc.* **2003**, *125*, 11510-11511. (b) Fiori, K. W.; Espino, C. G.; Brodsky, B. H.; Du Bois, J. *Tetrahedron*, **2009**, *65*, 3042-3051.

Chapter 2:

Tunable Differentiation of Tertiary C–H Bonds in Intramolecular Transition Metal-Catalyzed Nitrene Transfer Reactions

This chapter is adapted from sections published in:

Corbin, J. R.; Schomaker, J. M. *Chem. Commun.*, **2017**, 53, 4346-4349.

and

Huang, M.; Corbin, J. R.; Dolan, N. S.; Fry, C. G.; Vinokur, A. I.; Guzei, I. A.; Schomaker, J. M. *Inorg. Chem.*, **2017**, 56, 6725-6733.

The work described in this chapter focuses on work I did independently. After growing crystals of $[\text{Ag}(\text{Me}_4\text{phen})]\text{OTf}$ and $[\text{Ag}(\text{Me}_4\text{phen})_2]\text{OTf}$, the single X-ray crystal data was solved and analyzed by Dr. Anastasiya I. Vinokur and Dr. Ilia A. Guzei. This structural data is presented in Figure 2.2 in this chapter and represents some of my contributions to Huang, M., et al. applied in the context of the *Chem. Commun.* work; a more complete account can be found in the *Inorg. Chem.* paper cited on the previous page.

Chapter 2

Tunable Differentiation of Tertiary C–H Bonds in Intramolecular Transition Metal-Catalyzed Nitrene Transfer Reactions

2.1 Introduction

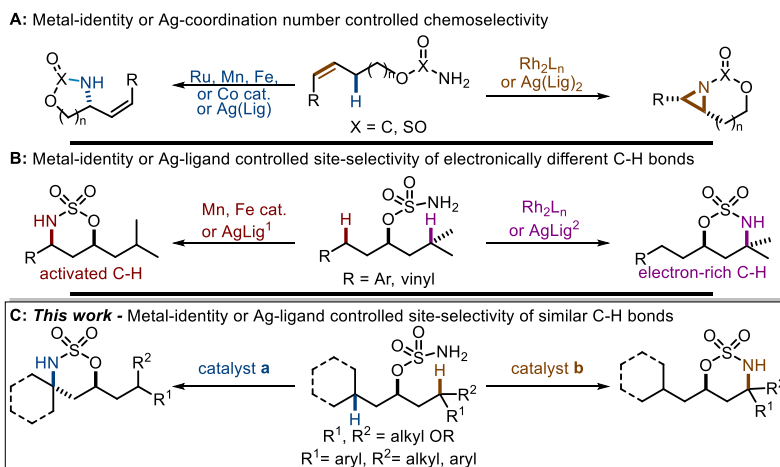
Transition metal-catalyzed nitrene transfer is a process that utilizes transient hyperelectrophilic metal-bound nitrenes for the direct conversion of ubiquitous and classically inert C–H bonds into valuable C–N bonds. Achieving both high yields and catalyst control in the manipulation of these reactive intermediates has been a major goal of research in homogenous transition-metal catalysis.^{1–9} In the presence of multiple competitive reactive sites, such as the situation presented in a substrate containing an alkene and an allylic C–H bond, a variety of transition metal catalysts have been shown to chemoselectively form either aziridine or amine products by exploiting differences in mechanism, substrate bias or ligand control (Figure 2.1A).^{9a–b} Orthogonal site-selectivity between C–H bonds in different steric or electronic environments can be achieved by exchanging the identity of the transition metal; for example, Mn catalysts favor reaction at benzylic methylenes while Rh₂L_n catalysts favor a tertiary methine (Figure 2.1B).^{2h,7a}

2.2. Background

Obtaining site-selectivity during C–H bond oxidation in the presence of competing sterically and electronically similar C–H bonds is extremely difficult. As a result, this area of C–H functionalization is underexplored and not well-understood. Oxidation of complex

molecule C–H bonds using stoichiometric amounts of oxidant often provides shockingly high selectivity for a single C–H bond in the presence of multiple similar ones. The underlying reasons for this substrate-controlled selectivity are often difficult to rationalize *a priori*. The challenges associated with overcoming the inherent substrate-controlled C–H selectivity are thus exacerbated because of this lack of understanding when attempting to override substrate bias and achieve reagent-control over a C–H oxidation.

Figure 2.1: Approaches to chemo- and site-selectivity in nitrene group transfer reactions



A powerful advance in this area would be represented by the development of catalyst-controlled methods for site-selective C–H oxidation of similar types. Examples of differentiating between aminations of competing 3° C–H bonds are scarce and no tunable examples have been reported as current strategies typically rely on conformationally or electronically biasing site-selectivity.^{2h,7a,9b} More interestingly, the Du Bois group has shown that the treatment of **2.1** with either Rh₂(OAc)₄ (**2.1**_{iPr}:**2.1**_{cHex} 2.0:1)^{2h} or Rh₂(TPA)₄ **2.5** (Table 2.1, entry 10) favors reaction at the 3° **iPr** over the 3° **cHex** C–H bond, presumably due to greater $\sigma_{C-H} \rightarrow \sigma_{C-H}^*$ at **iPr**, rendering that site more electron-rich. Selectivity for **2.1**_{iPr} increases from 2.0:1 to 2.4:1 to 11:1 in moving from OAc to the bulky and less electron-rich triphenylacetate (TPA) ligand for the Rh₂(II) catalyst.

2.3. Catalyst Screen and Substrate Scope

In this work, we sought to expand the utility of metal-catalyzed nitrene transfer to encompass the tunable amination of competing 3° C–H bonds in similar steric and/or electronic environments like **2.1** using a combination of ligand-controlled Ag(I) catalysis and known scaffolds based on other metals (Figure 2.1C). With a better understanding of how interactions between substrate and catalyst selectively differentiate tertiary C–H bonds, the development of second-generation catalysts able to install a C–N bond at a desired site in a complex molecule setting can be envisaged.

Table 2.1: Initial efforts to differentiate between similar tertiary C(sp³)–H bonds. ^aNMR yield, mesitylene internal standard. ^bSee the Supplementary Information for conditions using catalysts **2.4–2.7**. The reactions were run to complete conversion of the substrate **2.1**.

entry	lig/cat	Ag:L	yield ^a	cHex : iPr
1	BrBipy	1:3	38%	1.6 : 1
2	<i>t</i> BuBipy	1:3	91%	3.5 : 1
3	MeOBipy	1:3	91%	4.5 : 1
4	phen	1:3	97%	3.8 : 1
5	bp	1:3	96%	4.1 : 1
6	2.2	1:1.25	95%	5.0 : 1
7	tpa	1:1.25	99%	1 : 1.4
8	2.3	1:1.25	97%	1 : 3.9
9	2.4	-	98%	1 : 4.3
10	2.5	-	85%	1 : 6.0
11	2.6	-	46%	1 : 3.3
12	2.7	-	88%	1 : 4.1

X = *t*Bu **tBuBipy**

X = Br **BrBipy**

X = OMe **MeOBipy**

X, Y = H **phen**

X = Ph, Y = H **bp**

X, Y = Me **Me4phen 2.2**

tpa

Py5Me2 2.3

Rh₂(esp)₂ 2.4

Rh₂(TPA)₄ 2.5

Ru₂(hp)₄Cl 2.7

[Mn(*t*BuPc)]Cl 2.6

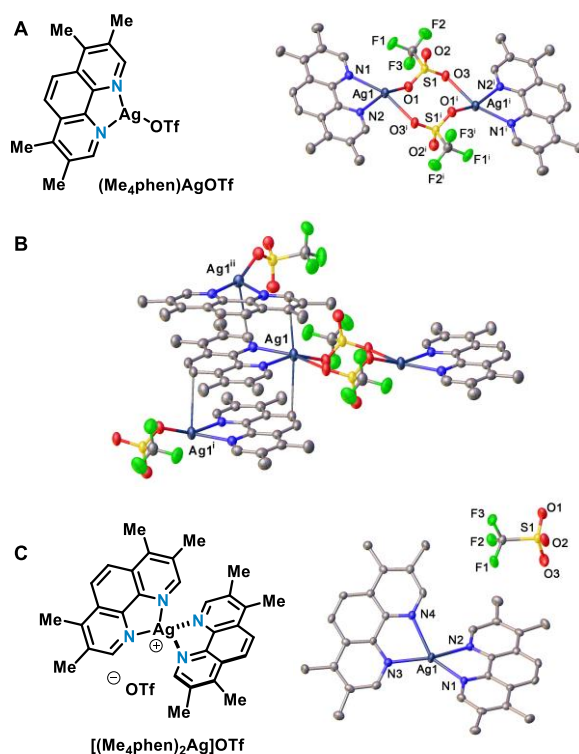
Investigations of a series of our Ag(I) catalysts (Table 2.1, entries 1-8) yielded interesting and unexpected results. A control reaction employing AgOTf and no ligand gave <3% of the aminated products in a ~1:1 ratio of **2.1_{cHex}**:**2.1_{iPr}**. More electron-rich 2,2'-bipyridine (bipy) ligands (compare entries 2-3 with entry 1) gave better selectivity and higher yields for **2.1_{cHex}**. More rigid 1,10-phenanthroline-based (phen) ligand scaffolds (entries 4-6), especially the electron-rich Me₄phen (entry 6), also exhibited selectivity for **2.1_{cHex}**.

Interestingly, identical results were obtained when using either a 1:3 ratio of AgOTf:Me₄phen or 1:1.25 AgOTf:Me₄phen (not shown in Table 2.1) suggesting that Ag(Me₄phen)OTf and Ag(Me₄phen)₂OTf provide similar selectivity, or only the lower coordinate complex can be accessed. Crystals were grown and single-crystal X-ray structures of compounds resulting from 1:1 and 1:2 mixtures of AgOTf:Me₄phen were obtained (Figure 2.2). Complex **Ag(Me₄phen)OTf** forms a three-dimensional framework in solid state (Figure 2.2A-2.2B), where the basic unit of the extended structure is a dimer (Me₄phen)Ag(μ-OTf)₂Ag(Me₄phen), with two triflates serving as bridging ligands. Each Ag center coordinates to two N atoms of the Me₄phen ligand and two bridging oxygen atoms from two different triflates. The geometry at Ag is best described as a distorted see-saw with index $\tau'_4 = 0.32$. The value $\tau'_4 = 0$ describes square planar complexes, whereas $\tau'_4 = 1$ corresponds to a tetrahedral geometry. The Ag–N distances are substantially different at 2.2795(18) and 2.3870(17) Å. The shorter bond is opposite to the shorter Ag1–O1 distance (2.2730(16) Å), whereas the longer Ag–N distance is *trans* to the substantially elongated Ag1–O3[1.5-*x*,0.5-*y*,1-*z*] bond of 2.6609(16) Å. There are also dative metal- π interactions between the Ag center and the phenanthroline ligands of neighboring molecules positioned on each side of the N1-N2-Ag-O1-O2 coordination plane. The Ag1...C1[1-*x*,*y*,0.5-*z*] and Ag1...C6[1-*x*,1-*y*,1-*z*] separations span 3.133(2) and 3.234(2) Å, lengths that are shorter than the sum of the silver vdW

radius and half-thickness of an aromatic ring (3.45 Å). Taking into account the latter interactions, the local geometry about the Ag center may appropriately be considered disordered octahedral. These distal Ag... π interactions connect the dimers into a three-dimensional structure (Figure 2.2B). In contrast, higher ligand loadings resulted in the crystallization of the 2:1 Me₄phen:AgOTf complex [Ag(Me₄phen)₂]OTf (Figure 2.2C), which does not dimerize. The Ag1 center is ligated by two Me₄phen ligands, whereas the triflate counterions are outer-sphere. The all-nitrogen metal coordination environment about the Ag center in [Ag(Me₄phen)₂]OTf corresponds to a distorted see-saw ($\tau'_4 = 0.43$). Both bidentate Me₄phen ligands bind asymmetrically, with one Ag–N distance being ~0.16 Å shorter than the other; however, all Ag–N distances fall within the expected range. The polymeric nature of [Ag(Me₄phen)OTf]_n in solution may result in similar steric environment around the metal center when compared to [Ag(Me₄phen)₂]OTf during catalysis. Though no solution NMR-studies were done to probe this, subjecting the grown crystals to the reaction mixture resulted in the same outcome as adding Me₄phen to AgOTf *in situ*. Regardless, similar selectivity during the amination of tertiary C–H bonds is observed suggesting changing the ratio of bidentate ligands to favor more sterically hindered catalysts will not be a solution to providing regioselectivity in this challenging system. Thus, going forward, the 1:1.25 AgOTf:Me₄phen system was considered optimal to conserve ligand.

Figure 2.2A. X-ray single crystal structure of a dimer of [Ag(Me₄phen)(OTf)]_n shown with 50% probability ellipsoids. Selected bond distances (Å) and angles (deg): Ag1–O1, 2.2730(16); Ag1–N1, 2.3870(17); Ag1–N2, 2.2795(18). O1–Ag1–N1, 114.87(6); O1–Ag1–N2, 157.43(6); N2–Ag1–N1, 71.56(6); S1–O1–Ag1, 127.08(10). Symmetry code: (i) 1.5-*x*, 0.5-*y*, 1-*z*. **2.2B.** Molecular drawing of [Ag(Me₄phen)(OTf)]_n, showing the metal- π interactions between the Ag

center and the phenanthroline ligands of neighboring molecules above and below. Symmetry code: (i) $1-x, y, 0.5-z$; (ii) $1-x, 1-y, 1-z$. **2.2C.** Molecular structure of $\text{Ag}(\text{Me}_4\text{phen})_2(\text{OTf})$ shown with 50% probability ellipsoids. Selected bond distances (Å) and angles (deg): Ag1–N1, 2.249(3); Ag1–N2, 2.398(3); Ag1–N3, 2.246(3); Ag1–N4, 2.410(3). N1–Ag1–N2, 71.69(12); N1–Ag1–N4, 145.21(12); N2–Ag1–N4, 95.20(11); N3–Ag1–N1, 132.42(11); N3–Ag1–N2, 151.81(11); N3–Ag1–N4, 71.87(11).



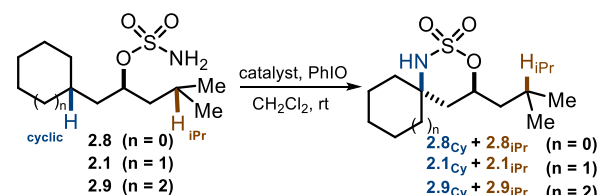
Switching to a higher denticity tris(2-pyridylmethyl)amine (tpa) ligand (entry 7) resulted in a modest switch in site-selectivity to favor **2.1_{iPr}**. A polydentate dimeric Ag catalyst based on **3** (entry 8) further improved selectivity for **2.1_{iPr}**, accomplishing tunable, catalyst-controlled nitrene transfer using a single metal (compare entries 6 and 8).

The reasons for the tunability between the *iPr* and *cHex* C–H bonds of **2.1** were not readily apparent. $[\text{Mn}(t\text{BuPc})]\text{Cl}$ **2.6** and $\text{Ru}_2(\text{hp})_4\text{Cl}$ **2.7** are known to promote step-wise nitrene transfer

pathways and also favored amination of the 3° *iPr* C–H bond of **2.1** (entries 11-12).^{3a} This is intriguing, as Rh₂(II) catalysts participate in *concerted* intramolecular nitrene transfer, yet show the same overall site-selectivity as **2.6-2.7**. The mechanism of Ag(I)-catalyzed nitrene transfer is necessarily step-wise, due to the lack of a vacant π^* orbital on the N of the metal nitrene.^{9d} However, we and others have shown that the nature of the ligand on Ag can impact whether the amination proceeds through HAT involving discrete radical intermediates, or undergoes a barrierless radical rebound that results in 'concerted-like' behavior in the nitrene transfer.⁸⁻⁹ This is reflected in the very different selectivities between catalysts **2.2** and **2.3**. Thus, rationalizing subtle differences in site-selectivity by invoking a broad picture of the mechanism of nitrene transfer cannot be applied in the same way as previous reports of chemoselective nitrene transfer (Figure 2.1A). Rather, subtle interactions between ligand architecture, substrate and catalyst electronics all play important, but poorly understood, roles in fine-tuning the steric and electronic environment of the metal-nitrene.

To gain further insight into the factors most important in influencing selectivity of nitrene transfer in these types of systems, substrates **2.8** and **2.9** were explored (Table 2.2) with catalysts **2.2-2.7**. Despite the observation that we could achieve tunability using ligand-controlled Ag(I) catalysis or by switching the metal identity, no trends in the selectivity were immediately apparent, requiring a more careful analysis of the interplay between the features of the substrate (electron density, C–H bond dissociation energy (BDE) and A-value of the alkyl group) and the catalyst (KIE, mechanism of nitrene transfer).

Table 2.2: Selectivity in the amination of carbocyclic *vs.* acyclic C–H bonds. ^aSee the Supplementary Information for detailed reaction conditions using catalysts **2.2–2.7**. ^bNMR yield, mesitylene internal standard. The reactions were run to complete conversion of the substrate.



entry	n, Cy	cat. ^a	yield ^b	Cy : <i>i</i> Pr	n = 1
1	0, cPent	2.2	93%	2.5 : 1	5.0 : 1
2	0, cPent	2.3	87%	1.8 : 1	1 : 3.9
3	0, cPent	2.4	98%	1.3 : 1	1 : 4.3
4	0, cPent	2.5	84%	1 : 2.1	1 : 6.0
5	0, cPent	2.6	56%	1 : 2.6	1 : 3.3
6	0, cPent	2.7	65%	1.0 : 1	1 : 4.1

entry	n, Cy	cat. ^a	yield ^b	Cy : <i>i</i> Pr
7	2, cHept	2.2	96%	7.3 : 1
8	2, cHept	2.3	96%	1.3 : 1
9	2, cHept	2.4	96%	1.2 : 1
10	2, cHept	2.5	96%	1 : 2.1
11	2, cHept	2.6	51%	1 : 1.2
12	2, cHept	2.7	78%	2.1 : 1

Catalysts with reported KIE values in the range of ~0-4, such as the dinuclear Rh₂(II) paddlewheel catalysts **2.4–2.5**, are thought to proceed through concerted nitrene transfer and favor the most electron-rich C–H bond (Figure 2.3A, reactivity trend: 3° > ethereal ≈ benzylic > 2° >> 1°).² Catalysts with KIEs > 4, as represented by **2.6** (KIE = 4.2) and **2.7** (KIE = 4.9), favor reaction at the weakest C–H bond (Figure 2.3A, reactivity trend: allylic > benzylic > ethereal > 3° > 2° >> 1°) due to the preference for a step-wise nitrene transfer pathway involving radical intermediates with significant lifetimes.^{3a,4c,7a} The two 3° C–H bonds of **2.1**, **2.8** and **2.9** have essentially the same BDEs, but the isopropyl C–H appears to be more electron-rich than the Cy C–H bonds, according to comparisons of the ¹³C chemical shifts (Figure 2.3B). An additional factor to consider is the conformational flexibility of the Cy ring; while cHex is likely to favour a distinct chair conformation, the flexibility of cPent and cHept may make the cyclic C–H bond more difficult to differentiate from an acyclic C–H bond.

2.2, entries 5-6 and 11-12). Use of **2.6** resulted in the more electron-rich carbon radical leading to **2.8iPr** (entry 11), but this is not always a selectivity-determining feature, as the use of **2.7** led to the formation of **2.9Cy** (entry 12). Using the trends in Rh, Ru and Mn catalysis to understand the behavior of our Ag catalysts **2.2-2.3** was instructive. It is worth noting that **2.3** (Table 2.1, entry 3 and Table 2.2, entries 2 and 8) displays similar behavior to **2.6-2.7**, implying that this Ag(I) complex proceeds through a nitrene transfer pathway involving HAT and the formation of long-lived radical intermediates.^{3a,7a} Indeed, the KIE for **2.3** was 5.7, in line with the values obtained for **2.6** (4.2) and **2.7** (4.9).^{3a,4c,7a} The most intriguing results involved the observation that Ag(Me₄phen)OTf **2.2** (Table 2.1, entry 6 and Table 2.2, entries 1 and 7) increasingly favored amination of the Cy C–H bond as the carbocycle increased in size from cPent to cHept, perhaps due to the fluxional nature of cHept and the greater rate of pseudo-equatorial C–H bond oxidation by strain release during the amination event.¹

Previous work in intramolecular nitrene transfer competition experiments generally attributes the preference for the amination of benzylic methylene C–H over 3° alkyl C(sp³) –H bonds to lower BDEs and stereoelectronic stabilization of the amination transition state (concerted or stepwise) by relatively large $\pi_{C=C} \rightarrow \sigma_{C-H}^*$ interactions.^{1,3a,4c,7a,9c} We were curious how a more electronically activated benzylic 3° C–H bond in **2.10-2.15** might compete with less activated, but more electron-rich, 3° alkyl C(sp³) –H bonds (Table 2.3). We chose to explore three catalysts, **2.2**, **2.3** and **2.5**, that display very different reactivity profiles as determined by our results described in Tables 2.1-2.2.

Substrates **2.10-2.12** were designed to compare the activation of a conformationally accessible cHex C–H bond with a series of different benzylic methane C–H bonds of decreasing BDE in moving from **2.10** to **2.12** (Table 2.3, entries 1-9). The substrates were utilized as ~1:1 mixtures

of diastereomers; however, evidence of tunable selectivity in the amination can still be assessed. Further studies to determine how the stereochemistry impacts the relative rates of C–H amination are underway and will be reported in due course. The preference of Ag(Me₄phen)OTf **2.2** for the most conformationally accessible cHex C–H bond (entries 1-3) decreased as the Bn C–H bond became weaker. AgOTf supported by Py₅Me₂ in catalyst **2.3** (entries 4-6) showed an increase in selectivity for the Bn C–H bond from 2.2:1 to 8.4:1 as the BDE was decreased, a trend that fits our mechanistic picture of step-wise nitrene transfer promoted by **2.3**.^{9c} Finally, the Rh₂(TPA)₄ catalyst **2.5** (entries 7-9) appeared to respond to decreasing electron density at the C–H bond by heavily favoring the cHex C–H bond in **2.12** (entry 9). Somewhat surprising was the lack of selectivity in **2.10** with **2.5** (entry 7), reflecting either similar electron density around the two 3° C–H bonds or a steric component to the site-selectivity.

Table 2.3: Competitive amination of activated C–H vs. tertiary C(sp³)–H bonds. ^aSee the Supplementary Information for conditions using catalysts **2.2-2.5**. ^bNMR yield, mesitylene internal standard. The reactions were run to complete conversion of the substrate.

entry	R ¹ , R ² , R ³	cat ^a	yield ^b	Alk:Bn (a:b)	entry	R ¹ , R ² , R ³	cat ^a	yield ^b	Alk:Bn (a:b)
1	-(CH ₂) ₅ -, Me, H	2.10	95%	3.8 : 1	10	Me, Me, H	2.13	89%	1 : 1.3
2	-(CH ₂) ₅ -, Me, OMe	2.11	90%	2.2 : 1	11	Me, Me, OMe	2.14	73%	1 : 2.6
3	-(CH ₂) ₅ -, Ph, H	2.12	83%	1.2 : 1	12	Me, Ph, H	2.15	89%	1 : 4.2
4		2.10	84%	1 : 2.2	13		2.13	91%	1.0 : 1
5		2.11	89%	1 : 3.4	14		2.14	90%	1 : 1.4
6		2.12	81%	1 : 8.4	15		2.15	83%	1 : 2.7
7		2.10	93%	1 : 1.1	16		2.13	94%	8.3 : 1
8		2.11	92%	1 : 1.8	17		2.15	93%	>19 : 1
9		2.12	70%	>19 : 1					

The effect of the conformational accessibility of a cHex C–H bond was removed in substrates **2.13-2.15**, where amination of a series of 3° benzylic methine C–H bonds were compared to an **iPr** C–H bond (Table 2.3, entries 10-17). Ag(Me₄phen)OTf **2.2** showed increased selectivity for the Bn C–H bond in moving from **2.13** to **2.15**, which is rationalized by adoption of a preferred conformation about the hindered and activated **Bn** C–H to maximize $\pi_{C=C} \rightarrow \sigma_{C-H}^*$ interactions. This suggests **2.2** favors kinetically accessible C–H bonds to a greater extent than the other catalysts tested in Table 2.3, an observation also made using **2.2** in Table 2.1. Catalyst **2.3** displayed less selectivity for **Bn** in **2.13-2.15** (entries 13-15) as compared to **2.10-2.12** (entries 5-7), suggesting **2.3** may be more sensitive to the electronics of the C–H bond than the kinetic accessibility. Finally, Rh₂(TPA)₄ **2.5** (entries 16-17) responded to the increased electron density at the **iPr** C–H.

It is worth noting that both Ag(I) catalysts **2.2** and **2.3** favor amination of the diphenyl methine C–H over the **iPr** C–H bond of **2.15**, even though it was more sterically encumbered (A-value of Ph = 3 vs. Me = 1.7). It appears that increasing the stereoelectronic bias against an acyclic 3° alkyl C–H bond improves the selectivity of Ag(I) catalysts for the activated C–H bond, due to the inherent stepwise nature of nitrene transfer in all Ag(I) catalysts. Thus, Ag(I) complexes are promising scaffolds for developing new catalysts that can select for any 'activated' 3° C–H bond over a typical 3° alkyl C(sp³)–H bond. Although Rh₂(II) catalysts are more substrate-dependent, they often favor 3° alkyl C(sp³)–H bonds, leading to success in the first examples of catalyst-controlled tunability between tertiary C–H bonds (Table 2.3, entries 6 vs. 9 and 12 vs. 17).

2.4 Conclusions

In conclusion, we report the first examples of site-selective and tunable C–H amination of substrates containing reactive 3° C–H bonds in similar steric and electronic

environments. In many cases, tunability could be achieved solely by changing the nature of an N-donor ligand supporting a Ag(I) complex; however, in challenging substrates, the orthogonal reactive site was favoured using Rh₂(TPA)₄. Though the underlying mechanistic rationale for the differentiation of these similar C–H bonds is still not completely understood, achieving this level of catalyst control is promising for the future development of site-selective and tunable intermolecular metal-nitrene transfer; a long-standing challenge in the field.

2.5. References

- 1 Selected reviews on metal-catalyzed nitrene transfer, see: (a) Roizen, J. L.; Harvey, M. E.; Du Bois, J. *Acc. Chem. Res.* **2012**, *45*, 911. (b) Zalatan, D. N.; Du Bois, J. *Top. Curr. Chem.* **2009**, *292*, 347. (c) Müller, P.; Fruit, C. *Chem. Rev.* **2003**, *103*, 2905. (d) Collet, F.; Lescot, C.; Dauban, P. *Chem. Soc. Rev.* **2011**, *40*, 1926. (e) Collet, F.; Lescot, C.; Liang, C.; Dauban, P. *Dalton Trans.* **2010**, *39*, 10401. (f) Scamp, R. J.; Rigoli, J. W.; Schomaker, J. M. *Pure Appl. Chem.* **2014**, *86*, 381. (g) Lu, H.; Zhang, X. P. *Chem. Soc. Rev.* **2011**, *40*, 1899. (h) Collet, F.; Dodd, R. H.; Dauban, P. *Chem. Commun.* **2009**, *34*, 5061.
- 2 Selected references on Rh-catalyzed nitrene transfer, see: (a) Espino, C. G.; Du Bois, J. *Angew. Chem., Int. Ed.* **2001**, *40*, 598. (b) Espino, C. G.; Fiori, K. W.; Kim, M.; Du Bois, J. *J. Am. Chem. Soc.* **2004**, *126*, 15378. (c) Zalatan, D. N.; Du Bois, J. *J. Am. Chem. Soc.* **2008**, *130*, 9220. (d) Liang, C.; Robert-Peillard, F.; Fruit, C.; Müller, P.; Dodd, R. H.; Dauban, P. *Angew. Chem., Int. Ed.* **2006**, *45*, 4641. (e) Fiori, K. W.; Du Bois, J. *J. Am. Chem. Soc.* **2007**, *129*, 562. (f) Lebel, H.; Spitz, C.; Leogane, O.; Trudel, C.; Parmentier, M. *Org. Lett.* **2011**, *13*, 5460. (g) Breslow, R.; Gellman, S. H. *J. Am. Chem. Soc.* **1983**,

- 105, 6728. (h) Fiori, K. W.; Espino, C. G.; Brodsky, B. H.; Du Bois, J. *Tetrahedron* **2009**, 65, 3042. (i) When, P. M.; Du Bois, J. *J. Am. Chem. Soc.* **2002**, 124, 12950.
- 3 For selected references on Ru-catalyzed nitrene transfer, see: (a) Harvey, M. E.; Musaev, D. J.; Du Bois, J. *J. Am. Chem. Soc.* **2011**, 133, 17207. (b) Milczek, E.; Boudet, N.; Blakey, S. *Angew. Chem., Int. Ed.* **2008**, 47, 6825.
- 4 For selected references on Fe-catalyzed nitrene transfer, see: (a) Nakanishi, M.; Salit, A.; Bolm, C. *Adv. Synth. Catal.* **2008**, 350, 1835. (b) Paradine, S. M.; White, M. C. *J. Am. Chem. Soc.* **2012**, 134, 2036. (c) Cramer, S. A.; Jenkins, D. M. *J. Am. Chem. Soc.* **2011**, 133, 19342. (d) Hennessy, E. T.; Liu, R. Y.; Iovan, D. A.; Duncan, R. A.; Betley, T. A. *Chem. Sci.* **2014**, 5, 1526.
- 5 For selected references on Co-catalyzed nitrene transfer, see: (a) Lu, H. J.; Subbarayan, V.; Tao, J. R.; Zhang, X. P. *Organometallics* **2010**, 29, 389. (b) Lu, H.-J.; Jiang, H.-L.; Hu, Y.; Wojtas, L.; Zhang, X. P. *Org. Lett.* **2012**, 14, 5158. (c) Lu, H.-J.; Jiang, H.-L.; Hu, Y.; Wojtas, L.; Zhang, X. P. *Chem. Sci.* **2011**, 2, 2361. (d) Lu, H.-J.; Jiang, H.-L.; Wojtas, L.; Zhang, X. P. *Angew. Chem. Int. Ed.* **2010**, 49, 10192. (e) Lu, H.-J.; Li, C.-Q.; Jiang, H.-L.; Lizardi, C. L.; Zhang, X. P. *Angew. Chem. Int. Ed.* **2014**, 53, 7028.
- 6 For selected references on Cu-catalyzed nitrene transfer, see: (a) Duran, F.; Leman, L.; Ghini, A.; Burton, G.; Dauban, P.; Dodd, R. H. *Org. Lett.* **2002**, 4, 2481. (b) Lebel, H.; Lectard, S.; Parmentier, M. *Org. Lett.* **2007**, 9, 4797. (c) Dauban, P.; Sanier, L.; Tarrade, A.; Dodd, R. H. *J. Am. Chem. Soc.* **2001**, 123, 7707. (d) Srivastava, R. S.; Tarver, N. R.; Nicholas, K. M. *J. Am. Chem. Soc.* **2007**, 129, 15250. (e) Barman, D. N.; Nicholas, K. M. *Eur. J. Org. Chem.* **2011**, 2011, 908. (f) Bagchi, V.; Paraskevopoulou, P.; Das, P.; Chi, L.;

Wang, Q.; Choudhury, A.; Mathieson, J. S.; Cronin, L.; Pardue, D. B.; Cundari, T. R.; Mitrikas, G.; Sanakis, Y.; Stavropoulos, P. *J. Am. Chem. Soc.* **2014**, *136*, 11362.

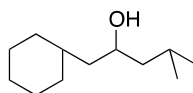
- 7 For selected references on Mn-catalyzed nitrene transfer, see: (a) Paradine, S. M.; Griffin, J. R.; Zhao, J.; Petronico, A. L.; Miller, S. M.; White, M. C. *Nat. Chem.* **2015**, *7*, 987–994. (b) Liang, S.; Jensen, M. P. *Organometallics*. **2012**, *31*, 8055. (c) Abu-Omar, M. M. *Dalton Trans.* **2011**, *40*, 3435–44. (d) Lai, T.-S.; Kwong, H.-L.; Che, C.-M.; Peng, S. M. *Chem. Commun.* **1997**, 2373.
- 8 For selected references on Ag-catalyzed nitrene transfer, see: (a) Diaz-Requejo, M. M.; Perez, P. *J. Chem. Rev.* **2008**, *108*, 3379. (b) Cui, Y.; He, C. *Angew. Chem., Int. Ed.* **2004**, *43*, 4210. (c) Li, Z.; Capretto, D. A.; Rahaman, R.; He, C. *Angew. Chem., Int. Ed.* **2007**, *46*, 5184. (d) Fructos, M. R.; Trofimenko, S.; Diaz-Requejo, M. M.; Perez, P. *J. Am. Chem. Soc.* **2006**, *128*, 11784. (e) Gomez-Emeterio, B. P.; Urbano, J.; Diaz-Requejo, M. M.; Perez, P. *J. Organometallics*. **2008**, *27*, 4126.
- 9 (a) Rigoli, J. W.; Weatherly, C. D.; Alderson, J. M.; Vo, B. T.; Schomaker, J. M. *J. Am. Chem. Soc.* **2013**, *135*, 17238. (b) Alderson, J. M.; Phelps, A. M.; Scamp, R. J.; Dolan, N. S.; Schomaker, J. M. *J. Am. Chem. Soc.* **2014**, *136*, 16720. (c) Scamp, R. J.; Jirak, J. G.; Dolan, N. S.; Guzei, I. A.; Schomaker, J. M. *Org. Lett.* **2016**, *18*, 3014. (d) Dolan, N. S.; Scamp, R. J.; Yang, T.; Berry, J. F.; Schomaker, J. M. *J. Am. Chem. Soc.* **2016**, *138*, 14658.

2.6. Experimental Details and Characterization

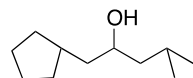
2.6.1 Synthesis of Alcohol Precursors

General procedure. A 250 mL round-bottom flask equipped with a reflux condenser was charged with 30 mL of diethyl ether and 0.97 g (40 mmol, 2 equiv) of Mg turnings. Alkyl bromide (40 mmol, 2 equiv) was added dropwise to keep a constant reflux, and the mixture was allowed to stir

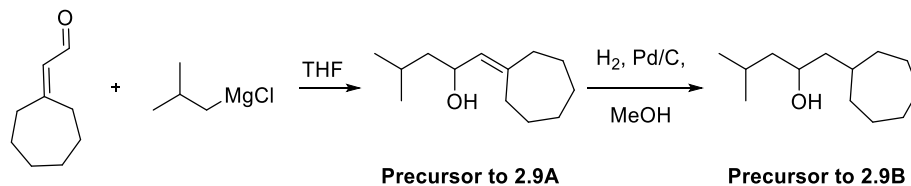
for 30 min. The reaction mixture was cooled to $-78\text{ }^{\circ}\text{C}$ in a dry ice/acetone bath and aldehyde (20 mmol, 1 equiv) in 30 mL of was added slowly via cannula. The reaction mixture was stirred 1 h at $-78\text{ }^{\circ}\text{C}$, and was then quenched by the gradual addition of aqueous 0.25 M HCl (60 mL). The layers were separated and the aqueous layer was extracted with two 30 mL portions of diethyl ether. The organic layers were combined, dried over MgSO_4 , and concentrated *in vacuo*. The crude residue was purified via column chromatography with an ethyl acetate/hexane gradient to give the pure alcohol product.



Precursor to Compound 2.1. The product was purified by column chromatography using a 0%–30% gradient of EtOAc in hexanes with 5% increments. The resulting colorless oil was obtained in 74% yield from isovaleraldehyde. Characterization data was consistent with the previously reported synthesis.^{9b}



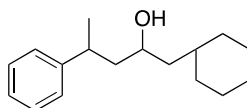
Precursor to Compound 2.8. Prepared from 2-cyclopentylacetaldehyde and commercial isobutylmagnesium chloride solution as in the procedure described for the precursor to Compound 2.9A (*vide infra*). The compound was isolated as a clear oil in 65% yield following column chromatography using a 0%-30% ethyl acetate in hexanes gradient, with 5% increments. **^1H NMR** (500 MHz, CDCl_3) δ 3.63 (m, 1H), 1.93 – 1.81 (m, 1H), 1.79 – 1.66 (m, 3H), 1.55 (m, 2H), 1.49 – 1.38 (m, 3H), 1.35 – 1.26 (m, 3H), 1.17 (m, 1H), 1.09 – 0.96 (m, 2H), 0.85 (dd, $J = 6.3, 4.3\text{ Hz}$, 6H). **^{13}C NMR** (126 MHz, CDCl_3) δ 69.3, 47.3, 44.6, 36.7, 33.3, 32.6, 25.1, 25.0, 24.6, 23.5, 22.10. **MS (EI)** m/z calculated for $\text{C}_{11}\text{H}_{22}\text{O}$ $[\text{M}-\text{H}]^-$ 169.1598; found, 169.1598.



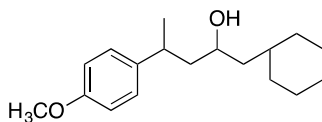
Precursor to Compound 2.9A. The aldehyde (9.97 mmol, 1 equiv) was dissolved in THF (0.33 M) in a dry 100 mL round-bottom flask under N₂. Commercially available isobutyl magnesium chloride (2 M in THF, 12 mmol, 1.2 equiv) was added to the stirring solution at -78 °C, the reaction mixture brought to room temperature, then stirred for 1-2 h or until TLC indicated complete consumption of the starting material. The reaction was quenched by the addition of 0.25 M HCl (30 mL). The layers were separated and the aqueous layer was extracted with two 30 mL portions of diethyl ether. The organic layers were combined, dried over MgSO₄, and concentrated *in vacuo*. The crude residue was purified by column chromatography using a 0%–30% gradient of EtOAc in hexanes with 5% increments. The pure, acid sensitive oil decomposes within hours in chloroform, and was isolated by silica column chromatography using a 0% -> 30% ethyl acetate/hexanes gradient in 84% yield, with 5% increments. The pure oil had a slight yellow hue. ¹H NMR (500 MHz, CDCl₃) δ 5.16 (dp, *J* = 8.8, 1.3 Hz, 1H), 4.44 (ddd, *J* = 8.8, 7.6, 6.1 Hz, 1H), 2.33 (td, *J* = 6.2, 1.4 Hz, 2H), 2.22 (td, *J* = 6.1, 1.2 Hz, 2H), 1.74 – 1.45 (m, 10H), 1.26 (ddd, *J* = 13.5, 7.4, 6.1 Hz, 1H), 1.19 (bs, 1H), 0.92 (dd, *J* = 9.0, 6.6 Hz, 6H). ¹³C NMR (126 MHz, CDCl₃) δ 144.4, 128.8, 66.5, 47.0, 37.8, 30.1, 29.6, 29.0, 29.0, 27.4, 24.7, 23.2, 22.6. MS (EI) *m/z* calculated for C₁₃H₂₄O [M-H]⁻ 195.1743; found, 195.1742.

Precursor to Compound 2.9B. Precursor to compound 2.9A (1 equiv, 9.8 mmol, 1.93 g) was dissolved in methanol (1 M, 10 mL) in a dry 100 mL round-bottom flask. After sparging the mixture with N₂, 5% Pd/C was added (10% by weight, 0.193 g) and the atmosphere was displaced with an H₂ balloon (1 atm). The compound was isolated in 46% yield by column chromatography

using a 0% to 30% ethyl acetate in hexanes gradient with 5% increments. The pure oil is slightly yellow. **¹H NMR** (500 MHz, CDCl₃) δ 3.74 (tt, *J* = 8.4, 4.5 Hz, 1H), 1.76 (m, 2H), 1.70 – 1.09 (m, 17H), 0.92 (dd, *J* = 6.6, 3.5 Hz, 6H). **¹³C NMR** (126 MHz, CDCl₃) δ 67.8, 47.5, 46.6, 35.7, 35.6, 33.9, 28.6, 28.4, 26.4, 26.3, 24.64, 23.48, 22.14. **MS (EI)** *m/z* calculated for C₁₃H₂₆O [M-OH]⁺ 197.1900; found, 197.1898.

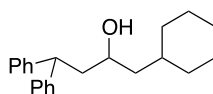


Precursor to Compound 2.10. Synthesized from 3-phenylbutanal according to the general procedure. The product was purified by column chromatography using a 0%–30% gradient of EtOAc in hexanes with 5% increments. The resulting clear oil was obtained in 73% yield as a 1.2:1 mixture of diastereomers. **¹H NMR** (500 MHz, CDCl₃) δ 7.29 (dd, *J* = 8.1, 7.1 Hz, 2H), 7.23 – 7.15 (m, 3H), 3.71 (tt, *J* = 8.3, 4.5 Hz, 0.5H), 3.44 (tt, *J* = 8.3, 3.8 Hz, 0.5H), 2.99 (dq, *J* = 14.1, 7.0, 5.0 Hz, 0.5H), 2.90 (h, *J* = 7.1 Hz, 0.5H), 1.77 – 1.57 (m, 7H), 1.56 – 1.50 (m, 0.5H), 1.46 – 1.29 (m, 2.5H), 1.26 (dd, *J* = 6.9, 3.9 Hz, 3H), 1.24 – 1.04 (m, 4H), 0.99 – 0.70 (m, 2H). **¹³C NMR** (126 MHz, CDCl₃) δ 147.7, 147.0, 128.7, 128.6, 127.3, 127.1, 126.3, 126.2, 67.8, 67.4, 47.1, 46.5, 46.2, 45.9, 37.0, 36.6, 34.5, 34.3, 34.2, 33.2, 33.0, 26.8, 26.7, 26.6, 26.5, 26.4, 23.5, 22.2. **MS (EI)** *m/z* calculated for C₁₇H₂₆O [M-OH]⁺ 229.1951; found, 229.1950.

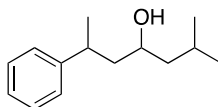


Precursor to Compound 2.11. Synthesized from 3-(4-methoxyphenyl)butanal according to the general procedure. The product was purified by column chromatography using a 0%–30% gradient of EtOAc in hexanes with 5% increments. The resulting clear oil was obtained in 75% yield as a

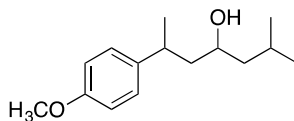
1.3:1 mixture of diastereomers. **¹H NMR** (500 MHz, CDCl₃) δ 7.16 – 7.09 (m, 2H), 6.87 – 6.81 (m, 2H), 3.79 (2x s, 3H), 3.71 (tq, *J* = 8.5, 4.4 Hz, 0.5H), 3.45 (tp, *J* = 8.5, 4.1 Hz, 0.5H), 3.00 – 2.90 (m, 0.5H), 2.85 (h, *J* = 7.1 Hz, 0.5H), 1.75 – 1.63 (m, 4H), 1.62 – 1.59 (m, 2.5H), 1.54 (m, 0.5H), 1.47 – 1.21 (m, 6H), 1.20 (m, 4H), 0.99 – 0.70 (m, 2H). **¹³C NMR** (126 MHz, CDCl₃) δ 158.1, 158.0, 139.7, 139.0, 128.1, 127.9, 114.1, 114.0, 68.0, 67.4, 55.43, 55.41, 47.3, 46.6, 46.2, 45.9, 36.3, 35.8, 34.5, 34.3, 34.23, 34.22, 33.2, 33.1, 26.8, 26.7, 26.6, 26.5, 26.4, 23.7, 22.5, 21.2. **MS (EI)** *m/z* calculated for C₁₇H₂₆O₂ [M-OH]⁺ 259.2056; found, 259.2055.



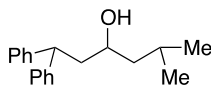
Precursor to Compound 2.12. Synthesized from 3,3-diphenylpropanal according to the general procedure. The product was purified by column chromatography using a 0%–30% gradient of EtOAc in hexanes with 5% increments. The resulting clear oil was obtained in 79% yield. **¹H NMR** (500 MHz, CDCl₃) δ 7.31 – 7.25 (m, 8H), 7.17 (dt, *J* = 11.1, 6.4, 2.4 Hz, 2H), 4.22 (dd, *J* = 9.8, 6.0 Hz, 1H), 3.58 (s, 1H), 2.21 (ddd, *J* = 13.6, 9.9, 3.6 Hz, 1H), 2.13 – 2.04 (m, 1H), 1.62 (tdd, *J* = 20.4, 12.5, 4.9 Hz, 5H), 1.43 – 1.28 (m, 3H), 1.27 – 1.07 (m, 4H), 0.95 – 0.72 (m, 2H). **¹³C NMR** (126 MHz, CDCl₃) δ 145.5, 144.3, 128.7, 128.7, 128.2, 127.9, 126.5, 126.4, 67.5, 47.9, 46.1, 44.0, 34.3, 34.3, 33.2, 26.7, 26.5, 26.4. **MS (EI)** *m/z* calculated for C₂₂H₂₈O [M-OH]⁺ 291.2107; found, 291.2104.



Precursor to Compound 2.13. Synthesized according to a previously reported procedure and the characterization data was consistent with the previously reported data.^{9b}



Precursor to Compound 2.14. Synthesized from 3-(4-methoxyphenyl)butanal using the procedure described for precursor to Compound 2.9A above with a solution of isobutyl magnesium chloride. The product was purified by column chromatography using a 0%–30% gradient of EtOAc in hexanes with 5% increments. The resulting clear oil was obtained in 60% yield as a 1.1:1 mixture of diastereomers. **¹H NMR** (500 MHz, CDCl₃) δ 7.15 – 7.11 (m, 2H), 6.87 – 6.82 (m, 2H), 3.78 (2x s, 3H), 3.67 (tt, *J* = 8.5, 4.3 Hz, 0.5H), 3.41 (tdd, *J* = 8.5, 4.8, 3.5 Hz, 0.5H), 2.95 (dq, *J* = 14.0, 7.0, 5.0 Hz, 0.5H), 2.86 (h, *J* = 7.1 Hz, 0.5H), 1.79 – 1.57 (m, 3H), 1.39 – 1.22 (m, 4H), 1.18 (ddd, *J* = 13.5, 8.2, 4.8 Hz, 2H), 0.88 (dd, *J* = 26.8, 6.6 Hz, 3H), 0.81 (dd, *J* = 6.6, 1.6 Hz, 3H). **¹³C NMR** (126 MHz, CDCl₃) δ 158.0, 158.0, 139.7, 139.0, 128.1, 127.9, 114.1, 114.0, 68.5, 68.0, 55.38, 55.37, 53.6, 47.5, 47.22, 47.16, 46.5, 36.2, 35.7, 24.8, 24.7, 23.69, 23.65, 23.4, 22.5, 22.4, 22.2, 21.2. **MS (EI)** *m/z* calculated for C₁₃H₂₄O₂ [M-OH]⁺ 219.1743; found, 219.1743.

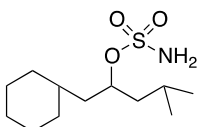


Precursor to Compound 2.15. Synthesized from 3,3-diphenylpropanal and a solution of isobutyl magnesium chloride according to the above procedure for precursor to compound 2.9A. The product was purified by column chromatography using a 0%–30% gradient of EtOAc in hexanes with 5% increments. The resulting clear oil was obtained in 57% yield. **¹H NMR** (500 MHz, CDCl₃) δ 7.25 – 7.19 (m, 8H), 7.11 (dddd, *J* = 12.4, 10.5, 5.3, 2.5 Hz, 2H), 4.17 (dd, *J* = 9.9, 5.9 Hz, 1H), 3.49 (tt, *J* = 8.5, 3.9 Hz, 1H), 2.17 (ddd, *J* = 13.6, 9.9, 3.5 Hz, 1H), 2.02 (ddd, *J* = 13.9, 9.0, 5.9 Hz, 1H), 1.66 (dh, *J* = 8.5, 6.6 Hz, 1H), 1.35 (ddd, *J* = 14.0, 8.5, 5.7 Hz, 1H), 1.24 (ddd, *J* = 13.4, 8.4, 4.6 Hz, 1H), 1.16 (bs, 1H), 0.77 (dd, *J* = 20.6, 6.6 Hz, 6H). **¹³C NMR** (126 MHz,

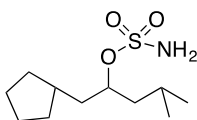
CDCl_3) δ 145.4, 144.3, 128.7, 128.7, 128.2, 127.9, 126.5, 126.4, 68.2, 47.8, 47.5, 43.9, 24.8, 23.5, 22.4. **MS (EI)** m/z calculated for $\text{C}_{19}\text{H}_{24}\text{O}$ $[\text{M}-\text{H}]^+$ 267.1743; found, 267.1739.

2.6.2. Synthesis of Sulfamate Esters

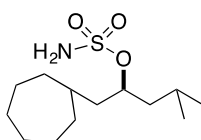
General Procedure. Formic acid (0.49 mL, 13 mmol, 2.5 equiv) was added dropwise to chlorosulfonyl isocyanate (3.0 equiv) cooled in an ice bath with vigorous stirring. Gas was evolved and the reaction mixture solidified within 5 min. To the resulting solid was added 10.4 mL of CH_3CN and the clear solution stirred in an ice bath for 30 min, allowed to warm to rt and stirred for an additional 4 h. The flask was placed in an ice bath and cooled to 0 °C. To the cold solution was added 5.2 mmol of the alcohol substrate in 8.7 mL of dimethylacetamide. The solution was warmed to rt and the mixture was stirred for 1 h. The reaction was quenched by the addition of 10 mL of H_2O and the aqueous layer was extracted with 3 x 50 mL portions of Et_2O . The combined organic layers were washed with 5 x 20 mL portions of H_2O , 1 x 25 mL brine, dried over MgSO_4 , filtered and concentrated under reduced pressure. The crude products were purified by silica gel column chromatography using a hexane/ EtOAc gradient.



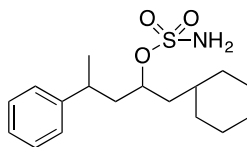
Compound 2.1. Synthesized according the the above general procedure. The product was purified by column chromatography using a 0%–30% gradient of EtOAc in hexanes with 5% increments. The resulting clear oil was obtained in 71% yield and became a white solid upon storing in a -30 °C freezer. The characterization data was consistent with the previously reported synthesis.^{9b}



Compound 2.8. Synthesized according to the general procedure. The product was purified by column chromatography using a 0%–30% gradient of EtOAc in hexanes in 5% increments. The resulting clear oil was obtained in 81% yield and became a white solid upon storing in a -30 °C freezer. **¹H NMR** (500 MHz, CDCl₃) δ 4.66 – 4.59 (m, 3H), 1.90 – 1.52 (m, 9H), 1.51 – 1.39 (m, 3H), 1.12 – 1.00 (m, 2H), 0.88 (dd, *J* = 11.2, 6.5 Hz, 7H). **¹³C NMR** (126 MHz, CDCl₃) δ 84.2, 43.8, 41.1, 36.4, 33.1, 32.9, 25.3, 25.2, 24.6, 23.0, 22.6. **MS (EI)** *m/z* calculated for C₁₁H₂₃NO₃S [M-H]⁻ 248.1326, found 248.1326.

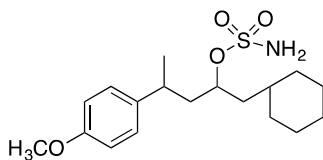


Compound 2.9. Synthesized according to the general procedure. The product was purified by column chromatography using a 0%–30% gradient of EtOAc in hexanes with 5% increments. The resulting clear oil was obtained in 55% yield and became a white solid upon storing in a -30 °C freezer. **¹H NMR** (500 MHz, CDCl₃) δ 4.65 (m, 3H), 1.74 – 1.48 (m, 10H), 1.48 – 1.33 (m, 6H), 1.20 – 1.08 (m, 2H), 0.88 (dd, *J* = 11.3, 6.5 Hz, 6H). **¹³C NMR** (126 MHz, CDCl₃) δ 83.2, 44.1, 43.1, 35.4, 35.1, 34.4, 28.7, 28.5, 26.5, 26.3, 24.7, 22.9, 22.7. **MS (EI)** *m/z* calculated for C₁₃H₂₇NO₃S [M+NH₄]⁺ 295.2050; found, 295.2048.

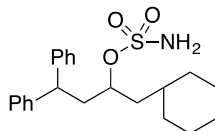


Compound 2.10. Synthesized according to the general procedure. The product was purified by column chromatography using a 0%–30% gradient of EtOAc in hexanes with 5% increments. The resulting clear oil was obtained in 72% yield as a 1.2:1 mixture of diastereomers. **¹H NMR** (500

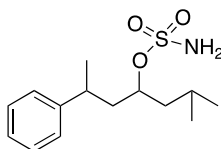
MHz, CDCl₃) δ 7.31 (ddd, J = 8.5, 7.0, 1.7 Hz, 2H), 7.24 – 7.19 (m, 3H), 4.58 – 4.50 (m, 1H), 4.50 – 4.47 (m, 1H), 4.42 (s, 1H), 2.96 (dt, J = 8.2, 6.8 Hz, 0.5H), 2.85 (dp, J = 8.8, 6.8 Hz, 0.5H), 2.18 (ddd, J = 14.2, 8.8, 6.5 Hz, 0.5H), 2.01 – 1.97 (m, 1H), 1.87 (dt, J = 14.2, 6.3 Hz, 0.5H), 1.75 – 1.60 (m, 5H), 1.53 – 1.41 (m, 1=2H), 1.41 – 1.25 (m, 4H), 1.23 – 1.05 (m, 3H), 1.00 – 0.74 (m, 2H). **¹³C NMR** (126 MHz, CDCl₃) δ 146.4, 146.3, 128.79, 128.77, 127.4, 127.2, 126.6, 82.4, 82.2, 42.9, 42.8, 42.5, 42.3, 37.0, 36.4, 34.1, 33.78, 33.77, 33.6, 33.2, 33.1, 26.6, 26.5, 26.32, 26.27, 26.22, 26.19, 23.4, 23.2, 21.3. **MS (EI)** m/z calculated for C₁₇H₂₇NO₃S [M+NH₄]⁺ 343.2050; found, 343.2045.



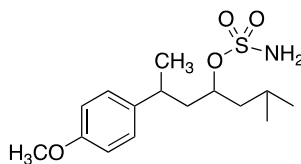
Compound 2.11. Synthesized according to the general procedure. The product was purified by column chromatography using a 0%–30% gradient of EtOAc in hexanes with 5% increments. The resulting clear oil was obtained in 87% yield as a 1.3:1 mixture of diastereomers. **¹H NMR** (500 MHz, CDCl₃) δ 7.16 – 7.11 (m, 2H), 6.87 – 6.80 (m, 2H), 4.72 (s, 1H), 4.68 (s, 1H), 4.56 – 4.43 (m, 1H), 3.78 (2x s, 3H), 2.97 – 2.86 (m, 0.5H), 2.78 (dq, J = 8.6, 6.7 Hz, 0.5H), 2.15 (ddd, J = 14.0, 8.7, 6.2 Hz, 0.5H), 2.01 – 1.78 (m, 2H), 1.76 – 1.56 (m, 4.5H), 1.54 – 1.37 (m, 2H), 1.34 – 1.07 (m, 7H), 0.97 – 0.72 (m, 2H). **¹³C NMR** (126 MHz, CDCl₃) δ 158.18, 158.17, 138.4, 138.2, 128.2, 128.0, 114.12, 114.10, 82.4, 82.1, 55.42, 55.41, 43.1, 43.0, 42.5, 42.2, 35.9, 35.6, 34.1, 33.8, 33.7, 33.6, 33.10, 33.05, 26.6, 26.5, 26.30, 26.25, 26.20, 26.15, 23.5, 23.2, 22.8, 21.2. **MS (EI)** m/z calculated for C₁₈H₂₉NO₄S [M+NH₄]⁺ 373.2156; found, 373.2150.



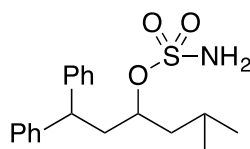
Compound 2.12. Synthesized according to the general procedure. The product was purified by column chromatography using a 0%–30% gradient of EtOAc in hexanes with 5% increments. The resulting clear oil was obtained in 38% and became a white solid upon storing in a -30 °C freezer. **¹H NMR** (500 MHz, CDCl₃) δ 7.33 – 7.26 (m, 8H), 7.21 – 7.17 (m, 2H), 4.57 (qd, *J* = 6.6, 5.0 Hz, 1H), 4.33 (s, 2H), 4.14 (dt, *J* = 8.3, 7.6 Hz, 1H), 2.54 (dt, *J* = 14.6, 7.3 Hz, 1H), 2.40 (ddd, *J* = 14.5, 8.3, 5.0 Hz, 1H), 1.71 (dt, *J* = 13.6, 6.6 Hz, 1H), 1.68 – 1.59 (m, 4H), 1.56 – 1.49 (m, 2H), 1.37 (tqd, *J* = 9.3, 6.0, 2.7 Hz, 1H), 1.23 – 1.08 (m, 3H), 0.94 – 0.76 (m, 2H). **¹³C NMR** (126 MHz, CDCl₃) δ 144.04, 143.86, 128.90, 128.82, 128.06, 127.98, 126.81, 126.72, 82.00, 47.76, 42.48, 40.56, 33.97, 33.42, 33.38, 26.53, 26.25, 26.22. **MS (EI)** *m/z* calculated for C₂₂H₂₉NO₃S [M+NH₄]⁺ 405.2206; found, 405.2206.



Compound 2.13. Synthesized according to the general procedure. The product was purified by column chromatography using a 0%–30% gradient of EtOAc in hexanes with 5% increments. The resulting clear oil was obtained in 72% yield as a 1.2:1 mixture of diastereomers. Characterization data consistent with the previously reported synthesis.^{9b}



Compound 2.14. Synthesized according the general procedure. The product was purified by column chromatography using a 0%–30% gradient of EtOAc in hexanes with 5% increments. The resulting clear oil was obtained in 83% yield as a 1.1:1 mixture of diastereomers. **¹H NMR** (500 MHz, CDCl₃) δ 7.19 – 7.08 (m, 2H), 6.92 – 6.76 (m, 2H), 4.64 (m, 2H), 4.53 – 4.42 (m, 1H), 3.79 (2x s, 3H), 2.92 (dp, *J* = 9.0, 6.8 Hz, 0.5H), 2.80 (dp, *J* = 8.7, 6.8 Hz, 0.5H), 2.19 – 2.11 (m, 0.5H), 2.00 – 1.89 (m, 1H), 1.84 (dt, *J* = 14.1, 6.6 Hz, 0.5H), 1.76 – 1.59 (m, 3H), 1.46 (ddd, *J* = 14.1, 8.1, 5.1 Hz, 1H), 1.30 – 1.21 (m, 4H), 0.90 (dd, *J* = 10.5, 6.4 Hz, 3H), 0.79 (dd, *J* = 29.2, 6.3 Hz, 3H). **¹³C NMR** (126 MHz, CDCl₃) δ 158.22, 158.21, 138.3, 138.2, 128.2, 128.0, 114.14, 114.12, 82.9, 82.7, 55.4, 44.0, 43.6, 43.1, 43.0, 36.0, 35.5, 24.7, 24.4, 23.6, 23.3, 23.2, 23.0, 22.4, 22.3, 21.2. **MS (EI)** *m/z* calculated for C₁₅H₂₅NO₄S [M+NH₄]⁺ 333.1843; found, 333.1837.



Compound 2.15. Synthesized according to the general procedure. The product was purified by column chromatography using a 0%–30% gradient of EtOAc in hexanes with 5% increments. The resulting clear oil was obtained in 30% and became a white solid upon storing in a -30 °C freezer. **¹H NMR** (500 MHz, CDCl₃) δ 7.32 – 7.27 (m, 8H), 7.20 (m, 2H), 4.54 (td, *J* = 7.0, 5.3 Hz, 1H), 4.32 (bs, 2H), 4.15 (t, *J* = 7.9 Hz, 1H), 2.54 (dt, *J* = 14.6, 7.3 Hz, 1H), 2.41 (ddd, *J* = 14.4, 8.3, 5.1 Hz, 1H), 1.77 – 1.67 (m, 2H), 1.55 – 1.52 (m, 1H), 0.85 (dd, *J* = 6.4, 2.9 Hz, 6H). **¹³C NMR** (126 MHz, CDCl₃) δ 144.0, 143.9, 128.9, 128.8, 128.1, 128.0, 126.8, 126.7, 82.5, 53.6, 47.7, 43.9, 40.5, 24.7, 22.7. **MS (EI)** *m/z* calculated for C₁₉H₂₅NO₃S [M+NH₄]⁺ 365.1893; found, 365.1891.

2.6.3 Nitrene Transfer Procedures and Characterization of C-H Amination Products

General procedure for the Ag-catalyzed C–H amination.^{9b} A pre-dried reaction flask was charged with silver triflate (6.4 mg, 0.025 mmol, 0.1 equiv) and ligand (7.4 mg Me₄phen, 0.03125

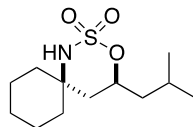
mmol, 0.125 equiv, or 9.1 mg tpa, 0.03125 mmol, 0.125 equiv, or 13.8 mg Py₅Me₂, 0.03125 mmol, 0.125 equiv). Dichloromethane (2.5 mL) was added and the mixture was stirred vigorously for 30 minutes. Then, 4Å molecular sieves (1 mmol substrate/g of sieves) were added, followed by a solution of the sulfamate substrate (0.25 mmol, 1 equiv) in dichloromethane (2.5 mL). Iodosobenzene (194 mg, 0.88 mmol, 3.5 equiv) was added in one portion and the reaction mixture was allowed to stir at room temperature for 30 minutes. The reaction mixture was filtered through a glass frit with dichloromethane and the filtrate was concentrated under reduced pressure. The crude products were purified by silica gel column chromatography using an EtOAc/hexane gradient (0–30% EtOAc/hexane unless otherwise specified). The reported yields were from the higher-yielding conditions for each product or by ¹H-NMR of the crude reaction mixture.

General procedure for Rh-catalyzed C–H amination. Procedures for Rh₂(OAc)₄ (2 mol% catalyst loading), Rh₂(TPA)₄ (2 mol% catalyst loading), and Rh₂(esp)₂ (1 mol% catalyst loading) have been reported by the Du Bois group using PhI(OAc)₂ as the oxidant (1.1 equiv), activated MgO as the base (2.3 equiv) and CH₂Cl₂ as the solvent (0.156 M). The reaction is refluxed at 45–50 °C for 1–2 h or until TLC indicates complete consumption of the starting material.^{2h}

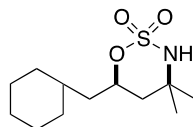
General procedure for Mn-catalyzed C–H amination. The White-Paradine catalyst was used according to the previously reported procedure. The reactions were done in the dark using 10 mol% [Mn(*t*BuPc)]Cl and 10 mol% AgSbF₆ that were stored in the glovebox prior to use. The reactions use PhI(OPiv)₂ as the oxidant (2 equiv), 4 Å mol sieves (40 mg) with a 9:1 solvent mixture of benzene:acetonitrile (0.5 M) using 0.15 mmol of substrate (1 equiv). The reaction takes place at room temperature over 8–24 h.^{7a}

General procedure for Ru-catalyzed C–H amination. The procedure for [Ru(hp)₄]Cl catalyzed amination (2.5 mol% catalyst loading) was followed as previously reported. The reaction uses

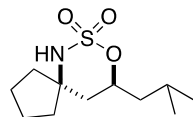
PhI(OPiv)₂ as the oxidant (1.4 equiv), 4 Å mol sieves as the dessicant (60 mg), and CH₂Cl₂ as the solvent (0.05 M). The reactions were refluxed at 45-50 °C for 24 h.^{3a}



Compound 2.1Cy. The product was purified by column chromatography using a 0%–30% gradient of EtOAc in hexanes with 5% increments to obtain pure regioisomers as previously reported. The compound is a white solid. Characterization data consistent with the previously reported synthesis.^{9b}

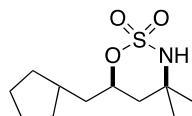


Compound 2.1Pr. The product was purified by column chromatography using a 0%–30% gradient of EtOAc in hexanes with 5% increments to obtain pure regioisomers as previously reported. The compound is a white solid. Characterization data consistent with the previously reported synthesis.^{9b}

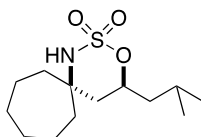


Compound 2.8Cy. The product was purified by column chromatography using a 0%–30% gradient of EtOAc in hexanes with 5% increments to obtain pure regioisomers. The compound is a white solid. ¹H NMR (500 MHz, CDCl₃) δ 4.78 (dddd, *J* = 11.3, 9.0, 4.3, 2.0 Hz, 1H), 4.07 (s, 1H), 2.48 – 2.40 (m, 1H), 1.90 – 1.76 (m, 2H), 1.75 – 1.50 (m, 9H), 1.29 (ddd, *J* = 14.2, 8.6, 4.3 Hz, 1H),

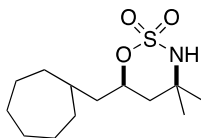
0.88 (dd, $J = 9.9, 6.7$ Hz, 6H). ^{13}C NMR (126 MHz, CDCl_3) δ 81.0, 66.6, 44.3, 42.7, 40.4, 35.6, 24.3, 24.0, 23.0, 22.7, 22.0. **MS (EI)** m/z calculated for $\text{C}_{11}\text{H}_{21}\text{NO}_3\text{S}$ $[\text{M}+\text{NH}_4]^+$ 265.1580; found, 265.1578.



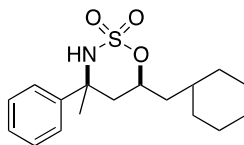
Compound 2.8_{IPr}. The product was purified by column chromatography using a 0%–30% gradient of EtOAc in hexanes with 5% increments to obtain pure regioisomers. The compound is a white solid. ^1H NMR (500 MHz, CDCl_3) δ 4.79 (dddd, $J = 11.5, 8.4, 4.6, 2.2$ Hz, 1H), 3.95 (s, 1H), 1.99 – 1.87 (m, 1H), 1.85 – 1.68 (m, 3H), 1.62 – 1.45 (m, 7H), 1.44 (s, 3H), 1.23 (s, 3H), 1.11 – 0.99 (m, 2H). ^{13}C NMR (126 MHz, CDCl_3) δ 81.0, 56.0, 42.1, 41.6, 35.9, 33.0, 32.6, 32.2, 25.3, 25.2, 25.0. **MS (EI)** m/z calculated for $\text{C}_{11}\text{H}_{21}\text{NO}_3\text{S}$ $[\text{M}+\text{NH}_4]^+$ 265.1580; found, 265.1578.



Compound 2.9_{Cy}. The product was purified by column chromatography using a 0%–30% gradient of EtOAc in hexanes with 5% increments to obtain pure regioisomers. The compound is a white solid. ^1H NMR (500 MHz, CDCl_3) δ 4.82 (dddd, $J = 11.8, 9.0, 4.2, 1.9$ Hz, 1H), 3.76 (s, 1H), 2.25 (dd, $J = 14.6, 9.1$ Hz, 1H), 1.88 – 1.51 (m, 11H), 1.49 – 1.31 (m, 4H), 1.31 – 1.24 (m, 1H), 0.88 (dd, $J = 10.0, 6.6$ Hz, 6H). ^{13}C NMR (126 MHz, CDCl_3) δ 79.4, 61.8, 45.0, 44.4, 42.1, 35.3, 29.4, 29.1, 24.0, 23.1, 22.2, 22.1, 21.9. **MS (EI)** m/z calculated for $\text{C}_{13}\text{H}_{25}\text{NO}_3\text{S}$ $[\text{M}+\text{NH}_4]^+$ 293.1893; found, 293.1890.

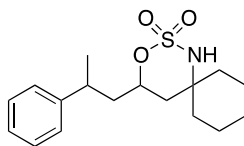


Compound 2.9_{iPr}. The product was purified by column chromatography using a 0%–30% gradient of EtOAc in hexanes with 5% increments to obtain pure regioisomers. The compound is a white solid. **¹H NMR** (500 MHz, CDCl₃) δ 4.89 (dddd, J = 11.1, 8.7, 4.1, 2.3 Hz, 1H), 3.90 (s, 1H), 1.82 – 1.75 (m, 2H), 1.75 – 1.67 (m, 2H), 1.67 – 1.57 (m, 6H), 1.51 (s, 3H), 1.49 – 1.39 (m, 5H), 1.29 (s, 3H), 1.18 (m, 1H), 0.94 (m, 1H). **¹³C NMR** (126 MHz, CDCl₃) δ 79.7, 56.1, 43.7, 42.4, 35.2, 34.6, 33.9, 32.3, 28.6, 28.6, 26.3, 26.2, 25.4. **MS (EI)** m/z calculated for C₁₃H₂₅NO₃S [M+NH₄]⁺ 293.1893; found, 293.1890.

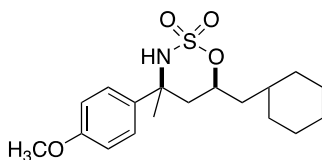


Compound 2.10_{Bn-syn}. The product was purified by column chromatography using a 0%–30% gradient of EtOAc in hexanes with 5% increments to obtain this pure diastereomer with nOe observed between the methyl group and O-methine. The compound is a white solid. The minor *anti*-diastereomer co-elutes as a mixture with **2.10_{Bn-syn}** and **2.10_{alk}** regioisomer with a clean ¹H-NMR signal at 4.93 (td, J = 8.7, 4.4, 1H) suitable for quantitative ¹H-NMR analysis. **Major (Bn-syn) ¹H NMR** (500 MHz, CDCl₃) δ 7.46 – 7.37 (m, 4H), 7.35 – 7.30 (m, 1H), 5.10 (dddd, J = 11.2, 9.0, 4.1, 2.0 Hz, 1H), 4.28 (s, 1H), 2.13 (dd, J = 14.1, 2.0 Hz, 1H), 2.08 – 2.00 (m, 1H), 1.87 (dt, J = 12.6, 3.7, 1.9 Hz, 1H), 1.80 (s, 3H), 1.77 – 1.65 (m, 4H), 1.64 – 1.58 (m, 1H), 1.50 (ddd, J = 14.0, 8.4, 4.0 Hz, 1H), 1.33 – 1.24 (m, 3H), 1.17 (qt, J = 12.8, 3.6 Hz, 1H), 1.05 – 0.92 (m, 2H). **¹³C NMR** (126 MHz, CDCl₃) δ 146.2, 129.3, 129.2, 128.4, 124.1, 78.9, 60.9, 53.6, 43.3, 40.6,

33.8, 33.3, 32.8, 27.5, 26.5, 26.3, 26.2. **MS (EI)** m/z calculated for $C_{17}H_{25}NO_3S$ $[M+NH_4]^+$ 341.1893; found, 341.1892.

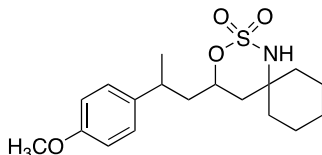


Compound 2.10_{alk}. The product was passed through column chromatography using a 0%–30% gradient of EtOAc in hexanes with 5% increments to obtain this pure regioisomer as a mixture of diastereomers. The compounds are white solids and were characterized as a 2.5:1 mixture of diastereomers. **1H NMR** (500 MHz, $CDCl_3$) δ 7.34 – 7.28 (m, 2H), 7.24 – 7.16 (m, 3H), 4.81 (dddd, $J = 11.8, 8.3, 5.2, 1.8$ Hz, 0.3H), 4.61 – 4.51 (m, 0.7H), 3.99 (s, 0.3H), 3.95 (s, 0.7H), 3.09 – 3.02 (m, 0.7H), 2.98 (dq, $J = 8.7, 6.9$ Hz, 0.3H), 2.36 – 2.31 (m, 0.3H), 2.26 – 2.19 (m, 0.7H), 2.11 – 2.04 (m, 0.3H), 2.00 (ddd, $J = 14.1, 9.3, 4.6$ Hz, 0.7H), 1.81 – 1.54 (m, 5H), 1.53 – 1.40 (m, 5H), 1.31 (d, $J = 7.3$ Hz, 2H), 1.29 – 1.18 (m, 3H). **^{13}C NMR** (126 MHz, $CDCl_3$) δ 146.1, 145.3, 128.8, 127.3, 126.9, 126.73, 126.65, 78.8, 78.4, 58.1, 58.0, 44.5, 43.67, 41.73, 40.6, 40.5, 35.5, 35.0, 32.94, 32.92, 25.72, 25.68, 22.44, 21.38, 21.2, 21.1, 21.0, 20.9. **MS (EI)** m/z calculated for $C_{17}H_{25}NO_3S$ $[M+NH_4]^+$ 341.1893; found, 341.1892.

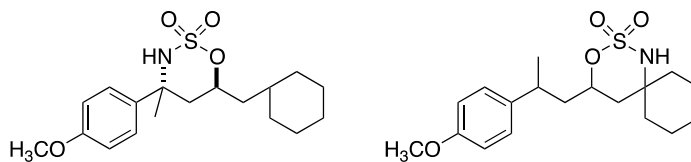


Compound 2.11_{Bn-syn}. The product was purified by column chromatography using a 0%–30% gradient of EtOAc in hexanes with 5% increments to obtain this pure diastereomer with nOe observed between the methyl group and O-methine. The compound is a white solid. **1H NMR** (500 MHz, $CDCl_3$) δ 7.40 – 7.36 (m, 2H), 6.96 – 6.92 (m, 2H), 5.11 (dddd, $J = 11.4, 9.0, 4.0, 2.5$ Hz,

1H), 4.21 (s, 1H), 3.84 (s, 3H), 2.13 – 2.01 (m, 2H), 1.92 – 1.86 (m, 1H), 1.81 (s, 3H), 1.80 – 1.60 (m, 6H), 1.55 – 1.48 (m, 1H), 1.30 (qq, $J = 14.7, 4.3, 3.9$ Hz, 2H), 1.24 – 1.13 (m, 1H), 1.06 – 0.90 (m, 2H). ^{13}C NMR (126 MHz, CDCl_3) δ 159.4, 138.3, 125.5, 114.4, 78.9, 60.5, 55.6, 43.3, 40.7, 33.9, 33.3, 32.8, 27.4, 26.57, 26.3, 26.2. **MS (EI)** m/z calculated for $\text{C}_{18}\text{H}_{27}\text{NO}_4\text{S}$ $[\text{M}+\text{NH}_4]^+$ 371.1999; found, 371.1997.

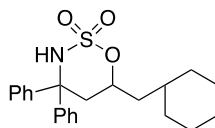


Compound 2.11_{alk-major diastereomer}. The product was passed through column chromatography using a 0%–30% gradient of EtOAc in hexanes with 5% increments to obtain this pure regioisomer as a mixture of diastereomers. The compounds are white solids. Characterized as a 2.5:1 mixture of diastereomers. Characterized as a 2:1 mix of regioisomers with **2.11_{Bn-syn}**. ^1H NMR (500 MHz, CDCl_3) δ 7.17 – 7.13 (m, 2H), 6.97 – 6.85 (m, 2H), 4.58 (tt, $J = 9.6, 3.5$ Hz, 1H), 3.82 (s, 3H), 3.77 (s, 1H), 3.08 – 3.00 (m, 1H), 1.79 – 1.60 (m, 6H), 1.55 – 1.47 (m, 3H), 1.33 (m, 3H), 1.17 – 1.05 (m, 2H), 0.99 (d, $J = 6.6$ Hz, 3H). ^{13}C NMR (126 MHz, CDCl_3) δ 158.3, 137.3, 128.2, 114.2, 78.8, 58.1, 55.4, 44.8, 40.8, 34.9, 34.6, 33.0, 25.7, 25.5, 22.6, 21.1, 20.9. **MS (EI)** m/z calculated for $\text{C}_{18}\text{H}_{27}\text{NO}_4\text{S}$ $[\text{M}+\text{NH}_4]^+$ 371.1999; found, 371.1995.

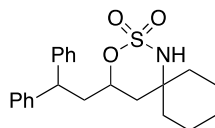


Compound 2.11_{Bn-anti} + Compound 2.11_{alk-minor diastereomer}. (3:1 Bn:alk). The product was passed through column chromatography using a 0%–30% gradient of EtOAc in hexanes with 5% increments to obtain the minor diastereomers of each regioisomer as a mixture. The compounds

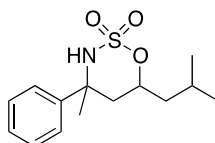
are white solids. Characterized as a 2.5:1 mixture of diastereomers and a 2:1 mix of regioisomers with **2.11_{Bn-syn}**. **¹H NMR** (500 MHz, CDCl₃) δ 7.40 – 7.36 (m, 1.4H), 7.11 – 7.08 (m, 0.4H), 6.93 – 6.83 (m, 2H), 4.80 (ddt, *J* = 10.1, 6.5, 2.0 Hz, 0.15H), 4.74 (dddd, *J* = 11.5, 9.0, 4.2, 1.4 Hz, 0.7H), 3.81 (s, 2H), 3.79 (s, 0.8H), 2.97 – 2.91 (m, 0.2H), 2.58 (dd, *J* = 14.9, 1.4 Hz, 0.7H), 1.84 (m, 1H), 1.77 – 1.58 (m, 7H), 1.54 – 1.47 (m, 2.4H), 1.45 (s, 2H), 1.43 (d, *J* = 1.3 Hz, 0.75H), 1.29 (m, 2H), 1.21 – 1.01 (m, 2H), 0.97 (d, *J* = 6.7 Hz, 1H). **¹³C NMR** (126 MHz, CDCl₃) δ 133.4, 127.8, 127.0, 114.3, 114.0, 79.7, 78.5, 58.2, 55.4, 43.9, 43.1, 40.8, 40.4, 35.7, 34.9, 34.7, 34.3, 33.8, 33.3, 33.0, 32.8, 27.1, 26.5, 26.3, 26.1, 25.7, 25.5, 21.7. **MS (EI)** *m/z* calculated for C₁₈H₂₇NO₄S [M+NH₄]⁺ 371.1999; found, 371.1995.



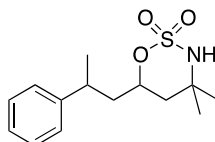
Compound 2.12_{Bn}. The product was purified by column chromatography using a 0%–30% gradient of EtOAc in hexanes with 5% increments to obtain pure regioisomers. The compound is a white solid. **¹H NMR** (500 MHz, CDCl₃) δ 7.56 – 7.29 (m, 8H), 7.28 – 7.20 (m, 2H), 4.86 (dddd, *J* = 11.5, 8.9, 4.1, 1.4 Hz, 1H), 4.81 (s, 1H), 3.02 (dd, *J* = 15.0, 1.3 Hz, 1H), 2.31 (dd, *J* = 14.9, 11.4 Hz, 1H), 1.86 – 1.77 (m, 1H), 1.77 – 1.61 (m, 5H), 1.61 – 1.51 (m, 2H), 1.31 – 1.20 (m, 3H), 1.20 – 1.08 (m, 1H), 1.00 – 0.91 (m, 1H). **¹³C NMR** (126 MHz, CDCl₃) δ 145.5, 140.1, 129.1, 128.6, 128.0, 127.7, 126.6, 124.6, 79.4, 66.7, 43.0, 39.6, 33.6, 33.2, 32.6, 26.3, 26.1, 25.9. **MS (EI)** *m/z* calculated for C₂₂H₂₇NO₃S [M+NH₄]⁺ 403.2050; found, 403.2050.



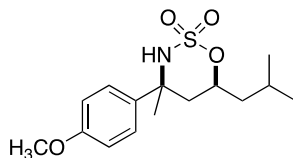
Compound 2.12_{alk}. The product was purified by column chromatography using a 0%–30% gradient of EtOAc in hexanes with 5% increments to obtain pure regioisomers. The compound is a white solid. **¹H NMR** (500 MHz, CDCl₃) δ 7.32 – 7.23 (m, 8H), 7.22 – 7.17 (m, 2H), 4.69 – 4.60 (m, 1H), 4.26 (dd, *J* = 10.6, 5.2 Hz, 1H), 3.84 (s, 1H), 2.45 (ddd, *J* = 14.0, 8.9, 5.2 Hz, 1H), 2.28 (ddd, *J* = 14.3, 10.6, 4.0 Hz, 1H), 2.21 (d, *J* = 13.9 Hz, 1H), 1.63 (dd, *J* = 14.4, 2.3 Hz, 2H), 1.57 – 1.53 (m, 2H), 1.49 (m, 4H), 1.40 – 1.32 (m, 1H), 1.24 – 1.15 (m, 2H). **¹³C NMR** (126 MHz, CDCl₃) δ 143.8, 143.1, 129.0, 128.8, 128.2, 127.7, 126.9, 126.7, 78.4, 58.1, 46.0, 41.7, 41.5, 40.7, 32.9, 25.7, 21.1, 20.9. **MS (EI)** *m/z* calculated for C₂₂H₂₇NO₃S [M+NH₄]⁺ 403.2050; found, 403.2050.



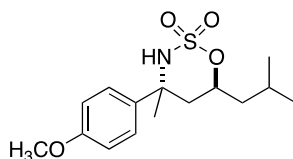
Compound 2.13_{Bn}. The product was purified by column chromatography using a 0%–30% gradient of EtOAc in hexanes with 5% increments and isolated as a mixture of diastereomers. The characterization data was consistent with the previously reported synthesis.^{9b}



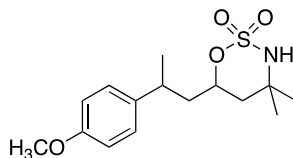
Compound 2.13_{alk}. The product was purified by column chromatography using a 0%–30% gradient of EtOAc in hexanes with 5% increments and isolated as a mixture of diastereomers. The characterization data was consistent with the previously reported synthesis.^{9b}



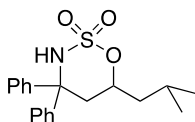
Compound 2.14_{Bn-syn}. The product was purified by column chromatography using a 0%–30% gradient of EtOAc in hexanes with 5% increments to obtain this pure diastereomer with nOe observed between the methyl group and O-methine. The compound is a white solid. **¹H NMR** (500 MHz, CDCl₃) δ 7.39 – 7.32 (m, 2H), 6.95 – 6.89 (m, 2H), 5.06 (dddd, *J* = 11.3, 9.0, 4.1, 2.4 Hz, 1H), 4.21 (s, 1H), 3.82 (s, 3H), 2.09 (dd, *J* = 14.1, 2.4 Hz, 1H), 1.99 – 1.81 (m, 2H), 1.79 (s, 3H), 1.53 – 1.43 (m, 2H), 0.99 (dd, *J* = 13.2, 6.4 Hz, 6H). **¹³C NMR** (126 MHz, CDCl₃) δ 159.4, 138.3, 125.5, 114.4, 79.4, 55.5, 44.5, 40.7, 34.9, 27.4, 24.0, 23.1, 22.1. **MS (EI)** *m/z* calculated for C₁₅H₂₃NO₄S [M+NH₄]⁺ 331.1686; found, 331.1683.



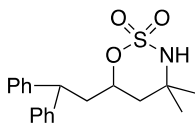
Compound 2.14_{Bn-anti}. The product was purified by column chromatography using a 0%–30% gradient of EtOAc in hexanes with 5% increments to obtain this pure diastereomer with no nOe observed between the methyl group and O-methine. The compound is a white solid. **¹H NMR** (500 MHz, CDCl₃) δ 7.39 (d, *J* = 8.9 Hz, 2H), 6.98 – 6.83 (m, 2H), 4.71 (dddd, *J* = 11.5, 8.7, 4.6, 1.4 Hz, 1H), 4.39 (s, 1H), 3.81 (s, 3H), 2.59 (dd, *J* = 15.0, 1.5 Hz, 1H), 1.91 – 1.82 (m, 2H), 1.79 – 1.69 (m, 2H), 1.45 (s, 3H), 0.95 (dd, *J* = 19.0, 6.6 Hz, 6H). **¹³C NMR** (126 MHz, CDCl₃) δ 159.0, 133.4, 127.0, 114.0, 80.2, 61.5, 55.4, 44.3, 40.2, 34.9, 25.5, 24.1, 23.0. **MS (EI)** *m/z* calculated for C₁₅H₂₃NO₄S [M+NH₄]⁺ 331.1686; found, 331.1681.



Compound 2.14_{alk-major diastereomer}. The product was purified by column chromatography using a 0%–30% gradient of EtOAc in hexanes with 5% increments to obtain the major diastereomer. The compound is a white solid. The minor alk diastereomer co-elutes as a mixture with **2.14_{Bn-anti}** and **2.14_{alk-major diastereomer}** isomers with a clean $^1\text{H-NMR}$ signal at 4.80 (dddd, $J = 11.6, 8.3, 5.2, 2.0$ Hz, 1H) suitable for quantitative $^1\text{H-NMR}$ analysis. **$^1\text{H NMR}$** (500 MHz, CDCl_3) δ 7.15 – 7.12 (m, 2H), 6.88 – 6.84 (m, 2H), 4.59 – 4.52 (m, 1H), 3.94 (s, 1H), 3.80 (s, 3H), 3.02 (dtt, $J = 11.3, 7.0, 3.5$ Hz, 1H), 1.99 (ddd, $J = 14.1, 9.6, 4.3$ Hz, 1H), 1.67 (ddd, $J = 14.0, 10.7, 3.1$ Hz, 1H), 1.55 – 1.42 (m, 2H), 1.34 (s, 3H), 1.27 (d, $J = 7.0$ Hz, 3H), 1.24 (s, 3H). **$^{13}\text{C NMR}$** (126 MHz, CDCl_3) δ 158.4, 137.3, 128.2, 114.2, 79.7, 56.0, 55.4, 44.7, 42.1, 34.5, 32.2, 25.3, 22.6. **MS (EI)** m/z calculated for $\text{C}_{15}\text{H}_{23}\text{NO}_4\text{S}$ $[\text{M}+\text{NH}_4]^+$ 331.1686; found, 331.1684.

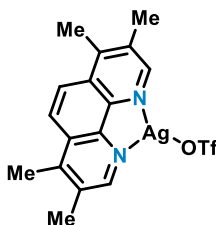


Compound 2.15_{Bn}. The product was purified by column chromatography using a 0%–30% gradient of EtOAc in hexanes with 5% increments to obtain pure regioisomers. The compound is a white solid. **$^1\text{H NMR}$** (500 MHz, CDCl_3) δ 7.47 – 7.42 (m, 2H), 7.30 – 7.25 (m, 2H), 7.24 – 7.11 (m, 6H), 4.77 – 4.66 (m, 2H), 2.94 (dd, $J = 14.8, 1.3$ Hz, 1H), 2.22 (dd, $J = 14.9, 11.4$ Hz, 1H), 1.86 – 1.69 (m, 2H), 1.47 – 1.40 (m, 1H), 0.84 (dd, $J = 10.1, 6.6$ Hz, 6H). **$^{13}\text{C NMR}$** (126 MHz, CDCl_3) δ 145.7, 140.3, 129.3, 128.7, 128.2, 127.9, 126.8, 124.8, 80.0, 66.9, 44.4, 39.7, 24.1, 23.0, 22.2. **MS (EI)** m/z calculated for $\text{C}_{19}\text{H}_{23}\text{NO}_3\text{S}$ $[\text{M}+\text{NH}_4]^+$ 363.1736; found, 363.1737.

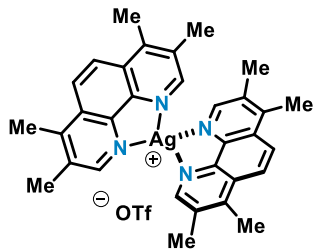


Compound 2.15_{alk}. The product was purified by column chromatography using a 0%–30% gradient of EtOAc in hexanes with 5% increments to obtain pure regioisomers. The compound is a white solid. $^1\text{H NMR}$ (500 MHz, CDCl_3) δ 7.29 – 7.20 (m, 6H), 7.19 – 7.12 (m, 4H), 4.60 (ddt, $J = 10.8, 9.0, 3.4$ Hz, 1H), 4.23 (dd, $J = 10.6, 5.1$ Hz, 1H), 3.96 (s, 1H), 2.41 (ddd, $J = 14.2, 9.0, 5.1$ Hz, 1H), 2.24 (ddd, $J = 14.3, 10.7, 3.8$ Hz, 1H), 1.59 (m, 1H), 1.55 – 1.51 (m, 1H), 1.27 (s, 3H), 1.21 (s, 3H). $^{13}\text{C NMR}$ (126 MHz, CDCl_3) δ 143.8, 143.1, 129.0, 128.8, 128.2, 127.8, 127.0, 126.7, 79.2, 56.0, 45.9, 41.9, 41.4, 32.1, 25.2. **MS (EI)** m/z calculated for $\text{C}_{19}\text{H}_{23}\text{NO}_3\text{S}$ $[\text{M}+\text{NH}_4]^+$ 363.1736; found, 363.1735.

2.6.4 Procedures for the synthesis of $[\text{Ag}(\text{Me}_4\text{phen})]\text{OTf}$ and $[\text{Ag}(\text{Me}_4\text{phen})_2]\text{OTf}$ crystals



$[(\text{Me}_4\text{phen})\text{Ag}]\text{OTf}$. The 1:1 $\text{AgOTf}:\text{Me}_4\text{phen}$ complex was prepared in an oven-dried scintillation vial equipped with a magnetic stir bar. Silver(I) triflate (10.9 mg, 0.04 mmol, 1 equiv) and 3,4,7,8- tetramethyl-1,10-phenanthroline (10.0 mg, 0.04 mmol, 1 equiv) were dissolved in CH_2Cl_2 (4 mL, 0.01 M). The resulting solution was stirred for 15 min at room temperature. Crystals suitable for X-ray crystallography were obtained by placing the scintillation vial in a sealed jar containing 15 mL pentane at room temperature for 14 h (72% yield).



[(Me₄phen)₂Ag]OTf. In an oven-dried scintillation vial equipped with a magnetic stir bar, the 1:2 AgOTf:Me₄phen complex was prepared by dissolving silver(I) triflate (10.9 mg, 0.04 mmol, 1 equiv) and 3,4,7,8-tetramethyl-1,10-phenanthroline (18.9 mg, 0.08 mmol, 2 equiv) in CH₂Cl₂ (4 mL, 0.01 M). The resulting solution was stirred for 15 min at room temperature. Crystals suitable for X-ray crystallography were obtained by placing the scintillation vial in a sealed jar containing 15 mL pentane and at room temperature for 30 h (89% yield).

Chapter 3:

Investigation of Transition Metal-Catalyzed Nitrene Transfer Reactions in Water

This chapter is reprinted (adapted) with permission from work published in:

Alderson, J. M.¹; Corbin, J. R.¹; Schomaker, J. M. *Bioorg.Med. Chem.* **2018**, 26, 5270-5273.

The work described in this chapter focuses on work I did in collaboration with Dr. Juliet M. Alderson as coauthors. Dr. Juliet M. Alderson was completing her PhD and just found that our group's nitrene transfer conditions work on water and made quick work of the optimization; I flushed out the scope, compared the results to those observed in traditional solvents, and helped complete the work for publication in the reference on the previous page. Additionally, I helped supply catalysts for Table 3.3 and helped run some of these catalyst comparisons and ran the reactions in buffered solvent in Table 3.4.

Chapter 3

Investigation of Transition Metal-Catalyzed Nitrene Transfer Reactions in Water

3.1 Introduction

Transition metal-catalyzed nitrene transfer is a powerful method for incorporating new C–N bonds into relatively unfunctionalized scaffolds. In this work, we report the first examples of site- and chemoselective C–H bond amination reactions in aqueous media. The unexpected ability to employ water as the solvent in these reactions is advantageous in that it eliminates toxic solvent use and enables reactions to be run at increased concentrations with lower oxidant loadings. Using water as the reaction medium has potential to expand the scope of nitrene transfer to encompass a variety of biomolecules and highly polar substrates, as well as enable pH control over the site-selectivity of C–H bond amination.

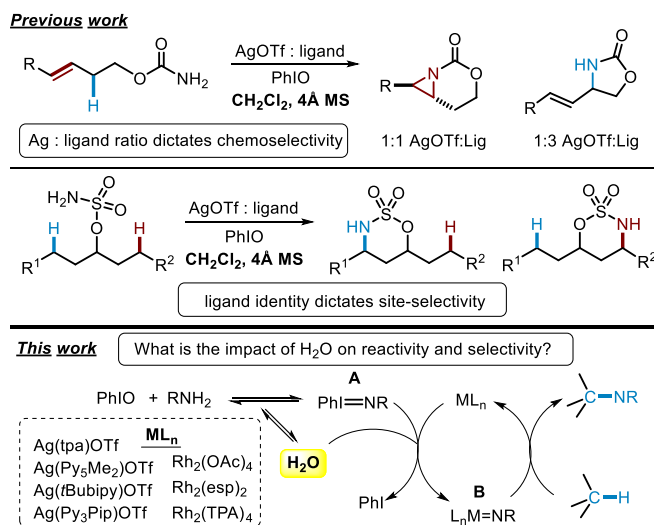
The development of selective carbon–nitrogen (C–N) bond-forming reactions is of great interest, as amines are present in a multitude of bioactive natural products and pharmaceuticals. While there are several synthetic methods available to introduce C–N bonds into organic substrates, transition metal-catalyzed nitrene transfer reactions are appealing for the direct amination of C–H bonds. An important challenge in nitrene transfer catalysis is to identify strategies that enable selective reaction at a desired site in the presence of multiple reactive C–H bonds. A variety of transition metal catalysts, including ones based on Rh, Ru, Fe, Mn, Cu, Ir, Co and Ag, have been studied with the goal of achieving predictable catalyst control over the C–N bond forming event.¹ In our own research program, we have successfully utilized the unique ability of Ag to adopt diverse

coordination geometries in solution to control nitrene transfer selectivity, based on simple changes to the reaction conditions. For example, we have developed tunable, chemoselective nitrene transfer protocols where the Ag:ligand ratio determines the selectivity between aziridination and C–H insertion in homoallylic and homoallenic carbamates (Scheme 3.1, top).² Additionally, site-selective C–H insertion of Ag-supported nitrenes derived from sulfamates have been developed where the selectivity is dictated and tuned by the identity of the ligand (Scheme 3.1, middle).³

In the context of transition metal-catalyzed nitrene transfer, general experimental protocols typically involve the use of anhydrous organic solvents, including isopropyl acetate, dichloromethane, chloroform or acetonitrile. Water has long been thought to be detrimental to nitrene transfer reactions, as there is potential to limit the formation of a critical imidoiodinane intermediate **A** (Scheme 3.1, bottom), change the catalyst geometry by serving as a ligand for the metal, promote catalyst death, or destroy the electrophilic metal nitrene **B**. For these reasons, molecular sieves or other desiccants are typically used; however, the impact of water on nitrene transfer has never been explicitly studied. Since Breslow's example of a successful Diels-Alder reaction in water, there have been efforts directed towards identifying other useful organic reactions that take place in water or 'on water'.⁴ In some cases, these reactions employ more environmentally benign conditions and display increased reactivity and/or selectivity.^{5,6} In light of these developments, we were curious whether our Ag-catalyzed nitrene transfer reactions might tolerate the presence of water and enable the utilization of highly polar substrates, eliminate the use of chlorinated solvents, decrease the current high loadings of PhIO oxidant and perhaps lead

to improved chemo- and site-selectivities. In this chapter, our investigations into how various metal-catalyzed C-H aminations are affected by the inclusion of water is described.

Scheme 3.1. Ag-catalyzed nitrene transfer.



3.2 Reaction Optimization

Initial experiments focused on tunable chemoselectivity using carbamates as the nitrene precursors (Table 3.1). In our previous work, a 1:1.25 ratio of AgOTf to 1,10-phenanthroline (phen) as the ligand furnished selective aziridination to **3.2** (entry 1), whereas employing a 1:3 ratio of AgOTf:phen resulted in the selective formation of the C–H insertion product **3.3** (entry 2) from **3.1**.² As expected, the exclusion of molecular sieves resulted in little product formation and recovery of the majority of the starting material **3.1** (entries 3-4). Although only minimal conversion was seen, it was interesting to note that the selectivity was similar to reactions run with molecular sieves. This observation suggests that water does not occupy a coordination site on the silver catalyst and has little effect on the coordination geometry of the purported silver nitrene. Rather, the difficulty of oxidizing carbamates to the key iminoiodinane intermediate **A** (Scheme 3.1, bottom) likely gives rise to an equilibrium that favors the starting materials over **A** when water

is not sequestered. The sensitivity of carbamate-derived iminoiodinanes to water prompted us to examine other nitrene precursors.

Table 3.1. Effect of water on carbamate nitrene transfer reagents.

entry	catalyst ^{a,b}	dessiccant	A : I	3.2	3.3	total yield ^c
1	1:1.25 AgOTf:phen	4 Å MS	15.7 : 1	67%	4%	71%
2	1:3 AgOTf:phen	4 Å MS	0 : 100	0%	93%	93%
3	1:1.25 AgOTf:phen	none	4.2 : 1	21%	5%	26% (70%)
4	1:3 AgOTf:phen	none	0 : 100	0%	3%	3% (93%)

^a Aziridination: 20 mol % AgOTf, 25 mol % phen, 2 equiv PhIO, CH₂Cl₂.
^b C-H insertion: 10 mol % AgOTf, 30 mol % phen, 3.5 equiv PhIO, CH₂Cl₂.
^c Recovered starting material **3.1** in parentheses.

Next, we investigated the effect of water on **3.4**, a sulfamate-derived nitrene precursor, where C–H insertion can occur at either a benzylic or tertiary alkyl C–H site (Table 3.2); Pérez has reported a single example of Cu-catalyzed styrene aziridination using PhI=NTs in water.⁷ Our previous work showed that a tris(2-pyridyl-methyl)amine (tpa) ligand favors benzylic insertion to furnish **3.4a** over **3.4b** (entry 1).^{1j,3} Interestingly, when the desiccant was excluded, there was essentially no impact on yield or selectivity (entry 2). This observation was encouraging, as it suggested that water is not as detrimental to C–H amination as had previously been thought. Even with the addition of water (entry 3), the reaction still proceeded smoothly with no change in the **3.4a:3.4b** ratio, indicating the geometry of the silver catalyst is likely not changing in the presence of water. When the nitrene transfer reaction of **3.4** was run in water as the solvent, full conversion to products **3.4a** and **3.4b** was noted, albeit in slightly lower yield compared to dichloromethane (entry 4), presumably due to the lower solubility of **3.4** in water. Heating the reaction to 40 °C increased the yield of **3.4a-3.4b** to 73%, with the remainder of the mass balance made up of starting material (entry 5). Heating the reaction also has the advantage of dissolving the polymeric PhIO oxidant, which is insoluble in dichloromethane; this enables a simpler workup procedure that does

not require a filtration step. Instead, extraction with either diethyl ether or ethyl acetate can be utilized, a greener alternative to the standard dichloromethane solvent. A control reaction in Et₂O resulted only in recovered **3.4**, indicating that the chemistry is happening in the aqueous medium and not during the extraction process. Heating these reactions resulted in an essentially biphasic mixture, suggesting the possibility that the chemistry may be happening 'on-water'.⁸ Organic reactions occurring at the organic-liquid water interface have the same economic and environmental benefits as those happening in solution, but on-water reactions allow for the use of substrates that are not soluble in aqueous systems. Overall, these results indicate that water does not hinder reactivity in Ag-catalyzed C-H bond amination reactions using sulfamates as the nitrogen source. This surprising result stimulated our curiosity as to whether other reported transition metal catalysts exhibit similar activity in water.

Table 3.2. Water tolerance of sulfamate nitrene transfer reagents.

entry	solvent ^a	desiccant	3.4a : 3.4b	total yield ^b
1	CH ₂ Cl ₂	4 Å MS	2.4 : 1	84% ^c
2	CH ₂ Cl ₂	none	3 : 1	100%
3 ^d	CH ₂ Cl ₂ + H ₂ O	none	2.9 : 1	94%
4	H ₂ O	none	2.7 : 1	66%
5 ^e	H ₂ O	none	2.9 : 1	73%

^a In CH₂Cl₂: 10 mol % AgOTf, 12.5 mol % tpa, 3.5 equiv PhIO, rt, 30 min.

^b NMR yields using a mesitylene internal standard. ^c Isolated yield. ^d 50 μL H₂O added. ^e Heated to 40 °C.

Table 3.3 describes results using **3.4** in the presence of a variety of other reported transition metal catalyst systems.^{1,9-12} Dinuclear Rh catalysts, including the popular Rh₂esp₂ (esp = α,α,α',α'-tetramethyl-1,3-benzenedipropanoate), all favored tertiary C(sp³)-H insertion to furnish **3.4b** (entries 1-3), mimicking the selectivity and activity observed in organic solvents.⁹ The preference for **3.4b** increased as the size of the carboxylate bridging ligand increased from OAc to esp to TPA

(triphenylacetate). Catalysts based on Ru, Fe, and Mn (entries 4-6) gave no product formation (entries 4-6).¹⁰⁻¹² Additional Ag(I) catalysts developed in our group, including (*t*BuBipy)₂AgOTf, [(Py₅Me₂)AgOTf]₂, and [α -Me-(*anti*)-Py₃PipAg]OTf were subjected to the same reaction conditions as (tpa)AgOTf (entries 7-9).¹³⁻¹⁶ (*t*BuBipy)₂AgOTf in water resulted in lower mass balance than reactions run in dichloromethane, perhaps due to the increased fluxionality of this complex, as compared to other Ag catalysts; the site-selectivity slightly favored **3.4b** (entry 7). Both [(Py₅Me₂)AgOTf]₂ and [α -Me-(*anti*)-Py₃PipAg]OTf delivered results similar to those observed for (tpa)AgOTf. These results show that by utilizing complementary Rh and Ag catalysts, tunable site-selective C-H amination can be achieved using water as the reaction medium.

Table 3.3. Catalyst activity in aqueous solvent.

entry	catalyst ^{a-c}	3.4a : 3.4b	total yield ^d
1	Rh ₂ esp ₂	1 : 6.5	90%
2	Rh ₂ (TPA) ₄	1 : 25	79%
3	Rh ₂ (OAc) ₄	1 : 1.5	60% (20%)
4	[Ru ₂ (hp) ₄ Cl]	---	0% (66%)
5	[FePc]Cl + AgSbF ₆	---	0% (70%)
6	[Mn(<i>t</i> BuPc)]Cl + AgSbF ₆	---	0% (54%)
7	(<i>t</i> Bubipy) ₂ AgOTf	1 : 1.8	45%
8	[(Py ₅ Me ₂)AgOTf] ₂	3.1 : 1	70%
9	[α -Me-(<i>anti</i>)-Py ₃ PipAg]OTf	2.6 : 1	83%

^a 10 mol % AgOTf, 12.5 mol % ligand, 3.5 equiv PhIO, H₂O. ^b 2 mol % Rh cat., 2 equiv PhIO, H₂O. ^c See the SI for conditions for entries 4-6. ^d NMR yields based on mesitylene as internal standard, recovered starting material **3.4** in parentheses.

***t*Bubipy**

Py₅Me₂

***anti*- α -Me-Py₃Pip**

Following initial catalyst screening, further optimization was carried out to determine if water enabled the use of less solvent, less oxidant and lower catalyst loadings, as compared to standard conditions (Table 3.4). The oxidant could be lowered to 2 equiv from the standard 3.5 equiv, but cutting the PhIO to 1 equiv resulted in incomplete conversion, even with longer reaction times

(entries 1-3). The stronger PhIO oxidant (entry 4) gave superior results to both PhI(OAc)₂ and PhI(OPiv)₂ (entries 5-6). Solvent concentration did not have a significant effect on selectivity or reactivity (compare entry 2 vs. 4, 7-8). However, the substitution of water for dichloromethane did allow reactions to be run at higher concentrations (0.4 M vs. 0.05 M). For ease of reaction setup, a 0.2 M concentration was preferred for studies of catalyst loading (entries 9-11). When the amount of (tpa)AgOTf was decreased to 5 mol % (entry 9), incomplete conversion was observed in the standard 30 min reaction time. This was easily corrected by running the reaction overnight (entry 8), enabling the catalyst loading to be further decreased to 2 mol % (entry 11), provided isolated (tpa)AgOTf is utilized to ensure the proper Ag:ligand stoichiometry. Furthermore, Ag-nitrene catalysis tolerated a variety of electrolytes in buffered solutions at a range of acidic and basic pH values (entries 12-14).

Table 3.4. Reaction optimization.

entry	equiv PhIO	conc.	mol % cat. ^a	3.4a : 3.4b	total yield ^b
1	3.5	0.05 M	10%	2.7 : 1	73%
2	2	0.05 M	10%	2.8 : 1	83%
3	1	0.05 M	10%	2.8 : 1	62% (20%)
4	2	0.1 M	10%	2.9 : 1	80%
5	2 PhI(OAc) ₂	0.1 M	10%	2.9 : 1	54%
6	2 PhI(OPiv) ₂	0.1 M	10%	2.7 : 1	51%
7	2	0.2 M	10%	3.4 : 1	82%
8	2	0.4 M	10%	3.2 : 1	80%
9	2	0.2 M	5%	2.6 : 1	65% (8%)
10 ^c	2	0.2 M	5%	3.0 : 1	80%
11 ^c	2	0.2 M	2%	3.0 : 1	79%
12 ^d	2	0.1 M	10%	2.9 : 1	52%
13 ^e	2	0.1 M	10%	2.7 : 1	77%
14 ^f	2	0.1 M	10%	3.2 : 1	75%

^a Standard conditions: 10 mol % AgOTf, 12.5 mol % tpa, 3.5 equiv PhIO, 0.05 M H₂O, 40°C, 30 min. ^b NMR yields based on mesitylene as internal standard, recovered **3.4** in parentheses. ^c The reaction was run overnight.

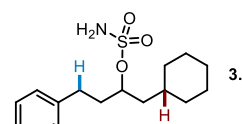
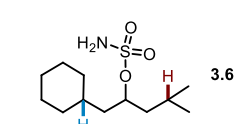
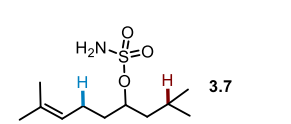
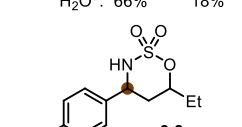
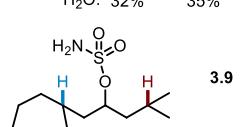
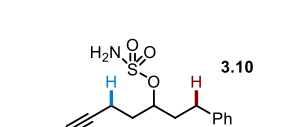
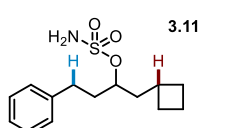
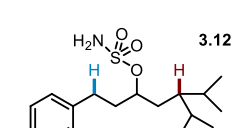
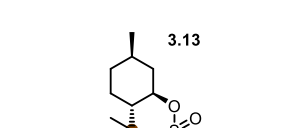
^d pH 2.8 Na₂HPO₄:citric acid hydrate buffer. ^e pH 5.0 NaOAc:HOAc buffer.

^f pH 9.5 Na₂CO₃:NaHCO₃ buffer.

3.3. Scope of C-H Amination Reactions in Water Compared to Halogenated Solvents

With optimized conditions in hand, other sulfamates were briefly investigated and the site-selectivity of the C-H amination compared to previous results in dichloromethane (Table 3.5). Another substrate **3.5**, displaying both benzylic C-H and tertiary C-H insertion sites, behaved similarly using (tpa)AgOTf in water as compared to dichloromethane, favoring benzylic insertion to **3.5a**. The nonpolar substrate **3.6**, featuring two very similar tertiary C-H bonds, resulted in minimal selectivity to favor insertion at the isopropyl C-H bond **3.6b**. The preferred insertion into the allylic C-H bond of **3.7** in water matched the previous results in dichloromethane; **3.8-3.13** were similarly well-behaved. Overall, these results indicate that although there is a slight sensitivity of (tpa)AgOTf to water, overall, the reactions are surprisingly similar to those carried out in organic solvents.

Table 3.5. Examples of intramolecular amination in water.

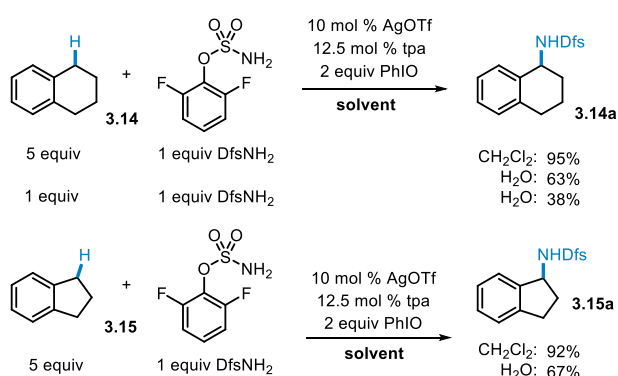
 <p>3.5</p> <p>CH₂Cl₂: 73% 3.5a 20% 3.5b H₂O^a: 66% 18%</p>	 <p>3.6</p> <p>CH₂Cl₂: 36% 3.6a 50% 3.6b H₂O: 32% 35%</p>	 <p>3.7</p> <p>CH₂Cl₂: 74% 3.7a 8% 3.7b H₂O: 58% 10%</p>
 <p>3.8</p> <p>H₂O: 62%</p>	 <p>3.9</p> <p>CH₂Cl₂: 69% 3.9a 29% 3.9b H₂O: 62% 31%</p>	 <p>3.10</p> <p>CHCl₃: 41%^a 3.10a 27% 3.10b H₂O: 36%^b 25%</p>
 <p>3.11</p> <p>CH₂Cl₂: 64% 3.11a 21% 3.11b H₂O: 51% 14%</p>	 <p>3.12</p> <p>CH₂Cl₂: 63% 3.12a 0% 3.12b H₂O: 72% 8%</p>	 <p>3.13</p> <p>H₂O: 87%</p>

Conditions: 10 mol % AgOTf, 12.5 mol % tpa, 2 equiv PhIO, 0.1 M H₂O, 40 °C. ^a*dr* = 6.5:1 *syn:anti* ^b*dr* = 7.0:1 *syn:anti*

Intermolecular nitrene transfer presents a greater challenge as compared to intramolecular reactions. However, water proved to be an effective solvent for the intermolecular amination of

1,2,3,4-tetrahydronaphthalene **3.14** and indane **3.15** using the sulfamate nitrene precursor DfsNH₂. The C–H insertion products **3.14a**–**3.15a** were furnished in moderate yields (Scheme 3.2). While an excess of the substrate **3.14** resulted in improved yields, product **3.14a** was still noted using only an equimolar amount of **3.14** and DfsNH₂. While modest, these results nonetheless showcase the first examples of intermolecular, silver-catalyzed C–H insertion in water.

Scheme 3.2. Intermolecular C-H amination in water



3.4. Concluding Remarks

An exploration of the effect of water on metal-catalyzed nitrene transfer showed that the long-held perception that this chemistry is sensitive to water is not always true. Both Ag and Rh catalysts give high yields of amine products, provided sulfamates are used as the nitrogen source. A decrease in the required amount of solvent, oxidant, and catalyst was tolerated with Ag catalysts; these conditions were general for sulfamate precursors. While the chemistry in water mimics intramolecular reactions in organic solvents more closely, intermolecular nitrene transfer was also reported for the first time. This study paves the way for applications of transition metal-catalyzed nitrene transfer reactions to highly polar biomolecules¹⁷ and the development of strategies that utilize simple changes in aqueous pH to tune the site-selectivity of C-H amination events.

3.4. References

1. For selected reviews on metal-catalyzed nitrene transfer reactions, see: (a) Dauban, P.; Dodd, R. H. *Synlett*. **2003**, *11*, 1571. (b) Díaz-Requejo, M. M.; Pérez, P. J. *Chem. Rev.* **2008**, *108*, 3379. (c) Collet, F.; Dodd, R. H.; Dauban, P. *Chem. Commun.* **2009**, *34*, 5061. (d) Zalatan, D. N.; Du Bois, J. *Top. Curr. Chem.* **2010**, *292*, 347. (e) Davies, H. M. L.; Du Bois, J.; Yu, J. Q. *Chem. Soc. Rev.* **2011**, *40*, 1855. (f) Collet, F.; Lescot, C.; Dauban, P. *Chem. Soc. Rev.* **2011**, *40*, 1926. (g) Dequierez, G.; Pons, V.; Dauban, P. *Angew. Chem. Int. Ed.* **2012**, *51*, 7384. (h) Che, C. -M.; Lo, V. K. -Y.; Zhou, C. -Y. *Comprehensive Organic Synthesis II*, 2nd ed. (Ed.:P. Knochel), Elsevier, Amsterdam, **2014**, 26–85. (i) Darses, B.; Rodrigues, R.; Neuville, L.; Mazurais, M.; Dauban, P. *Chem. Commun.* **2017**, *53*, 493, and references therein. (j) Alderson, J.M.; Corbin, J.R.; Schomaker, J.M. *Acc. Chem. Res.* **2017**, *50*, 2147-2158.
2. Rigoli, J.W.; Weatherly, C.D.; Alderson, J.; Vo, B.T.; Schomaker, J.M. *J. Am. Chem. Soc.* **2013**, *135*, 17238-41.
3. Scamp, R.; Alderson, J.M.; Phelps, A.M.; Dolan, N.S.; Schomaker, J.M. *J. Am. Chem. Soc.* **2014**, *136*, 16720-23.
4. (a) Breslow, R. *Acc. Chem. Res.* **1991**, *24*, 159. (b) Breslow, R. *Acc. Chem. Res.* **2004**, *37*, 471.
5. For selected references, see: (a) Genin, E.; Michelet, V. in Green Process Engineering Poux, M.; Cognet, P.; Gourdon, C. Ed.; **2015**, 292-324. (b) Kobayashi, S. *Science of Synthesis* **2012**, 855-867. (c) Li, C.-J. *Chem. Rev.* **1993**, *93*, 2023. (d) Genet, J. P.; Savignac, M. *J. Organomet. Chem.* **1999**, *576*, 305. (e) Lindström, U. M. *Chem. Rev.* **2002**, *102*, 2751. (f) Kobayashi, S.; Manabe, K. *Acc. Chem. Res.* **2002**, *35*, 209. (g) Li, C.-J. *Chem. Rev.* **2005**, *105*, 3095. (h) Li, C.-J.; Chen, L. *Chem. Soc. Rev.* **2006**, *35*, 68. (i)

- Raj, M.; Singh, V. K. *Chem. Commun.* **2009**, 6687. (j) Simon, M.-O.; Li, C.-J. *Chem. Soc. Rev.* **2012**, *41*, 1415. (k) Butler, R. N.; Coyne, A. G. *Chem. Rev.* **2010**, *110*, 6302.
6. (a) Pirrung, M. C. *Chem.–Eur. J.* **2006**, *12*, 1312. (b) Otto, S.; Engberts, J. B. F. N. *Org. Biomol. Chem.* **2003**, *1*, 2809. (c) Aplander, K.; Ding, R.; Lindström, U. M.; Wennerberg, J.; Schultz, S. *Angew. Chem. Int. Ed.* **2007**, *46*, 4543. (d) Simon, M.-O.; Li, C.-J. *Chem. Soc. Rev.* **2012**, *41*, 1415. (e) Liu, P. N.; Deng, J. G.; Tu, Y. Q.; Wang, S. H. *Chem. Commun.* **2004**, 2070. (f) Liu, P.-N.; Gu, P.-M.; Deng, J.-G.; Tu, Y.-Q.; Ma, Y.-P. *Eur. J. Org. Chem.* **2005**, 3221. (g) Anastas, P.; Eghbali, N. *Chem. Soc. Rev.* **2010**, *39*, 301, and references therein.
7. Álvarez, M.; Gava, R.; Rodríguez, M. R.; Rull, S. G.; Pérez, P. J. *ACS Catal.* **2017**, *7*, 3707.
8. (a) Narayan, S.; Muldoon, J.; Finn, M. G.; Fokin, V. V.; Kolb, H. C.; Sharpless, K. B. *Angew. Chem. Int. Ed.* **2005**, *44*, 3275. (b) Butler, R. N.; Coyne, A. G. *Org. Biomol. Chem.*, **2016**, *14*, 9945, and references therein. (c) Hayashi, Y.; *Angew. Chem. Int. Ed.* **2006**, *45*, 8013-04.
9. Fiori, K. W.; Espino, C. G.; Brodsky, B. H.; Du Bois, J. *Tetrahedron* **2009**, *65*, 3042.
10. Harvey, M. E.; Musaev, D. G.; Du Bois, J. *J. Am. Chem. Soc.* **2011**, *133*, 17207.
11. Paradine, S. M.; White, M. C. *J. Am. Chem. Soc.* **2012**, *134*, 2036
12. Paradine, S. M.; Griffin, J. R.; Zhao, J.; Petronico, A. L.; Miller, S. M.; White, M. C. *Nature Chem.* **2015**, *7*, 987.
13. Scamp, R. J.; Jirak, J. G.; Dolan, N. S.; Guzei, I. A.; Schomaker, J. M. *Org. Lett.* **2016**, *18*, 3014.
14. Huang, M.; Corbin, J. R.; Dolan, N. S.; Fry, C. G.; Vinokur, A. I.; Guzei, I. A.; Schomaker, J. M. *Inorg. Chem.* **2017**, *56*, 6725–6733.

15. Dolan, N. S.; Scamp, R. J.; Yang, T.; Berry, J. F.; Schomaker, J. M. *J. Am. Chem. Soc.* **2016**, *138*, 14658.
16. Huang, M.; Yang, T.; Paretsky, J.; Berry, J.F.; Schomaker, J.M. *J. Am. Chem. Soc.* **2017**, *139*, 17376-17386.
17. Li, J.; Cisar, J.S.; Zhou, C.-Y.; Vera, B.; Williams, H.; Rodríguez, A.B.; Cravatt, B.F.; Romo, D. *Nature Chem.* **2013**, *5*, 510-517.
18. Alderson, J. M.; Schomaker, J. M. *Chem. Eur. J.* **2017**, *23*, 8571-8576.
19. Corbin, J. R.; Schomaker, J. M. *Chem. Commun.* **2017**, *53*, 4346-4349.

3.6. Experimental Details and Characterization

3.6.1. Synthesis of homoallylic carbamates.

The homoallylic alcohol (between 0.5 g and 3.0 g, 1 equiv) was dissolved in dichloromethane (0.3 M) and placed in an ice bath. Trichloroacetylisocyanate (1.2 equiv) was slowly added dropwise. The reaction was stirred with cooling in the ice bath until TLC indicated complete consumption of the starting material. The solvent was then removed and the crude reaction was dissolved in methanol (0.4 M). Potassium carbonate (0.5 equiv) was then added to the reaction and the mixture stirred at room temperature until TLC indicated complete consumption of the starting material. Water was added to the reaction and the mixture was extracted with three portions of dichloromethane. The organic phase was dried with sodium sulfate and concentrated under reduced pressure. The crude products were purified by silica gel column chromatography. Characterization data for carbamate **1** matched previous characterization.²

3.6.2. Synthesis of homoallylic sulfamates.

Formic acid (0.49 mL, 13 mmol, 2.5 equiv) was added dropwise to chlorosulfonyl isocyanate (3.0 equiv) in an ice bath with vigorous stirring. Gas was evolved and the reaction mixture

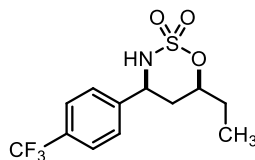
solidified within 5 min. To the solid was added 10.4 mL of CH₃CN and the resulting clear solution was stirred in an ice bath for 30 minutes and allowed to warm to room temperature and stir at room temperature for four hours. The flask was placed in an ice bath and to the cold solution was added 5.2 mmol alcohol substrate in 8.7 mL of dimethylacetamide. The solution was warmed to room temperature and the mixture was stirred for 1 h. The reaction was quenched with the addition of 10 mL of H₂O. The aqueous layer was extracted with 3 x 50 mL of Et₂O. The combined organic layers were washed with 5 x 20 mL H₂O, 1 x 25 mL saturated aqueous sodium chloride, dried over MgSO₄, filtered and concentrated under reduced pressure. The crude products were purified by silica gel column chromatography using a hexane/EtOAc gradient. Characterization data for compounds matched previous characterization.^{3,16,1819}

3.6.3. Synthesis of C-H insertion products.

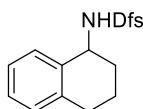
General procedure for Ag-catalyzed nitrene insertion in water.

A reaction flask was charged with silver triflate (5.1 mg, 0.02 mmol, 0.1 equiv) and tpa ligand (7.3 mg, 0.025 mmol, 0.125 equiv). Water (0.5 mL) was added and the mixture was stirred vigorously for 30 minutes. Then, the substrate (0.2 mmol, 1 equiv) was added along with additional water (0.5 mL). Iodosobenzene (88 mg, 0.4 mmol, 2 equiv) was added in one portion and the reaction mixture was heated to 40 °C in an oil bath and stirred for 30 min (or overnight for lower catalyst loadings). Upon completion and cooling to room temperature, the reaction mixture was transferred to a separatory funnel, and the reaction flask was rinsed with water and Et₂O. The aqueous layer was extracted three times with Et₂O and the combined organic layers were dried over Na₂SO₄ before being concentrated under reduced pressure. The crude products were analyzed by ¹H NMR and yields were based off mesitylene (10 µL) as an internal standard. For characterization, crude products were purified by silica gel column chromatography using an

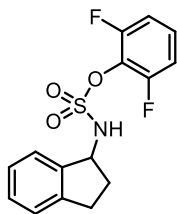
EtOAc/hexanes gradient. Characterization data for all products matched previously published data.^{2,3,12,16,19}



Compound 3.8. The product was purified by column chromatography using a 0 → 40% gradient of EtOAc in hexanes with 10% increments. The product was obtained as a white solid. **¹H NMR** (500 MHz, Chloroform-*d*) δ 7.67 (d, *J* = 8.1 Hz, 2H), 7.49 (d, *J* = 8.1 Hz, 2H), 4.90 – 4.79 (m, 2H), 4.41 (d, *J* = 9.4 Hz, 1H), 2.10 (dt, *J* = 14.2, 2.5 Hz, 1H), 1.95 – 1.72 (m, 3H), 1.05 (t, *J* = 7.5 Hz, 3H). **¹³C NMR** (126 MHz, CDCl₃) δ 142.0 (q, *J* = 1.4 Hz), 131.2 (q, *J* = 32.8 Hz), 127.0, 126.3 (q, *J* = 3.7 Hz), 123.9 (q, *J* = 272.3 Hz), 85.7, 58.0, 35.8, 28.5, 9.2. **HRMS** (ESI) *m/z* calculated for C₁₂H₁₄F₃NO₃ S [M-H][−] 308.0574, found 308.0573.



Compound 3.14a. The product was purified by column chromatography using a 0 → 30% gradient of EtOAc in hexanes with 6% increments. The product was obtained as a white solid. **¹H NMR** (500 MHz, Chloroform-*d*) δ 7.58 – 7.47 (m, 1H), 7.25 – 7.17 (m, 3H), 7.14 – 7.08 (m, 1H), 7.06 – 6.97 (m, 2H), 5.04 – 4.83 (m, 2H), 2.85 (dt, *J* = 17.0, 5.8 Hz, 1H), 2.76 (ddd, *J* = 17.0, 8.2, 5.9 Hz, 1H), 2.23 – 2.11 (m, 2H), 1.99 – 1.81 (m, 2H). **¹³C NMR** (126 MHz, CDCl₃) δ 156.2 (dd, *J* = 253.1, 3.5 Hz), 137.9, 134.6, 129.5, 129.4, 128.3, 127.6 (t, *J* = 15.6 Hz), 127.4 (t, *J* = 9.2 Hz), 126.7, 112.7 (dd, *J* = 18.3, 4.3 Hz), 54.0, 30.4, 29.1, 19.2. **HRMS** (ESI) *m/z* calculated for C₁₆H₁₄F₂NO₃ S [M-H][−] 338.0668, found 338.0671.



Compound 3.15a. The product was purified by a SiO₂ column using a 0 → 40% gradient of EtOAc in hexanes with 10% increments. The product was obtained as a white solid. **¹H NMR** (500 MHz, Chloroform-*d*) δ 7.49 (d, *J* = 6.7 Hz, 1H), 7.32 – 7.19 (m, 4H), 7.02 (dd, *J* = 8.6, 7.6 Hz, 2H), 5.22 (q, *J* = 7.4 Hz, 1H), 4.97 (d, *J* = 8.4 Hz, 1H), 3.05 (ddd, *J* = 16.1, 8.7, 4.4 Hz, 1H), 2.89 (dt, *J* = 15.9, 7.8 Hz, 1H), 2.73 – 2.66 (m, 1H), 2.15 (ddt, *J* = 13.7, 8.5, 7.0, 1H). **¹³C NMR** (126 MHz, CDCl₃) δ 156.2 (dd, *J* = 253.3, 3.5 Hz), 143.4, 141.1, 129.0, 127.5 (t, *J* = 9.0 Hz), 127.2, 125.1, 124.6, 112.7 (dd, *J* = 18.2, 4.2 Hz), 60.7, 34.3, 30.1. **HRMS** (ESI) *m/z* calculated for C₁₅H₁₃F₂NO₃S [M-H][−] 324.0511, found 324.0512.

Chapter 4:

Amine-Substituted Allyl Cations: Brief Overview and Uses in 4π -Electrocyclizations

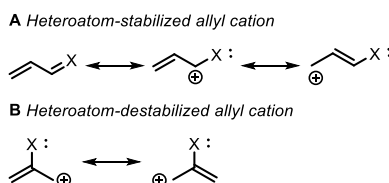
Chapter 4

Amine-Substituted Allyl Cations: Brief Overview and Use in 4 π -Electrocyclizations

4.1 Introduction

Allyl cations are useful intermediates in the synthesis of organic compounds due to the increased stabilization of the electron-deficient cation afforded by delocalization of π electrons. Methods for generating heteroatom-substituted allyl cations are desirable for their potential in synthesizing functionalized carbocyclic frameworks; the positioning and identity of the heteroatom substituent impacts the stability and reactivity of the cationic intermediate (Figure 4.1). Most frequently, heteroatom-substituted allyl cations are employed as dienophilic three carbon units in [4+3]-cycloaddition reactions for the direct synthesis of seven-membered carbocycles while pentadienyl cations are primed for stereospecific 4 π -electrocyclization reactions in the synthesis of five-membered rings. A brief introduction to [4+3]-cycloaddition reactions will be discussed with an emphasis on methods that generate *N*-substituted allyl cations before providing a brief overview of 4 π -electrocyclization reactions with a particular emphasis on methods that contain C–N bonds in the final cyclopentanes.

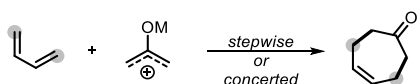
Figure 4.1. Heteroatom positioning impacts allyl cation stability *via* lone-pair conjugation.



4.2. [4+3]-Cycloaddition Reactions of Allyl Cations

The [4+3]-cycloaddition reaction is one of the relatively few methods available for stereoselectively forming cycloheptanes efficiently.¹ The most common heteroatom-substituted three-carbon π -system used in [4+3]-cycloaddition reactions are oxyallyl cations, while a diene acts as the four-carbon unit (Scheme 4.1A). This is due to the relatively mild generation of oxyallyl cations, such as exposing easily obtained α,α' -dihaloketones to a mild base, reductant, or photolysis to access these reactive intermediates.² Reactions typically work best with cyclic and electron-rich dienes.

Scheme 4.1. Generic [4+3]-cycloaddition between an oxyallyl cation and butadiene and oxyallyl cation generation.



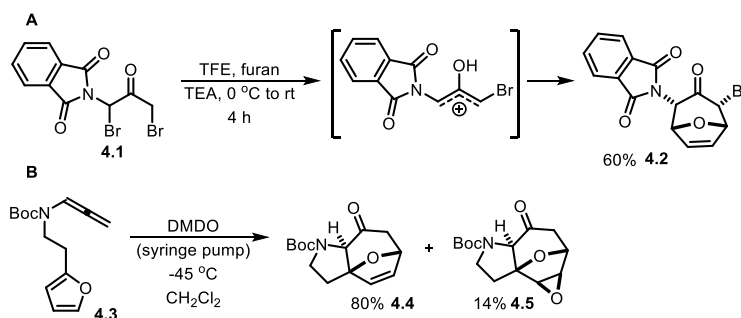
4.2.1. [4+3]-Cycloaddition of 1-Amidoallyl Cations

In contrast to the multitude of methods to access and utilize oxyallyl cations in [4+3]-cycloaddition reactions, there is a small number of useful methods for generating *N*-substituted allyl cations. The nitrogen atom is more often retained after reactions involving 1-amidoallyl cations compared to 2-amidoallyl cations (Figure 4.1A vs 4.1B), and reactions work best with an *O*-atom at C-2.

The most successful strategy of accessing 1-amidoallyl cation involves accessing a 2-oxyallyl cation with an amino-substituent at C-1. For example, Walters demonstrated that the 1,3-dibromoketone **4.1** could be treated with TFE/TEA in the presence of furan to give **4.2** (Scheme 4.2A).³ Hsung further expanded this sort of chemistry by treating allenamides with tethered furans

of the form **4.3** with DMDO to give **4.4** by allene oxidation (Scheme 4.2B). Trace overoxidation to **4.5** was observed in this case.⁴ These *N*-stabilized 2-oxyallyl cation intermediates have been used for diastereoselective reactions with a chiral auxiliary on nitrogen.^{5a-b}

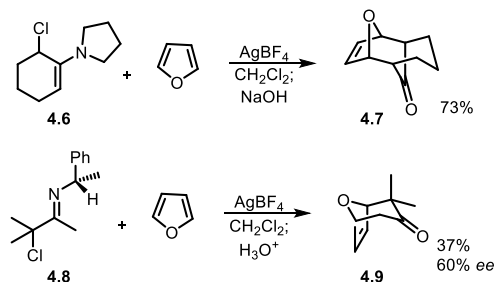
Scheme 4.2. Generation and utility of 1-amido-2-oxyallyl cation intermediates.



4.2.2. [4+3]-Cycloaddition of 2-Amidoallyl Cations

Typically, if the *N*-group is positioned at the 2-position of the allyl cation as in Figure 4.1B, the nitrogen is not retained in the product after [4+3]-cycloaddition. One successful way of accessing this intermediate is by ionization of α -chloroenamines or α -chloroimines (Scheme 4.3).

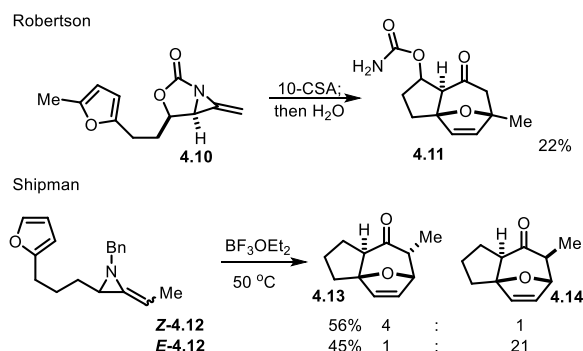
Scheme 4.3. Ag(I)-promoted chloride abstraction to form 2-amidoallyl cation intermediates.



Treatment of either α -chloroenamine **4.6** or α -chloroimine **4.8** gives modest yields of [4+3]-cycloadducts **4.7** and **4.9**. The use of a chiral auxiliary on imine **4.8** afforded modestly diastereoselective cycloaddition; hydrolysis of the resulting iminium provided **4.9** in 60% *ee*.^{6a-e}

The Shipman and Robertson groups showed that strain-promoted ring opening of methyleneaziridines **4.10** and **4.12** is a useful strategy for accessing 2-amidoallyl cations under mild conditions (Scheme 4.4). Intramolecular trapping of the intermediate cations by furan furnished cycloheptenones **4.11** and **4.13-4.14** following imine hydrolysis in modest yields.^{7b-e}

Scheme 4.4. Methyleneaziridines as intermediates towards 2-amidoallyl cations.

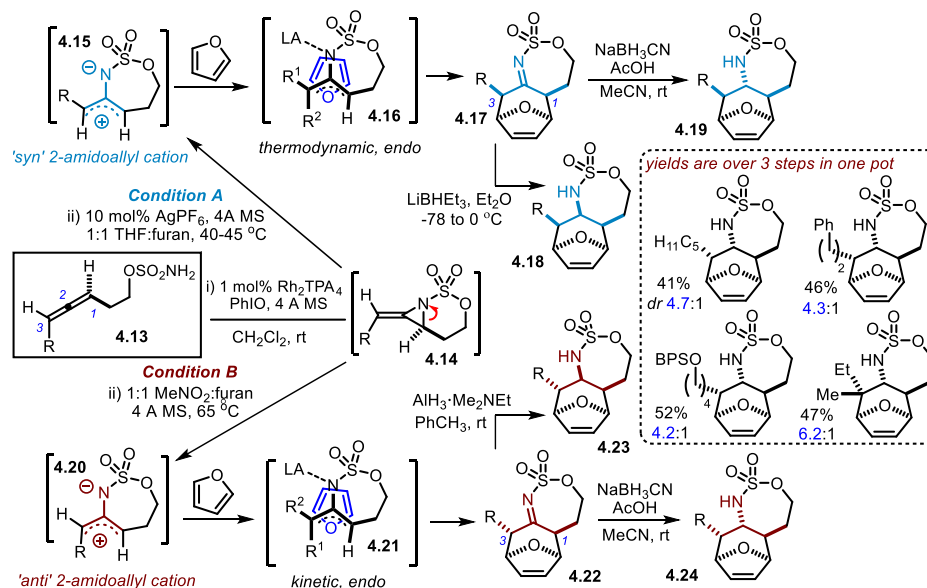


The Schomaker group greatly expanded the utility of this strategy to 2-amidoallyl cations by employing an allene aziridination/[4+3]-cycloaddition sequence that engages methyleneaziridines with furan intermolecularly (Scheme 4.5).^{7a} Treatment of homoallenic sulfamate **4.13** with a hypervalent iodine oxidant in the presence of Rh₂TPA₄ as a nitrene transfer catalyst results in bicyclic methylene aziridine **4.14** with complete (*E*)-selectivity. Treatment of **4.14** with furan and THF as a nucleophilic polar aprotic cosolvent (*Condition A*) results in opening of the aziridine and isomerization of the 2-amidoallyl cation to minimize A^{1,3}-strain to give **4.15**; this thermodynamic amidoallyl cation undergoes [4+3]-cycloaddition with furan via an *endo* transition state **4.16** to give 1,3-*syn* **4.17**. Reagent-controlled reduction can then furnish 1,2-*syn*-2,3-*syn* **4.18** or 1,2-*anti*-2,3-*anti* **4.19**.

Alternatively, if methyleneaziridine **4.14** is treated with furan in the presence of a non-nucleophilic MeNO₂ cosolvent the kinetic amidoallyl cation **4.20** will undergo [4+3]-cycloaddition to yield 1,3-*anti* **4.22** via *endo* transition state **4.21**. Reagent-controlled reduction in this case

furnishes 1,2-*syn*-2,3-*anti* **4.23** or 1,2-*anti*-2,3-*syn* **4.24** allowing for selective access to any *endo* diastereomer of this cycloaddition/reduction sequence.

Scheme 4.5. Allene aziridination/[4+3]-reaction: strategy to obtain complete stereodivergence.

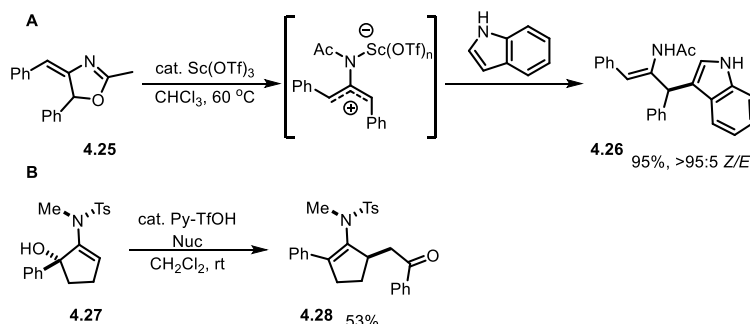


4.3. Other Methods Utilizing Amidoallyl Cations

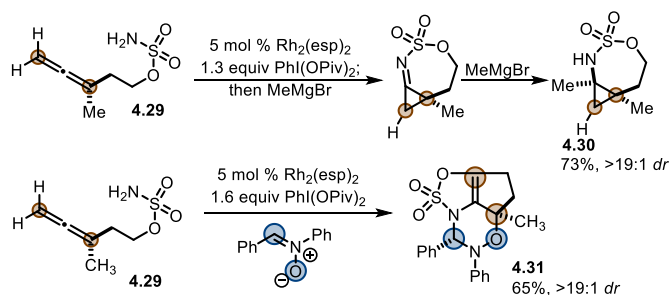
Nucleophilic trapping of 2-amidoallyl cations generated *in situ* is a common mode of reactivity as well. Nitrogen is typically retained in these reaction products so generating 2-amidoallyl cations in this regime could be considered *umpolung* reactivity of the typically nucleophilic α -enamine or α -imine carbon. For example, heterocyclic oxazoline derivatives similar to **4.25** (either *E* or *Z*) decompose to a 2-amidoallyl cation in the presence of a catalytic amount of Lewis acidic Sc(OTf)₃.^{6g} The intermediate 2-amidoallyl cation was then trapped with indole derivatives producing **4.26** with excellent (*Z*)-selectivity regardless of the alkene geometry of the starting material (Scheme 4.6A). Kartika has been developing this chemistry to expand the utility to more convenient starting materials that tolerate a broader range of nucleophiles including alcohols,

enolates, indoles, thiols, and pyrroles (Scheme 4.6B).^{6f} These 2-amidoallyl cations were generated by protonating α -hydroxyenamines.

Scheme 4.6. *Umpolung* reactivity of enamine α -carbons by nucleophilic trapping of 2-amidoallyl cations.



Scheme 4.7. Oxidative allene amination to generated 2-amidoallyl cations from 1,1-disubstituted allenes.



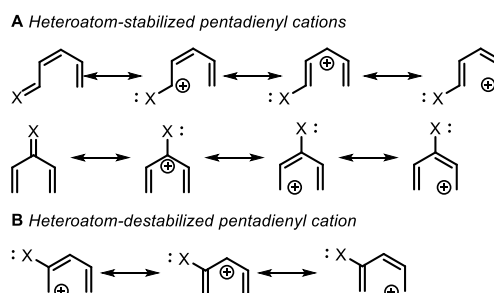
Blakey demonstrated that oxidative nitrene transfer to 1,1-disubstituted allenes generates 2-amidoallyl cations (Scheme 4.7). Oxidative amination of **4.29** yields an iminocyclopropane intermediate that was trapped diastereoselectively with Grignard nucleophiles to yield highly-substituted aminocyclopropanes **4.30** while simultaneously avoiding hydrolysis of the C=N bond.^{8a} Alternatively, oxidative amination of **4.29** in the presence of dipolarophiles, such as benzaldehyde or nitrone, yielded interesting [n+3]-aminoheterocycles **4.31** in high *dr*, in which the nitrogen of the enamine attacked the electrophilic moiety of nitrone instead of carbon.^{8b} While

bicyclic methyleneaziridine intermediates were never observed in these reactions, their intermediacy along the reaction pathway have not been ruled out.

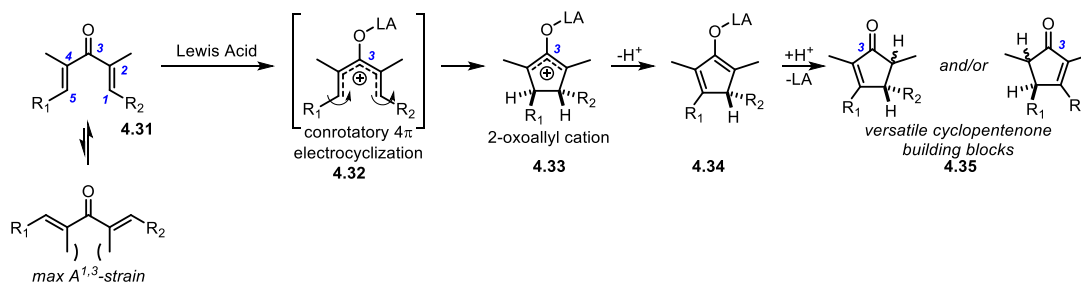
4.4. Brief Introduction to Nazarov Electrocyclization Reactions

Extending the conjugation of allyl cations results in useful pentadienyl cation intermediates for the preparation of stereodefined cyclopentene intermediates through a stereospecific 4π -electrocyclization process. Placing a heteroatom on the pentadienyl cation results in either lone-pair stabilization of this intermediate (Figure 4.2A) or inductive destabilization (Figure 4.2B).

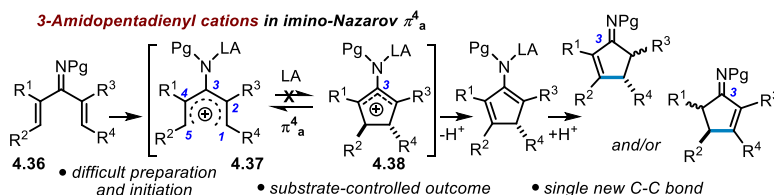
Figure 4.2. Heteroatom placement on pentadienyl cation and resonance effects.



Most commonly, divinyl ketones **4.31** are treated with a harsh Lewis or Brønsted acid resulting in a pentadienyl cation with oxygen substitution at C-3 (Scheme 4.8).⁹ Following a stereospecific conrotatory 4π -electrocyclization of this intermediate **4.32**, a cyclic 2-oxyallyl cation intermediate **4.33** is formed. Substrate-controlled elimination and tautomerization of the resulting enolate **4.34** produces highly-substituted and useful cyclopentenone **4.35**. Unfortunately, elimination from 2-oxyallyl cation is not regioselective and this elimination ablates a stereocenter that was made in a stereocontrolled way. Tautomerization of enolate is not stereospecific, so mixtures of alkene isomers and diastereomers of **4.35** may form if there are no built in substrate biases. Additionally, typical conditions for promoting these reactions are harshly acidic which directly impacts the functional group tolerance of this process.

Scheme 4.8. The classic Nazarov reaction of 3-oxypentadienyl cations.

In contrast to the 3-oxy-Nazarov cyclization, which is well-developed and continues to see creative new solutions to the issues associated with the process outlined above, the analogous 3-imino-Nazarov cyclization of divinyl imines has seen little development (Table 4.1).¹⁰⁻¹¹ In part, this is due to the dearth of methods to generate the divinyl imine starting material **4.36**. Additionally, calculations by Smith and Ulmer suggest 4π -electrocyclization of **4.37** is thermodynamically and kinetically disfavored due to increased *N*-stabilization of 3-amidopentadienyl cation **4.37** vs. 2-amidoallyl cation **4.38**, as suggested in Figure 4.1 B vs Figure 4.2A, and the better lone-pair stabilization afforded by *N*- vs *O*-substitution (Table 4.1).¹⁰ As such, researchers have had to develop creative ways of generating amidopentadienyl cation intermediates to explore electrocycloization of these species.¹¹

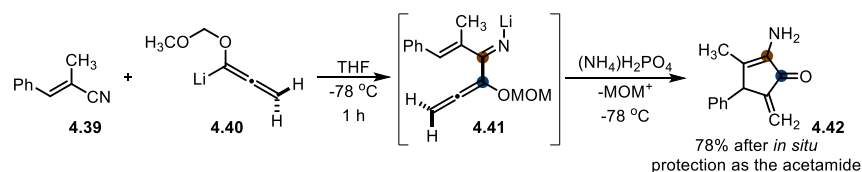
Table 4.1. Thermodynamic and kinetic barriers to 3-amidopentadienyl cation electrocycloization.

	Energy of Activation (kcal/mol)				Energy of Cyclization (kcal/mol)		
	RHF/3-21G(*)	MP2/G-31G**// RHF/3-21G(*)	MP2/6-31G*		RHF/3-21G(*)	MP2/G-31G**// RHF/3-21G(*)	MP2/6-31G*
NH ₂	36.26	22.58	23.29	NH ₂	16.15	6.97	6.80
OH	30.67	15.56	15.94	OH	5.59	-3.19	-3.83

4.4.1 Aza-Nazarov Reactions and Aza-Piancatelli Reactions

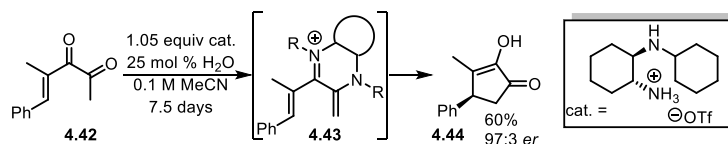
Despite the difficulty of performing 3-amidopentadienyl cation electrocyclization reactions, various workarounds have spurred development in this area, though α,β -unsaturated cyclopentenimines are typically not the product. Tius was the first to report a successful electrocyclization with an *N*-substituent on a 2-oxy-3-amidopentadienyl cation by adding allenyl lithium **4.40** to α,β -unsaturated nitrile **4.39** (Scheme 4.9).^{11e} This reaction is thought to be driven by irreversible loss of the methoxymethyl cation *O*-protecting group and allene strain upon aqueous acidic work-up of **4.41** in $(\text{NH}_4)_2\text{H}_2\text{PO}_4$ yielding amine-substituted cyclopentenone **4.42**.

Scheme 4.9. 2-oxy-3-amidopentadienyl cation electrocyclization.



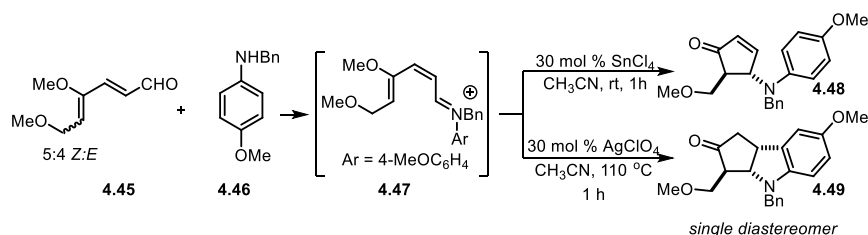
Tius followed up with this work by subjecting diketone **4.42** to an asymmetric diamine promoter (Scheme 4.10). In this work, a 2,3-diaminopentadienyl cation **4.43** undergoes diastereoselective electrocyclization yielding α -hydroxycyclopentenone **4.44** in high *ee* demonstrating a rare example of an asymmetric Nazarov in addition to the ability of this class of pentadienyl cations to undergo efficient electrocyclization.^{11f} Unfortunately, this process is not catalytic in chiral diamine, no C-N bonds remain in the product, and the reaction rate is extremely slow.

Scheme 4.10. Chiral diamine-promoted electrocyclization of diketones.



Liu demonstrated that 1-amino-4-oxypentadienyl cations **4.47** produced from condensation of aniline **4.46** on a *Z:E* mixture of polyunsaturated aldehyde **4.45** in the presence of catalytic Lewis acid results in 4-aminocyclopent-2-en-1-one **4.48** (Scheme 4.11).^{11g} Tautomerization of any *syn*-**4.48** to the more stable *anti*-**4.48** under the harshly acidic conditions is suggested as the cause of diastereoenrichment from **4.45**. Depending on the Lewis acid used, diastereoselective conjugate addition of the electron-rich *N*-aryl substituent could take place in a single operation to provide polycycle **4.49**.

Scheme 4.11. Tandem condensation/electrocyclization of 1-amino-4-oxypentadienyl cations.



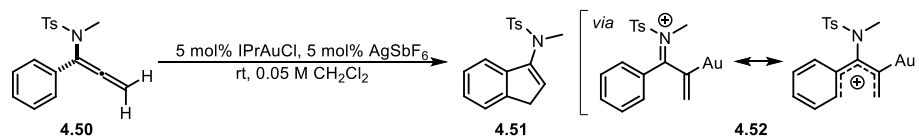
4.4.2 Imino-Nazarov Reactions

Despite the preliminary discoveries that placing multiple heteroatoms on a pentadienyl cation can promote electrocyclization reactions that are tolerant of nitrogen substituents, none of the aza-Nazarov reactions resulted in the synthetically versatile 2-cyclopenten-1-imine products that are analogous to the classic cyclopentenone Nazarov product **4.35** (Scheme 4.8). This is unfortunate as the 3-oxo-Nazarov electrocyclization has been demonstrated to be useful in the synthesis of a wide range of bioactive oxygenated cyclopentane-containing natural products.⁹

To start approaching this issue, Hsung subjected arylallenamide **4.50** to a cationic NHC-supported Au(I) catalyst producing 1-aminoindene **4.51** (Scheme 4.12).^{11b} Electrocyclization of the intermediate 3-amidopentadienyl cation **4.52** is thought to be promoted by the electron-withdrawing sulfonamide protecting group in addition to coordination of the cationic Au(I)-

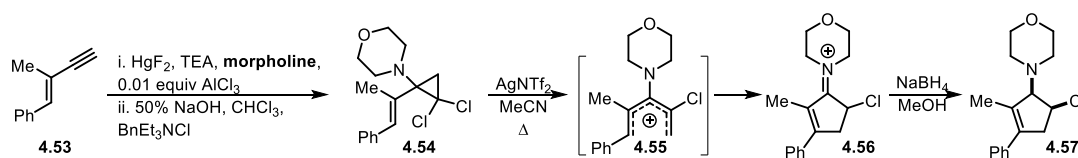
catalyst to the central allene carbon (C-2 of the cation) combatting the increased electron-donating ability of nitrogen at C-3.

Scheme 4.12. Electrocyclization of arylallenamides via Au(I) catalysis



Another interesting approach was reported by West in which simple enyne **4.53** was taken through a two-step aminomercuration-demercuration/dichlorocyclopropanation sequence to form aminodichlorocyclopropane **4.54** (Scheme 4.13).^{11c} When treated with a stoichiometric amount of AgNTf₂, chloride abstraction promoted opening of the cyclopropane to 2-chloro-3-aminopentadienyl cation **4.55** that underwent smooth electrocyclization to furnish a-chloroiminium **4.56**. This cyclization is perhaps promoted by the strain-energy released by the cyclopropane opening and the pentadienyl cation is additionally destabilized by the electronegative chlorine substituent at C-2. *In situ* reduction of **4.56** by NaBH₄ was necessary to prevent hydrolysis to isolate aminocyclopentenes **4.57**.

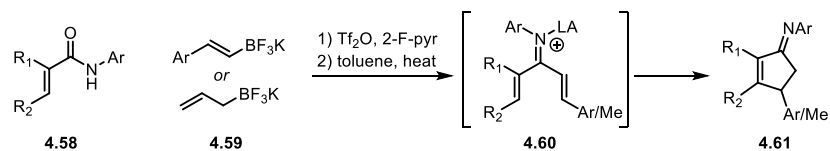
Scheme 4.13. Cyclization of 2-chloro-3-aminopentadienyl cations.



Recently, Huang reported the closest example of a true 3-imino-Nazarov electrocycylation (Scheme 4.14).^{11a} Huang discovered reductive alkenyliminylation of α,β -unsaturated amides **4.58** with potassium organotrifluoroborates **4.59** in the presence of Tf₂O and 2-fluoropyridine was a reliable route to synthesizing divinylimines related to iminium **4.60**. A one-pot procedure was devised by heating the reductive alkenyliminylation crude in toluene to promote electrocyclization

of the divinyl imines *in situ*; isolation of the imine and treatment with a Lewis acid was an alternative procedure if the imine is isolable. Electrocyclization of 3-amidopentadienyl cation **4.60** occasionally was efficient, though the reaction was not general and very limited in scope of both amide substitution patterns and potassium organotrifluoroborates. The reaction would often halt at the divinyl imine. Nevertheless, this was an impressive advance that demonstrated 3-imino-Nazarov electrocyclizations may not be as difficult as previously thought. However, this process suffers from the same drawbacks as the traditional 3-oxy-Nazarov electrocyclization due to the intermediacy of a cyclic 2-amidoallyl cation following controtatory electrocyclic ring closure of **4.55**. Substrate-controlled elimination and tautomerization are operable in this manifold, no examples of substitution at C-5 were reported and improvements to tolerated substitution-patterns are much needed.

Scheme 4.14. 3-imino-Nazarov electrocyclization of divinyl imines.

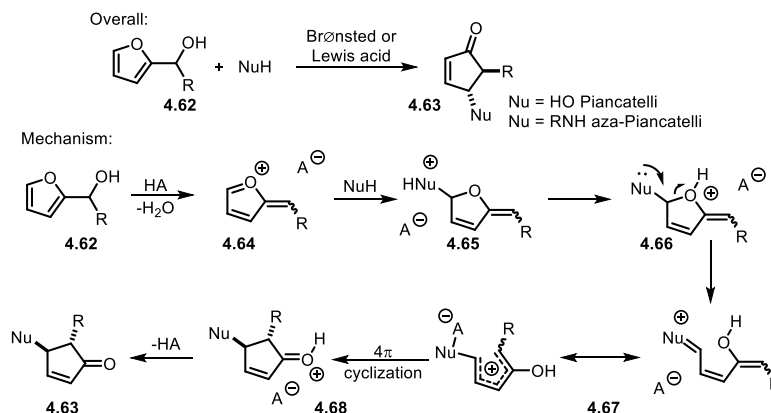


An alternative approach to accessing amine-substituted cyclopentenones via an electrocyclization reaction is the aza-Piancatelli reaction. The generally proposed mechanism of the Piancatelli is shown in Scheme 4.15.

In contrast to the Nazarov reaction, 2-furylcarbinol **4.62** is treated with an acid additive to promote dehydration to **4.64**. At this point, NuH adds to the oxocarbenium ion to form an acetal or hemiaminal **4.65** (NuH = H_2O for Piancatelli or RNH_2 for aza-Piancatelli, respectively). Ring opening of **4.66** after a series of proton transfers affords 1-hetero-4-oxypentadienyl cation **4.67** which undergoes 4p-electrocyclization to **4.68** readily due to the push-pull effect of the heteroatom

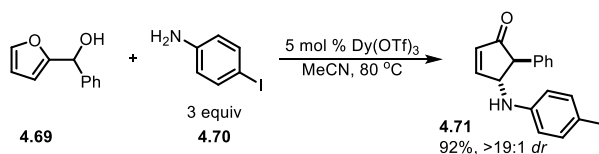
substitution pattern. This electrocyclization produces a 1-oxyallyl cation that provides predictable positioning of the olefin without disturbing any stereocenters formed during the conrotatory cyclization overcoming the issues of substrate-controlled elimination and tautomerization in Nazarov cyclizations. However, deprotonation gives amine-substituted cyclopentenone **4.63** instead of an α,β -unsaturated cyclopentenimine.

Scheme 4.15. Mechanism of the Piancatelli and aza-Piancatelli rearrangement.



An example aza-Piancatelli is shown in Scheme 4.16. In this process, $\text{Dy}(\text{OTf})_3$ -catalyzed dehydration of **4.69** in refluxing MeCN results in **4.71** after trapping the dehydration intermediate **4.64** with **4.70**.

Scheme 4.16. Example aza-Piancatelli rearrangement from aniline trapping a 2-furylcarbinol dehydration intermediate.

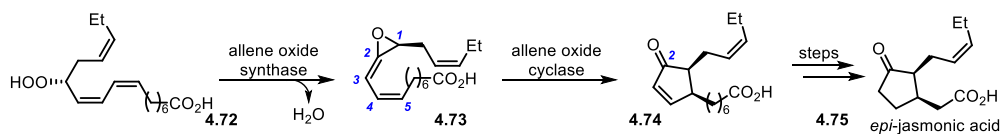


4.5. Allene Oxide Cyclization and Oxidation-Initiated Nazarov Reactions

A related cyclization takes place in the synthesis of jasmonates in plants (Scheme 4.17).¹³ Lipid hydroperoxide **4.72** undergoes an enzyme catalyzed dehydration to form conjugated allene oxide

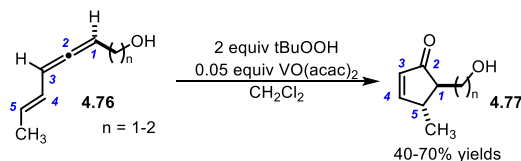
4.73. Allene oxide cyclase then catalyzes a diastereo- and enantioselective 2-oxypentadienyl cation cyclization furnishing enone **4.74** prior to a series of β -oxidations and reduction to *epi*-jasmonic acid **4.75**.

Scheme 4.17. Allene oxide cyclization in plant biosynthesis of jasmonates.

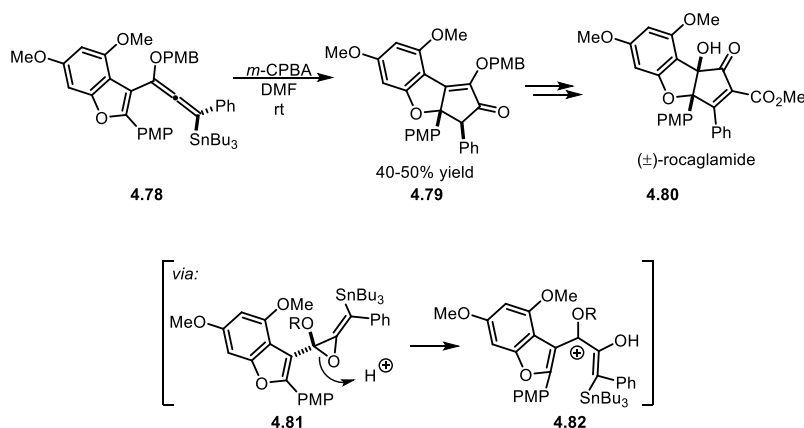


Appealingly, this reaction has been mimicked synthetically by subjecting conjugated allenic or homoallenic alcohols **4.76** to directed epoxidation conditions.¹⁴ Presumably, allene oxide intermediates like **4.73** are involved and 2-oxypentadienyl cation cyclization furnishes cyclopentenone **4.77** in modest yields and excellent *dr*.^{14a} This is due to intermediacy of cyclic 1-oxallyl cation, analogous to that in the Piantatelli rearrangement, precluding both substrate-controlled elimination and ablation of stereocenters following conrotatory cyclization.

Scheme 4.18. Oxidation-initiated 2-oxo-Nazarov electrocyclization of eneallenes.



The Frontier group demonstrated that Nazarov cyclizations initiated by the oxidation of eneallenes constitutes a synthetically useful approach to the synthesis of densely functionalized oxygenated cyclopentanes in their synthesis of racemic rocaglamide **4.80** (Scheme 4.19).^{14d-e} Epoxidation of conjugated allene ether **4.78** results in diastereoselective cyclization to **4.79**, presumably through allene oxide **4.81** opening to trioxygenated pentadienyl cation **4.82** prior to engaging in the stereospecific 4π -electrocyclization reaction.

Scheme 4.19. Synthetic utility of eneallene oxidation-initiated oxy-Nazarov electrocyclicization.

4.6. Conclusions

Heteroatom-substituted allyl cations are useful intermediates for the stereocontrolled synthesis of functionalized carbocyclic rings, particularly odd seven and five-membered rings. While reactions of 2-oxyallyl cations and oxygen-substituted pentadienyl cations are well-explored and continue to be developed at a faster rate, a great deal more remains to be discovered about 2-amidoallyl cations and amine-substituted pentadienyl cations. Moreover, frequently in reactions of amine-substituted allyl cations, the C-N bond is not retained in the product. New methods for generating amine-substituted allyl cations creatively tend to spur the development of interesting reactions; the development of methods that retain the C-N bond will certainly be useful in synthesizing amine-containing bioactive compounds and natural products or amino-derivatives of oxygenated natural products. The wide-range of structurally diverse amine-containing cyclopentanes as well as the challenges associated with amine-substituted 4π -electrocyclization reactions provided the impetus to investigate 2-amidopentadienyl cations analogous to **4.73** described in the next chapter.

4.7 References

1. For selected reviews on [4+3]-cycloadditions, see: a) I. V. Hartung, H. M. R. Hoffmann, *Angew. Chem. Int. Ed.* **2004**, *43*, 1934; *Angew. Chem.* **2004**, *116*, 1968; b) M. Harmata, *Acc. Chem. Res.* **2001**, *34*, 595; c) H. M. R. Hoffmann, *Angew. Chem. Int. Ed. Engl.* **1984**, *23*, 1; *Angew. Chem.* **1984**, *96*, 29. d) Harmata, M. *Chem. Commun.*, **2010**, *46*, 8886-8903.
2. For selected reviews on heteroatom-substituted allyl cations in [4+3]-cycloadditions, see: a) A. G. Lohse, R. P. Hsung, *Chem. Eur. J.* **2011**, *17*, 3812; b) Harmata, M. *Chem. Commun.*, **2010**, *46*, 8904-8922.
3. Walters, M. A.; Arcand, H. R.; and Lawrie, D. J., *Tetrahedron Lett.*, **1995**, *36*, 23–26.
4. Xiong, H.; Huang, J.; Ghosh, S. K.; and Hsung, R. P., *J. Am. Chem. Soc.*, **2003**, *125*, 12694–12695.
5. For examples of diastereoselective reactions of 1-amido-2-oxyallyl cation being chiral auxiliaries on nitrogen, see: (a) Myers, A. G.; and Barbay, J. K., *Org. Lett.*, **2001**, *3*, 425–428. (b) Xiong, H.; Hsung, R. P.; Shen, L.; and Hahn, J. M., *Tetrahedron Lett.*, **2002**, *43*, 4449–4453.
6. Other methods to generate 2-amidoallyl cations: (a) Schmid, R.; Schmid H. Silberioneninduzierte Reaktion von 3-Chlor-2-pyrrolidino-cyclohexen mit 1,3-Dienen. *Helv. Chim. Acta* **1974**, *57*, 1883. (b) Kim, H.; Ziani-Cherif, C.; Oh, J.; Cha, J. K. New [4+3] cycloaddition approach to *cis*-2,8-disubstituted oxocanes. *J. Org. Chem.* **1995**, *60*, 792. (c) Kende, A. S.; Huang, H. Asymmetric [4+3] cycloadditions from chiral α -chloro imines. *Tetrahedron Lett.* **1997**, *38*, 3353. (d) De Kimpe, N; Stevens, C. Silver ion-induced reactions of α -haloimines. *Tetrahedron* **1990**, *46*, 6753. (e) De Kimpe, N.; Palamareva, M.; Verhe, R.; Debuyck, L.; Schamp, N. Silver-induced conversion of α -chloro ketimines into 2,2-dimethyl-3-(N-alkyl) imino-8-

oxabicyclo[3.2.1]oct-6-enes. Presumptive evidence for the [3+4] cycloaddition of intermediate 2-aminoallylcarbenium ions with furan. *J. Chem. Res.* **1986**, 190. (f) Saputra, M. A.; Dange, N. S.; Cleveland, A. H.; Malone, J. A.; Fronczek, F. R.; Kartika, R. Regioselective functionalization of enamides at the α -Carbon via unsymmetrical 2-amidoallyl cations. *Org. Lett.* **2017**, *19*, 2414. (g) Schlegel, M.; Schneider, C. Lewis acid-catalyzed nucleophilic addition of indoles to in situ-generated 2-amidoallyl cations. *J. Org. Chem.* **2017**, *82*, 5986.

(7) Amidoallyl cations via allene amination and methyleneaziridine ring opening: (a) Gerstner, N. C.; Adams, C. S.; Tretbar, M.; Schomaker, J. M. Stereocontrolled syntheses of seven-membered carbocycles by tandem allene aziridination/[4+3] reaction. *Angew. Chem. Int. Ed.* **2016**, *55*, 13240. (b) Prié, G.; Prévost, N.; Twin, H.; Fernandes, S. A.; Hayes, J. F.; Shipman, A. A Lewis acid catalyzed intramolecular [4+3] cycloaddition route to polycyclic systems that contain a seven-membered ring. *Angew. Chem. Int. Ed.* **2004**, *43*, 6517. (c) Griffin, K.; Montagne, C.; Hoang, C. T.; Clarkson, G. J.; Shipman, M. Lewis acid promoted intramolecular (3+2) 'cycloadditions' of methyleneaziridines with alkene and alkyne acceptors. *Org. Biomol. Chem.* **2012**, *10*, 1032. (d) Feast, G. C.; Page, L. W.; Robertson, J. The intramolecular amination of allenes. *Chem. Commun.* **2010**, *46*, 2835. (e) Robertson, J.; Feast, G. C.; White, L. V.; Steadman, V. A.; Claridge, T. D. W. Structure and reactivity of bicyclic methylene aziridines prepared by intramolecular aziridination of allenes. *Org. Biomol. Chem.* **2010**, *8*, 3060.

(8) Amidoallyl cations by amination of 1,1-disubstituted allenes: (a) Stoll, A. H.; Blakey, S. B. Rhodium catalyzed allene amination: Diastereoselective synthesis of aminocyclopropanes via a 2-amidoallylcation intermediate. *J. Am. Chem. Soc.* **2010**, *132*, 2108. (b) Stoll, A. H.; Blakey, S. B. Rhodium catalyzed allene amidation: a facile entry into 2-amidoallylcations for unusual [3+3] annulation reactions. *Chem. Sci.* **2011**, *2*, 112.

(9) For selected reviews on Nazarov reactions, see: (a) Vinogradov, M. G.; Turova, O. V.; Zlotin, S. G. Nazarov reaction: current trends and recent advances in the synthesis of natural compounds and their analogs. *Org. Biomol. Chem.* **2017**, *15*, 8245. (b) Di Grandi, M. J. Nazarov-like cyclization reactions. *Org. Biomol. Chem.* **2014**, *12*, 5331. (c) Frontier, A. J.; Collison, C. The Nazarov cyclization in organic synthesis. Recent advances. *Tetrahedron* **2005**, *61*, 7577. (d) Tius, M. A. Allene ether Nazarov cyclization. *Chem. Soc. Rev.* **2014**, *43*, 2979.

(10) For substituent effects and retro-Nazarov reactivity, see: (a) Harmata, M.; Lee, D. R. The Retro-Nazarov Reaction. *J. Am. Chem. Soc.* **2002**, *124*, 14328. (b) Smith, D. A.; Ulmer, C. W. Effects of Substituents in the 3-Position on the [2+2] Pentadienyl Cation Electrocyclization. *J. Org. Chem.*, **1997**, *62*, 5110-5115.

(11) For examples of state-of-the-art imino-Nazarov reactions, see: (a) Fan, T.; Wang, A.; Li, J.-Q.; Ye, J.-L.; Zheng, X.; Huang, P.-Q. Versatile one-pot synthesis of polysubstituted cyclopent-2-enimines from α,β -unsaturated amides: imino-Nazarov reaction. *Angew. Chem. Int. Ed.* **2018**, *57*, 10352. (b) Ma, Z.-X.; He, S.; Song, W.; Hsung, R. P. α -Aryl-substituted allenamides in an imino-Nazarov cyclization cascade catalyzed by Au(I). *Org. Lett.* **2012**, *14*, 5736. (c) Bonderoff, S. A.; Grant, T. N.; West, F. G.; Tremblay, M. Nazarov reactions of vinyl cyclopropylamines: an approach to the imino-Nazarov problem. *Org. Lett.* **2013**, *15*, 2888. (d) Suárez-Pantiga, S.; Rubio, E.; Alvarez-Rúa, González, J. M. Intermolecular reaction of internal alkynes and imines: propargyl tosylates as key partners in a gold-catalyzed [4+1] unusual cyclization leading to cyclopent-2-enimines. *Org. Lett.* **2009**, *11*, 13. (e) Tius, M. A.; Chu, C. C.; Nieves-Colberg, R. An imino Nazarov cyclization. *Tetrahedron Lett.* **2001**, *42*, 2419. (f) Bow, W. F.; Basak, A. K.; Jolit, A.; Vicic, D. A.; Tius, M. A. Enamine-iminium ion Nazarov cyclization of α -ketoenones. *Org. Lett.* **2010**, *12*, 440. (g) William, R.; Wang, S.; Ding, F.; Arviana, E. N.; Liu, X.-W. Interrupted imino-

Nazarov cyclization of 1-aminopentadienyl cation and related cascade process. *Angew. Chem. Int. Ed.* **2014**, *53*, 10742.

(12) For selected references on Piancatelli and aza-Piancatelli reactions, see: (a) Veits, G. K.; Wenz, D. R.; Read de Alaniz, J. Versatile method for the synthesis of 4-aminocyclopentenones: Dysprosium(III) triflate catalyzed aza-Piancatelli rearrangement. *Angew. Chem. Int. Ed.* **2010**, *49*, 9484. (b) Yu, D.; Thai, V. T.; Palmer, L. I.; Veits, G. K.; Cook, J. E.; Read de Alaniz, J.; Hein, J. E. Importance of off-cycle species in the acid-catalyzed aza-Piancatelli rearrangement. *J. Org. Chem.* **2013**, *78*, 12784. (c) Faza, O. N.; López, C. S.; Álvarez, R.; de Lera, Á. R. Theoretical study of the electrocyclic ring closure of hydroxypentadienyl cations. *Chem. Eur. J.* **2004**, *10*, 4324-4333. (d) Davis, R. L.; Tantillo, D. J. Theoretical studies on pentadienyl cation electrocyclizations. *Curr. Org. Chem.* **2010**, *14*, 1561-1577.

(13) Mechanistic studies of strain-promoted 2-oxypentadienyl cation cyclization of allene oxides in Nature: (a) Turner, J. G.; Ellis, C.; Devoto, A. The jasmonate signal pathway. *Plant Cell* **2002**, *14*, S153. (b) López, C. S.; Faza, O. N.; York, D. M.; de Lera, Á. R. Theoretical study of the vinyl allene oxide to cyclopent-2-en-1-one rearrangement: Mechanism, torquoselectivity and solvent effects. *J. Org. Chem.* **2004**, *69*, 3635. (c) González-Pérez, A. B.; Grechkin, A.; de Lera, Á. R. A unifying mechanism for the rearrangement of vinyl allene oxide geometric isomers to cyclopentenones. *Org. Biomol. Chem.* **2014**, *12*, 7694.

(14) Eneallene oxidation-initiated Nazarov cyclization: (a) Kim, S. J.; Cha, J. K. An efficient cyclopentenone formation via an allene oxide. *Tetrahedron Lett.* **1988**, *29*, 5613. (b) Doutheau, A.; Gore, J.; Malacria, M. Preparation et Epoxydation de Trienes-1,2,4ynes-6 (alleneenynes). *Tetrahedron*, **1977**, *33*, 2393. (c) Dulcere, J.-P.; Grimaldi, J.; Santelli, M. Synthesis of silyl-substituted vinylallenes. *Tetrahedron Lett.* **1981**, *22*, 3179. (d) Malona, J. A.; Cariou, K.; Spencer,

W. T.; Frontier, A. J. Total synthesis of (\pm)-rocaglamide via oxidation-initiated Nazarov cyclization. *J. Org. Chem.* **2012**, *77*, 1891. (e) Spencer, W. T.; Levin, M. D.; Frontier, A. J. Oxidation-initiated Nazarov cyclization of vinyl alkoxyallenes. *Org. Lett.* **2011**, *13*, 414. (f) Fradette, R. J.; Kang, M.; West, F. G. Oxidation-initiated cyclizations of pentadienyl ethers: an alternative entry to the Nazarov reaction. *Angew. Chem. Int. Ed.* **2017**, *56*, 6335.

Chapter 5:

Biomimetic 2-Imino-Nazarov Electrocyclizations via Eneallene Aziridination

This chapter is reprinted (adapted) with permission from work published in:

Corbin, J. R.; Ketelboeter, D. R.; Fernández, I.; Schomaker, J. M. *J. Am. Chem. Soc.*, **2020**, *142*,
5568-5573.

The work described in this chapter focuses on work I did in collaboration with my mentee Devin Ketelboeter and Prof. Isra Fernández. Under my direction as his graduate student mentor and with his input, Devin assisted me with preparing substrates, probing the scope by cyclizing the substrates he made, and collecting characterization data which permitted us to try some challenging substrates, many of which did not get included in the final publication but are included in this chapter. Prof. Fernández provided all computational work and insight; his contribution led us to the hypothesis that provided a proof-of-concept for an asymmetric variation. I explored reactions to diversify the product scaffold, performed stereochemical determinations, and investigated strategies for asymmetric variations.

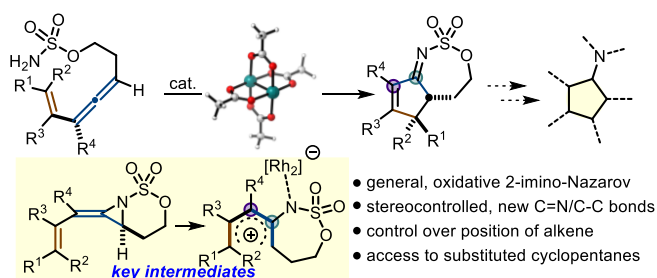
Chapter 5

Biomimetic 2-Imino-Nazarov Cyclizations via Eneallene Aziridination

5.1 Introduction

Amidoallyl cations are appealing three-carbon synthons for the preparation of complex amine-containing carbocycles; however, methods to generate and utilize these reactive species are limited and underexplored compared to those for oxallyl cations. Here we disclose a bioinspired strain-driven ring opening of bicyclic methyleneaziridines to 2-amidopentadienyl cation intermediates that readily engage in Nazarov cyclizations (Figure 5.1). Advantages of this strategy include ease of generation and improved reactivity compared to 3-pentadienyl cations, control over the ultimate position of the alkene, the potential for high dr between vicinal stereocenters, and the ability to further elaborate the products to fully substituted aminocyclopentanes. Experimental and computational studies support a dual role for the Rh_2L_n complex as both a nitrene transfer catalyst and a Lewis acid promoter, insight that provides a framework for the future development of asymmetric 2-imino-Nazarov cyclizations.

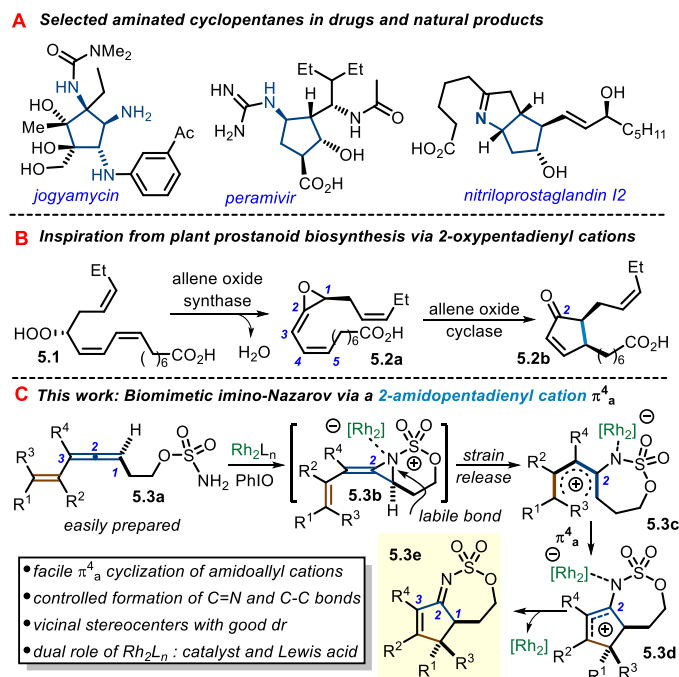
Figure 5.1. 2-Imino-Nazarov Electrocyclization described in this work.



5.2 Background

Flexible methods to construct functionalized, densely substituted carbocycles have long been of intense interest to the synthetic community, as these motifs occur frequently in useful bioactive molecules and natural products. For example, amine-bearing cyclopentanes are found in diverse natural products and pharmaceuticals, including the antiprotozoal compound jogyamycin, the anti-influenza drug peramivir, and nitroloprostaglandin I2 (PGI2), which is used in the treatment of arteriosclerosis, cardiac failure, and thrombosis (Scheme 5.1A).

Scheme 5.1. Background and proposed 2-Imino-Nazarov reaction



The aza version of the classic Nazarov cyclization¹ of divinyl ketones to prepare 2-cyclopenten-1-imines is challenging. This is due to better stabilization of the key pentadienyl cation in a “3-imino-Nazarov” reaction compared with the 3-oxyallyl cation intermediates implicated in a typical Nazarov reaction.² Tius, Hsung, West, Huang, and others have reported creative solutions to overcome this issue;³ nonetheless, reaction development has been hampered by the dearth of

methods for convenient generation of 3-amidoallyl cation intermediates.⁴ The aza-Piancatelli reaction, which moves the N to C1, has also been used to address this challenge;⁵ however, it benefits from a “push–pull” enol–iminium intermediate that ultimately furnishes the amine-substituted cyclopentenone product.

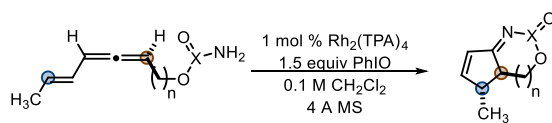
Our work was inspired by the biosynthesis of epi-jasmonic acid (Scheme 5.1B), which proceeds via a Nazarov-type electrocyclization of allene oxide **5.2a** to furnish α,β -unsaturated cyclopentenone **5.2b**. This enzyme-catalyzed process readily controls the site of unsaturation in the product and yields excellent *dr* and *ee* of the new vicinal stereocenters.⁶ We envisaged that a nitrogen version of this process could be readily mimicked by a tandem allene aziridination/electrocyclization (Scheme 5.1C) from easily obtained eneallenes of the form **5.3a**. Rh₂-catalyzed nitrene transfer yields conjugated bicyclic methyleneaziridine **5.3b**, analogous to **5.2a**. The ring strain inherent in **5.3b** (~35 kcal/mol) provides kinetically competent access to versatile 2-amidoallyl cation intermediate **5.3c** without the need for stoichiometric Lewis or Brønsted acids⁷ or competing formation of iminocyclopropanes.^{7d,f} Additionally, the modified 2-N positioning in **5.3c** reduces stabilization of the pentadienyl cation relative to traditional 3-amidopentadienyl cations to facilitate productive cyclization. A 4π conrotatory electrocyclization of **5.3c** to **5.3d** and subsequent loss of the Rh complex furnishes **5.3e**, ideally with high *dr*. The intermediacy of **5.3d** enables the formation of **5.3e** with predictable positioning of the alkene, as substrate-controlled elimination present in the typical Nazarov reaction is not operative here. In fact, no elimination or tautomerization is required from **5.3d** in this oxidative manifold, which avoids loss of stereochemical information between the vicinal stereocenters installed in the conrotatory cyclization of **5.3c**.⁸ This chapter describes the successful implementation of this strategy to develop a new “2-imino-Nazarov” reaction, including factors influencing the

mechanism and stereoselectivity of the cyclization, the elaboration of the products to increase molecular complexity from simple precursors, and potential strategies to secure enantioenriched products.

5.3. Reaction Optimization

Hydrozirconation/ $\text{Zr}=\text{O}$ elimination of allyl propargyl alcohol with Schwartz's reagent enables rapid access to eneallene **5.4** (Table 5.2, top).⁹ Preliminary studies found that sulfamates were the best nitrene precursors and that a two carbon tether between the allene and the sulfamate was optimal (Table 5.1).

Table 5.1. *N*-Group transfer tether optimization

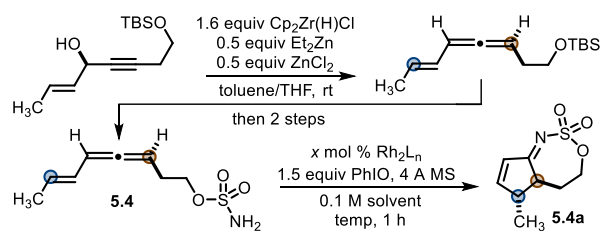


entry	n	X	yield, <i>dr</i>
1	1	C	4%, >19:1
2	1	S(O)	11%, >19:1
3	2	C	trace
4	2	S(O)	24%, >19:1

Nitrene transfer conditions previously reported by our group served as a starting point for investigating the feasibility of the 2-imino-Nazarov reaction of **5.4**.^{7a} Catalytic $\text{Rh}_2(\text{TPA})_4$ (TPA = triphenylacetate) transformed **5.4** to **5.4a** in 24% yield with >19:1 *dr* (entry 1). Varying the concentration (entries 2 and 3) had little impact; however, increasing the temperature to 50 °C (entry 1 vs 4) improved the yield of **5.4a** to 41%. Adding the catalyst last, as opposed to the oxidant, was not beneficial (entry 5). Switching the oxidant to $\text{PhI}(\text{OAc})_2$ (entry 6) or the solvent to MeNO_2 (entry 7) gave low yields of 21% and 23%, respectively. However, increasing the loading of $\text{Rh}_2(\text{TPA})_4$ to 5 mol % (entries 8 and 9) in CH_2Cl_2 improved the yield of **5.4a** to 58%; further increases in temperature in DCE (entry 10) were not beneficial. Interestingly, $\text{Rh}_2(\text{OAc})_4$ (entry

11) and $\text{Rh}_2(\text{esp})_2$ (entry 12) were inferior to $\text{Rh}_2(\text{TPA})_4$. Computations of the LUMO energies for $\text{Rh}_2(\text{TPA})_4$ (−2.90 eV), $\text{Rh}_2(\text{OAc})_4$ (−2.68 eV), and $\text{Rh}_2(\text{esp})_2$ (−2.71 eV) suggested that Lewis acidity of the catalyst was important to reaction success (see the Appendix for computational details).

Table 5.2. Selected optimization studies



entry	solvent	catalyst (mol %)	temp (°C)	% yield ^a	notes
1	CH_2Cl_2	$\text{Rh}_2(\text{TPA})_4$ (1)	rt	24	15% rsm
2	CH_2Cl_2 (0.2 M)	$\text{Rh}_2(\text{TPA})_4$ (1)	rt	28	-
3	CH_2Cl_2 (0.05 M)	$\text{Rh}_2(\text{TPA})_4$ (1)	rt	33	-
4	CH_2Cl_2	$\text{Rh}_2(\text{TPA})_4$ (1)	50	41	-
5	CH_2Cl_2	$\text{Rh}_2(\text{TPA})_4$ (1)	50	33	catalyst added last
6	CH_2Cl_2	$\text{Rh}_2(\text{TPA})_4$ (1)	50	21	$\text{PhI}(\text{OAc})_2$
7	MeNO_2	$\text{Rh}_2(\text{TPA})_4$ (1)	45	23	-
8	CH_2Cl_2	$\text{Rh}_2(\text{TPA})_4$ (5)	50	55	LUMO = −2.90 eV
9	CH_2Cl_2	$\text{Rh}_2(\text{TPA})_4$ (5)	50	58	0.05 equiv PhIOx3 added every 20 min
10	$\text{ClCH}_2\text{CH}_2\text{Cl}$	$\text{Rh}_2(\text{TPA})_4$ (5)	80	49	-
11	CH_2Cl_2	$\text{Rh}_2(\text{OAc})_4$ (5)	50	42	LUMO = −2.68 eV
12	CH_2Cl_2	$\text{Rh}_2(\text{esp})_2$ (5)	50	41	LUMO = −2.71 eV

^aNMR yields using mesitylene as internal standard

5.4. Reaction Scope

With the optimized conditions in hand, the scope of the tandem allene aziridination/2-imino-Nazarov reaction was explored (Table 5.3). All of the substrates were either racemic or a 1:1 racemic mixture of diastereomers. Freshly prepared **5.4** provided **5.4a** in 63% yield with >19:1 *dr*, bearing an *anti* relationship between the hydrogens at the two newly formed stereocenters through a thermally allowed conrotatory 4π electrocyclozation (Table 5.3, entry 1). Engaging *cis*-eneallene **5.5** gave **5.5a** in moderate yield (entry 2), favoring the *syn* isomer (NOESY-NMR studies detailed in the Appendix); we considered that the lower *dr* compared to **5.4a** could result from isomerization of the alkene geometry in **5.5**, partial epimerization of **5.5a** under the reaction

conditions, or a competing “non-Nazarov” pathway. Control experiments confirmed that the alkene of **5.5** does not isomerize in the presence of Rh₂TPA₄ or PhIO, while epimerization of **5.5a** is unlikely, as we would expect a similar *dr* for **5.4a** if this pathway were operative. Isomerization of intermediate species or a competing non-Nazarov pathway cannot be ruled out. Isopropyl substitution was tolerated in **5.6** to give **5.6a** in 74% yield with excellent *dr* (entry 3). To our delight, the preparation of **5.6a** could be run on a 1 g scale to give a 79% yield with >19:1 *dr*. Protected alcohols were suitable precursors, with **5.7** giving **5.7a** in 65% yield with >19:1 *dr* (entry 4). The ability of the external stereocenter in **5.8** to control the *dr* in the all-carbon stereotriad in **5.8a** was investigated (entry 5); while the *dr* between *a* and *b* was >19:1, the *dr* between *a/b* and *c* was only moderately improved to 1.2:1.

Substitution at C-3 (R⁴) and C-4 (R²) in **5.9** and **5.10** (entries 6-7) gave **5.9a** and **5.10a** in good yield; NOE correlations for **5.10a** show *anti* stereochemistry in the major diastereomer. Here, moderate *dr* may result from isomerization of either the precursor or intermediates, although a competing non-Nazarov pathway is also possible. Extending the conjugation of the alkene in styrenyl allene **5.11** (entry 8) resulted in an unoptimized 36% yield of **5.11a** in >19:1 *dr*, though this substrate was prone to decomposition at high temperatures. Increased steric congestion in eneallenes **5.12** (entry 9), where both R¹ and R³ are alkyl substituents, gave lower yields, but excellent *dr* in forming a challenging all-carbon quaternary center in **5.12a**. Eneallenes **5.13-5.15**, where both R¹ and R² are substituted, gave good yields of the 2-cyclopenten-1-imines **5.13a-5.15a**. As the alkene in these cases cannot undergo isomerization, the less-than-perfect *dr* is puzzling. Prolonged exposure of **5.14a** as a mixture to the reaction conditions revealed no change in *dr* over 24 h, while resubjecting diastereomerically pure *anti*-**5.14a** (*dr* >19:1) to the reaction conditions gave no change in the *dr*, providing support for lack of epimerization of the imine itself (see the

Appendix for details). The isopropenyl substituent on cyclohexene **5.15a** promotes high *anti* selectivity between adjacent stereocenters *a/b*.

Table 5.3. Scope of the tandem allene aziridination/2-imino-Nazarov reaction.

entry	R ¹ -R ⁴	product	% yield ^a , dr	entry	R ¹ -R ⁴	product	% yield ^a , dr	entry	R ¹ -R ⁴	product	% yield ^a , dr
1	R ¹ = Me R ² = H R ³ , R ⁴ = H		5.4a 63% ^c dr > 19:1	5	R ¹ = Ph(CH) ₂ CH ₃ R ² , R ³ = H R ⁴ = H		5.8a 71% dr _{a,b} > 19:1 dr _{ab,c} 1.2:1	9	R ¹ = (E)-C ₁₁ H ₁₉ R ² = H R ³ = Me R ⁴ = H		5.12a 31% dr > 19:1
2	R ¹ = H R ² , R ⁴ = H R ³ = Me		5.5a 36% dr = 2.4:1	6	R ¹ = Me R ² = H R ³ = H R ⁴ = Me		5.9a 65% dr 4.1:1	10	R ¹ , R ² = (CH ₂) ₃ R ³ = H R ⁴ = H		5.13a 62% dr = 14:1
3	R ¹ = ⁱ Pr R ² = H R ³ , R ⁴ = H		5.6a > 74% dr > 19:1 79%, 1 g scale	7	R ¹ = Me R ² = Me R ³ , R ⁴ = H		5.10a 46% ^b dr = 3.9:1	11	R ¹ , R ² = (CH ₂) ₄ R ³ = H R ⁴ = H		5.14a 74% dr = 3.0:1
4	R ¹ = (CH ₂) ₃ OBPS R ² = H R ³ = H R ⁴ = H		5.7a 65% dr > 19:1	8	R ¹ = Ph R ² = H R ³ = H R ⁴ = H		5.11a 36% dr > 19:1	12	R ¹ , R ² = ring R ³ = H R ⁴ = H		5.15a 77% dr _{a,b} > 19:1 dr _{ab,c} 1.2:1
Challenging substitution patterns											
entry	R ¹ -R ³	product	% yield ^a , dr	entry	R ¹ -R ³	product	% yield ^a , dr	entry	R ¹ -R ³	product	% yield ^a , dr
13	R ¹ = Me R ² = H R ³ = Me		5.16a 34%	15	R ¹ = CH(CH ₂) ₂ R ² = H R ³ = H		5.18a 25% ^d dr > 19:1	17	R ¹ = H R ² = H R ³ = H		5.20a 41%
14	R ¹ = Me R ² = H R ³ = C ₆ H ₁₁		trace	16	R ¹ = (E)-C ₃ H ₅ R ² = H R ³ = H		5.19a 25% dr = 5.9:1	18			5.21a 62% dr = 7.7 : 4.6 : 4.2 : 1

^aIsolated yield. ^bUsed 1 mol % Rh₂(TPA)₄. ^cYield decreases as allene ages. ^d53% mass balance

Additional iminocyclopentene scaffolds with all-carbon quaternary centers were sought by cyclizing eneallenes **5.16-5.17** (entries 13-14), furnishing cyclized **5.16a** in modest yield;

increasing the steric bulk of the *cis*-substituent R³ in **5.17a** results in poor reaction efficiency. Surprisingly, cyclopropyl-containing **5.18a** also resulted in a modest yield after subjecting **5.18** to the reaction conditions. Extending the conjugation of the alkene in **5.19** (entry 16) resulted in an unoptimized 25% yield of **5.19a** with electronically differentiated alkene handles, though this substrate was prone to decomposition at high temperatures. Additionally, substitution at C-5 is not required, as **5.20** (entry 17) furnishes **5.20a** in moderate yield. Lastly, terpene-derived substrate **5.21** with a bicyclo[3.1.1]heptane moiety furnished all possible diastereomers of **5.21a** unselectively (entry 18). Though the efficiency of some of these reactions was less than desirable, these unique scaffolds would be difficult to obtain by other means. In general, reactions were run to full consumption of starting material; no other identifiable products were observed in the NMR crude, with the exception of PhI and catalyst.

5.5. Experimental and Computational Mechanistic Investigation

DFT calculations (see Appendix for computational details) were carried out to gain more insight into the mechanism of this unusual 2-imino-Nazarov reaction (Figure 5.2). The fate of the methyleneaziridine **5.22**, readily formed upon reaction of eneallene **5.4a** with Rh₂-catalyst in the presence of PhIO, was explored first. Exothermic coordination of the aziridine nitrogen to the Rh₂-catalyst leads to **INT1**, which evolves to amidoallyl cation **INT2** through **TS1**, a saddle point associated with aziridine ring-opening ($\Delta E^\ddagger = 13.6$ kcal/mol). The intermediacy of this achiral intermediate was supported by subjecting enantioenriched **5.4** (92% *ee*, see Appendix for details) to the standard conditions and noting degradation of the axial chirality to only 12% *ee* in the product **5.4a**. Ring closure converts **INT2** into bicyclic **INT3** via **TS2**, which is associated with the formation of a new C–C bond. The lower barrier ($\Delta E^\ddagger = 5.0$ kcal/mol) of this step is consistent with its computed high exothermicity ($\Delta E_R = -39.8$ kcal/mol); however, the barrier is similar to an

aza-Piancatelli reaction, with the N at C1, highlighting the favorable electronic benefits of positioning the N at C2 *vs.* C3.⁵ Decoordination of the Rh₂-fragment gives the observed product **5.4a** and releases the catalyst. The reaction profile for the corresponding *Z*-eneallene isomer **5.22-Z** was computed to be higher in energy than the energies computed for **5.22** along the entire reaction coordinate. In addition, the *E/Z* isomerization barriers computed for either **INT1** or **INT2** are much higher (>20 kcal/mol, see Figure 5S-2 in the computational portion of the Appendix) than the barriers associated with the ring opening and subsequent cyclization. This finding could help to explain the higher yields and *dr* noted with **5.4** *vs.* **5.5**.

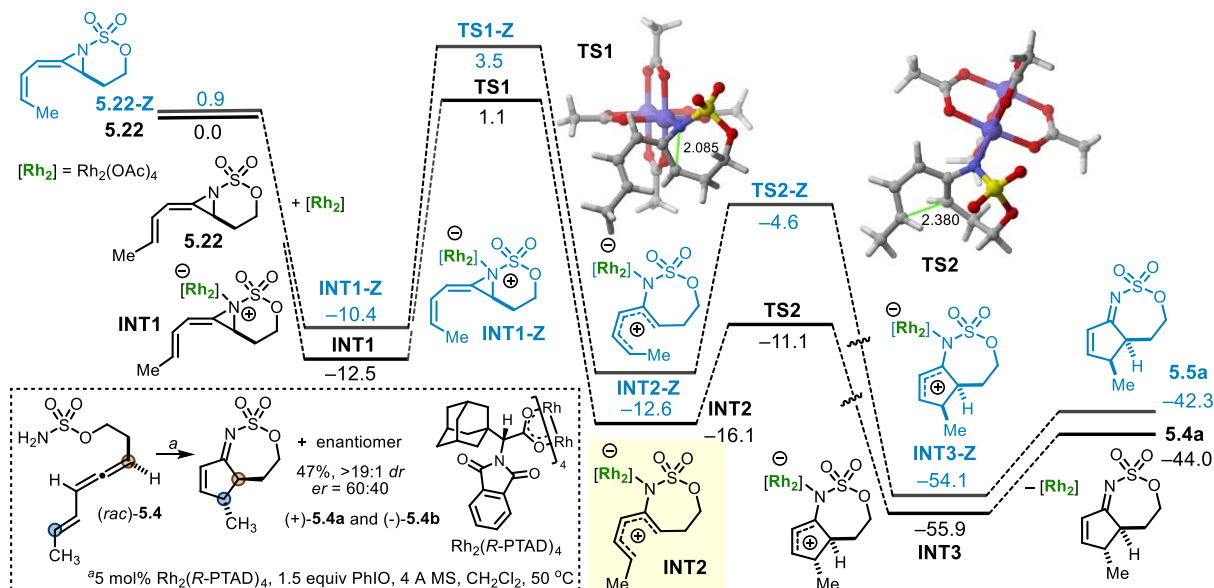


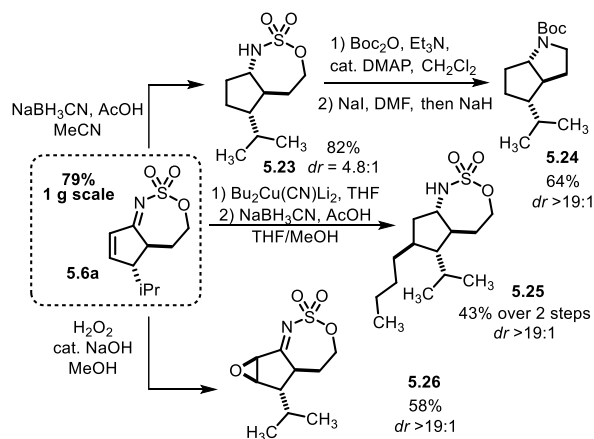
Figure 5.2. Computed reaction profile for the 2-imino-Nazarov of aziridine **5.22**. Relative energies and bond distances given in kcal/mol and angstroms, respectively. All data computed SMD(CH₂Cl₂)-B3LYP-D3/def2-TZVPP//SMD(CH₂Cl₂)-B3LYP-D3/def2-SVP level.

The dual role of the Rh₂L_n nitrene transfer catalyst as a Lewis acid promoter was intriguing; while these modes of reactivity are preceded individually, there are few examples where both features of a Lewis acidic dinuclear Rh catalyst are utilized in a synergistic fashion.¹⁰ During

optimization studies, higher catalyst loadings of the most Lewis acidic Rh_2L_n complex gave more efficient cyclization. Dissociation of Rh_2OAc_4 prior to cyclization had a prohibitively large computed energy barrier, leading to the hypothesis that the use of a racemic allene with a chiral Rh_2L_n catalyst might generate enantioenriched products. Indeed, subjecting (*rac*)-**5.4** (Figure 5.2, inset) to the reaction conditions using $\text{Rh}_2(\text{R-PTAD})_4$ produced (+)-**5.4a** and (-)-**5.4b** in a 60:40 *er*, a promising result when considering the large distance between the catalyst and the site of the stereodetermining C–C bond formation event. Efforts to identify better chiral Rh_2L_n catalysts and counteranions for accessing enantioenriched, densely functionalized aminocyclopentenes are currently underway. This result also provides compelling evidence that Rh_2 is involved in promoting cyclization as a Lewis acid, in addition to facilitating the nitrene transfer.

5.6. Product Utility

Finally, the 2-cyclopenten-1-imine products of tandem allene aziridination/2-imino-Nazarov reaction proved flexible intermediates for preparation of complex aminated cyclopentanes. As shown in Scheme 5.2, a variety of transformations were successfully carried out on **6a** (see the Appendix for conditions). Global reduction of **5.6a** with NaBH_3CN produces **5.23** in 82% yield and 4.8:1 *dr*. Boc-protection of the amine, separation of the diastereomers, and double displacement with NaI/NaH , generates fused pyrrolidine **5.24** in 64% yield over two steps (>19:1 *dr*), showcasing one of many potential uses of the tether.^{6a} Higher-order cuprates, such as $\text{Bu}_2\text{Cu}(\text{CN})\text{Li}_2$, gave diastereoselective 1,4-addition to **5.6a**; subsequent protonation of the metalloenamine and imine reduction affords **5.25** in >19:1 *dr*. Lastly, to demonstrate the application of **5.6a** to the synthesis of fully-substituted aminated cyclopentanes, nucleophilic epoxidation with H_2O_2 and catalytic NaOH provides **5.26** in 58% yield and >19:1 *dr*.

Scheme 5.2. Flexible transformations of **5.6a**.

5.7. Conclusion

In conclusion, we have developed an efficient 2-imino-Nazarov cyclization reaction from simple precursors. Stereocontrolled, site-selective Rh₂-catalyzed eneallene aziridination initiates an electrocyclization that furnishes structurally diverse α,β -iminocyclopentene scaffolds in good yield and *dr*. Investigation of the reaction mechanism suggests formation of discrete achiral intermediates, implying strain-promoted methyleneaziridine ring opening to a 2-amidopentadienyl cation is operative. Computations indicate that the nitrene transfer catalyst remains associated during cyclization as a mild Lewis acid, providing a new framework for developing asymmetric 2-imino-Nazarov electrocyclizations.

5.8. References

- (1) For selected reviews on Nazarov reactions, see: (a) Vinogradov, M. G.; Turova, O. V.; Zlotin, S. G. Nazarov reaction: current trends and recent advances in the synthesis of natural compounds and their analogs. *Org. Biomol. Chem.* **2017**, *15*, 8245. (b) Di Grandi, M. J. Nazarov-like cyclization reactions. *Org. Biomol. Chem.* **2014**, *12*, 5331. (c) Frontier, A. J.; Collison, C. The

Nazarov cyclization in organic synthesis. Recent advances. *Tetrahedron* **2005**, *61*, 7577. (d) Tius, M. A. Allene ether Nazarov cyclization. *Chem. Soc. Rev.* **2014**, *43*, 2979.

(2) For substituent effects and retro-Nazarov reactivity, see: Harmata, M.; Lee, D. R. The Retro-Nazarov Reaction. *J. Am. Chem. Soc.* **2002**, *124*, 14328.

(3) For examples of state-of-the-art imino-Nazarov reactions, see: (a) Fan, T.; Wang, A.; Li, J.-Q.; Ye, J.-L.; Zheng, X.; Huang, P.-Q. Versatile one-pot synthesis of polysubstituted cyclopent-2-enimines from α,β -unsaturated amides: imino-Nazarov reaction. *Angew. Chem. Int. Ed.* **2018**, *57*, 10352. (b) Ma, Z.-X.; He, S.; Song, W.; Hsung, R. P. α -Aryl-substituted allenamides in an imino-Nazarov cyclization cascade catalyzed by Au(I). *Org. Lett.* **2012**, *14*, 5736. (c) Bonderoff, S. A.; Grant, T. N.; West, F. G.; Tremblay, M. Nazarov reactions of vinyl cyclopropylamines: an approach to the imino-Nazarov problem. *Org. Lett.* **2013**, *15*, 2888. (d) Suárez-Pantiga, S.; Rubio, E.; Alvarez-Rúa, González, J. M. Intermolecular reaction of internal alkynes and imines: propargyl tosylates as key partners in a gold-catalyzed [4+1] unusual cyclization leading to cyclopent-2-enimines. *Org. Lett.* **2009**, *11*, 13. (e) Tius, M. A.; Chu, C. C.; Nieves-Colberg, R. An imino Nazarov cyclization. *Tetrahedron Lett.* **2001**, *42*, 2419. (f) Bow, W. F.; Basak, A. K.; Jolit, A.; Vicic, D. A.; Tius, M. A. Enamine-iminium ion Nazarov cyclization of α -ketoenones. *Org. Lett.* **2010**, *12*, 440. (g) William, R.; Wang, S.; Ding, F.; Arviana, E. N.; Liu, X.-W. Interrupted imino-Nazarov cyclization of 1-aminopentadienyl cation and related cascade process. *Angew. Chem. Int. Ed.* **2014**, *53*, 10742.

(4) Other methods to generate amidoallyl cations: (a) Schmid, R.; Schmid H. Silberioneninduzierte Reaktion von 3-Chlor-2-pyrrolidino-cyclohexen mit 1,3-Dienen. *Helv. Chim. Acta* **1974**, *57*, 1883.

(b) Kim, H.; Ziani-Cherif, C.; Oh, J.; Cha, J. K. New [4+3] cycloaddition approach to *cis*-2,8-disubstituted oxocanes. *J. Org. Chem.* **1995**, *60*, 792. (c) Kende, A. S.; Huang, H. Asymmetric

[4+3] cycloadditions from chiral α -chloro imines. *Tetrahedron Lett.* **1997**, 38, 3353. (d) De Kimpe, N.; Stevens, C. Silver ion-induced reactions of α -haloimines. *Tetrahedron* **1990**, 46, 6753. (e) De Kimpe, N.; Palamareva, M.; Verhe, R.; Debuyck, L.; Schamp, N. Silver-induced conversion of α -chloro ketimines into 2,2-dimethyl-3-(N-alkyl) imino-8-oxabicyclo[3.2.1]oct-6-enes. Presumptive evidence for the [3+4] cycloaddition of intermediate 2-aminoallylcarbenium ions with furan. *J. Chem. Res.* **1986**, 190. (f) Saputra, M. A.; Dange, N. S.; Cleveland, A. H.; Malone, J. A.; Fronczek, F. R.; Kartika, R. Regioselective functionalization of enamides at the α -Carbon via unsymmetrical 2-amidoallyl cations. *Org. Lett.* **2017**, 19, 2414. (g) Schlegel, M.; Schneider, C. Lewis acid-catalyzed nucleophilic addition of indoles to in situ-generated 2-amidoallyl cations. *J. Org. Chem.* **2017**, 82, 5986.

(5) For selected references on Piancatelli and aza-Piancatelli reactions, see: (a) Veits, G. K.; Wenz, D. R.; Read de Alaniz, J. Versatile method for the synthesis of 4-aminocyclopentenones: Dysprosium(III) triflate catalyzed aza-Piancatelli rearrangement. *Angew. Chem. Int. Ed.* **2010**, 49, 9484. (b) Yu, D.; Thai, V. T.; Palmer, L. I.; Veits, G. K.; Cook, J. E.; Read de Alaniz, J.; Hein, J. E. Importance of off-cycle species in the acid-catalyzed aza-Piancatelli rearrangement. *J. Org. Chem.* **2013**, 78, 12784. (c) Faza, O. N.; López, C. S.; Álvarez, R.; de Lera, Á. R. Theoretical study of the electrocyclic ring closure of hydroxypentadienyl cations. *Chem. Eur. J.* **2004**, 10, 4324-4333. (d) Davis, R. L.; Tantillo, D. J. Theoretical studies on pentadienyl cation electrocyclizations. *Curr. Org. Chem.* **2010**, 14, 1561-1577.

(6) Mechanistic studies of strain-promoted 2-oxypentadienyl cation cyclization of allene oxides in Nature: (a) Turner, J. G.; Ellis, C.; Devoto, A. The jasmonate signal pathway. *Plant Cell* **2002**, 14, S153. (b) López, C. S.; Faza, O. N.; York, D. M.; de Lera, Á. R. Theoretical study of the vinyl allene oxide to cyclopent-2-en-1-one rearrangement: Mechanism, torquoselectivity and solvent

effects. *J. Org. Chem.* **2004**, *69*, 3635. (c) González-Pérez, A. B.; Grechkin, A.; de Lera, Á. R. A unifying mechanism for the rearrangement of vinyl allene oxide geometric isomers to cyclopentenones. *Org. Biomol. Chem.* **2014**, *12*, 7694.

(7) Amidoallyl cations via allene amination and methyleneaziridine ring opening: (a) Gerstner, N. C.; Adams, C. S.; Tretbar, M.; Schomaker, J. M. Stereocontrolled syntheses of seven-membered carbocycles by tandem allene aziridination/[4+3] reaction. *Angew. Chem. Int. Ed.* **2016**, *55*, 13240.

(b) Prié, G.; Prévost, N.; Twin, H.; Fernandes, S. A.; Hayes, J. F.; Shipman, A. A Lewis acid catalyzed intramolecular [4+3] cycloaddition route to polycyclic systems that contain a seven-membered ring. *Angew. Chem. Int. Ed.* **2004**, *43*, 6517. (c) Griffin, K.; Montagne, C.; Hoang, C.

T.; Clarkson, G. J.; Shipman, M. Lewis acid promoted intramolecular (3+2) 'cycloadditions' of methyleneaziridines with alkene and alkyne acceptors. *Org. Biomol. Chem.* **2012**, *10*, 1032. (d)

Feast, G. C.; Page, L. W.; Robertson, J. The intramolecular amination of allenes. *Chem. Commun.* **2010**, *46*, 2835. (e) Robertson, J.; Feast, G. C.; White, L. V.; Steadman, V. A.; Claridge, T. D. W.

Structure and reactivity of bicyclic methylene aziridines prepared by intramolecular aziridination of allenes. *Org. Biomol. Chem.* **2010**, *8*, 3060. (f) Stoll, A. H.; Blakey, S. B. Rhodium catalyzed allene amination: Diastereoselective synthesis of aminocyclopropanes via a 2-amidoallylcation intermediate. *J. Am. Chem. Soc.* **2010**, *132*, 2108. (g) Stoll, A. H.; Blakey, S. B. Rhodium catalyzed

allene amidation: a facile entry into 2-amidoallylcations for unusual [3+3] annulation reactions. *Chem. Sci.* **2011**, *2*, 112. (h) Takahashi, H.; Yasui, S.; Tsunoi, S.; Shibata, I. Catalytic

cycloaddition of 2-methyleneaziridines with 1,1-Dicyanoalkenes. *Org. Lett.* **2014**, *16*, 1192.

(8) Eneallene oxidation-initiated Nazarov cyclization: (a) Kim, S. J.; Cha, J. K. An efficient cyclopentenone formation via an allene oxide. *Tetrahedron Lett.* **1988**, *29*, 5613. (b) Doutheau, A.; Gore, J.; Malacria, M. Preparation et Epoxydation de Trienes-1,2,4ynes-6 (alleneenyne).

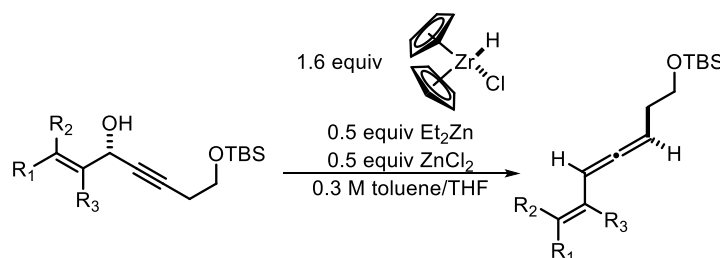
Tetrahedron, **1977**, 33, 2393. (c) Dulcere, J.-P.; Grimaldi, J.; Santelli, M. Synthesis of silyl-substituted vinylallenes. *Tetrahedron Lett.* **1981**, 22, 3179. (d) Malona, J. A.; Cariou, K.; Spencer, W. T.; Frontier, A. J. Total synthesis of (±)-rocaglamide via oxidation-initiated Nazarov cyclization. *J. Org. Chem.* **2012**, 77, 1891. (e) Spencer, W. T.; Levin, M. D.; Frontier, A. J. Oxidation-initiated Nazarov cyclization of vinyl alkoxyallenes. *Org. Lett.* **2011**, 13, 414. (f) Fradette, R. J.; Kang, M.; West, F. G. Oxidation-initiated cyclizations of pentadienyl ethers: an alternative entry to the Nazarov reaction. *Angew. Chem. Int. Ed.* **2017**, 56, 6335.

(9) Methods to prepare eneallenes: (a) Pu, X.; Ready, J. M. Direct and stereospecific synthesis of allenes via reduction of propargylic alcohols with $\text{Cp}_2\text{Zr(H)Cl}$. *J. Am. Chem. Soc.* **2008**, 130, 10874. (b) Myers, A. G.; Zheng, B. New and stereospecific synthesis of allenes in a single step from propargylic alcohols. *J. Am. Chem. Soc.* **1996**, 118, 4492.

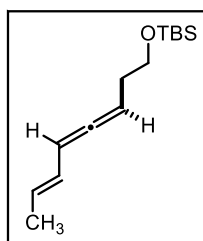
(10) Rh_2L_n catalysts as Lewis acids: (a) Dequirez, G.; Ciesielski, J.; Retailleau, P.; Dauban, P. Catalytic intermolecular alkene oxyamination with nitrenes. *Chem. Eur. J.* **2015**, 20, 8929. (b) Ciesielski, J.; Dequirez, G.; Retailleau, P.; Gandon, V.; Dauban, P. Rhodium-catalyzed alkene difunctionalization with nitrenes. *Chem. Eur. J.* **2016**, 22, 9338.

5.9. Experimental Details and Characterization

5.9.1. General procedure for eneallene synthesis:



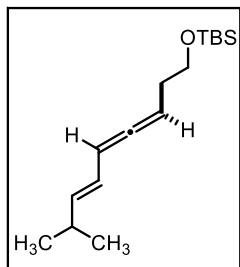
A round-bottom flask equipped with a stir bar was charged with ZnCl_2 (0.5 equiv) and the solid was freshly fused by flame torching under vacuum. After cooling to room temperature under a slight positive pressure of nitrogen, Et_2Zn (1 M in toluene, 0.5 equiv) was added, followed by anhydrous THF (3 M with respect to Et_2Zn). This mixture was stirred at room temperature for 30 minutes until solid ZnCl_2 was completely dissolved, then toluene was added (0.3 M with respect to ROH). The solution was cooled to 0 °C before allyl propargyl alcohol (1.0 equiv) in toluene (0.3 M with respect to Et_2Zn) was added to the EtZnCl solution. The mixture was stirred for 20 min before the addition of $\text{Cp}_2\text{Zr(H)Cl}$ (1.6 equiv) in a single portion under the protection of nitrogen atmosphere. The reaction was stirred vigorously for 12-24 hours until starting material was consumed according to TLC. The process was quenched by adding saturated NaHCO_3 . The aqueous phase was extracted thrice with ether, and the combined organic layers were dried by Na_2SO_4 before concentrating under reduced pressure. The desired eneallene was easily purified by SiO_2 column chromatography using hexanes/ EtOAc or pentane/ Et_2O solvent systems. **NOTE:** While some substrates in the report by Ready could be synthesized using EtMgCl as the base instead of EtZnCl , the eneallene class of substrates could not be prepared successfully using EtMgCl .



OTBS Precursor to Compound 5.4. Following the general procedure (14.3 mmol scale), **OTBS Precursor to Compound 5.4** was purified on silica gel using a 0-30% hexanes: EtOAc solvent system with increasing 5% increments of EtOAc to provide a yellow oil (2.33 g, 9.8 mmol, 69% yield). **^1H NMR** (500

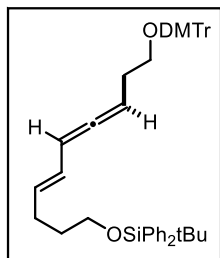
MHz, $\text{Chloroform-}d$) δ 5.87 – 5.81 (m, 1H), 5.75 (ddt, J = 10.3, 5.8, 2.7 Hz, 1H), 5.61 (dq, J = 14.8, 6.7, 1.4 Hz, 1H), 5.28 (dtd, J = 8.4, 5.8, 1.4 Hz, 1H), 3.67 (t, J = 6.7 Hz, 2H), 2.23 (qd, J = 6.8, 2.7 Hz, 2H), 1.73 (dt, J = 6.7, 1.6 Hz, 3H), 0.90 (s, 9H), 0.06 (s, 6H). **^{13}C NMR** (126 MHz,

CDCl_3) δ 206.8, 127.1, 127.0, 94.0, 88.9, 63.0, 32.8, 26.1, 18.5, 18.2, -5.1. **HRMS** (ASAP-MS) m/z calculated for $\text{C}_{14}\text{H}_{26}\text{OSi}$ $[\text{M}+\text{H}]^+$ 239.1826, measured 239.1822 (1.7 ppm).



OTBS Precursor to Compound 5.6. Following the general procedure (14 mmol scale), **OTBS Precursor to Compound 5.6** was purified on silica gel using a 0-25% hexanes:EtOAc solvent system with increasing 5% increments of EtOAc to provide a deep yellow oil (1.37 g, 5.1 mmol, 37% yield). **^1H**

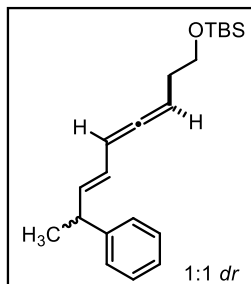
NMR (500 MHz, Chloroform- d) δ 5.83 – 5.73 (m, 2H), 5.59 (ddd, J = 14.8, 6.6, 1.4 Hz, 1H), 5.33 – 5.26 (m, 1H), 3.68 (t, J = 6.7 Hz, 2H), 2.33 (dqt, J = 13.4, 6.7, 1.2 Hz, 1H), 2.24 (qd, J = 6.8, 2.5 Hz, 2H), 1.00 (d, J = 6.7 Hz, 6H), 0.90 (s, 9H), 0.06 (s, 6H). **^{13}C NMR** (126 MHz, CDCl_3) δ 207.0, 139.5, 122.8, 94.0, 88.8, 62.8, 32.6, 31.1, 25.9, 22.33, 22.31, 18.3, -5.3. **HRMS** (ASAP-MS) m/z calculated for $\text{C}_{16}\text{H}_{30}\text{OSi}$ $[\text{M}+\text{H}]^+$ 267.2139, measured 267.2138 (0.4 ppm).



OTBS Precursor to Compound 5.7. The *O*-TBS protected homopropargyl acetylide was replaced with a 4,4'-dimethoxytrityl *O*-protecting group. Following the general procedure (5 mmol scale), **OTBS Precursor to Compound 5.7** was purified on silica gel using a 0-30% hexanes:EtOAc

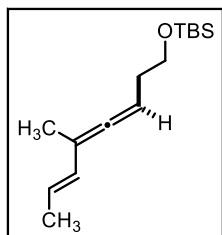
solvent system with increasing 5% increments of EtOAc to provide a light yellow oil (1.829 g, 2.6 mmol, 52% yield). **^1H NMR** (500 MHz, Chloroform- d) δ 7.67 (dt, J = 7.7, 1.7 Hz, 4H), 7.47 – 7.31 (m, 13H), 7.28 (d, J = 7.4 Hz, 1H), 7.21 – 7.17 (m, 1H), 6.83 – 6.80 (m, 4H), 5.82 (dd, J = 15.1, 10.3 Hz, 1H), 5.76 – 5.68 (m, 1H), 5.57 (dt, J = 14.5, 6.8 Hz, 1H), 5.38 – 5.31 (m, 1H), 3.78 (s, 6H), 3.66 (t, J = 6.3 Hz, 2H), 3.13 (t, J = 6.5 Hz, 2H), 2.31 (qd, J = 6.7, 2.5 Hz, 2H), 2.16 (q, J = 7.3 Hz, 2H), 1.64 (p, J = 6.8 Hz, 2H), 1.05 (d, J = 2.0 Hz, 9H). **^{13}C NMR** (126 MHz, CDCl_3) δ 207.1, 158.5, 145.4, 136.7, 135.7, 134.2, 132.1, 130.2, 129.7, 128.4, 127.7, 126.8, 126.1, 113.1,

94.1, 89.4, 86.0, 63.4, 63.2, 55.3, 32.4, 30.3, 29.1, 27.0, 19.4, 0.1. **HRMS** (ESI-MS) m/z calculated for $C_{47}H_{52}O_4Si$ $[M+H]^+$ 731.3527, measured 731.3522 (0.7 ppm).



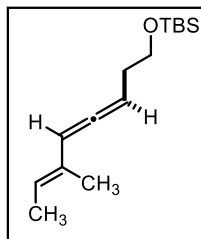
OTBS Precursor to Compound 5.8. Following the general procedure (2.9 mmol scale), **OTBS Precursor to Compound 5.8** was purified on silica gel using a 0-30% hexanes:EtOAc solvent system with increasing 5% increments of EtOAc to provide a yellow oil (0.830 g, 2.5 mmol, 87% yield).

1H NMR (500 MHz, Chloroform- d) δ 7.32 – 7.28 (m, 2H), 7.22 – 7.18 (m, 3H), 5.91 – 5.74 (m, 3H), 5.34 – 5.27 (m, 1H), 3.68 (td, J = 6.7, 4.7 Hz, 2H), 3.50 (q, J = 6.9 Hz, 1H), 2.27 – 2.21 (m, 2H), 1.38 (dd, J = 7.0, 1.3 Hz, 3H), 0.90 (s, 9H), 0.06 (s, 6H). **^{13}C NMR** (126 MHz, $CDCl_3$) δ 207.4, 136.8, 128.6, 127.4, 126.3, 124.8, 124.7, 94.0, 89.1, 62.9, 42.5, 32.7, 26.1, 21.3, 18.5, -5.1. **HRMS** (ASAP-MS) m/z calculated for $C_{21}H_{32}OSi$ $[M+H]^+$ 329.2295, measured 329.2290 (1.5 ppm).



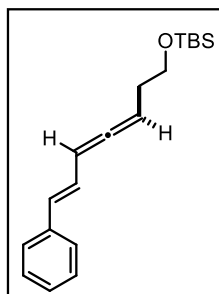
OTBS Precursor to Compound 5.9. Following the general procedure (15 mmol scale), **OTBS Precursor to Compound 5.9** was purified on silica gel using a 0-30% hexanes:EtOAc solvent system with increasing 5% increments of EtOAc to provide a clear oil (1.726 g, 6.8 mmol, 45% yield).

1H NMR (500 MHz, Chloroform- d) δ 6.04 – 5.93 (m, 1H), 5.52 (dq, J = 14.7, 6.7, 1.4 Hz, 1H), 5.23 – 5.13 (m, 1H), 3.67 (t, J = 6.7 Hz, 2H), 2.21 (q, J = 6.8 Hz, 2H), 1.77 (dt, J = 3.8, 1.6 Hz, 6H), 0.90 (s, 9H), 0.06 (s, 6H). **^{13}C NMR** (126 MHz, $CDCl_3$) δ 206.7, 130.1, 123.7, 99.9, 87.0, 63.2, 33.0, 26.1, 18.5, 18.4, 15.8, -5.1. **HRMS** (ASAP-MS) m/z calculated for $C_{15}H_{28}OSi$ $[M+H]^+$ 253.1982, measured 253.1978 (1.6 ppm).



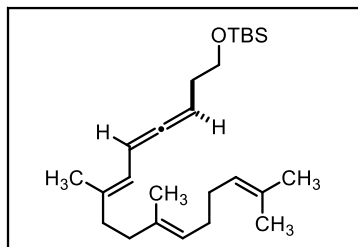
OTBS Precursor to Compound 5.10. Following the general procedure (27 mmol scale), **OTBS Precursor to Compound 5.10** was purified on silica gel using a 0-25% hexanes:EtOAc solvent system with increasing 5% increments of EtOAc to provide a deep yellow oil (4.83 g, 19.1 mmol, 70% yield). **¹H NMR**

(500 MHz, Chloroform-*d*) δ 5.84 (dt, J = 6.0, 2.8 Hz, 1H), 5.47 – 5.36 (m, 2H), 3.69 (t, J = 6.8 Hz, 2H), 2.26 (qd, J = 6.9, 2.8 Hz, 2H), 1.70 (dt, J = 7.0, 1.3 Hz, 3H), 1.67 (d, J = 1.4 Hz, 3H), 0.90 (d, J = 1.0 Hz, 9H), 0.06 (d, J = 0.9 Hz, 6H). **¹³C NMR** (126 MHz, CDCl₃) δ 205.2, 130.9, 123.0, 99.4, 90.7, 63.1, 33.1, 26.1, 18.5, 14.1, 13.4, -5.1. **HRMS** (ASAP-MS) m/z calculated for C₁₅H₂₈OSi [M+H]⁺ 253.1982, measured 253.1977 (2.0 ppm).



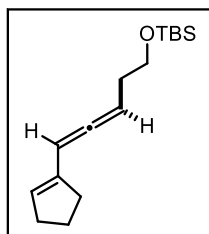
OTBS Precursor to Compound 5.11. Following the general procedure (14.5 mmol scale), **OTBS Precursor to Compound 5.11** was purified on silica gel using a 0-30% hexanes:EtOAc solvent system with increasing 5% increments of EtOAc to provide a light yellow oil (2.40 g, 8.0 mmol, 41% yield). **¹H NMR**

(500 MHz, Chloroform-*d*) δ 7.40 – 7.35 (m, 2H), 7.30 (t, J = 7.7 Hz, 2H), 7.23 – 7.18 (m, 1H), 6.59 (ddd, J = 15.7, 10.3, 1.0 Hz, 1H), 6.48 (dd, J = 15.8, 1.4 Hz, 1H), 6.02 – 5.94 (m, 1H), 5.42 (q, J = 6.8 Hz, 1H), 3.72 (t, J = 6.6 Hz, 2H), 2.30 (qd, J = 6.7, 2.7 Hz, 2H), 0.92 (s, 9H), 0.08 (s, 6H). **¹³C NMR** (126 MHz, CDCl₃) δ 208.9, 137.5, 130.1, 128.7, 127.4, 126.3, 125.4, 94.7, 89.5, 62.8, 32.7, 26.1, 18.5, -5.1. **HRMS** (ASAP-MS) m/z calculated for C₁₉H₂₈OSi [M+H]⁺ 301.1982, measured 301.1979 (1.0 ppm).



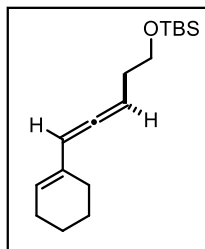
OTBS Precursor to Compound 5.12. Following the general procedure (15 mmol scale), **OTBS Precursor to Compound 5.12** was purified on silica gel using a 0-30% hexanes:EtOAc solvent system with increasing 5% increments of EtOAc to provide a deep

yellow/orange oil (4.70 g, 12.1 mmol, 80% yield). **¹H NMR** (500 MHz, Chloroform-*d*) δ 5.97 (ddt, $J = 10.8, 6.3, 2.7$ Hz, 1H), 5.62 (dp, $J = 10.9, 1.3$ Hz, 1H), 5.32 – 5.26 (m, 1H), 5.14 – 5.07 (m, 2H), 3.68 (t, $J = 6.7$ Hz, 2H), 2.24 (qd, $J = 6.8, 2.7$ Hz, 2H), 2.15 – 2.03 (m, 6H), 1.98 (dd, $J = 9.1, 6.1$ Hz, 2H), 1.72 (d, $J = 1.3$ Hz, 3H), 1.68 (d, $J = 1.5$ Hz, 3H), 1.60 (d, $J = 1.3$ Hz, 6H), 0.90 (s, 9H), 0.06 (s, 6H). **¹³C NMR** (126 MHz, CDCl₃) δ 207.8, 137.6, 135.4, 131.4, 124.5, 124.0, 119.7, 90.6, 88.5, 63.0, 40.1, 39.9, 32.9, 26.9, 26.7, 26.1, 25.8, 18.5, 17.8, 16.6, 16.1, -5.1. **HRMS** (ASAP-MS) m/z calculated for C₂₅H₄₄OSi [M+H]⁺ 389.3234, measured 389.3231 (0.8 ppm).



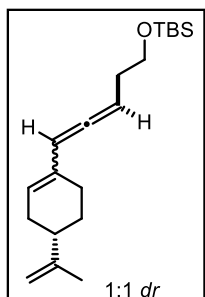
OTBS Precursor to Compound 5.13. Following the general procedure (11 mmol scale), **OTBS Precursor to Compound 5.13** was purified on silica gel using a 0-30% hexanes:EtOAc solvent system with increasing 10% increments of EtOAc to provide a deep yellow oil (2.9 g, 11 mmol, quantitative yield). **¹H**

NMR (500 MHz, Chloroform-*d*) δ 6.03 – 6.01 (m, 1H), 5.62 (d, $J = 2.3$ Hz, 1H), 5.38 – 5.32 (m, 1H), 3.68 (t, $J = 6.8$ Hz, 2H), 2.40 (ddt, $J = 9.8, 4.8, 2.3$ Hz, 2H), 2.34 – 2.30 (m, 2H), 2.25 (qd, $J = 6.9, 2.7$ Hz, 2H), 1.89 (p, $J = 7.6$ Hz, 2H), 0.90 (s, 9H), 0.06 (s, 6H). **¹³C NMR** (126 MHz, CDCl₃) δ 207.1, 138.6, 127.9, 91.4, 89.5, 63.1, 33.3, 32.9, 32.8, 26.1, 23.3, 18.5, -5.1. **HRMS** (ASAP-MS) m/z calculated for C₁₆H₂₈OSi [M+H]⁺ 265.1982, measured 265.1977 (1.9 ppm).



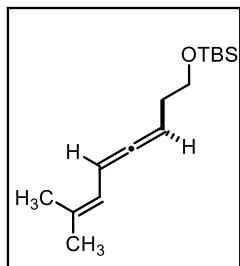
OTBS Precursor to Compound 5.14. Following the general procedure (15.0 mmol scale), **OTBS Precursor to Compound 5.14** was purified on silica gel using a 0-30% hexanes:EtOAc solvent system with increasing 5% increments of EtOAc to provide a yellow oil (2.89 g, 10.4 mmol, 69% yield). **¹H NMR** (500

MHz, Chloroform-*d*) δ 5.80 (dt, J = 5.9, 2.8 Hz, 1H), 5.64 (ddt, J = 5.1, 3.7, 1.8 Hz, 1H), 5.41 – 5.34 (m, 1H), 3.68 (t, J = 6.8 Hz, 2H), 2.25 (qd, J = 6.9, 2.8 Hz, 2H), 2.09 (dh, J = 5.9, 1.9 Hz, 2H), 2.02 (dp, J = 6.3, 2.0 Hz, 2H), 1.69 – 1.56 (m, 4H), 0.90 (s, 9H), 0.06 (s, 6H). **¹³C NMR** (126 MHz, CDCl₃) δ 204.9, 132.4, 125.7, 97.8, 90.8, 63.1, 33.1, 26.1, 26.0, 25.9, 22.7, 22.6, 18.5, -5.1. **HRMS** (ASAP-MS) m/z calculated for C₁₇H₃₀OSi [M+H]⁺ 279.2139, measured 279.2136 (1.0 ppm).



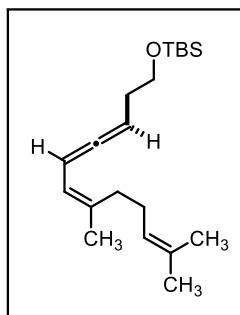
OTBS Precursor to Compound 5.15. Following the general procedure (15.0 mmol scale), **OTBS Precursor to Compound 5.15** was purified on silica gel using a 0-30% hexanes:EtOAc solvent system with increasing 5% increments of EtOAc to provide a yellow oil (3.93 g, 12.3 mmol, 82% yield). **¹H NMR** (500

MHz, Chloroform-*d*) δ 5.87 – 5.82 (m, 1H), 5.69 – 5.65 (m, 1H), 5.40 (dq, J = 13.0, 6.6, 6.2 Hz, 1H), 4.77 – 4.73 (m, 2H), 3.70 (tt, J = 6.8, 1.5 Hz, 2H), 2.31 – 2.15 (m, 5H), 2.12 – 2.00 (m, 2H), 1.86 (ddd, J = 10.6, 5.4, 2.6 Hz, 1H), 1.76 (d, J = 1.2 Hz, 3H), 1.55 – 1.47 (m, 1H), 0.92 (s, 9H), 0.08 (s, 6H). **¹³C NMR** (126 MHz, CDCl₃) δ 205.1, 205.0, 149.81, 149.78, 132.1, 132.0, 126.7, 126.6, 124.87, 124.85, 108.7, 97.3, 97.2, 90.8, 90.7, 63.0, 62.9, 41.3, 41.2, 33.0, 32.9, 31.4, 31.3, 27.53, 27.51, 26.3, 26.2, 26.0, 20.82, 20.81, 18.38, 18.37, -5.23, -5.24. **HRMS** (ASAP-MS) m/z calculated for C₂₀H₃₄OSi [M+H]⁺ 319.2452, measured 319.2447 (1.6 ppm).



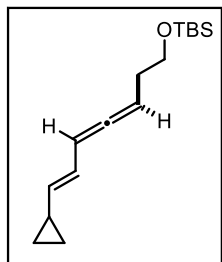
OTBS Precursor to Compound 5.16. Following the general procedure (22.1 mmol scale), **OTBS Precursor to Compound 5.16** was purified on silica gel using a 0-30% hexanes:EtOAc solvent system with increasing 5% increments of EtOAc to provide a light yellow oil (3.269 g, 12.9 mmol, 59%

yield). **¹H NMR** (500 MHz, Chloroform-*d*) δ 5.95 (ddd, $J = 11.4, 6.1, 2.9$ Hz, 1H), 5.63 – 5.57 (m, 1H), 5.32 – 5.25 (m, 1H), 3.68 (t, $J = 6.7$ Hz, 2H), 2.23 (qd, $J = 6.9, 2.7$ Hz, 2H), 1.77 (d, $J = 1.4$ Hz, 3H), 1.71 (d, $J = 1.3$ Hz, 3H), 0.90 (s, 9H), 0.06 (s, 6H). **¹³C NMR** (126 MHz, CDCl₃) δ 207.6, 134.0, 120.0, 90.6, 88.6, 63.0, 32.9, 26.13, 26.09, 18.5, 18.2, -5.1. **HRMS** (ASAP-MS) m/z calculated for C₁₅H₂₈OSi [M+H]⁺ 253.1982, measured 253.1978 (1.6 ppm).



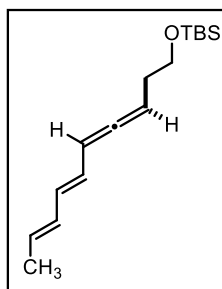
OTBS Precursor to Compound 5.17. Following the general procedure (15 mmol scale), **OTBS Precursor to Compound 5.17** was purified on silica gel using a 0-30% hexanes:EtOAc solvent system with increasing 5% increments of EtOAc to provide a deep yellow oil (2.83 g, 8.8 mmol, 59% yield). **¹H**

NMR (500 MHz, Chloroform-*d*) δ 5.97 (ddt, $J = 11.3, 5.8, 2.7$ Hz, 1H), 5.61 (dt, $J = 11.0, 1.3$ Hz, 1H), 5.30 – 5.25 (m, 1H), 5.12 (tdt, $J = 5.5, 2.8, 1.5$ Hz, 1H), 3.67 (t, $J = 6.8$ Hz, 2H), 2.23 (qd, $J = 6.9, 2.7$ Hz, 2H), 2.13 – 2.08 (m, 4H), 1.77 (s, 3H), 1.69 (d, $J = 1.3$ Hz, 3H), 1.61 (d, $J = 1.4$ Hz, 3H), 0.90 (s, 9H), 0.06 (s, 6H). **¹³C NMR** (126 MHz, CDCl₃) δ 207.7, 137.8, 132.1, 124.1, 120.4, 90.4, 88.5, 63.0, 32.9, 32.4, 26.8, 26.1, 25.9, 24.0, 18.5, 17.8, -5.1. **HRMS** (ASAP-MS) m/z calculated for C₂₀H₃₆OSi [M+H]⁺ 321.2608, measured 321.2607 (0.3 ppm).



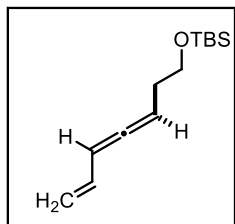
OTBS Precursor to Compound 5.18. Following the general procedure (5 mmol scale), **OTBS Precursor to Compound 5.18** was purified on silica gel using a 0-30% hexanes:EtOAc solvent system with increasing 5% increments of EtOAc to provide a gold-yellow oil (1.186 g, 4.5 mmol, 90% yield). **¹H**

NMR (500 MHz, Chloroform-*d*) δ 5.90 (dd, $J = 15.1, 10.4$ Hz, 1H), 5.74 (ddt, $J = 10.6, 5.9, 2.7$ Hz, 1H), 5.29 (q, $J = 6.8$ Hz, 1H), 5.17 (ddd, $J = 15.2, 8.8, 1.4$ Hz, 1H), 3.67 (t, $J = 6.7$ Hz, 2H), 2.23 (qd, $J = 6.8, 2.7$ Hz, 2H), 1.41 (qt, $J = 8.6, 4.8$ Hz, 1H), 0.90 (s, 9H), 0.75 – 0.71 (m, 2H), 0.39 (dt, $J = 6.3, 4.3$ Hz, 2H), 0.06 (s, 6H). **¹³C NMR** (126 MHz, CDCl₃) δ 206.8, 136.0, 123.4, 94.0, 89.1, 63.0, 32.8, 26.1, 18.5, 14.2, 7.3, -5.1. **HRMS** (ASAP-MS) m/z calculated for C₁₆H₂₈OSi [M+H]⁺ 265.1982, measured 265.1981 (0.4 ppm).



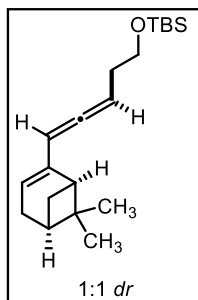
OTBS Precursor to Compound 5.19. Following the general procedure (15.0 mmol scale), **OTBS Precursor to Compound 5.19** was purified on silica gel using a 0-30% hexanes:EtOAc solvent system with increasing 5% increments of EtOAc to provide a light yellow oil (2.64 g, 10.0 mmol, 67% yield). **¹H**

NMR (500 MHz, Chloroform-*d*) δ 6.17 – 6.02 (m, 2H), 5.94 – 5.86 (m, 1H), 5.80 (ddt, $J = 10.9, 5.9, 2.7$ Hz, 1H), 5.67 (dq, $J = 13.6, 6.8$ Hz, 1H), 5.34 (q, $J = 7.0$ Hz, 1H), 3.68 (t, $J = 6.7$ Hz, 2H), 2.24 (qd, $J = 6.8, 2.7$ Hz, 2H), 1.78 – 1.75 (m, 3H), 0.90 (s, 9H), 0.06 (s, 6H). **¹³C NMR** (126 MHz, CDCl₃) δ 208.3, 131.6, 131.0, 129.2, 126.2, 94.6, 89.2, 62.9, 32.7, 26.1, 18.5, 18.4, -5.1. **HRMS** (ASAP-MS) m/z calculated for C₁₆H₂₈OSi [M+H]⁺ 265.1982, measured 265.1928 (0.8 ppm).



OTBS Precursor to Compound 5.20. Following the general procedure (15 mmol scale), **OTBS Precursor to Compound 5.20** was purified on silica gel using a 0-100% pentane:Et₂O solvent system with increasing 20% increments of ether to provide a light yellow oil (2.22 g, 9.9 mmol, 66% yield). **¹H NMR**

(500 MHz, Chloroform-*d*) δ 6.16 (dtd, $J = 16.9, 10.2, 1.0$ Hz, 1H), 5.85 – 5.74 (m, 1H), 5.36 – 5.29 (m, 1H), 5.15 (dd, $J = 17.0, 1.6$ Hz, 1H), 4.94 (dq, $J = 10.0, 1.4$ Hz, 1H), 3.67 (t, $J = 6.6$ Hz, 2H), 2.24 (qd, $J = 6.8, 2.7$ Hz, 2H), 0.89 (s, 9H), 0.05 (s, 6H). **¹³C NMR** (126 MHz, CDCl₃) δ 208.0, 133.5, 115.2, 94.6, 89.2, 62.9, 32.5, 26.1, 18.5, -5.1. **HRMS** (ASAP-MS) m/z calculated for C₁₃H₂₄OSi [M+H]⁺ 225.1669, measured 225.1668 (0.4 ppm).

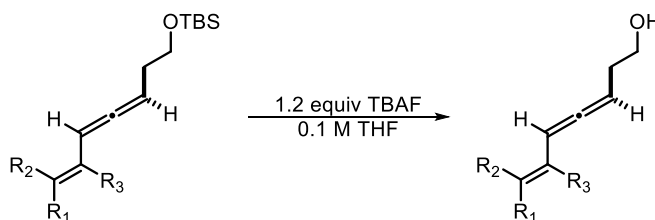


OTBS Precursor to Compound 5.21. Following the general procedure (10.8 mmol scale), **OTBS Precursor to Compound 5.21** was purified on silica gel using a 0-30% hexanes:EtOAc solvent system with increasing 5% increments of EtOAc to provide a yellow oil (2.47 g, 8.1 mmol, 75% yield). **¹H NMR** (500 MHz, Chloroform-*d*) δ 5.85 (tt, $J = 6.0, 2.7$ Hz, 1H), 5.45 (dt, $J = 3.8, 1.8$ Hz, 1H), 5.37 (tddd, $J = 9.0, 6.7, 4.2, 1.9$ Hz, 1H), 3.69 – 3.62 (m, 2H), 2.41 – 2.19 (m, 6H), 2.10 (dp, $J = 7.9, 2.9$ Hz, 1H), 1.29 (s, 3H), 1.16 (dd, $J = 8.6, 0.9$ Hz, 1H), 0.90 (d, $J = 0.8$ Hz, 9H), 0.81 (d, $J = 3.3$ Hz, 3H), 0.06 (s, 6H). **¹³C NMR** (126 MHz, CDCl₃) δ 205.3, 205.2, 142.6, 142.3, 120.5, 120.4, 96.7, 96.5, 91.1, 90.9, 63.13, 63.11, 42.61, 42.58, 41.0, 40.9, 38.01, 37.98, 32.9, 32.7, 32.04, 32.01, 31.6, 31.5, 26.5, 26.4, 26.1, 21.02, 20.97, 18.5, -5.09, -5.11. **HRMS** (ASAP-MS) m/z

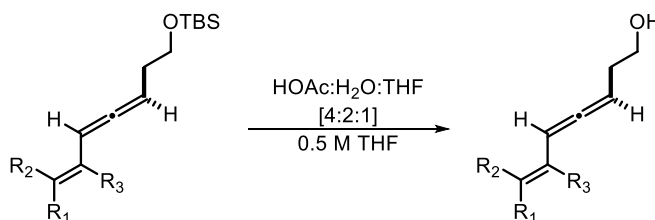
calculated for C₂₀H₃₄OSi [M+H]⁺ 319.2452, measured 319.2449 (0.9 ppm).

5.9.2. Procedures for alcohol deprotection:

NOTE: The acidic deprotection (method B, *vide infra*) must be used on the indicated substrates instead of the basic method A or the formation of undesired alkylidene THF was observed (*i.e.* intramolecular addition of alkoxide into the allene).

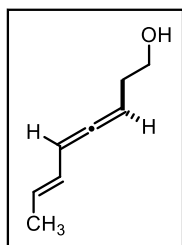


Method A – A dry round-bottom flask equipped with a stirbar was charged with the homoallenyl silyl ether (1.0 equiv) and diluted in anhydrous tetrahydrofuran (0.1 M). The solution was stirred and tetrabutylammonium fluoride (1 M in THF, 1.2 equiv) was added. The reaction stirred for 30–60 min until complete consumption of starting material was observed by TLC. At this point water was added to quench the reaction and the aqueous layer was extracted thrice with ether. The combined organic extracts were dried over Na_2SO_4 before concentrating the volatiles under reduced pressure. The crude mixture was purified by SiO_2 column chromatography using pentane/ Et_2O or hexanes/ EtOAc as eluent.



Method B – A round-bottom flask equipped with a stirbar was charged with the homoallenyl silyl ether (1.0 equiv) and diluted in tetrahydrofuran (0.5 M). The solution was stirred and DI H_2O (twice the amount of THF by volume) was added, followed by HOAc (four times the amount of THF by volume). The reaction stirred until starting material was completely consumed by TLC.

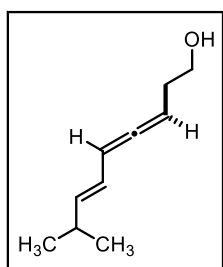
At this point the reaction was quenched slowly with a large excess of saturated NaHCO_3 solution and transferred to a separatory funnel. The organic layer was washed with portions of NaHCO_3 until the formation of bubbles stopped and all AcOH was removed. The organic layer was dried over Na_2SO_4 before concentrating the volatiles under reduced pressure. The pure homoallenlic alcohol was purified by SiO_2 column chromatography using pentane/ether or hexanes/ EtOAc as eluent.



ROH Precursor to Compound 5.4. Following method A (17.9 mmol scale),

ROH Precursor to Compound 5.4 was purified on silica gel using a 0-30% hexanes: EtOAc solvent system with increasing 5% increments of EtOAc to provide a yellow oil (1.83 g, 14.7 mmol, 76% yield). ^1H NMR (500 MHz,

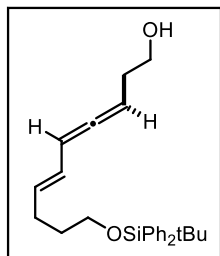
Chloroform-d) δ 5.89 – 5.77 (m, 2H), 5.68 – 5.59 (m, 1H), 5.30 (dddd, $J = 7.8, 6.2, 4.3, 2.3$ Hz, 1H), 3.70 (t, $J = 6.2$ Hz, 2H), 2.28 (qd, $J = 6.4, 2.6$ Hz, 2H), 1.74 (dt, $J = 6.3, 1.4$ Hz, 3H). ^{13}C NMR (126 MHz, CDCl_3) δ 206.8, 127.8, 126.6, 94.6, 88.7, 62.1, 32.4, 18.2. HRMS (ASAP-MS) m/z calculated for $\text{C}_8\text{H}_{12}\text{O}$ $[\text{M}+\text{H}]^+$ 125.0961, measured 125.0959 (1.6 ppm).



ROH Precursor to Compound 5.6. Following method A (5.1 mmol scale),

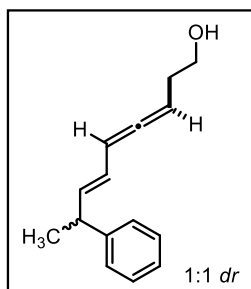
ROH Precursor to Compound 5.6 was purified on silica gel using a 0-30% hexanes: EtOAc solvent system with increasing 5% increments of EtOAc to provide a yellow oil (0.761 g, 5.0 mmol, 98% yield). ^1H NMR (500 MHz,

Chloroform-d) δ 5.85 – 5.75 (m, 2H), 5.62 (ddd, $J = 14.8, 6.6, 1.4$ Hz, 1H), 5.33 – 5.29 (m, 1H), 3.72 (q, $J = 5.9$ Hz, 2H), 2.36 – 2.25 (m, 3H), 1.59 (s, 1H), 1.00 (d, $J = 6.8$ Hz, 6H). ^{13}C NMR (126 MHz, CDCl_3) δ 207.1, 140.4, 122.4, 94.9, 88.7, 62.1, 32.4, 31.3, 25.8, 22.4. HRMS (ASAP-MS) m/z calculated for $\text{C}_{10}\text{H}_{16}\text{O}$ $[\text{M}+\text{H}]^+$ 153.1274, measured 153.1273 (0.7 ppm).



ROH Precursor to Compound 5.7. Method B (2.4 mmol scale) was slightly modified. Allene was dissolved in THF and AcOH/H₂O were added. After 1 h, additional THF (5 mL) and AcOH (20 mL) were added to obtain a homogenous 67% AcOH solution. The reaction progress was monitored closely by TLC and

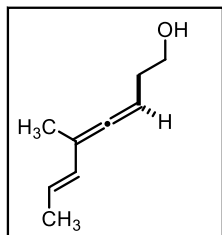
the reaction was quenched after complete consumption of starting material as described above (1 h after extra AcOH was added). **ROH Precursor to Compound 5.7** was purified on silica gel using a 0-30% hexanes:EtOAc solvent system with increasing 5% increments of EtOAc to provide a viscous yellow oil (0.199 g, 0.5 mmol, 20% yield). Up to 1.6 mmol of additional product was collected as a mixture with DMTrOH byproduct that is more easily purified after converting the homoallynic alcohol to the corresponding sulfamate. **¹H NMR** (500 MHz, Chloroform-*d*) δ 7.68 – 7.66 (m, 4H), 7.42 – 7.36 (m, 6H), 5.87 – 5.78 (m, 2H), 5.62 (dtd, J = 14.3, 6.9, 1.5 Hz, 1H), 5.31 (tdd, J = 6.9, 5.6, 1.6 Hz, 1H), 3.72 (t, J = 6.3 Hz, 2H), 3.67 (t, J = 6.3 Hz, 2H), 2.29 (tt, J = 6.5, 3.2 Hz, 2H), 2.22 – 2.16 (m, 2H), 1.69 – 1.62 (m, 2H), 1.50 (bs, 1H), 1.05 (s, 9H). **¹³C NMR** (126 MHz, CDCl₃) δ 207.0, 135.7, 132.8, 129.7, 127.7, 125.6, 113.3, 94.7, 88.8, 63.4, 62.1, 32.4, 32.3, 29.1, 27.0, 19.4. **HRMS** (ASAP-MS) m/z calculated for C₂₆H₃₄O₂Si [M+H]⁺ 407.2401, measured 407.2401 (<0.1 ppm).



ROH Precursor to Compound 5.8. Following method A (2.5 mmol scale), **ROH Precursor to Compound 5.8** was purified on silica gel using a 0-30% hexanes:EtOAc solvent system with increasing 5% increments of EtOAc to provide a yellow oil (0.478 g, 2.2 mmol, 89% yield). **¹H NMR** (500 MHz,

Chloroform-*d*) δ 7.33 – 7.28 (m, 2H), 7.20 (tt, J = 7.1, 1.5 Hz, 3H), 5.91 – 5.78 (m, 3H), 5.32 (tdd, J = 8.0, 6.0, 3.3 Hz, 1H), 3.73 (q, J = 5.4 Hz, 2H), 3.51 (p, J = 6.8 Hz, 1H), 2.30 (tdd, J = 9.0, 7.0, 4.4 Hz, 2H), 1.51 (bs, 1H), 1.38 (d, J = 7.0 Hz, 3H). **¹³C NMR** (126 MHz, CDCl₃) δ 207.42,

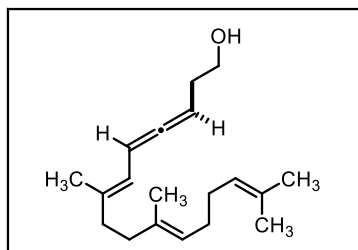
207.41, 145.74, 145.71, 137.54, 137.51, 128.61, 128.60, 127.35, 126.33, 126.32, 124.29, 124.25, 94.67, 94.66, 88.88, 88.87, 62.11, 62.10, 42.49, 42.48, 32.34, 32.33, 21.32, 21.26. **HRMS** (ASAP-MS) m/z calculated for $C_{15}H_{18}O$ $[M+H]^+$ 215.1430, measured 215.1428 (0.9 ppm).



ROH Precursor to Compound 5.9. Following method A (6.8 mmol scale),

ROH Precursor to Compound 5.9 was purified on silica gel using a 0-30% hexanes:EtOAc solvent system with increasing 5% increments of EtOAc to provide a yellow oil (0.691 g, 5.0 mmol, 74% yield). **1H NMR** (500 MHz,

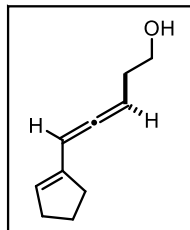
Chloroform- d) δ 5.97 (dd, J = 15.6, 2.3 Hz, 1H), 5.60 – 5.50 (m, 1H), 5.22 – 5.16 (m, 1H), 3.71 – 3.67 (m, 2H), 2.26 (q, J = 6.1 Hz, 2H), 1.79 (d, J = 2.7 Hz, 3H), 1.78 – 1.75 (m, 3H), 1.70 – 1.58 (bs, 1H). **^{13}C NMR** (126 MHz, $CDCl_3$) δ 206.7, 129.5, 124.5, 100.7, 86.7, 62.2, 32.5, 18.4, 15.9. **HRMS** (ASAP-MS) m/z calculated for $C_9H_{14}O$ $[M+H]^+$ 139.1117, measured 119.1117 (<0.1 ppm).



ROH Precursor to Compound 5.12. Following method A (12.1 mmol scale), **ROH Precursor to Compound 5.12** was purified on silica gel using a 0-30% hexanes:EtOAc solvent system with increasing 5% increments of EtOAc to provide a yellow oil (2.670

g, 9.7 mmol, 80% yield). **1H NMR** (500 MHz, Chloroform- d) δ 5.94 (ddt, J = 11.0, 6.0, 3.0 Hz, 1H), 5.51 (dq, J = 10.9, 1.3 Hz, 1H), 5.20 (q, 1H), 5.04 – 4.95 (m, 2H), 3.61 (t, J = 6.1 Hz, 2H), 2.18 (qd, J = 6.5, 2.9 Hz, 2H), 1.97 (ddd, J = 19.2, 13.5, 6.8 Hz, 7H), 1.87 (dd, J = 9.1, 6.2 Hz, 2H), 1.62 (d, J = 1.3 Hz, 3H), 1.57 (d, J = 1.7 Hz, 3H), 1.49 (s, 6H). **^{13}C NMR** (126 MHz, $CDCl_3$) δ 207.8, 138.4, 135.5, 131.4, 124.5, 123.9, 119.2, 91.3, 88.3, 62.1, 40.1, 39.8, 32.4, 26.8, 26.6,

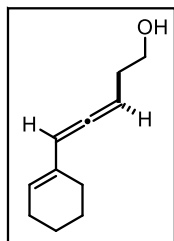
25.8, 17.8, 16.6, 16.1. **HRMS** (ASAP-MS) m/z calculated for $C_{19}H_{30}O$ $[M+H]^+$ 275.2369, measured 275.2365 (1.5 ppm).



ROH Precursor to Compound 5.13. Following method A (11.0 mmol scale),

ROH Precursor to Compound 5.13 was purified on silica gel using a 0-30% hexanes:EtOAc solvent system with increasing 5% increments of EtOAc to provide a yellow oil (1.054 g, 7.0 mmol, 64% yield). **1H NMR** (500 MHz,

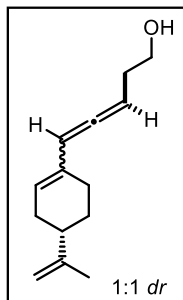
Chloroform- d) δ 6.08 (dt, J = 6.2, 2.9 Hz, 1H), 5.64 (q, J = 2.1 Hz, 1H), 5.36 (dt, J = 10.5, 6.7 Hz, 1H), 3.72 (t, J = 6.2 Hz, 2H), 2.40 (tt, J = 7.4, 2.5 Hz, 2H), 2.30 (dddd, J = 12.8, 9.3, 6.7, 2.6 Hz, 4H), 1.89 (p, J = 7.5 Hz, 2H), 1.71 – 1.66 (s, 1H). **^{13}C NMR** (126 MHz, $CDCl_3$) δ 207.1, 138.1, 128.7, 92.1, 89.3, 62.1, 33.3, 32.7, 32.5, 23.3. **HRMS** (ASAP-MS) m/z calculated for $C_{10}H_{14}O$ $[M+H]^+$ 151.1117, measured 151.1117 (<0.1 ppm).



ROH Precursor to Compound 5.14. Following method A (10.4 mmol scale),

ROH Precursor to Compound 5.14 was purified on silica gel using a 0-30% hexanes:EtOAc solvent system with increasing 5% increments of EtOAc to provide an yellow oil (1.186 g, 7.2 mmol, 69% yield). **1H NMR** (500 MHz,

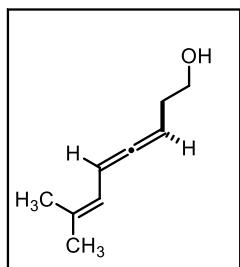
Chloroform- d) δ 5.87 (dt, J = 6.0, 2.9 Hz, 1H), 5.66 (dt, J = 5.3, 2.5 Hz, 1H), 5.39 (tt, J = 7.8, 4.0 Hz, 1H), 3.72 (t, J = 6.3 Hz, 2H), 2.29 (qd, J = 6.4, 2.9 Hz, 2H), 2.13 – 1.94 (m, 4H), 1.68 – 1.55 (m, 5H). **^{13}C NMR** (126 MHz, $CDCl_3$) δ 205.0, 131.9, 126.4, 98.5, 90.6, 62.2, 32.6, 26.0, 25.9, 22.6, 22.5. **HRMS** (ASAP-MS) m/z calculated for $C_{11}H_{16}O$ $[M+H]^+$ 165.1274, measured 165.1275 (0.6 ppm).



ROH Precursor to Compound 5.15. Following method A (12.3 mmol scale),

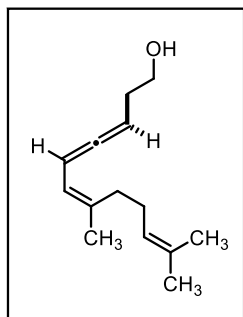
ROH Precursor to Compound 5.15 was purified on silica gel using a 0-30% hexanes:EtOAc solvent system with increasing 5% increments of EtOAc to provide a yellow oil (2.052 g, 10.0 mmol, 82% yield). $^1\text{H NMR}$ (500 MHz, Chloroform-*d*) δ 5.88 (dt, J = 5.5, 2.8 Hz, 1H), 5.70 – 5.64 (m, 1H), 5.39 (tdd, J

= 13.2, 6.6, 1.8 Hz, 1H), 4.74 – 4.69 (m, 2H), 3.72 (t, J = 6.2 Hz, 2H), 2.33 – 2.08 (m, 6H), 2.04 (m, 1H), 1.85 (ddp, J = 12.8, 4.9, 2.3 Hz, 1H), 1.73 (t, J = 1.1 Hz, 3H), 1.63 (s, 1H), 1.49 (dtt, J = 12.7, 11.0, 5.3 Hz, 1H). $^{13}\text{C NMR}$ (126 MHz, CDCl_3) δ 205.2, 205.1, 149.9, 149.8, 131.72, 131.67, 125.74, 125.69, 108.84, 108.83, 98.04, 98.02, 90.7, 90.6, 62.2, 62.1, 41.2, 41.2, 32.63, 32.55, 31.42, 31.40, 27.58, 27.56, 26.4, 26.3, 20.92, 20.91. **HRMS** (ASAP-MS) m/z calculated for $\text{C}_{14}\text{H}_{20}\text{O}$ $[\text{M}+\text{H}]^+$ 205.1587, measured 205.1586 (0.5 ppm).



ROH Precursor to Compound 5.16. Following method A (12.9 mmol scale), **ROH Precursor to Compound 5.16** was purified on silica gel using a 0-30% hexanes:EtOAc solvent system with increasing 5% increments of EtOAc to provide a yellow oil (1.318 g, 9.5 mmol, 74% yield). $^1\text{H NMR}$ (500

MHz, Chloroform-*d*) δ 6.01 (ddd, J = 11.5, 6.3, 3.0 Hz, 1H), 5.59 (dq, J = 10.8, 1.5 Hz, 1H), 5.28 (dd, J = 10.1, 4.2 Hz, 1H), 3.70 (t, J = 6.3 Hz, 2H), 2.27 (qd, J = 6.3, 2.8 Hz, 2H), 1.79 – 1.68 (m, 6H). $^{13}\text{C NMR}$ (126 MHz, CDCl_3) δ 207.5, 134.8, 119.5, 91.3, 88.4, 62.1, 32.4, 26.1, 18.2. **HRMS** (ASAP-MS) m/z calculated for $\text{C}_9\text{H}_{14}\text{O}$ $[\text{M}+\text{H}]^+$ 119.1117, measured 119.1116 (0.7 ppm).

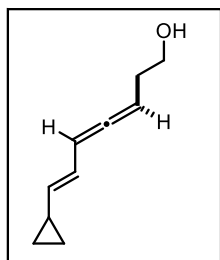


ROH Precursor to Compound 5.17. Following method A (8.8 mmol scale),

ROH Precursor to Compound 5.17 was purified on silica gel using a 0-30% hexanes:EtOAc solvent system with increasing 5% increments of EtOAc to provide a yellow oil (1.196 g, 5.8 mmol, 66% yield). **¹H NMR** (500 MHz, Chloroform-*d*) δ 6.05 (ddt, J = 11.6, 6.0, 2.8 Hz, 1H), 5.61 (dt, J =

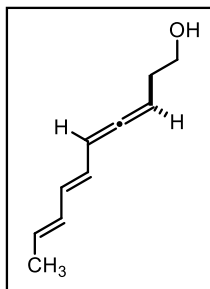
11.0, 1.3 Hz, 1H), 5.30 (q, J = 3.4 Hz, 1H), 5.12 (ddt, J = 8.5, 5.5, 1.4 Hz, 1H), 3.72 (q, J = 5.8 Hz, 2H), 2.29 (qd, J = 6.4, 2.9 Hz, 2H), 2.17 – 2.06 (m, 5H), 1.78 (t, J = 1.5 Hz, 3H), 1.69 (d, J =

1.3 Hz, 3H), 1.63 – 1.60 (m, 3H). **¹³C NMR** (126 MHz, CDCl₃) δ 207.8, 138.7, 132.2, 124.0, 119.9, 91.1, 88.4, 62.1, 32.46, 32.44, 26.8, 25.8, 24.0, 17.8.



HRMS (ASAP-MS) m/z calculated for C₁₄H₂₂O [M+H]⁺ 207.1743, measured 207.1743 (<0.1 ppm).

ROH Precursor to Compound 5.18. Following method A (4.5 mmol scale), **ROH Precursor to Compound 5.18** was purified on silica gel using a 0-30% hexanes:EtOAc solvent system with increasing 5% increments of EtOAc to provide a yellow oil (0.541 g, 3.6 mmol, 80% yield). **¹H NMR** (500 MHz, Chloroform-*d*) δ 5.94 – 5.86 (m, 1H), 5.80 (ddt, J = 10.5, 6.0, 2.8 Hz, 1H), 5.31 (qt, J = 6.6, 1.2 Hz, 1H), 5.19 (ddd, J = 15.0, 8.8, 1.4 Hz, 1H), 3.71 (t, J = 6.2 Hz, 2H), 2.28 (qd, J = 6.3, 2.8 Hz, 2H), 1.58 (bs, 1H), 1.46 – 1.37 (m, 1H), 0.77 – 0.70 (m, 2H), 0.43 – 0.37 (m, 2H). **¹³C NMR** (126 MHz, CDCl₃) δ 206.8, 136.9, 122.9, 94.7, 88.9, 62.1, 32.4, 14.2, 7.3. **HRMS** (ASAP-MS) m/z calculated for C₁₀H₁₄O [M+H]⁺ 151.1117, measured 119.1118 (0.7 ppm).

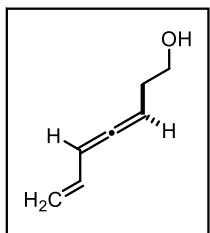


ROH Precursor to Compound 5.19. Following method B (10.0 mmol scale),

ROH Precursor to Compound 5.19 was purified on silica gel using a 0-30% hexanes:EtOAc solvent system with increasing 5% increments of EtOAc to provide an orange oil (0.595 g, 4.0 mmol, 40% yield). **¹H NMR** (500 MHz,

Chloroform-*d*) δ 6.19 – 5.99 (m, 2H), 5.97 – 5.82 (m, 2H), 5.69 (dq, J = 13.9, 6.8 Hz, 1H), 5.39 – 5.32 (m, 1H), 3.71 (t, J = 6.2 Hz, 2H), 2.29 (qd, J = 6.4, 2.5 Hz, 2H), 1.76 (dd, J = 6.8, 1.7 Hz, 3H). **¹³C NMR** (126 MHz, CDCl₃) δ 208.3, 131.7, 131.5, 129.7, 125.5, 95.2, 89.0, 62.1, 32.3, 18.4.

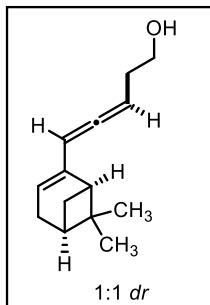
HRMS (ASAP-MS) m/z calculated for C₁₀H₁₄O [M+H]⁺ 151.1117, measured 151.1116 (0.7 ppm).



ROH Precursor to Compound 5.20. Following method A (9.9 mmol scale),

ROH Precursor to Compound 5.20 was purified on silica gel using a 0-30% hexanes:EtOAc solvent system with increasing 5% increments of EtOAc to provide an yellow oil (0.948 g, 8.6 mmol, 87% yield). **¹H NMR** (500 MHz,

Chloroform-*d*) δ 6.16 (dtd, J = 17.1, 10.2, 1.0 Hz, 1H), 5.85 (ddt, J = 10.1, 6.1, 2.9 Hz, 1H), 5.34 (dddd, J = 8.1, 6.7, 5.4, 1.4 Hz, 1H), 5.18 (dq, J = 17.1, 1.1 Hz, 1H), 4.98 (dq, J = 10.1, 1.3 Hz, 1H), 3.72 (t, J = 6.3 Hz, 2H), 2.30 (qd, J = 6.4, 2.9 Hz, 2H), 1.61 (s, 1H). **¹³C NMR** (126 MHz, CDCl₃) δ 208.0, 133.0, 115.9, 95.2, 88.9, 62.0, 32.1. **HRMS** (ASAP-MS) m/z calculated for C₇H₁₀O [M+H]⁺ 111.0804, measured 111.0803 (0.9 ppm).



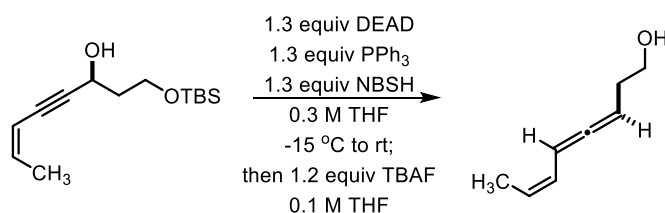
ROH Precursor to Compound 5.21. Following method B (7.1 mmol scale),

ROH Precursor to Compound 5.21 was purified on silica gel using a 0-30% hexanes:EtOAc solvent system with increasing 5% increments of EtOAc to provide a yellow oil (1.028 g, 5.0 mmol, 70% yield). **¹H NMR** (500 MHz,

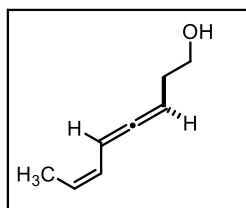
Chloroform-*d*) δ 5.92 (ddt, J = 9.2, 6.3, 3.1 Hz, 1H), 5.51 – 5.45 (m, 1H), 5.40

(dqq, $J = 8.6, 6.4, 2.1$ Hz, 1H), 3.70 (q, $J = 6.2$ Hz, 2H), 2.42 – 2.22 (m, 7H), 2.13 – 2.08 (m, 1H), 1.28 (s, 3H), 1.16 (dd, $J = 8.7, 5.1$ Hz, 1H), 0.81 (d, $J = 2.3$ Hz, 3H). ^{13}C NMR (126 MHz, CDCl_3) δ 205.2, 205.1, 141.94, 141.86, 121.18, 121.16, 97.4, 97.2, 91.01, 90.93, 62.1, 62.0, 42.7, 42.6, 40.99, 40.86, 38.1, 38.0, 32.43, 32.38, 32.1, 32.0, 31.51, 31.46, 26.4, 26.3, 21.00, 20.92. **HRMS** (ASAP-MS) m/z calculated for $\text{C}_{14}\text{H}_{20}\text{O}$ $[\text{M}+\text{H}]^+$ 205.1587, measured 205.1586 (0.5 ppm).

5.9.3. Procedure for (Z)-eneallene substrate:



A portion of THF (0.325 M with respect to DEAD) was used to dissolve PPh_3 and the solution was cooled to -15°C before adding DEAD dropwise. After 10 min, alcohol in THF (0.33 M with respect to ROH) was added to the yellow mixture. After another 10 min, a solution of *o*-nitrobenzenesulfonylhydrazide (NBSH) in THF (0.65 M with respect to NBSH) was added. The temperature was held at -15°C for 1-2 h until starting material was consumed according to TLC analysis. The reaction was warmed to room temperature and the mixture stirred overnight (>8 h). At this point the crude mixture was concentrated and directly purified by SiO_2 column chromatography. The resulting alcohol was immediately deprotected according to method A using TBAF (*vide supra*).

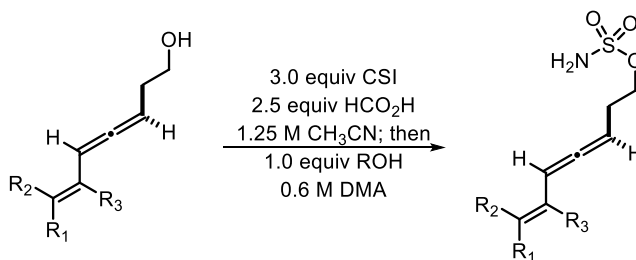


ROH Precursor to Compound 5.5. The Mitsunobu outlined above was conducted twice on 10 mmol scale and purified on silica gel using a 0-15% hexanes:EtOAc solvent system with increasing 5% increments of EtOAc

providing ~4.7 mmol (47% yield) of allene each run. The deprotection was conducted following

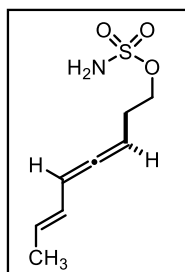
method A (8.4 mmol scale), **ROH Precursor to Compound 5.5** was purified on silica gel using a 0-30% hexanes:EtOAc solvent system with increasing 5% increments of EtOAc to provide a yellow oil (0.463 g, 3.7 mmol, 44% yield). $^1\text{H NMR}$ (500 MHz, Chloroform-*d*) δ 6.10 (dddq, $J = 10.7, 5.9, 2.9, 1.5$ Hz, 1H), 5.80 (tq, $J = 11.0, 1.5$ Hz, 1H), 5.46 (ddt, $J = 10.4, 8.8, 6.2$ Hz, 1H), 5.32 (q, $J = 6.8$ Hz, 1H), 3.70 (tt, $J = 6.3, 1.6$ Hz, 2H), 2.28 (qd, $J = 6.3, 5.3, 2.5$ Hz, 2H), 1.72 (dd, $J = 7.0, 1.6$ Hz, 3H). $^{13}\text{C NMR}$ (126 MHz, CDCl_3) δ 208.3, 125.9, 124.6, 90.0, 88.5, 62.0, 32.2, 13.3. **HRMS** (ASAP-MS) m/z calculated for $\text{C}_8\text{H}_{12}\text{O}$ $[\text{M}+\text{H}]^+$ 125.0961, measured 125.0960 (0.8 ppm).

5.9.4. General procedure for the synthesis of homoallenenic sulfamates:

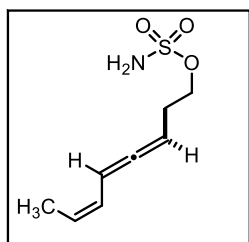


A dry, 3-necked round-bottom flask was equipped with a stirbar and chlorosulfonyl isocyanate (3.0 equiv) was added and cooled to 0 °C. At this temperature, formic acid (2.5 equiv) was added dropwise with vigorous stirring. Gas evolves and the reaction mixture solidified within 5 minutes. Acetonitrile (1.25 M with respect to formic acid) was then added and the solution stirs at 0 °C for 30 min before warming to room temperature for 4-6 hours. At this point the flask was cooled to 0 °C and to the cold solution was added alcohol (1.0 equiv) in *N,N*-dimethylacetamide (0.6 M with respect to alcohol). The solution was warmed to room temperature and the mixture was stirred for 1-2 hours or until starting material was completely consumed according to TLC. The reaction was quenched by the addition of H_2O and the aqueous phase was extracted thrice with ether. The

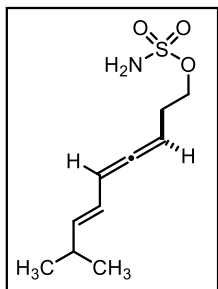
combined organic extracts were then washed with five portions of water, once with brine, then dried over Na_2SO_4 before concentrating under reduced pressure. The crude products were purified by SiO_2 column chromatography using a pentane/ether gradient. The purified sulfamate was dried for 1-2 hours to remove residual solvent before being stored in a $-78\text{ }^\circ\text{C}$ freezer. **NOTE:** The homoallenic sulfamates change color if left under vacuum overnight, so the use of diethyl ether instead of EtOAc for these purifications was critical for fast solvent removal.



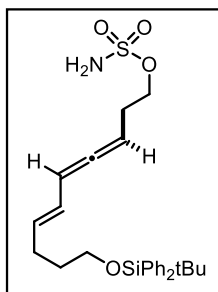
Compound 5.4. Following the general procedure (7.0 mmol scale), **5.4** was purified on silica gel using a 0-100% pentane: Et_2O solvent system with increasing 20% increments of Et_2O to provide an off-white solid upon drying and freezing at $-78\text{ }^\circ\text{C}$ (0.978 g, 4.8 mmol, 69% yield). **^1H NMR** (500 MHz, Chloroform- d) δ 5.88 – 5.80 (m, 2H), 5.70 – 5.61 (m, 1H), 5.33 – 5.27 (m, 1H), 5.02 – 4.93 (s, 2H), 4.25 (td, J = 6.7, 1.1 Hz, 2H), 2.46 (qd, J = 6.6, 2.2 Hz, 2H), 1.74 (dt, J = 7.0, 1.6 Hz, 3H). **^{13}C NMR** (126 MHz, CDCl_3) δ 206.9, 128.4, 126.2, 95.4, 87.2, 70.3, 28.4, 18.2. **HRMS** (ESI-MS) m/z calculated for $\text{C}_8\text{H}_{13}\text{NO}_3\text{S}$ $[\text{M}-\text{H}]^-$ 202.0543, measured 202.0544 (0.5 ppm).



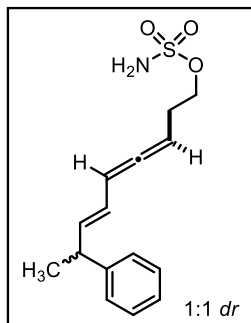
Compound 5.5. Following the general procedure (3.7 mmol scale), **5.5** was purified on silica gel using a 0-100% pentane: Et_2O solvent system with increasing 20% increments of Et_2O to provide a yellow oil that solidified upon storing at $-78\text{ }^\circ\text{C}$ (0.597 g, 2.9 mmol, 79% yield). **^1H NMR** (500 MHz, Chloroform- d) δ 6.14 (ddtd, J = 10.8, 6.1, 2.9, 1.4 Hz, 1H), 5.84 – 5.77 (m, 1H), 5.49 (dddd, J = 10.7, 8.7, 7.0, 5.5 Hz, 1H), 5.32 (ddtd, J = 7.6, 5.1, 2.4, 1.2 Hz, 1H), 4.96 (s, 2H), 4.26 (t, J = 6.7 Hz, 2H), 2.47 (qd, J = 6.6, 2.9 Hz, 2H), 1.72 (dt, J = 7.1, 1.5 Hz, 3H). **^{13}C NMR** (126 MHz, CDCl_3) δ 208.5, 126.5, 124.3, 90.7, 87.0, 70.3, 28.3, 13.3. **HRMS** (ESI-MS) m/z calculated for $\text{C}_8\text{H}_{13}\text{NO}_3\text{S}$ $[\text{M}-\text{H}]^-$ 202.0543, measured 202.0544 (0.5 ppm).



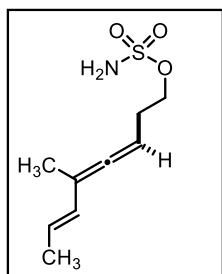
Compound 5.6. Following the general procedure (5.0 mmol scale), **5.6** was purified on silica gel using a 0-100% pentane:Et₂O solvent system with increasing 20% increments of Et₂O to provide a clear, yellow-tinted oil (0.882 g, 3.8 mmol, 76% yield). **¹H NMR** (500 MHz, Chloroform-*d*) δ 5.87 – 5.75 (m, 2H), 5.64 (ddd, *J* = 14.5, 6.6, 1.3 Hz, 1H), 5.30 (q, *J* = 6.4 Hz, 1H), 4.87 (s, 2H), 4.26 (t, *J* = 6.7 Hz, 2H), 2.47 (qd, *J* = 6.6, 2.7 Hz, 2H), 2.34 (dddd, *J* = 13.4, 7.9, 6.8, 5.5 Hz, 1H), 1.00 (d, *J* = 6.7 Hz, 6H). **¹³C NMR** (126 MHz, CDCl₃) δ 207.2, 141.0, 122.1, 95.6, 87.2, 70.3, 31.3, 28.4, 22.38, 22.36. **HRMS** (ESI-MS) *m/z* calculated for C₁₀H₁₇NO₃S [M-H]⁻ 230.0856, measured 230.0858 (0.9 ppm).



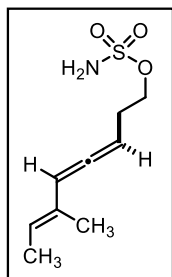
Compound 5.7. Following the general procedure (0.8 mmol scale), **5.7** was purified on silica gel using a 0-100% pentane:Et₂O solvent system with increasing 20% increments of Et₂O to provide a red oil (94.8 mg, 0.2 mmol, 25% yield). **¹H NMR** (500 MHz, Chloroform-*d*) δ 7.68 – 7.65 (m, 4H), 7.45 – 7.35 (m, 6H), 5.86 – 5.79 (m, 2H), 5.67 – 5.58 (m, 1H), 5.35 – 5.28 (m, 1H), 4.64 (bs, 2H), 4.26 (t, *J* = 6.7 Hz, 2H), 3.67 (t, *J* = 6.3 Hz, 2H), 2.47 (qd, *J* = 6.7, 2.3 Hz, 2H), 2.22 – 2.16 (m, 2H), 1.69 – 1.62 (m, 2H), 1.05 (s, 9H). **¹³C NMR** (126 MHz, CDCl₃) δ 207.2, 135.7, 134.2, 133.5, 129.7, 127.8, 125.3, 95.5, 87.2, 70.3, 63.3, 32.2, 29.1, 28.4, 27.0, 19.4. **HRMS** (ESI-MS) *m/z* calculated for C₂₆H₃₅NO₄S [M+Na]⁺ 508.1948, measured 508.1946 (0.4 ppm).



Compound 5.8. Following the general procedure (2.2 mmol scale), **5.8** was purified on silica gel using a 0-100% pentane:Et₂O solvent system with increasing 20% increments of Et₂O to provide a white solid (0.423 g, 1.4 mmol, 66% yield). **¹H NMR** (500 MHz, Chloroform-*d*) δ 7.33 – 7.29 (m, 2H), 7.22 – 7.18 (m, 3H), 5.90 – 5.81 (m, 3H), 5.36 – 5.30 (m, 1H), 4.67 (bs, 2H), 4.26 (q, *J* = 6.5 Hz, 2H), 3.51 (h, *J* = 6.7 Hz, 1H), 2.51 – 2.44 (m, 2H), 1.39 (dd, *J* = 7.0, 2.2 Hz, 3H). **¹³C NMR** (126 MHz, CDCl₃) δ 207.55, 207.54, 145.7, 145.6, 138.15, 138.13, 128.68, 128.65, 127.4, 127.3, 126.41, 126.39, 123.95, 123.90, 95.41, 95.36, 87.39, 87.36, 70.24, 70.18, 42.55, 42.47, 28.4, 28.3, 21.3, 21.2. **HRMS** (ESI-MS) *m/z* calculated for C₁₅H₁₉NO₃S [M+Na]⁺ 316.0978, measured 316.0974 (1.3 ppm).

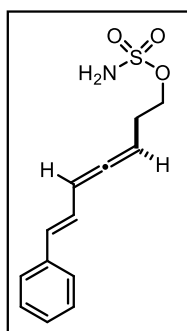


Compound 5.9. Following the general procedure (5.0 mmol scale), **5.9** was purified on silica gel using a 0-100% pentane:Et₂O solvent system with increasing 20% increments of Et₂O to provide a yellow oil (0.225 g, 1.0 mmol, 20% yield). **¹H NMR** (500 MHz, Chloroform-*d*) δ 6.00 – 5.93 (m, 1H), 5.62 – 5.52 (m, 1H), 5.19 (dddd, *J* = 6.4, 5.0, 3.2, 1.5 Hz, 1H), 4.86 (bs, 2H), 4.24 (t, *J* = 6.7 Hz, 2H), 2.44 (q, *J* = 6.6 Hz, 2H), 1.78 (dd, *J* = 7.7, 2.3 Hz, 6H). **¹³C NMR** (126 MHz, CDCl₃) δ 206.8, 129.2, 125.0, 101.5, 85.2, 70.5, 28.6, 18.4, 15.7. **HRMS** (ESI-MS) *m/z* calculated for C₉H₁₅NO₃S [M-H]⁻ 216.0700, measured 216.0701 (0.5 ppm).



Compound 5.10. The sulfamate was characterized over two steps from **OTBS Precursor to Compound 5.10** after being deprotected using method A. Following the general procedure (10.0 mmol scale), **5.10** was purified on silica gel using a 0-100% pentane:Et₂O solvent system with increasing 20% increments of Et₂O to

provide an orange oil (0.629 g, 2.9 mmol, 29% yield over two steps). **¹H NMR** (500 MHz, Chloroform-*d*) δ 5.92 (dt, J = 6.1, 3.0 Hz, 1H), 5.47 (qq, J = 7.0, 1.3 Hz, 1H), 5.42 – 5.36 (m, 1H), 4.81 (s, 2H), 4.27 (t, J = 6.6 Hz, 2H), 2.48 (qdd, J = 6.7, 2.9, 1.1 Hz, 2H), 1.70 (dt, J = 6.9, 1.3 Hz, 3H), 1.69 – 1.66 (m, 3H). **¹³C NMR** (126 MHz, CDCl₃) δ 205.4, 130.3, 124.3, 100.9, 89.0, 70.3, 28.7, 14.1, 13.34. **HRMS** (ESI-MS) m/z calculated for C₉H₁₅NO₃S [M–H][–] 216.0700, measured 216.0701 (0.5 ppm).

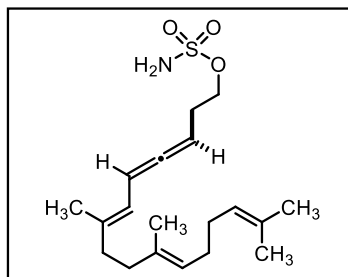


Compound 5.11. The sulfamate was characterized over two steps from **OTBS**

Precursor to Compound 5.11 after being deprotected using method B.

Following the general procedure (2.8 mmol scale), **5.11** was purified on silica gel using a 0-100% pentane:Et₂O solvent system with increasing 20% increments of Et₂O to provide a light yellow solid (0.237 g, 0.9 mmol, 32% yield over two

steps). **¹H NMR** (500 MHz, Chloroform-*d*) δ 7.40 – 7.36 (m, 2H), 7.31 (t, J = 7.7 Hz, 2H), 7.22 (dd, J = 7.8, 5.9 Hz, 1H), 6.64 – 6.44 (m, 2H), 6.06 (ddt, J = 9.4, 6.0, 2.8 Hz, 1H), 5.44 (q, J = 6.5 Hz, 1H), 4.70 (s, 2H), 4.31 (t, J = 6.6 Hz, 2H), 2.53 (qd, J = 6.6, 2.9 Hz, 2H). **¹³C NMR** (126 MHz, CDCl₃) δ 209.0, 137.2, 131.3, 128.8, 127.7, 126.4, 124.4, 96.1, 87.8, 70.2, 28.4. **HRMS** (ESI-MS) m/z calculated for C₁₃H₁₅NO₃S [M–H][–] 264.0700, measured 264.0700 (<0.1 ppm).

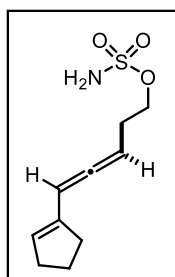


Compound 5.12. Following the general procedure (9.7 mmol scale),

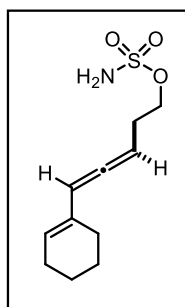
5.12 was purified on silica gel using a 0-100% pentane:Et₂O solvent system with increasing 20% increments of Et₂O to provide a yellow-orange oil (1.944 g, 5.5 mmol, 57% yield).

¹H NMR (500 MHz, Chloroform-*d*) δ 6.07 (ddt, J = 10.8, 6.1, 2.9 Hz, 1H), 5.61 (dt, J = 10.9, 1.3 Hz, 1H), 5.30 (q, J = 4.9 Hz, 1H), 5.09 (qt, J = 7.0, 1.5 Hz, 2H), 4.86 (s, 2H), 4.26 (t, J = 6.7 Hz, 2H), 2.47 (qd, J = 6.7,

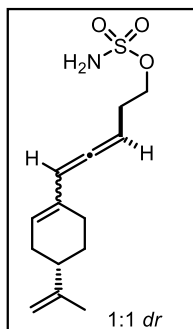
2.9 Hz, 2H), 2.16 – 2.02 (m, 6H), 1.97 (dd, $J = 9.1, 6.1$ Hz, 2H), 1.72 (d, $J = 1.3$ Hz, 3H), 1.68 (d, $J = 1.6$ Hz, 3H), 1.60 (d, $J = 1.4$ Hz, 6H). **^{13}C NMR** (126 MHz, CDCl_3) δ 208.0, 139.1, 135.6, 131.5, 124.5, 123.9, 118.9, 92.0, 86.8, 70.4, 40.1, 39.8, 28.5, 26.8, 26.6, 25.8, 17.8, 16.7, 16.1. **HRMS** (ESI-MS) m/z calculated for $\text{C}_{19}\text{H}_{31}\text{NO}_3\text{S}$ $[\text{M}-\text{H}]^-$ 352.1952, measured 352.1948 (1.1 ppm).



Compound 5.13. Following the general procedure (7.0 mmol scale), **5.13** was purified on silica gel using a 0-100% pentane: Et_2O solvent system with increasing 20% increments of Et_2O to provide a dark red-brown oil (0.474 g, 2.1 mmol, 30% yield). **^1H NMR** (500 MHz, $\text{Chloroform-}d$) δ 6.11 (dt, $J = 6.2, 3.0$ Hz, 1H), 5.67 (q, $J = 2.1$ Hz, 1H), 5.41 – 5.33 (m, 1H), 4.91 (s, 2H), 4.26 (t, $J = 6.7$ Hz, 2H), 2.48 (qd, $J = 6.6, 3.0$ Hz, 2H), 2.41 (ddt, $J = 7.4, 5.0, 2.3$ Hz, 2H), 2.32 (tt, $J = 7.3, 1.8$ Hz, 2H), 1.95 – 1.85 (m, 2H). **^{13}C NMR** (126 MHz, CDCl_3) δ 207.2, 137.9, 129.3, 92.8, 87.8, 70.2, 33.3, 32.7, 28.5, 23.3. **HRMS** (ESI-MS) m/z calculated for $\text{C}_{10}\text{H}_{15}\text{NO}_3\text{S}$ $[\text{M}-\text{H}]^-$ 228.0700, measured 228.0703 (0.5 ppm).

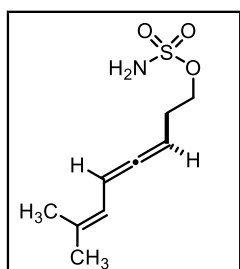


Compound 5.14. Following the general procedure (7.2 mmol scale), **5.14** was purified on silica gel using a 0-100% pentane: Et_2O solvent system with increasing 20% increments of Et_2O to provide an orange oil (1.293 g, 5.3 mmol, 74% yield). **^1H NMR** (500 MHz, $\text{Chloroform-}d$) δ 5.89 (dd, $J = 6.3, 3.1$ Hz, 1H), 5.68 (dq, $J = 4.6, 2.0$ Hz, 1H), 5.41 – 5.35 (m, 1H), 4.86 (s, 2H), 4.26 (dd, $J = 8.0, 5.4$ Hz, 2H), 2.47 (qq, $J = 6.9, 2.3$ Hz, 2H), 2.10 (dtq, $J = 6.5, 4.6, 2.2$ Hz, 2H), 2.00 (ddt, $J = 7.1, 4.9, 2.7$ Hz, 2H), 1.69 – 1.55 (m, 4H). **^{13}C NMR** (126 MHz, CDCl_3) δ 205.1, 131.9, 127.0, 99.3, 89.0, 70.3, 28.6, 26.0, 25.8, 22.6, 22.5. **HRMS** (ESI-MS) m/z calculated for $\text{C}_{11}\text{H}_{17}\text{NO}_3\text{S}$ $[\text{M}-\text{H}]^-$ 242.0856, measured 242.0858 (0.8 ppm).



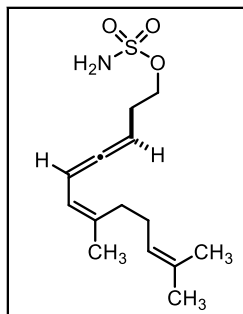
Compound 5.15. Following the general procedure (10.0 mmol scale), **5.15** was purified on silica gel using a 0-100% pentane:Et₂O solvent system with increasing 20% increments of Et₂O to provide an orange oil that becomes solid after storing at -78 °C (1.921 g, 6.8 mmol, 68% yield). **¹H NMR** (500 MHz, Chloroform-*d*) δ 5.91 (dt, *J* = 6.4, 3.0 Hz, 1H), 5.69 (d, *J* = 5.1 Hz, 1H), 5.39 (dq,

J = 13.4, 6.6 Hz, 1H), 4.94 – 4.77 (m, 2H), 4.75 – 4.70 (m, 2H), 4.26 (tt, *J* = 6.6, 2.0 Hz, 2H), 2.48 (ddt, *J* = 7.2, 5.0, 2.7 Hz, 2H), 2.28 – 2.11 (m, 3H), 2.10 – 1.99 (m, 2H), 1.89 – 1.82 (m, 1H), 1.74 (s, 3H), 1.55 – 1.43 (m, 1H). **¹³C NMR** (126 MHz, CDCl₃) δ 205.33, 205.29, 149.80, 149.77, 131.60, 131.58, 126.26, 126.25, 108.91, 108.90, 98.78, 98.77, 89.10, 89.09, 70.30, 70.26, 41.17, 41.16, 31.41, 31.40, 28.67, 28.65, 28.61, 27.5, 26.3, 26.2, 20.94, 20.93. **HRMS** (ESI-MS) *m/z* calculated for C₁₄H₂₁NO₃S [M-H]⁻ 282.1169, measured 282.1168 (0.4 ppm).



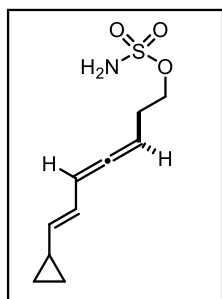
Compound 5.16. Following the general procedure (11.3 mmol scale), **5.16** was purified on silica gel using a 0-100% pentane:Et₂O solvent system with increasing 20% increments of Et₂O to provide a yellow oil that solidifies upon storage at -78 °C (1.406 g, 6.5 mmol, 58% yield). **¹H NMR** (500 MHz,

Chloroform-*d*) δ 6.04 (ddt, *J* = 11.7, 6.1, 2.9 Hz, 1H), 5.59 (dq, *J* = 10.9, 1.4 Hz, 1H), 5.33 – 5.25 (m, 1H), 5.03 (s, 2H), 4.25 (t, *J* = 6.7 Hz, 2H), 2.45 (qd, *J* = 6.7, 2.9 Hz, 2H), 1.77 (d, *J* = 1.6 Hz, 3H), 1.71 (s, 3H). **¹³C NMR** (126 MHz, CDCl₃) δ 207.7, 135.4, 119.1, 91.9, 86.8, 70.4, 28.5, 26.1, 18.2. **HRMS** (ESI-MS) *m/z* calculated for C₉H₁₅NO₃S [M-H]⁻ 216.0700, measured 216.0700 (<0.1 ppm).



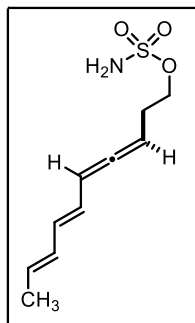
Compound 5.17. Following the general procedure (3.6 mmol scale), **5.17** was purified on silica gel using a 0-100% pentane:Et₂O solvent system with increasing 20% increments of Et₂O to provide a yellow-orange oil (0.542 g, 1.9 mmol, 53% yield). **¹H NMR** (500 MHz, Chloroform-*d*) δ 6.07 (ddt, *J* = 11.6, 6.1, 2.9 Hz, 1H), 5.65 – 5.58 (m, 1H), 5.30 (dd, *J* = 7.8, 5.2 Hz, 1H),

5.11 (tdd, *J* = 7.2, 3.1, 1.5 Hz, 1H), 4.77 (s, 2H), 4.27 (t, *J* = 6.7 Hz, 2H), 2.47 (qd, *J* = 6.6, 2.9 Hz, 2H), 2.16 – 2.06 (m, 4H), 1.78 (d, *J* = 1.5 Hz, 3H), 1.69 (s, 3H), 1.61 (d, *J* = 1.2 Hz, 3H). **¹³C NMR** (126 MHz, CDCl₃) δ 207.9, 139.3, 132.3, 123.9, 119.6, 91.8, 86.8, 70.4, 32.4, 28.5, 26.8, 25.9, 24.0, 17.8. **HRMS** (ESI-MS) *m/z* calculated for C₁₄H₂₃NO₃S [M-H]⁻ 284.1326, measured 284.1324 (0.7 ppm).

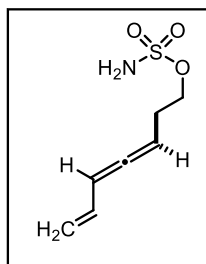


Compound 5.18. Following the general procedure (4.5 mmol scale), **5.18** was purified on silica gel using a 0-100% pentane:Et₂O solvent system with increasing 20% increments of Et₂O to provide a white solid after drying and storing at -78 °C (0.485 g, 2.1 mmol, 47% yield). **¹H NMR** (500 MHz, Chloroform-*d*) δ 5.89 (dd, *J* = 14.8, 10.4 Hz, 1H), 5.82 (ddd, *J* = 10.4, 6.0, 2.9

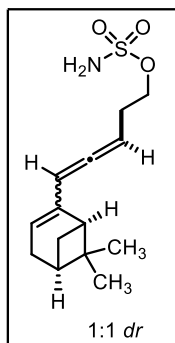
Hz, 1H), 5.34 – 5.30 (m, 1H), 5.20 (ddd, *J* = 14.8, 9.0, 1.3 Hz, 1H), 4.88 (bs, 2H), 4.26 (t, *J* = 6.7 Hz, 2H), 2.46 (qd, *J* = 6.6, 2.9 Hz, 2H), 1.42 (qt, *J* = 8.5, 4.8 Hz, 1H), 0.74 (ddd, *J* = 9.4, 3.7, 2.8 Hz, 2H), 0.41 (tq, *J* = 4.7, 2.2 Hz, 2H). **¹³C NMR** (126 MHz, CDCl₃) δ 206.9, 137.5, 122.5, 95.4, 87.3, 70.3, 28.4, 14.2, 7.4. **HRMS** (ESI-MS) *m/z* calculated for C₁₀H₁₅NO₃S [M+Na]⁺ 252.0665, measured 252.0663 (0.8 ppm).



Compound 5.19. Following the general procedure (4.0 mmol scale), **5.19** was purified on silica gel using a 0-100% pentane:Et₂O solvent system with increasing 20% increments of Et₂O to provide a yellow oil that solidified upon storing at -78 °C (0.219 g, 0.96 mmol, 24% yield). **¹H NMR** (500 MHz, Chloroform-*d*) δ 6.20 – 6.12 (m, 1H), 6.07 (dddd, *J* = 14.9, 13.3, 3.9, 2.2 Hz, 1H), 5.92 – 5.86 (m, 2H), 5.71 (dq, *J* = 13.9, 6.8 Hz, 1H), 5.36 (q, *J* = 6.5, 5.9 Hz, 1H), 4.67 (s, 2H), 4.27 (t, *J* = 6.7 Hz, 2H), 2.48 (qd, *J* = 6.7, 2.4 Hz, 2H), 1.77 (dd, *J* = 6.6, 1.6 Hz, 3H). **¹³C NMR** (126 MHz, CDCl₃) δ 208.4, 132.2, 131.4, 130.2, 125.0, 96.0, 87.6, 70.2, 28.3, 18.4. **HRMS** (ESI-MS) *m/z* calculated for C₁₀H₁₅NO₃S [M-H]⁻ 228.0700, measured 228.0702 (0.9 ppm).



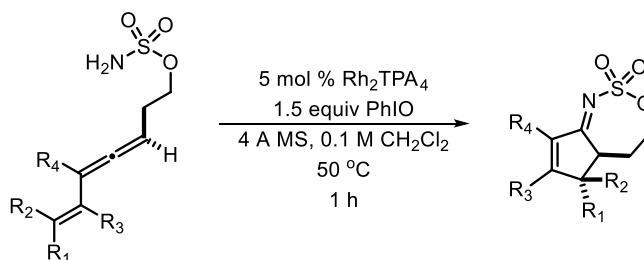
Compound 5.20. Following the general procedure (8.6 mmol scale), **5.20** was purified on silica gel using a 0-100% pentane:Et₂O solvent system with increasing 20% increments of Et₂O to provide a light-yellow oil (0.993 g, 5.2 mmol, 60% yield). **¹H NMR** (500 MHz, Chloroform-*d*) δ 6.16 (dtd, *J* = 17.1, 10.3, 1.0 Hz, 1H), 5.88 (ddt, *J* = 9.7, 6.1, 2.9 Hz, 1H), 5.34 (dddd, *J* = 7.8, 6.4, 5.2, 1.4 Hz, 1H), 5.23 – 5.18 (m, 1H), 5.05 – 4.99 (m, 1H), 4.98 (s, 2H), 4.26 (t, *J* = 6.6 Hz, 2H), 2.48 (qd, *J* = 6.6, 2.9 Hz, 2H). **¹³C NMR** (126 MHz, CDCl₃) δ 208.1, 132.7, 116.5, 96.0, 87.5, 70.1, 28.1. **HRMS** (ESI-MS) *m/z* calculated for C₇H₁₁NO₃S [M-H]⁻ 188.0387, measured 188.0387 (<0.1 ppm).



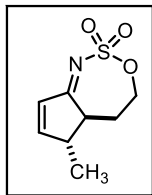
Compound 5.21. Following the general procedure (5.0 mmol scale), **5.21** was purified on silica gel using a 0-100% pentane:Et₂O solvent system with increasing 20% increments of Et₂O to provide an orange oil (0.620 g, 2.2 mmol, 44% yield). **¹H NMR** (500 MHz, Chloroform-*d*) δ 5.94 (dq, *J* = 6.4, 3.2 Hz, 1H), 5.50 (td, *J* = 3.5, 1.7 Hz, 1H), 5.43 – 5.35 (m, 1H), 4.82 (s, 2H), 4.27 – 4.20 (m, 2H), 2.47 (ddt,

$J = 9.6, 6.6, 2.9$ Hz, 2H), 2.40 (ddq, $J = 11.1, 5.5, 3.3, 2.8$ Hz, 1H), 2.36 – 2.25 (m, 3H), 2.11 (tdd, $J = 5.9, 4.2, 2.8$ Hz, 1H), 1.29 (d, $J = 1.9$ Hz, 3H), 1.15 (dd, $J = 8.8, 4.0$ Hz, 1H), 0.81 (d, $J = 7.2$ Hz, 3H). **^{13}C NMR** (126 MHz, CDCl_3) δ 205.5, 205.4, 141.8, 141.6, 121.74, 121.71, 98.1, 97.9, 89.4, 89.3, 70.4, 70.3, 42.7, 42.6, 40.9, 40.8, 38.04, 37.99, 32.06, 32.05, 31.6, 31.5, 28.58, 28.55, 26.4, 26.3, 20.99, 20.98. **HRMS** (ESI-MS) m/z calculated for $\text{C}_{14}\text{H}_{21}\text{NO}_3\text{S}$ $[\text{M}-\text{H}]^-$ 282.1169, measured 282.1169 (<0.1 ppm).

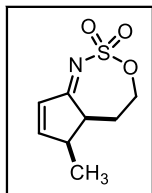
5.9.5. Procedure for eneallene aziridination/electrocyclization:



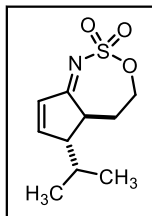
A dry round-bottom flask equipped with a stir bar was charged with 4 Å molecular sieves before adding Rh_2TPA_4 (5 mol %, 0.05 equiv) and homoallenic sulfamate (1.0 equiv) using anhydrous CH_2Cl_2 (0.1 M) to transfer quantitatively. The solution was placed in an oil bath preheated to 50 °C and stirred vigorously. As soon as boiling starts, PhIO (1.5 equiv) was added in a single portion and the reaction was fit with a reflux condenser and stirred for 1 h at which point all allene is consumed by ^1H NMR analysis of reaction aliquots or TLC. The reaction was cooled to room temperature, diluted with CH_2Cl_2 , and filtered over a fritted funnel. The filtrate was concentrated under reduced pressure and the crude mixture was purified by SiO_2 column chromatography using a gradient of either hexanes/EtOAc or pentane/Et₂O.



Compound 5.4a. Following the general procedure (0.3 mmol scale), **5.4a** was purified on silica gel using a 0-60% hexanes:EtOAc solvent system with increasing 10% increments of EtOAc to provide a light-yellow oil (38.2 mg, 0.19 mmol, 63% yield, >19:1 *dr*). **¹H NMR** (500 MHz, Chloroform-*d*) δ 7.33 (dd, J = 5.5, 2.3 Hz, 1H), 6.29 (dd, J = 5.5, 2.0 Hz, 1H), 4.73 – 4.66 (m, 1H), 4.50 (dt, J = 12.0, 3.9 Hz, 1H), 2.99 (ddd, J = 10.4, 6.1, 2.3 Hz, 1H), 2.80 (dddd, J = 9.5, 7.3, 5.0, 2.2 Hz, 1H), 2.08 (ddd, J = 10.4, 7.7, 4.2 Hz, 2H), 1.28 (d, J = 7.2 Hz, 3H). **¹³C NMR** (126 MHz, CDCl₃) δ 193.2, 167.1, 132.9, 71.3, 52.2, 47.8, 29.6, 18.1. **HRMS** (ESI-MS) m/z calculated for C₈H₁₁NO₃S [M+H]⁺ 202.0532, measured 202.0530 (1.0 ppm).

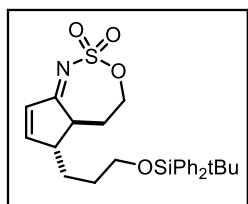


Compound 5.5a. Following the general procedure (0.5 mmol scale), **5.5a** was purified on silica gel using a 0-60% hexanes:EtOAc solvent system with increasing 10% increments of EtOAc to provide a yellow solid (35.9 mg, 0.18 mmol, 36% yield, 2.4:1 *syn:anti*). **Major (*syn*) diastereomer** **¹H NMR** (500 MHz, Chloroform-*d*) δ 7.43 (dd, J = 5.5, 2.7 Hz, 1H), 6.32 (dd, J = 5.5, 1.9 Hz, 1H), 4.64 (dd, J = 11.2, 4.2 Hz, 1H), 4.57 – 4.52 (m, 1H), 3.52 (ddd, J = 11.0, 6.0, 4.0 Hz, 1H), 3.38 – 3.31 (m, 1H), 2.03 – 1.95 (m, 2H), 1.14 (d, J = 7.5 Hz, 3H). **¹³C NMR** (126 MHz, CDCl₃) δ 193.8, 168.6, 132.5, 71.2, 46.7, 43.2, 26.4, 15.7. **HRMS** (ESI-MS) m/z calculated for C₈H₁₁NO₃S [M+H]⁺ 202.0532, measured 202.0531 (1.4 ppm). **NOTE:** the minor (*anti*) diastereomer is characterized as compound **5.4a**.



Compound 5.6a. Following the general procedure (3.26 mmol scale), **5.6a** was purified on silica gel using a 0-60% hexanes:EtOAc solvent system with increasing 10% increments of EtOAc to provide a light-brown oil (0.553 g, 2.4 mmol, 74% yield, >19:1 *dr*). **¹H NMR** (500 MHz, Chloroform-*d*) δ 7.44 (dd, J = 5.6, 2.4 Hz, 1H), 6.32 (dd, J

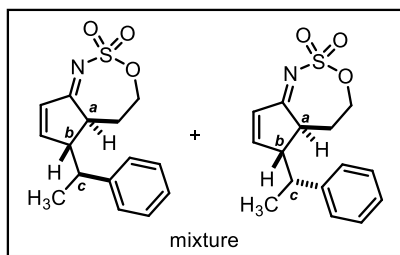
= 5.6, 2.0 Hz, 1H), 4.70 (td, J = 11.8, 3.7 Hz, 1H), 4.46 (ddd, J = 12.0, 4.9, 2.5 Hz, 1H), 3.20 (ddd, J = 11.8, 3.6, 2.1 Hz, 1H), 2.59 (dq, J = 6.4, 2.1 Hz, 1H), 2.11 – 1.97 (m, 2H), 1.87 (dp, J = 13.5, 6.7 Hz, 1H), 1.00 (dd, J = 10.8, 6.8 Hz, 6H). **^{13}C NMR** (126 MHz, CDCl_3) δ 193.7, 165.4, 133.6, 71.1, 59.6, 47.4, 31.3, 30.7, 20.5, 20.0. **HRMS** (ESI-MS) m/z calculated for $\text{C}_{10}\text{H}_{15}\text{NO}_3\text{S}$ $[\text{M}+\text{H}]^+$ 230.0845, measured 230.0844 (0.4 ppm).



Compound 5.7a. Following the general procedure (0.195 mmol scale), **5.7a**

was purified on silica gel using a 0-60% hexanes:EtOAc solvent system with increasing 10% increments of EtOAc to provide a yellow oil (61.2 mg, 0.127

mmol, 65% yield, $dr >19:1$ *anti:syn*). **^1H NMR** (500 MHz, Chloroform- d) δ 7.65 (dt, J = 6.7, 1.6 Hz, 4H), 7.46 – 7.37 (m, 6H), 7.34 (dd, J = 5.6, 2.3 Hz, 1H), 6.28 (dd, J = 5.5, 2.0 Hz, 1H), 4.65 (td, J = 11.9, 3.5 Hz, 1H), 4.45 (ddd, J = 12.0, 5.0, 2.3 Hz, 1H), 3.73 – 3.68 (m, 2H), 3.04 (ddd, J = 12.1, 3.4, 2.1 Hz, 1H), 2.71 (ddq, J = 6.8, 4.6, 2.4 Hz, 1H), 2.02 – 1.91 (m, 2H), 1.64 (ddq, J = 12.2, 6.2, 3.8, 2.9 Hz, 4H), 1.06 (s, 9H). **^{13}C NMR** (126 MHz, CDCl_3) δ 193.2, 166.0, 135.7, 133.8, 133.2, 129.9, 127.9, 71.1, 63.4, 52.7, 50.2, 30.3, 30.1, 29.8, 27.0, 19.3. **HRMS** (ESI-MS) m/z calculated for $\text{C}_{26}\text{H}_{33}\text{NO}_4\text{SSi}$ $[\text{M}+\text{H}]^+$ 484.1972, measured 484.1968 (0.8 ppm).

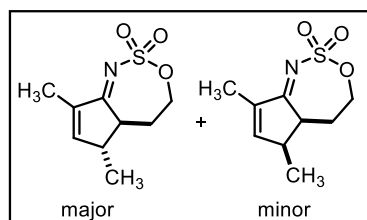


Compound 5.8a. Following the general procedure (0.259 mmol

scale), **5.8a** was purified on silica gel using a 0-60% hexanes:EtOAc solvent system with increasing 10% increments of EtOAc to provide a yellow oily solid (55.2 mg, 0.189 mmol,

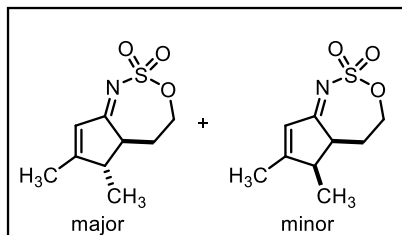
73% yield, $dr_{a,b} >19:1$ *anti:syn* and $dr_{ab,c} = 1.2:1$). **^1H NMR** (500 MHz, Chloroform- d) δ 7.58 (dd, J = 5.6, 2.3 Hz, 1H), 7.35 (td, J = 7.7, 2.2 Hz, 4H), 7.29 – 7.23 (m, 4H), 7.21 – 7.16 (m, 3H), 6.36 (dd, J = 5.6, 2.0 Hz, 1H), 6.26 (d, J = 5.6 Hz, 1H), 4.55 (td, J = 12.1, 3.3 Hz, 1H), 4.38 (ddd, J =

12.0, 5.1, 2.2 Hz, 1H), 4.18 – 4.09 (m, 2H), 3.23 (dd, $J = 12.5, 2.9$ Hz, 1H), 3.08 (dt, $J = 12.2, 2.6$ Hz, 1H), 2.99 – 2.93 (m, 2H), 2.84 (dq, $J = 9.9, 2.2$ Hz, 1H), 2.79 – 2.69 (m, 1H), 2.04 – 1.96 (m, 2H), 1.81 (ddt, $J = 14.6, 11.6, 5.9$ Hz, 1H), 1.70 (dq, $J = 14.9, 2.9$ Hz, 1H), 1.45 (d, $J = 6.8$ Hz, 3H), 1.36 (d, $J = 5.1$ Hz, 3H). **^{13}C NMR** (126 MHz, CDCl_3) δ 193.2, 192.6, 165.5, 164.3, 143.9, 143.2, 134.0, 133.4, 129.1, 129.0, 127.5, 127.3, 127.14, 127.05, 70.8, 60.0, 59.4, 49.2, 47.6, 44.1, 43.1, 30.5, 29.8, 19.1, 18.5. **HRMS** (ESI-MS) m/z calculated for $\text{C}_{15}\text{H}_{17}\text{NO}_3\text{S}$ $[\text{M}+\text{H}]^+$ 292.1002, measured 292.0999 (1.0 ppm). **NOTE:** Relative stereochemistry of the major diastereomers was determined by analogy to other substrates with nOe data and by comparing coupling constants. $J_{a,b} = 2\text{--}3$ Hz is consistent with *anti* cyclopentene while $J_{a,b} = 6\text{--}8$ Hz for *syn* cyclopentene.



Compound 5.9a. Following the general procedure (0.32 mmol scale), **5.9a** was purified on silica gel using a 0–60% hexanes:EtOAc solvent system with increasing 10% increments of

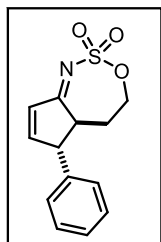
EtOAc to provide a light-yellow oil (44.4 mg, 0.21 mmol, 65% yield, $dr = 4.1:1$ *anti:syn*). **Major (*anti*) diastereomer** **^1H NMR** (500 MHz, Chloroform- d) δ 7.01 (s, 1H), 4.67 (qd, $J = 10.7, 10.1, 5.3$ Hz, 1H), 4.55 – 4.43 (m, 1H), 3.01 – 2.95 (m, 1H), 2.63 (dtt, $J = 9.7, 5.0, 2.4$ Hz, 1H), 2.08 – 2.01 (m, 2H), 1.83 (q, $J = 2.3, 1.8$ Hz, 3H), 1.21 (d, $J = 7.3$ Hz, 3H). **^{13}C NMR** (126 MHz, CDCl_3) δ 192.1, 161.2, 139.6, 70.3, 51.5, 43.9, 28.5, 17.1, 10.35. **Minor (*syn*) diastereomer** **^1H NMR** (500 MHz, Chloroform- d) δ 7.10 (d, $J = 2.8$ Hz, 1H), 4.65 – 4.60 (m, 1H), 4.52 (dt, $J = 9.6, 2.9$ Hz, 1H), 3.52 (dt, $J = 10.9, 5.3$ Hz, 1H), 3.20 – 3.15 (m, 1H), 2.03 (d, $J = 3.5$ Hz, 2H), 1.83 (s, 3H), 1.08 (d, $J = 7.4$ Hz, 3H). **^{13}C NMR** (126 MHz, CDCl_3) δ 192.4, 162.4, 139.2, 70.1, 46.0, 39.3, 25.4, 14.9, 10.38. **HRMS** (ESI-MS) m/z calculated for $\text{C}_9\text{H}_{13}\text{NO}_3\text{S}$ $[\text{M}+\text{H}]^+$ 216.0689, measured 216.0687 (0.9 ppm).



Compound 5.10a. Following the general procedure (0.5 mmol scale), **5.10a** was purified on silica gel using a 0-60% hexanes:EtOAc solvent system with increasing 10% increments of EtOAc to provide a yellow-brown oil (45.9 mg, 0.21 mmol,

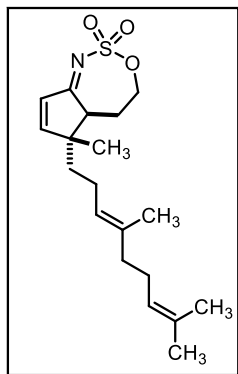
46% yield, 2.0:1 *anti:syn*). **NOTE:** Using 1 mol % Rh₂TPA₄ seemed to improve the *dr* to 3.9:1.

Major (Anti) diastereomer ¹H NMR (500 MHz, Chloroform-*d*) δ 6.02 (t, *J* = 1.5 Hz, 1H), 4.66 (ddd, *J* = 11.8, 9.1, 6.8 Hz, 1H), 4.44 (dt, *J* = 12.0, 3.8 Hz, 1H), 3.04 (ddd, *J* = 8.6, 6.7, 2.4 Hz, 1H), 2.59 (tdd, *J* = 8.9, 4.8, 1.9 Hz, 1H), 2.10 (d, *J* = 1.3 Hz, 3H), 2.05 – 2.00 (m, 2H), 1.24 (d, *J* = 7.4 Hz, 3H). **Minor (Syn) diastereomer ¹H NMR** (500 MHz, Chloroform-*d*) δ 6.07 (t, *J* = 1.5 Hz, 1H), 4.63 – 4.55 (m, 1H), 4.49 (dt, *J* = 11.9, 3.8 Hz, 1H), 3.54 (dt, *J* = 8.6, 6.3 Hz, 1H), 3.12 (p, *J* = 7.4 Hz, 1H), 2.13 (s, 3H), 1.98 – 1.93 (m, 2H), 1.12 (d, *J* = 7.5 Hz, 3H). **Mixed ¹³C NMR** (126 MHz, CDCl₃) δ 193.4, 192.7, 182.9, 181.8, 129.3, 129.2, 71.2, 70.8, 53.1, 50.2, 47.7, 45.9, 30.0, 26.5, 17.7, 17.2, 16.8, 14.8. **HRMS** (ESI-MS) *m/z* calculated for C₉H₁₃NO₃S [M+H]⁺ 216.0689, measured 216.0688 (0.5 ppm).



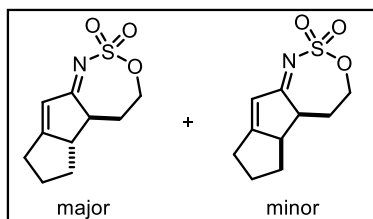
Compound 5.11a. Following the general procedure (0.2 mmol scale), **5.11a** was purified on silica gel using a 0-60% hexanes:EtOAc solvent system with increasing 10% increments of EtOAc to provide a light-yellow oil (19.0 mg, 0.072 mmol, 36% yield, >19:1 *anti:syn*). **¹H NMR** (500 MHz, Chloroform-*d*) δ 7.42 – 7.32 (m, 4H),

7.15 (dd, *J* = 6.9, 1.8 Hz, 2H), 6.49 (dd, *J* = 5.5, 2.2 Hz, 1H), 4.56 (td, *J* = 11.6, 4.3 Hz, 1H), 4.48 (ddd, *J* = 12.0, 5.1, 2.5 Hz, 1H), 3.87 (q, *J* = 2.5 Hz, 1H), 3.33 – 3.27 (m, 1H), 2.29 – 2.17 (m, 2H). **¹³C NMR** (126 MHz, CDCl₃) δ 192.4, 164.1, 138.9, 134.1, 129.5, 128.4, 127.3, 71.0, 58.3, 54.0, 29.5. **HRMS** (ESI-MS) *m/z* calculated for C₁₃H₁₃NO₃S [M+H]⁺ 262.0543, measured 262.0543 (<0.1 ppm).



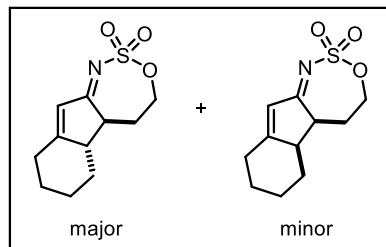
Compound 5.12a. Following the general procedure (0.5 mmol scale), **5.12a** was purified on silica gel using a 0-60% hexanes:EtOAc solvent system with increasing 10% increments of EtOAc to provide a yellow solid (56.2 mg, 0.16 mmol, 31% yield, >19:1 *anti:syn*). **¹H NMR** (500 MHz, Chloroform-*d*) δ 7.29 (d, J = 5.5 Hz, 1H), 6.24 (d, J = 5.6 Hz, 1H), 5.07 (qdt, J = 5.3, 2.7, 1.4 Hz, 2H), 4.59 – 4.51 (m, 2H), 3.14 (dd, J = 12.3, 2.7 Hz, 1H), 2.17 – 2.02 (m, 4H),

2.00 – 1.88 (m, 4H), 1.68 (d, J = 1.5 Hz, 3H), 1.57 (m, 8H), 1.11 (s, 3H). **¹³C NMR** (126 MHz, CDCl₃) δ 192.2, 171.2, 136.7, 131.8, 131.1, 124.2, 123.1, 70.8, 52.2, 52.0, 40.0, 39.8, 26.8, 26.7, 25.9, 23.5, 22.6, 17.8, 16.3. **HRMS** (ESI-MS) m/z calculated for C₁₉H₂₉NO₃S [M+H]⁺ 352.1941, measured 352.1936 (1.4 ppm).



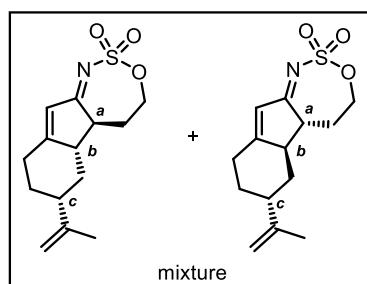
Compound 5.13a. Following the general procedure (0.21 mmol scale), **5.13a** was purified on silica gel using a 0-60% hexanes:EtOAc solvent system with increasing 10% increments of

EtOAc to provide an off-white solid (28.9 mg, 0.13 mmol, 62% yield, 13.7:1 *anti:syn*). **Major (Anti) diastereomer** **¹H NMR** (500 MHz, Chloroform-*d*) δ 6.05 (d, J = 1.9 Hz, 1H), 4.61 (td, J = 12.1, 3.3 Hz, 1H), 4.46 (ddd, J = 11.9, 5.0, 2.1 Hz, 1H), 3.11 (dt, J = 12.3, 3.1 Hz, 1H), 2.90 – 2.83 (m, 1H), 2.61 (m, 2H), 2.24 – 2.07 (m, 4H), 1.35 – 1.24 (m, 2H). **¹³C NMR** (126 MHz, CDCl₃) δ 195.4, 190.6, 124.5, 70.4, 58.5, 50.9, 30.8, 29.7, 26.6, 26.4. **HRMS** (ESI-MS) m/z calculated for C₁₀H₁₃NO₃S [M+H]⁺ 228.0688, measured 228.0683 (2.2 ppm).



Compound 5.14a. Following the general procedure (0.5 mmol scale), **5.14a** was purified on silica gel using a 0-60% hexanes:EtOAc solvent system with increasing 10% increments of EtOAc to provide an off-white solid (89.8 mg, 0.37 mmol, 74%

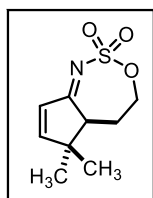
yield, 3.0:1 *anti:syn*). Characterized as the mixture of diastereomers before isolating and characterizing pure *anti*-**5.14a**. **Mix 5.14a** ^1H NMR (500 MHz, Chloroform-*d*) δ 6.02 (m, 1H), 4.75 – 4.60 (m, 1H), 4.47 (m, 1H), 3.63 – 3.06 (m, 1H), 2.99 – 2.82 (m, 1H), 2.45 – 2.21 (m, 3H), 2.10 – 1.99 (m, 3H), 1.96 – 1.87 (m, 1H), 1.53 – 1.32 (m, 2H), 1.28 – 1.14 (m, 1H). ^{13}C NMR (126 MHz, CDCl_3) δ 194.1, 193.0, 185.0, 183.6, 126.3, 126.0, 71.2, 71.0, 53.0, 51.8, 48.5, 47.0, 33.30, 33.29, 31.3, 30.9, 30.3, 27.3, 26.5, 26.1, 25.1, 24.9. **Compound anti-5.14a.** ^1H NMR (500 MHz, Chloroform-*d*) δ 6.00 (d, $J = 1.8$ Hz, 1H), 4.74 – 4.65 (m, 1H), 4.45 (dt, $J = 12.1, 3.9$ Hz, 1H), 3.13 – 3.05 (m, 1H), 2.84 (ddt, $J = 14.0, 3.9, 1.9$ Hz, 1H), 2.45 – 2.38 (m, 1H), 2.33 – 2.20 (m, 2H), 2.08 – 1.99 (m, 3H), 1.94 – 1.87 (m, 1H), 1.51 – 1.32 (m, 2H), 1.23 – 1.17 (m, 1H). ^{13}C NMR (126 MHz, CDCl_3) δ 193.0, 183.6, 126.3, 71.2, 53.0, 51.8, 33.3, 30.9, 30.3, 26.5, 24.9. **HRMS** (ESI-MS) m/z calculated for $\text{C}_{11}\text{H}_{15}\text{NO}_3\text{S}$ $[\text{M}+\text{H}]^+$ 242.0845, measured 228.0843 (0.8 ppm).



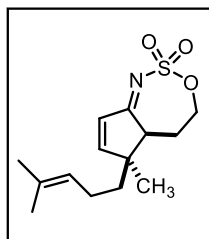
Compound 5.15a. Following the general procedure (0.5 mmol scale), **5.15a** was purified on silica gel using a 0-60% hexanes:EtOAc solvent system with increasing 10% increments of EtOAc to provide a light-brown oil (108.2 mg, 0.385 mmol, 77%

yield, $dr_{a,b} > 19:1$ *anti:syn* and $dr_{ab,c} = 1.2:1$). Characterized as a mixture of diastereomers. ^1H NMR (500 MHz, Chloroform-*d*) δ 6.03 (dt, $J = 3.5, 1.7$ Hz, 1H), 5.99 (d, $J = 1.7$ Hz, 1H), 5.03 (q, $J = 1.5$ Hz, 1H), 4.89 (s, 1H), 4.76 (p, $J = 1.5$ Hz, 1H), 4.73 – 4.66 (m, 3H), 4.45 (dddd, $J = 12.2,$

5.8, 4.8, 2.6 Hz, 2H), 3.11 (ddt, $J = 7.8, 5.6, 2.4$ Hz, 1H), 3.06 (dt, $J = 11.7, 3.0$ Hz, 1H), 2.90 (ddd, $J = 14.3, 4.3, 2.2$ Hz, 1H), 2.68 (ddd, $J = 14.5, 4.6, 2.6$ Hz, 1H), 2.62 – 2.46 (m, 5H), 2.42 – 2.28 (m, 2H), 2.27 – 2.15 (m, 2H), 2.09 – 2.05 (m, 1H), 2.03 – 1.93 (m, 4H), 1.80 (d, $J = 3.4$ Hz, 3H), 1.74 – 1.72 (m, 3H), 1.68 – 1.61 (m, 1H), 1.46 (td, $J = 13.0, 4.7$ Hz, 1H), 1.42 – 1.33 (m, 1H), 1.28 – 1.23 (m, 1H). **^{13}C NMR** (126 MHz, CDCl_3) δ 193.1, 192.9, 184.2, 182.5, 147.8, 144.6, 126.5, 125.9, 112.0, 110.2, 71.19, 71.16, 52.7, 51.9, 51.8, 48.7, 43.9, 38.1, 37.9, 34.8, 31.5, 30.4, 30.3, 30.2, 28.2, 26.9, 22.6, 20.9. **HRMS** (ESI-MS) m/z calculated for $\text{C}_{14}\text{H}_{19}\text{NO}_3\text{S}$ $[\text{M}+\text{H}]^+$ 282.1158, measured 282.1157 (0.4 ppm). **NOTE:** Trace amounts of a third diastereomer could be detected (major:minor = 22.2:1). Relative stereochemistry of the major diastereomers was determined by analogy to other substrates with nOe data and by comparing coupling constants.

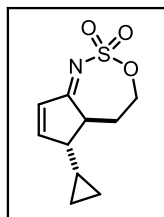


Compound 5.16a. Following the general procedure (0.5 mmol scale), **5.16a** was purified on silica gel using a 0-60% hexanes:EtOAc solvent system with increasing 10% increments of EtOAc to provide a yellow solid (37.0 mg, 0.17 mmol, 34% yield). **^1H NMR** (500 MHz, Chloroform- d) δ 7.26 (d, $J = 5.5$ Hz, 1H), 6.22 (d, $J = 5.5$ Hz, 1H), 4.60 – 4.55 (m, 2H), 3.01 (dd, $J = 12.4, 2.9$ Hz, 1H), 2.12 (ddt, $J = 14.8, 12.5, 8.9$ Hz, 1H), 1.96 (dq, $J = 14.8, 2.9$ Hz, 1H), 1.27 (s, 3H), 1.12 (s, 3H). **^{13}C NMR** (126 MHz, CDCl_3) δ 191.9, 171.8, 130.8, 70.9, 54.5, 48.8, 27.2, 26.4, 24.5. **HRMS** (ESI-MS) m/z calculated for $\text{C}_9\text{H}_{13}\text{NO}_3\text{S}$ $[\text{M}+\text{H}]^+$ 216.0689, measured 216.0687 (0.9 ppm).



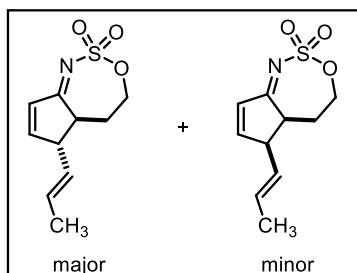
Compound 5.17a. Following the general procedure (0.5 mmol scale), crude **5.17a** was subjected to silica gel chromatography using a 0-60% hexanes:EtOAc solvent system with increasing 10% increments of EtOAc to

provide a trace amount of impure **5.17a** that was unsuitable for full characterization (<10% yield, see NMR data).



Compounds 5.18a. Following the general procedure (0.5 mmol scale), a 1.2:1 mixture of iminocyclopentene:unknown compound was generated. Iminocyclopentene **5.18a** was purified on silica gel using a 0-60% hexanes:EtOAc

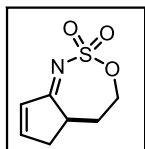
solvent system with increasing 10% increments of EtOAc to provide a light-yellow oil (41.7 mg, 0.18 mmol, 37% yield, >19:1 *dr*). The captured unknown was generated in 28% NMR yield as a 3.2:1 mixture of diastereomers with the minor decomposing completely on silica gel and was not fully characterized. **¹H NMR** (500 MHz, Chloroform-*d*) δ 7.37 (dd, *J* = 5.6, 2.4 Hz, 1H), 6.29 (dd, *J* = 5.5, 2.0 Hz, 1H), 4.76 – 4.69 (m, 1H), 4.51 – 4.46 (m, 1H), 3.28 (ddd, *J* = 10.1, 5.4, 2.3 Hz, 1H), 2.13 – 2.10 (m, 1H), 2.09 – 2.04 (m, 2H), 0.83 – 0.76 (m, 1H), 0.62 (dddd, *J* = 13.3, 12.4, 6.3, 3.5 Hz, 2H), 0.37 – 0.30 (m, 1H), 0.27 – 0.20 (m, 1H). **¹³C NMR** (126 MHz, CDCl₃) δ 193.2, 165.1, 133.3, 71.23, 57.5, 51.0, 30.4, 13.9, 3.9, 2.8. **HRMS** (ESI-MS) *m/z* calculated for C₁₀H₁₃NO₃S [M+H]⁺ 228.0689, measured 228.0688 (0.4 ppm).



Compound 5.19a. Following the general procedure (0.5 mmol scale), **5.19a** was purified on silica gel using a 0-60% hexanes:EtOAc solvent system with increasing 10% increments of EtOAc to provide a light-yellow oil (28.1 mg, 0.125 mmol, 25%

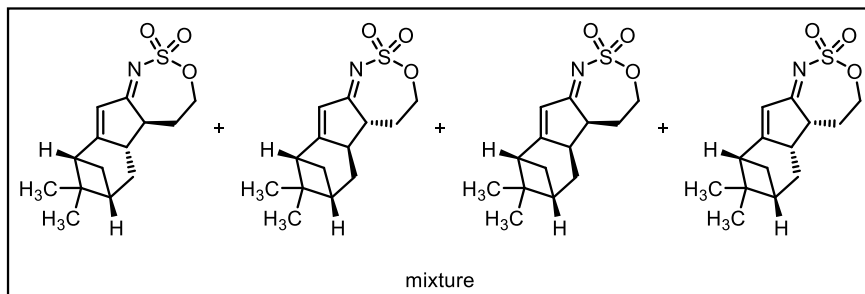
yield, 5.9:1 *anti:syn*). **Major (anti) diastereomer** **¹H NMR** (500 MHz, Chloroform-*d*) δ 7.17 (dd, *J* = 5.7, 2.5 Hz, 1H), 6.20 (dd, *J* = 5.5, 2.1 Hz, 1H), 5.55 (dq, *J* = 15.3, 6.5 Hz, 1H), 5.27 – 5.19 (m, 1H), 4.55 (dddd, *J* = 12.0, 8.9, 6.1, 3.5 Hz, 1H), 4.39 (dt, *J* = 11.9, 3.9 Hz, 1H), 3.16 (dt, *J* = 8.2, 2.5 Hz, 1H), 2.99 (ddd, *J* = 8.9, 6.5, 2.6 Hz, 1H), 2.01 – 1.96 (m, 2H), 1.61 (dd, *J* = 6.5, 1.7

Hz, 3H). **¹³C NMR** (126 MHz, CDCl₃) δ 192.6, 165.0, 133.3, 129.7, 127.9, 71.3, 56.0, 51.1, 29.2, 18.0. **HRMS** (ESI-MS) *m/z* calculated for C₁₀H₁₃NO₃S [M+H]⁺ 228.0689, measured 228.0688 (0.4 ppm).



Compound 5.20a. Following the general procedure (0.3 mmol scale), **5.20a** was purified on silica gel using a 0-60% hexanes:EtOAc solvent system with increasing 10% increments of EtOAc to provide an off-white solid (23.1 mg, 0.123 mmol, 41%

yield). **¹H NMR** (500 MHz, Chloroform-*d*) δ 7.48 (dt, *J* = 5.5, 2.7 Hz, 1H), 6.37 (dt, *J* = 5.5, 2.1 Hz, 1H), 4.75 (td, *J* = 11.6, 4.4 Hz, 1H), 4.48 (ddd, *J* = 12.1, 4.6, 2.7 Hz, 1H), 3.63 – 3.55 (m, 1H), 3.20 (ddt, *J* = 19.8, 6.4, 2.4 Hz, 1H), 2.52 (dq, *J* = 19.8, 2.3 Hz, 1H), 2.11 – 1.99 (m, 2H). **¹³C NMR** (126 MHz, CDCl₃) δ 194.2, 162.6, 134.3, 71.3, 43.6, 40.5, 30.7. **HRMS** (ESI-MS) *m/z* calculated for C₇H₉NO₃S [M+Na]⁺ 210.0195, measured 210.0194 (0.5 ppm).



Compound 5.21a. Following the general procedure (0.5 mmol scale), **5.21a** was purified on silica gel using a 0-60%

hexanes:EtOAc solvent system with increasing 10% increments of EtOAc to provide a yellow solid (87.8 mg, 0.312 mmol, 62% yield, *dr* = 7.7:4.6:4.2:1). Characterized as a mixture of diastereomers. **¹H NMR** (500 MHz, Chloroform-*d*) δ 5.96 – 5.84 (m, 1H), 4.80 – 4.50 (m, 1H), 4.50 – 4.41 (m, 1H), 3.98 – 3.50 (m, 0.5H), 3.28 – 3.14 (m, 1H), 3.14 – 2.86 (m, 2H), 2.53 – 2.37 (m, 0.5H), 2.33 – 2.04 (m, 3H), 2.01 – 1.57 (m, 2H), 1.39 – 1.21 (m, 3H), 1.12 – 0.86 (m, 3H), 0.64 – 0.57 (m, 1H). **¹³C NMR** (126 MHz, CDCl₃) δ 196.1, 195.8, 194.4, 192.3, 191.6, 191.2,

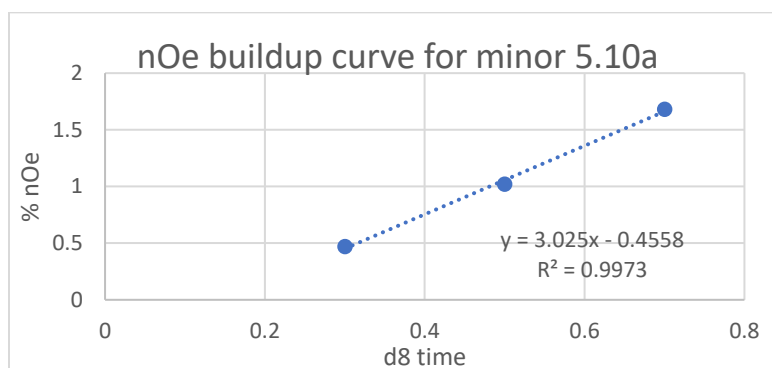
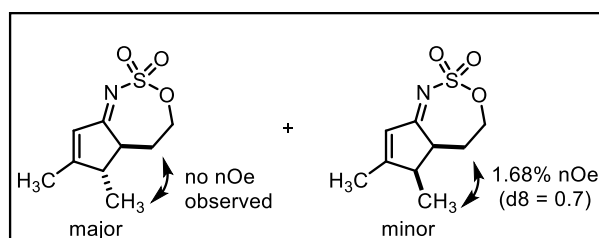
190.8, 190.1, 124.5, 124.2, 122.3, 121.9, 71.8, 71.2, 70.5, 70.4, 55.6, 52.0, 50.3, 50.1, 48.7, 48.3, 47.7, 47.1, 46.4, 46.32, 46.27, 45.9, 42.5, 42.2, 41.8, 40.9, 40.7, 40.1, 39.1, 38.9, 38.2, 30.9, 30.3, 30.2, 29.7, 28.1, 27.2, 27.1, 27.0, 26.8, 26.62, 26.57, 26.52, 26.0, 24.5, 23.6, 23.4, 22.1, 21.8, 21.1.

HRMS (ESI-MS) m/z calculated for $C_{14}H_{19}NO_3S$ $[M+H]^+$ 282.1158, measured 282.1158 (<0.1 ppm).

5.9.6. Representative nOe studies:

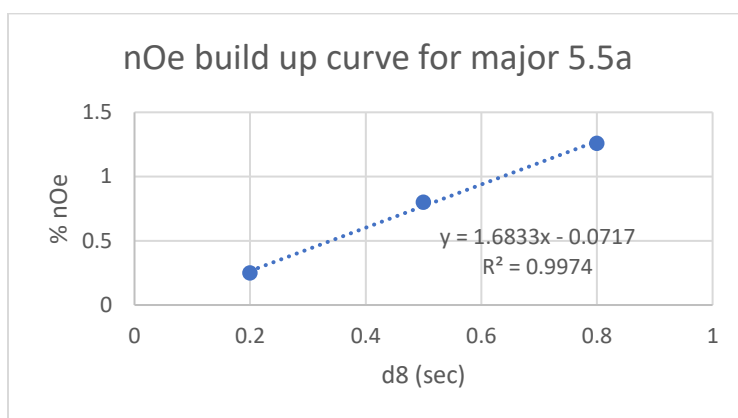
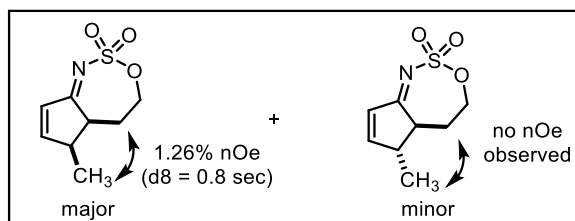
Selective 1-D NOESY to determine relative stereochemistry for major & minor diastereomers of

5.10a

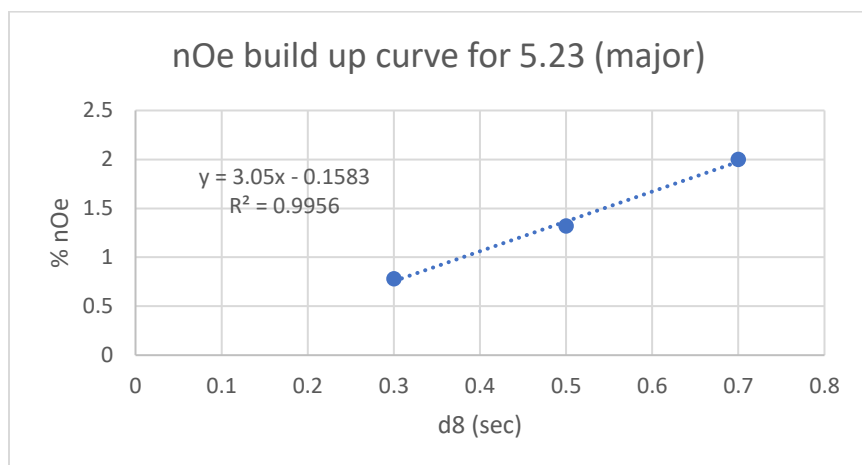
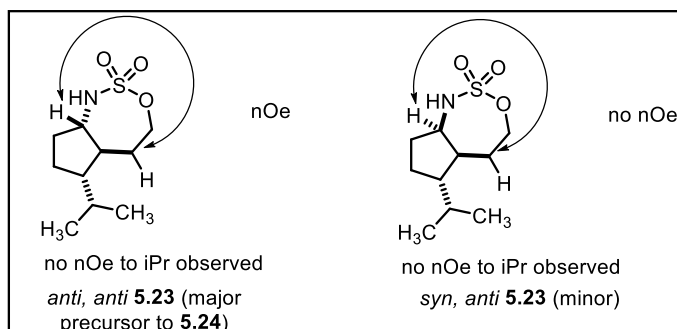


Selective 1-D NOESY to determine relative stereochemistry for major & minor diastereomers of

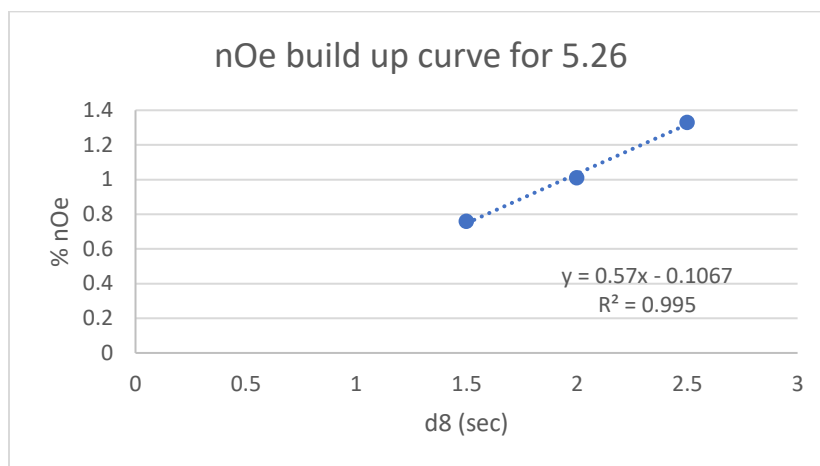
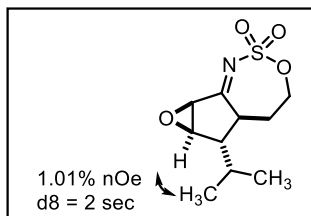
5.5a



Selective 1-D NOESY to determine relative stereochemistry for **5.23** and linear build-up curve

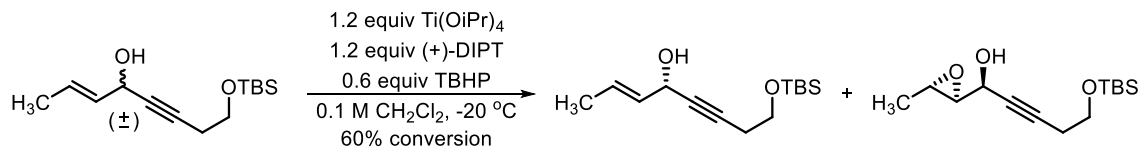


Selective 1-D NOESY to determine relative stereochemistry for 5.26 and linear build-up curve



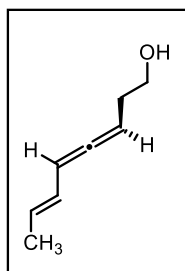
5.9.7. Axial-to-point chirality transfer and asymmetric catalysis experiments:

Chiral substrate preparation: Enantioenriched allyl propargyl alcohol was prepared by Sharpless kinetic resolution.



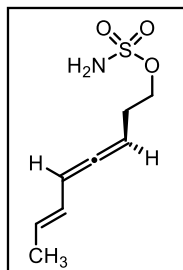
A dry round-bottom flask equipped with a stir bar was charged with anhydrous CH_2Cl_2 (0.1 M) and cooled to $-20\text{ }^\circ\text{C}$. At this temperature, $\text{Ti}(\text{OiPr})_4$ (1.2 equiv) was added followed by (+)-diisopropyl tartrate (1.2 equiv) and stir 10 min. Alcohol (1.0 equiv) was then added, followed by

tert-butyl hydroperoxide (0.6 equiv). The reaction was maintained at -20 °C for 48 h at which point ^1H NMR aliquot showed 60% conversion to the undesired epoxide (alternatively, reaction can be monitored by titration of residual TBHP). The reaction was then quenched with acetone (90 mL) containing water (3 mL) precooled to -20 °C and the mixture was warmed to room temperature over 1 h before filtering the salts over celite. The filtrate was evaporated and the residue was taken up in Et_2O and treated with 1 N NaOH solution at 0 °C. After stirring for 30 min, the organic layer was separated, washed with brine, dried over Na_2SO_4 , and concentrated under reduced pressure. The resulting oil was purified by SiO_2 column chromatography using hexanes/ EtOAc to collect pure, enantioenriched allyl propargyl alcohol. The enantioenriched alcohol was then taken forward to the UV-active homoallenenic sulfamate before determining *ee*. **NOTE:** During the stereospecific reduction of propargyl alcohols using the Schwartz reagent, Ready warns that ZnCl_2 will erode axial chirality. Besides being a precursor to EtZnCl , ZnCl_2 is a byproduct of the reaction between ROZnCl and $\text{Cp}_2\text{Zr(H)Cl}$ to generate Cp_2ZrO and ZnCl_2 .² Deprotection of the TBS-ether was conducted using Method A before using the alcohol in the general procedure for synthesizing sulfamate esters (*vide supra*).



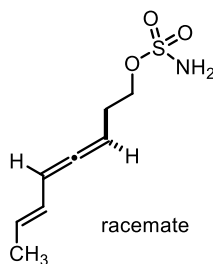
ROH Precursor to Enantioenriched 5.4. The described Sharpless kinetic resolution was ran to 55% conversion to further increase the *ee* of the recovered allyl propargyl alcohol. Following the general procedure for allene formation and deprotection using Method A (*vide supra*), **ROH Precursor to Enantioenriched**

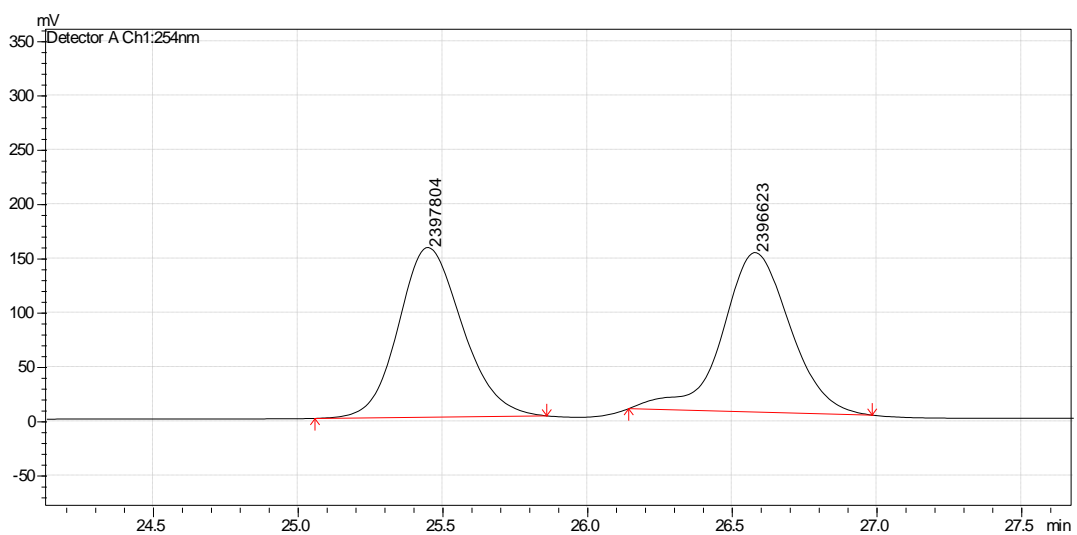
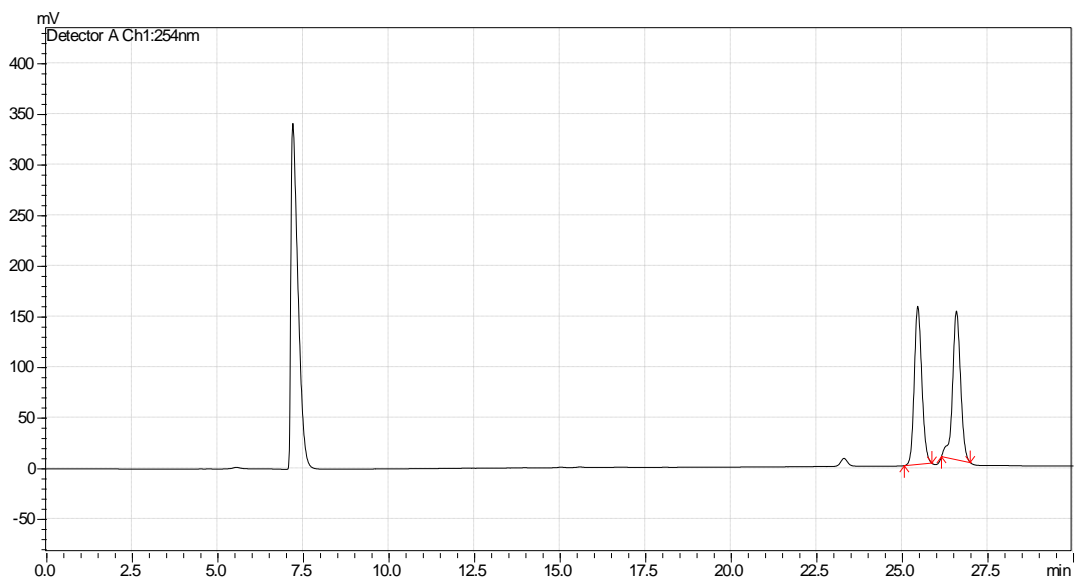
5.4 was isolated as described for the racemate to provide an orange oil (0.563 g, 4.5 mmol, 86% yield). The spectroscopic and HRMS data was consistent with that reported for racemic **ROH Precursor to 5.4**. Axial chirality is drawn by analogy to that reported by Ready invoking Sharpless's mnemonic.



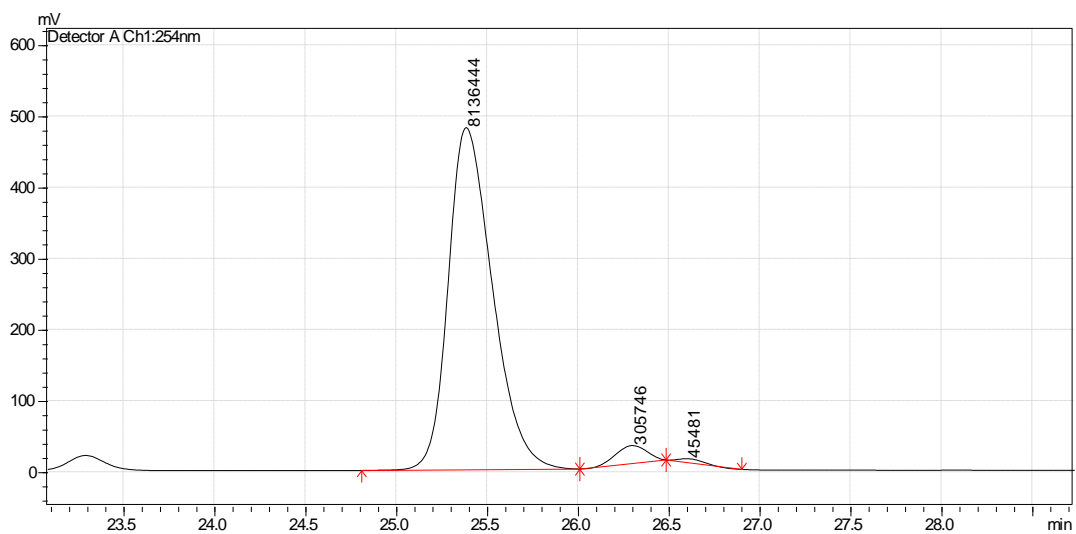
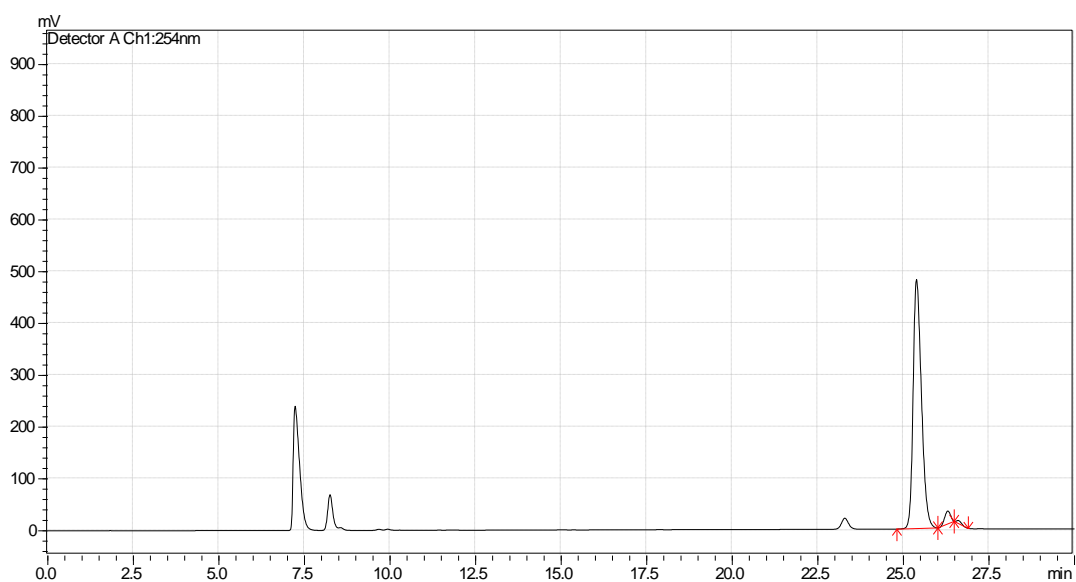
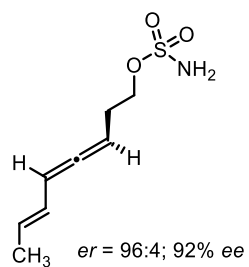
Enantioenriched Compound 5.4. Following the general procedure for synthesizing sulfamate esters (4.5 mmol scale), **Enantioenriched 5.4** was isolated as described for **5.4** to provide a white solid (0.644 g, 3.2 mmol, 70% yield, 92% *ee* [see chromatograms below]). The spectroscopic and HRMS data was consistent with that reported for racemic **5.4**.

Separation of eneallene enantiomers and HPLC traces: HPLC conditions – chromatograms were acquired on a Shimadzu Prominence HPLC equipped with a Chiracel OJ-H column. Flow rate: 1.00 mL/min.; Oven temp: 40.0 °C; Solvent: 5:95 iPrOH:hexane held for 2 min and polarity was increased to 20:80 iPrOH:hexane over 20 minutes. The eluent composition was held at this ratio for another 5 minutes before dropping back down to 5:95 iPrOH:hexane over 30 sec. The solvent composition stayed at this ratio for 2.5 min to complete the 30 min analysis. Detector: UV 254 nm and 210 nm.





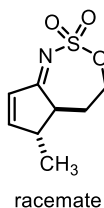
Major Peak Area	Minor Peak Area	<i>er</i> (major:minor)	% <i>ee</i>
2397804	2396623	50:50	0

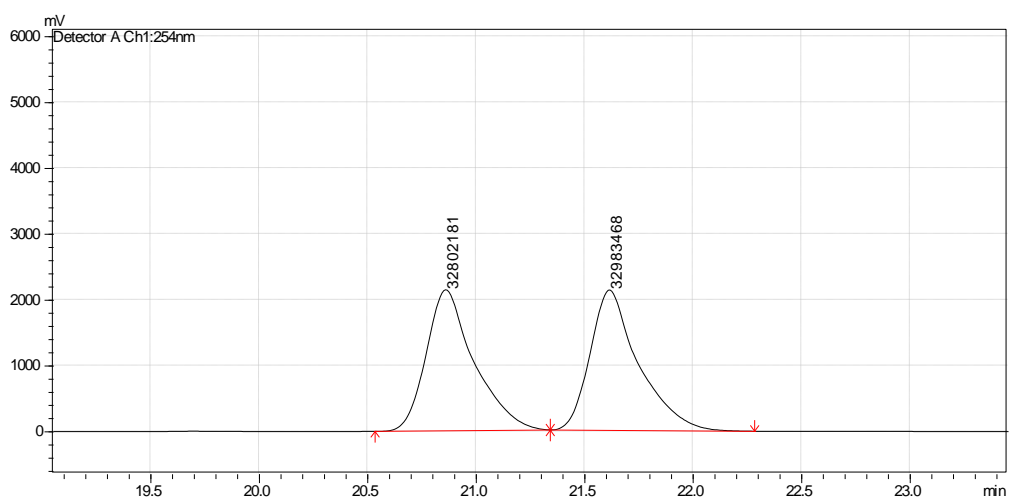
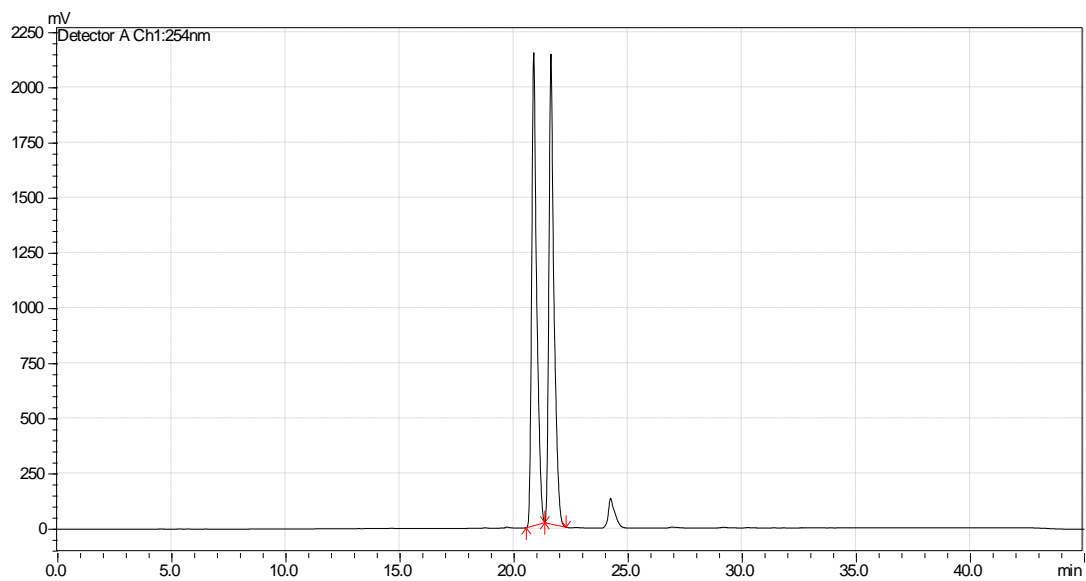


Major Peak Area	Minor Peak Area	<i>er</i> (major:minor)	% <i>ee</i>
8136444	305746	96:4	92
8136444	45481	99:1	98

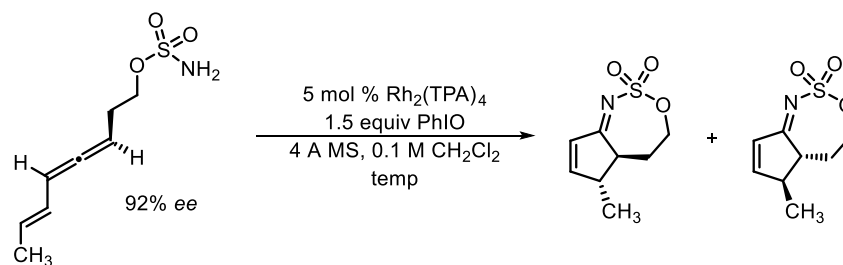
NOTE: We reported the lower *ee* despite this assignment likely being incorrect. Even though the higher *ee* is likely the correct peak assignment by comparison to racemate retention times, we were able to confirm significant erosion of *ee* following amination and cyclization regardless the peak assignment.

Separation of cyclopentene enantiomers and HPLC traces: HPLC conditions – chromatograms were acquired on a Shimadzu Prominence HPLC equipped with a Chiracel AD-H column. Flow rate: 1.00 mL/min.; Oven temp: 40.0 °C; Solvent: 5:95 iPrOH:hexane held for 2 min and polarity was increased to 50:50 iPrOH:hexane over 33 minutes. The eluent composition was held at this ratio for another 3 minutes before dropping back down to 5:95 iPrOH:hexane over 30 sec. The solvent composition stayed at this ratio for 2.5 min to complete the 40 min analysis. Detector: UV 254 nm and 210 nm.





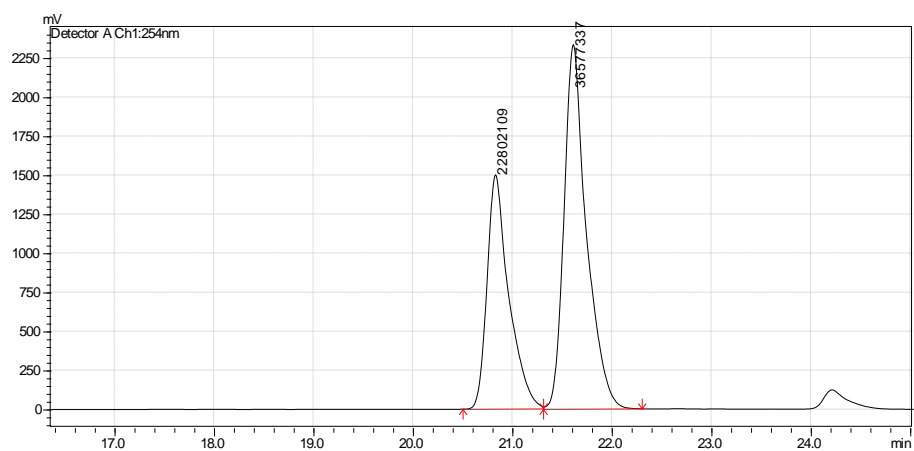
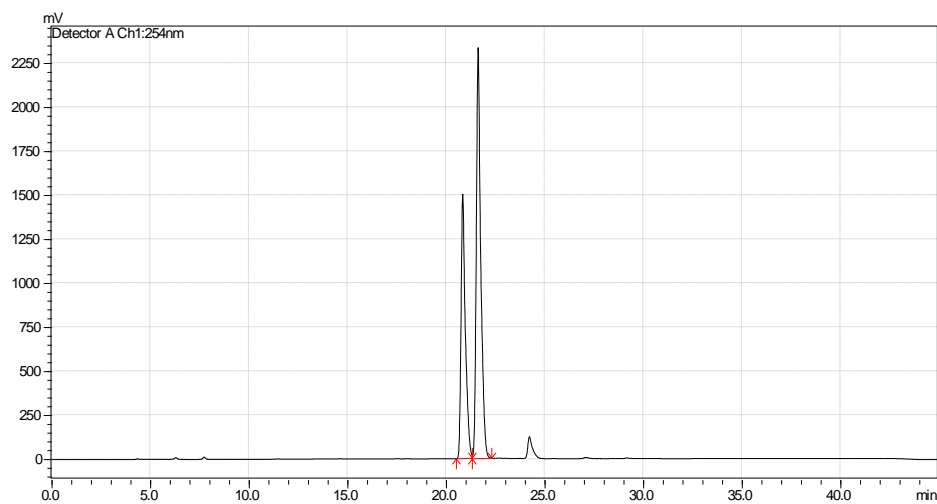
Major Peak Area	Minor Peak Area	<i>er</i> (major:minor)	% <i>ee</i>
32802181	32983468	50:50	0



entry	temperature (°C)	% yield ^a	er	% ee
1	23	63	62:38	24
2	50	57	56:44	12

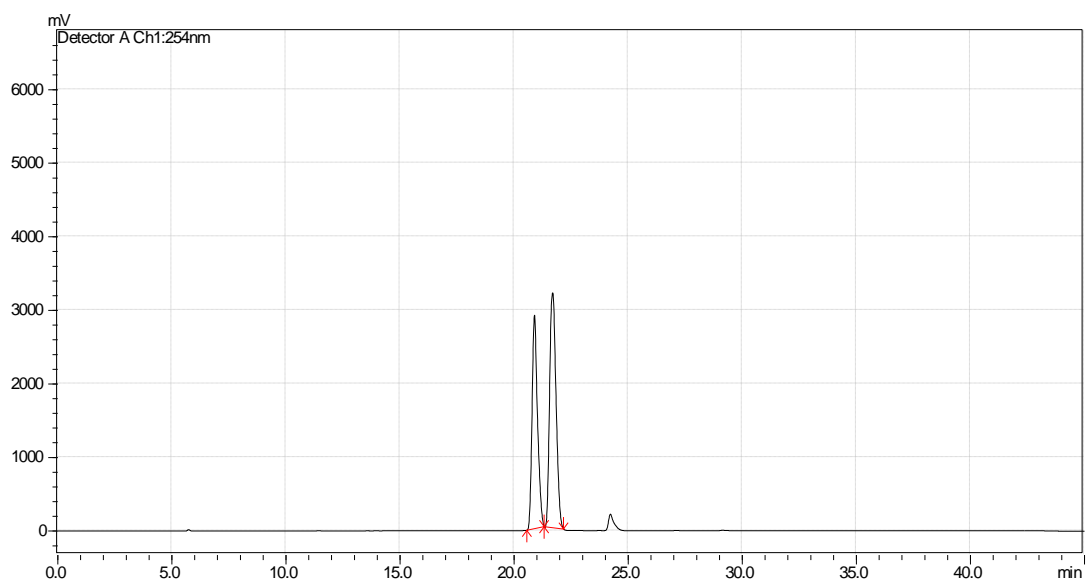
^a Isolated yields

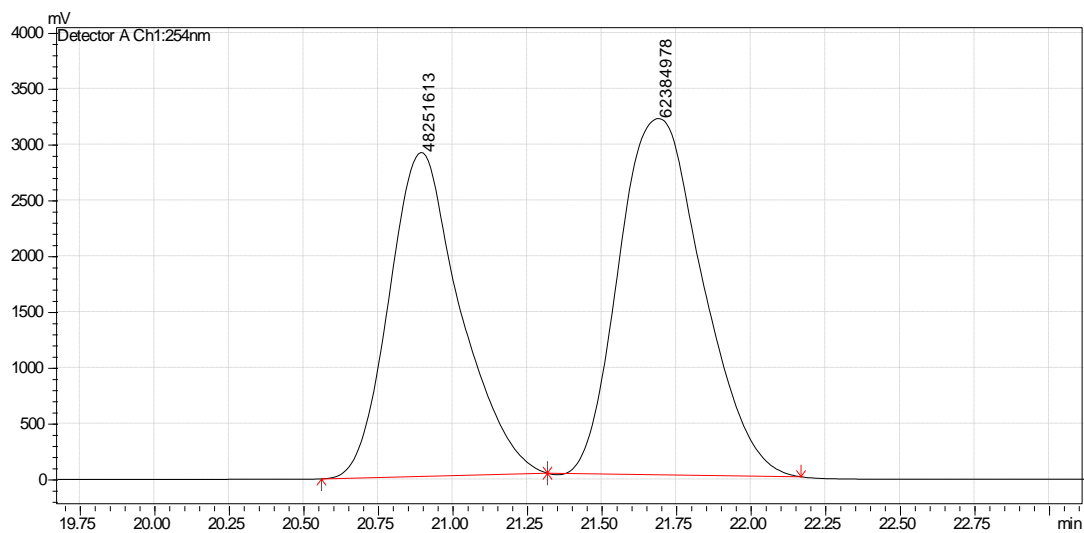
Room temperature (entry 1)



Major Peak Area	Minor Peak Area	<i>er</i> (major:minor)	% <i>ee</i>
36577337	22802109	62:38	24

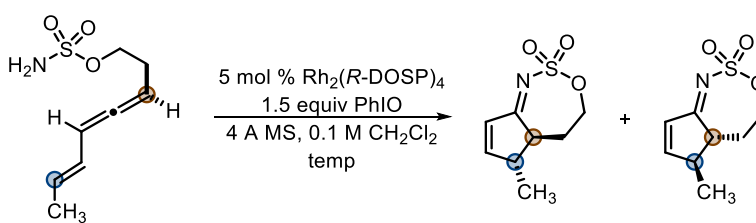
Elevated temperature (entry 2)





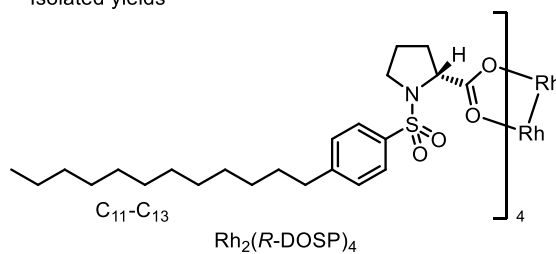
Major Peak Area	Minor Peak Area	<i>er</i> (major:minor)	% <i>ee</i>
62384978	48251613	56:44	12

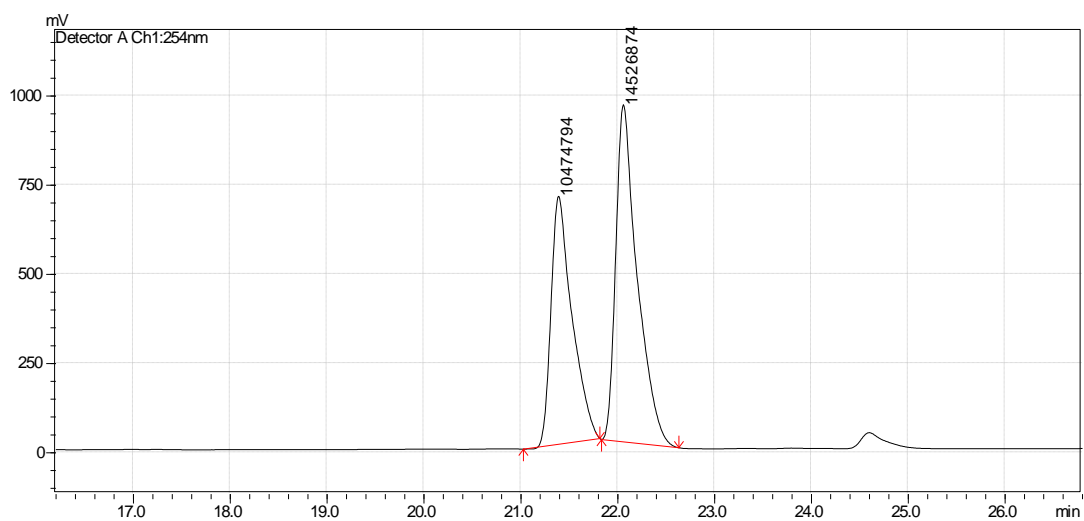
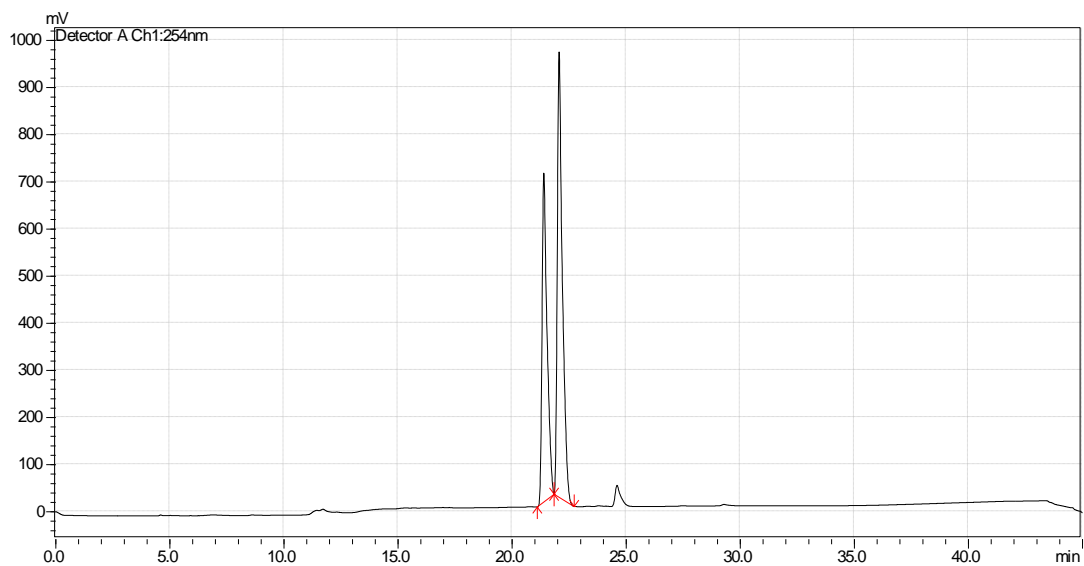
Asymmetric catalysis with racemic substrate.



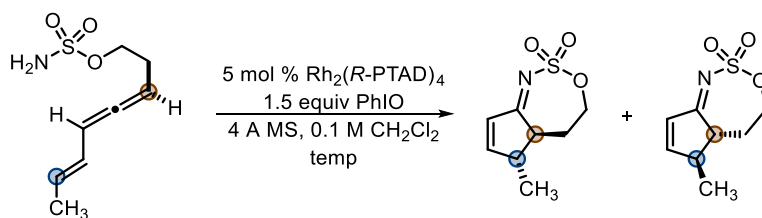
entry	temperature (° C)	% yield ^a	<i>er</i>	% <i>ee</i>
1	50	54	58:42	16

^a Isolated yields



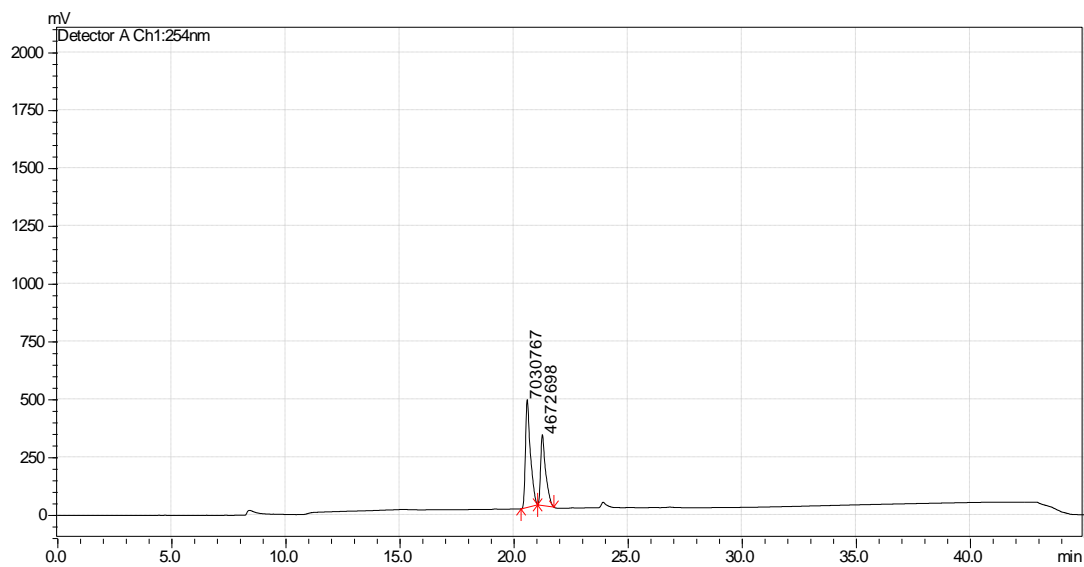
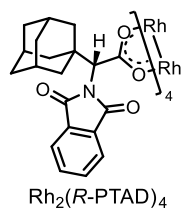


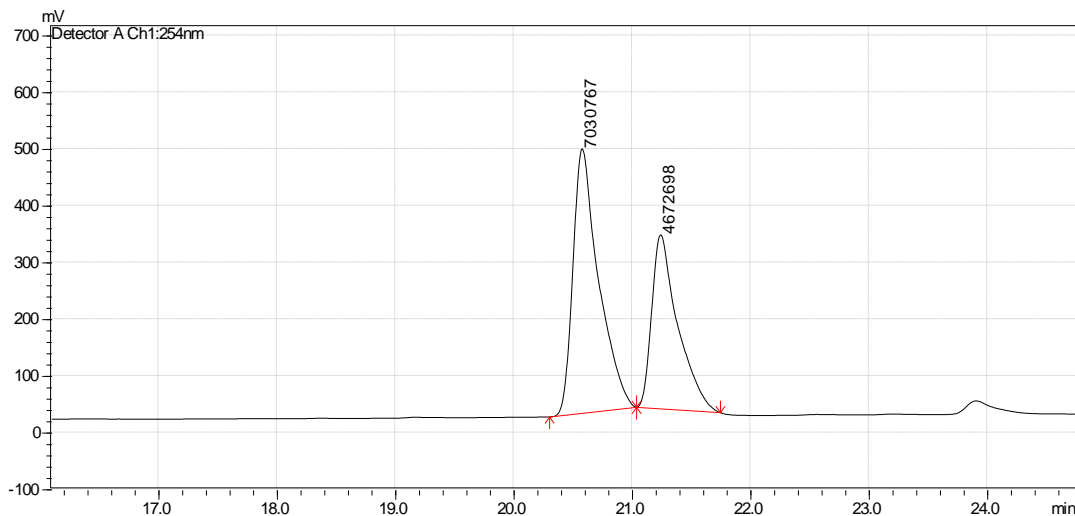
Major Peak Area	Minor Peak Area	<i>er</i> (major:minor)	% <i>ee</i>
14526872	10474794	58:42	16



entry	temperature (° C)	% yield ^a	er	% ee
1	50	47	60:40	20

^a Isolated yields

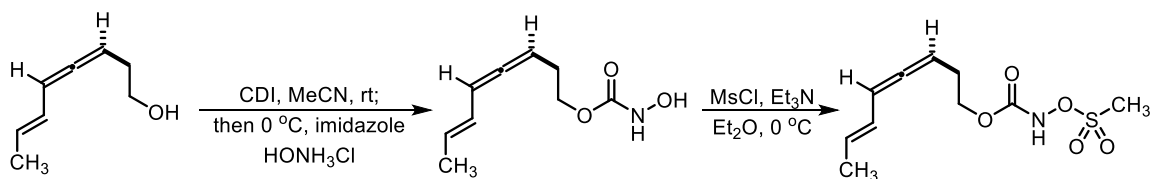




Major Peak Area	Minor Peak Area	<i>er</i> (major:minor)	% <i>ee</i>
7030767	4672698	60:40	20

5.9.8. Tether length/*N*-source optimization and reaction monitoring

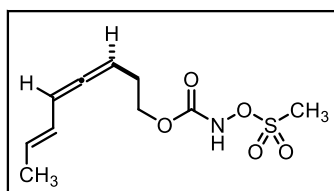
Synthesis of homoallenic N-mesyloxycarbamate and procedure for nitrene transfer



Solid 1,1'-carbonyldiimidazole (8.2 mmol, 1.2 equiv) was added to a solution of **ROH Precursor to 5.4** (6.8 mmol, 1.0 equiv) in acetonitrile (36 mL, 0.19 M) and the clear solution stirred at room temperature for 2 hours. The resulting mixture was cooled to 0 °C and hydroxylamine-HCl (27.2 mmol, 4.0 equiv) was added, followed by imidazole (20.4 mmol, 3.0

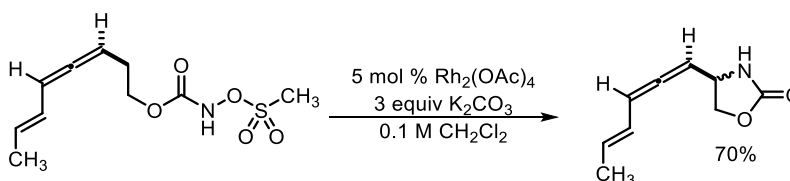
equiv) and vigorous stirring was maintained for 1 hour at 0 °C. After the reaction is complete according to TLC analysis, the suspension was concentrated. The white residue was dissolved in a 1:1 mixture of EtOAc:10% HCl (aq). The layers were separated and the aqueous layer was extracted twice with EtOAc. The combined organic layers were washed with brine, dried over Na₂SO₄ and concentrated. The resulting *N*-hydroxycarbamate is obtained as a white solid and was sufficiently pure to be used in the next step.

The resulting *N*-hydroxycarbamate (3.4 mmol, 1.0 equiv) was dissolved in Et₂O and cooled to 0 °C. The solution is stirred and MsCl (3.4 mmol, 1.0 equiv) is added dropwise, followed by Et₃N (3.4 mmol, 1.0 equiv). The resulting white suspension stirs for 1 h at 0 °C. The mixture was quenched with H₂O and the aqueous layer was extracted three times with Et₂O. The combined organic layers were washed with brine, dried over Na₂SO₄, and concentrated. The crude material was columned over SiO₂ using hexanes:EtOAc gradient (0 to 25% EtOAc with increasing 5% increments) followed by recrystallization in CHCl₃/hexanes to give *N*-mesyloxycarbamate **S5.1**.

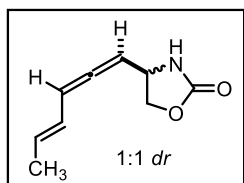


Compound S5.1. Following the described procedure, **S5.1** was obtained as a clear oil (0.130 g, 0.5 mmol, 15% yield). ¹H NMR (500 MHz, Chloroform-*d*) δ 8.47 – 8.28 (m, 1H), 5.85 – 5.78 (m, 2H), 5.70

– 5.59 (m, 1H), 5.28 – 5.21 (m, 1H), 4.30 (td, *J* = 6.6, 1.7 Hz, 2H), 3.17 (s, 3H), 2.39 (qd, *J* = 6.7, 3.7 Hz, 2H), 1.77 – 1.72 (m, 3H). ¹³C NMR (126 MHz, CDCl₃) δ 206.9, 156.0, 128.3, 126.2, 95.2, 87.4, 66.5, 36.4, 28.4, 18.2. HRMS (ESI-MS) *m/z* calculated for C₁₀H₁₅NO₅S [M+NH₄]⁺ 279.1009, measured 279.1006 (1.1 ppm).

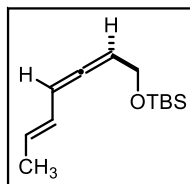
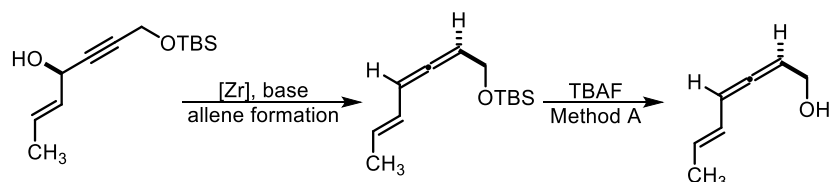


To a solution of **S5.1** (0.15 mmol, 1.0 equiv) in CH_2Cl_2 (1.5 mL, 0.1 M) was added K_2CO_3 (0.45 mmol, 3.0 equiv) and $\text{Rh}_2(\text{OAc})_4$ (0.0075 mmol, 0.05 equiv). The resulting suspension stirs until complete consumption of starting material is observed by TLC. The crude solution is washed with water and the aqueous layer is extracted three times with CH_2Cl_2 , dried over Na_2SO_4 , and concentrated. Allenic C–H amination product **S5.2** was observed (70% ^1H -NMR yield with respect to mesitylene internal standard) instead of the desired eneallene aziridination/electrocyclization.



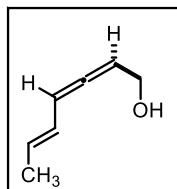
Compound S5.2. Characterized as a 1:1 mix of diastereomers. ^1H NMR (500 MHz, Chloroform-*d*) δ 6.01 (tdd, $J = 10.3, 6.2, 1.7$ Hz, 1H), 5.88 – 5.78 (m, 1H), 5.73 (ddd, $J = 15.2, 6.3, 1.2$ Hz, 1H), 5.40 – 5.32 (m, 1H), 5.02 (s, 1H), 4.55 (td, $J = 8.4, 1.8$ Hz, 1H), 4.43 – 4.34 (m, 1H), 4.19 (dt, $J = 8.6, 5.3$ Hz, 1H), 1.77 (dt, $J = 6.5, 1.6$ Hz, 3H). ^{13}C NMR (126 MHz, CDCl_3) δ 206.1, 206.0, 158.9, 158.8, 130.41, 130.39, 124.89, 124.86, 98.10, 98.07, 92.67, 92.65, 70.4, 70.3, 52.10, 52.07, 18.34, 18.33. HRMS (ESI-MS) m/z calculated for $\text{C}_9\text{H}_{11}\text{NO}_2$ $[\text{M}+\text{H}]^+$ 166.0863, measured 166.0861 (1.2 ppm).

Synthesis of allenic carbamate and procedure for nitrene transfer

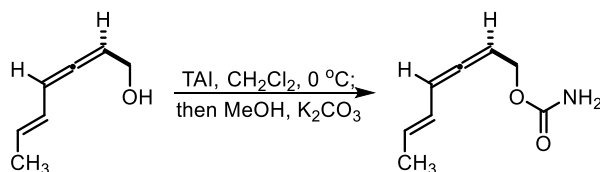


Compound S5.3. Following the general procedure for allene formation (36.9 mmol scale), **S5.3** was isolated a dark yellow/orange oil (4.98 g, 22.2 mmol, 60% yield). ^1H NMR (500 MHz, Chloroform-*d*) δ 5.90 – 5.81 (m, 2H), 5.64 (ddtd, $J = 15.9, 8.1, 6.6, 1.5$ Hz, 1H), 5.39 (dt, $J = 8.1, 4.5, 1.5$ Hz, 1H), 4.22 – 4.17 (m, 2H), 1.74 (dt, $J =$

6.7, 1.5 Hz, 3H), 0.90 (s, 9H), 0.08 (d, $J = 2.2$ Hz, 6H). ^{13}C NMR (126 MHz, CDCl_3) δ 205.6, 127.9, 126.3, 95.4, 93.2, 61.9, 26.1, 18.5, 18.2, -4.9. **HRMS** (ASAP-MS) m/z calculated for $\text{C}_{13}\text{H}_{24}\text{OSi}$ $[\text{M}+\text{H}]^+$ 225.1669, measured 225.1665 (1.8 ppm).

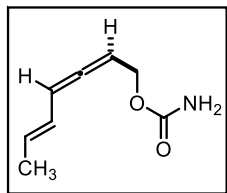


Compound S5.4. Following Method A for TBS-ether deprotection (9.6 mmol scale), **S5.4** was isolated as a yellow oil (0.822 g, 6.6 mmol, 69% yield). ^1H NMR (500 MHz, $\text{Chloroform-}d$) δ 5.93 (ddt, $J = 11.5, 5.7, 2.7$ Hz, 1H), 5.89 – 5.81 (m, 1H), 5.71 – 5.62 (m, 1H), 5.49 (tdd, $J = 9.2, 5.0, 1.9$ Hz, 1H), 4.14 – 4.11 (m, 2H), 1.92 – 1.78 (m, 1H), 1.76 – 1.72 (m, 3H). ^{13}C NMR (126 MHz, CDCl_3) δ 205.1, 128.5, 125.9, 96.6, 93.1, 60.6, 18.1. **HRMS** (ASAP-MS) m/z calculated for $\text{C}_7\text{H}_{10}\text{O}$ $[\text{M}+\text{H}]^+$ 111.0804, measured 111.0803 (0.9 ppm).

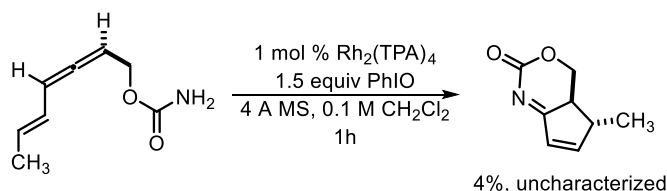


Allenic alcohol **S5.4** (0.165 g, 1.5 mmol, 1 equiv) was dissolved in CH_2Cl_2 (5 mL, 0.3 M) and placed in an ice bath. Trichloroacetyl isocyanate (TAI, 0.2 mL, 1.5 mmol, 1 equiv) was then added slowly dropwise. The reaction was stirred at 0 °C until starting material was consumed by TLC (~20 min). At this point the solvent was removed and the crude reaction was redissolved in MeOH (3.8 mL, 0.4 M). Potassium carbonate (0.104 g, 0.75 mmol, 0.5 equiv) was added and the mixture stirs at room temperature until TLC shows complete consumption of the starting material (~3 h). At this point H_2O was added to the reaction and the mixture was extracted with three portions of CH_2Cl_2 . The organic extracts were dried over Na_2SO_4 , the salts were filtered, and then the solvent was removed under decreased pressure. The crude material was purified using silica column

chromatography using hexanes:EtOAc with a 0% to 30% EtOAc gradient using increasing 5% EtOAc increments.

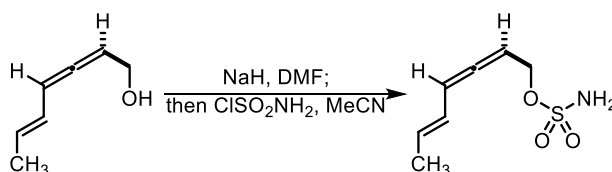


Compound S5.5. Allenic carbamate was isolated as an orange solid (0.165 g, 1.1 mmol, 72% yield). **¹H NMR** (500 MHz, Chloroform-*d*) δ 5.95 – 5.81 (m, 2H), 5.73 – 5.64 (m, 1H), 5.45 (q, J = 6.6 Hz, 1H), 4.56 (dd, J = 6.6, 2.2 Hz, 4H), 1.75 (dt, J = 6.8, 1.6 Hz, 3H). **¹³C NMR** (126 MHz, CDCl₃) δ 207.4, 156.5, 128.9, 125.6, 95.9, 88.7, 63.1, 18.3. **HRMS** (ESI-MS) m/z calculated for C₈H₁₁NO₂ [M+Na]⁺ 176.0682, measured 176.0681 (0.6 ppm).



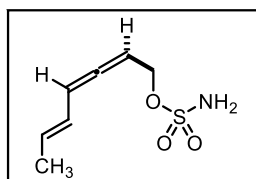
The general eneallene aziridination/electrocyclization was followed on **S5.5** with the following exceptions (0.1 mmol scale). Only 1 mol % Rh₂TPA₄ was used (1.4 mg, 0.001 mmol), and the reaction was not heated. This resulted in ~4-15% imino-Nazarov electrocyclization product (uncharacterized) and ~38% recovered starting material according to quantitative analysis of the crude ¹H-NMR using mesitylene as an internal standard.

Synthesis of allenic sulfamate and nitrene transfer



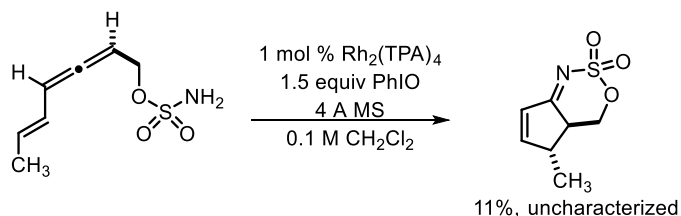
NaH (60% dispersion in mineral oil) was washed 3 times with 10 mL Et₂O to remove the mineral oil (92 mg, 2.31 mmol, 1.1 equiv) and then suspended in DMF (2.1 mL). A solution of allenic

alcohol **S5.4** (0.231 g, 2.1 mmol, 1.0 equiv) in DMF (1.6 mL, final concentration of 0.56 M) was added dropwise at 0 °C. The reaction was stirred for 1 h at room temperature. At this point, the reaction was cooled to 0 °C and a solution of ClSO₂NH₂ in MeCN (3 mL, 0.7 M) was added dropwise and the resulting solution stirs for ~2 h. The reaction is quenched with 10 mL H₂O and extracted 3 times with 30 mL Et₂O. The combined organic extracts were washed 5 times with 20 mL H₂O, 1 time with 25 mL brine, and dried over Na₂SO₄ before concentrating. The crude mixture was purified by silica chromatography using pentane/Et₂O solvent gradient (0% to 100% Et₂O with increasing 20% increments). This provided pure **S5.6** (87 mg, 0.5 mmol, 24% yield). Significant elimination to the triene is observed and is the only product using the general sulfamate ester synthesis using acidic CSI described above.



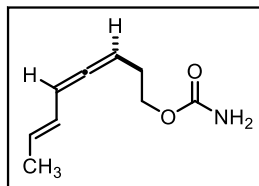
Compound S5.6. Isolated as a yellow oil. ¹H NMR (500 MHz, Chloroform-*d*) δ 6.02 – 5.96 (m, 1H), 5.89 – 5.81 (m, 1H), 5.78 – 5.68 (m, 1H), 5.52 (q, *J* = 6.9 Hz, 1H), 4.74 – 4.66 (m, 4H), 1.77 (dt, *J* = 6.5, 1.5 Hz, 3H). ¹³C

NMR (126 MHz, CDCl₃) δ 208.7, 130.2, 124.6, 96.4, 87.3, 69.6, 18.4. HRMS (ESI-MS) *m/z* calculated for C₇H₁₁NO₃S [M+H]⁺ 188.0387, measured 188.0387 (<0.1 ppm).

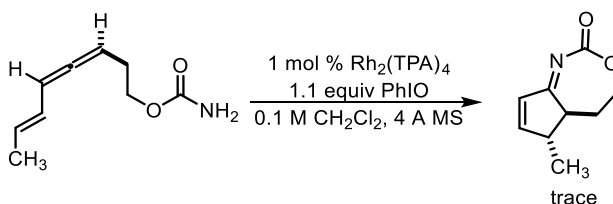


The general eneallene aziridination/electrocyclization was followed on **S5.6** with the following exceptions (0.1 mmol scale). Only 1 mol % Rh₂TPA₄ was used (1.4 mg, 0.001 mmol), and the reaction was not heated. This resulted in ~11% imino-Nazarov electrocyclization product

(uncharacterized) and no recovered starting material according to quantitative analysis of the crude ^1H -NMR using mesitylene as an internal standard.

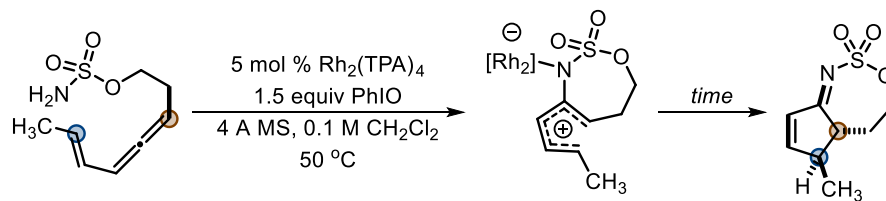


Compound S5.7. Following the procedure for synthesizing the allenic carbamate above (1.0 mmol scale), homoallenic carbamate **S5.7** was isolated as a yellow oil that solidifies upon dryness (107.8 mg, 0.64 mmol, 64% yield). ^1H NMR (500 MHz, Chloroform- d) δ 5.87 – 5.77 (m, 2H), 5.67 – 5.59 (m, 1H), 5.27 (ddd, J = 8.7, 6.9, 3.5 Hz, 1H), 4.57 (s, 2H), 4.13 (t, J = 6.7 Hz, 2H), 2.34 (qd, J = 6.8, 2.6 Hz, 2H), 1.74 (dt, J = 6.4, 1.4 Hz, 3H). ^{13}C NMR (126 MHz, CDCl_3) δ 206.9, 156.8, 127.7, 126.6, 94.8, 88.1, 64.4, 28.8, 18.3. HRMS (ESI-MS) m/z calculated for $\text{C}_9\text{H}_{13}\text{NO}_2$ $[\text{M}+\text{Na}]^+$ 190.0839, measured 190.0836 (1.6 ppm).



The general eneallene aziridination/electrocyclization was followed on **S5.7** with the following exceptions (0.15 mmol scale). Only 1 mol % Rh_2TPA_4 was used (1.4 mg, 0.001 mmol) with 1.1 equiv PhIO, and the reaction was not heated. This resulted in trace amounts of imino-Nazarov electrocyclization product (uncharacterized) and no recovered starting material according to quantitative analysis of the crude ^1H -NMR using mesitylene as an internal standard.

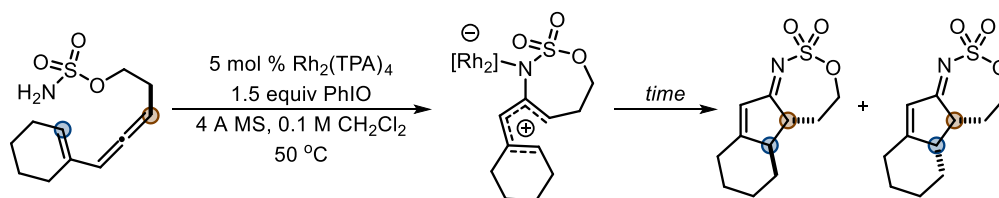
Monitoring mass balance by quantitative ^1H -NMR using 1,3,5-trimethoxybenzene as internal standard



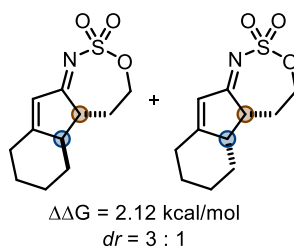
entry	time	% rsm	% yield ^a	% mass balance
1	18 min	33	15	48
2	33 min	24	22	45
3	48 min	7	29	36
4	63 min	5	37	42
5	117 min	2	48	50

^aNMR yields using 1,3,5-trimethoxybenzene as internal standard

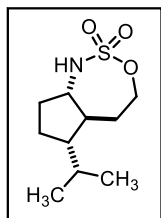
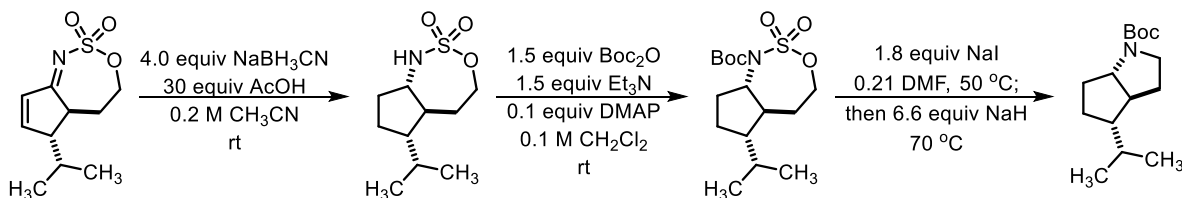
Monitoring the diastereomeric ratio over time to investigate epimerization under the reaction conditions



entry	time	<i>anti</i> : <i>syn</i>
1	15 min	3.0 : 1
2	30 min	3.0 : 1
3	45 min	2.9 : 1
4	60 min	3.1 : 1
5	120 min	3.0 : 1
6	180 min	2.9 : 1
7	300 min	3.0 : 1
8	24 h	3.0 : 1



5.9.9. Procedures for functionalization of α,β -unsaturated iminocyclopentene 5.6a



Compound 5.23. Iminocyclopentene **5.6a** was added to a dry round-bottom flask

equipped with a stirbar (75.3 mg, 0.3 mmol, 1.0 equiv). After adding CH_3CN (0.2

M), NaBH_3CN (50.3 mg, 0.8 mmol, 4.0 equiv) was added in a single portion,

followed by the dropwise addition of AcOH (0.34 mL, 6 mmol, 30 equiv). The reaction was stirred

at room temperature until starting material was consumed according to TLC analysis (12 h). The

reaction was quenched with the dropwise addition of saturated aqueous NaHCO_3 and extracted

thrice with EtOAc . The organic extracts were washed once with brine before drying over Na_2SO_4 ,

filtering the salts, and evaporating the volatiles *in vacuo*. The crude mixture was purified on silica

gel using a 0-50% EtOAc :hexanes gradient with increasing 10% EtOAc increments. Amine **5.23**

was isolated as a white solid (57 mg, 0.246 mmol, 82% yield, 4.8:1 *dr*). **Major diastereomer:** ^1H

NMR (500 MHz, $\text{Chloroform-}d$) δ 4.86 (d, $J = 7.0$ Hz, 1H), 4.32 – 4.20 (m, 2H), 3.84 (ddt, $J =$

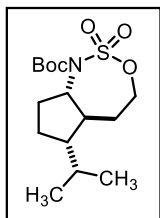
10.7, 8.9, 6.8 Hz, 1H), 2.22 (dddd, $J = 11.8, 9.4, 7.4, 2.8$ Hz, 1H), 2.09 – 1.97 (m, 2H), 1.78 (dddd,

$J = 17.8, 9.6, 5.6, 1.8$ Hz, 2H), 1.59 – 1.49 (m, 1H), 1.39 (m, 2H), 1.28 – 1.17 (m, 1H), 0.92 (d, $J =$

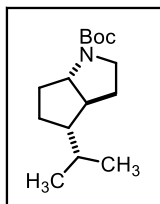
6.7 Hz, 3H), 0.84 (d, $J = 6.7$ Hz, 3H). ^{13}C **NMR** (126 MHz, CDCl_3) δ 71.1, 56.7, 53.9, 47.5,

33.0, 32.2, 31.9, 27.6, 21.8, 19.4. **HRMS** (ESI-MS) m/z calculated for $\text{C}_{10}\text{H}_{19}\text{NO}_3\text{S}$ $[\text{M-H}]^-$

232.1013, measured 232.1014 (0.4 ppm).

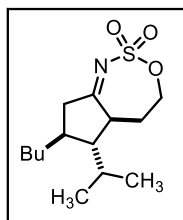
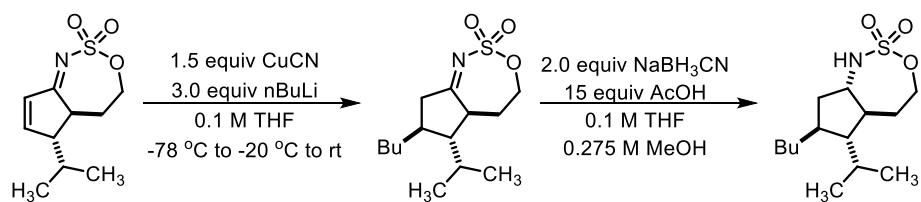


Precursor to 5.24. Aminocyclopentane **5.23** (46.7 mg, 0.2 mmol, 1 equiv) was dissolved as in dry CH_2Cl_2 (0.1 M) in a dry round-bottom flask equipped with a stirbar as a 4.8:1 mixture of diastereomers. The solution was stirred and Boc_2O (65.8 mg, 0.3 mmol, 1.5 equiv), Et_3N (0.05 mL, 0.3 mmol, 1.5 equiv), and DMAP (3.2 mg, 0.02 mmol, 0.1 equiv) were added in sequence. When the starting material was consumed according to TLC analysis (~40 min), the reaction was quenched with saturated aqueous NH_4Cl and extracted thrice with CH_2Cl_2 . The combined organic extracts were washed once with saturated NH_4Cl , followed by brine. The organic extracts were dried over Na_2SO_4 , the salts were filtered, and the volatiles were concentrated *in vacuo*. The crude mixture was purified on silica gel using a 0-50% CH_2Cl_2 :pentane gradient with increasing 10% CH_2Cl_2 increments. The column was then flushed with 100% CH_2Cl_2 (one column volume). This provided Boc-protected amine **Precursor to 5.24** as a clear oil (40.8 mg, 0.122 mmol, 74%, >19:1 *dr*). $^1\text{H NMR}$ (500 MHz, CHCl_3 -*d*) δ 4.81 (td, $J = 11.2, 7.8$ Hz, 1H), 4.56 (ddd, $J = 11.4, 6.5, 1.7$ Hz, 1H), 4.34 (td, $J = 12.0, 5.0$ Hz, 1H), 2.33 – 2.22 (m, 2H), 2.17 – 2.00 (m, 2H), 1.93 – 1.81 (m, 2H), 1.73 (ddt, $J = 11.8, 9.4, 6.3$ Hz, 1H), 1.54 (s, 10H), 1.13 (qd, $J = 12.4, 6.6$ Hz, 1H), 0.96 (d, $J = 6.8$ Hz, 3H), 0.89 (d, $J = 6.7$ Hz, 3H). $^{13}\text{C NMR}$ (126 MHz, CDCl_3) δ 151.8, 85.0, 69.8, 61.4, 46.9, 39.9, 31.9, 29.4, 28.0, 27.5, 26.1, 21.9, 19.8. **HRMS** (ESI-MS) m/z calculated for $\text{C}_{15}\text{H}_{27}\text{NO}_5\text{S}$ $[\text{M}+\text{NH}_4]^+$ 351.1948, measured 351.1942 (1.7 ppm).



Compound 5.24. *N*-Boc protected **Precursor to 5.24** (38 mg, 0.116 mmol, 1 equiv) was dissolved in dry DMF (0.21 M) in a scintillation vial equipped with a stirbar, followed by the addition of NaI (33.0 mg, 0.22 mmol, 1.8 equiv). The solution was capped and warmed to 50 °C in an oil bath with stirring and this temperature was maintained for 15 minutes. At this point, unwashed NaH (60% dispersion in mineral oil, 31.6 mg, 0.79 mmol, 6.6

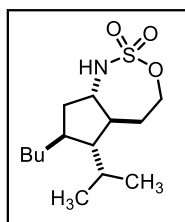
equiv) was added and the solution turned yellow. The oil bath temperature was raised to 70 °C and this temperature was maintained until the reaction was complete (15 h). The yellow color fades over the course of the reaction. The reaction is then placed in an ice bath to cool to 0 °C, prior to cautiously quenching with the dropwise addition of H₂O. The aqueous layer was extracted thrice with Et₂O and the combined organic extracts were dried over Na₂SO₄ before filtering the salts and concentrating the volatiles *in vacuo*. The crude mixture was purified on silica gel using a 0-50% Et₂O:pentane gradient with increasing 10% Et₂O increments. This provided pyrrolidine **5.24** as a clear oil (25.6 mg, 0.101 mmol, 87% yield). **¹H NMR** (500 MHz, Chloroform-*d*) δ 4.16 – 3.95 (m, 1H), 3.57 – 3.39 (m, 1H), 3.36 – 3.26 (m, 1H), 2.29 (qd, *J* = 7.4, 3.4 Hz, 1H), 2.19 – 2.02 (m, 1H), 1.91 (dq, *J* = 12.5, 8.1 Hz, 1H), 1.80 (dtd, *J* = 12.6, 6.4, 2.8 Hz, 1H), 1.62 (ddt, *J* = 11.8, 7.0, 4.5 Hz, 2H), 1.45 (s, 10H), 1.38 – 1.30 (m, 1H), 1.24 – 1.16 (m, 1H), 0.93 (d, *J* = 6.7 Hz, 3H), 0.87 (d, *J* = 6.7 Hz, 3H). **¹³C NMR** (126 MHz, CDCl₃) δ 154.6, 78.9, 63.0, 52.5, 47.8, 45.8, 33.9, 32.6, 30.8, 30.6, 28.7, 21.9, 20.6. **HRMS** (ESI-MS) *m/z* calculated for C₁₅H₂₇NO₂ [M+H]⁺ 254.2115, measured 254.2110 (2.0 ppm).



Precursor to Compound 5.25. A flame-dried round-bottom flask equipped with a stir bar was cooled under N₂. The reaction vessel was charged with CuCN (26.9 mg, 0.3 mmol, 1.5 equiv) and diluted with anhydrous THF (1 mL). The solution was cooled to -78 °C with stirring, and recently titrated nBuLi (2.5 M in hexanes,

0.24 mL, 0.6 mmol, 3.0 equiv) was added dropwise. These components are stirred for 1 h to generate the higher-order cuprate Bu₂Cu(CN)Li₂. The cuprate solution was then warmed to -20 °C

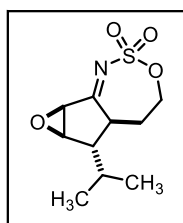
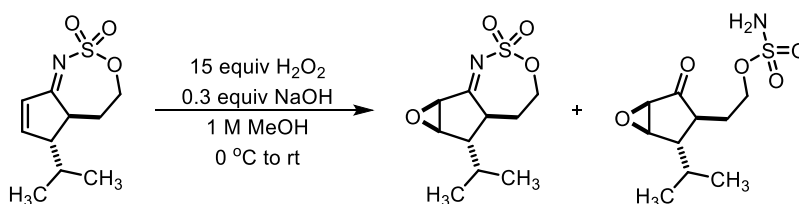
prior to the dropwise addition of iminocyclopentene **5.6a** (45.9 mg, 0.2 mmol, 1 equiv) in 1 mL THF to bring the final reaction concentration to 0.1 M. The reaction was stirred at -20 °C for 1 h prior to warming to rt for 1 h. The reaction was then quenched with saturated aqueous NH₄Cl. The aqueous layer was extracted thrice with Et₂O and the combined organic extracts were dried over Na₂SO₄, the salts were filtered, and the volatiles were removed under reduced pressure. The crude mixture was purified on silica gel using a 0-20% EtOAc/hexanes gradient with increasing 5% EtOAc increments. This was followed by a 20-50% EtOAc/hexanes gradient with increasing 10% EtOAc increments. This resulted in the isolation of imine **Precursor to 5.25** as a light-yellow oil (31.2 mg, 0.11 mmol, 55% yield, >19:1 *dr*). **¹H NMR** (500 MHz, Chloroform-*d*) δ 4.55 – 4.42 (m, 2H), 2.98 – 2.91 (m, 1H), 2.80 (ddd, *J* = 18.8, 7.2, 1.5 Hz, 1H), 2.31 (ddd, *J* = 18.8, 10.7, 1.1 Hz, 1H), 2.05 (dtd, *J* = 14.8, 11.6, 5.7 Hz, 1H), 1.93 (m, 3H), 1.70 – 1.63 (m, 1H), 1.56 (td, *J* = 9.5, 3.3 Hz, 1H), 1.32 (tdd, *J* = 11.7, 8.1, 5.9 Hz, 3H), 1.27 – 1.16 (m, 2H), 0.99 (d, *J* = 7.0 Hz, 6H), 0.90 (t, *J* = 6.9 Hz, 3H). **¹³C NMR** (126 MHz, CDCl₃) δ 199.4, 70.8, 56.4, 48.8, 44.5, 38.7, 34.6, 31.1, 29.9, 28.5, 22.9, 20.5, 20.0, 14.1. **HRMS** (ESI-MS) *m/z* calculated for C₁₄H₂₅NO₃S [M+H]⁺ 288.1628, measured 288.1631 (1.0 ppm).



Compound 5.25. Imine **Precursor to 5.25** (25 mg, 0.085 mmol, 1 equiv) was dissolved in THF (0.1 M with respect to the imine) and the solution was cooled to 0 °C with stirring. At this point, a solution of NaBH₃CN (12.8 mg, 0.2 mmol, 2.0 equiv) and AcOH (0.09 mL, 1.65 mmol, 15 equiv) in MeOH (0.275 M with

respect to the hydride) was added in a single portion and the solution was warmed to room temperature. The reaction was stirred until starting material was consumed according to TLC analysis (~2 h). The reaction was transferred to a separatory funnel using Et₂O prior to cautiously quenching with sat. aq. NaHCO₃. The organic layer was washed twice more with sat. aq. NaHCO₃

before washing once with brine. The organic extracts were dried over Na_2SO_4 , the salts were filtered, and the volatiles were removed under reduced pressure. The crude mixture was purified on silica gel using a 0-100% Et_2O :pentane gradient with increasing 20% Et_2O increments. This provided amine **19** as a white solid (19.0 mg, 0.066 mmol, 78% yield, >19:1 *dr*). **^1H NMR** (500 MHz, CDCl_3) δ 4.72 (d, J = 5.8 Hz, 1H), 4.27 – 4.17 (m, 2H), 3.70 (ddt, J = 11.9, 8.7, 6.1 Hz, 1H), 2.38 (dddd, J = 11.4, 8.3, 5.8, 2.2 Hz, 1H), 2.18 – 2.05 (m, 2H), 1.74 (pd, J = 6.9, 4.3 Hz, 1H), 1.67 – 1.62 (m, 2H), 1.61 – 1.51 (m, 2H), 1.30 (ddt, J = 12.8, 9.1, 5.9 Hz, 2H), 1.19 (dt, J = 10.0, 5.2 Hz, 2H), 1.14 – 1.05 (m, 2H), 0.89 (dd, J = 15.8, 6.9 Hz, 9H). **^{13}C NMR** (126 MHz, CDCl_3) δ 71.2, 59.5, 55.4, 46.0, 40.1, 38.6, 35.2, 34.4, 30.6, 29.8, 23.0, 21.6, 18.7, 14.2. **HRMS** (ESI-MS) m/z calculated for $\text{C}_{14}\text{H}_{27}\text{NO}_3\text{S}$ $[\text{M}+\text{NH}_4]^+$ 307.2050, measured 307.2048 (0.7 ppm).

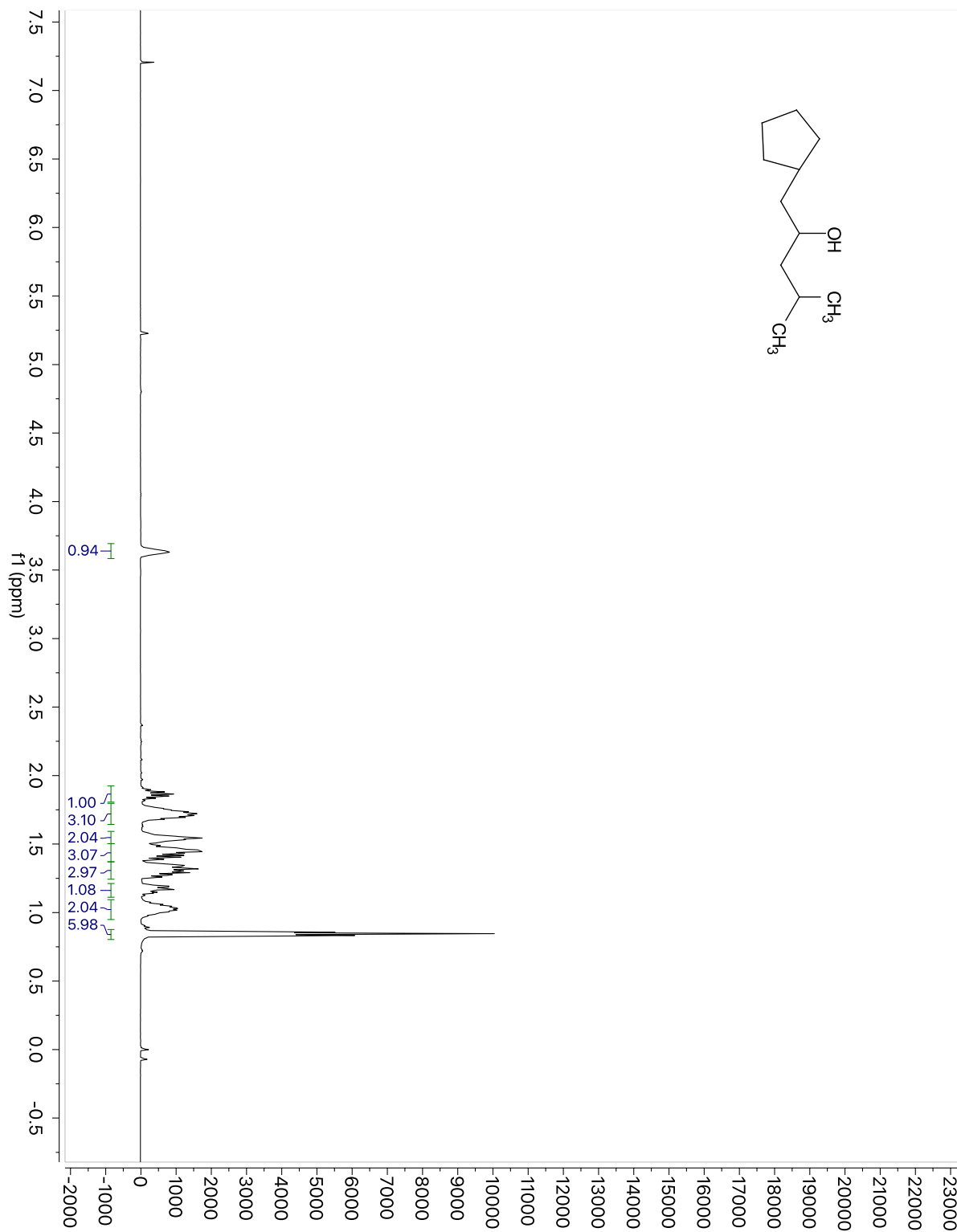


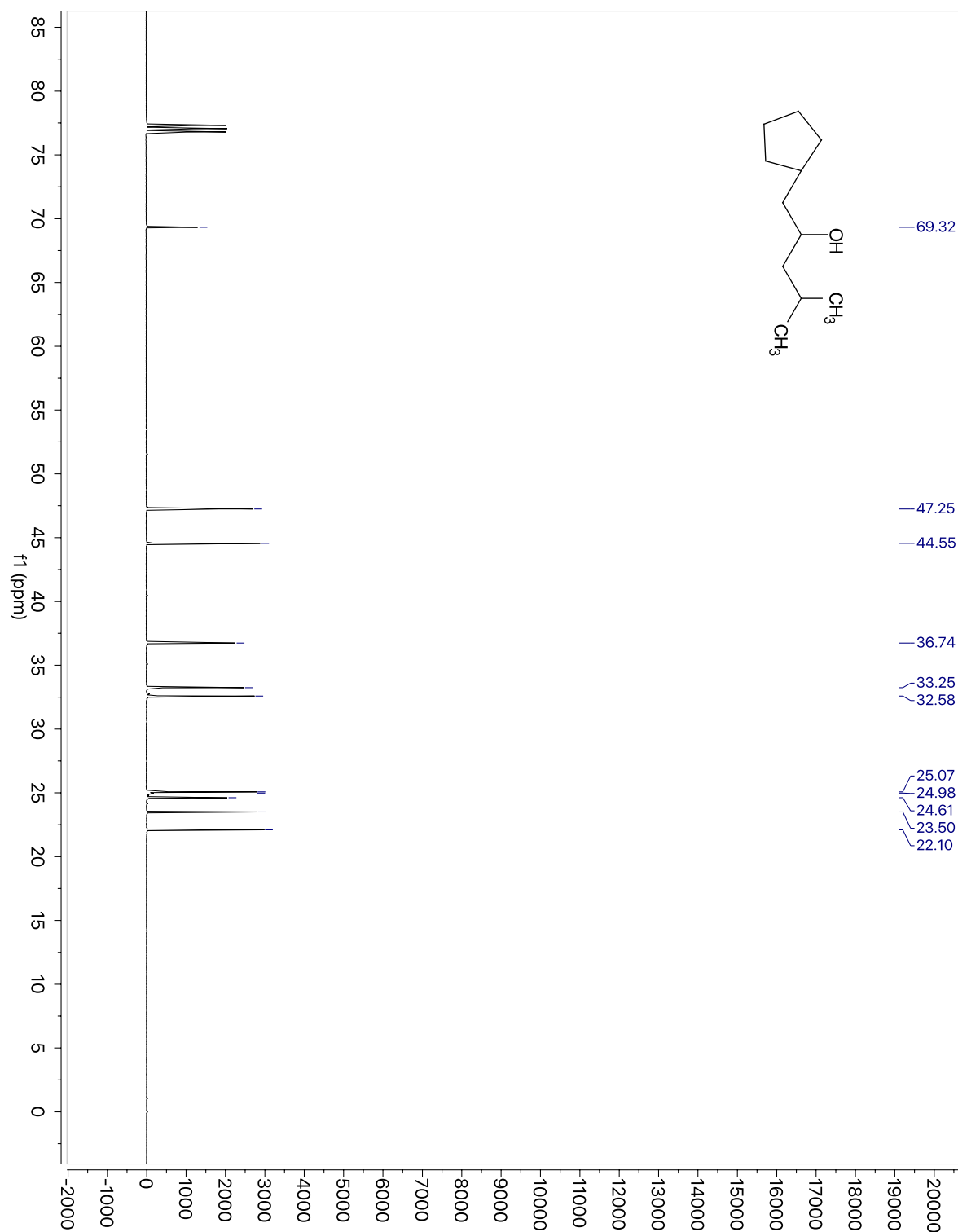
Compound 5.26. Iminocyclopentene **5.6a** (71.1 mg, 0.31 mmol, 1 equiv) was added to a round-bottom flask equipped with a stir bar and dissolved in MeOH (1 M). The solution was cooled to 0 °C with vigorous stirring prior to adding H_2O_2 (30% aqueous solution, 0.5 mL, 4.65 mmol, 15 equiv). A grain of solid NaOH

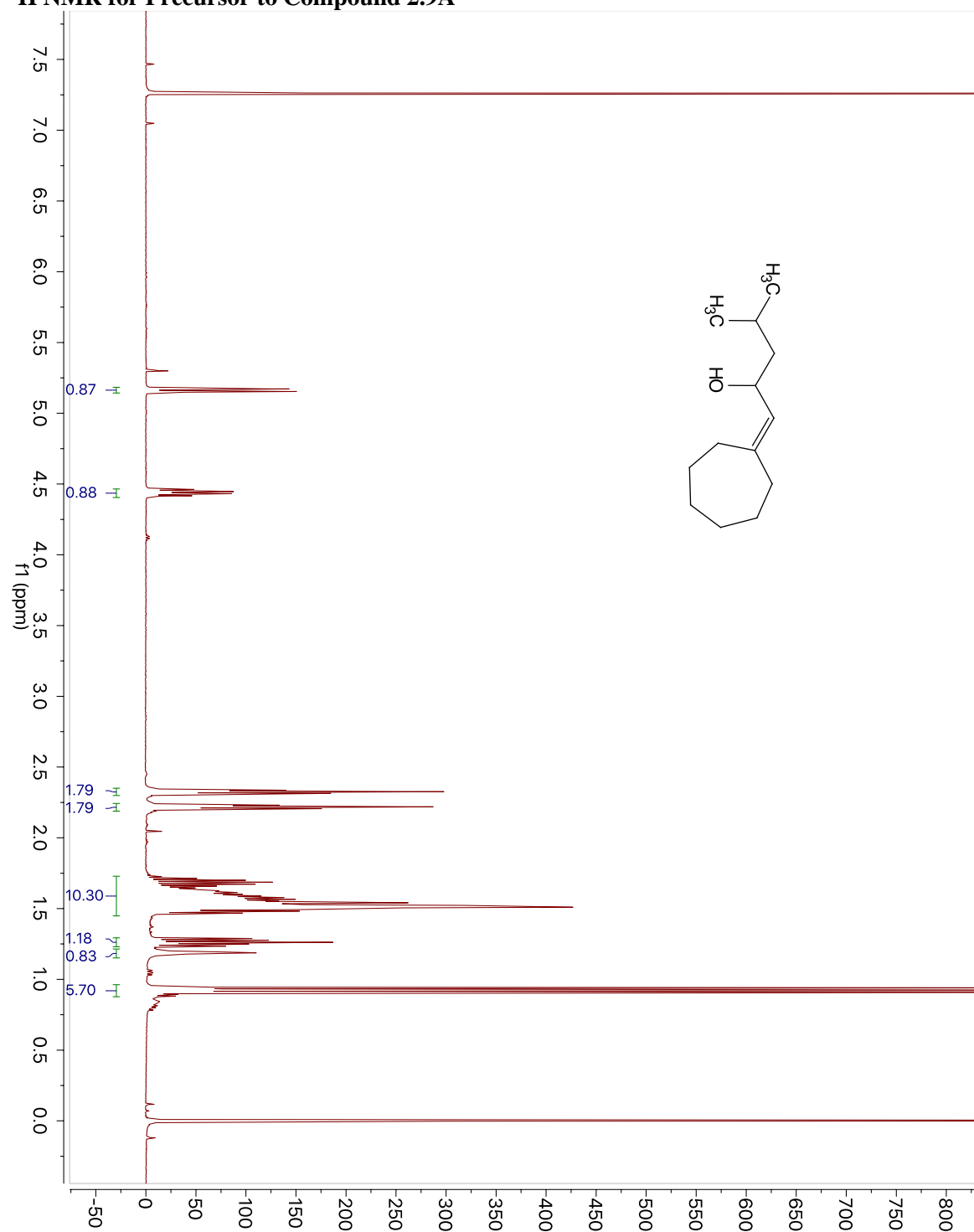
was then added (1-3 mg, 0.09 mmol, 0.3 equiv) and the reaction stirred for 3.5 h with no additional ice added to the water bath. At this point, complete consumption of starting material was observed according to TLC analysis and the reaction was poured into an ice-filled beaker of brine to quench. The aqueous layer was extracted thrice with CH_2Cl_2 before drying the combined organic extracts over Na_2SO_4 , filtering the salts, and removing the volatiles under reduced pressure (70% NMR yield, 4.8:1 mixture). The crude was sufficiently pure to recommend carrying forward in

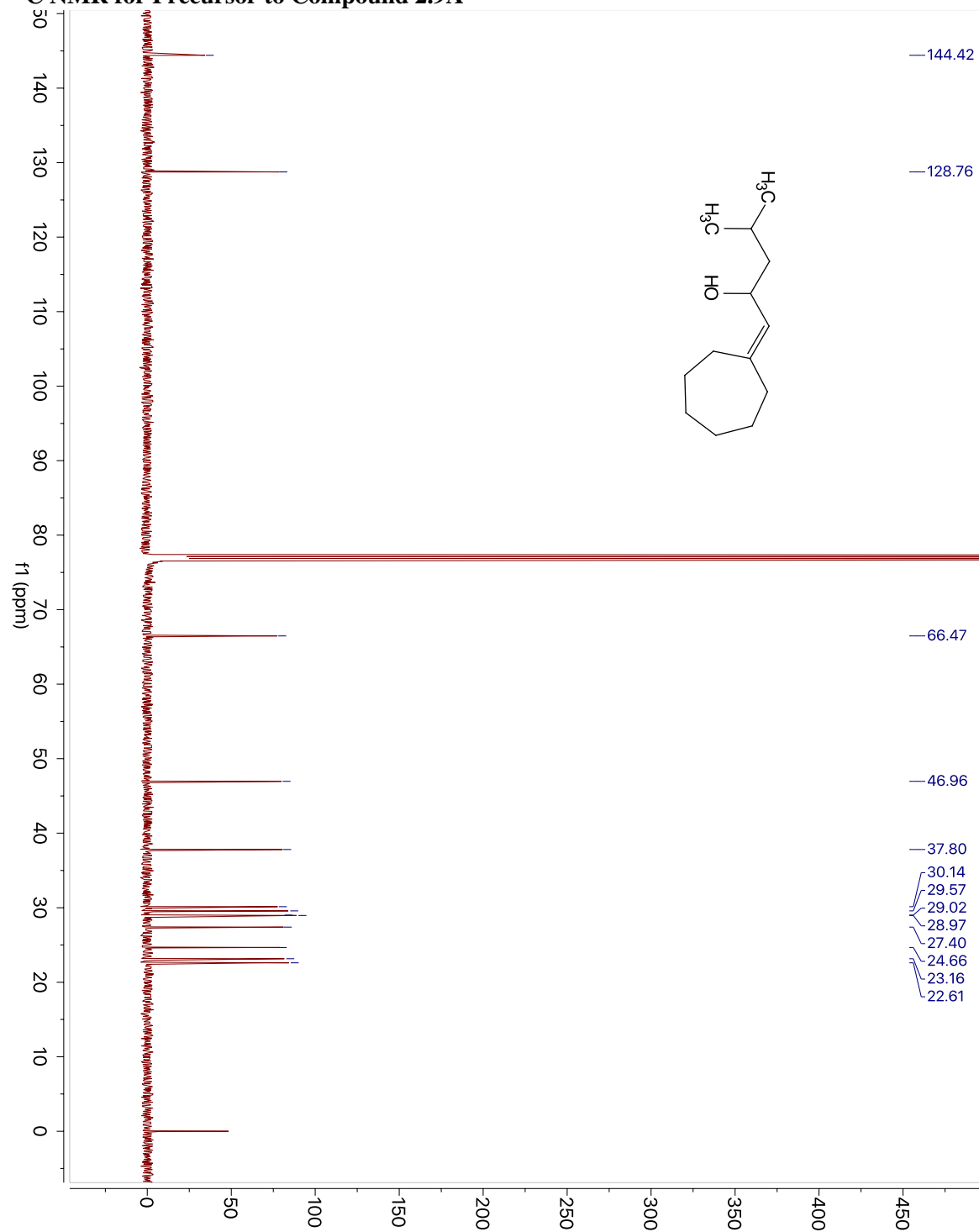
subsequent transformations; notably, further imine hydrolysis was observed when purifying over silica gel or Al₂O₃. **Compound 5.26** was an off-white/yellow solid (74.8 mg total, 0.24 mmol, 58% yield, >19:1 *dr* of epoxyimine). **¹H NMR** (500 MHz, Chloroform-*d*) δ 4.31 (dt, *J* = 12.2, 3.9 Hz, 1H), 4.25 (td, *J* = 11.7, 2.7 Hz, 1H), 4.01 (d, *J* = 2.6 Hz, 1H), 3.55 (d, *J* = 2.6 Hz, 1H), 2.44 – 2.33 (m, 1H), 2.24 – 2.15 (m, 1H), 1.77 – 1.73 (m, 2H), 1.61 (dq, *J* = 15.7, 2.8 Hz, 1H), 1.01 (d, *J* = 5.9 Hz, 3H), 0.95 (d, *J* = 6.2 Hz, 3H). **¹³C NMR** (126 MHz, CDCl₃) δ 211.5, 70.8, 60.6, 59.4, 55.8, 48.8, 35.0, 29.2, 21.2, 20.7. **HRMS** (ESI-MS) *m/z* calculated for C₁₀H₁₅NO₄S [M+H]⁺ 246.0795, measured 246.0792 (1.2 ppm).

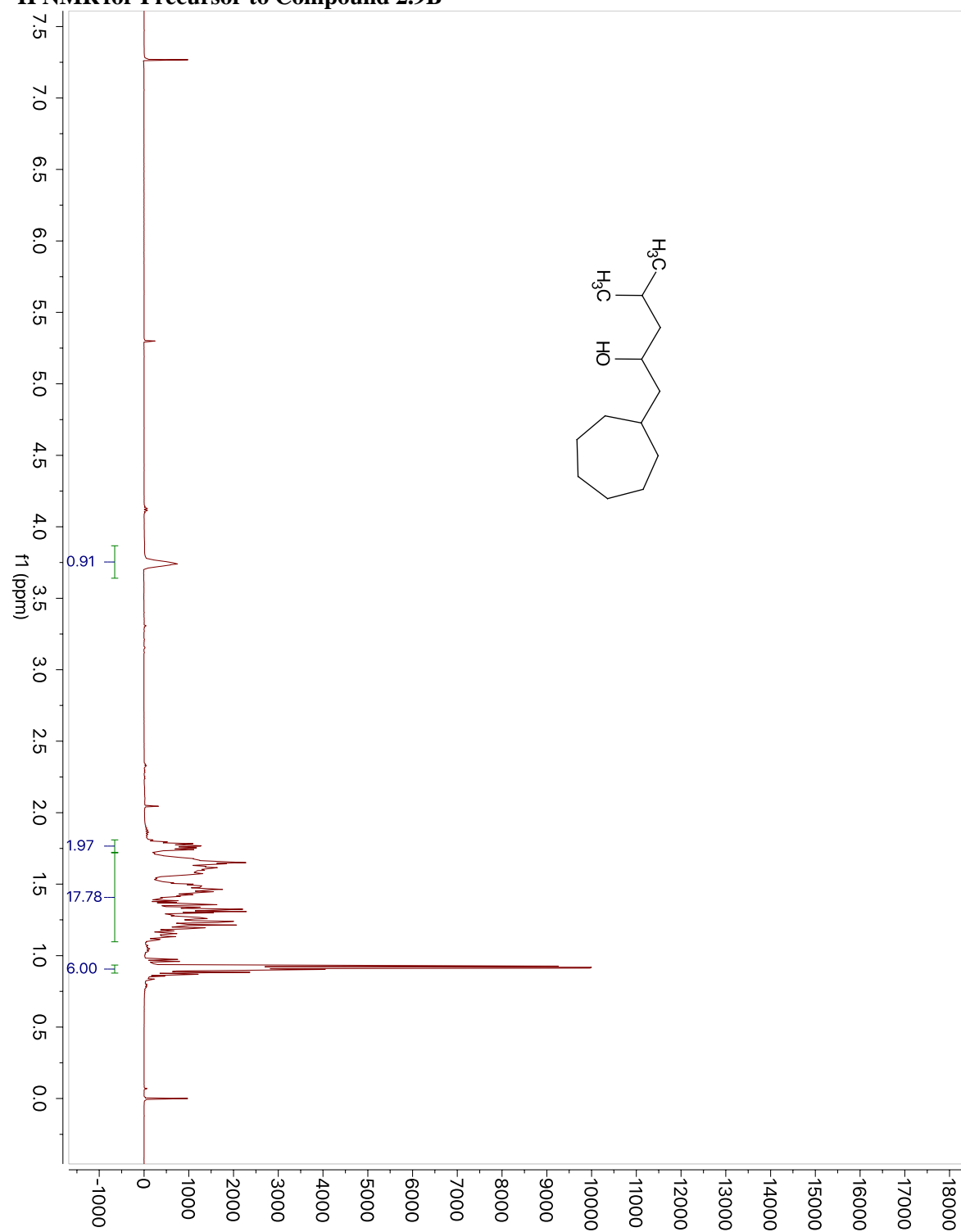
Appendix: ^1H - and ^{13}C -NMR Data, X-Ray Data, and Computational Data

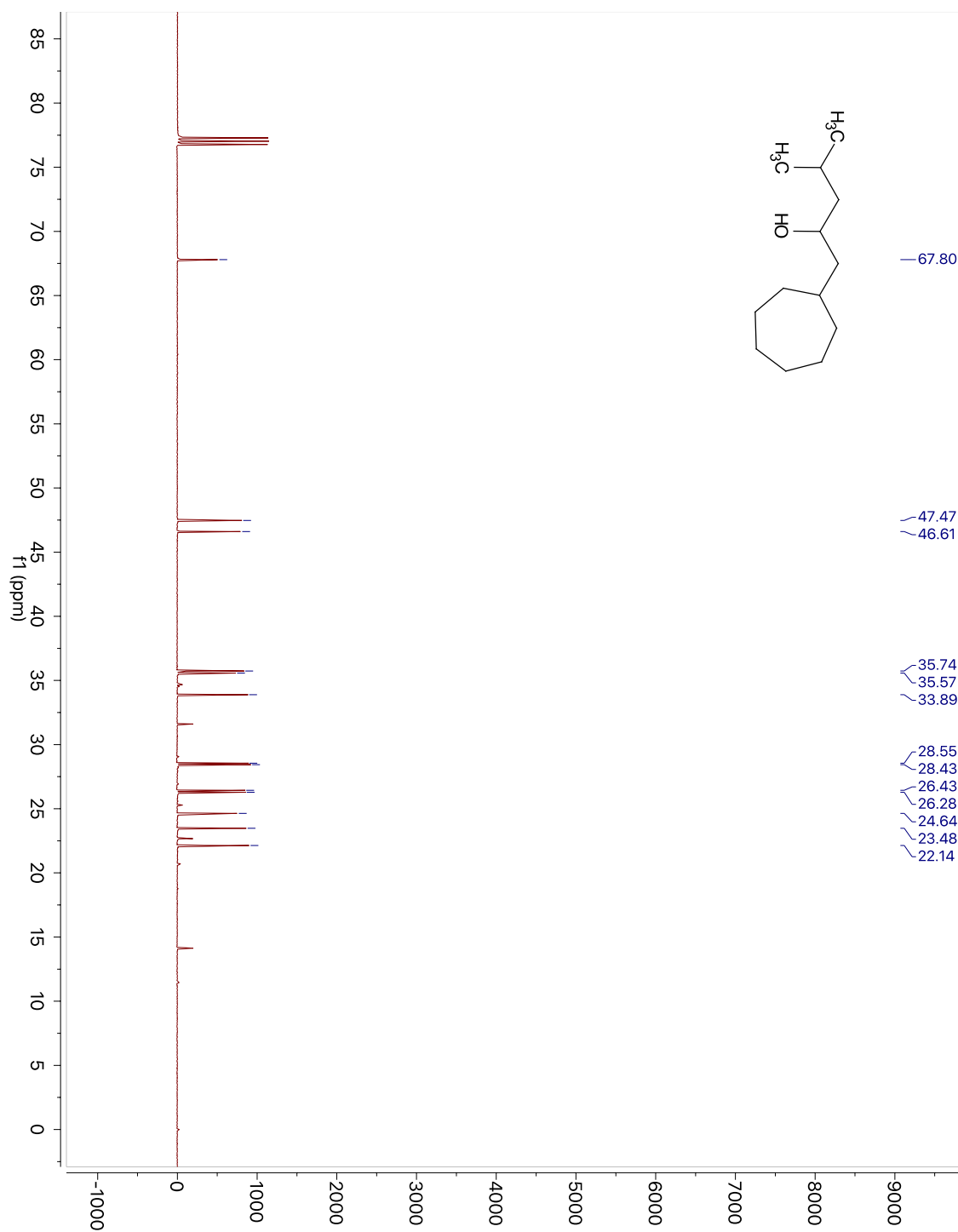
Chapter 2 ^1H - and ^{13}C -NMR Data ^1H NMR for Precursor to Compound 2.8

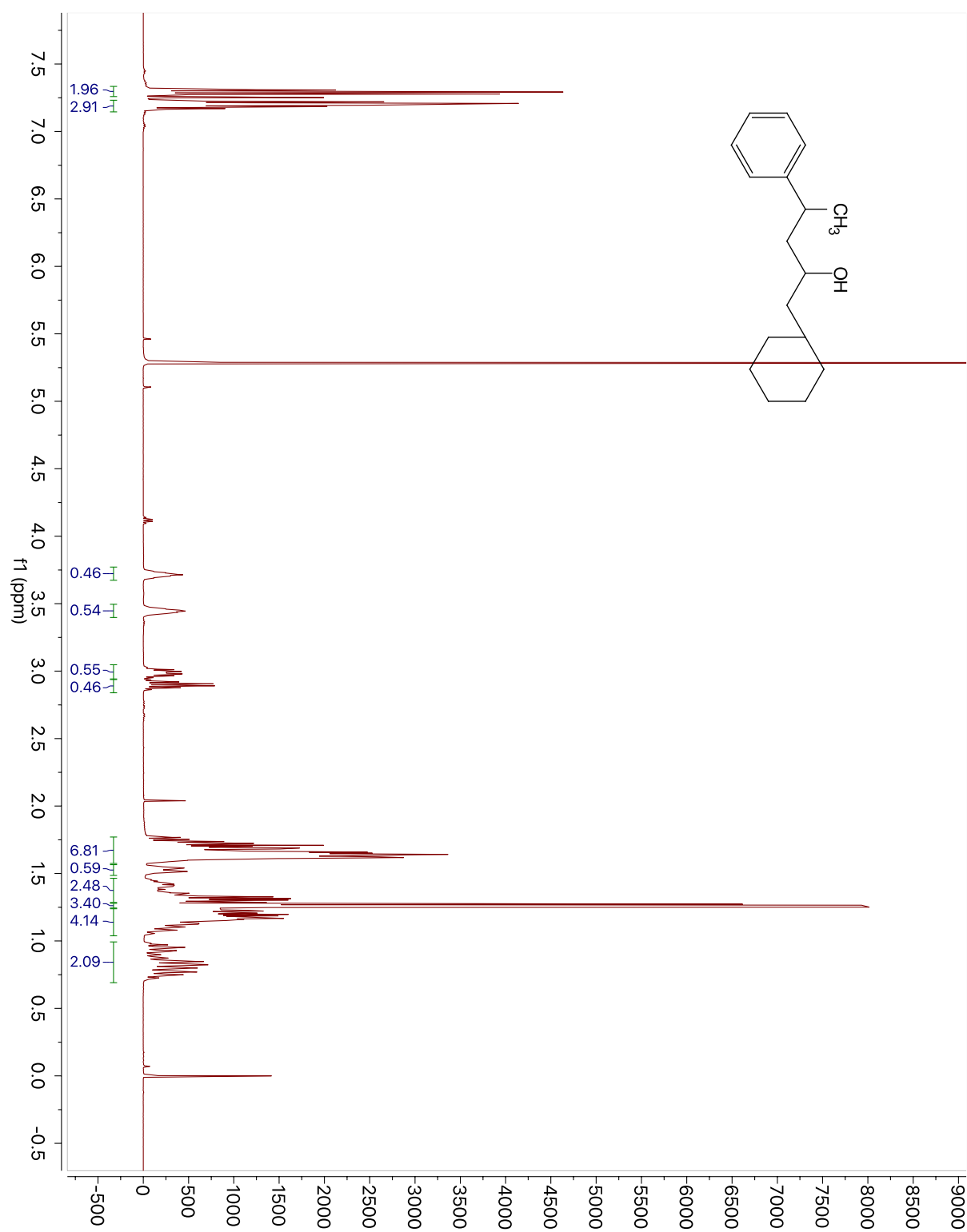
^{13}C NMR for Precursor to Compound 2.8

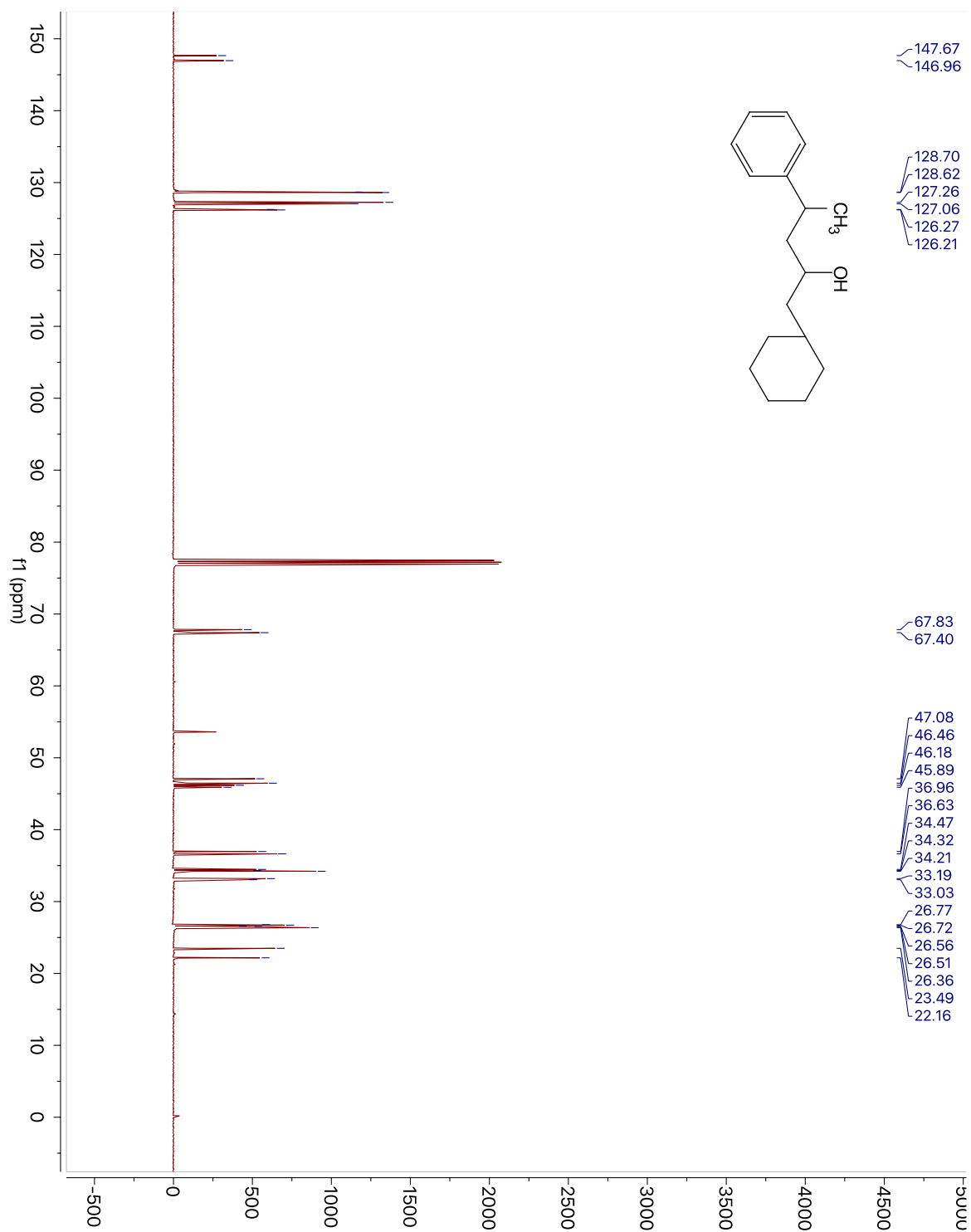
¹H NMR for Precursor to Compound 2.9A

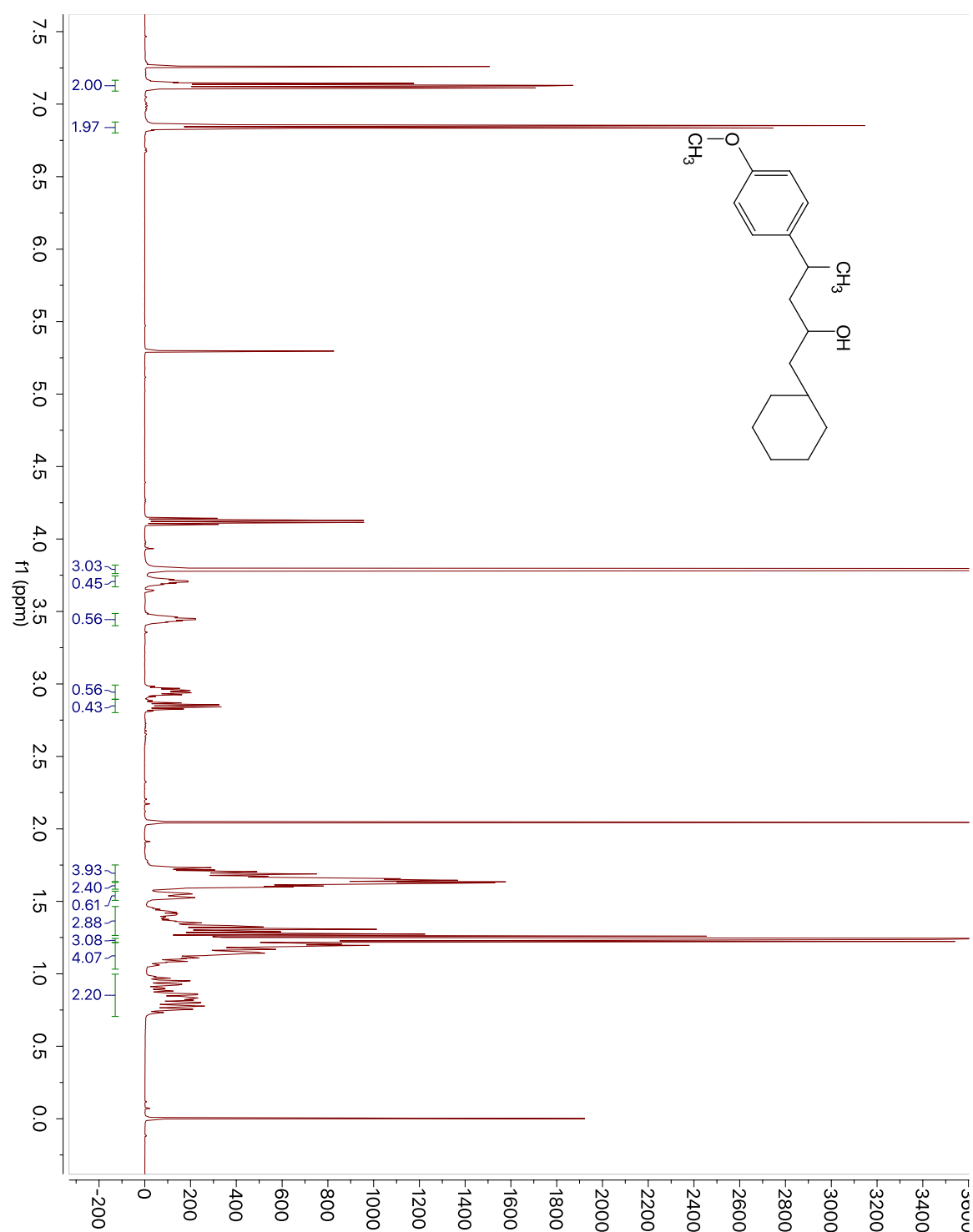
^{13}C NMR for Precursor to Compound 2.9A

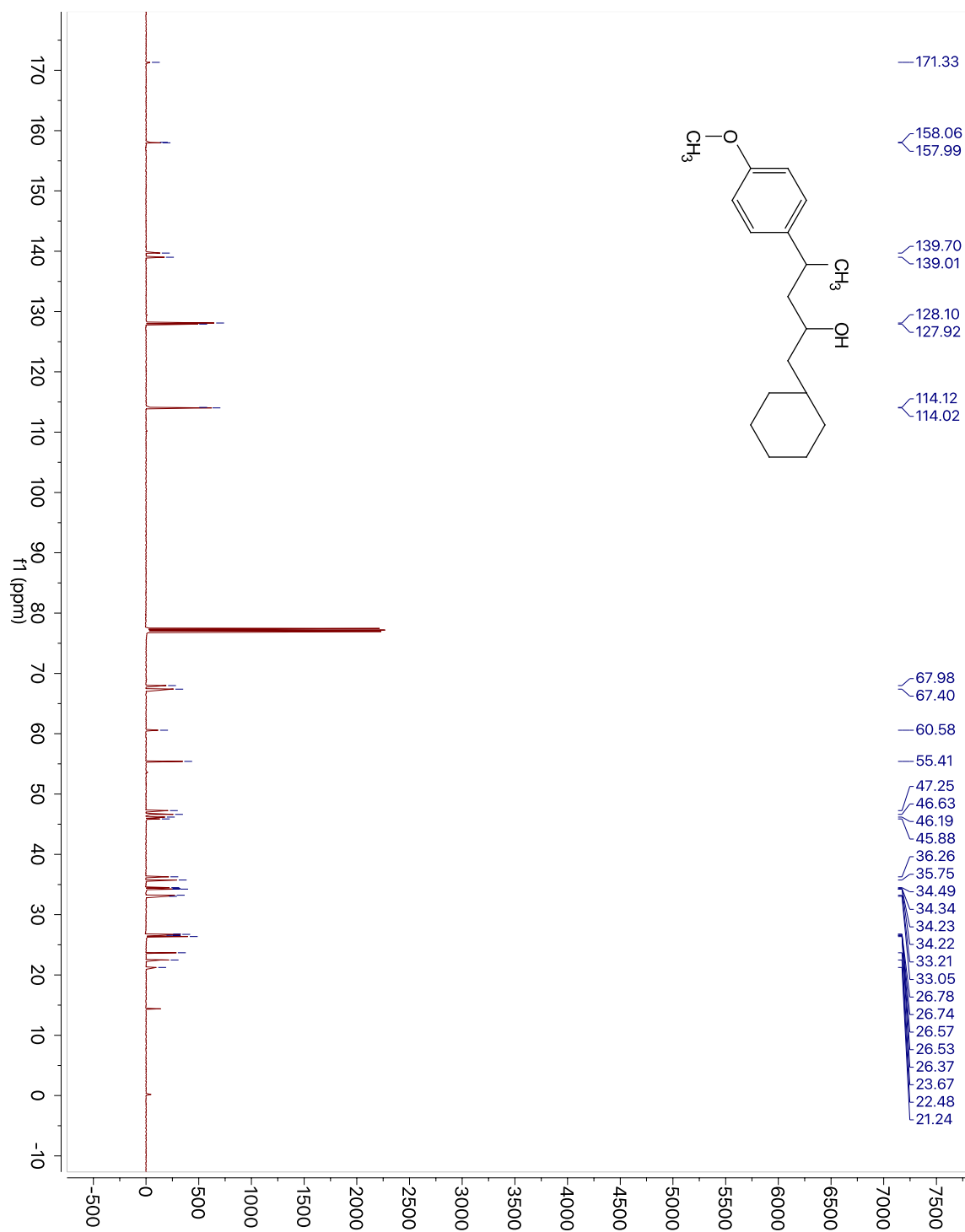
^1H NMR for Precursor to Compound 2.9B

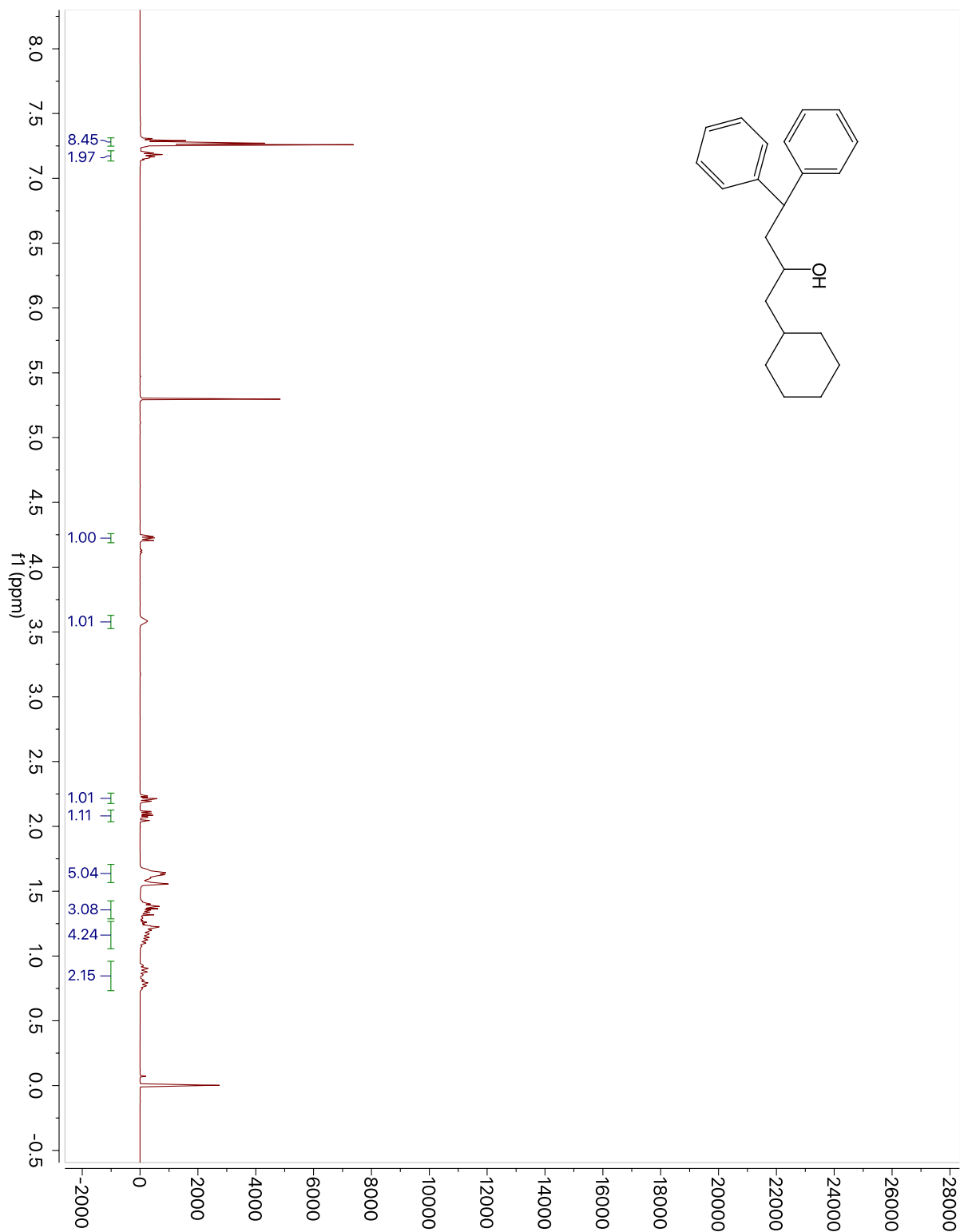
^{13}C NMR for Precursor to Compound 2.9B

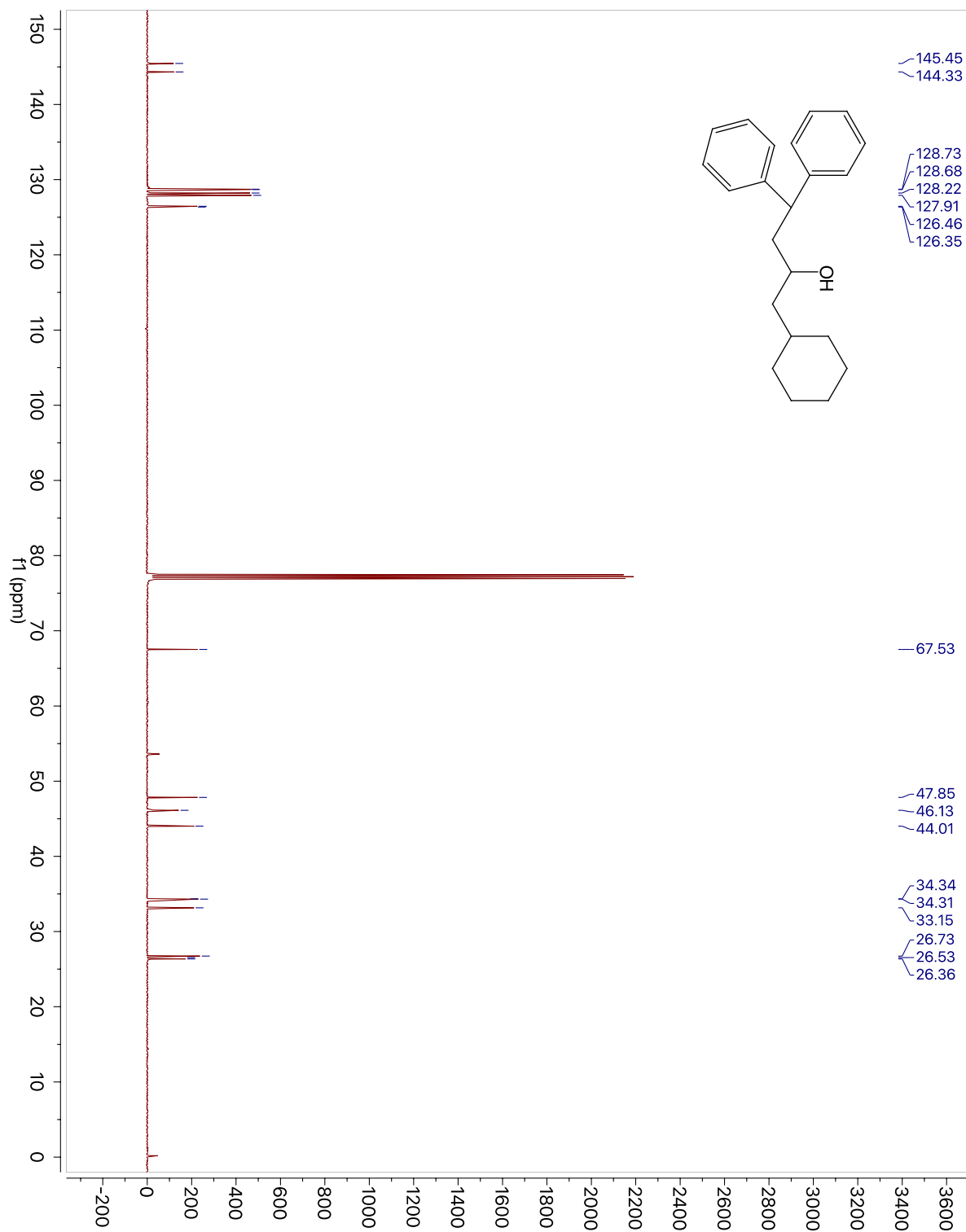
¹H NMR for Precursor to Compound 2.10

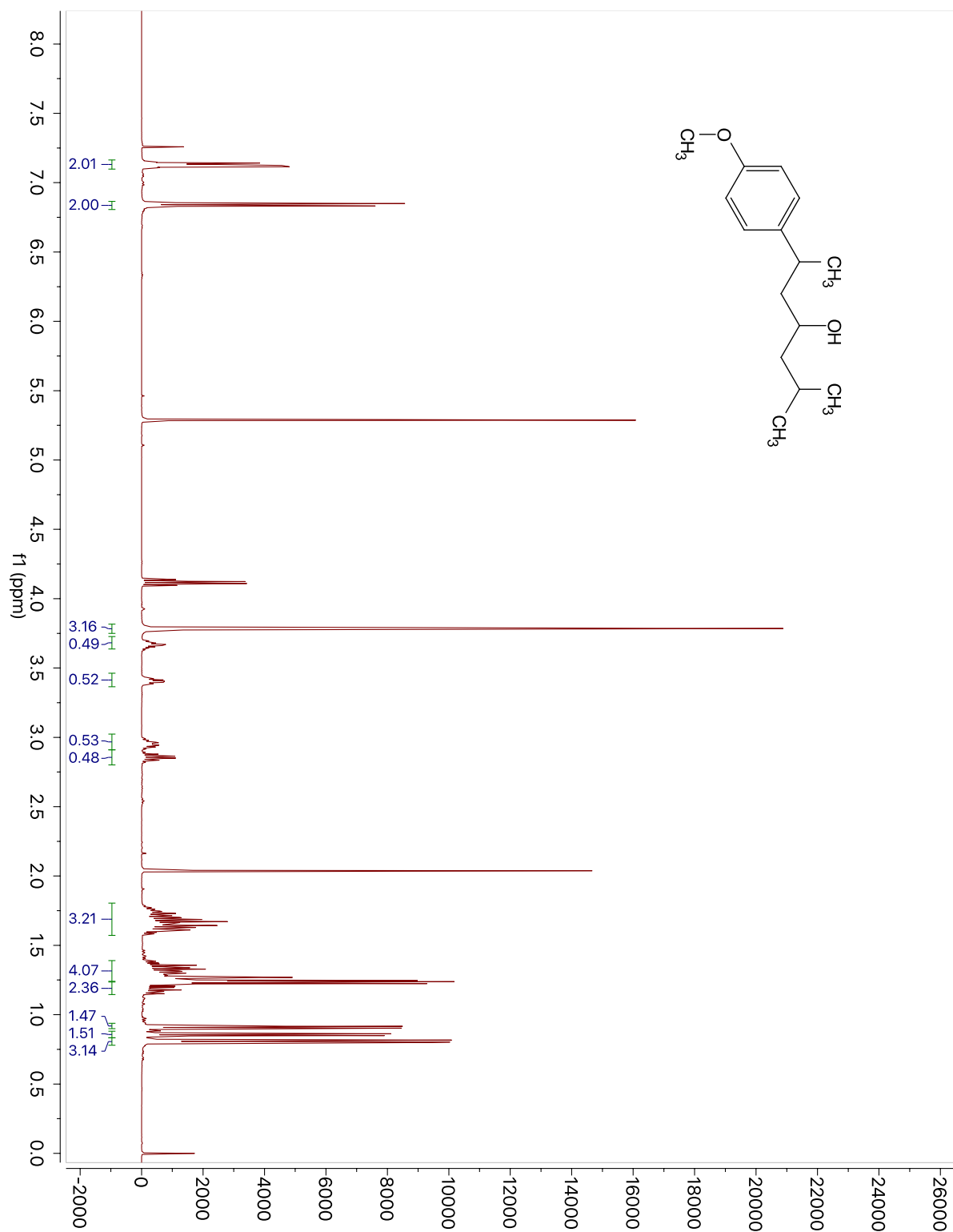
^{13}C NMR for Precursor to Compound 2.10

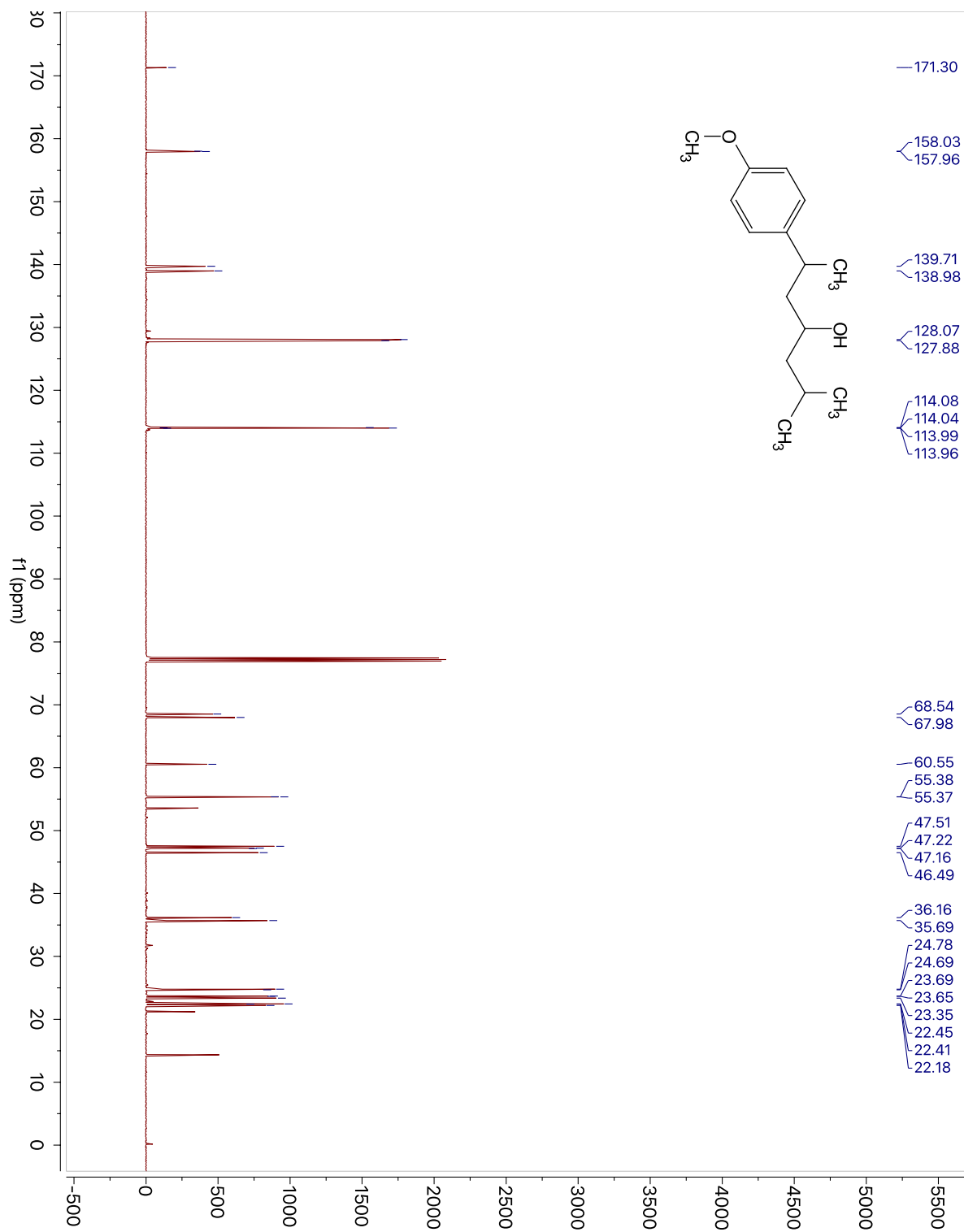
¹H NMR for Precursor to Compound 2.11

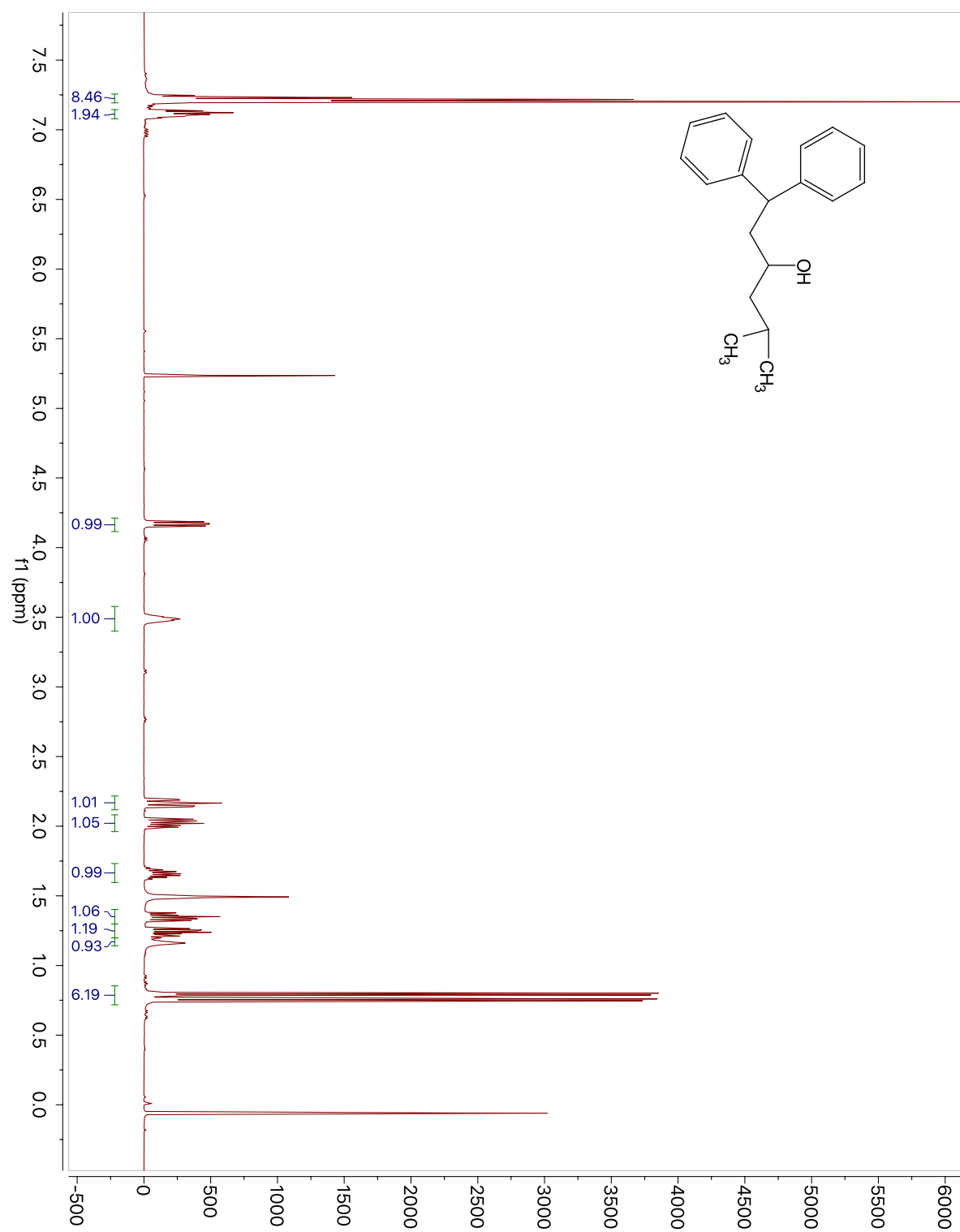
^{13}C NMR for Precursor to Compound 2.11

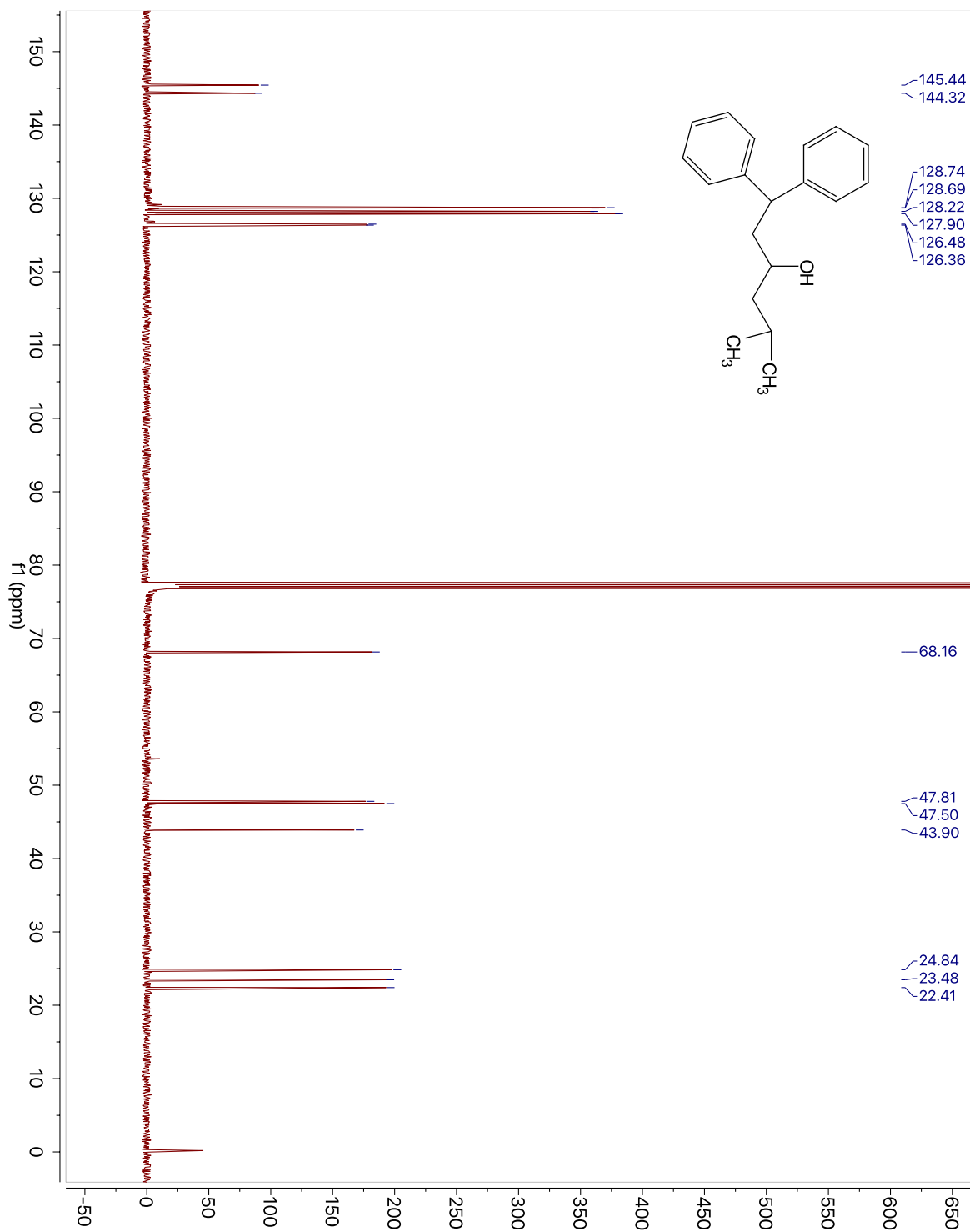
^1H NMR for Precursor to Compound 2.12.

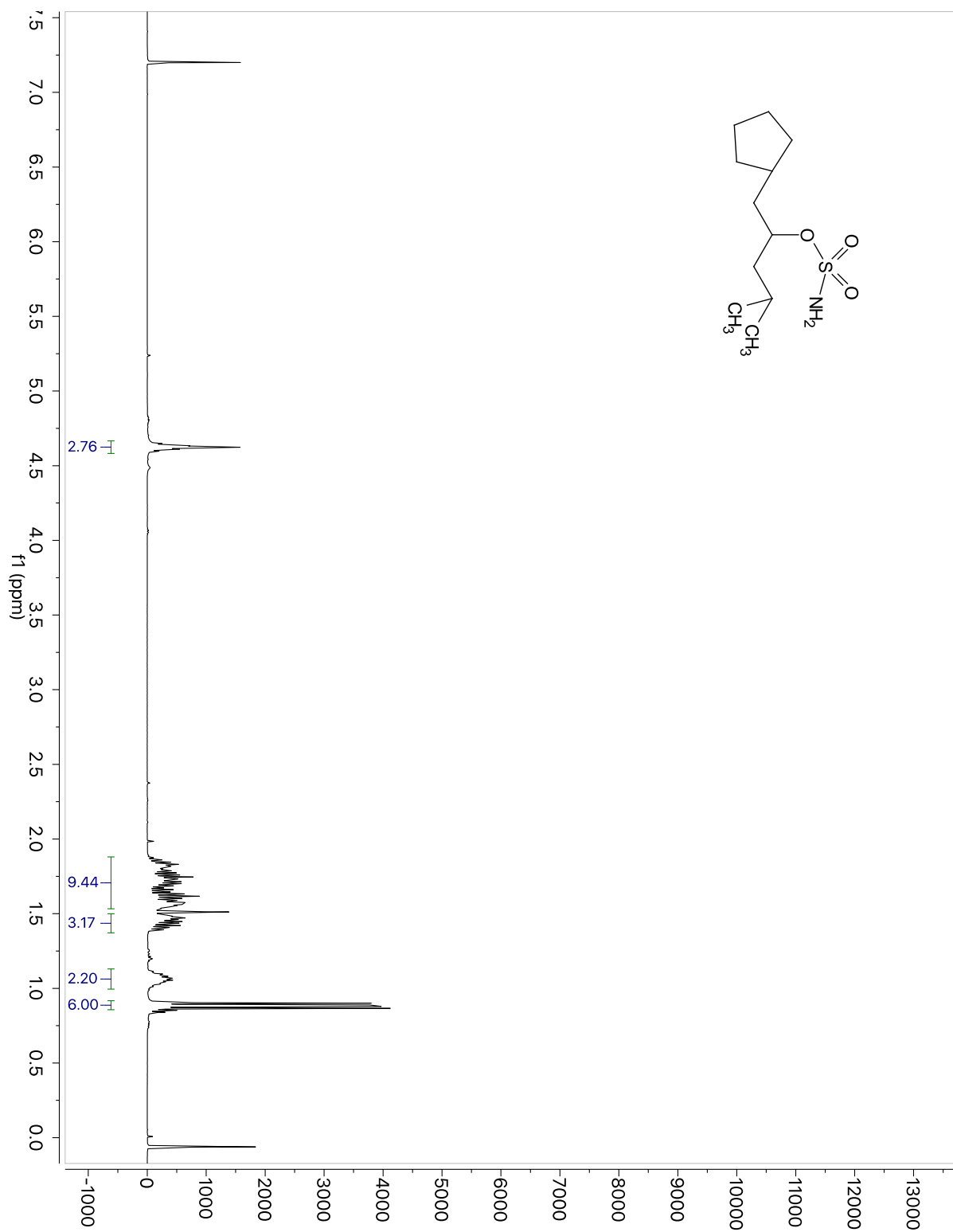
^{13}C NMR for Precursor to Compound 2.12

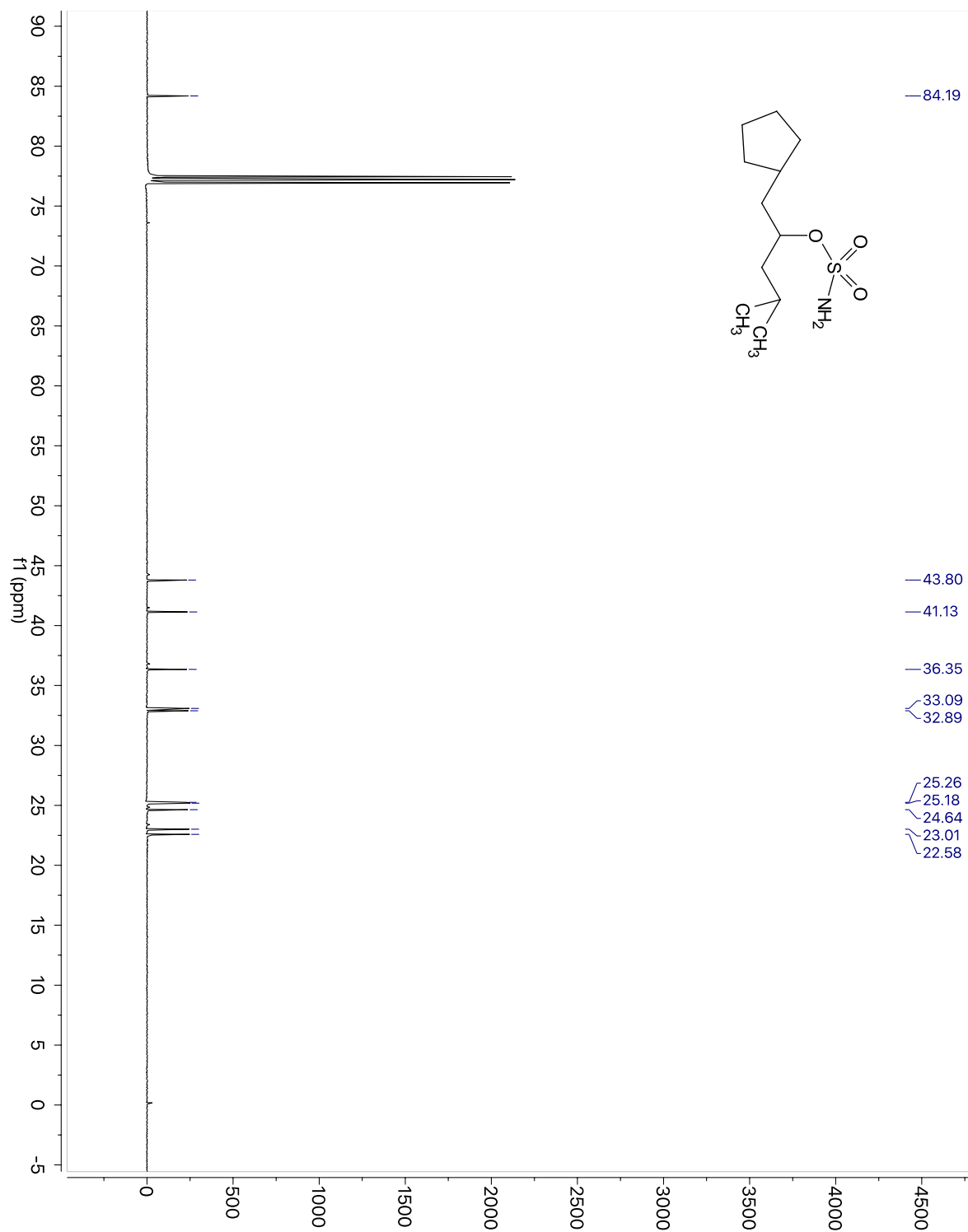
¹H NMR for Precursor to Compound 2.14

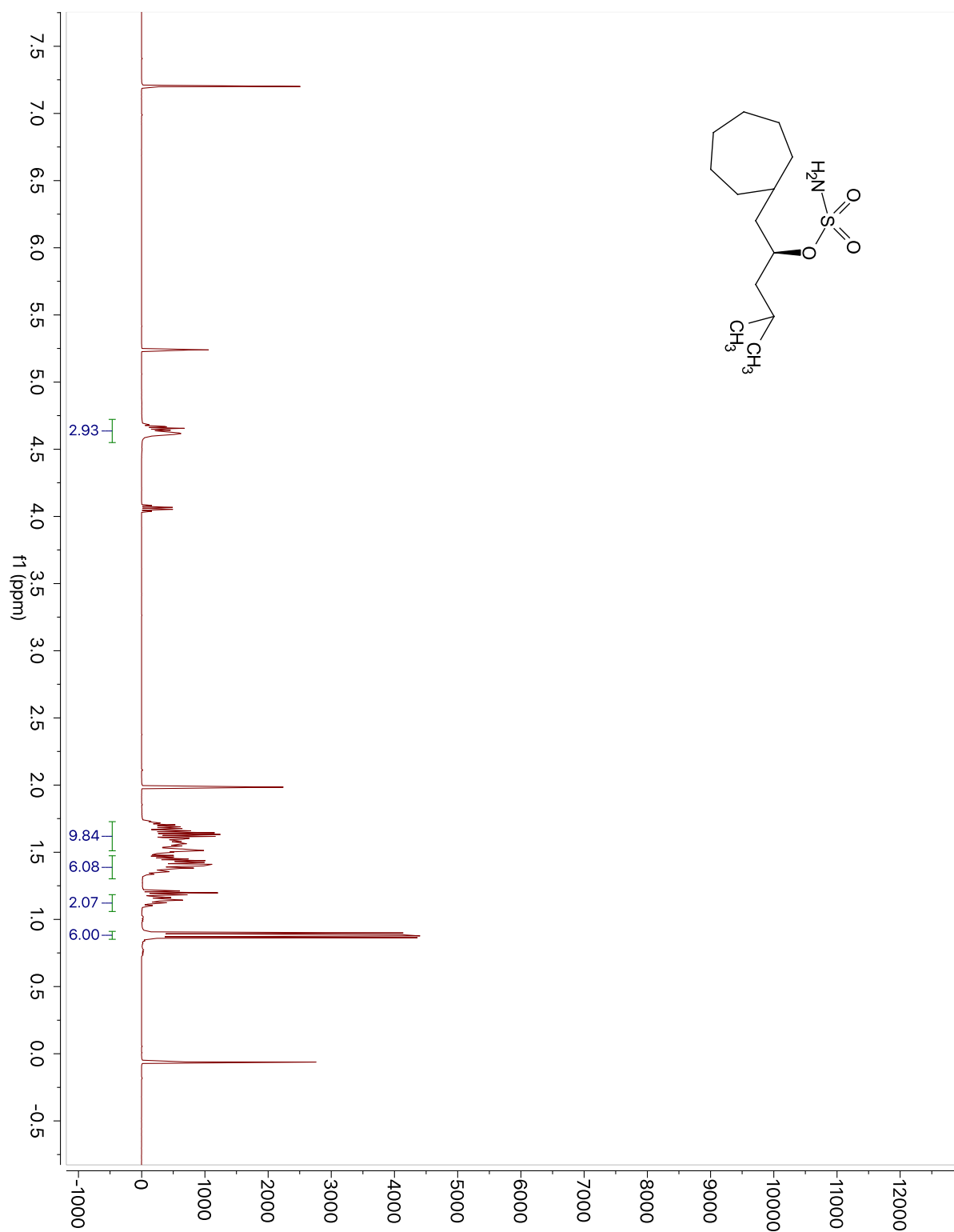
^{13}C NMR for Precursor to Compound 2.14

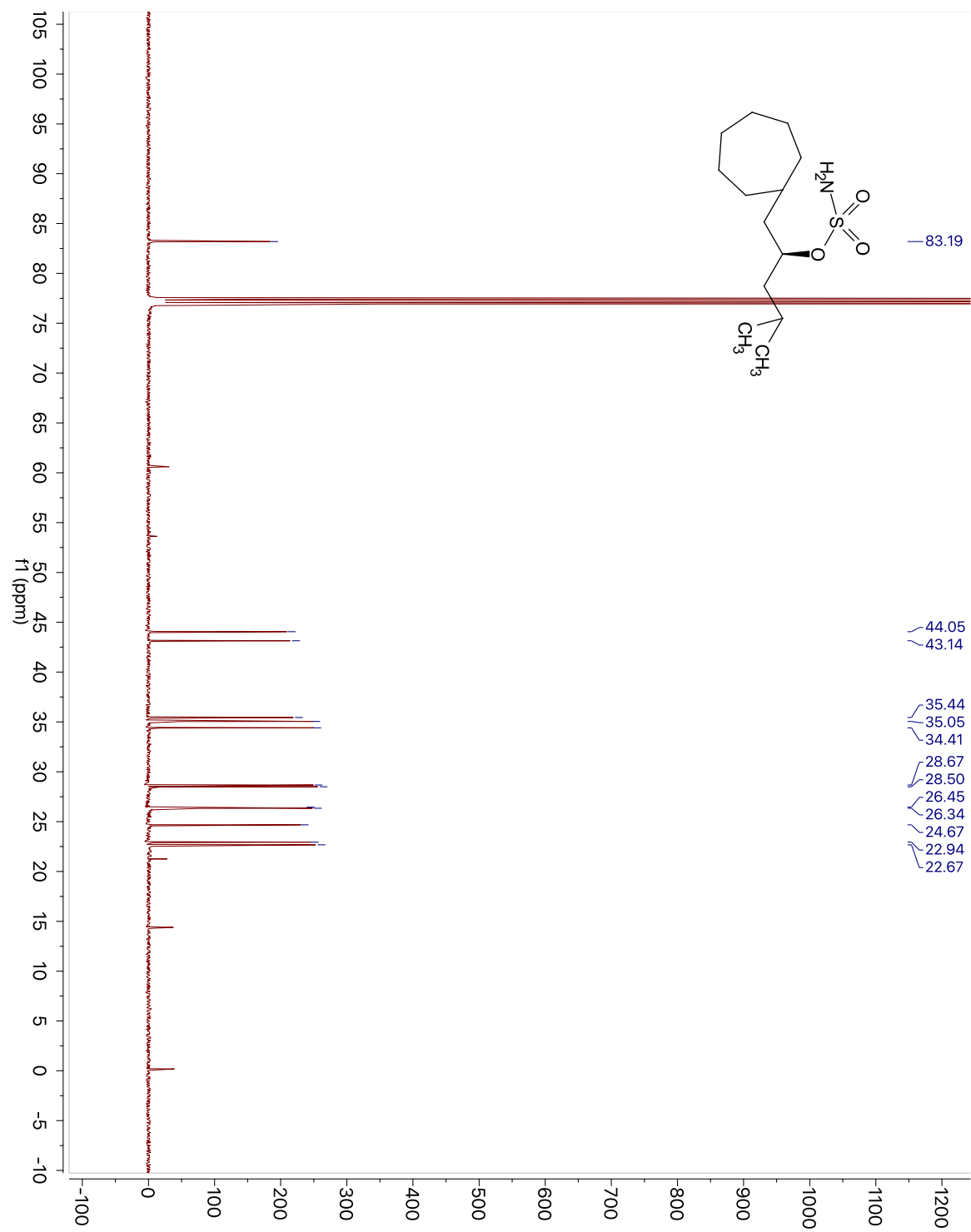
¹H NMR for Precursor to Compound 2.15

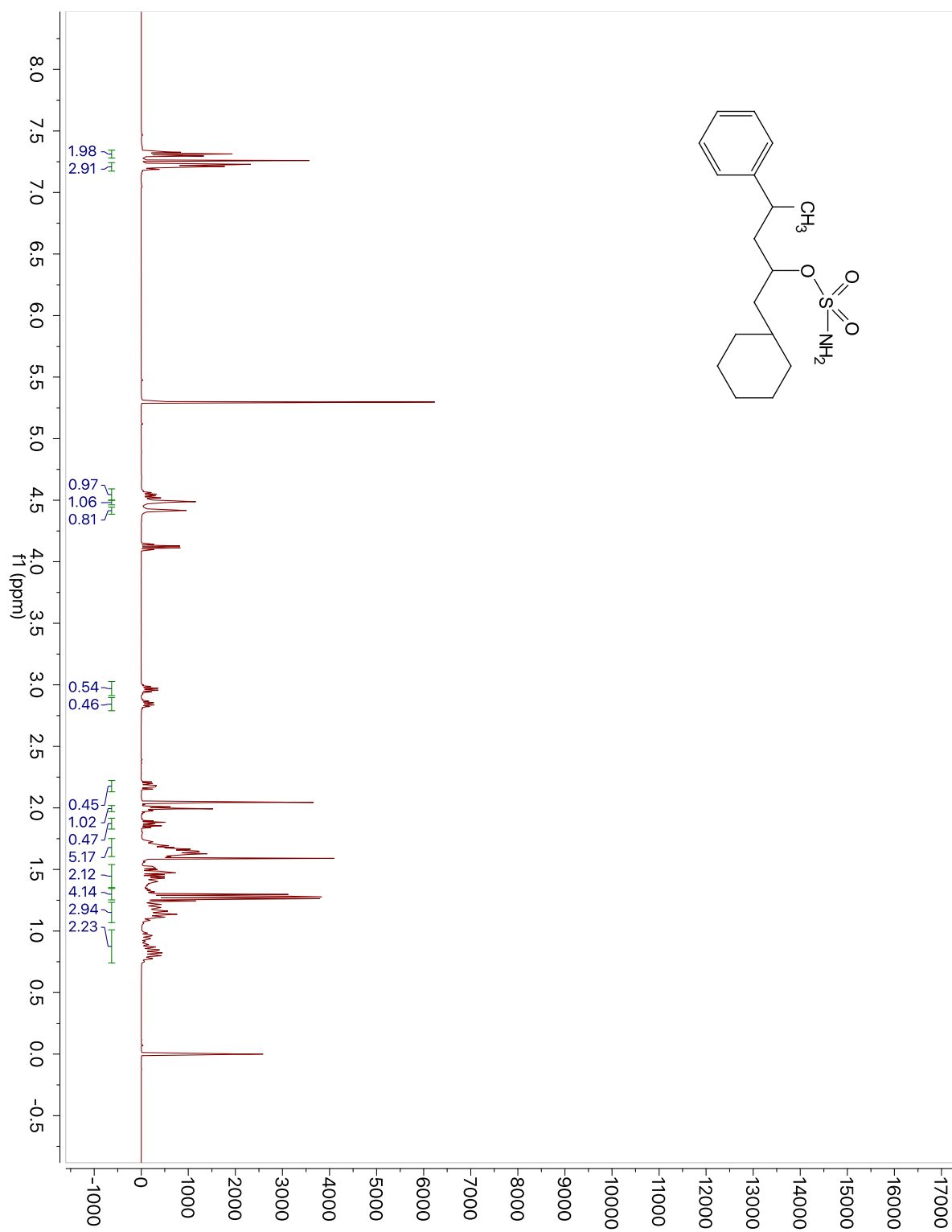
^{13}C NMR for Precursor to Compound 2.15.

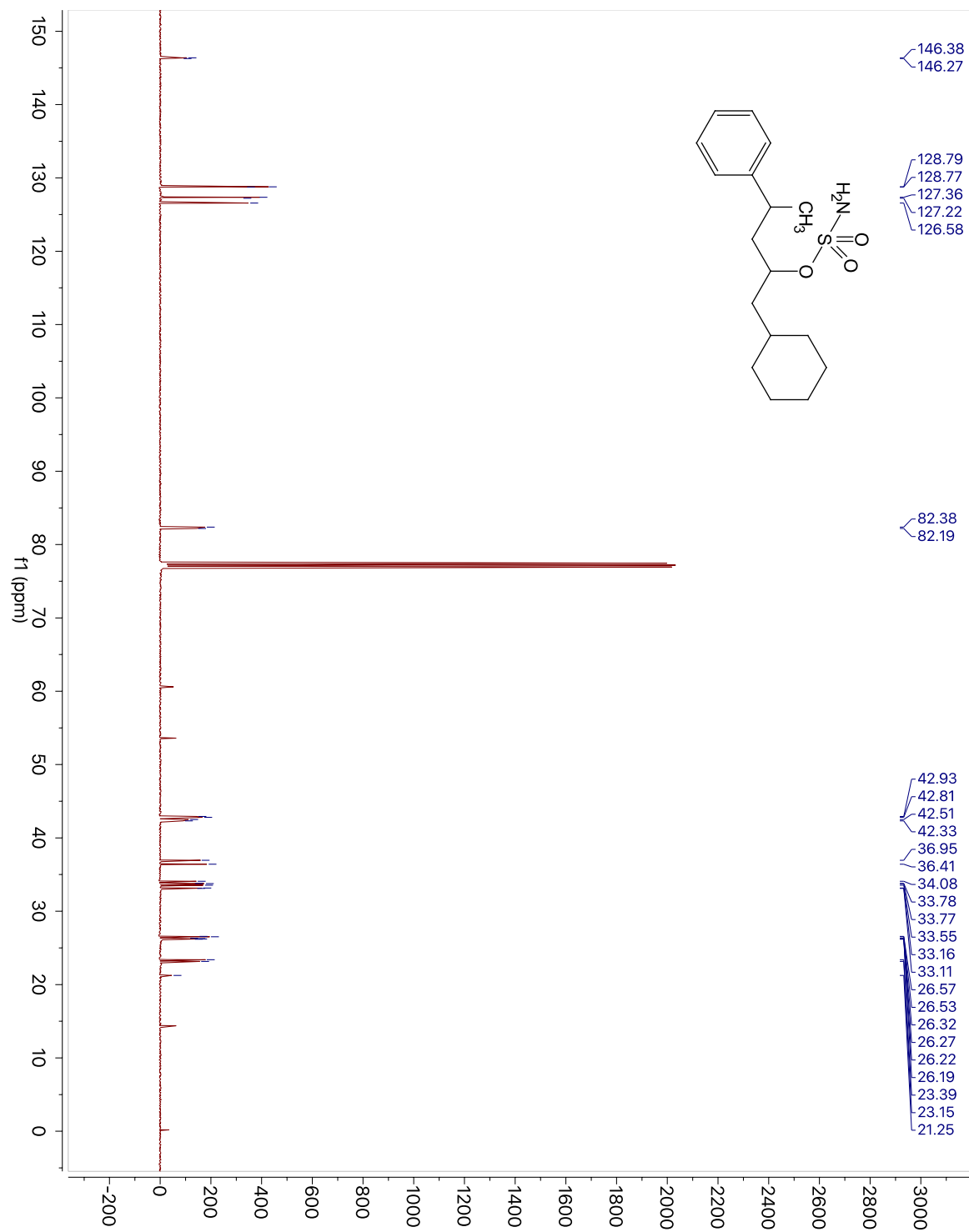
¹H NMR for Compound 2.8.

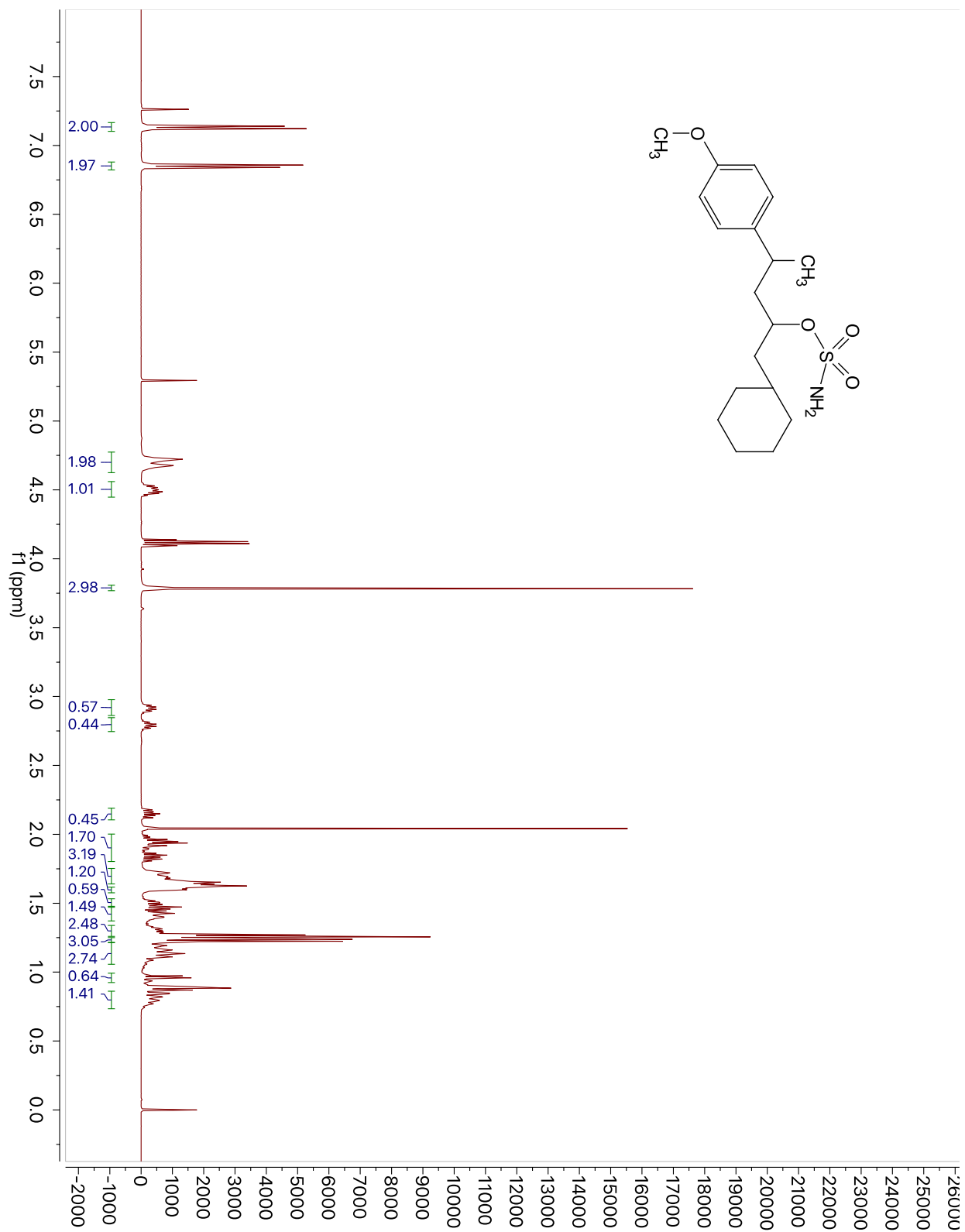
^{13}C NMR for Compound 2.8.

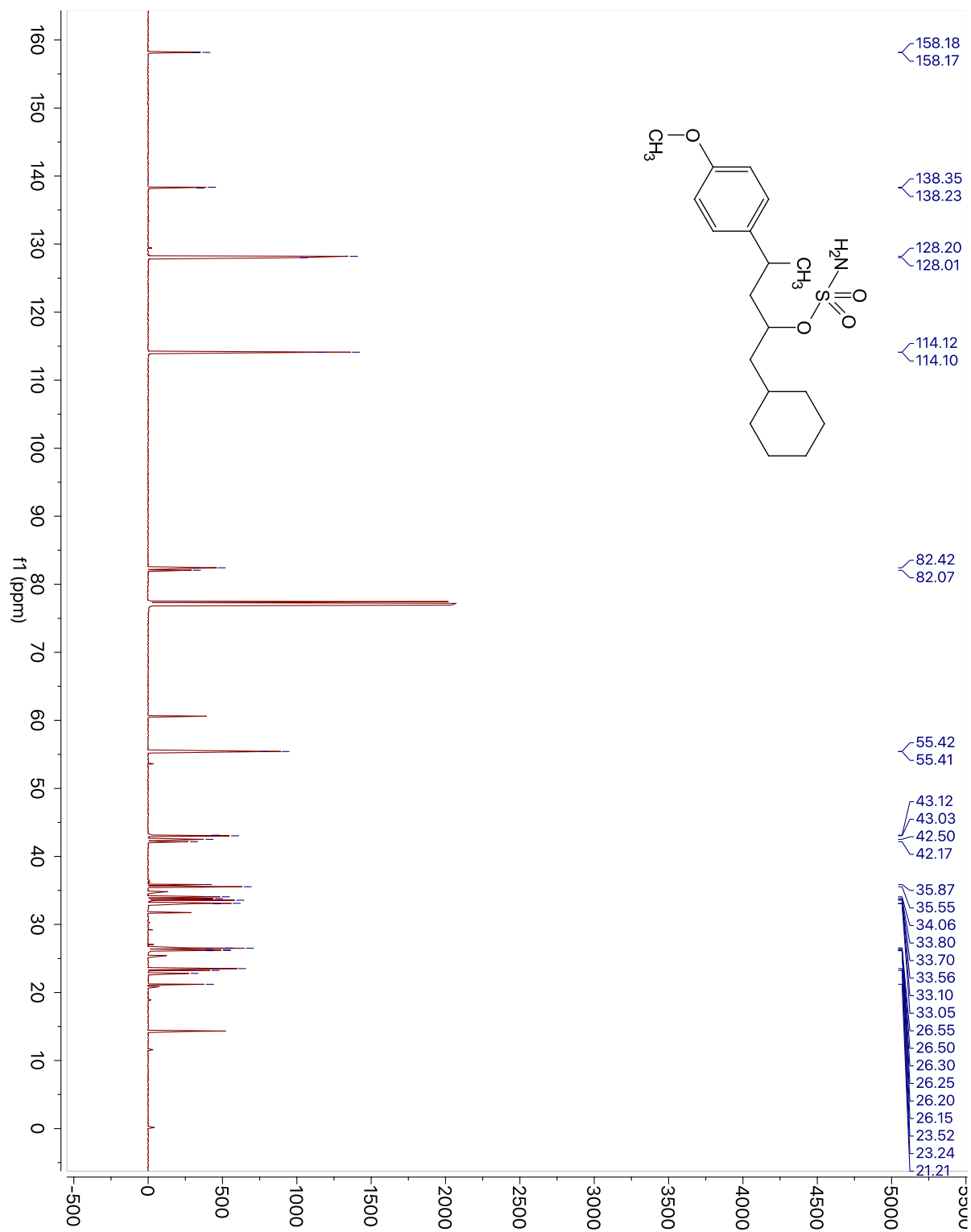
¹H NMR for Compound 2.9.

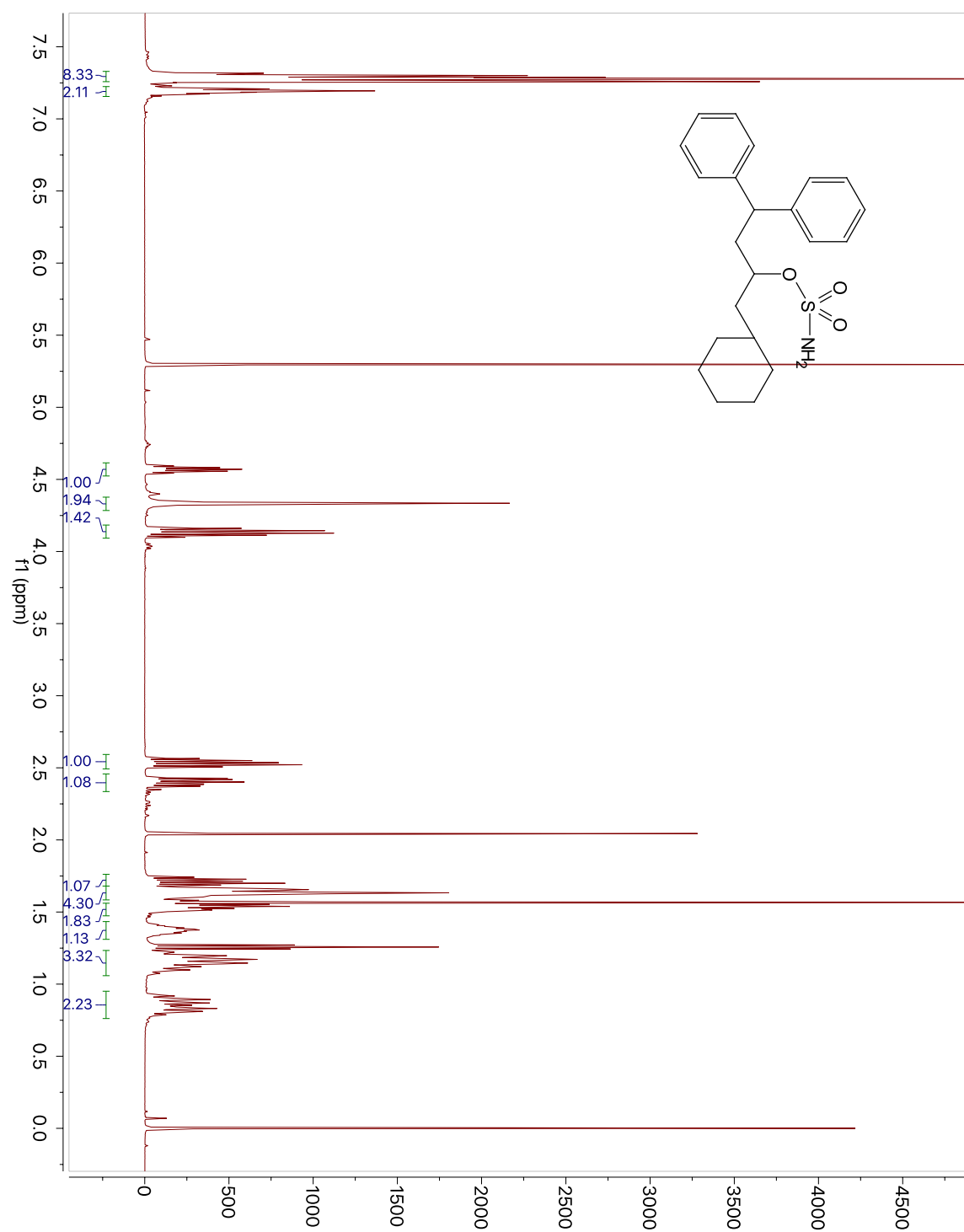
^{13}C NMR for Compound 2.9.

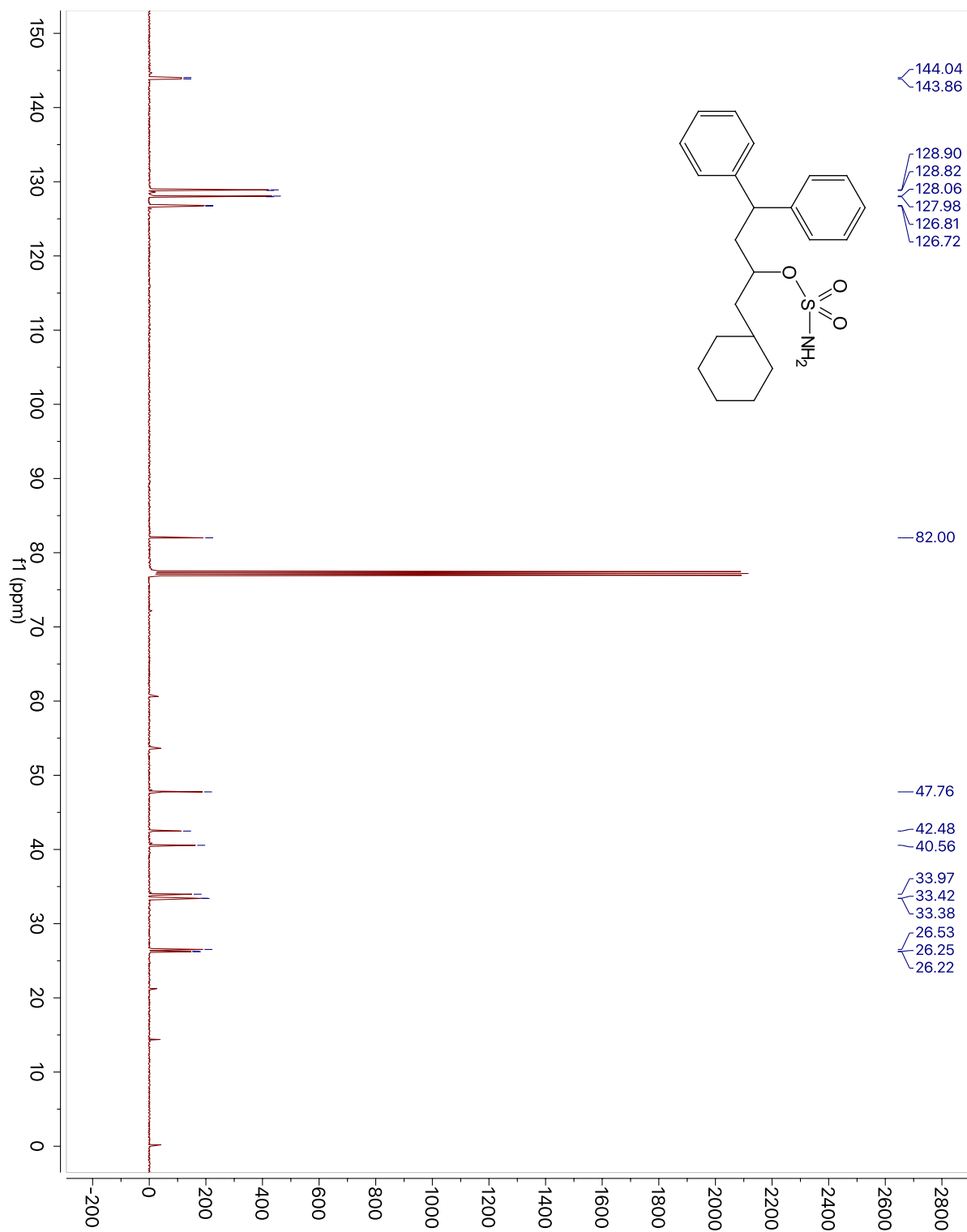
¹H NMR for Compound 2.10.

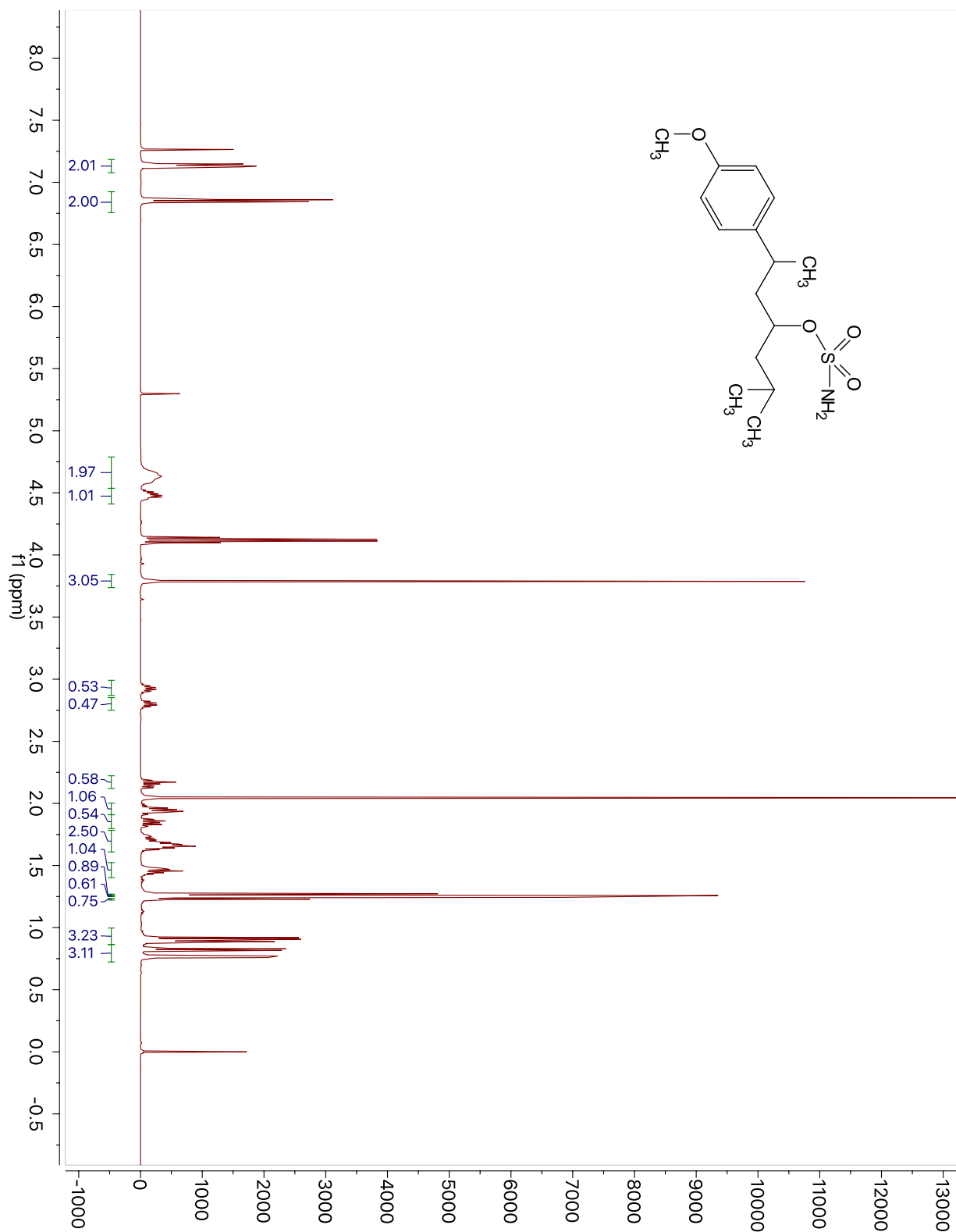
^{13}C NMR for Compound 2.10.

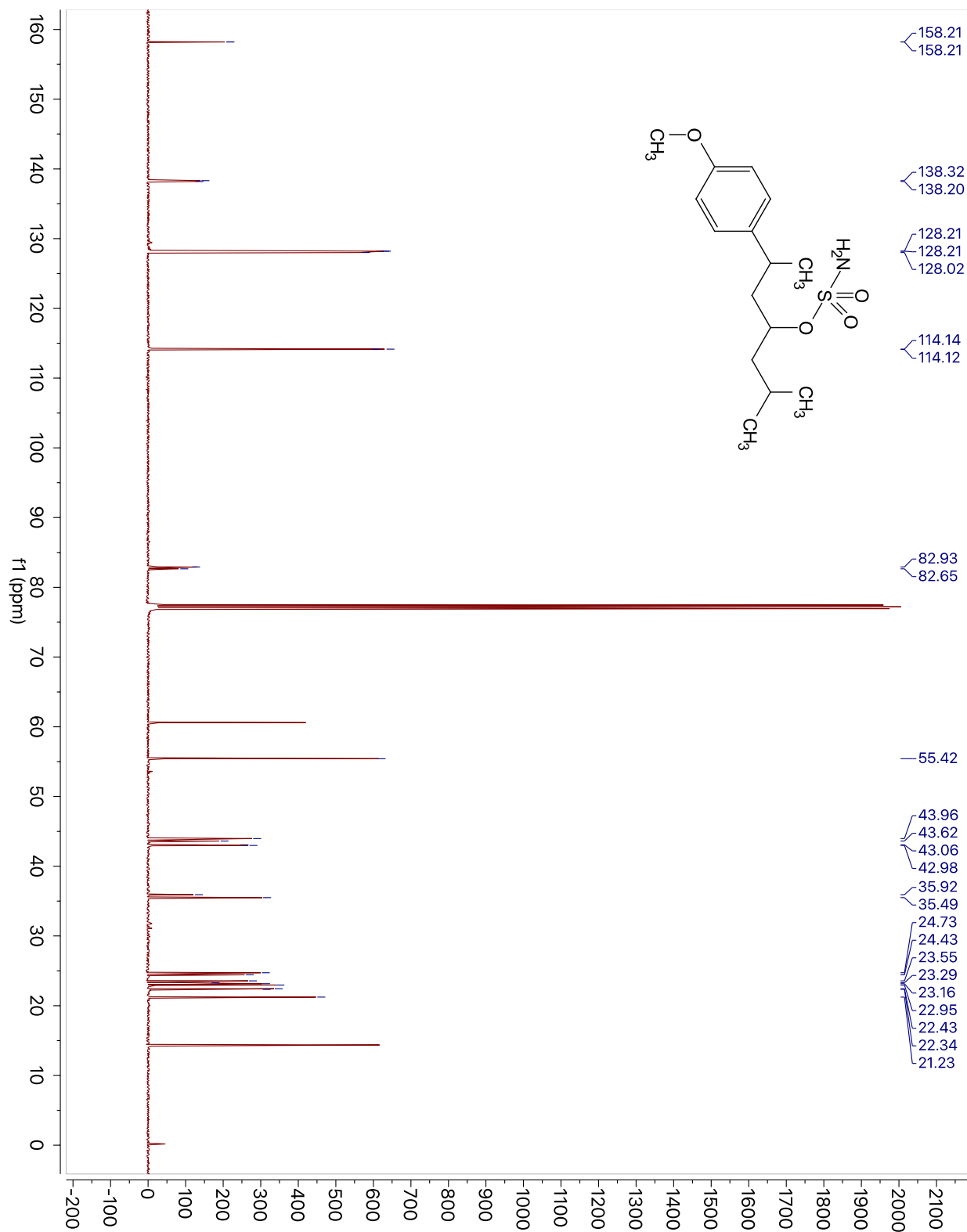
¹H NMR for Compound 2.11.

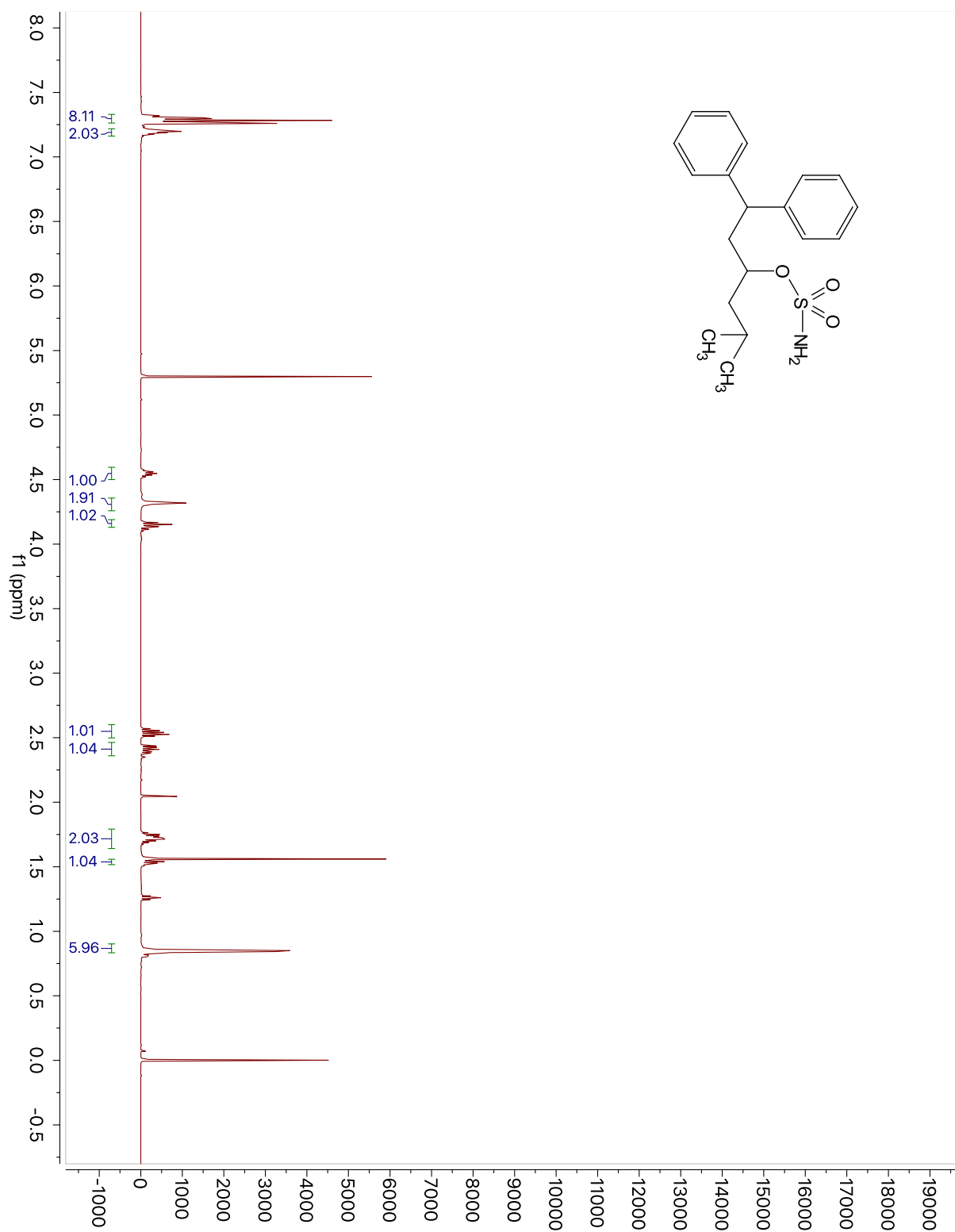
^{13}C NMR for Compound 2.11.

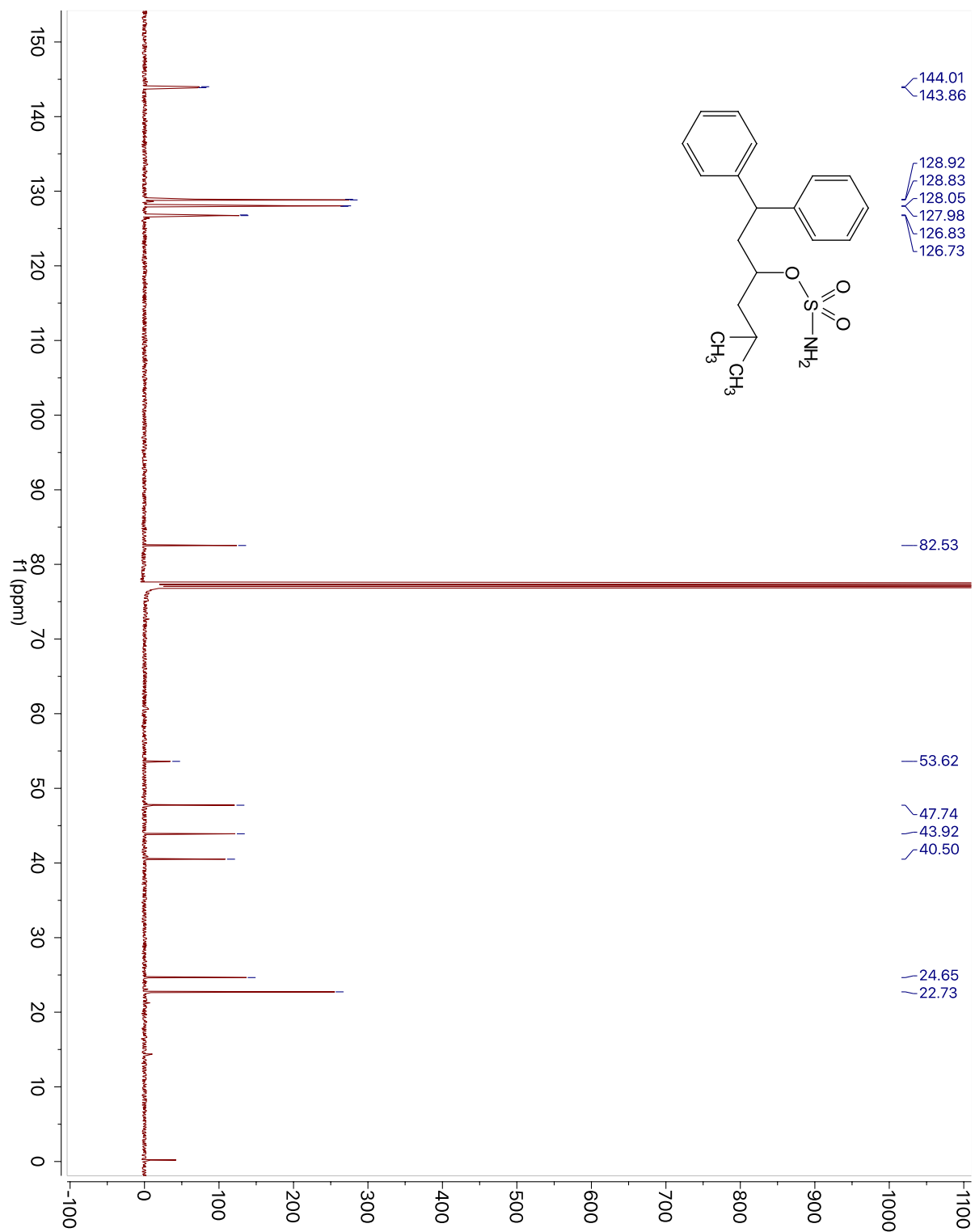
¹H NMR for Compound 2.12.

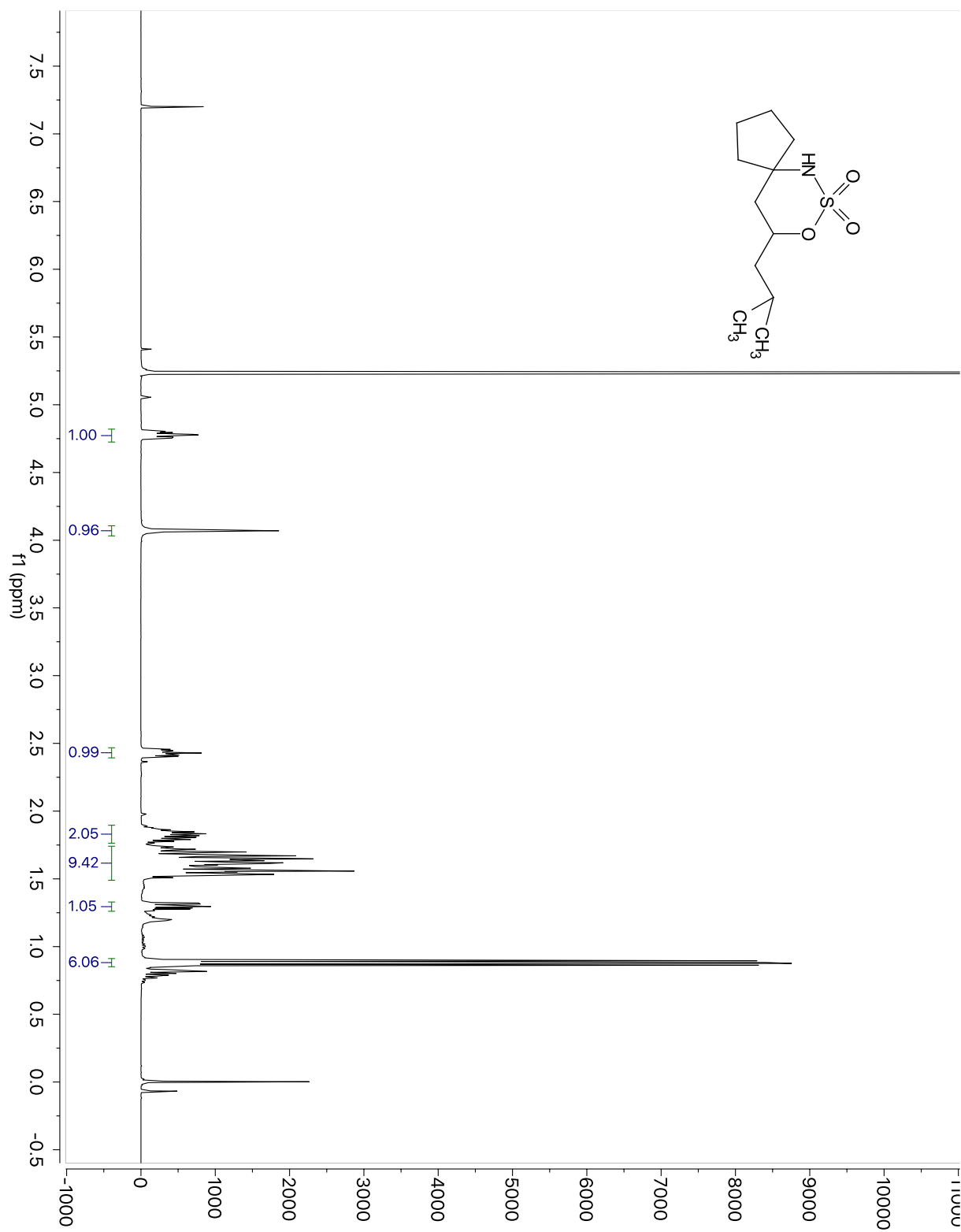
^{13}C NMR for Compound 2.12.

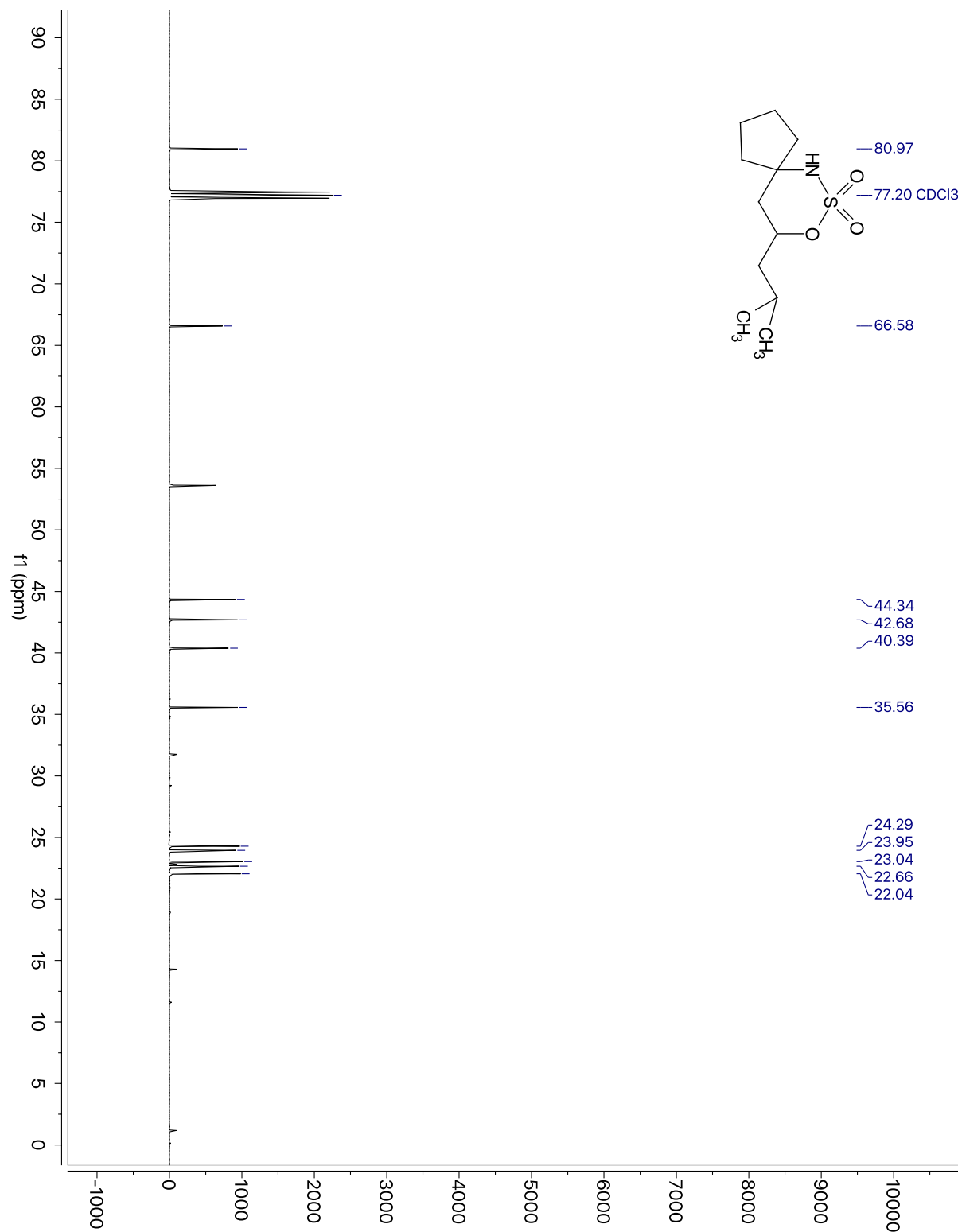
¹H NMR for Compound 2.14.

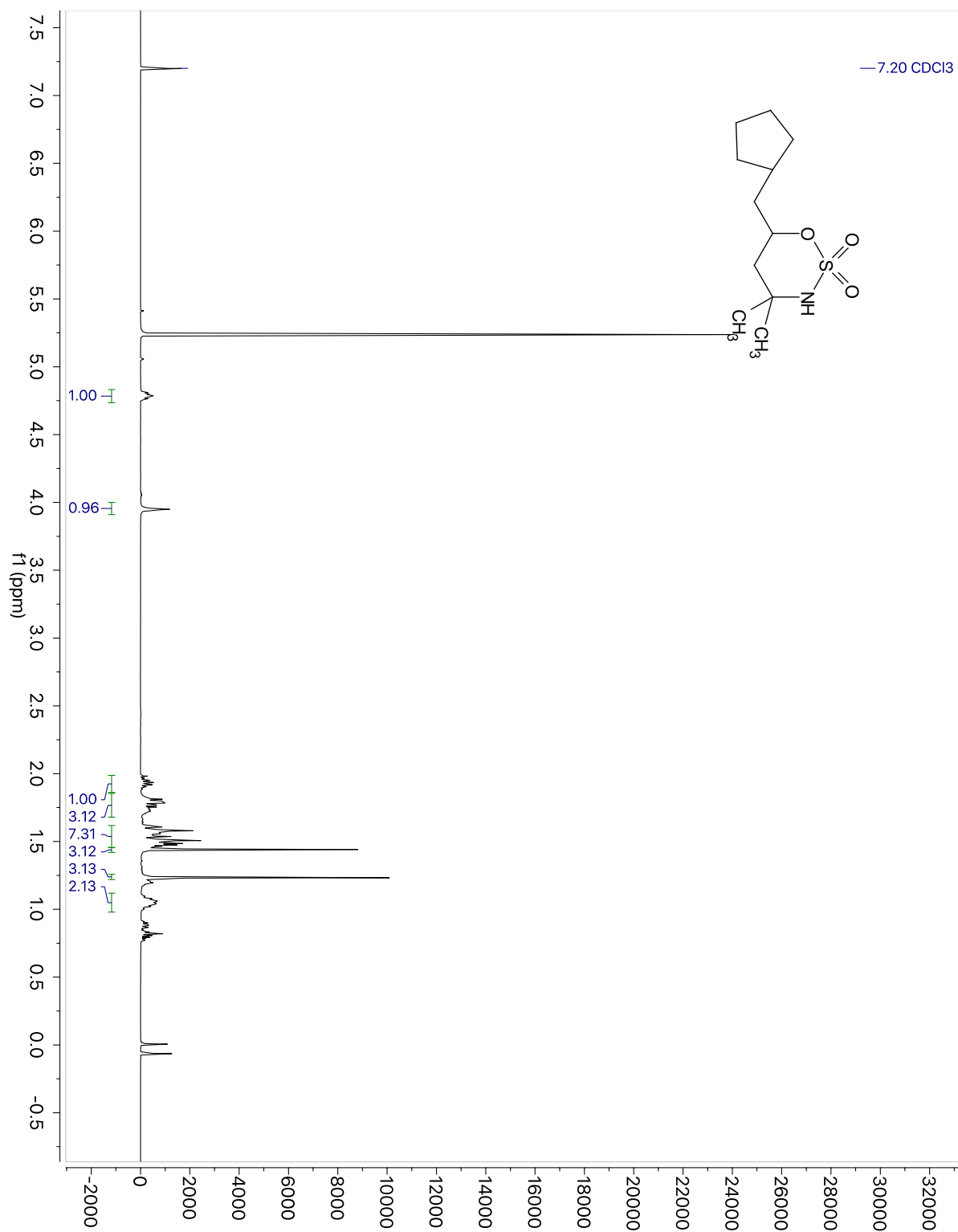
^{13}C NMR for Compound 2.14.

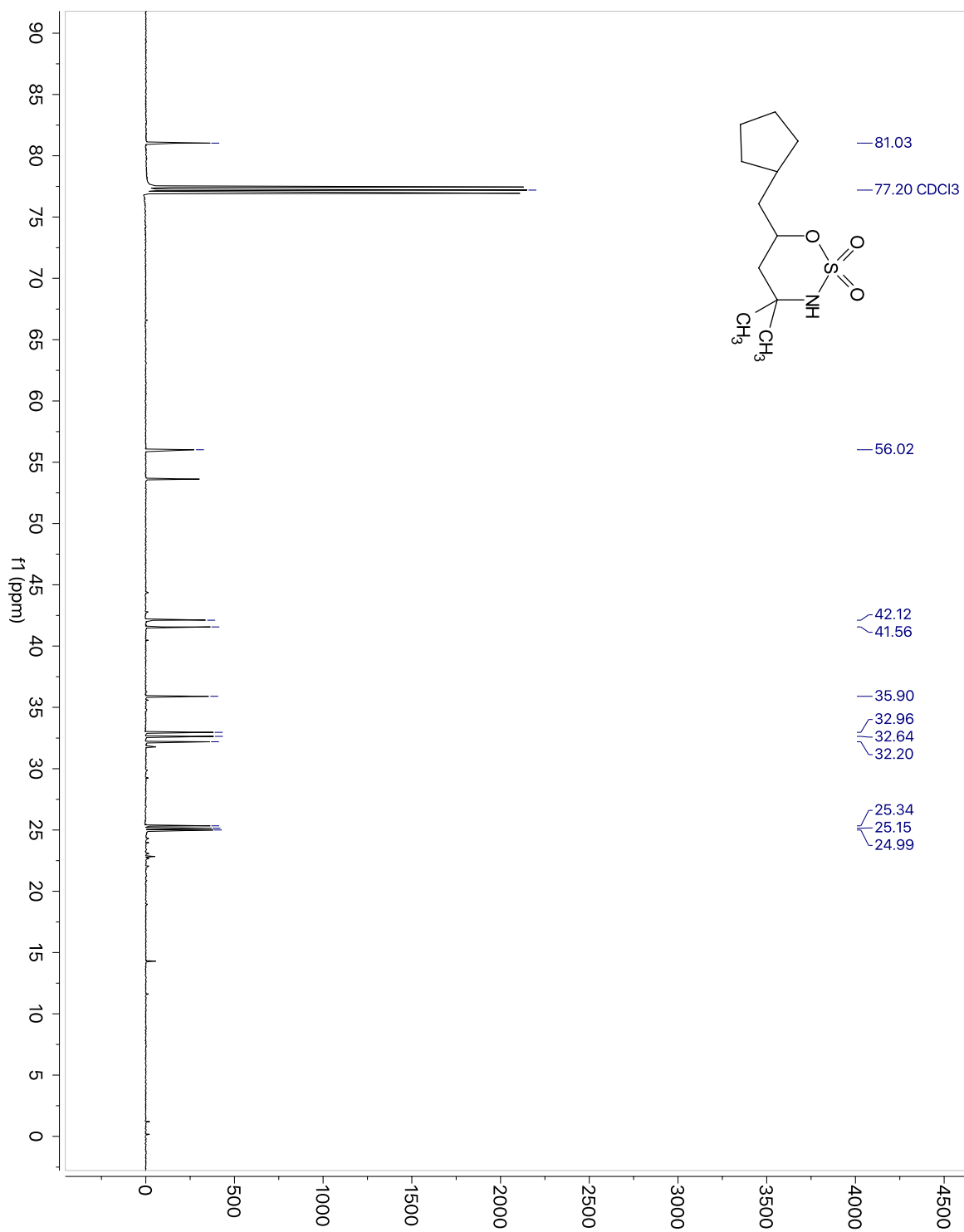
¹H NMR for Compound 2.15.

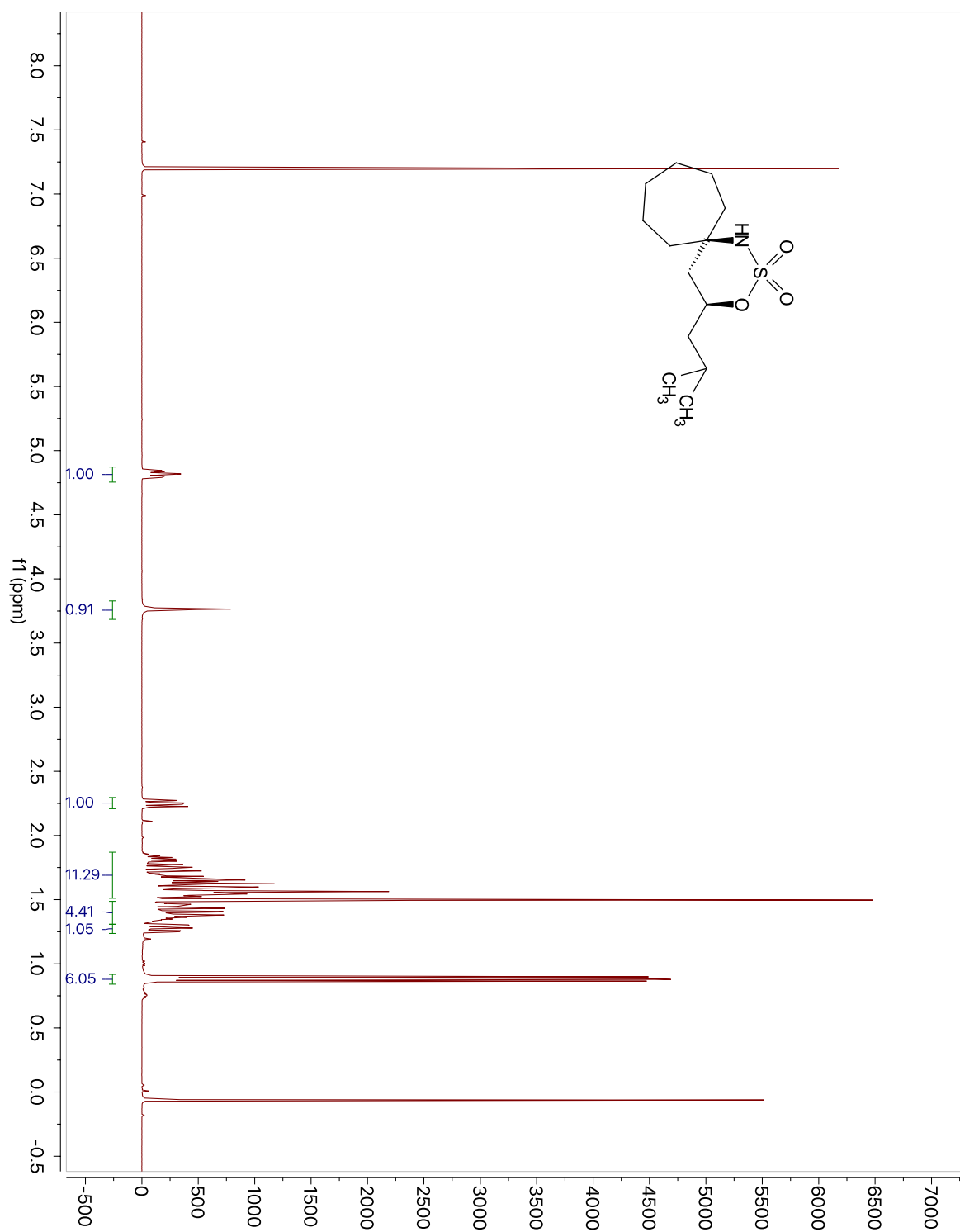
^{13}C NMR for Compound 2.15.

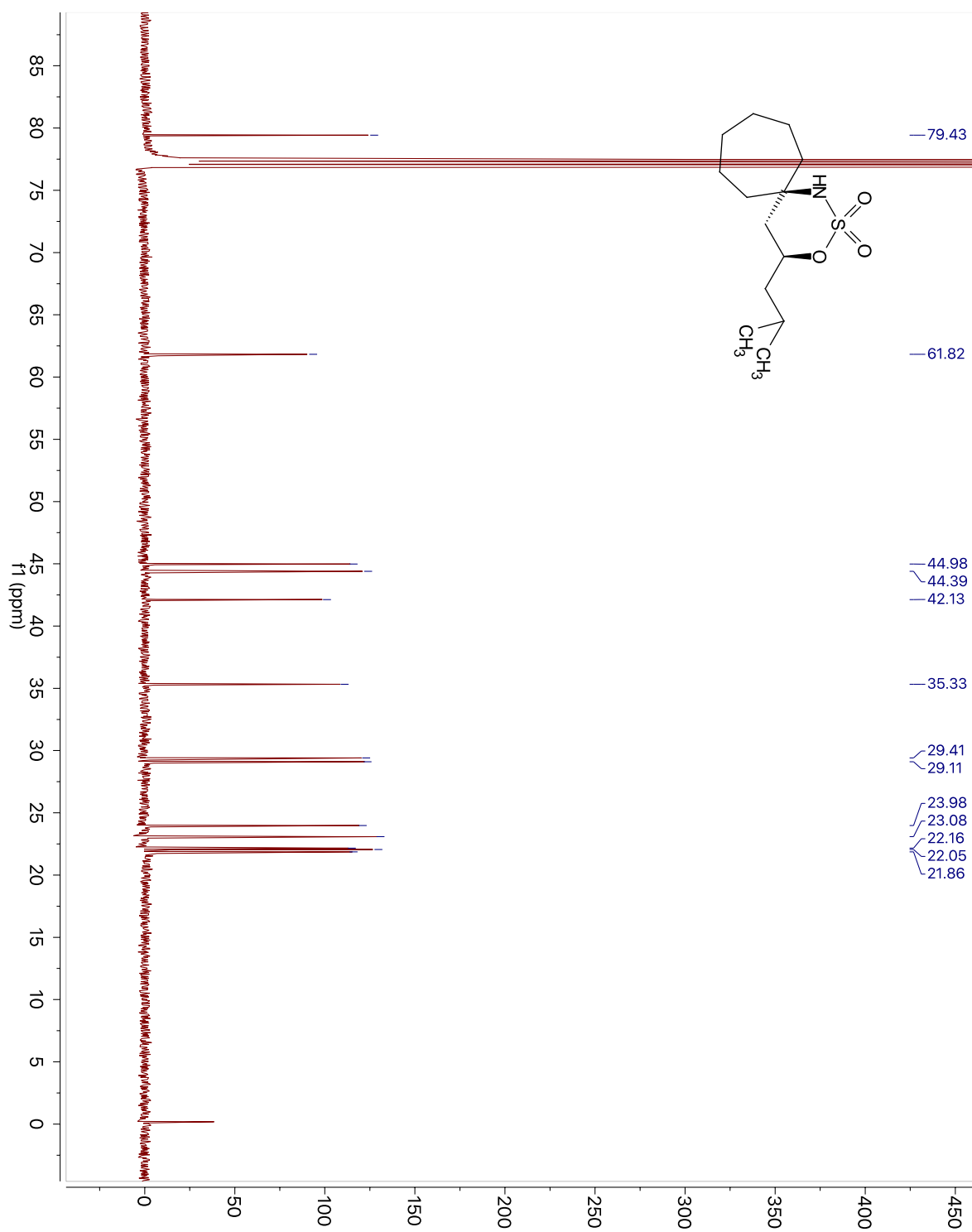
¹H NMR for Compound 2.8_{Cy}.

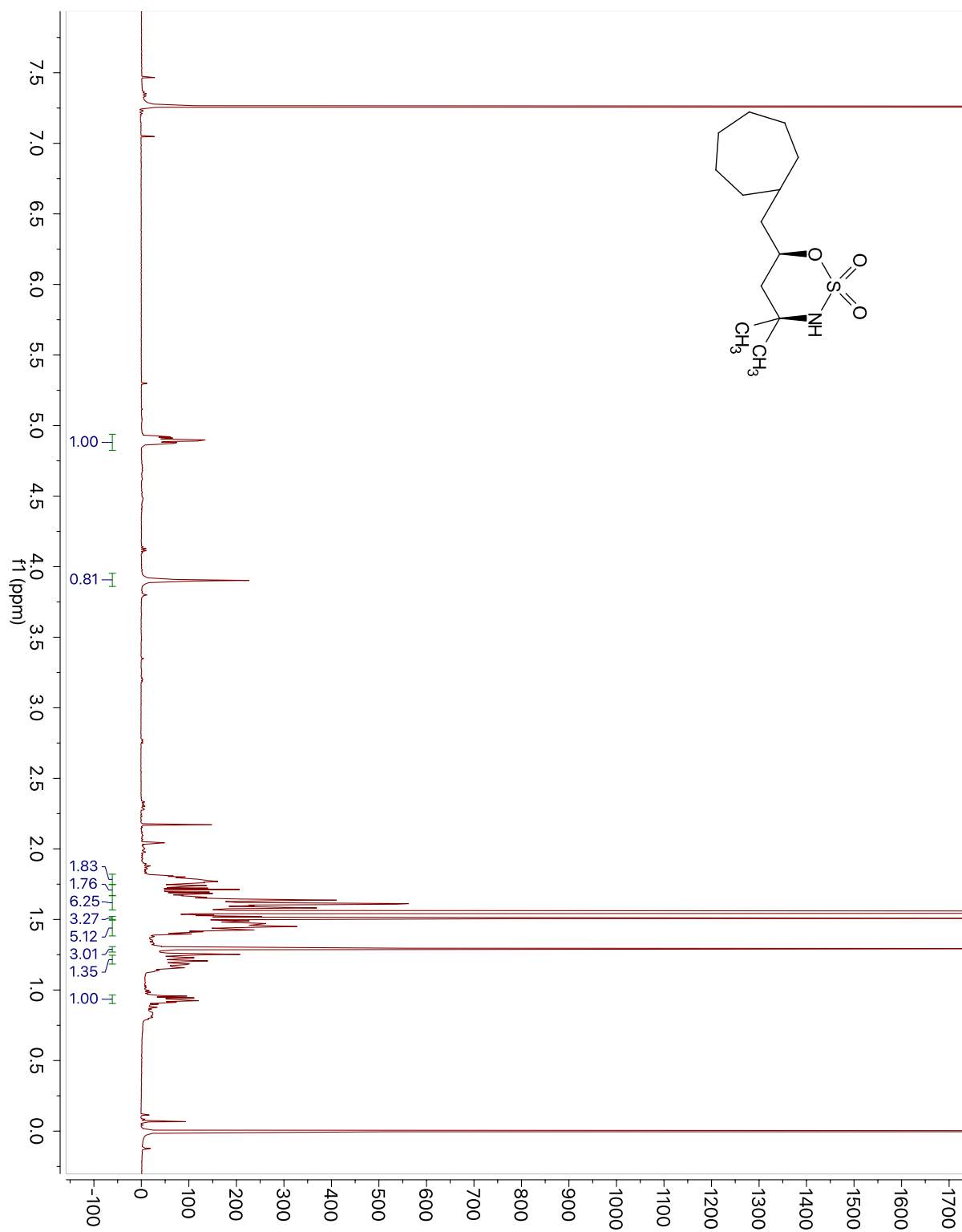
^{13}C NMR for Compound 2.8_{Cy}.

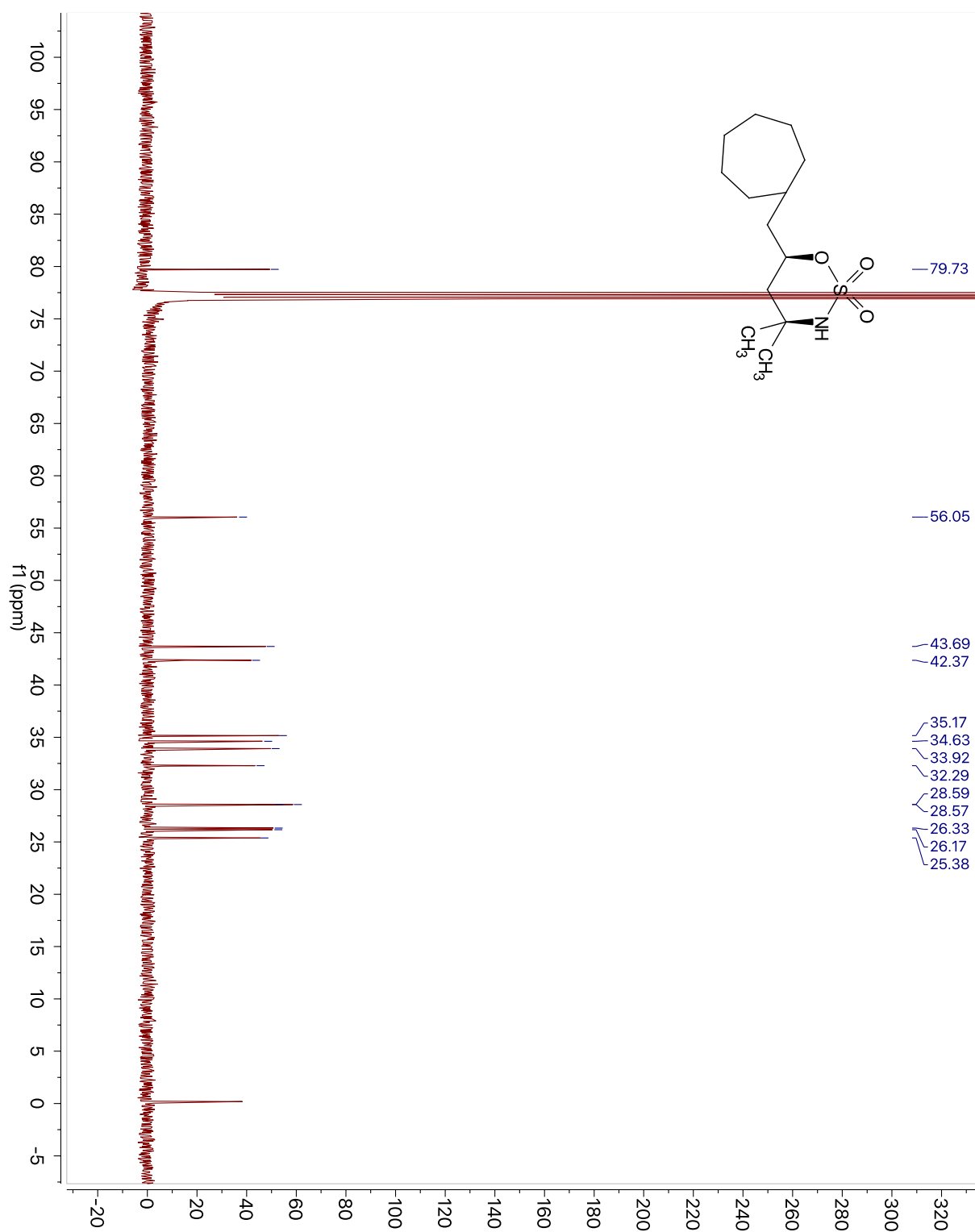
¹H NMR for Compound 2.8_{Pr}.

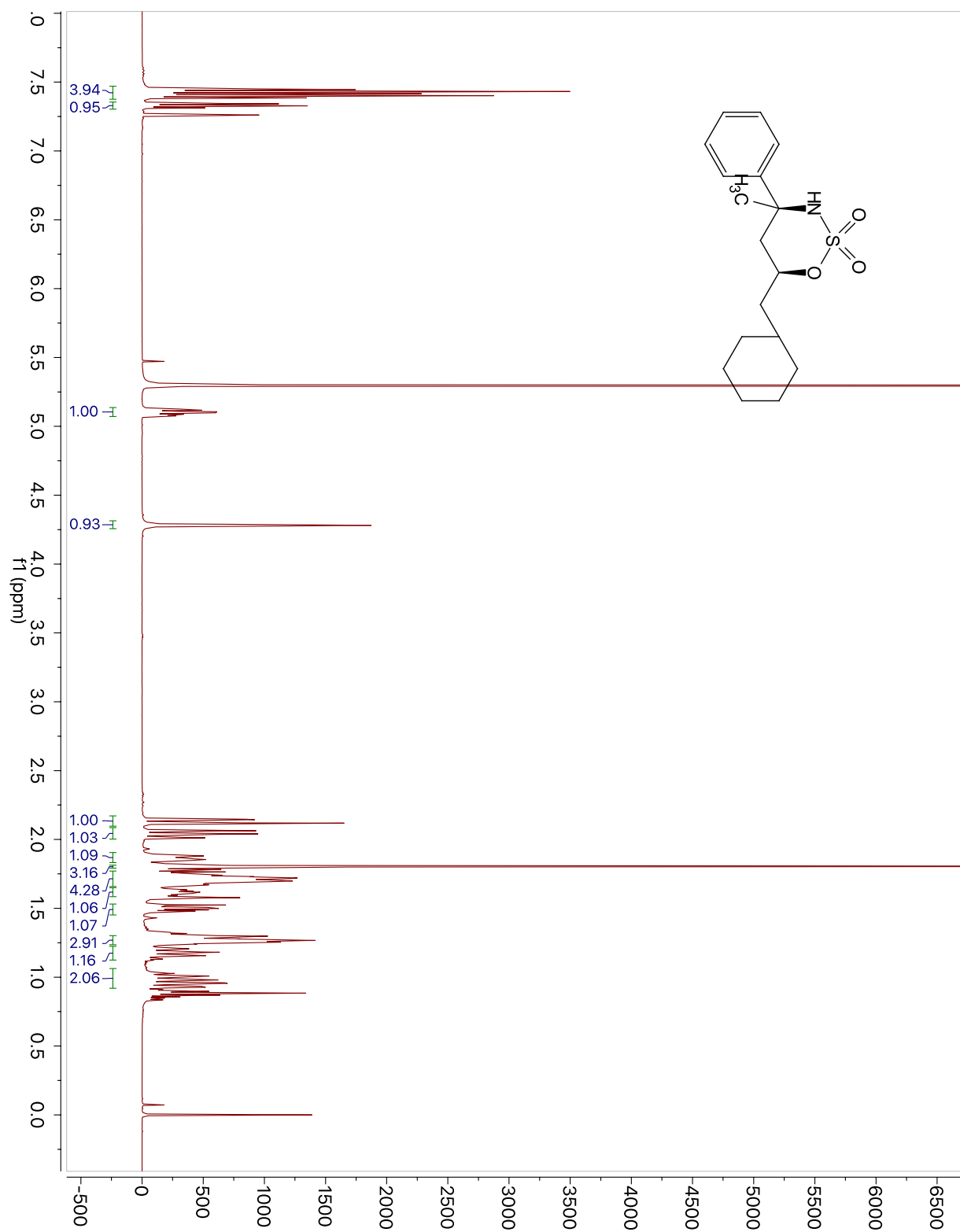
^{13}C NMR for Compound 2.8_{iPr}.

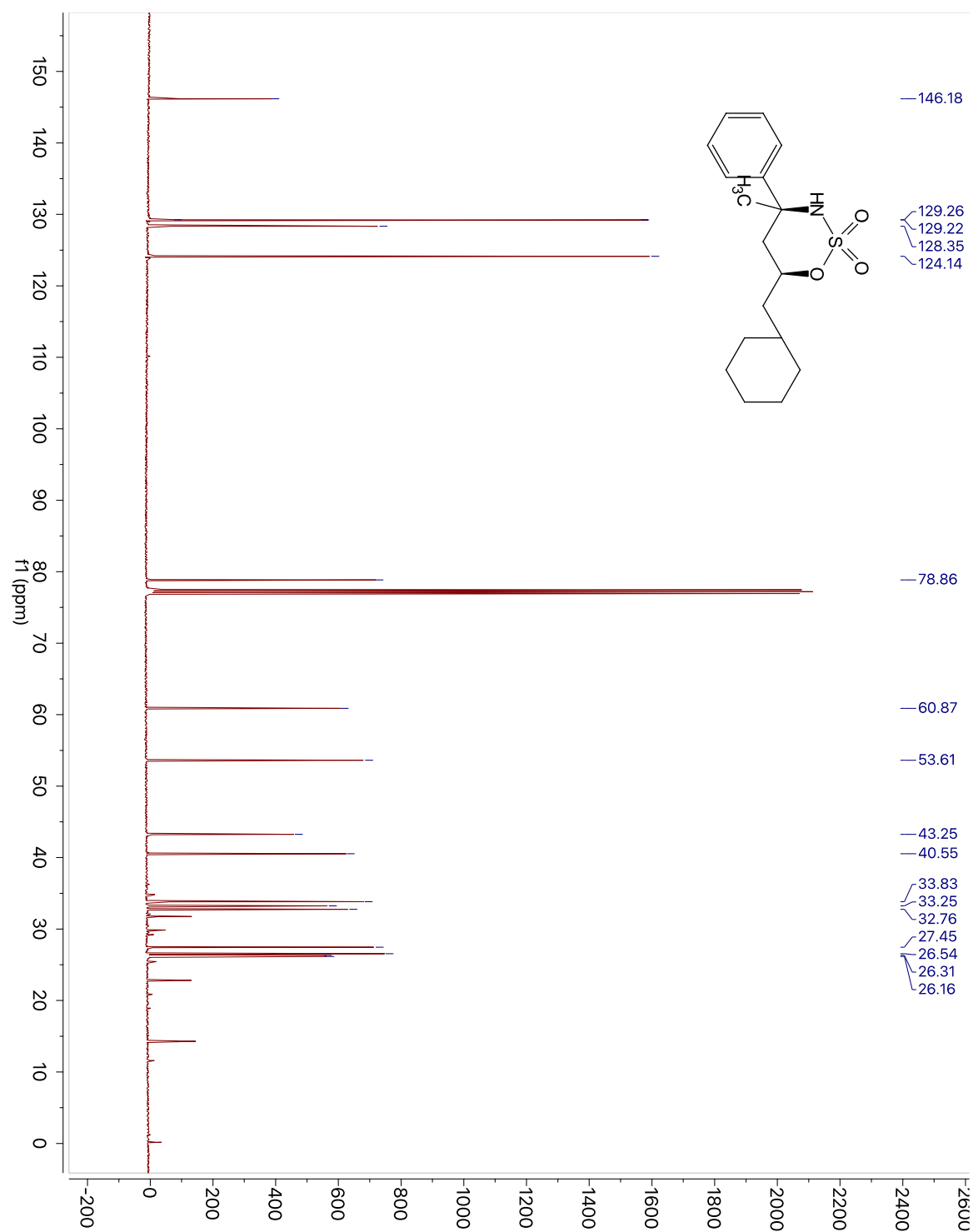
¹H NMR for Compound 2.9_{Cy}.

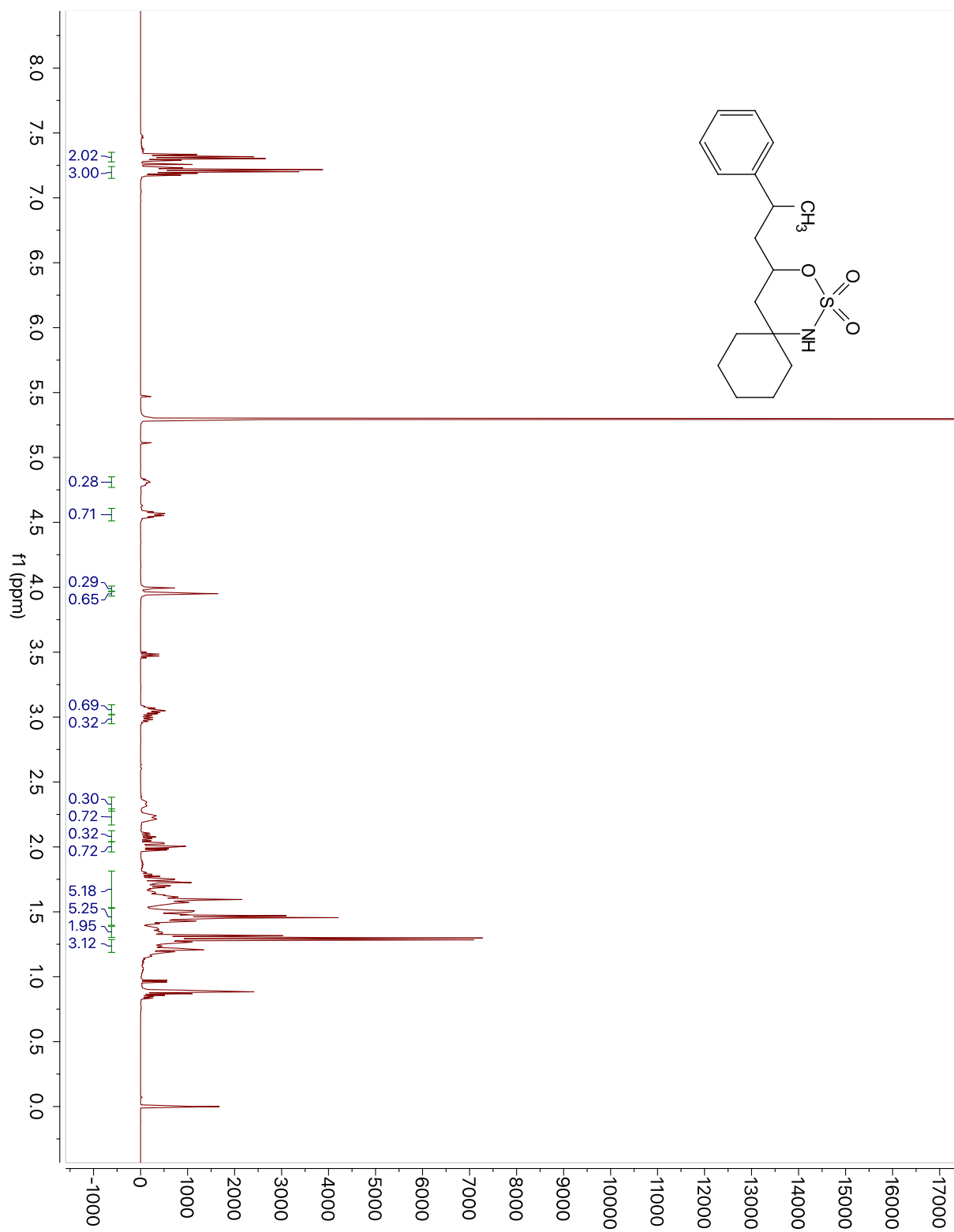
^{13}C NMR for Compound 2.9_{Cy}.

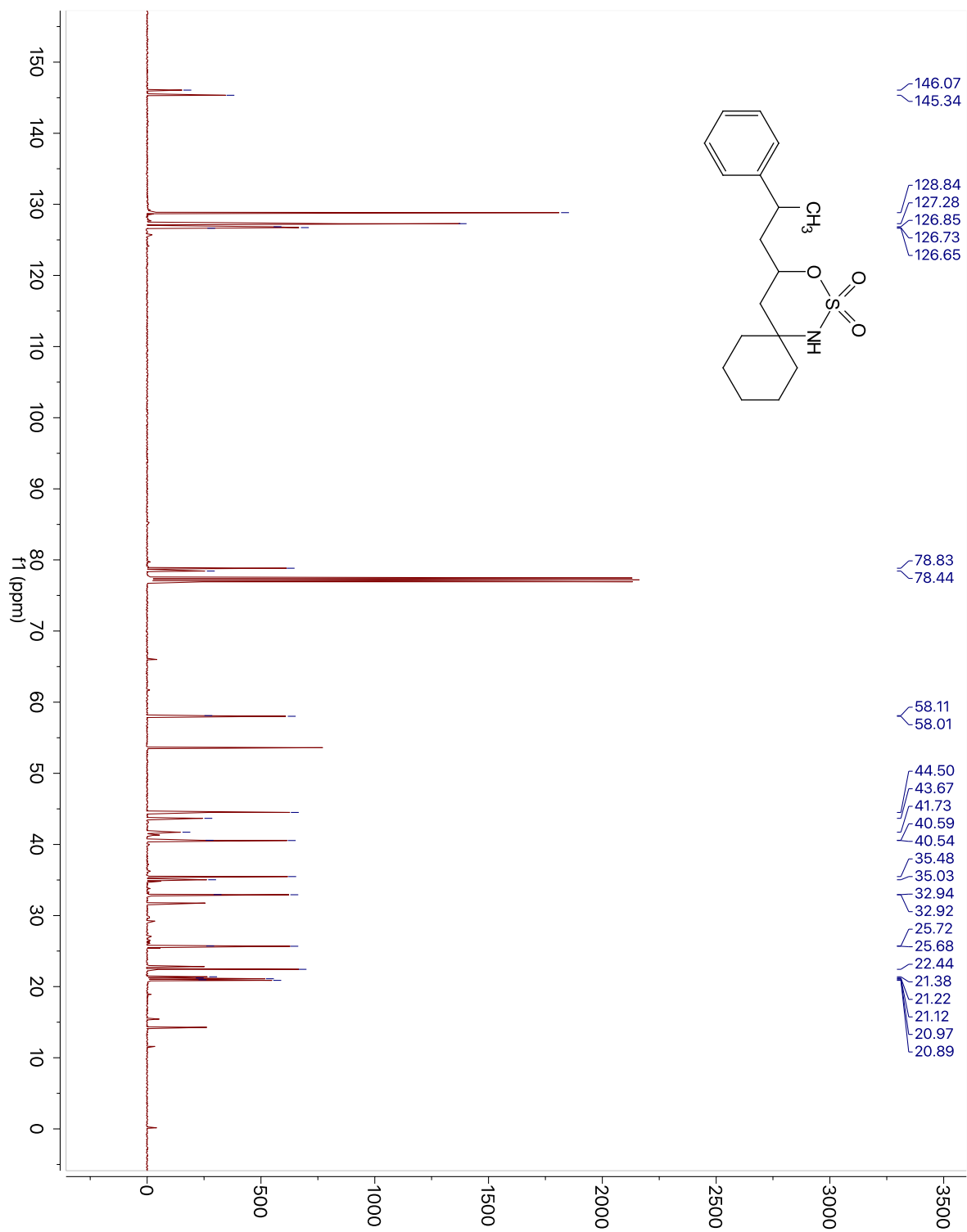
¹H NMR for Compound 2.9_{iPr}.

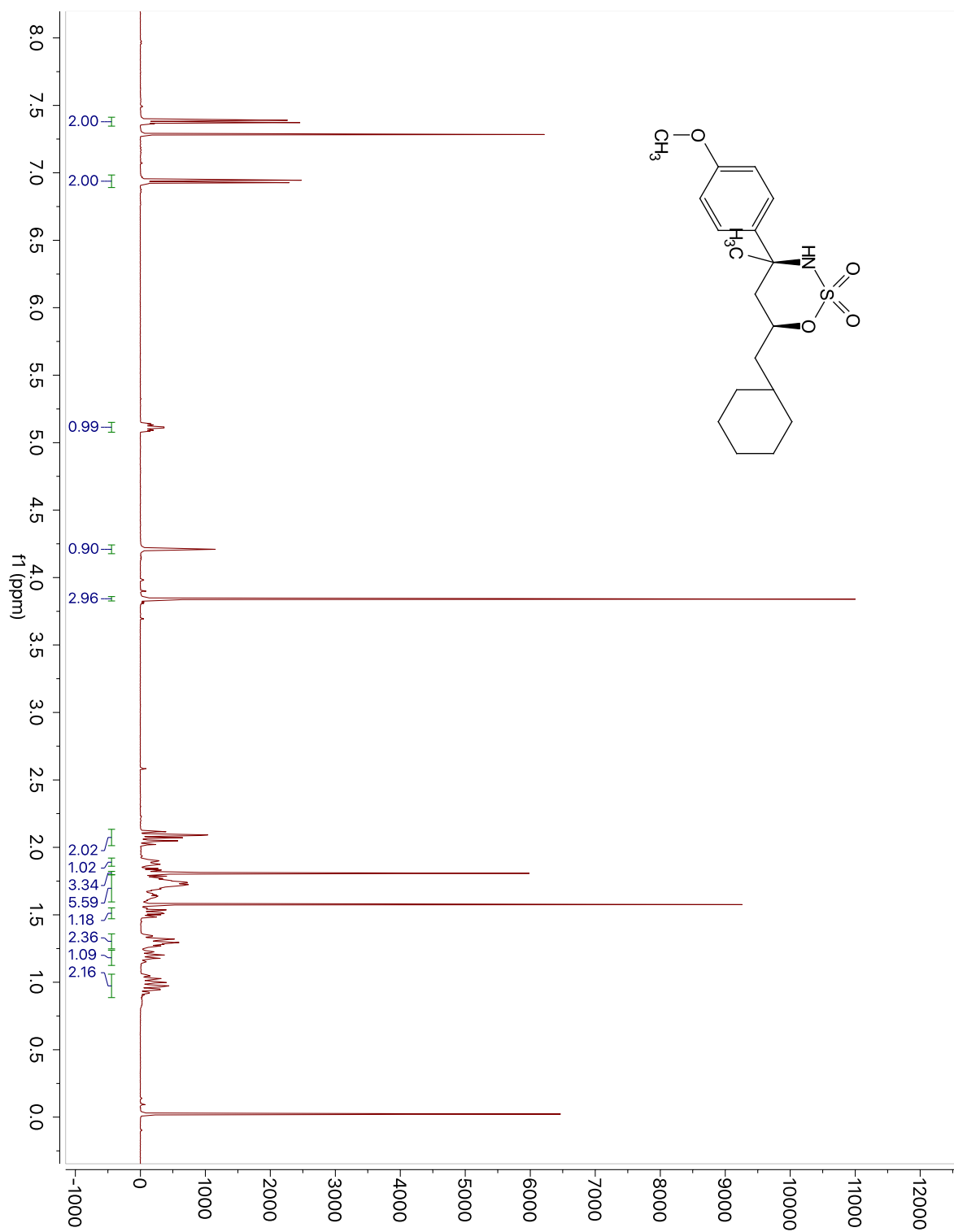
^{13}C NMR for Compound 2.9_{iPr}.

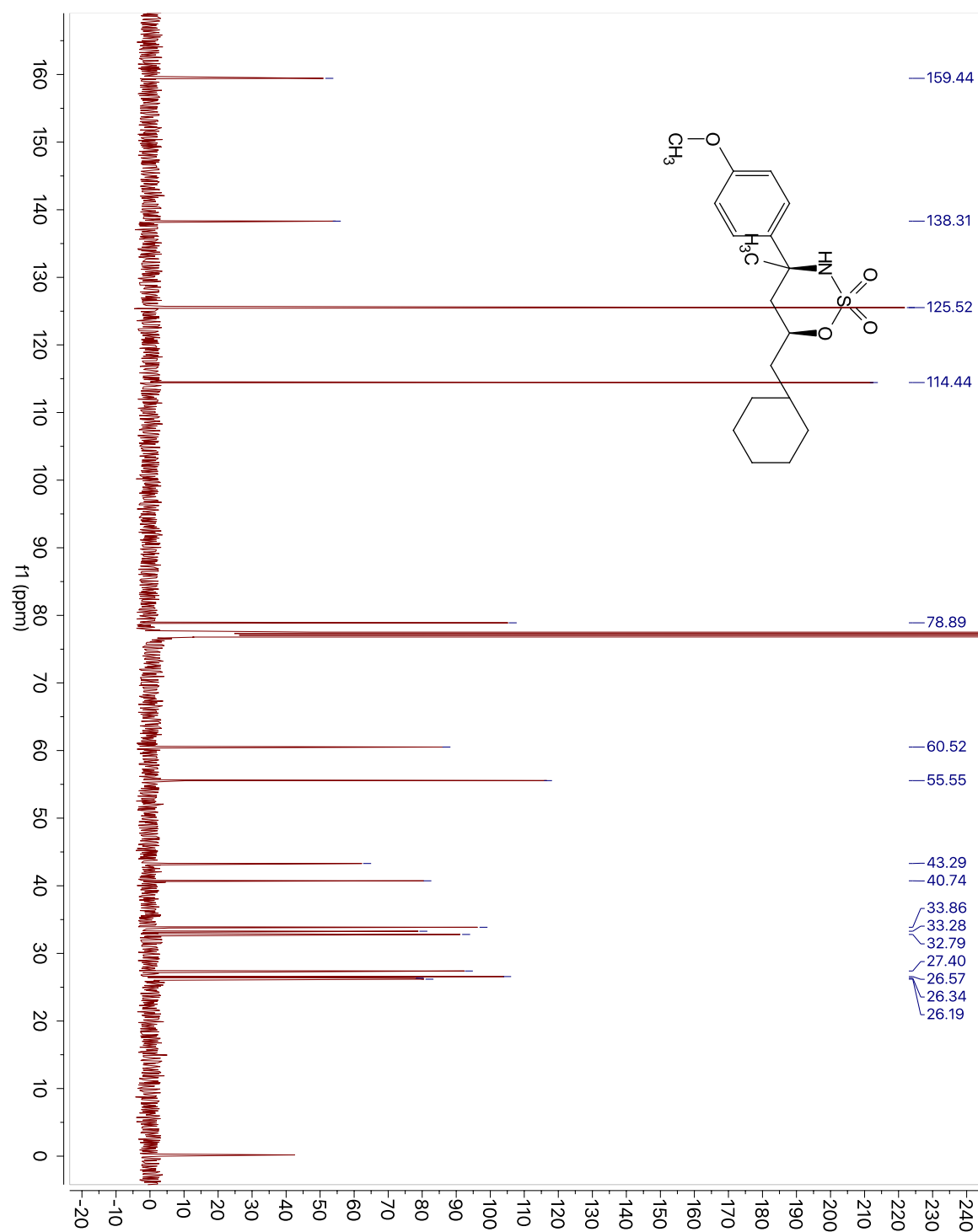
¹H NMR for Compound 2.10_{Bn-syn}.

^{13}C NMR for Compound 2.10_{Bn-syn.}

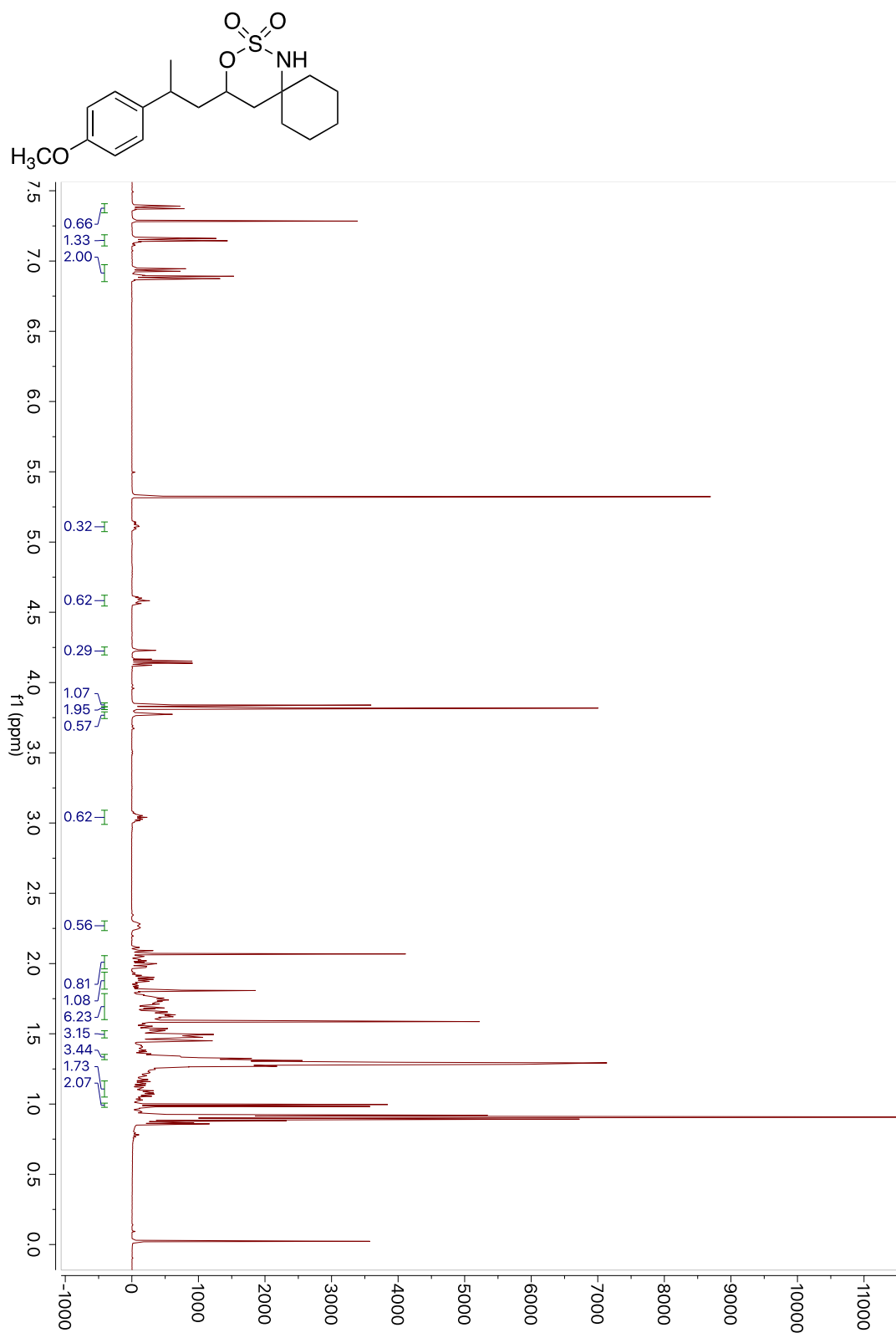
¹H NMR for Compound 2.10_{alk}.

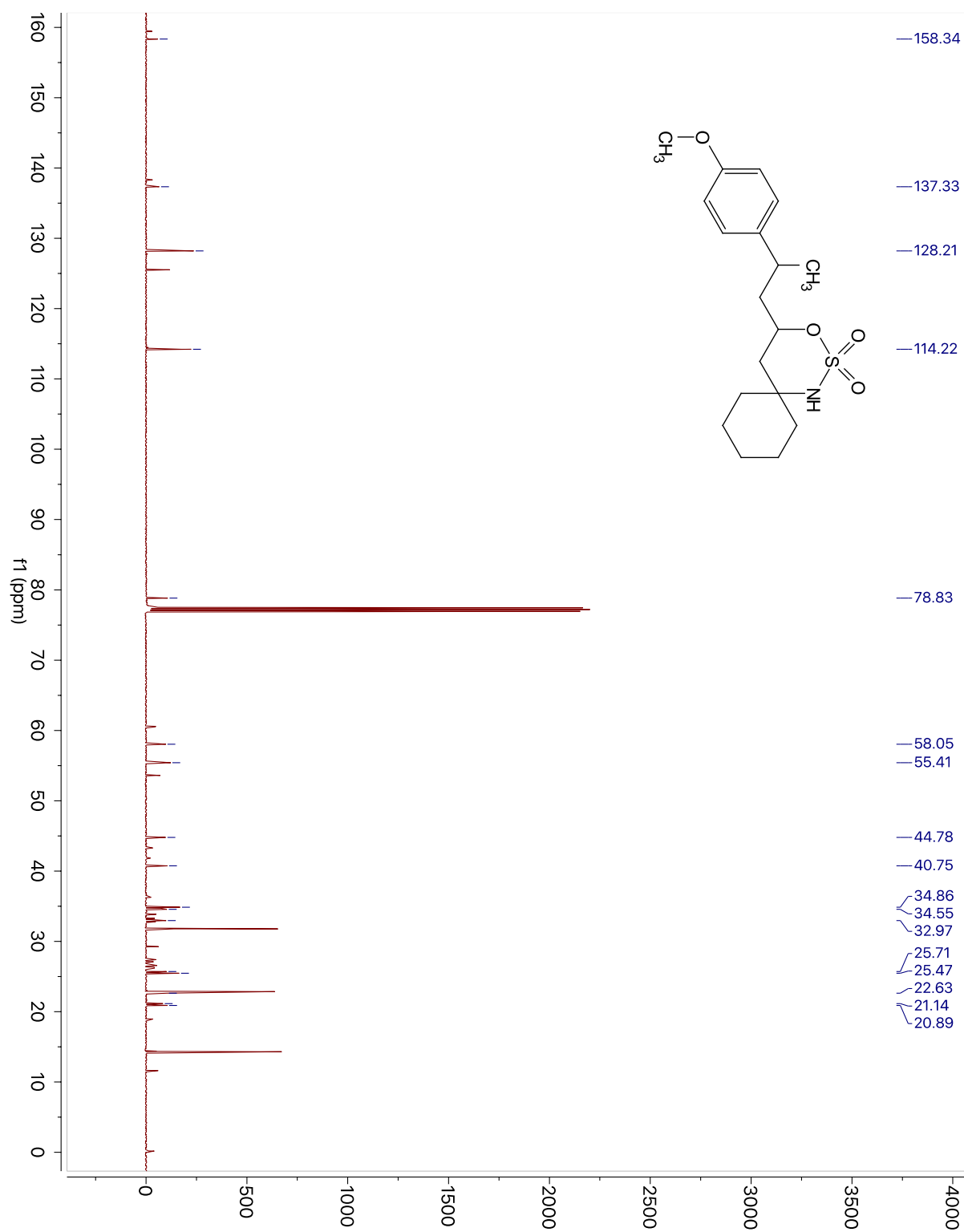
^{13}C NMR for Compound 2.10_{alk.}

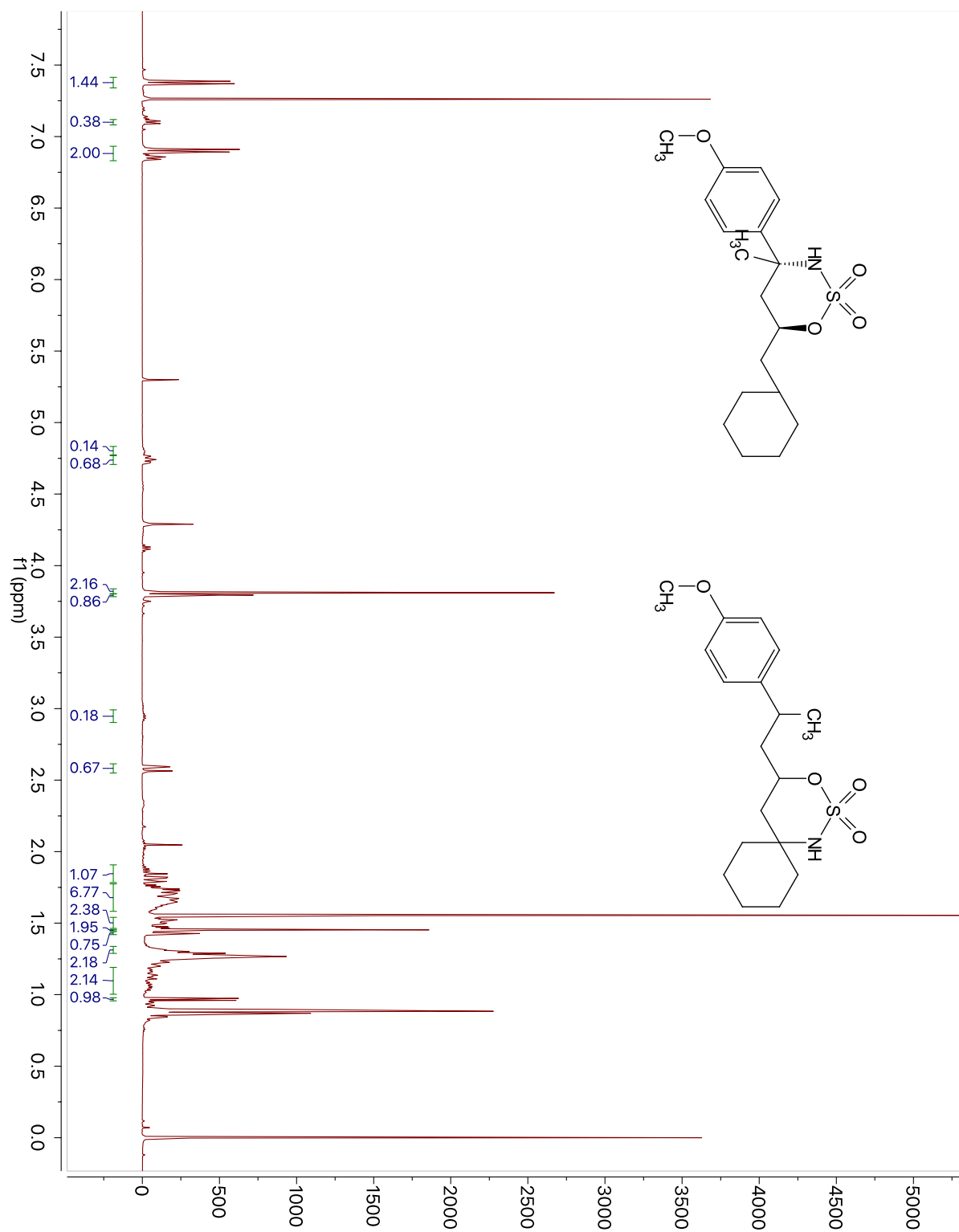
¹H NMR for Compound 2.11_{Bn-syn}.

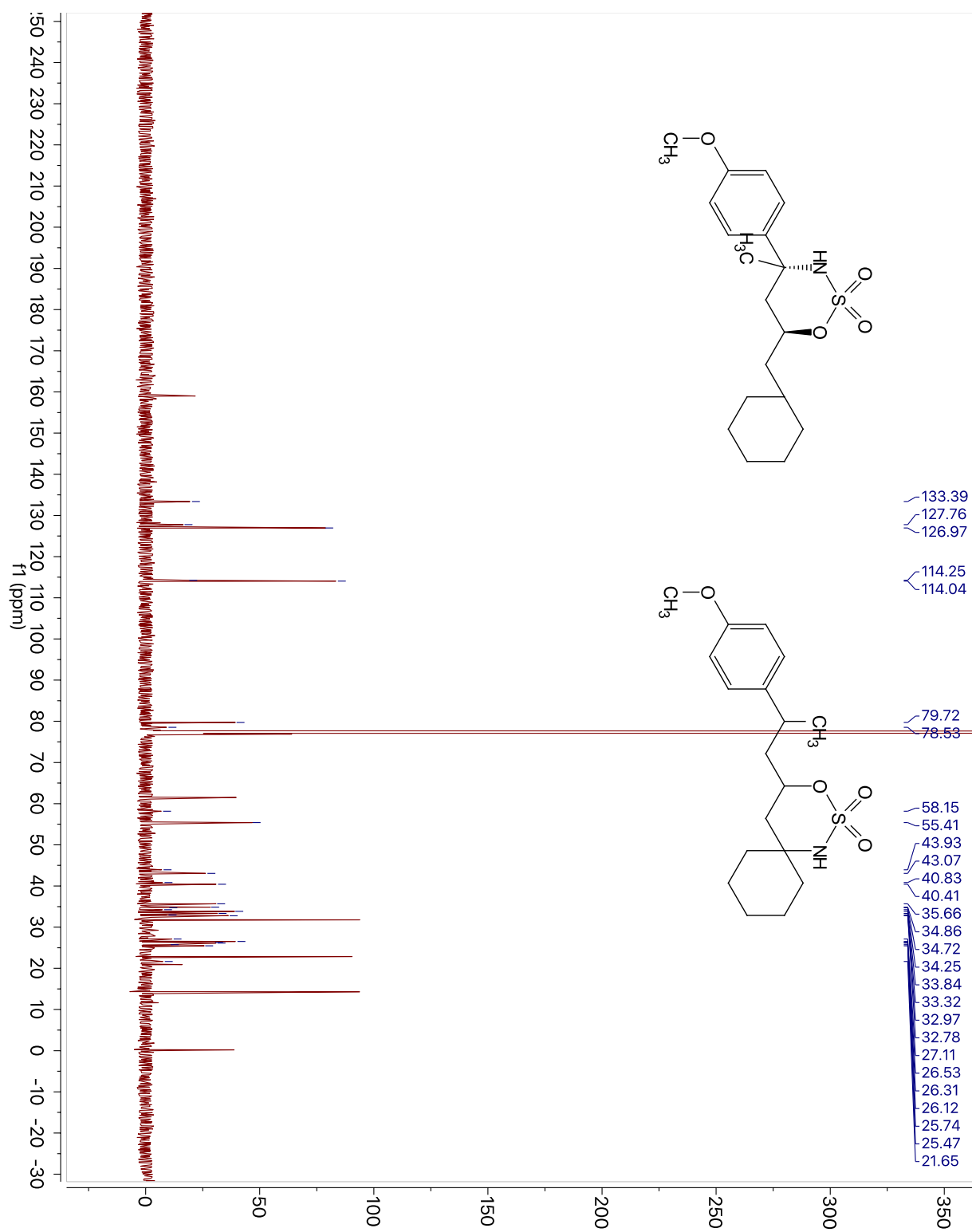
^{13}C NMR for Compound 2.11_{Bn-syn}.

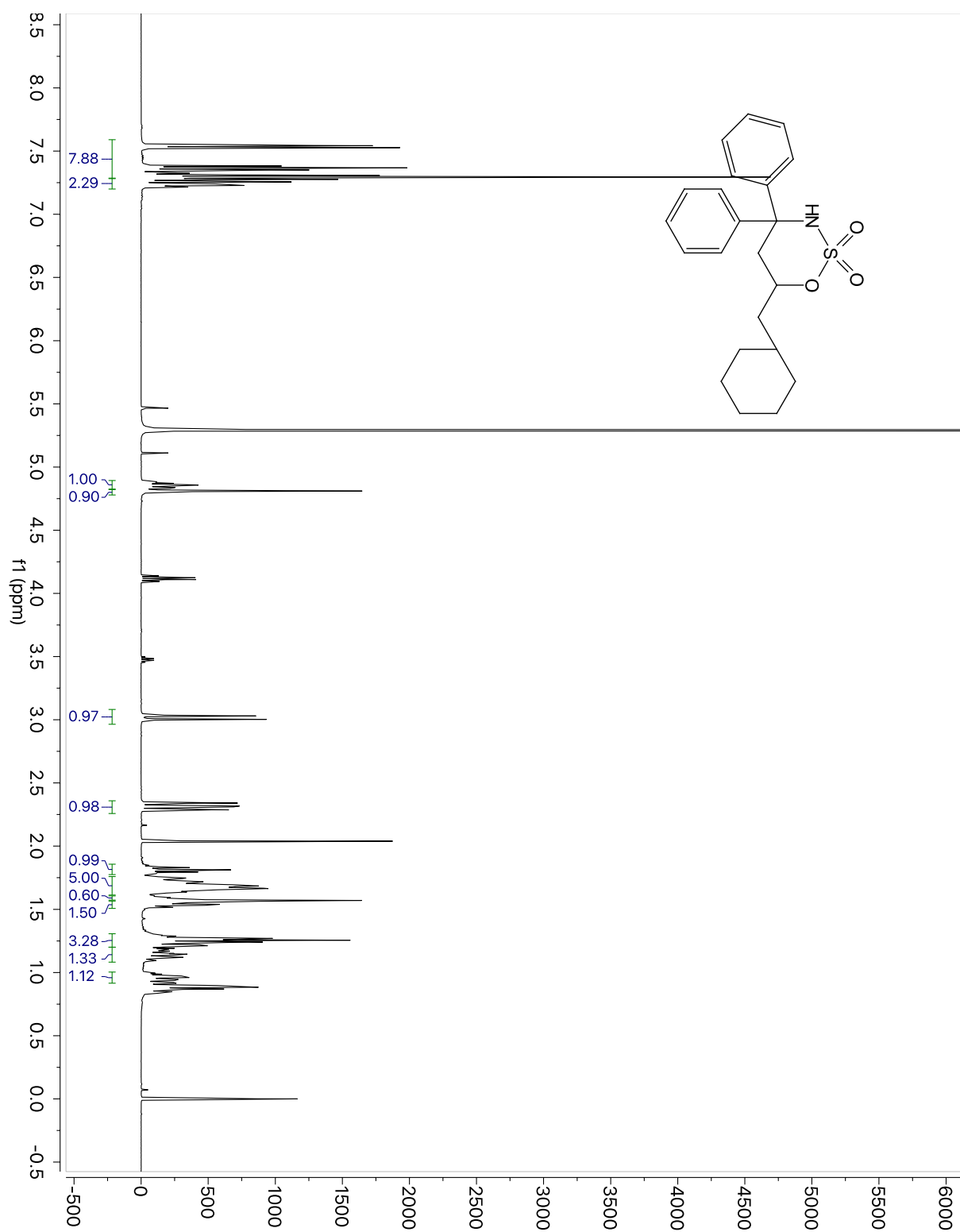
¹H NMR for Compound 2.11_{alk-major} diastereomer. 2:1 mix with Compound 2.11_{syn}.

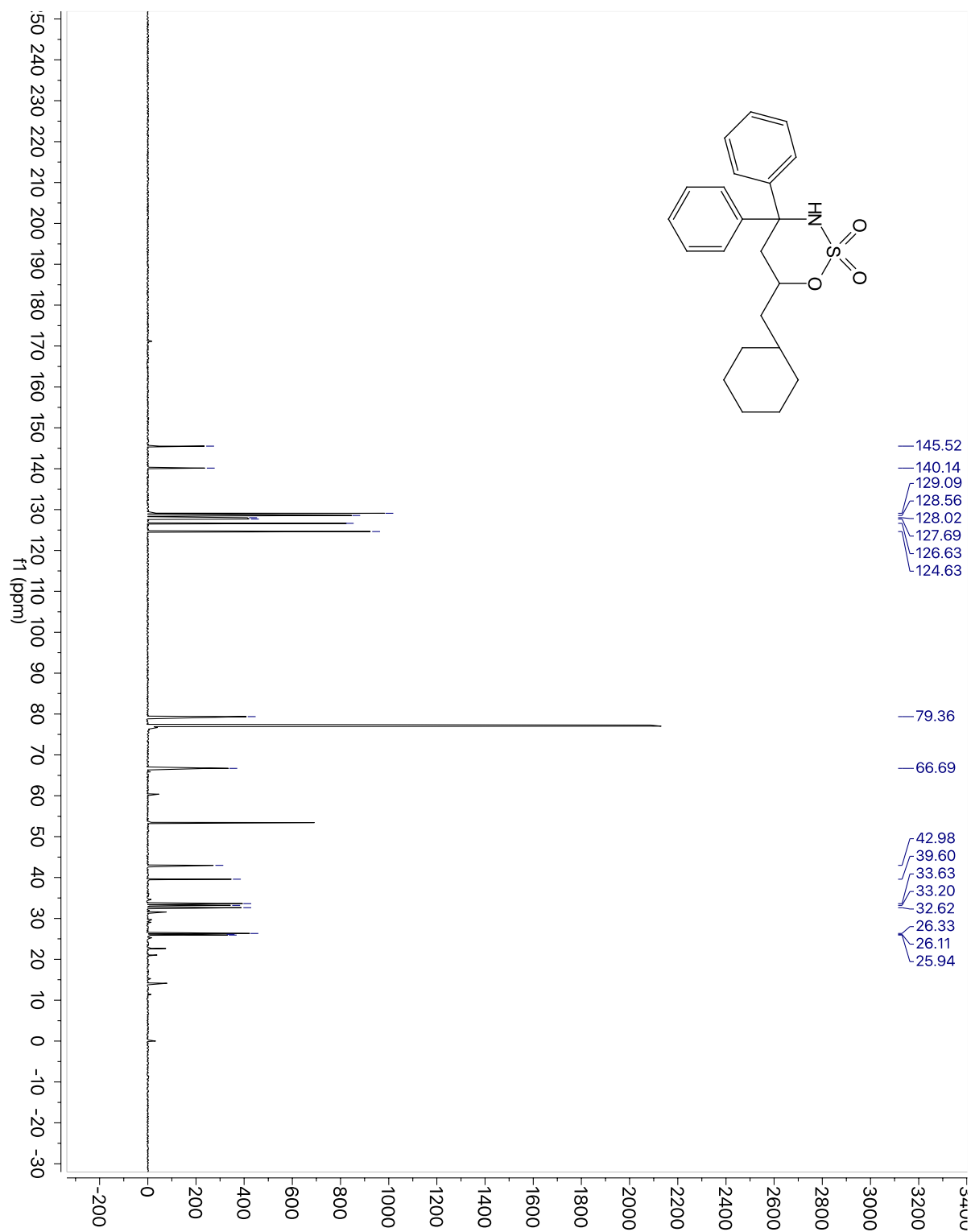


^{13}C NMR for Compound 2.11_{alk-majordiastereomer} 2:1 mix with Compound 2.11_{syn}.

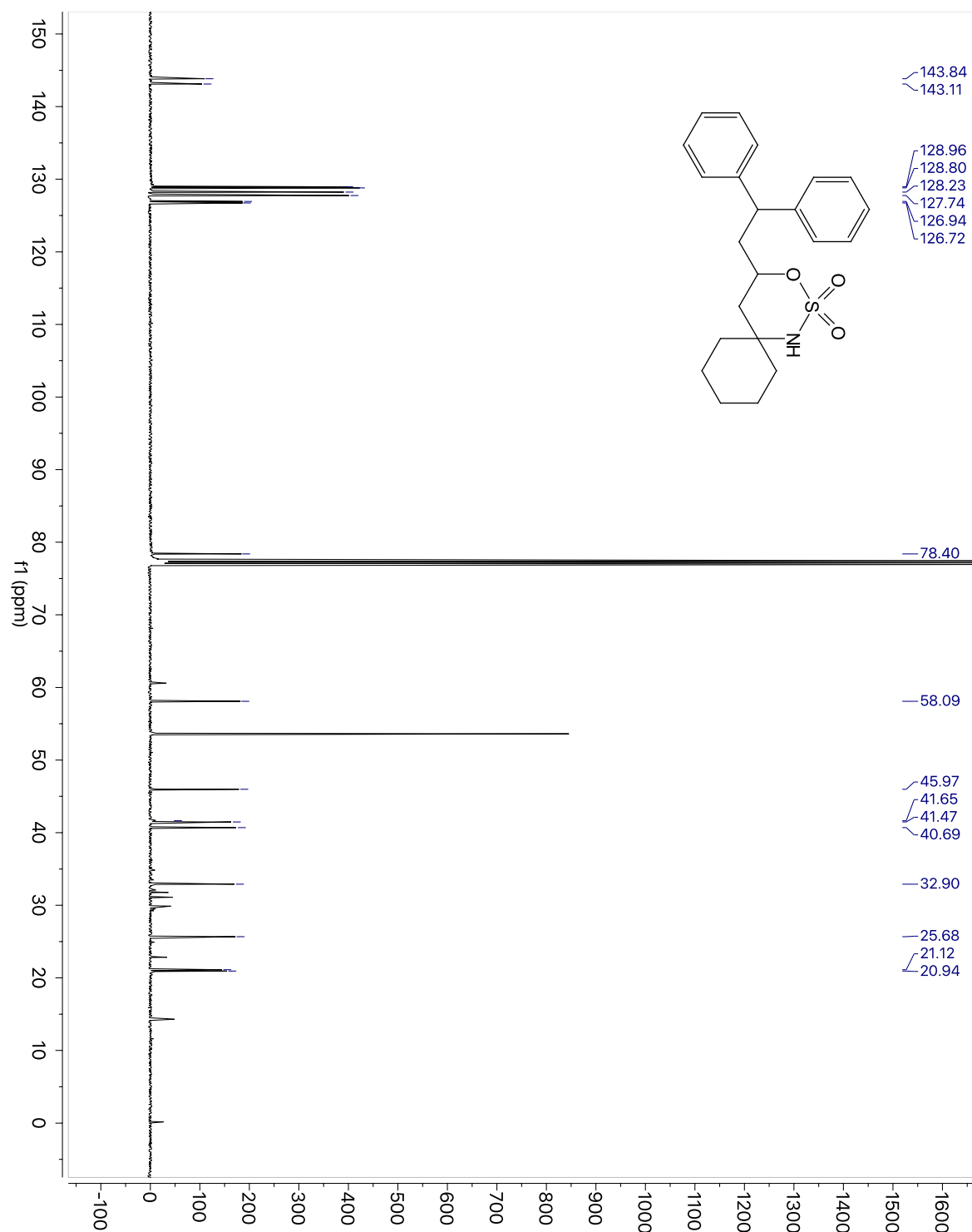
¹H NMR for Compound 2.11_{minor-diastereomers}

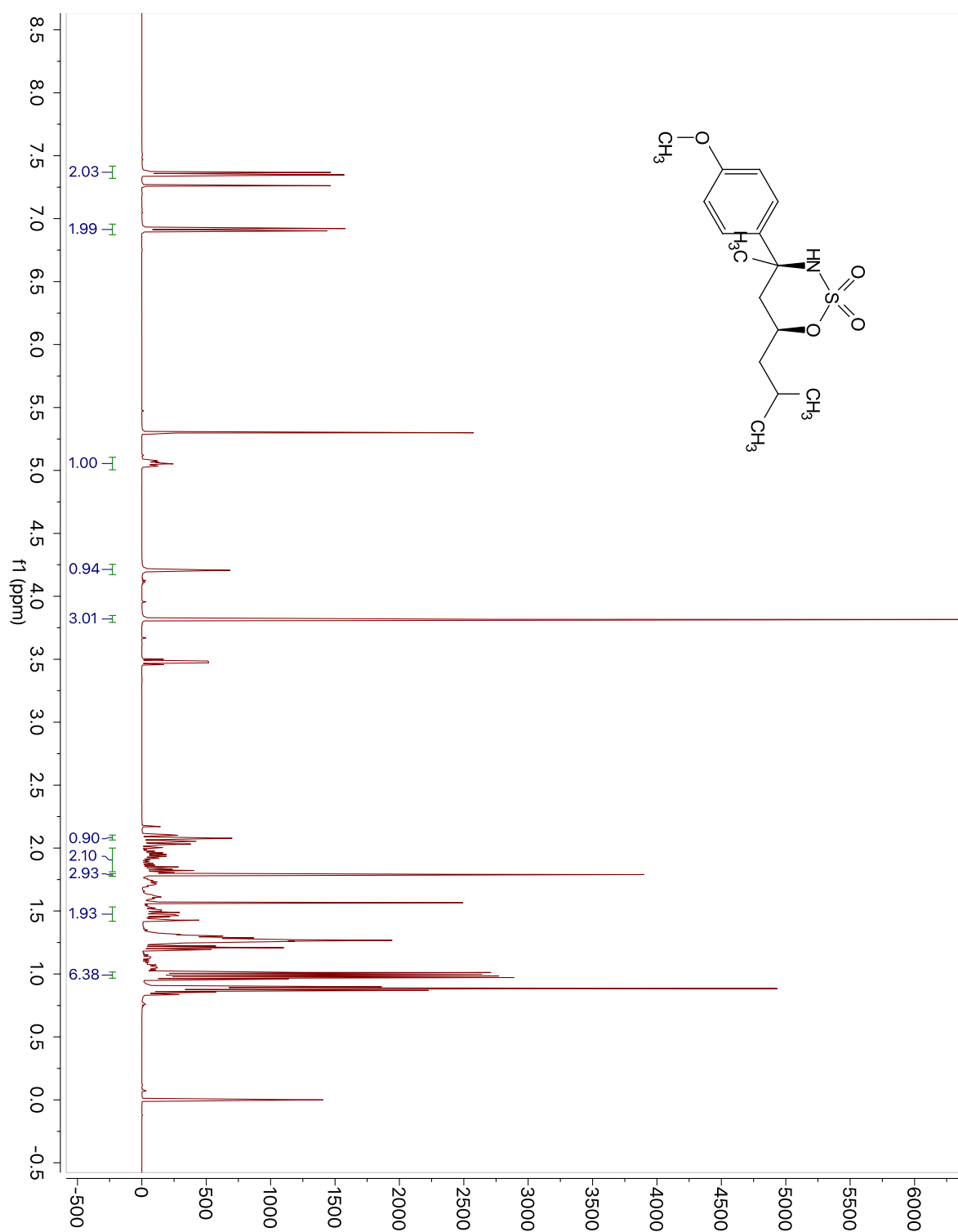
^{13}C NMR for Compound 2.11_{minor-diastereomers}.

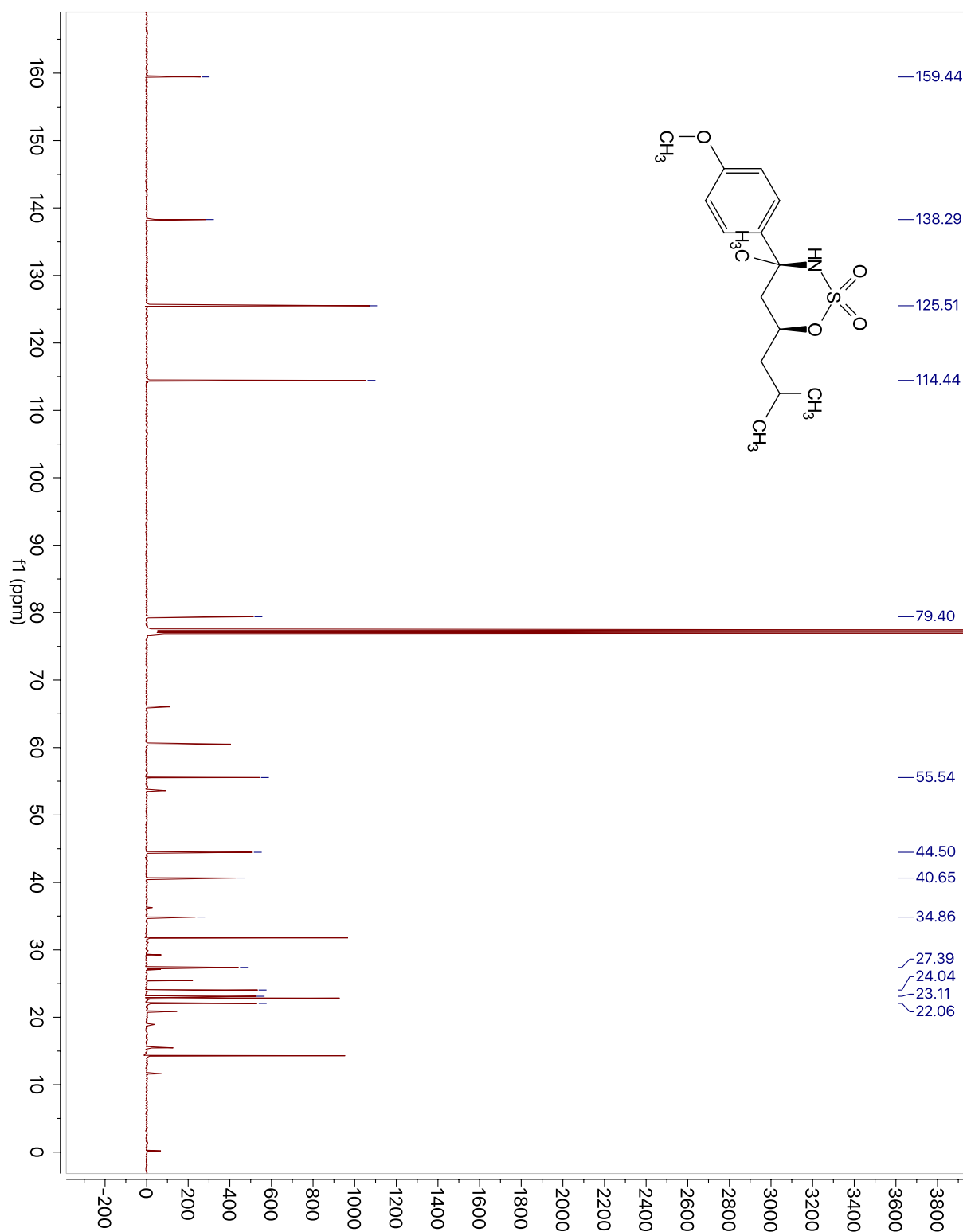
¹H NMR for Compound 2.12_{Bn}.

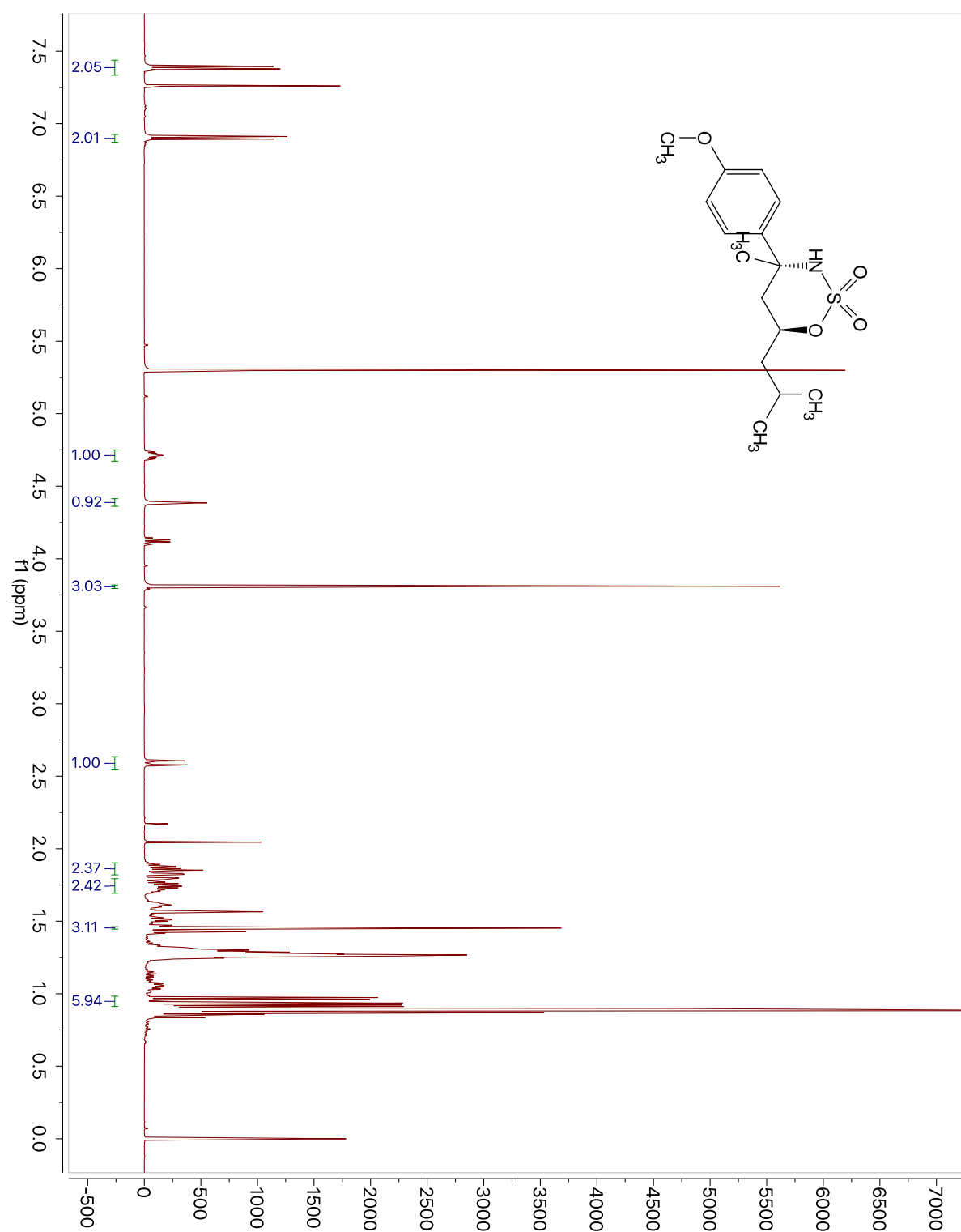
^{13}C NMR for Compound 2.12_{Bn}.

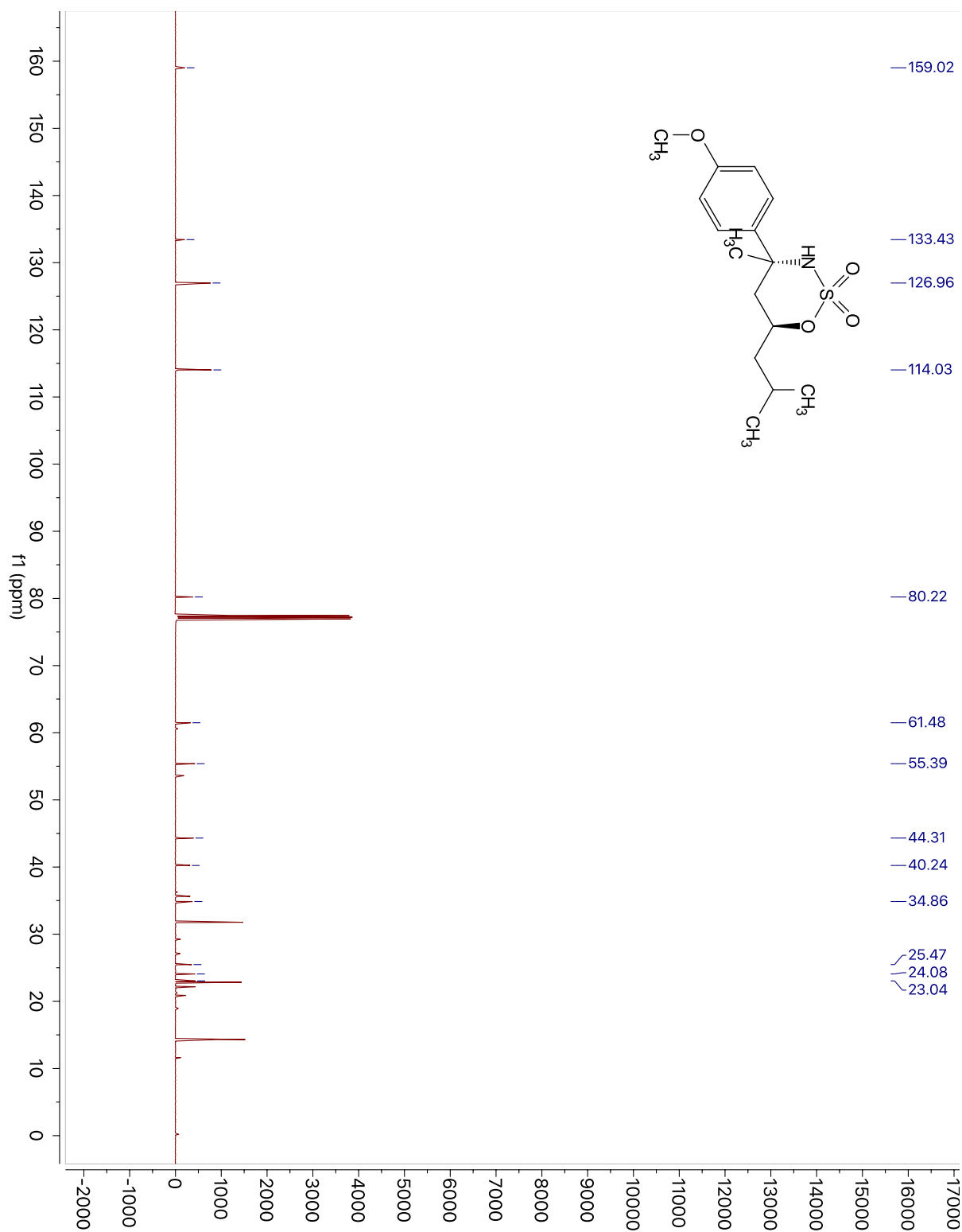
¹H NMR for Compound 2.12_{Cy}.

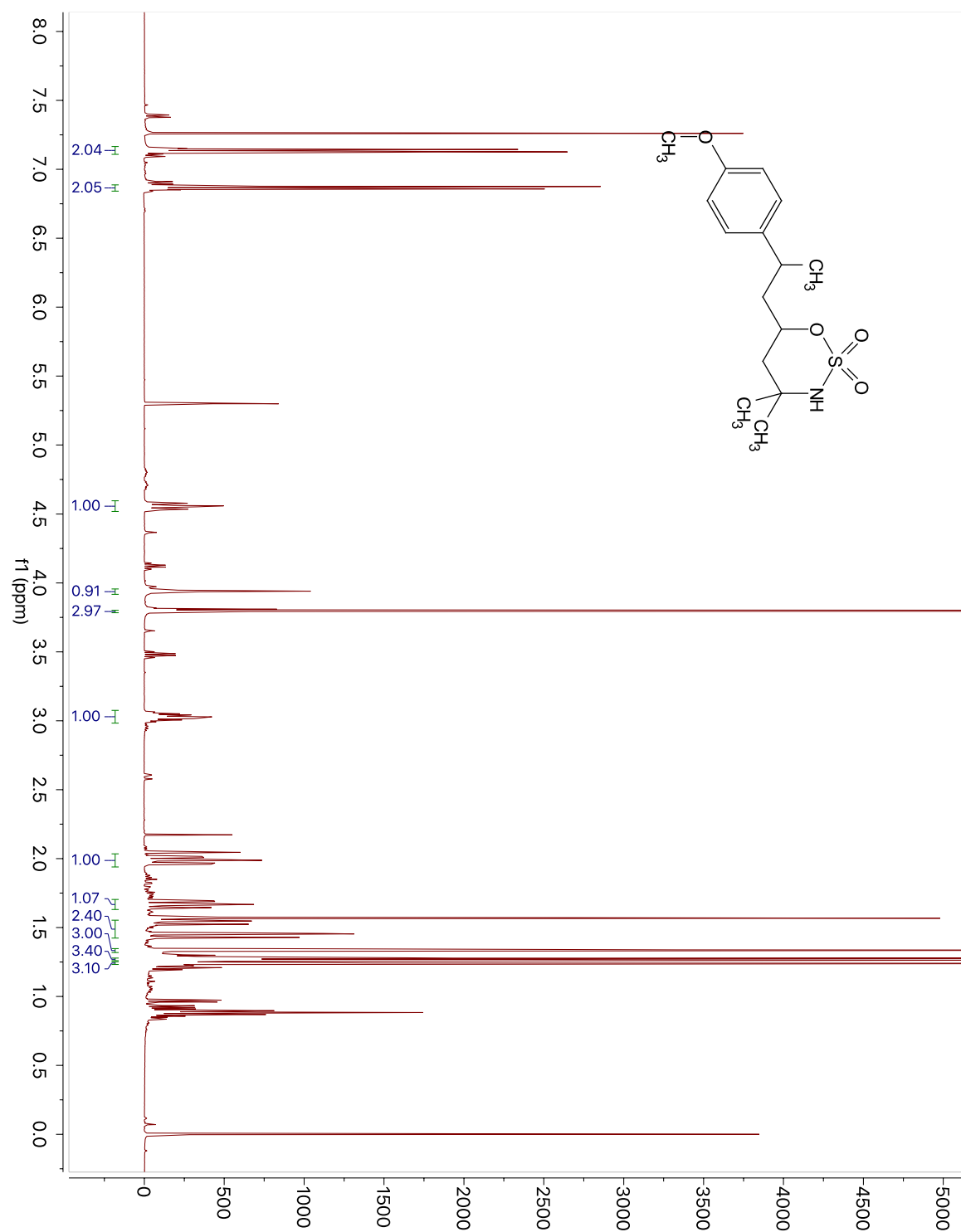
^{13}C NMR for Compound 2.12_{Cy}.

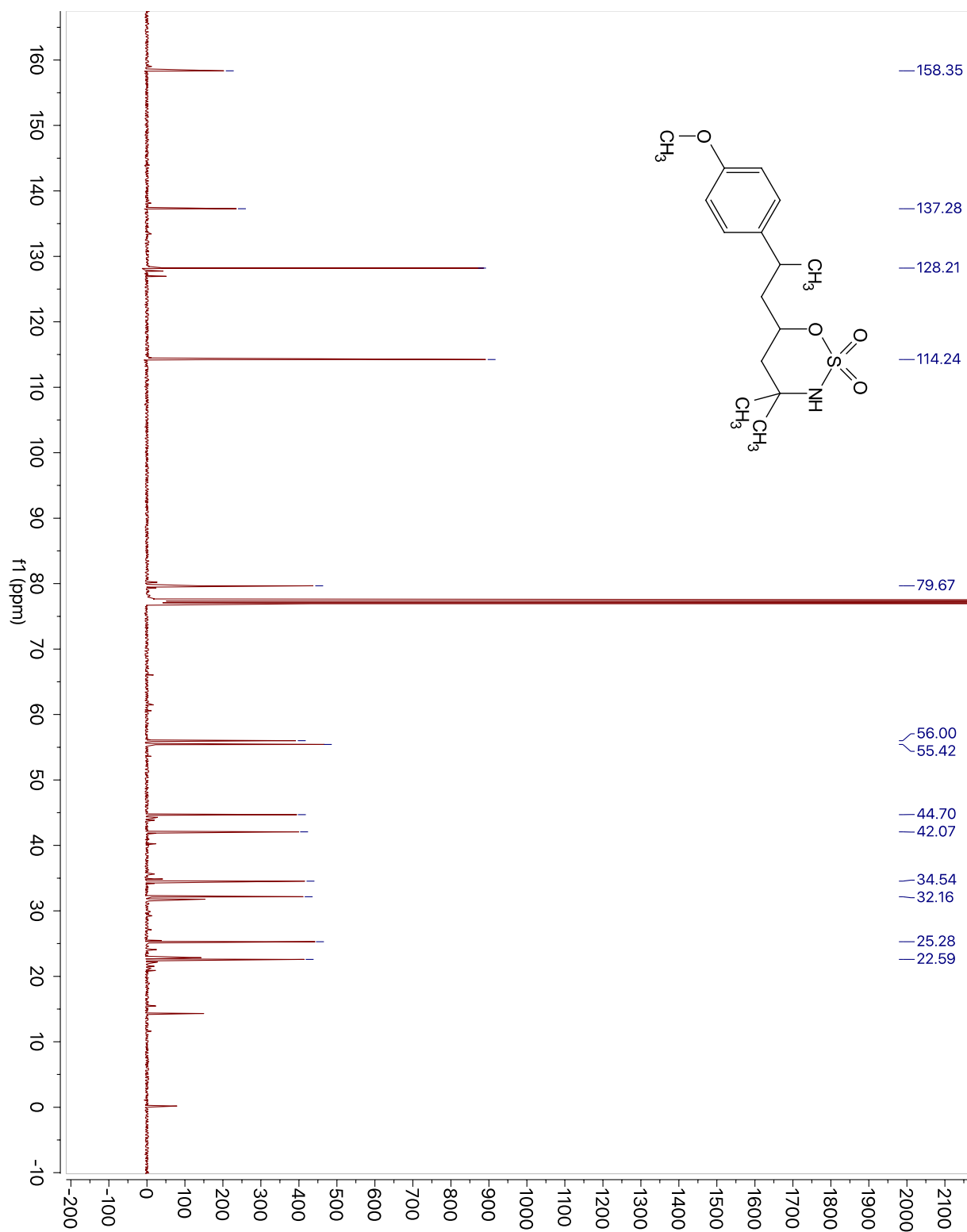
¹H NMR for Compound 2.14_{Bn-syn}.

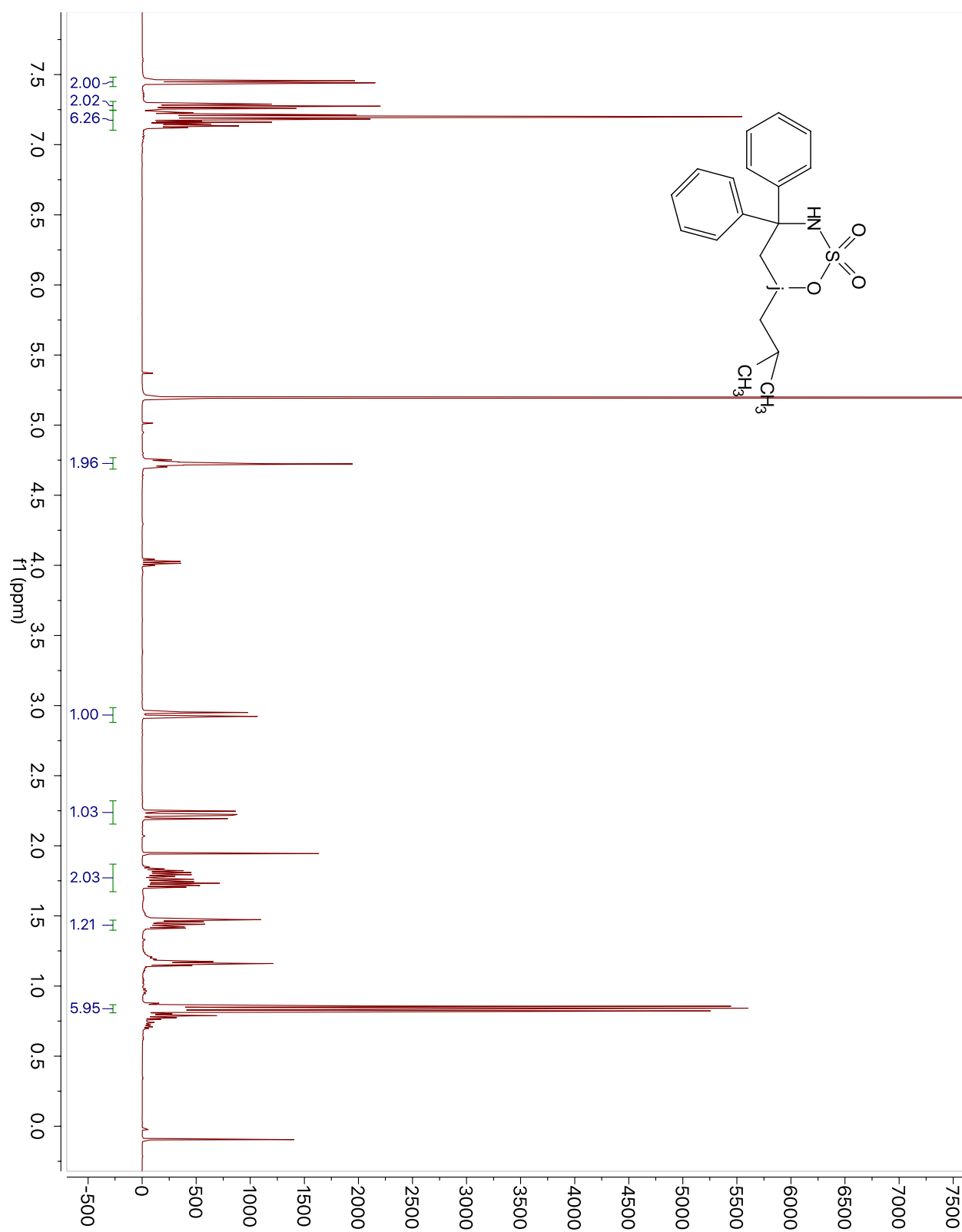
^{13}C NMR for Compound 2.14_{Bn-syn}.

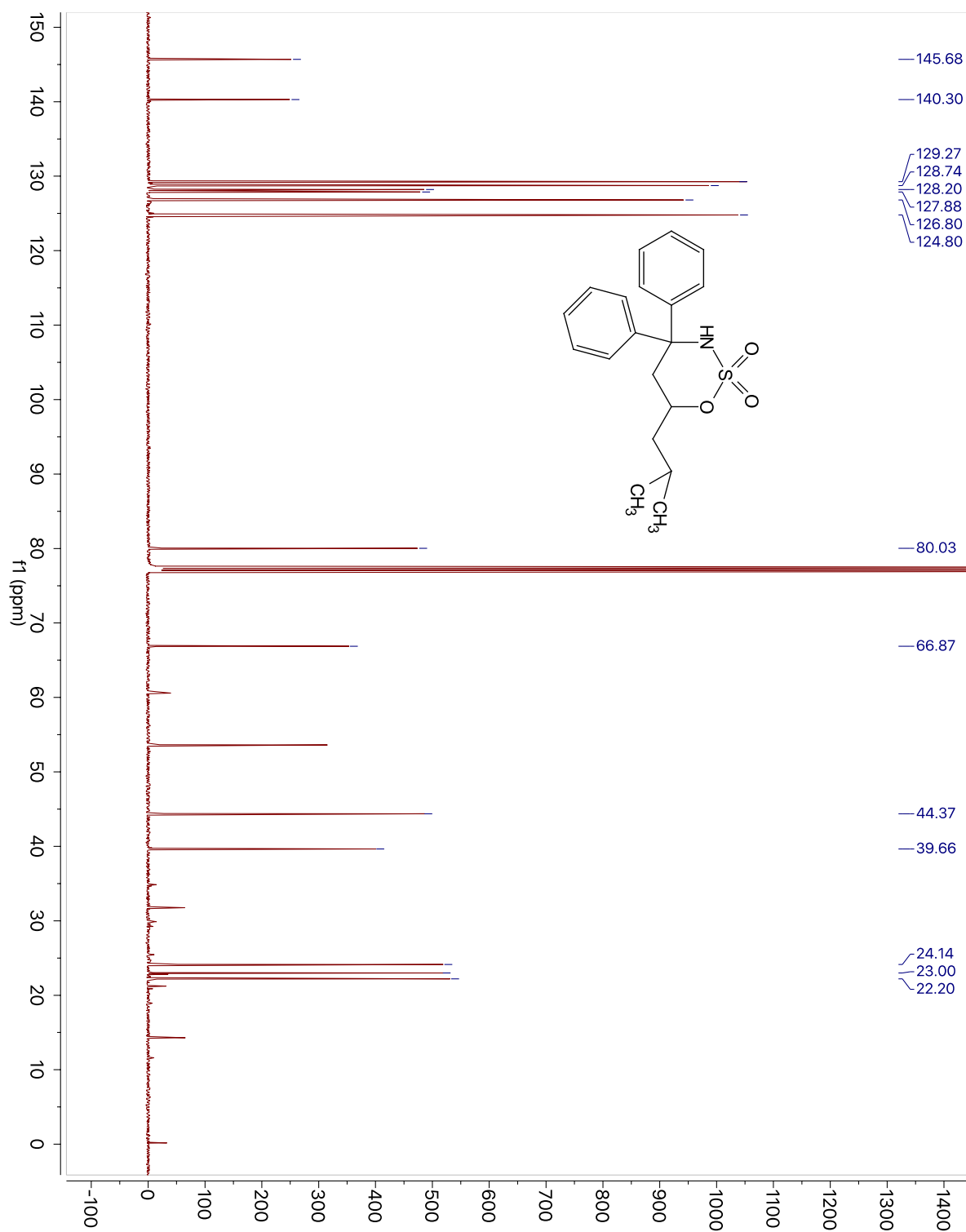
¹H NMR for Compound 2.14_{Bn-anti}.

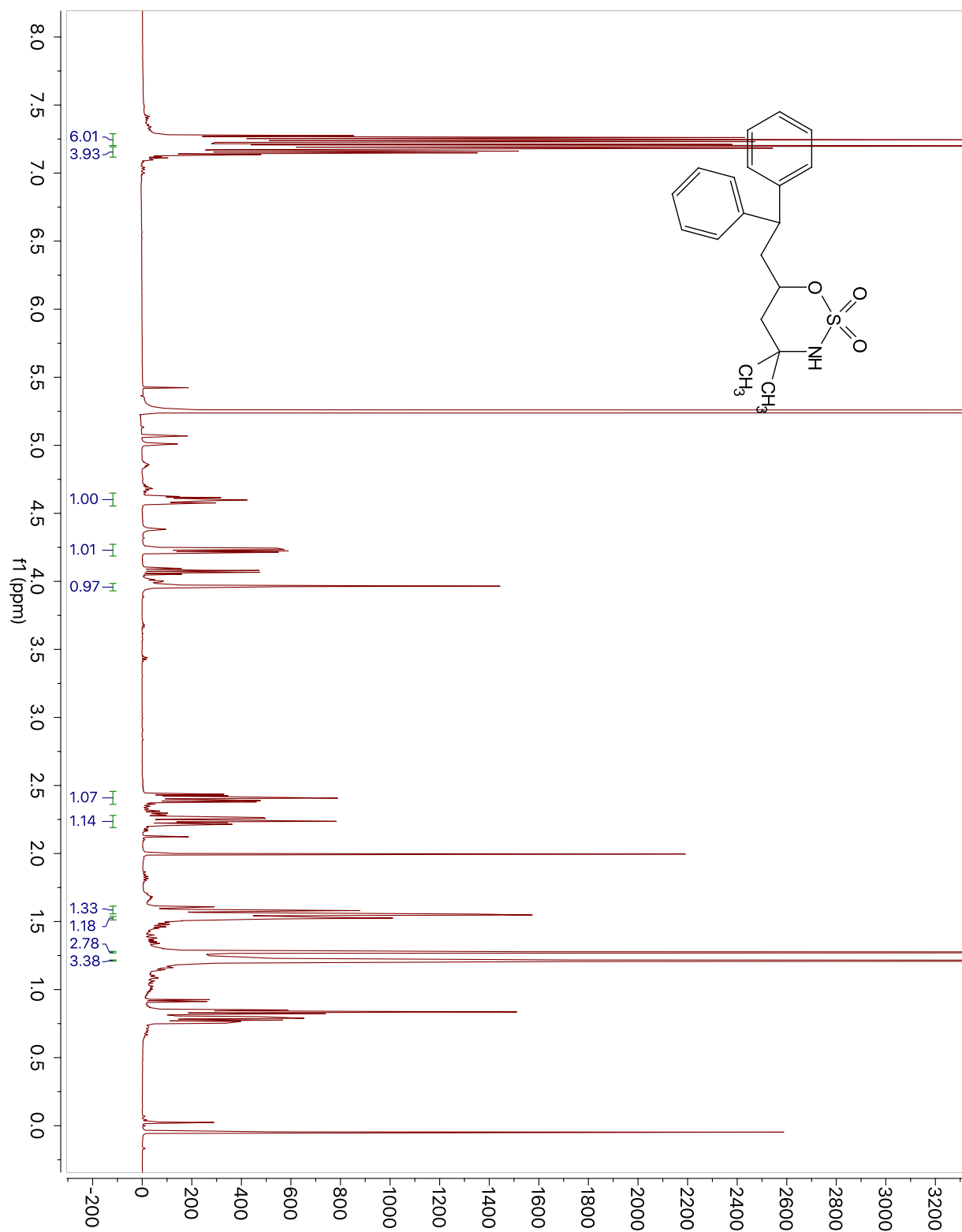
^{13}C NMR for Compound 2.14_{Bn-anti}

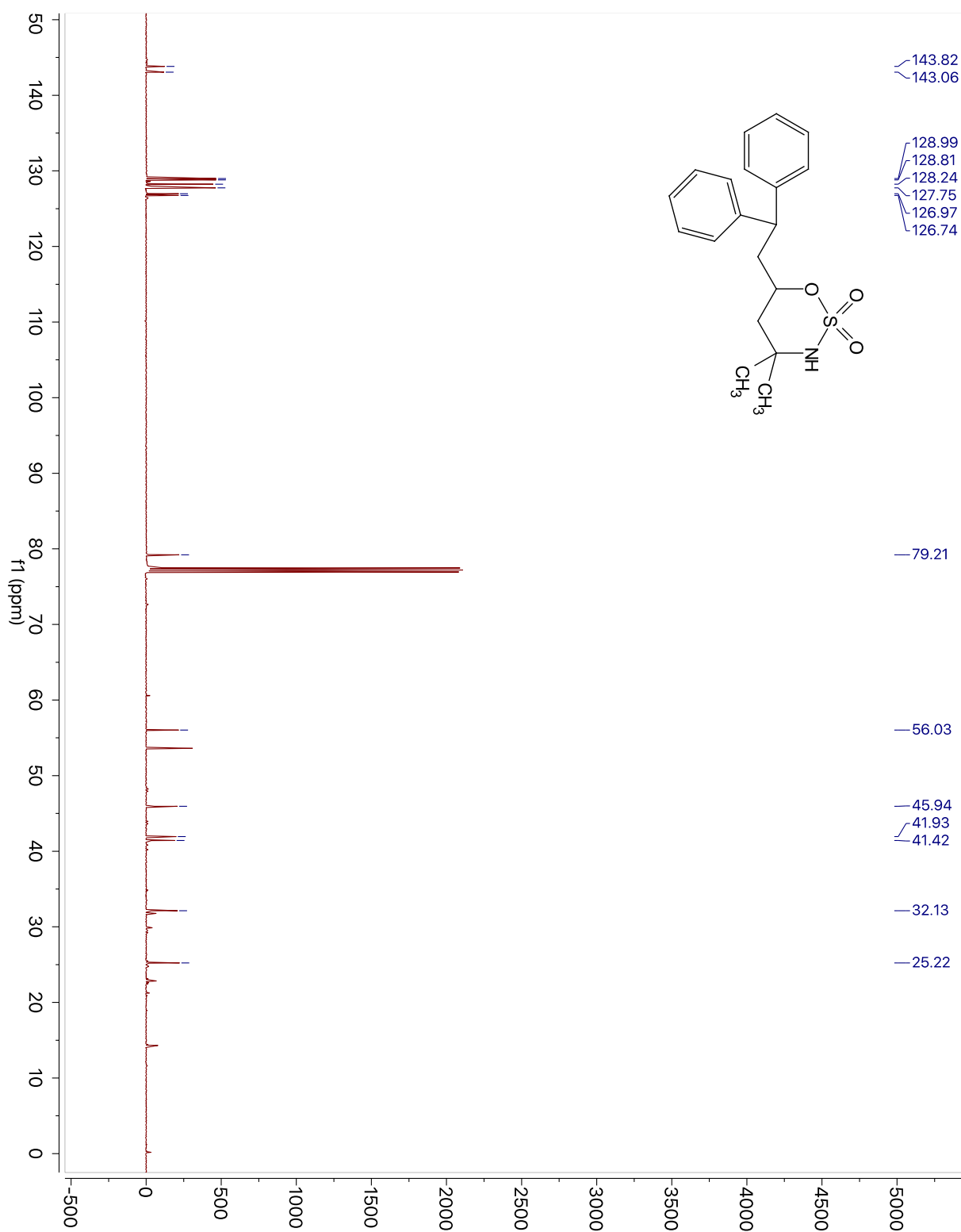
¹H NMR for Compound 2.14_{alk-major diastereomer}.

^{13}C NMR for Compound 2.14_{alk-major diastereomer}.

¹H NMR for Compound 2.15_{Bn}.

^{13}C NMR for Compound 2.15_{Bn}.

¹H NMR for Compound 2.15_{iPr}.

^{13}C NMR for Compound 2.15_{iPr}.

Chapter 2 X-Ray Data

Crystal structure for [Ag(Me₄phen)]OTf

Data Collection. A colorless crystal with approximate dimensions $0.4 \times 0.135 \times 0.13$ mm³ was selected under oil under ambient conditions and attached to the tip of a MiTeGen MicroMount®. The crystal was mounted in a stream of cold nitrogen at 100(1) K and centered in the X-ray beam by using a video camera. The crystal evaluation and data collection were performed on a Bruker SMART APEXII diffractometer with Cu K α ($\lambda = 1.54178$ Å) radiation and the diffractometer to crystal distance of 4.03 cm. The initial cell constants were obtained from three series of ω scans at different starting angles. Each series consisted of 25 frames collected at intervals of 1.0° in a 25° range about ω with the exposure time of 1 second per frame. The reflections were successfully indexed by an automated indexing routine built in the APEXII program. The final cell constants were calculated from a set of 9577 strong reflections from the actual data collection. The data were collected by using the full sphere data collection routine to survey the reciprocal space to the extent of a full sphere to a resolution of 0.8 Å. A total of 30037 data were harvested by collecting 19 sets of frames with 0.5° scans in ω and ϕ with an exposure time 2-5 sec per frame. These highly redundant datasets were corrected for Lorentz and polarization effects. The absorption correction was based on fitting a function to the empirical transmission surface as sampled by multiple equivalent measurements.

Structure Solution and Refinement. The systematic absences in the diffraction data were consistent for the space groups C2/c and Cc. The E-statistics strongly suggested the centrosymmetric space group C2/c that yielded chemically reasonable and computationally stable results of refinement. A successful solution by the direct methods provided most non-hydrogen atoms from the E-map. The remaining non-hydrogen atoms were located in an alternating series of least-squares cycles and difference Fourier maps. All nonhydrogen atoms were refined with anisotropic displacement coefficients. All hydrogen atoms were included in the structure factor calculation at idealized positions and were allowed to ride on the neighboring atoms with relative isotropic displacement coefficients. The final least-squares refinement of 248 parameters against 3530 data resulted in residuals R (based on F² for $I \geq 2\sigma$) and wR (based on F² for all data) of 0.0243 and 0.0674, respectively. The final difference Fourier map was featureless.

Summary. Crystal Data for C₁₇H₁₆AgF₃N₂O₃S (M = 493.25 g/mol): monoclinic, space group C2/c (no. 15), $a = 14.5857(11)$ Å, $b = 18.287(2)$ Å, $c = 13.4986(10)$ Å, $\beta = 101.928(4)^\circ$, $V = 3522.7(6)$ Å³, $Z = 8$, $T = 100.0$ K, $\mu(\text{CuK}\alpha) = 10.778$ mm⁻¹, $D_{\text{calc}} = 1.860$ g/cm³, 30037 reflections measured ($7.858^\circ \leq 2\theta \leq 147.264^\circ$), 3530 unique ($R_{\text{int}} = 0.0308$, $R_{\text{sigma}} = 0.0144$) which were used in all calculations. The final R_1 was 0.0243 ($I > 2\sigma(I)$) and wR_2 was 0.0674 (all data).

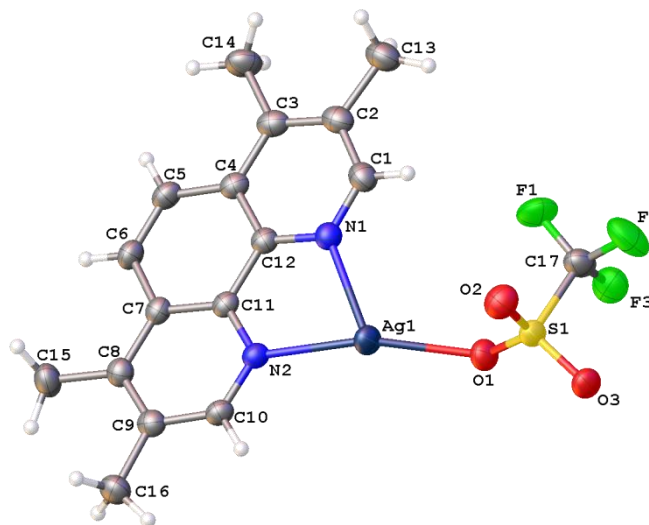


Figure S2-1. A molecular drawing of [Ag(Me₄phen)]OTf shown with 50% probability ellipsoids.

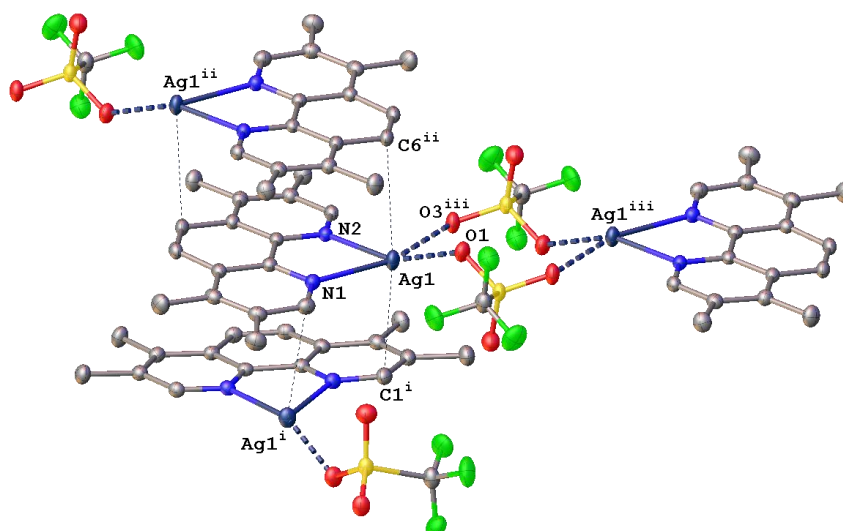


Figure S2-2. A molecular drawing of [Ag(Me₄phen)]OTf shown with 30% probability ellipsoids. The entire coordination environment of Ag1 is shown. Symmetry codes: i = 1-x, y, 1/2 - z; ii = 1-x, 1-y, 1-z; iii = 3/2 - x, 1/2 - y, 1-z.

Table S2-1. Crystal data and structure refinement for [Ag(Me₄phen)]OTf.

Identification code	schomaker75
Empirical formula	C ₁₇ H ₁₆ AgF ₃ N ₂ O ₃ S
Formula weight	493.25
Temperature/K	100.0

Crystal system	monoclinic
Space group	C2/c
a/Å	14.5857(11)
b/Å	18.287(2)
c/Å	13.4986(10)
$\alpha/^\circ$	90
$\beta/^\circ$	101.928(4)
$\gamma/^\circ$	90
Volume/Å ³	3522.7(6)
Z	8
$\rho_{\text{calc}}/\text{cm}^3$	1.860
μ/mm^{-1}	10.778
F(000)	1968.0
Crystal size/mm ³	0.4 × 0.135 × 0.13
Radiation	CuK α (λ = 1.54178)
2 Θ range for data collection/ $^\circ$	7.858 to 147.264
Index ranges	-18 ≤ h ≤ 18, -22 ≤ k ≤ 20, -16 ≤ l ≤ 16
Reflections collected	30037
Independent reflections	3530 [R_{int} = 0.0308, R_{sigma} = 0.0144]
Data/restraints/parameters	3530/0/248
Goodness-of-fit on F^2	1.105
Final R indexes [$I \geq 2\sigma(I)$]	R_1 = 0.0243, wR_2 = 0.0671
Final R indexes [all data]	R_1 = 0.0248, wR_2 = 0.0674
Largest diff. peak/hole / e Å ⁻³	0.51/-0.35

Table S2-2. Fractional Atomic Coordinates ($\times 10^4$) and Equivalent Isotropic Displacement Parameters (Å² $\times 10^3$) for [Ag(Me₄phen)]OTf. U_{eq} is defined as 1/3 of the trace of the orthogonalised U_{IJ} tensor.

Atom	x	y	z	U(eq)
Ag1	6095.3(2)	3532.8(2)	4180.5(2)	38.15(8)
S1	6437.0(3)	1719.7(3)	4382.9(4)	32.51(12)
F1	4619.8(11)	1606(1)	3761.5(14)	60.8(4)
F2	5354.6(13)	579.9(10)	3881.3(16)	70.0(5)
F3	5141.8(10)	1135(1)	5217.4(13)	55.1(4)
O1	6270.7(11)	2397.4(8)	4879.3(13)	40.5(3)
O2	6533.3(12)	1797.7(10)	3354.9(13)	46.8(4)
O3	7102.1(11)	1245.4(9)	5012.4(13)	40.4(4)
N1	4516.8(12)	3869.3(10)	3461.6(13)	30.9(4)
N2	5999.9(11)	4777(1)	4137.4(11)	27.7(3)
C1	3793.6(17)	3431.1(13)	3108.4(17)	35.7(5)
C2	2869.2(16)	3674.0(13)	2764.0(16)	35.8(4)
C3	2686.1(15)	4411.0(13)	2772.2(15)	34.4(4)
C4	3443.5(14)	4895.2(12)	3135.3(14)	29.4(4)
C5	3333.8(14)	5673.0(12)	3185.5(15)	32.3(4)
C6	4070.4(14)	6120.0(12)	3514.3(15)	31.6(4)
C7	5006.5(14)	5842.6(11)	3827.7(14)	28.1(4)
C8	5797.7(15)	6304.3(12)	4137.5(16)	31.4(4)
C9	6667.2(14)	5982.2(12)	4428.7(15)	31.5(4)
C10	6724.3(13)	5218.0(12)	4428.4(14)	29.0(4)
C11	5144.3(13)	5080.4(11)	3826.6(13)	26.3(4)
C12	4350.8(14)	4595.4(11)	3469.7(14)	27.6(4)
C13	2108.9(18)	3114.7(15)	2412(2)	46.5(6)
C14	1703.9(15)	4698.4(15)	2407(2)	45.3(5)
C15	5673.2(17)	7120.8(13)	4134(2)	43.1(5)
C16	7563.6(17)	6416.4(13)	4726(2)	40.7(5)

C17 5330.0(16) 1230.3(14) 4301(2) 42.4(5)

Table S2-3. Anisotropic Displacement Parameters ($\text{\AA}^2 \times 10^3$) for [Ag(Me₄phen)]OTf. The Anisotropic displacement factor exponent takes the form: $-2\pi^2[h^2a^{*2}U_{11}+2hka^*b^*U_{12}+\dots]$.

Atom	U_{11}	U_{22}	U_{33}	U_{23}	U_{13}	U_{12}
Ag1	33.42(11)	27.02(11)	50.98(12)	0.35(6)	1.68(8)	6.53(5)
S1	25.4(2)	27.3(3)	42.6(3)	0.29(19)	1.92(19)	4.04(18)
F1	29.9(7)	74.6(11)	70.1(11)	9.4(8)	-7.7(7)	3.7(7)
F2	57.2(10)	50(1)	102.1(14)	-28.6(9)	15.0(9)	-15.9(8)
F3	41.7(8)	59.7(10)	65.1(10)	10.7(8)	13.8(7)	-4.9(7)
O1	39.6(8)	27.9(8)	52.0(9)	-1.2(6)	4.9(7)	5.2(6)
O2	44.9(9)	48.3(10)	47.4(9)	3.5(7)	9.9(7)	6.9(8)
O3	30.5(7)	32.4(8)	55.3(10)	2.7(7)	2.0(7)	7.3(6)
N1	31.7(9)	28.8(9)	31.8(8)	-0.8(7)	5.4(7)	1.9(7)
N2	26.1(8)	29.3(9)	27.1(8)	-0.5(6)	4.4(6)	3.3(6)
C1	39.3(12)	32.7(11)	35.0(11)	-2.6(8)	7.8(9)	-3.6(9)
C2	34.1(11)	42.0(12)	31.3(10)	-2.9(9)	6.7(8)	-6.7(9)
C3	28.7(10)	45.6(12)	28.8(9)	0.1(8)	5.9(8)	-0.4(9)
C4	27.4(9)	35.4(11)	25.7(9)	0.3(7)	6.2(7)	2.7(8)
C5	27.2(9)	37.2(11)	32.3(10)	4.1(8)	5.6(8)	7.9(8)
C6	32.4(10)	28.7(10)	33.8(10)	3.5(8)	6.8(8)	7.6(8)
C7	29.6(9)	28.3(10)	26.9(9)	2.7(7)	7.4(7)	3.6(8)
C8	32(1)	31.1(10)	32.2(10)	1.6(8)	8.8(8)	0.8(9)
C9	30.3(10)	35.2(11)	29.5(9)	1.5(8)	7.0(7)	-1.5(8)
C10	24.2(9)	33.4(11)	29.2(9)	1.1(7)	4.6(7)	3.6(8)
C11	26.5(9)	29.8(10)	23.0(8)	1.6(7)	6.3(7)	3.5(7)
C12	28.2(9)	30.3(10)	24.6(8)	0.0(7)	6.4(7)	1.1(8)
C13	40.7(12)	49.2(15)	47.4(13)	-4.9(11)	4.1(10)	-11.8(11)

C14	26.7(10)	52.7(15)	53.9(14)	-4.1(11)	2.1(10)	0.2(10)
C15	40.9(12)	29.3(11)	58.9(14)	3.3(10)	9.5(10)	-1.4(9)
C16	32.4(11)	40.0(13)	48.6(13)	2.0(9)	5.6(10)	-6.2(9)
C17	30.7(11)	38.6(12)	54.7(14)	-3.2(10)	1(1)	0.4(9)

Table S2-4. Bond Lengths for [Ag(Me₄phen)]OTf.

Atom Atom Length/Å			Atom Atom Length/Å		
Ag1	O1	2.2730(16)	C1	C2	1.404(3)
Ag1	O3 ¹	2.6609(16)	C2	C3	1.374(3)
Ag1	N1	2.3870(17)	C2	C13	1.511(3)
Ag1	N2	2.2795(18)	C3	C4	1.422(3)
Ag1	C6 ²	3.233(2)	C3	C14	1.510(3)
S1	O1	1.4528(16)	C4	C5	1.434(3)
S1	O2	1.4304(18)	C4	C12	1.417(3)
S1	O3	1.4404(16)	C5	C6	1.350(3)
S1	C17	1.829(2)	C6	C7	1.436(3)
F1	C17	1.328(3)	C7	C8	1.421(3)
F2	C17	1.321(3)	C7	C11	1.408(3)
F3	C17	1.332(3)	C8	C9	1.380(3)
N1	C1	1.332(3)	C8	C15	1.504(3)
N1	C12	1.350(3)	C9	C10	1.400(3)
N2	C10	1.323(3)	C9	C16	1.511(3)
N2	C11	1.351(2)	C11	C12	1.459(3)
C1	Ag1 ³	3.133(2)			

¹3/2-X,1/2-Y,1-Z; ²1-X,1-Y,1-Z; ³1-X,+Y,1/2-Z

Table S2-5. Bond Angles for [Ag(Me₄phen)]OTf.

Atom Atom Atom Angle/°			Atom Atom Atom Angle/°		
------------------------	--	--	------------------------	--	--

O1	Ag1	O3 ¹	87.27(5)	C2	C3	C14	120.8(2)
O1	Ag1	N1	114.87(6)	C4	C3	C14	120.9(2)
O1	Ag1	N2	157.43(6)	C3	C4	C5	123.21(19)
O1	Ag1	C6 ²	78.72(6)	C12	C4	C3	118.47(19)
O3 ¹	Ag1	C6 ²	80.80(5)	C12	C4	C5	118.32(18)
N1	Ag1	O3 ¹	156.29(6)	C6	C5	C4	121.80(19)
N1	Ag1	C6 ²	94.76(5)	C5	C6	C7	121.78(19)
N2	Ag1	O3 ¹	84.74(5)	C8	C7	C6	122.80(19)
N2	Ag1	N1	71.56(6)	C11	C7	C6	118.46(19)
N2	Ag1	C6 ²	79.18(5)	C11	C7	C8	118.74(18)
O1	S1	C17	102.45(11)	C7	C8	C15	119.9(2)
O2	S1	O1	114.94(11)	C9	C8	C7	118.2(2)
O2	S1	O3	116.31(10)	C9	C8	C15	121.9(2)
O2	S1	C17	104.64(12)	C8	C9	C10	118.51(19)
O3	S1	O1	113.44(10)	C8	C9	C16	123.0(2)
O3	S1	C17	102.67(11)	C10	C9	C16	118.44(19)
S1	O1	Ag1	127.08(10)	N2	C10	C9	124.39(18)
C1	N1	Ag1	128.04(15)	N2	C11	C7	121.94(18)
C1	N1	C12	117.68(19)	N2	C11	C12	118.16(18)
C12	N1	Ag1	114.19(13)	C7	C11	C12	119.90(17)
C10	N2	Ag1	124.07(13)	N1	C12	C4	122.35(19)
C10	N2	C11	118.16(18)	N1	C12	C11	117.99(17)
C11	N2	Ag1	117.74(13)	C4	C12	C11	119.66(18)
N1	C1	Ag1 ³	96.82(13)	F1	C17	S1	111.01(18)
N1	C1	C2	124.3(2)	F1	C17	F3	106.9(2)
C2	C1	Ag1 ³	84.06(13)	F2	C17	S1	111.36(17)
C1	C2	C13	118.8(2)	F2	C17	F1	108.5(2)

C3	C2	C1	118.8(2)	F2	C17	F3	108.0(2)
C3	C2	C13	122.3(2)	F3	C17	S1	110.90(16)
C2	C3	C4	118.4(2)				
$^1/3$ -X, $^1/2$ -Y, 1 -Z; 2 -X, 1 -Y, 1 -Z; 3 -X,+Y, $^1/2$ -Z							

Table S2-6. Torsion Angles for [Ag(Me₄phen)]OTf.

A	B	C	D	Angle/°	A	B	C	D	Angle/°
Ag1	N1	C1	Ag1 ¹	-97.42(14)	C4	C5	C6	C7	0.3(3)
Ag1	N1	C1	C2	175.14(16)	C5	C4	C12	N1	179.15(18)
Ag1	N1	C12	C4	-175.87(14)	C5	C4	C12	C11	-1.6(3)
Ag1	N1	C12	C11	4.9(2)	C5	C6	C7	C8	177.38(19)
Ag1	N2	C10	C9	-178.27(14)	C5	C6	C7	C11	-2.6(3)
Ag1	N2	C11	C7	176.39(13)	C6	C7	C8	C9	179.74(18)
Ag1	N2	C11	C12	-4.4(2)	C6	C7	C8	C15	-0.7(3)
Ag1 ¹	C1	C2	C3	-93.25(19)	C6	C7	C11	N2	-178.16(17)
Ag1 ¹	C1	C2	C13	87.62(19)	C6	C7	C11	C12	2.7(3)
O1	S1	C17	F1	60.3(2)	C7	C8	C9	C10	-1.5(3)
O1	S1	C17	F2	-178.63(19)	C7	C8	C9	C16	177.10(19)
O1	S1	C17	F3	-58.30(19)	C7	C11	C12	N1	178.66(17)
O2	S1	O1	Ag1	2.59(16)	C7	C11	C12	C4	-0.6(3)
O2	S1	C17	F1	-59.9(2)	C8	C7	C11	N2	1.9(3)
O2	S1	C17	F2	61.1(2)	C8	C7	C11	C12	-177.28(17)
O2	S1	C17	F3	-178.56(17)	C8	C9	C10	N2	2.1(3)
O3	S1	O1	Ag1	139.84(11)	C10	N2	C11	C7	-1.5(3)
O3	S1	C17	F1	178.19(18)	C10	N2	C11	C12	177.74(16)
O3	S1	C17	F2	-60.8(2)	C11	N2	C10	C9	-0.6(3)
O3	S1	C17	F3	59.55(19)	C11	C7	C8	C9	-0.3(3)
N1	C1	C2	C3	1.0(3)	C11	C7	C8	C15	179.24(19)

N1	C1	C2	C13	-178.2(2)	C12N1	C1	Ag1	¹ 86.11(17)
N2	C11	C12	N1	-0.5(3)	C12N1	C1	C2	-1.3(3)
N2	C11	C12	C4	-179.83(16)	C12C4	C5	C6	1.8(3)
C1	N1	C12	C4	1.1(3)	C13C2	C3	C4	178.8(2)
C1	N1	C12	C11	-178.17(17)	C13C2	C3	C14	-1.1(3)
C1	C2	C3	C4	-0.3(3)	C14C3	C4	C5	0.3(3)
C1	C2	C3	C14	179.8(2)	C14C3	C4	C12	179.96(19)
C2	C3	C4	C5	-179.53(19)	C15C8	C9	C10	178.9(2)
C2	C3	C4	C12	0.1(3)	C15C8	C9	C16	-2.4(3)
C3	C4	C5	C6	-178.58(19)	C16C9	C10	N2	-176.60(19)
C3	C4	C12	N1	-0.5(3)	C17S1	O1	Ag1	-110.25(13)
C3	C4	C12	C11	178.74(17)				
¹ 1-X,+Y,1/2-Z								

Table S2-7. Hydrogen Atom Coordinates ($\text{\AA}\times 10^4$) and Isotropic Displacement Parameters ($\text{\AA}^2\times 10^3$) for $[\text{Ag}(\text{Me}_4\text{phen})]\text{OTf}$.

Atom	x	y	z	U(eq)
H1	3911	2921	3088	43
H5	2726	5879	2982	39
H6	3967	6632	3539	38
H10	7324	5002	4652	35
H13A	1842	3189	1691	70
H13B	1616	3170	2801	70
H13C	2376	2622	2515	70
H14A	1345	4635	2939	68
H14B	1399	4428	1801	68
H14C	1730	5219	2243	68
H15A	6271	7354	4437	65

H15B 5202	7249	4527	65
H15C 5466	7292	3436	65
H16A 7673	6694	4141	61
H16B 8089	6082	4957	61
H16C 7510	6755	5275	61

Crystal structure for [Ag(Me₄phen)₂]OTf

Data Collection. A colorless crystal with approximate dimensions 0.138 x 0.07 x 0.01 mm³ was selected under oil under ambient conditions and attached to the tip of a MiTeGen MicroMount©. The crystal was mounted in a stream of cold nitrogen at 100(1) K and centered in the X-ray beam by using a video camera.

The crystal evaluation and data collection were performed on a Bruker Quazar SMART APEXII diffractometer with Mo K_α ($\lambda = 0.71073$ Å) radiation and the diffractometer to crystal distance of 4.96 cm.

The initial cell constants were obtained from three series of ω scans at different starting angles. Each series consisted of 12 frames collected at intervals of 0.5° in a 6° range about ω with the exposure time of 10 seconds per frame. The reflections were successfully indexed by an automated indexing routine built in the APEX3 program suite. The final cell constants were calculated from a set of 5350 strong reflections from the actual data collection.

The data were collected by using the full sphere data collection routine to survey the reciprocal space to the extent of a full sphere to a resolution of 0.73 Å. A total of 66919 data were harvested by collecting 5 sets of frames with 0.6° scans in ω and ϕ with exposure times of 40 sec per frame. These highly redundant datasets were corrected for Lorentz and polarization effects. The absorption correction was based on fitting a function to the empirical transmission surface as sampled by multiple equivalent measurements.

Structure Solution and Refinement.

The systematic absences in the diffraction data were uniquely consistent for the space group $P2_12_12_1$ that yielded chemically reasonable and computationally stable results of refinement.

A successful solution by the direct methods provided most non-hydrogen atoms from the *E*-map. The remaining non-hydrogen atoms were located in an alternating series of least-squares cycles and difference Fourier maps. All non-hydrogen atoms were refined with anisotropic displacement coefficients.

All hydrogen atoms were included in the structure factor calculation at idealized positions and were allowed to ride on the neighboring atoms with relative isotropic displacement coefficients.

The asymmetric unit contains one cationic Ag complex and one trifluoromethanesulfonate anion.

The final least-squares refinement of 414 parameters against 8140 data resulted in residuals R (based on F^2 for $I \geq 2\sigma$) and wR (based on F^2 for all data) of 0.0382 and 0.0786, respectively. The final difference Fourier map was featureless.

Summary.

Crystal Data for $\text{C}_{33}\text{H}_{32}\text{AgF}_3\text{N}_4\text{O}_3\text{S}$ ($M = 729.55$ g/mol): orthorhombic, space group $P2_12_12_1$ (no. 19), $a = 7.321(3)$ Å, $b = 14.785(6)$ Å, $c = 27.845(11)$ Å, $V = 3014.1(19)$ Å³, $Z = 4$, $T = 100.0$ K, $\mu(\text{MoK}\alpha) = 0.799$ mm⁻¹, $D_{\text{calc}} = 1.608$ g/cm³, 66919 reflections measured ($2.926^\circ \leq 2\theta \leq 58.372^\circ$), 8140 unique ($R_{\text{int}} = 0.0885$, $R_{\text{sigma}} = 0.0607$) which were used in all calculations. The final R_1 was 0.0382 ($I > 2\sigma(I)$) and wR_2 was 0.0786 (all data).

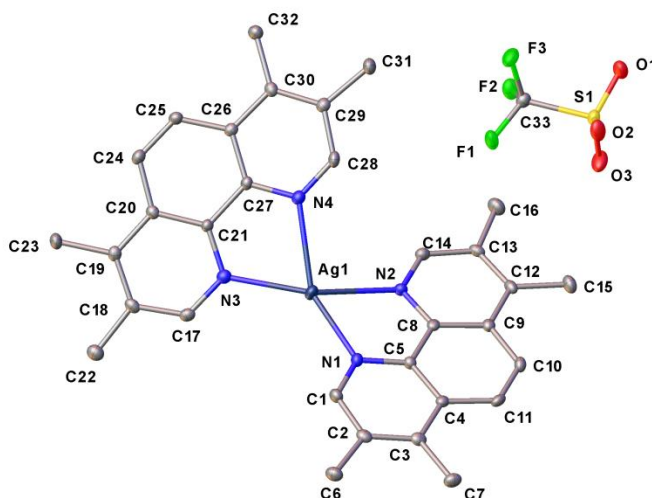


Figure S2-3. A molecular drawing of $[\text{Ag}(\text{Me}_4\text{phen})_2]\text{OTf}$ shown with 50% probability ellipsoids. All H atoms are omitted.

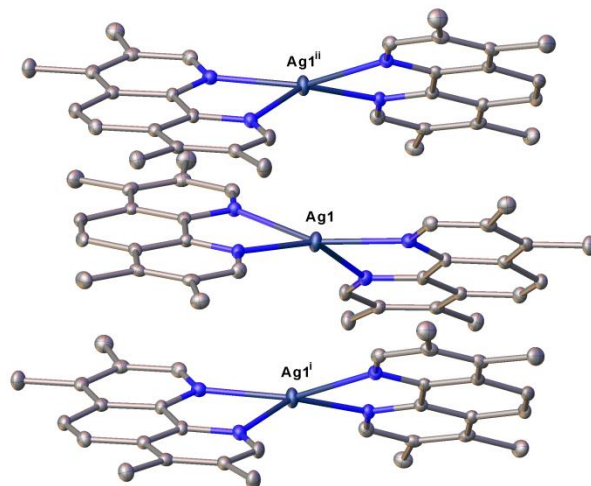


Figure S2-4. A molecular drawing of $[\text{Ag}(\text{Me}_4\text{phen})_2]\text{OTf}$ showing the stacking of the cationic Ag complex shown with 50% probability ellipsoids. All H atoms and counterions are omitted for clarity. Symmetry codes: i (0.5+x, 0.5-y, 1-z), ii (-0.5+x, 0.5-y, 1-z).

Table S2-8. Crystal data and structure refinement for $[\text{Ag}(\text{Me}_4\text{phen})_2]\text{OTf}$.

Identification code	Schomaker77
Empirical formula	$\text{C}_{33}\text{H}_{32}\text{AgF}_3\text{N}_4\text{O}_3\text{S}$
Formula weight	729.55
Temperature/K	100.0
Crystal system	orthorhombic
Space group	$P2_12_12_1$
a/Å	7.321(3)
b/Å	14.785(6)
c/Å	27.845(11)
$\alpha/^\circ$	90
$\beta/^\circ$	90
$\gamma/^\circ$	90
Volume/Å ³	3014.1(19)
Z	4

$\rho_{\text{calc}}/\text{cm}^3$	1.608
μ/mm^{-1}	0.799
F(000)	1488.0
Crystal size/ mm^3	$0.138 \times 0.07 \times 0.01$
Radiation	MoK α ($\lambda = 0.71073$)
2 Θ range for data collection/ $^\circ$	2.926 to 58.372
Index ranges	$-10 \leq h \leq 10, -20 \leq k \leq 20, -38 \leq l \leq 38$
Reflections collected	66919
Independent reflections	8140 [$R_{\text{int}} = 0.0885, R_{\text{sigma}} = 0.0607$]
Data/restraints/parameters	8140/0/414
Goodness-of-fit on F^2	1.057
Final R indexes [$I \geq 2\sigma(I)$]	$R_1 = 0.0382, wR_2 = 0.0748$
Final R indexes [all data]	$R_1 = 0.0555, wR_2 = 0.0786$
Largest diff. peak/hole / $\text{e } \text{\AA}^{-3}$	0.59/-0.45
Flack parameter	0.001(14)

Table S2-9. Fractional Atomic Coordinates ($\times 10^4$) and Equivalent Isotropic Displacement Parameters ($\text{\AA}^2 \times 10^3$) for **[Ag(Me₄phen)₂]OTf**. U_{eq} is defined as 1/3 of the trace of the orthogonalised U_{ij} tensor.

Atom	<i>x</i>	<i>y</i>	<i>z</i>	U(eq)
Ag1	3896.5(5)	2835.2(2)	5068.3(2)	27.31(9)
N1	4272(4)	1907(2)	4436.0(11)	19.3(7)
N2	2968(5)	3626(2)	4357.2(12)	19.2(7)
N3	3752(5)	2581(2)	5862.7(12)	21.9(8)
N4	5035(5)	4159(2)	5475.4(11)	21.4(8)
C1	4859(5)	1057(3)	4469.1(15)	23.0(9)
C2	5205(5)	490(3)	4079.4(15)	21.5(9)

C3	4964(5)	822(3)	3620.2(15)	21.0(9)
C4	4340(5)	1732(3)	3570.9(14)	18.0(8)
C5	3991(5)	2243(3)	3990.6(12)	17.6(7)
C6	5844(6)	-470(3)	4177.8(16)	27.6(10)
C7	5322(6)	273(3)	3177.2(16)	27.3(10)
C8	3318(5)	3164(3)	3947.0(14)	17.7(8)
C9	3061(5)	3556(3)	3490.4(14)	19.2(8)
C10	3476(5)	3015(3)	3074.7(14)	22.5(10)
C11	4074(6)	2152(3)	3114.9(13)	22.5(8)
C12	2460(6)	4462(3)	3458.9(15)	20.9(9)
C13	2129(6)	4924(3)	3881.0(15)	22.3(9)
C14	2407(5)	4469(3)	4318.7(15)	21.7(9)
C15	2225(6)	4924(3)	2983.0(16)	30.7(11)
C16	1521(7)	5909(3)	3892.2(18)	33.9(11)
C17	3165(6)	1805(3)	6053.6(16)	21.6(9)
C18	3128(6)	1618(3)	6549.0(16)	21.7(9)
C19	3719(6)	2284(3)	6861.9(14)	20.9(9)
C20	4334(5)	3113(3)	6669.4(14)	18.7(9)
C21	4338(5)	3235(3)	6165.4(13)	17.3(8)
C22	2440(6)	713(3)	6717.9(17)	29.6(11)
C23	3681(6)	2130(3)	7399.6(13)	28.4(9)
C24	4942(6)	3853(3)	6963.7(14)	22.1(9)
C25	5413(5)	4658(3)	6772.8(15)	20.3(9)
C26	5445(5)	4809(3)	6266.9(14)	18.9(8)
C27	4957(5)	4089(3)	5961.7(13)	17.8(8)
C28	5541(6)	4941(3)	5295.8(14)	22.9(9)

C29	5992(6)	5714(3)	5561.5(14)	21.6(8)
C30	5937(6)	5655(3)	6058.4(14)	20.4(8)
C31	6472(6)	6573(3)	5297.9(15)	29.8(10)
C32	6372(6)	6447(3)	6373.1(15)	25.6(9)
S1	6623.5(14)	7095.2(8)	3227.9(4)	24.9(2)
F1	6498(4)	6089.9(18)	4010.3(9)	39.5(7)
F2	5057(4)	7344.1(18)	4072.5(9)	37.6(7)
F3	7970(4)	7338.3(19)	4095.5(9)	38.7(7)
O1	6770(5)	8051(2)	3167.0(11)	39.8(9)
O2	8224(5)	6602(2)	3097.5(11)	38.1(8)
O3	4936(5)	6704(3)	3079.0(12)	50(1)
C33	6546(6)	6955(3)	3882.2(14)	23.8(9)

Table S2-10. Anisotropic Displacement Parameters ($\text{\AA}^2 \times 10^3$) for **[Ag(Me₄phen)₂OTf]**. The Anisotropic displacement factor exponent takes the form: $-2\pi^2[h^2a^{*2}U_{11}+2hka^*b^*U_{12}+\dots]$.

Atom	U ₁₁	U ₂₂	U ₃₃	U ₂₃	U ₁₃	U ₁₂
Ag1	41.06(19)	24.92(14)	15.95(13)	-2.37(13)	-2.09(14)	0.03(16)
N1	21.5(19)	20.0(17)	16.5(16)	-0.1(12)	-0.8(13)	-0.6(13)
N2	22.7(18)	14.3(16)	20.6(18)	-0.3(13)	-0.9(14)	2.2(14)
N3	23.2(19)	21.4(18)	21.1(17)	-0.9(13)	0.0(16)	0.3(16)
N4	24(2)	21.9(18)	18.1(17)	0.1(14)	-1.8(15)	0.9(15)
C1	25(2)	19(2)	25(2)	4.0(17)	-2.0(18)	-0.5(17)
C2	16(2)	19(2)	30(2)	1.1(17)	1.0(18)	-3.1(16)
C3	15(2)	22(2)	26(2)	-2.8(17)	2.5(17)	-1.3(16)
C4	18(2)	17(2)	19(2)	-2.0(15)	1.4(15)	-2.5(15)
C5	16.8(18)	18.1(18)	17.7(17)	1.2(16)	-0.4(17)	1(2)

C6	28(3)	19(2)	36(2)	0.3(18)	-2(2)	0.0(18)
C7	28(2)	23(2)	30(2)	-8.0(19)	3(2)	0.4(18)
C8	16(2)	21(2)	16.1(19)	-0.4(16)	-0.5(15)	-4.8(16)
C9	17(2)	21(2)	20(2)	0.7(17)	-0.8(17)	-2.6(17)
C10	22(2)	30(3)	15.1(18)	4.1(16)	-0.8(15)	-4.4(17)
C11	24(2)	26(2)	17.4(17)	-6.0(18)	-1.2(16)	-5(2)
C12	19(2)	19(2)	25(2)	6.6(18)	-2.6(17)	-2.4(16)
C13	20(2)	16(2)	30(2)	2.1(17)	-0.9(18)	-0.3(16)
C14	22(2)	20(2)	23(2)	-2.6(17)	1.1(17)	-1.7(16)
C15	34(3)	30(2)	29(2)	12(2)	0(2)	2(2)
C16	37(3)	25(2)	40(3)	6(2)	-2(2)	3(2)
C17	20(2)	19(2)	25(2)	-4.4(17)	-0.7(18)	1.7(17)
C18	19(2)	17(2)	30(2)	4.8(17)	2.9(18)	3.3(17)
C19	20(2)	21(2)	21.4(19)	2.1(16)	0.7(17)	6.7(19)
C20	16(2)	17(2)	23(2)	1.6(15)	0.1(15)	2.7(15)
C21	19(2)	18.3(19)	14.6(19)	-2.0(15)	1.6(15)	0.5(15)
C22	32(3)	21(2)	36(3)	3.6(19)	0(2)	0.8(19)
C23	40(3)	25(2)	19.7(18)	3.6(18)	-0.1(18)	-2(2)
C24	22(2)	27(2)	17(2)	-4.5(17)	-1.5(17)	0.9(18)
C25	23(2)	17(2)	21(2)	-2.2(16)	-2.6(17)	0.7(16)
C26	17(2)	20(2)	20(2)	-1.1(16)	0.3(16)	0.6(16)
C27	18(2)	19(2)	16.6(19)	-0.1(16)	-1.2(16)	2.4(16)
C28	25(2)	28(2)	15.5(19)	3.3(17)	0.2(16)	1.3(17)
C29	21(2)	23(2)	20.9(19)	0.3(15)	-0.5(19)	1.3(19)
C30	18(2)	22(2)	21.4(19)	3.2(15)	-1.5(18)	0.7(17)
C31	39(3)	29(2)	21(2)	4.8(17)	2(2)	-4(2)

C32	29(3)	22(2)	25(2)	0.8(17)	-1(2)	0.8(19)
S1	31.7(6)	25.3(5)	17.7(4)	2.0(4)	-0.5(4)	0.8(5)
F1	68(2)	25.1(13)	25.4(14)	6.0(11)	7.8(14)	8.2(14)
F2	38.8(15)	39.8(17)	34.3(14)	2.0(12)	11.1(12)	9.5(12)
F3	40.3(15)	49.4(18)	26.3(13)	-2.3(13)	-7.2(12)	-8.6(13)
O1	66(2)	25.5(18)	27.5(17)	5.0(13)	2.0(16)	2.9(16)
O2	52(2)	35.4(18)	27.0(17)	3.7(14)	13.6(15)	12.7(16)
O3	47(2)	75(3)	28.2(19)	9.8(18)	-9.8(16)	-24(2)
C33	25(2)	27(2)	20(2)	-1.2(16)	-0.4(17)	3.5(17)

Table S2-11. Bond Lengths for [Ag(Me₄phen)₂]OTf.

Atom	Atom	Length/Å	Atom	Atom	Length/Å
Ag1	N1	2.249(3)	C13	C14	1.407(6)
Ag1	N2	2.398(3)	C13	C16	1.523(6)
Ag1	N3	2.246(3)	C17	C18	1.407(6)
Ag1	N4	2.410(3)	C18	C19	1.384(6)
N1	C1	1.332(5)	C18	C22	1.505(6)
N1	C5	1.352(5)	C19	C20	1.411(5)
N2	C8	1.355(5)	C19	C23	1.515(5)
N2	C14	1.316(5)	C20	C21	1.415(5)
N3	C17	1.335(5)	C20	C24	1.438(5)
N3	C21	1.352(5)	C21	C27	1.457(5)
N4	C27	1.359(5)	C24	C25	1.348(6)
N4	C28	1.313(5)	C25	C26	1.427(6)
C1	C2	1.394(6)	C26	C27	1.408(5)

C2	C3	1.381(6)	C26	C30	1.425(5)
C2	C6	1.520(6)	C28	C29	1.401(6)
C3	C4	1.428(6)	C29	C30	1.387(5)
C3	C7	1.499(6)	C29	C31	1.508(6)
C4	C5	1.415(5)	C30	C32	1.497(6)
C4	C11	1.427(5)	S1	O1	1.428(3)
C5	C8	1.453(6)	S1	O2	1.427(3)
C8	C9	1.410(6)	S1	O3	1.426(4)
C9	C10	1.439(6)	S1	C33	1.834(4)
C9	C12	1.413(6)	F1	C33	1.329(5)
C10	C11	1.353(6)	F2	C33	1.341(5)
C12	C13	1.381(6)	F3	C33	1.327(5)
C12	C15	1.501(6)			

Table S2-12. Bond Angles for [Ag(Me₄phen)₂]OTf.

Atom	Atom	Atom	Angle/°	Atom	Atom	Atom	Angle/°
N1	Ag1	N2	71.69(12)	C12	C13	C16	122.8(4)
N1	Ag1	N4	145.21(12)	C14	C13	C16	118.8(4)
N2	Ag1	N4	95.20(11)	N2	C14	C13	124.6(4)
N3	Ag1	N1	132.42(11)	N3	C17	C18	124.5(4)
N3	Ag1	N2	151.81(11)	C17	C18	C22	119.2(4)
N3	Ag1	N4	71.87(11)	C19	C18	C17	118.1(4)
C1	N1	Ag1	124.1(3)	C19	C18	C22	122.7(4)
C1	N1	C5	117.4(3)	C18	C19	C20	118.6(4)
C5	N1	Ag1	118.4(2)	C18	C19	C23	120.6(4)

C8	N2	Ag1	113.4(3)	C20	C19	C23	120.8(4)
C14	N2	Ag1	128.1(3)	C19	C20	C21	119.2(4)
C14	N2	C8	117.9(4)	C19	C20	C24	122.9(4)
C17	N3	Ag1	123.4(3)	C21	C20	C24	117.9(4)
C17	N3	C21	117.9(4)	N3	C21	C20	121.8(4)
C21	N3	Ag1	118.6(3)	N3	C21	C27	118.4(3)
C27	N4	Ag1	113.1(3)	C20	C21	C27	119.8(3)
C28	N4	Ag1	129.3(3)	C25	C24	C20	121.8(4)
C28	N4	C27	117.3(4)	C24	C25	C26	122.1(4)
N1	C1	C2	124.9(4)	C27	C26	C25	118.2(4)
C1	C2	C6	118.5(4)	C27	C26	C30	118.8(4)
C3	C2	C1	119.0(4)	C30	C26	C25	123.0(4)
C3	C2	C6	122.6(4)	N4	C27	C21	117.8(3)
C2	C3	C4	117.7(4)	N4	C27	C26	122.2(4)
C2	C3	C7	123.2(4)	C26	C27	C21	120.0(3)
C4	C3	C7	119.1(4)	N4	C28	C29	125.7(4)
C5	C4	C3	118.8(4)	C28	C29	C31	119.0(4)
C5	C4	C11	118.5(4)	C30	C29	C28	117.9(4)
C11	C4	C3	122.6(4)	C30	C29	C31	123.1(4)
N1	C5	C4	122.2(4)	C26	C30	C32	120.1(3)
N1	C5	C8	118.2(3)	C29	C30	C26	118.0(4)
C4	C5	C8	119.5(3)	C29	C30	C32	121.9(4)
N2	C8	C5	117.8(3)	O1	S1	C33	103.42(19)
N2	C8	C9	121.9(4)	O2	S1	O1	114.4(2)
C9	C8	C5	120.4(4)	O2	S1	C33	102.75(18)
C8	C9	C10	118.0(4)	O3	S1	O1	115.6(2)

C8	C9	C12	119.1(4)	O3	S1	O2	115.5(2)
C12	C9	C10	122.9(4)	O3	S1	C33	102.5(2)
C11	C10	C9	121.7(4)	F1	C33	S1	112.1(3)
C10	C11	C4	121.9(4)	F1	C33	F2	106.6(3)
C9	C12	C15	121.5(4)	F2	C33	S1	111.7(3)
C13	C12	C9	118.1(4)	F3	C33	S1	111.8(3)
C13	C12	C15	120.4(4)	F3	C33	F1	108.2(3)
C12	C13	C14	118.4(4)	F3	C33	F2	106.2(3)

Table S2-13. Torsion Angles for [Ag(Me₄phen)₂]OTf.

A	B	C	D	Angle/°	A	B	C	D	Angle/°
Ag1	N1	C1	C2	-175.9(3)	C12	C9	C10	C11	179.1(4)
Ag1	N1	C5	C4	174.7(3)	C12	C13	C14	N2	0.1(7)
Ag1	N1	C5	C8	-4.9(5)	C14	N2	C8	C5	178.1(3)
Ag1	N2	C8	C5	6.6(4)	C14	N2	C8	C9	-1.3(6)
Ag1	N2	C8	C9	-172.8(3)	C15	C12	C13	C14	-178.6(4)
Ag1	N2	C14	C13	170.6(3)	C15	C12	C13	C16	-0.1(6)
Ag1	N3	C17	C18	177.4(3)	C16	C13	C14	N2	-178.4(4)
Ag1	N3	C21	C20	-178.2(3)	C17	N3	C21	C20	-0.1(6)
Ag1	N3	C21	C27	2.7(5)	C17	N3	C21	C27	-179.2(3)
Ag1	N4	C27	C21	3.9(4)	C17	C18	C19	C20	-0.3(6)
Ag1	N4	C27	C26	-175.8(3)	C17	C18	C19	C23	178.8(4)
Ag1	N4	C28	C29	172.2(3)	C18	C19	C20	C21	-0.4(6)
N1	C1	C2	C3	1.2(6)	C18	C19	C20	C24	178.8(4)
N1	C1	C2	C6	-179.1(4)	C19	C20	C21	N3	0.6(6)

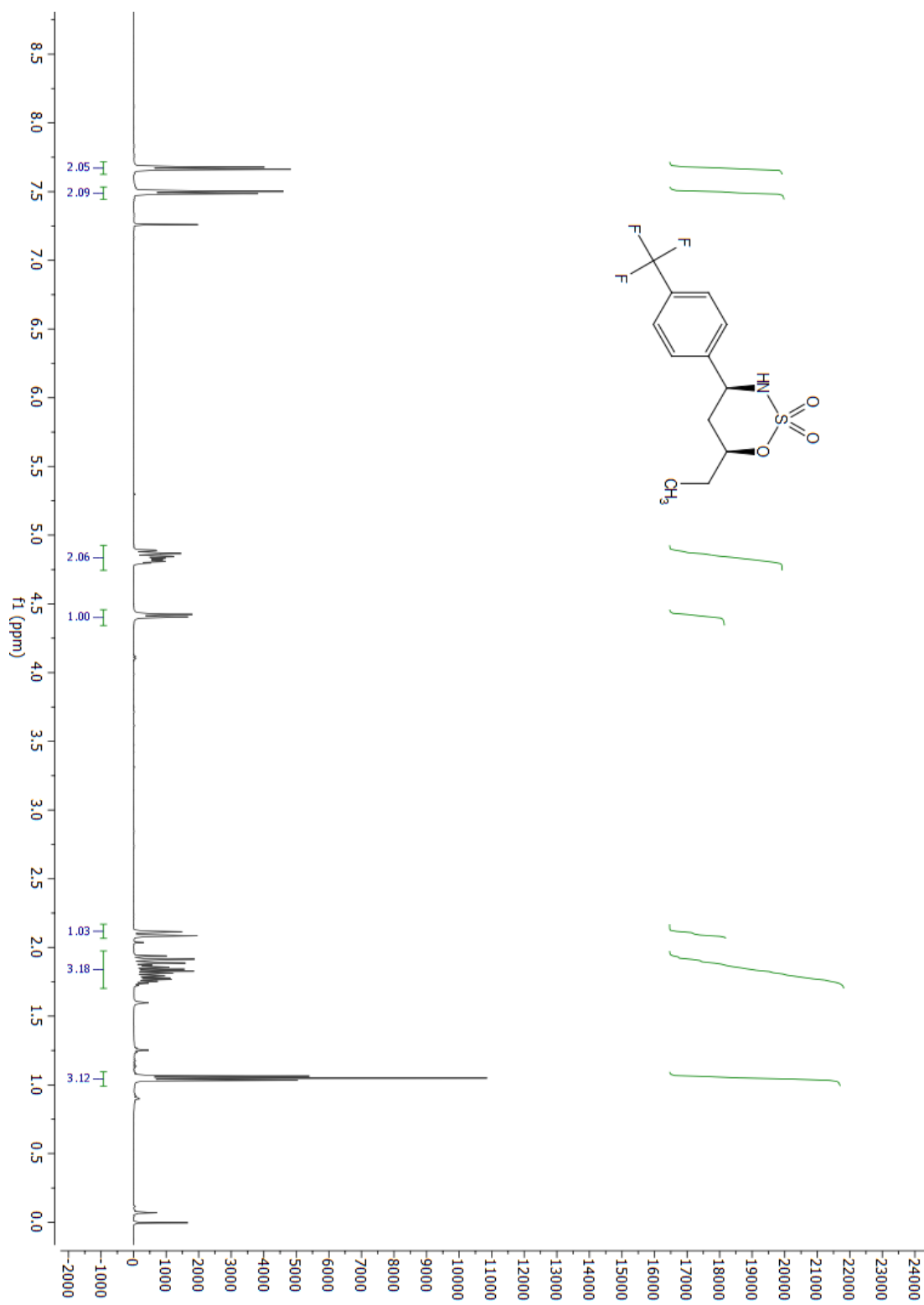
N1 C5 C8 N2 -1.6(5) C19 C20 C21 C27 179.6(4)
 N1 C5 C8 C9 177.9(4) C19 C20 C24 C25 -175.7(4)
 N2 C8 C9 C10 179.7(4) C20 C21 C27 N4 176.4(4)
 N2 C8 C9 C12 1.4(6) C20 C21 C27 C26 -3.9(6)
 N3 C17 C18 C19 0.8(6) C20 C24 C25 C26 -3.9(6)
 N3 C17 C18 C22 -179.7(4) C21 N3 C17 C18 -0.6(6)
 N3 C21 C27 N4 -4.6(5) C21 C20 C24 C25 3.5(6)
 N3 C21 C27 C26 175.2(4) C22 C18 C19 C20 -179.7(4)
 N4 C28 C29 C30 1.1(7) C22 C18 C19 C23 -0.6(6)
 N4 C28 C29 C31 -177.5(4) C23 C19 C20 C21 -179.5(4)
 C1 N1 C5 C4 -1.5(6) C23 C19 C20 C24 -0.3(6)
 C1 N1 C5 C8 178.9(3) C24 C20 C21 N3 -178.6(4)
 C1 C2 C3 C4 -1.0(6) C24 C20 C21 C27 0.4(6)
 C1 C2 C3 C7 179.1(4) C24 C25 C26 C27 0.3(6)
 C2 C3 C4 C5 -0.4(6) C24 C25 C26 C30 180.0(4)
 C2 C3 C4 C11 178.8(4) C25 C26 C27 N4 -176.7(4)
 C3 C4 C5 N1 1.7(6) C25 C26 C27 C21 3.6(6)
 C3 C4 C5 C8 -178.7(4) C25 C26 C30 C29 177.4(4)
 C3 C4 C11 C10 179.8(4) C25 C26 C30 C32 -2.7(6)
 C4 C5 C8 N2 178.8(4) C27 N4 C28 C29 -0.6(6)
 C4 C5 C8 C9 -1.7(6) C27 C26 C30 C29 -2.9(6)
 C5 N1 C1 C2 0.1(6) C27 C26 C30 C32 177.0(4)
 C5 C4 C11 C10 -1.0(6) C28 N4 C27 C21 177.9(4)
 C5 C8 C9 C10 0.3(6) C28 N4 C27 C26 -1.8(6)
 C5 C8 C9 C12 -178.0(4) C28 C29 C30 C26 0.7(6)
 C6 C2 C3 C4 179.4(4) C28 C29 C30 C32 -179.2(4)

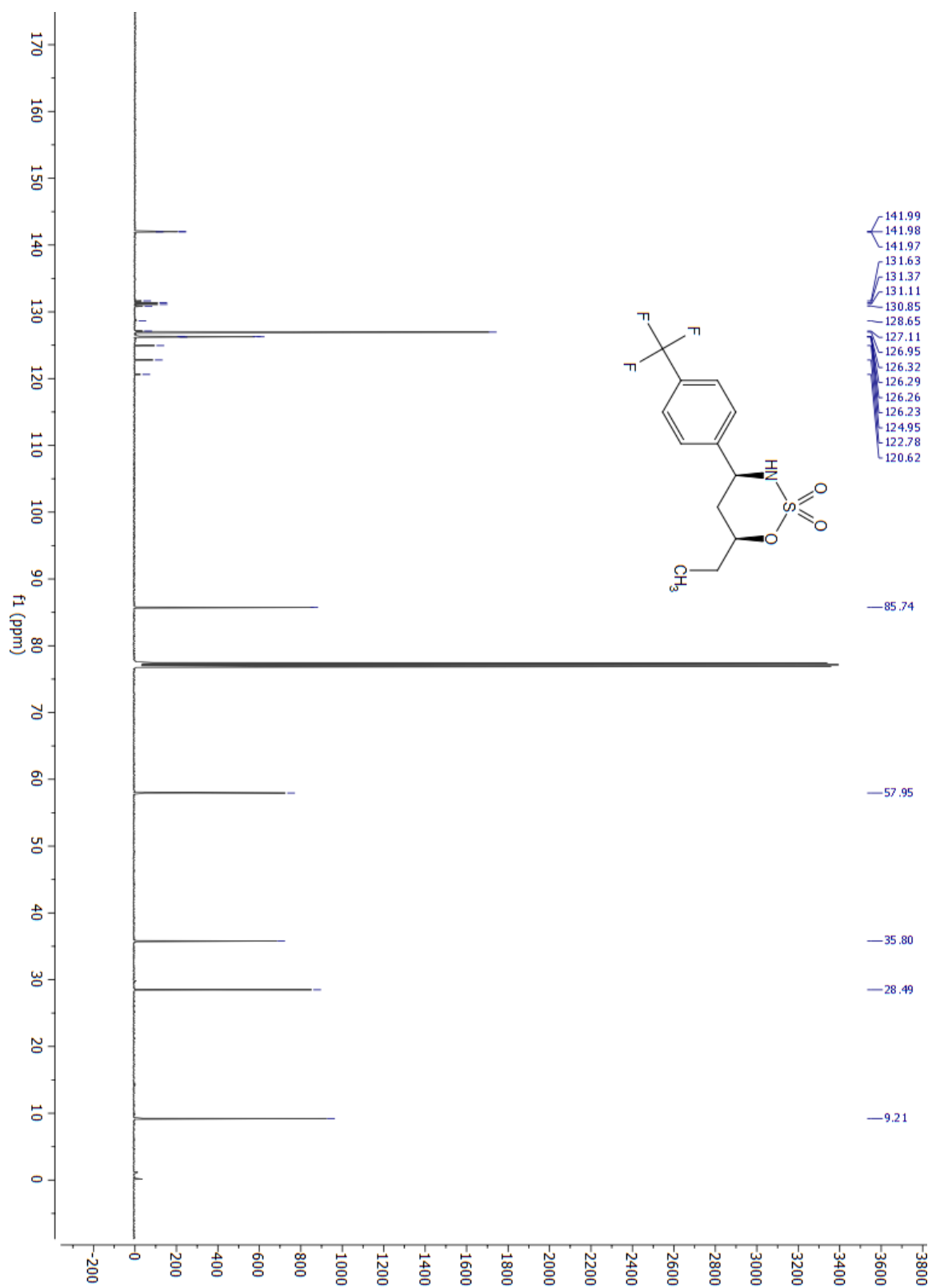
C6	C2	C3	C7	-0.5(6)	C30	C26	C27	N4	3.6(6)
C7	C3	C4	C5	179.5(4)	C30	C26	C27	C21	-176.1(4)
C7	C3	C4	C11	-1.3(6)	C31	C29	C30	C26	179.3(4)
C8	N2	C14	C13	0.5(6)	C31	C29	C30	C32	-0.6(7)
C8	C9	C10	C11	0.9(6)	O1	S1	C33	F1	-176.9(3)
C8	C9	C12	C13	-0.7(6)	O1	S1	C33	F2	63.6(3)
C8	C9	C12	C15	177.9(4)	O1	S1	C33	F3	-55.3(3)
C9	C10	C11	C4	-0.5(6)	O2	S1	C33	F1	-57.6(3)
C9	C12	C13	C14	0.0(6)	O2	S1	C33	F2	-177.0(3)
C9	C12	C13	C16	178.5(4)	O2	S1	C33	F3	64.1(3)
C10	C9	C12	C13	-178.9(4)	O3	S1	C33	F1	62.6(3)
C10	C9	C12	C15	-0.3(6)	O3	S1	C33	F2	-56.9(3)
C11	C4	C5	N1	-177.5(4)	O3	S1	C33	F3	-175.8(3)
C11	C4	C5	C8	2.1(5)					

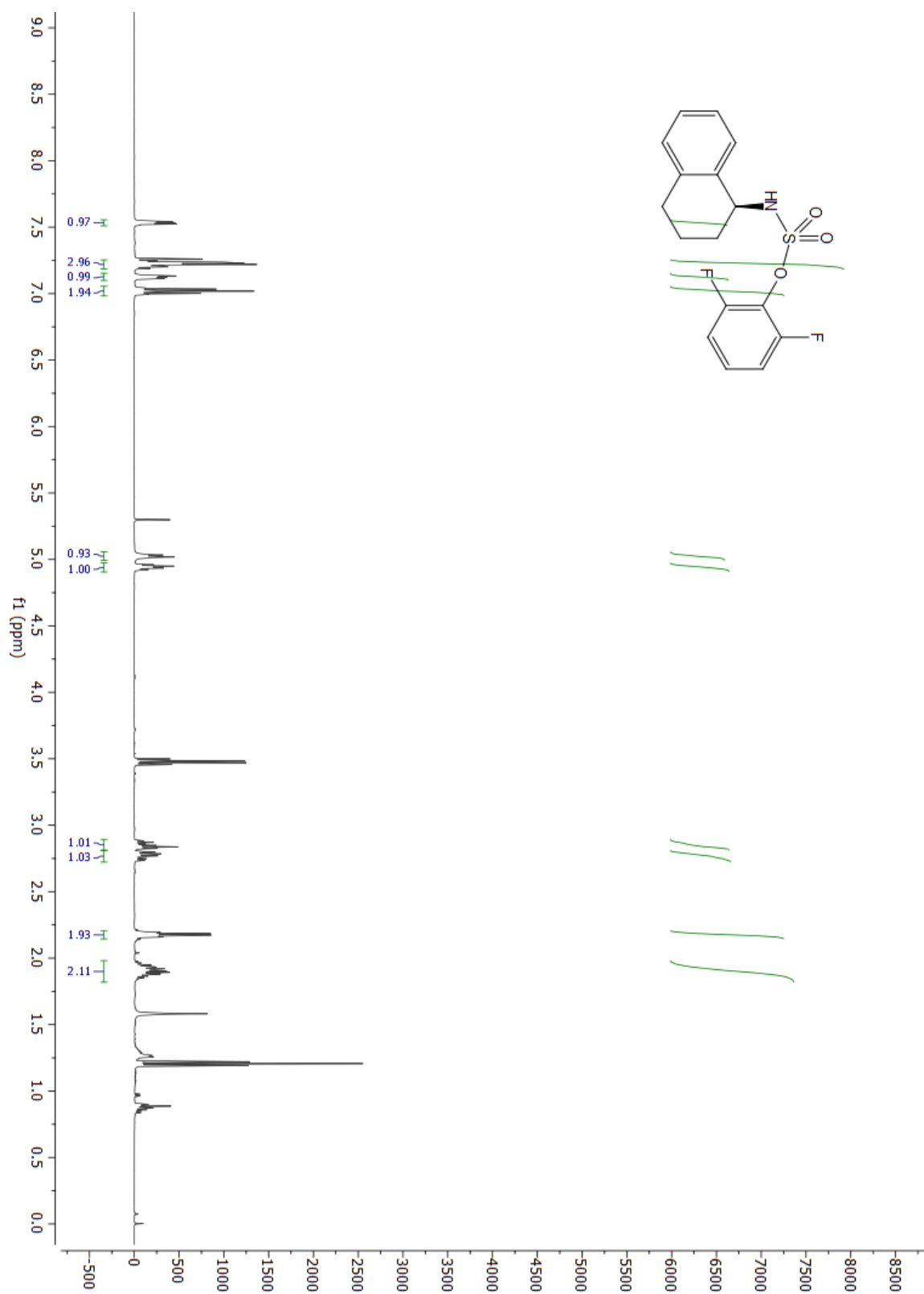
Table S2-14. Hydrogen Atom Coordinates ($\text{\AA} \times 10^4$) and Isotropic Displacement Parameters ($\text{\AA}^2 \times 10^3$) for **[Ag(Me₄phen)₂]OTf**.

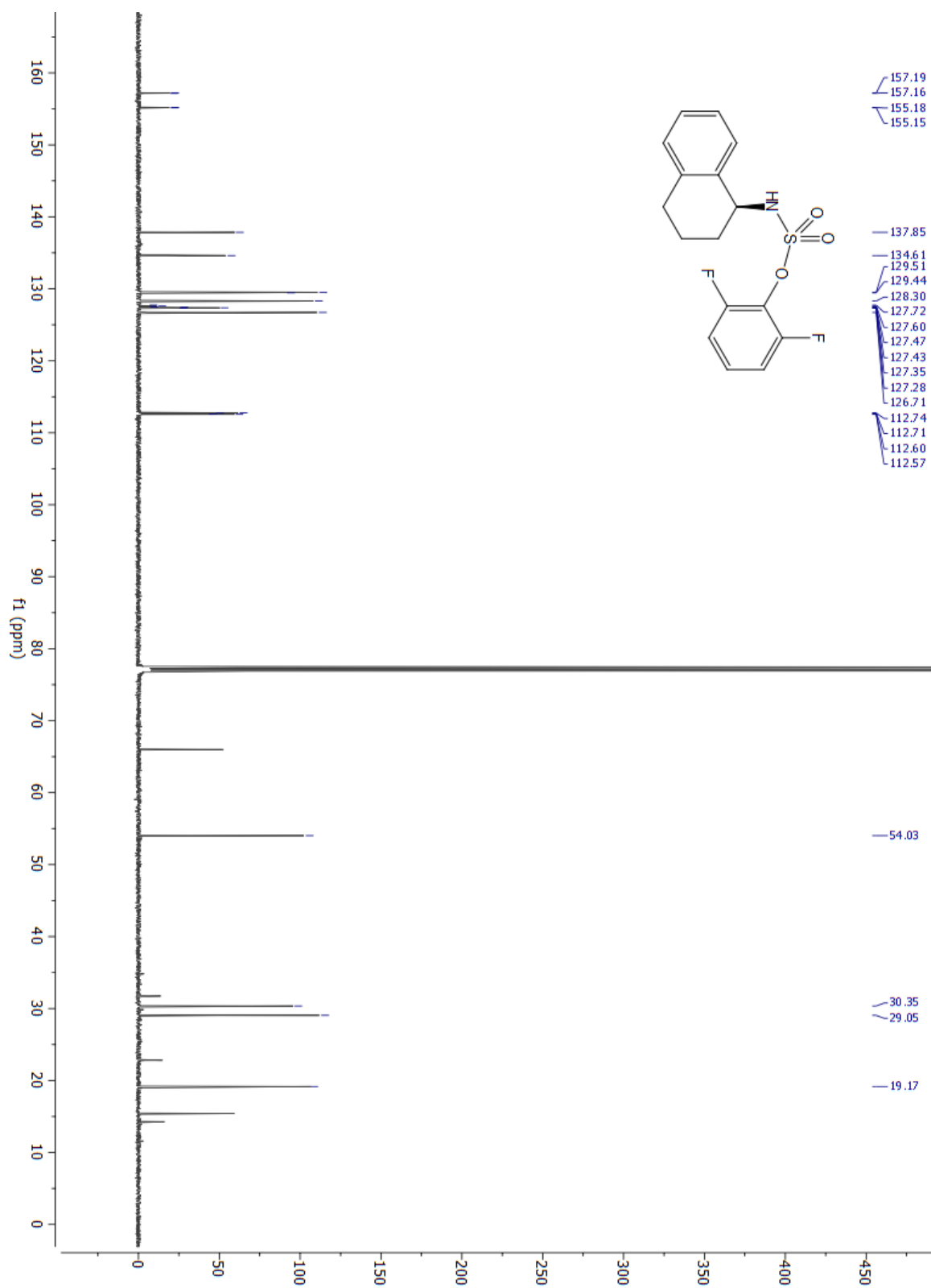
Atom	<i>x</i>	<i>y</i>	<i>z</i>	U(eq)
H1	5057	818	4782	28
H6A	4986	-900	4033	41
H6B	5896	-572	4525	41
H6C	7061	-559	4039	41
H7A	4228	271	2974	41
H7B	5627	-349	3269	41
H7C	6344	539	2999	41
H10	3328	3270	2764	27

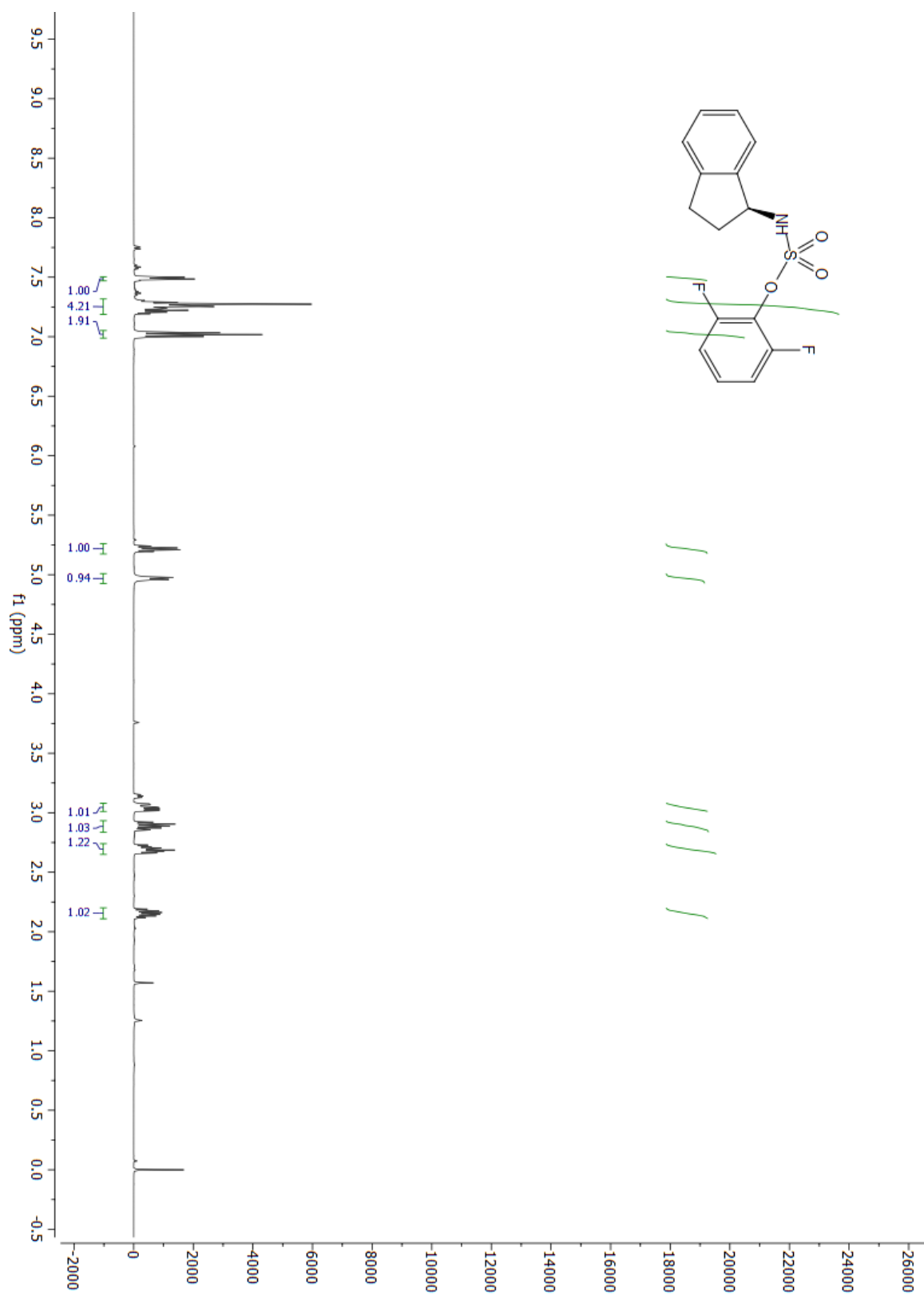
H11	4323	1816	2831	27
H14	2173	4792	4607	26
H15A	3408	5156	2873	46
H15B	1363	5427	3017	46
H15C	1752	4490	2748	46
H16A	2456	6287	3740	51
H16B	1351	6101	4226	51
H16C	367	5972	3718	51
H17	2743	1349	5841	26
H22A	1900	386	6447	44
H22B	1514	802	6967	44
H22C	3459	361	6849	44
H23A	4891	2254	7534	43
H23B	3344	1501	7466	43
H23C	2781	2536	7547	43
H24	5015	3773	7302	26
H25	5733	5140	6982	24
H28	5606	4987	4956	27
H31A	5545	7034	5364	45
H31B	6514	6453	4952	45
H31C	7668	6789	5406	45
H32A	5318	6583	6578	38
H32B	6654	6974	6173	38
H32C	7429	6302	6575	38

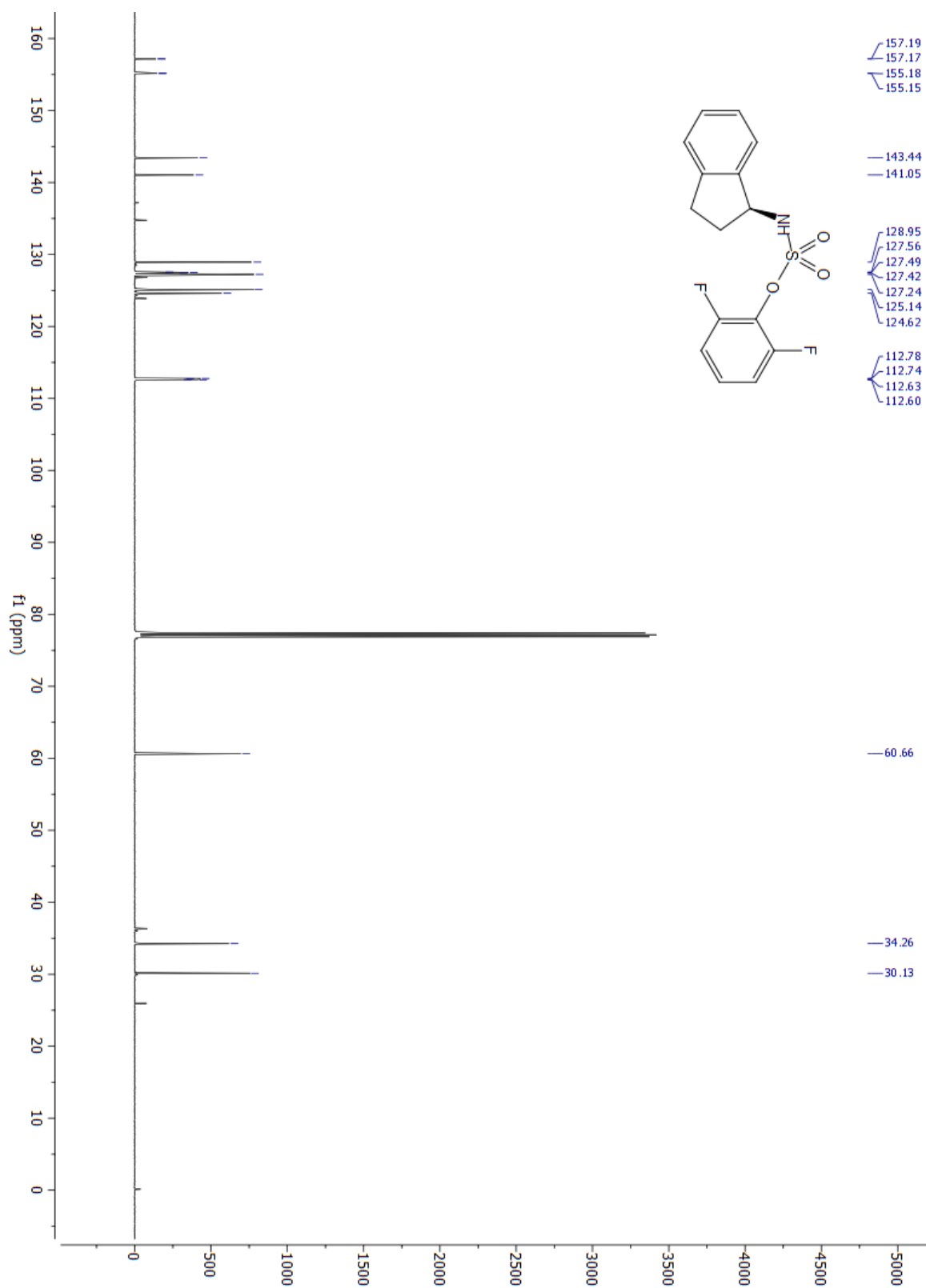
Chapter 3 ^1H - and ^{13}C -NMR Data ^1H -NMR for Compound 3.8

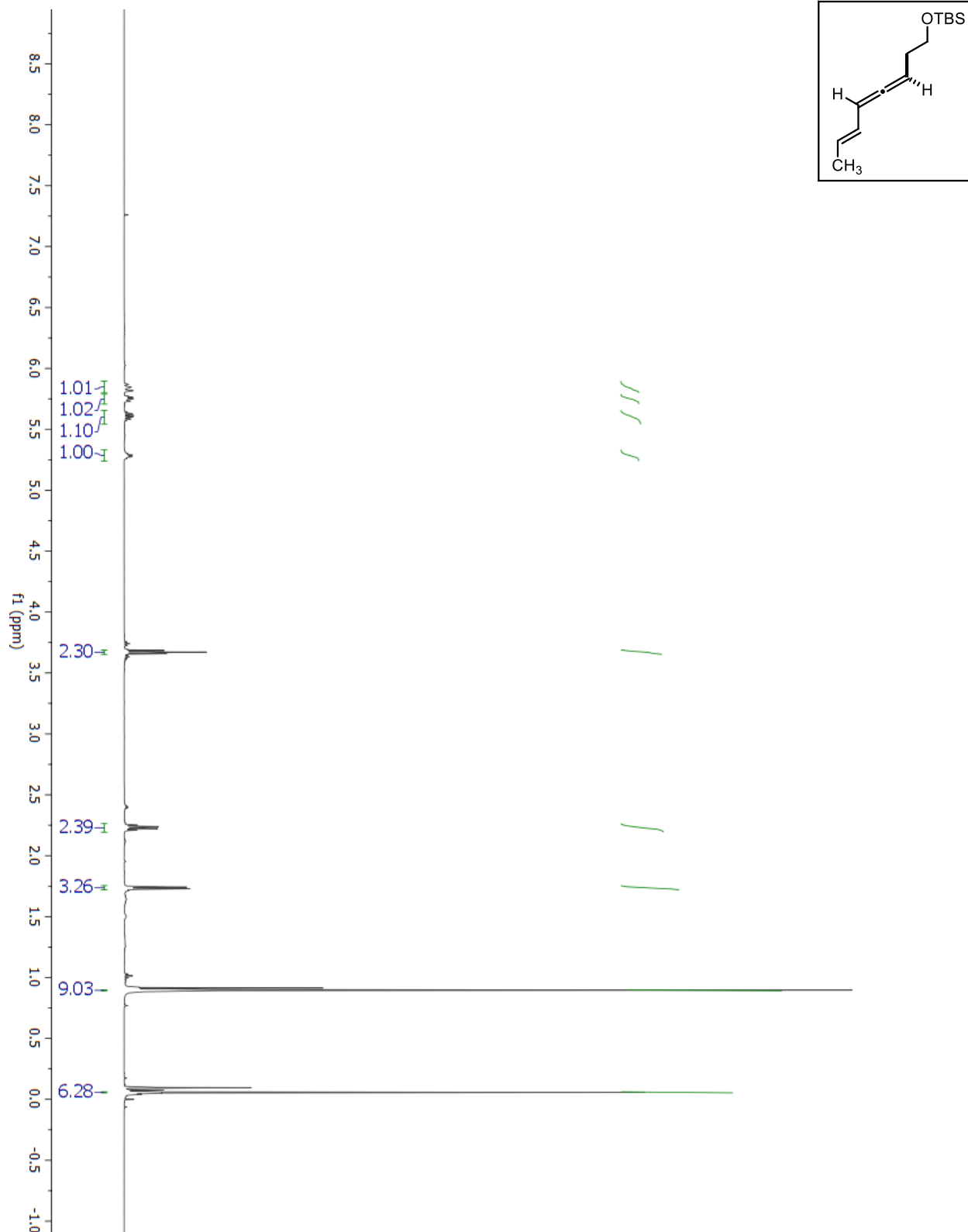
^{13}C -NMR for Compound 3.8

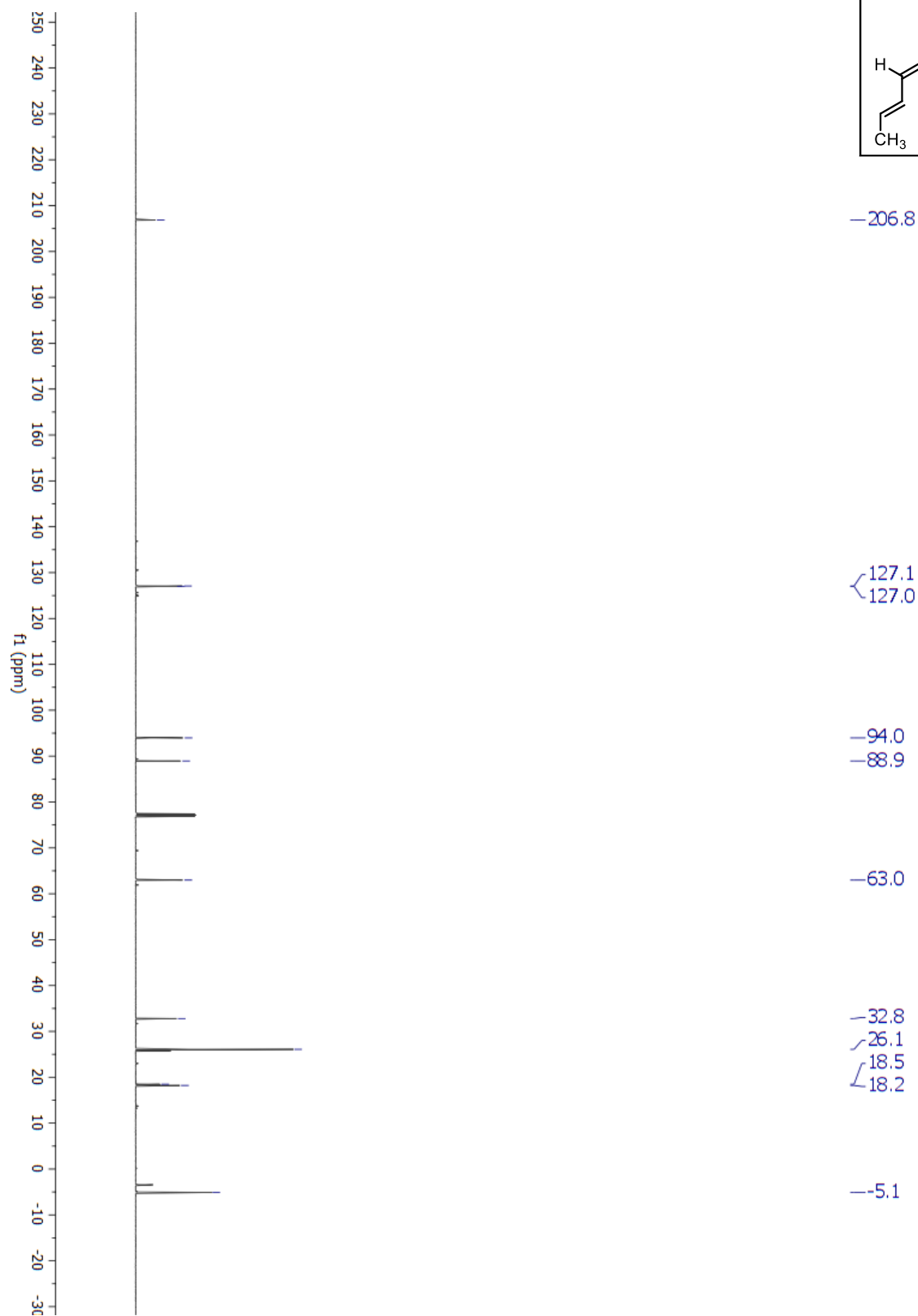
¹H-NMR for Compound 3.14a

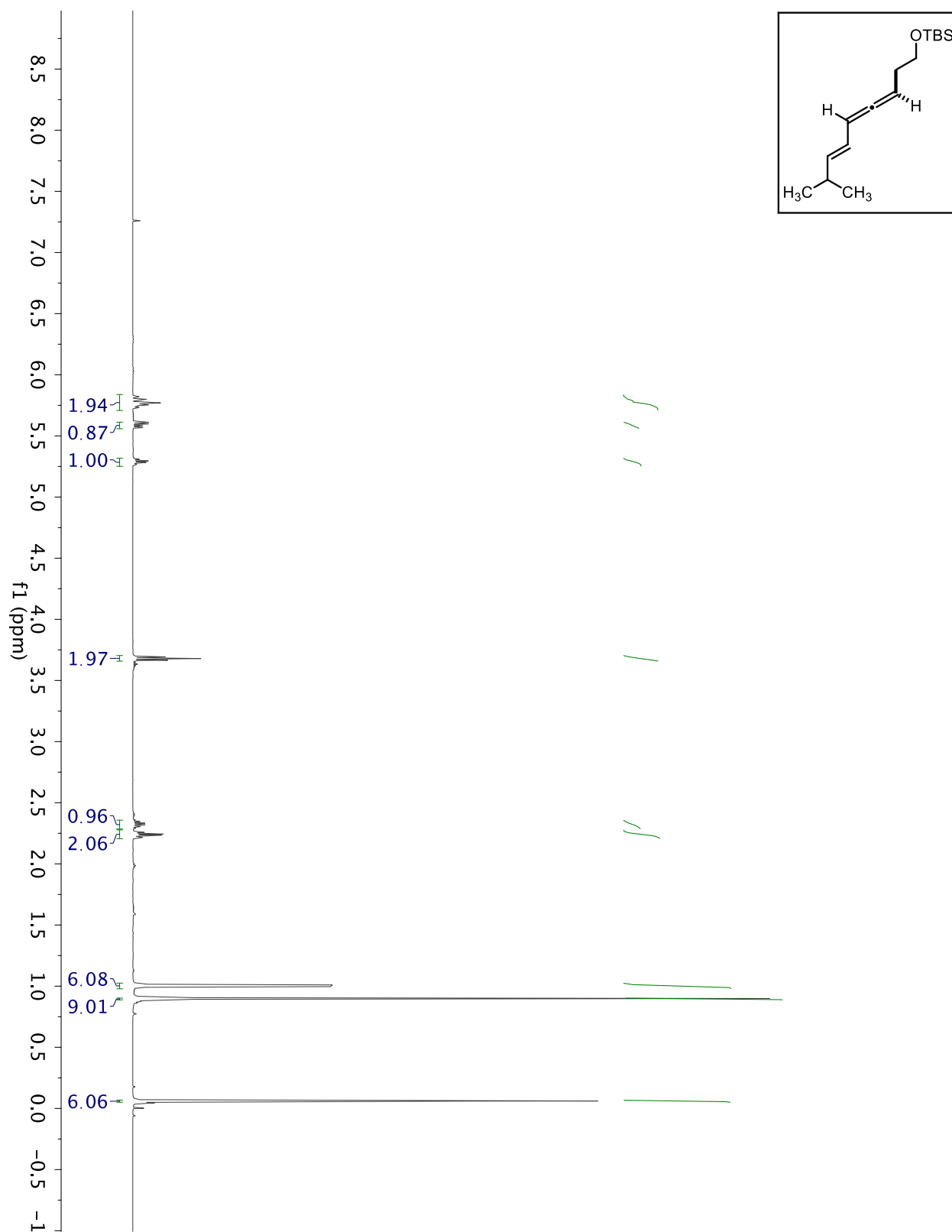
^{13}C -NMR for Compound 3.14a

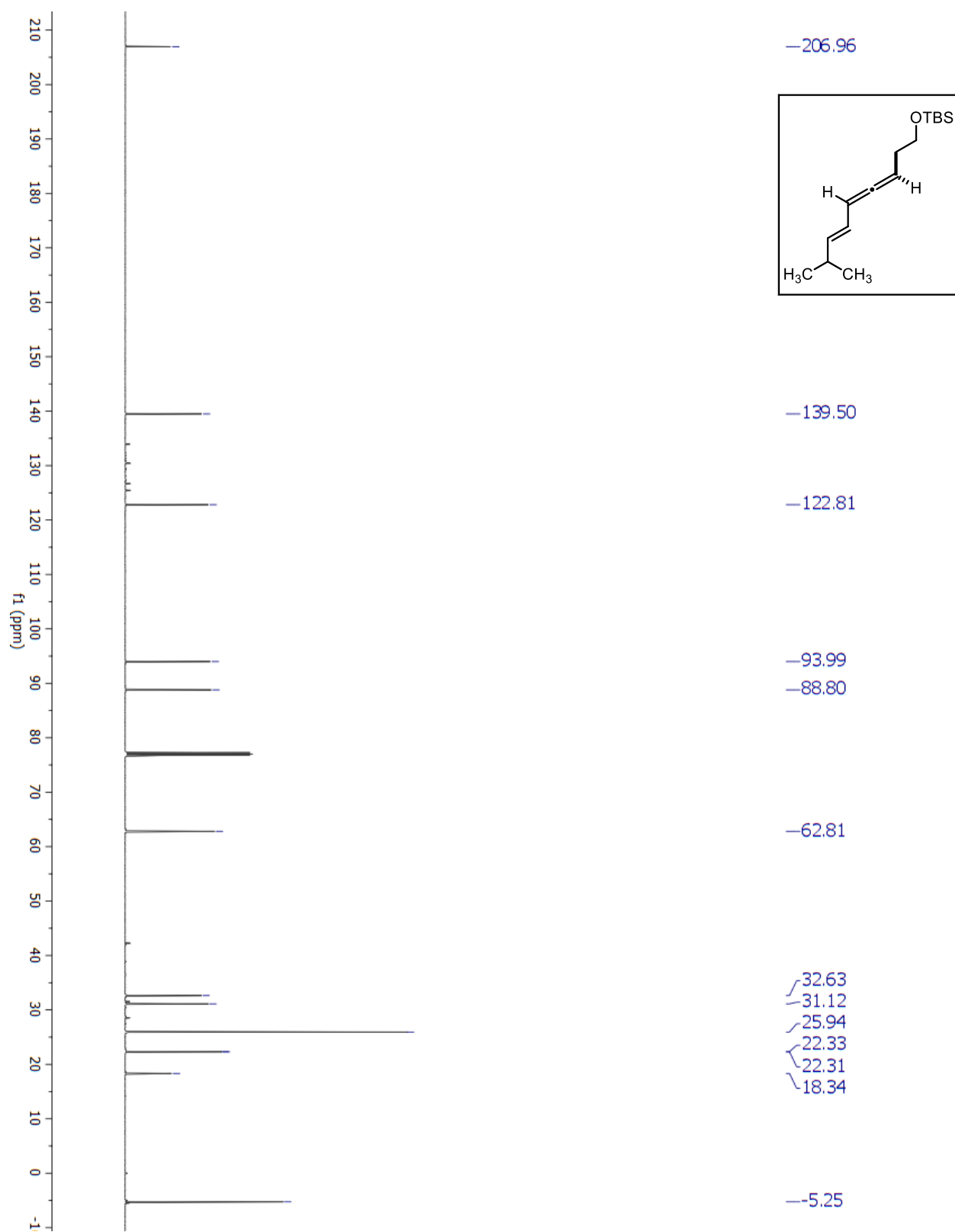
¹H-NMR for Compound 3.15a

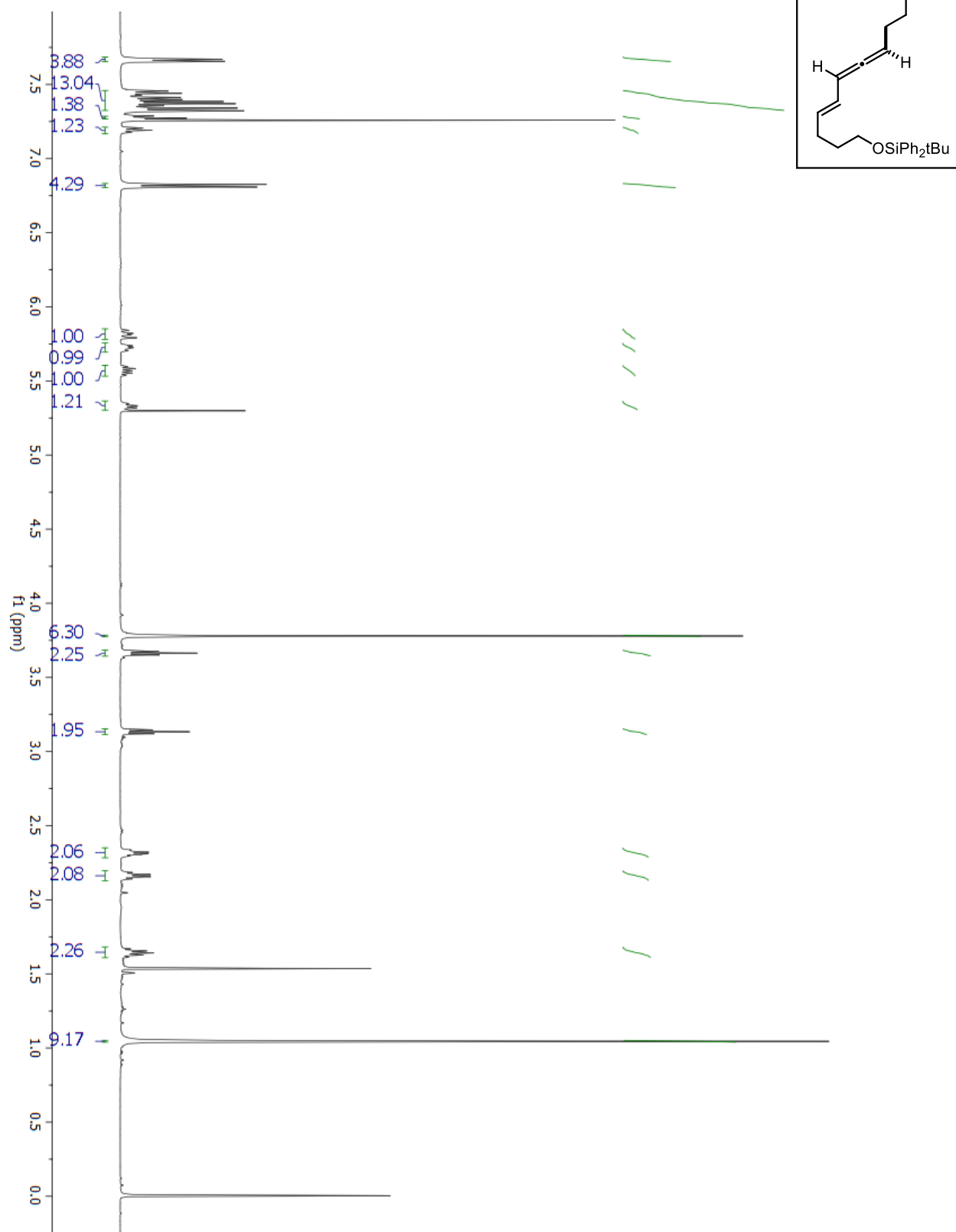
^{13}C -NMR for Compound 3.15a

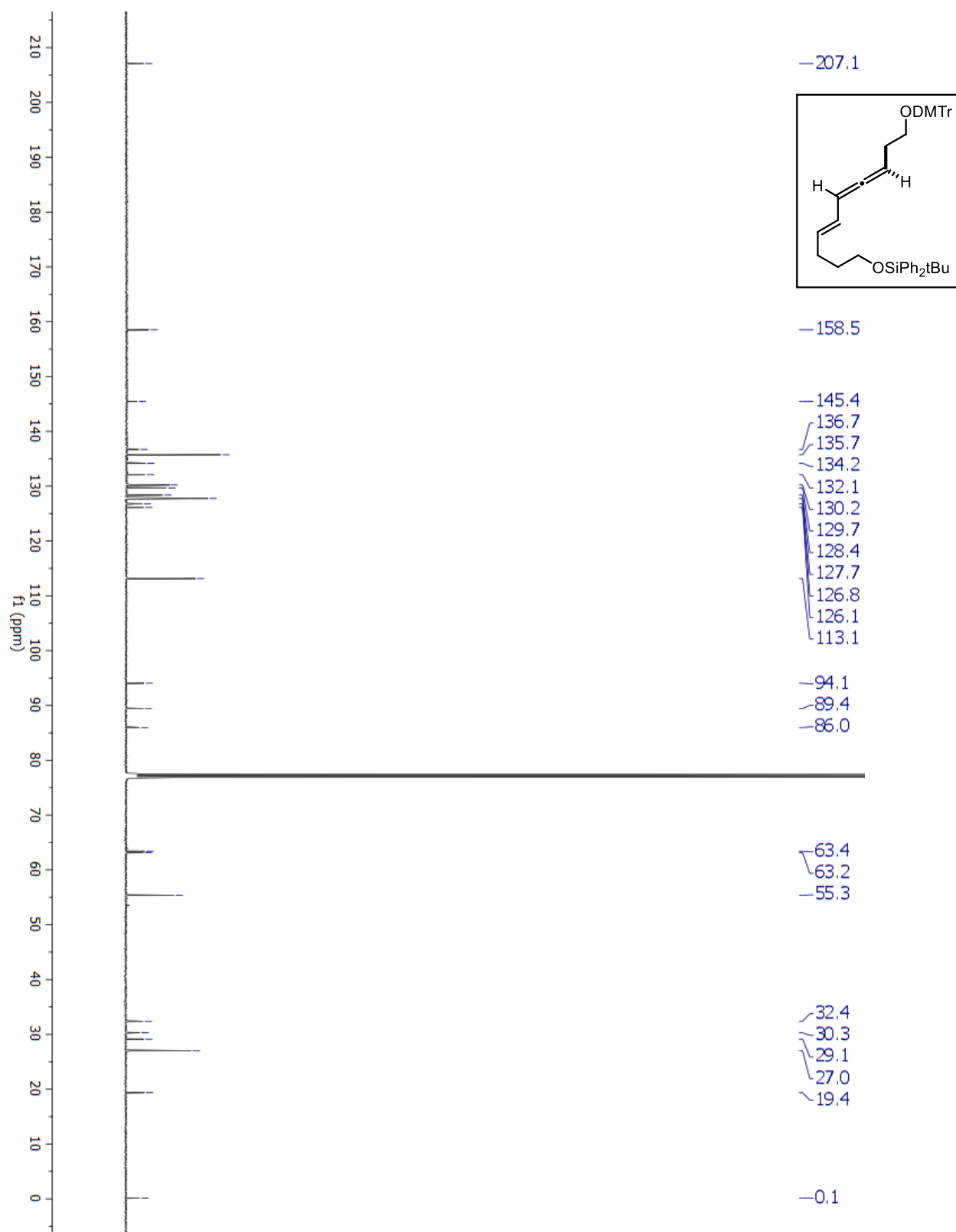
Chapter 5 ^1H - and ^{13}C -NMR Data ^1H -NMR for OTBS Precursor to 5.4

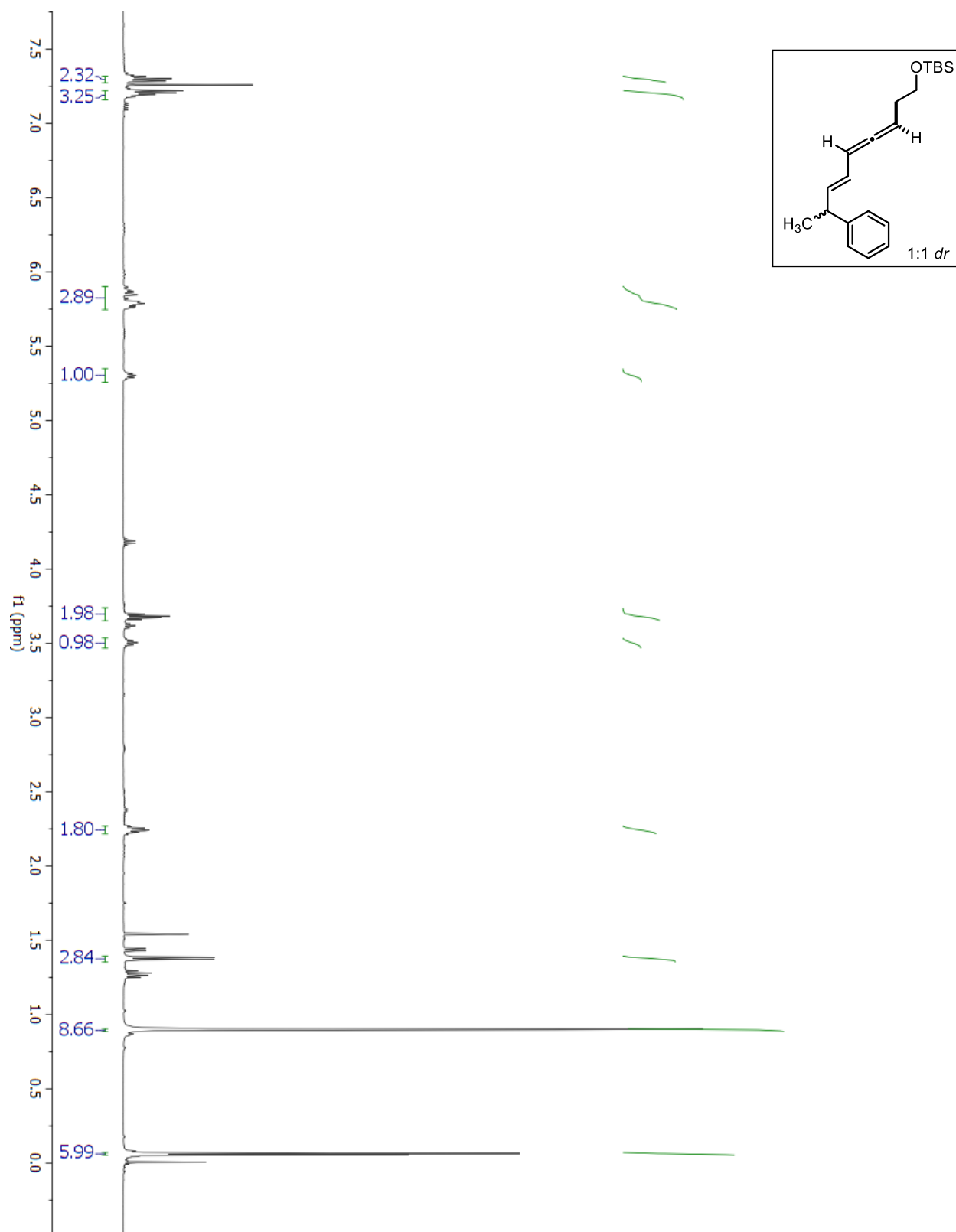
^{13}C -NMR for OTBS Precursor to 5.4

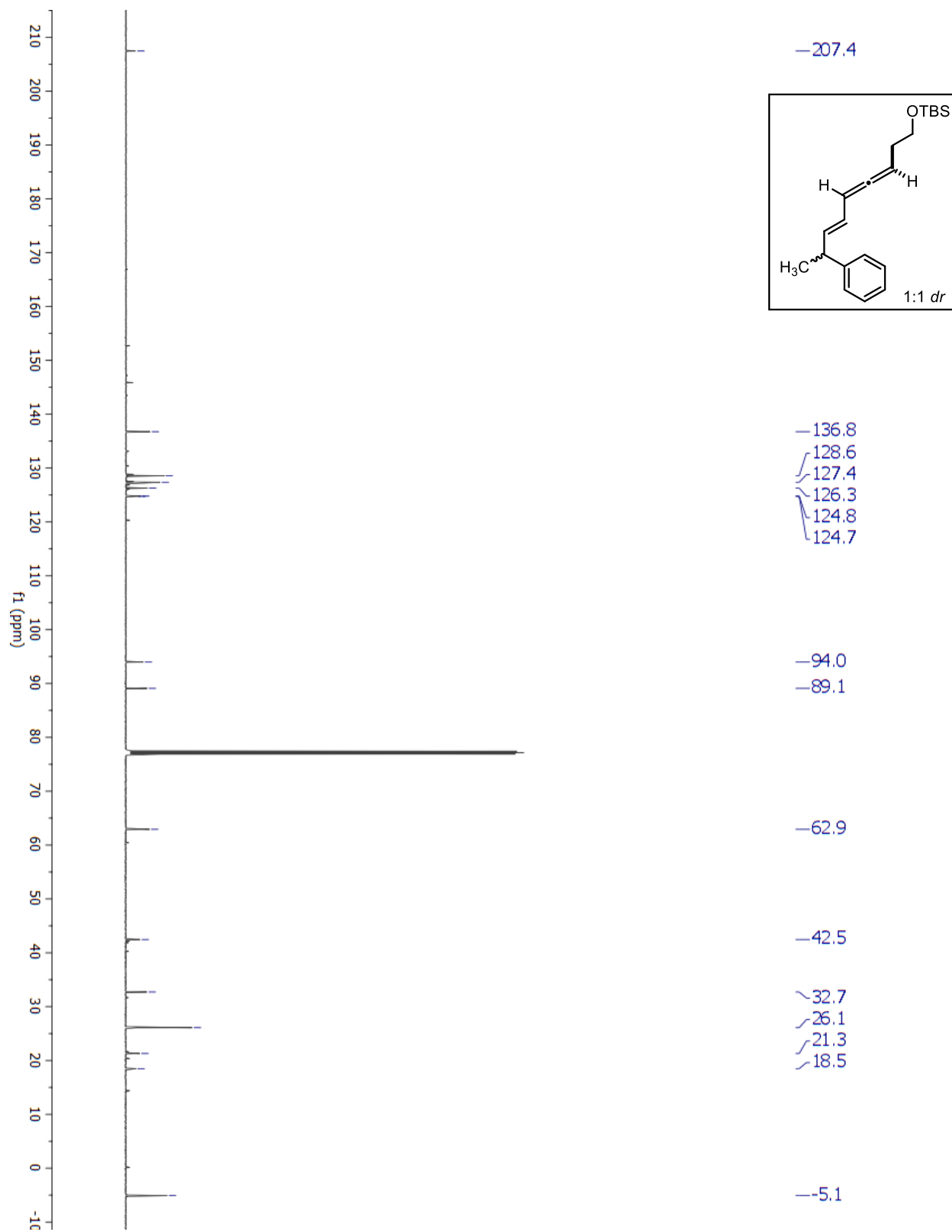
¹H-NMR for OTBS Precursor to 5.6

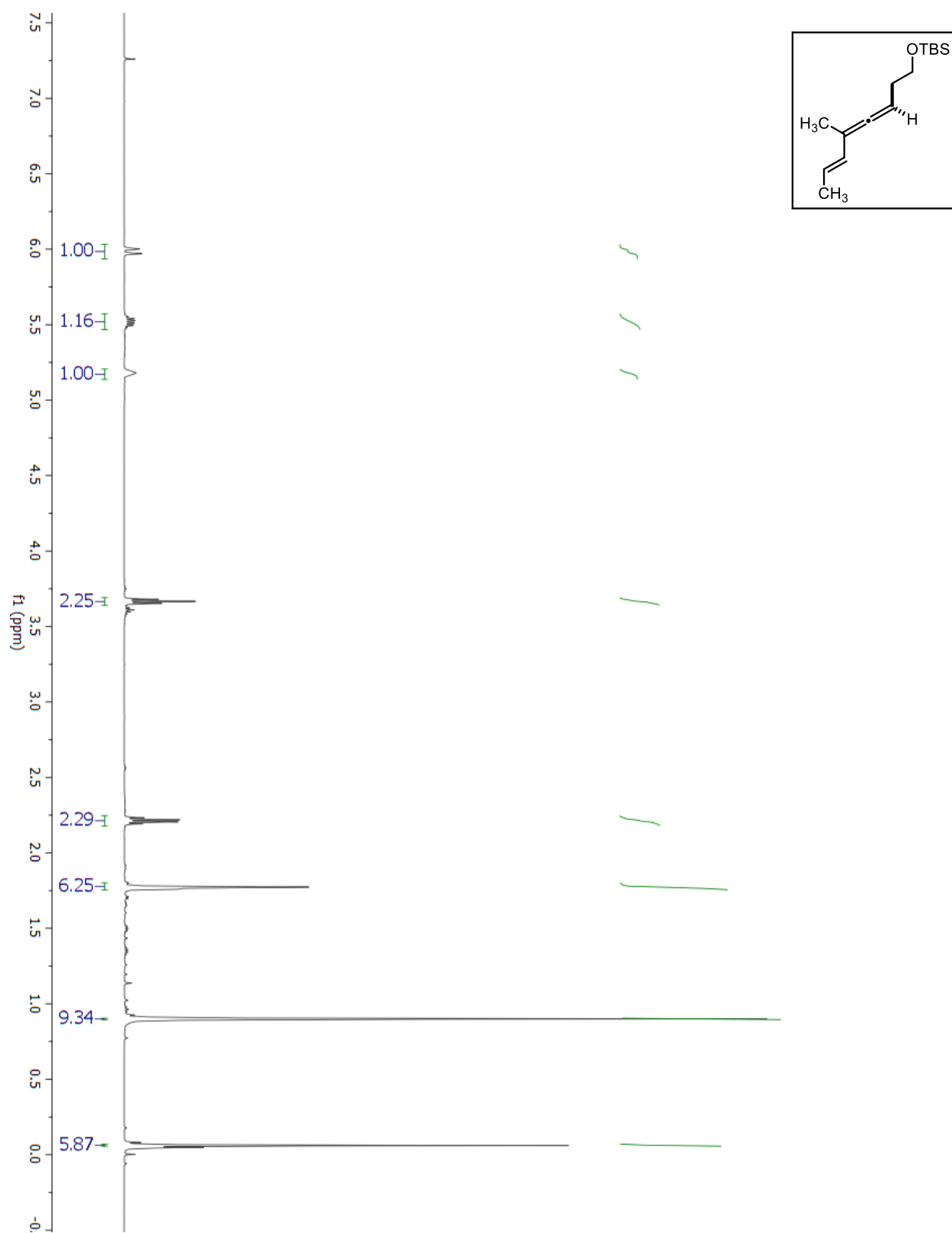
^{13}C -NMR for OTBS Precursor to 5.6

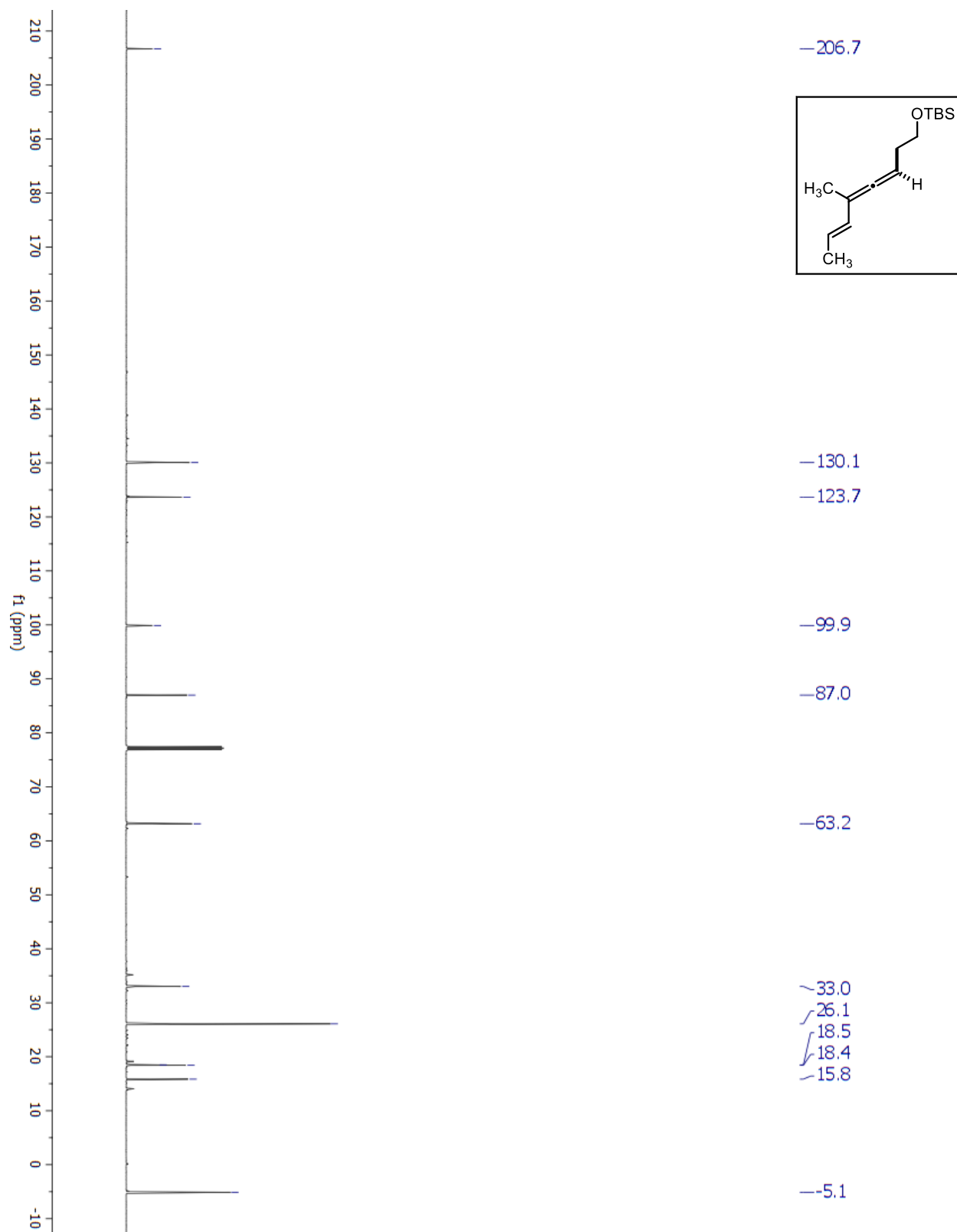


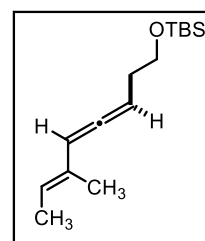
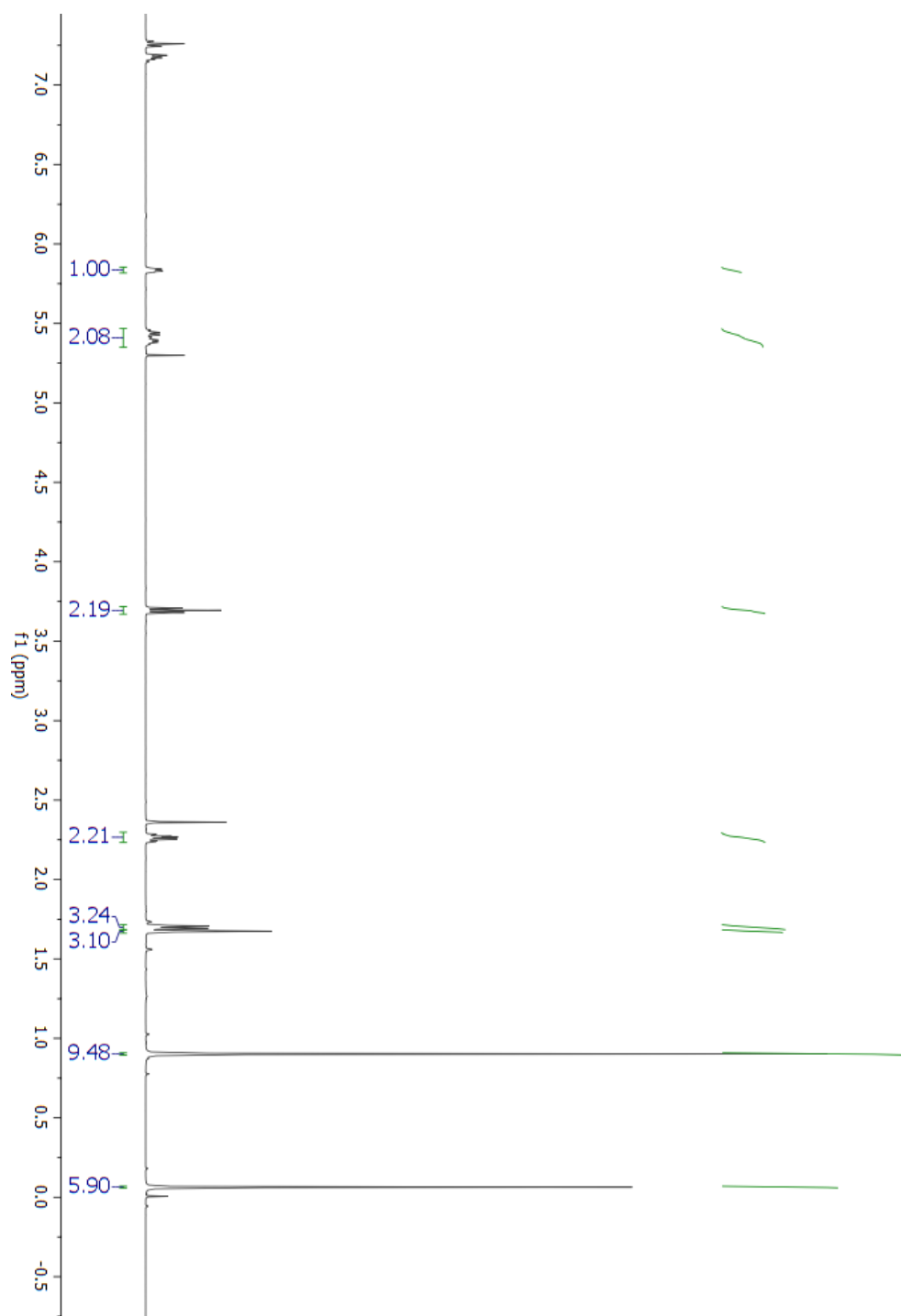


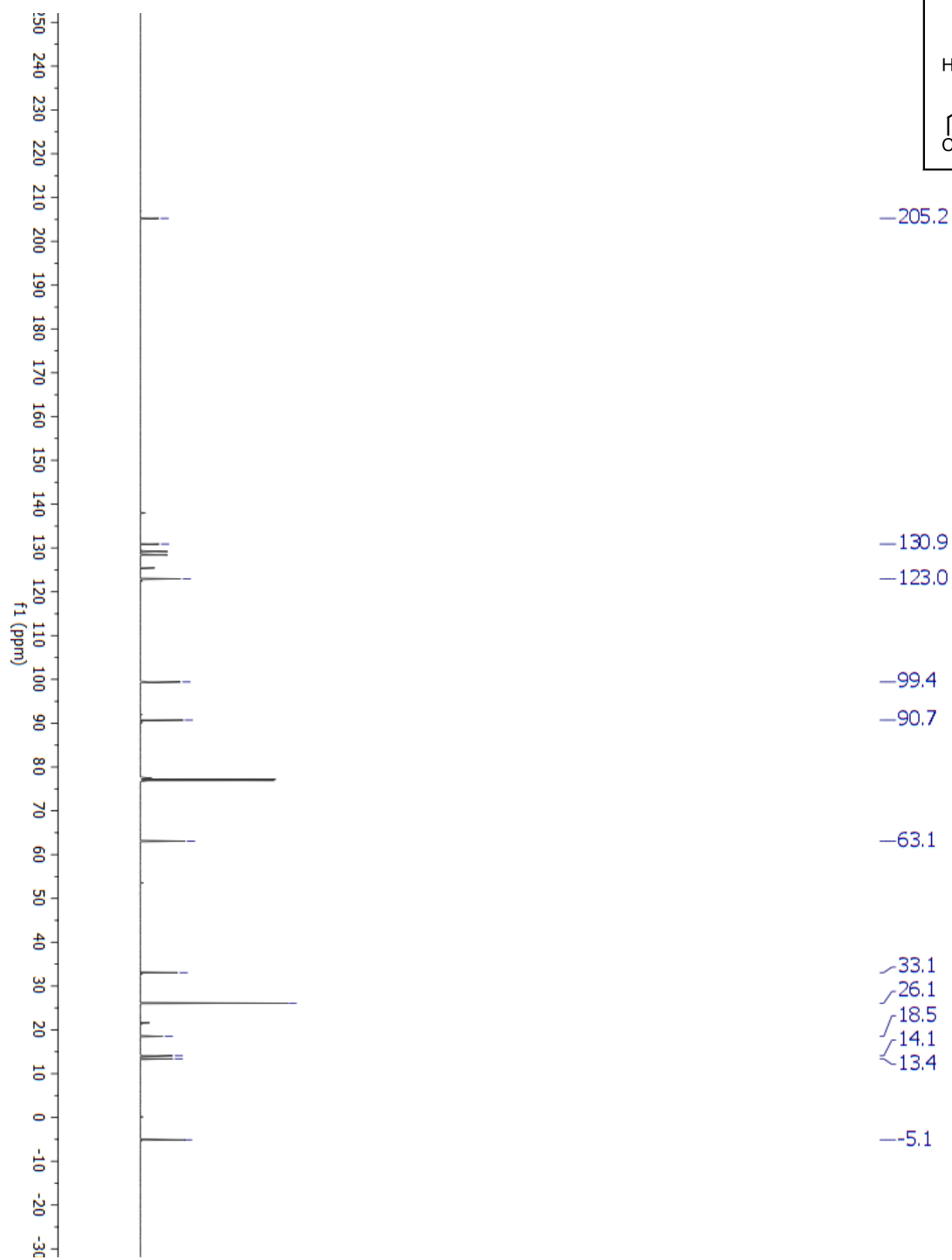
¹H-NMR for OTBS Precursor to 5.8

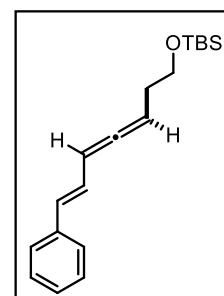
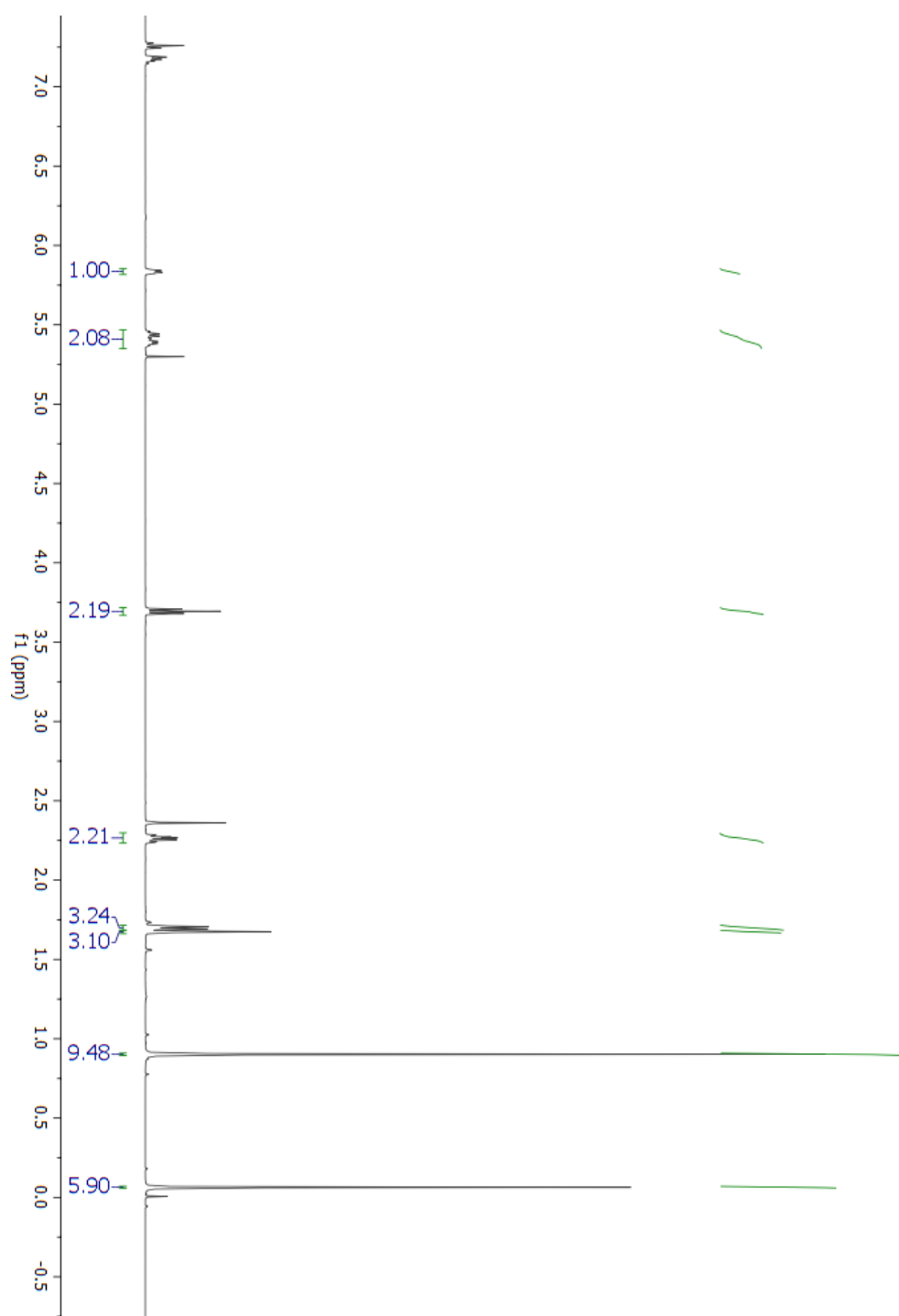
^{13}C -NMR for OTBS Precursor to 5.8

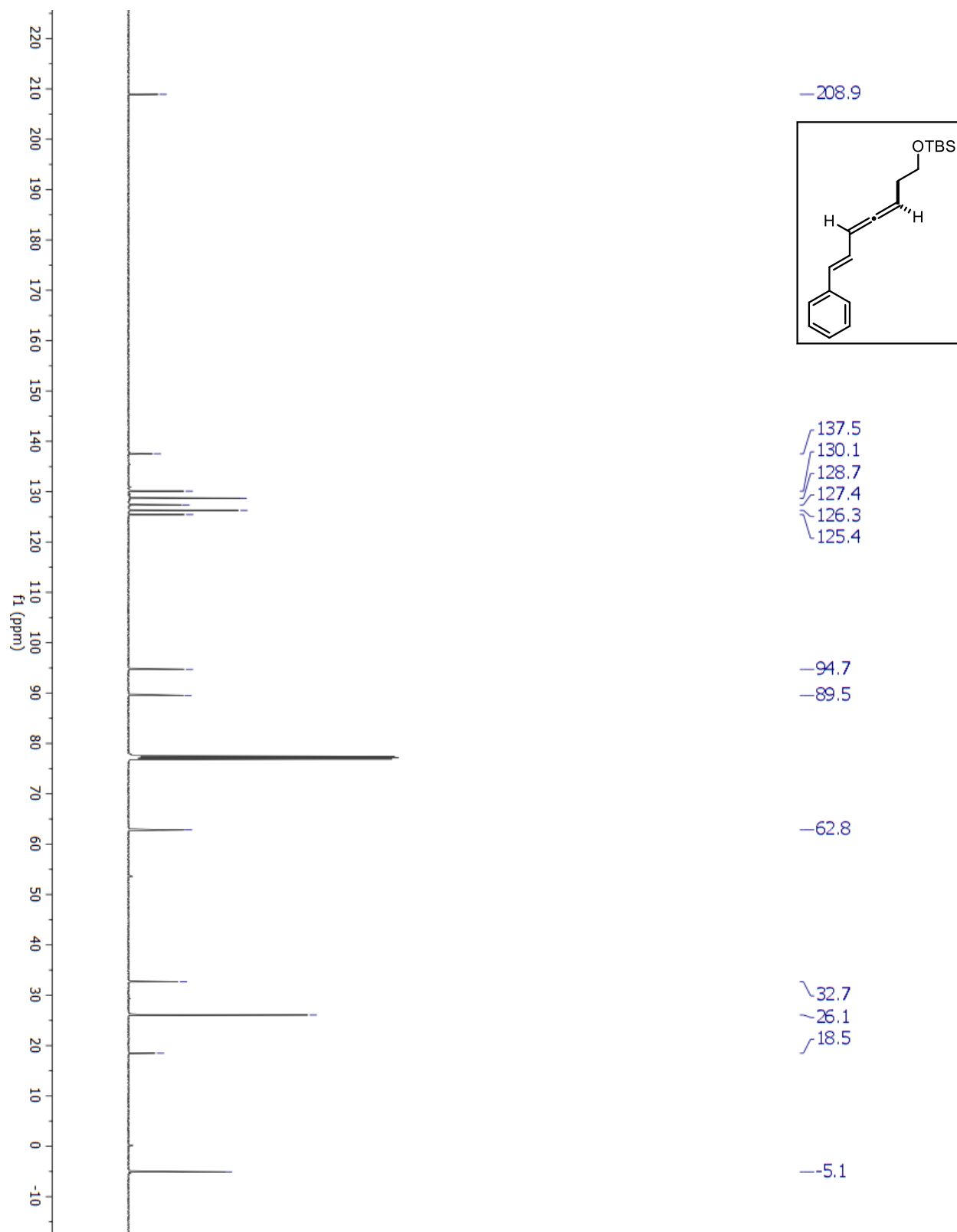


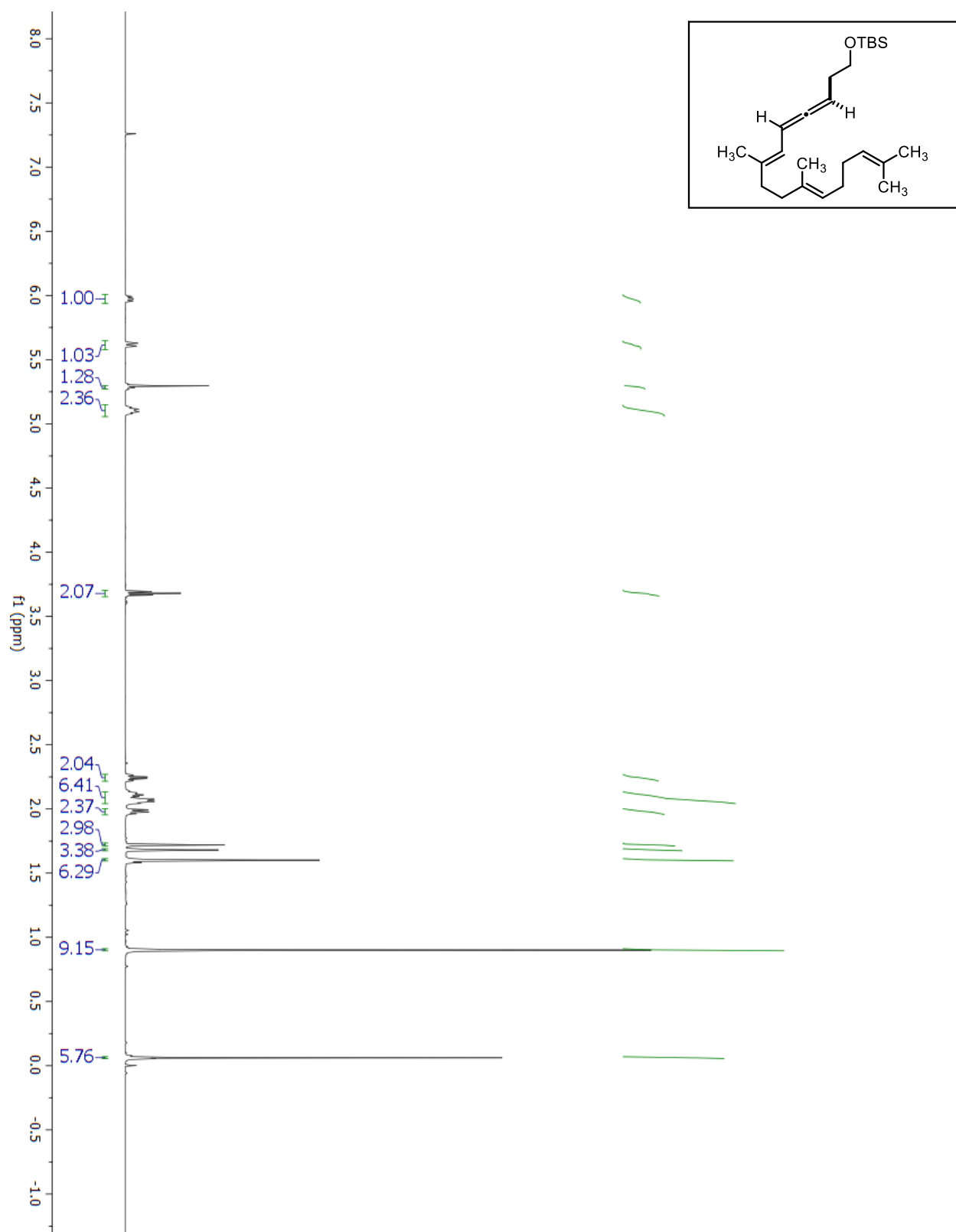
^{13}C -NMR for OTBS Precursor to 5.9

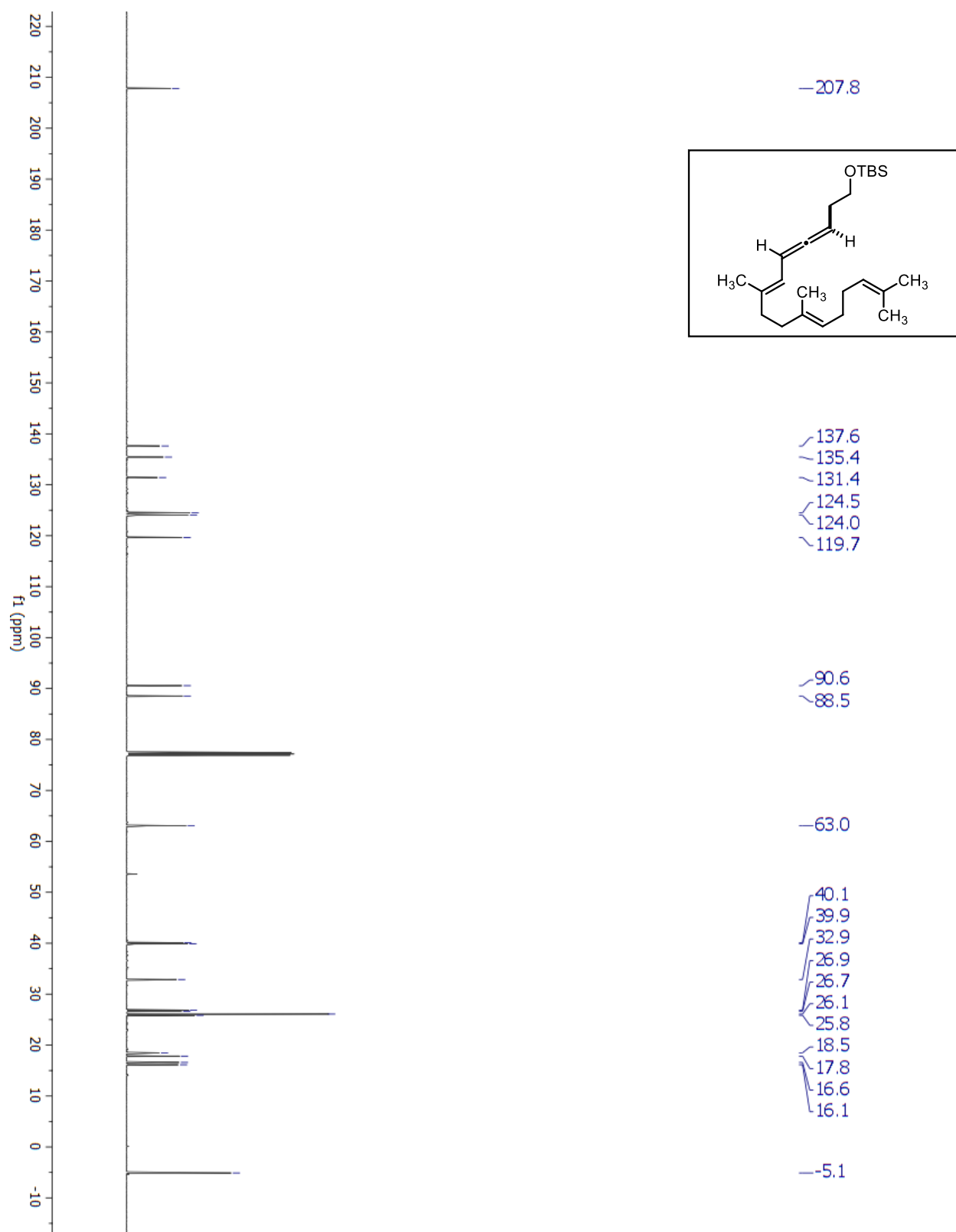
¹H-NMR for OTBS Precursor to 5.10

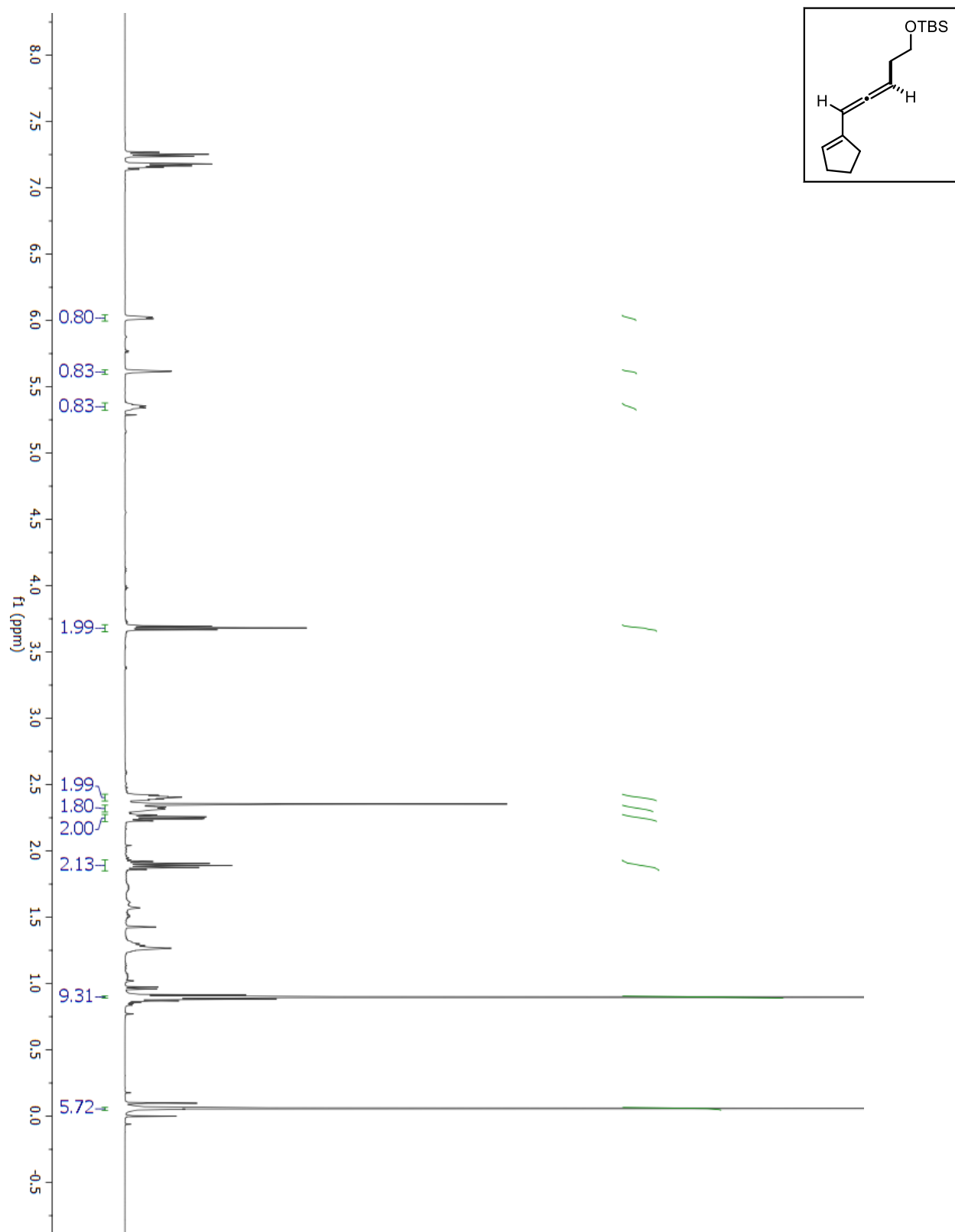
^{13}C -NMR for OTBS Precursor to 5.10

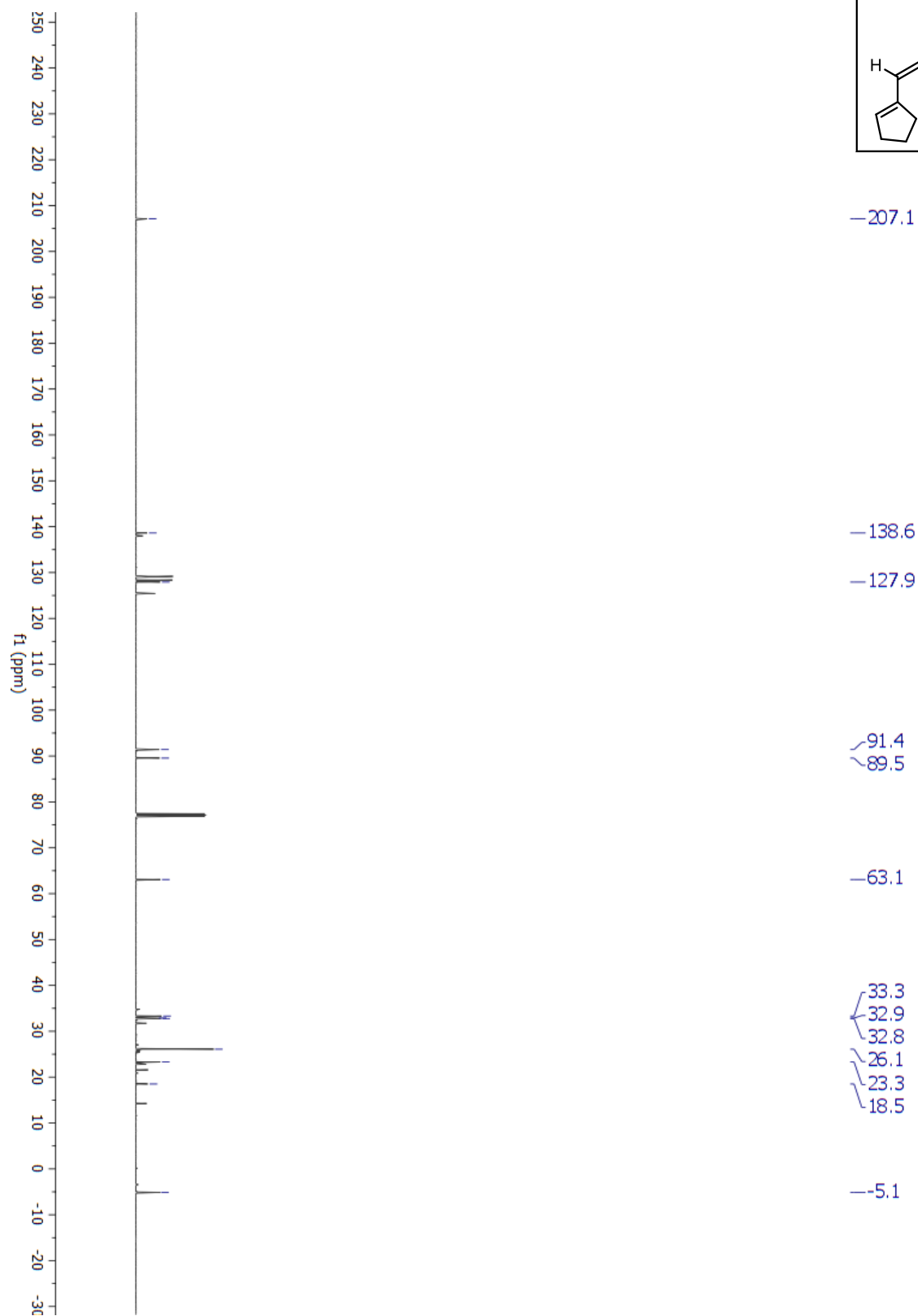
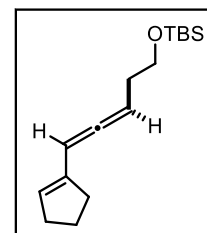
¹H-NMR for OTBS Precursor to 5.11

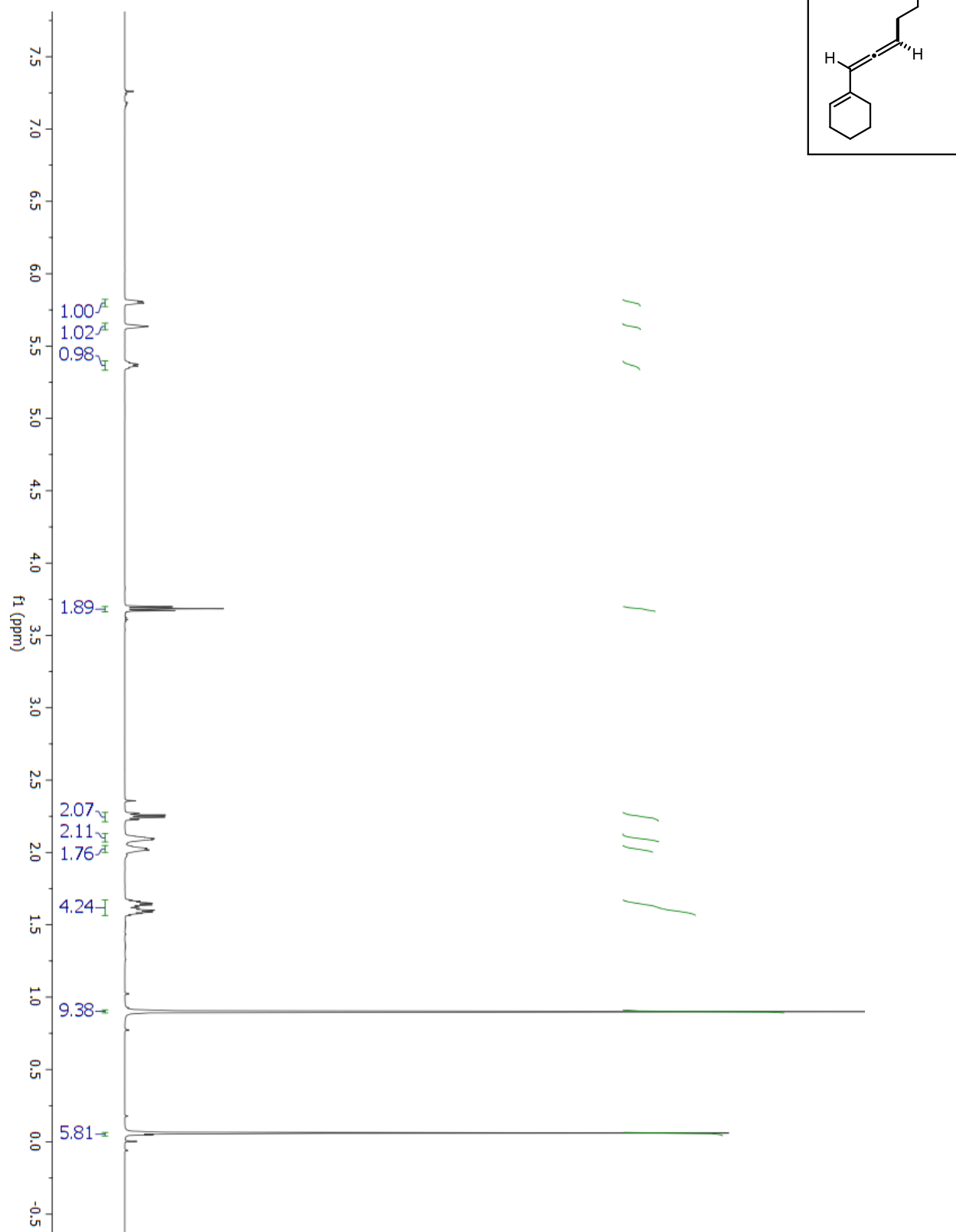
^{13}C -NMR for OTBS Precursor to 5.11

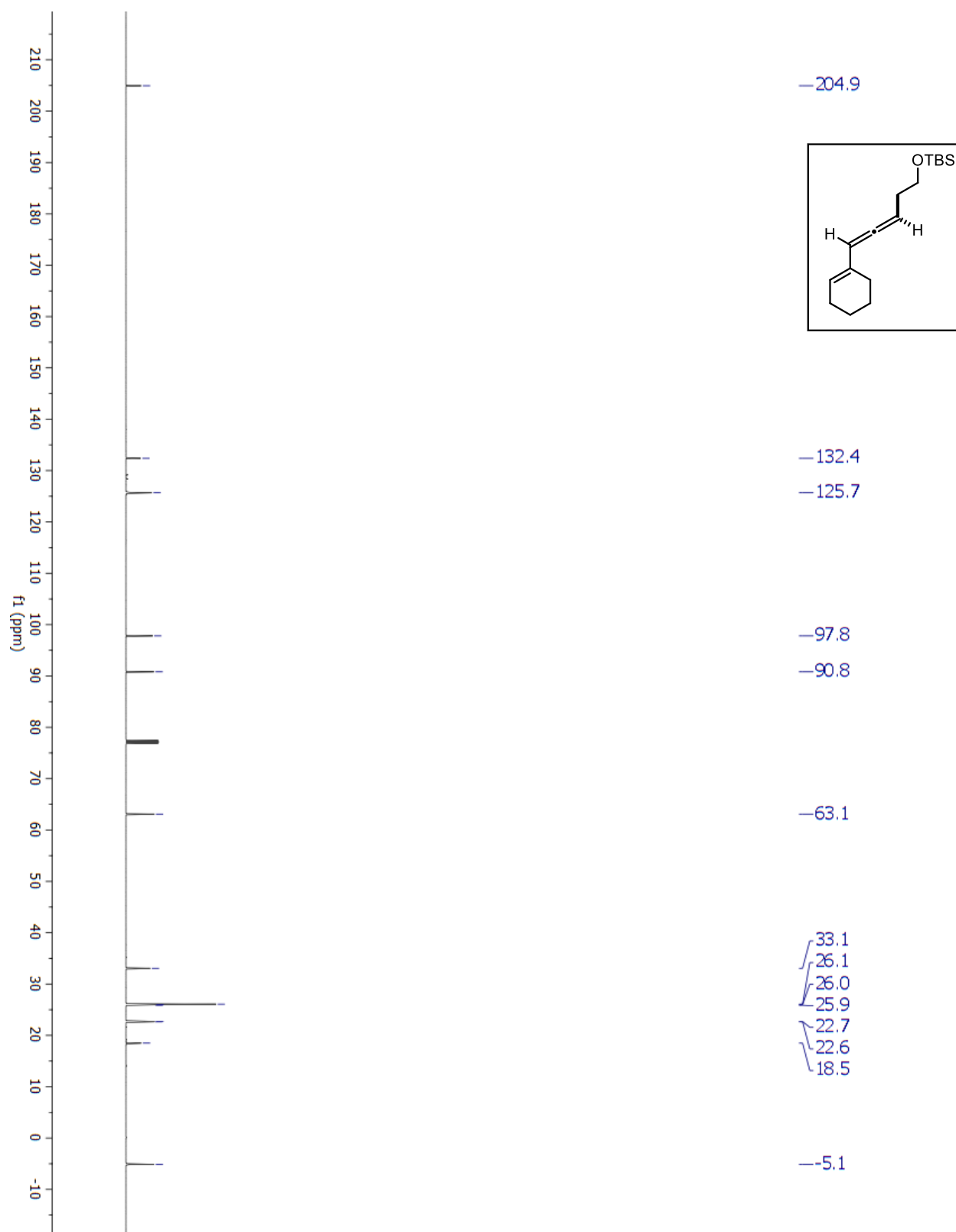
¹H-NMR for OTBS Precursor to 5.12

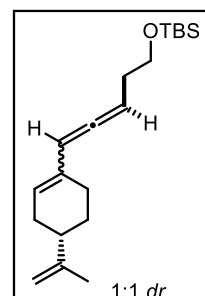
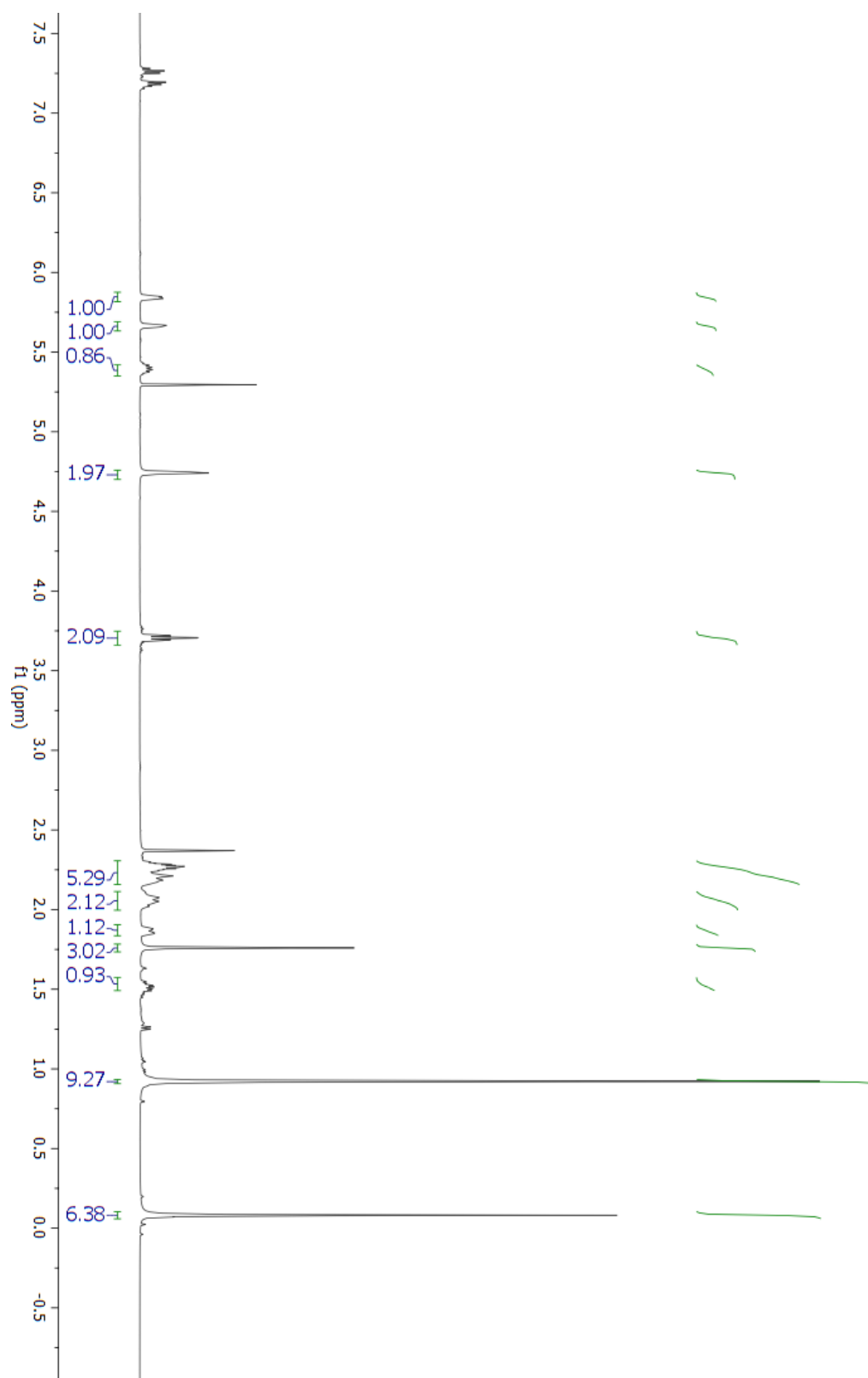


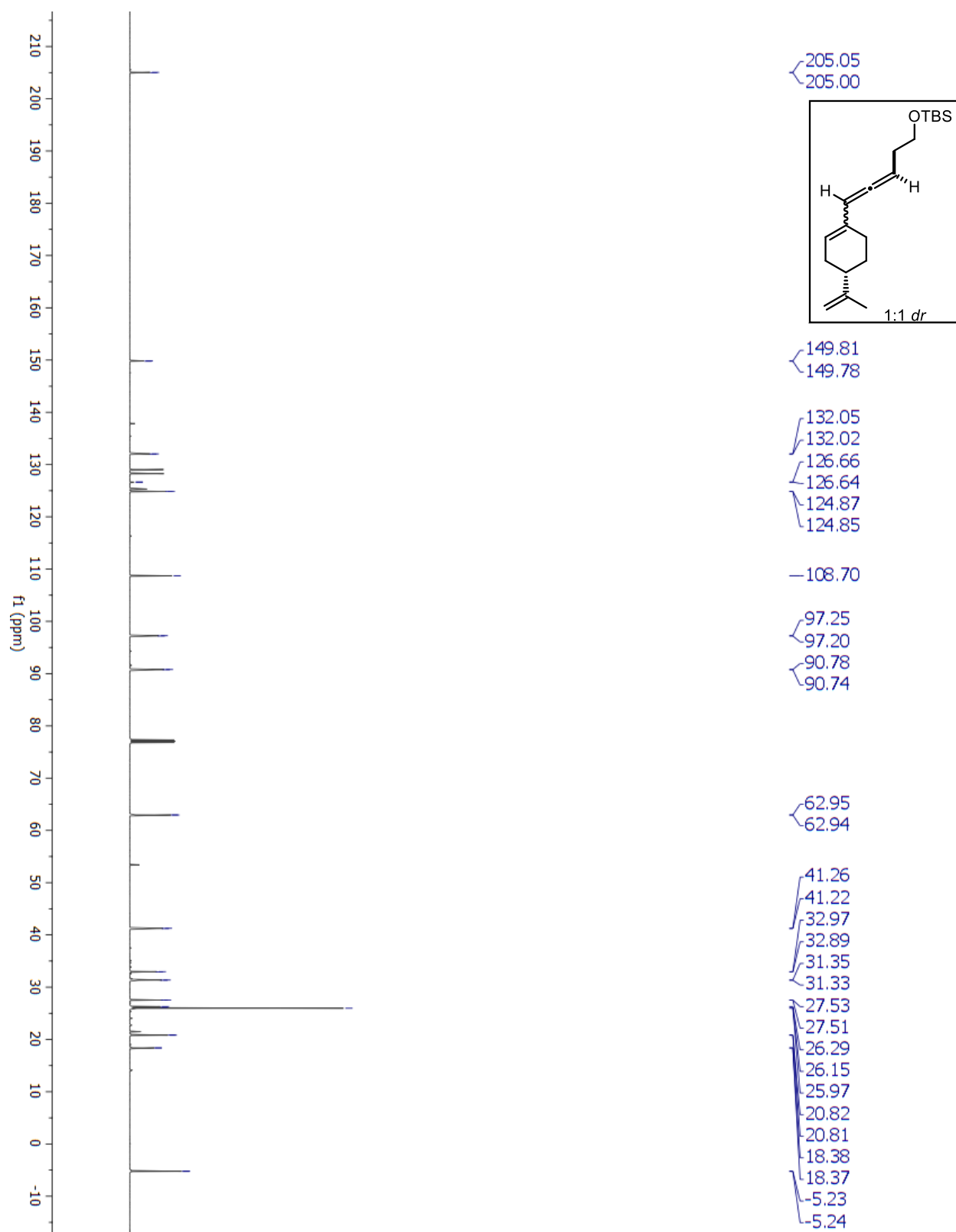
¹H-NMR for OTBS Precursor to 5.13

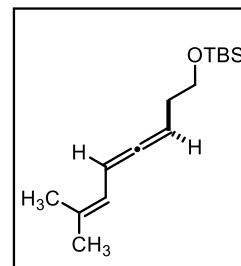
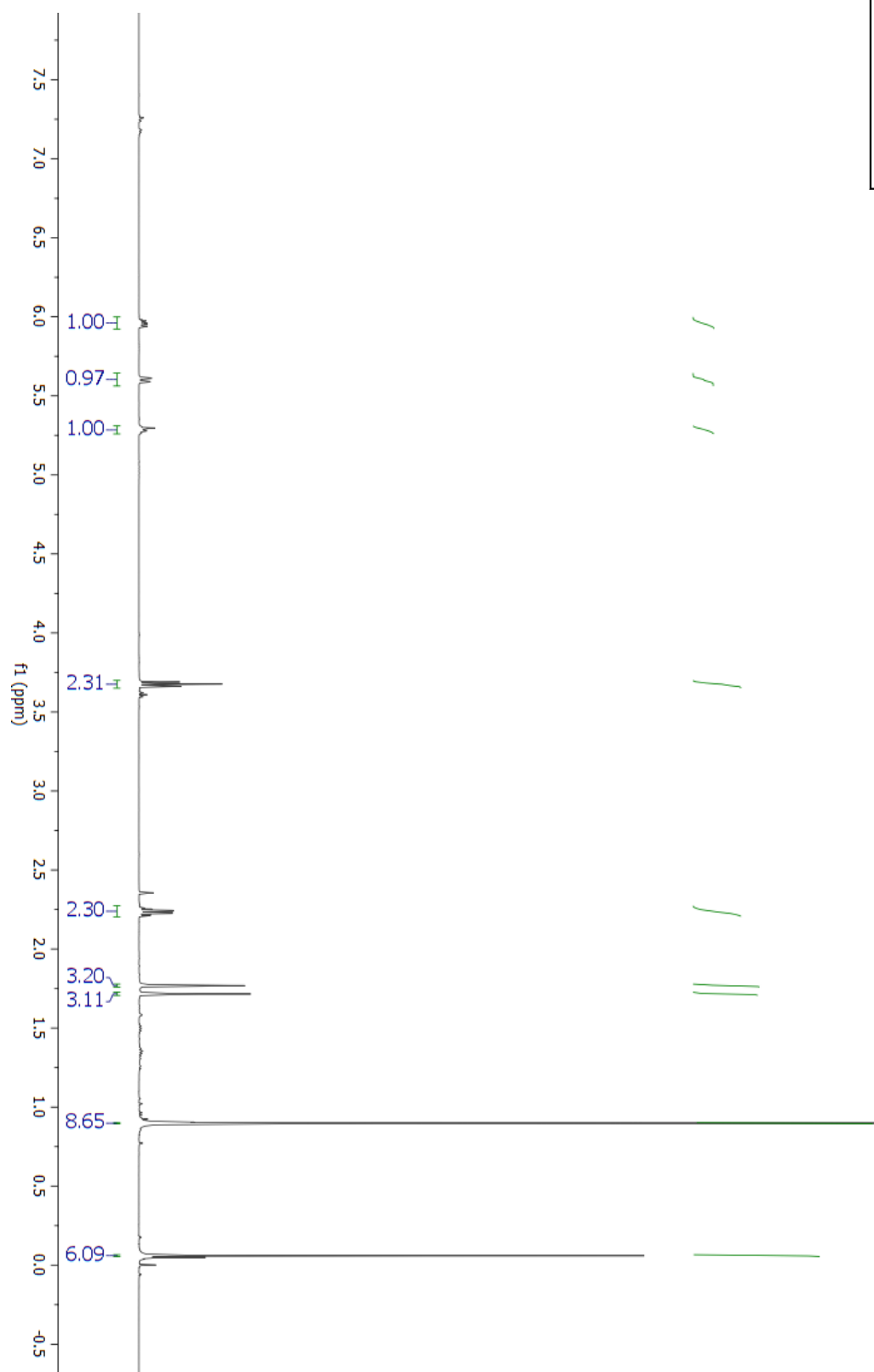
^{13}C -NMR for OTBS Precursor to 5.13

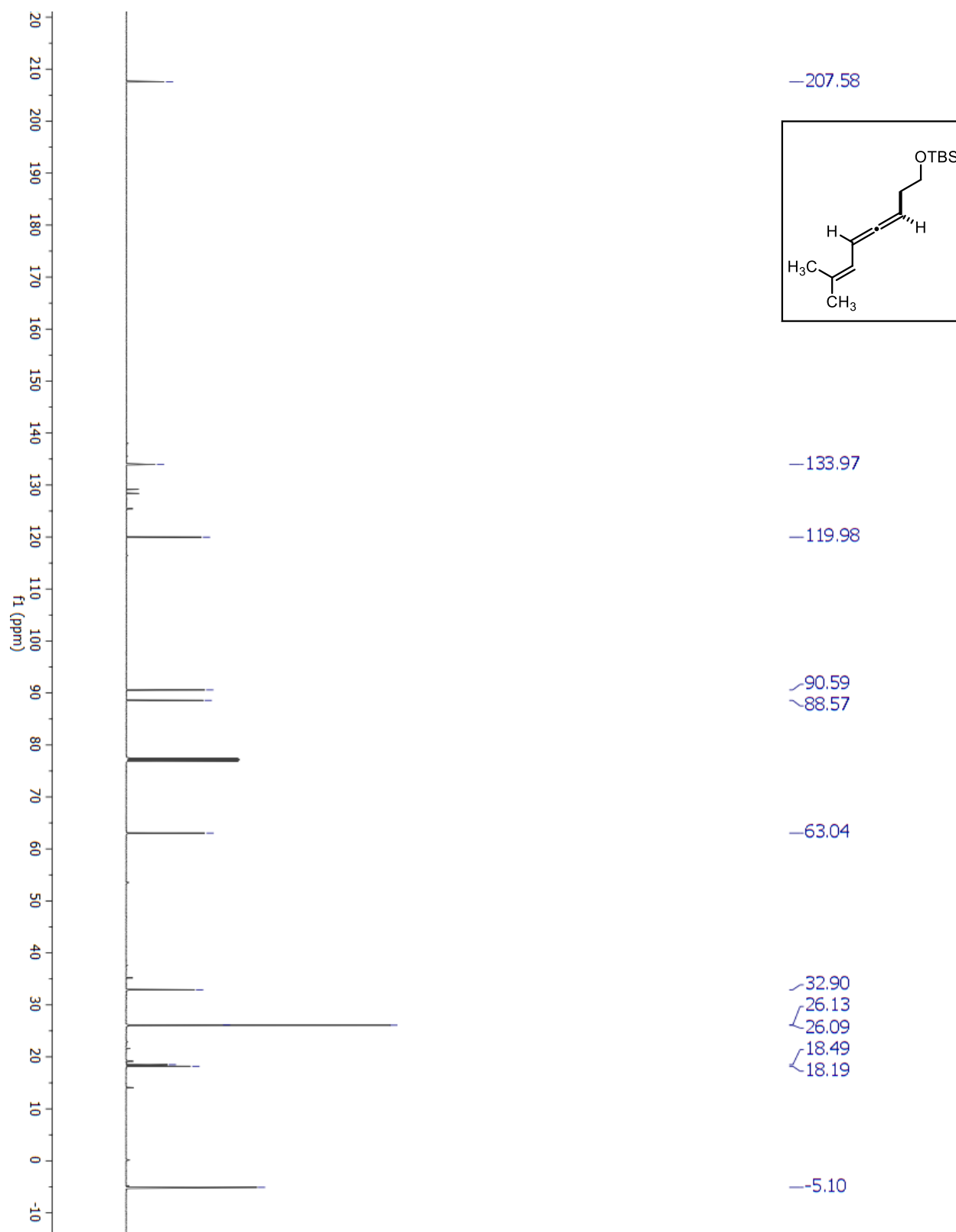
¹H-NMR for OTBS Precursor to 5.14

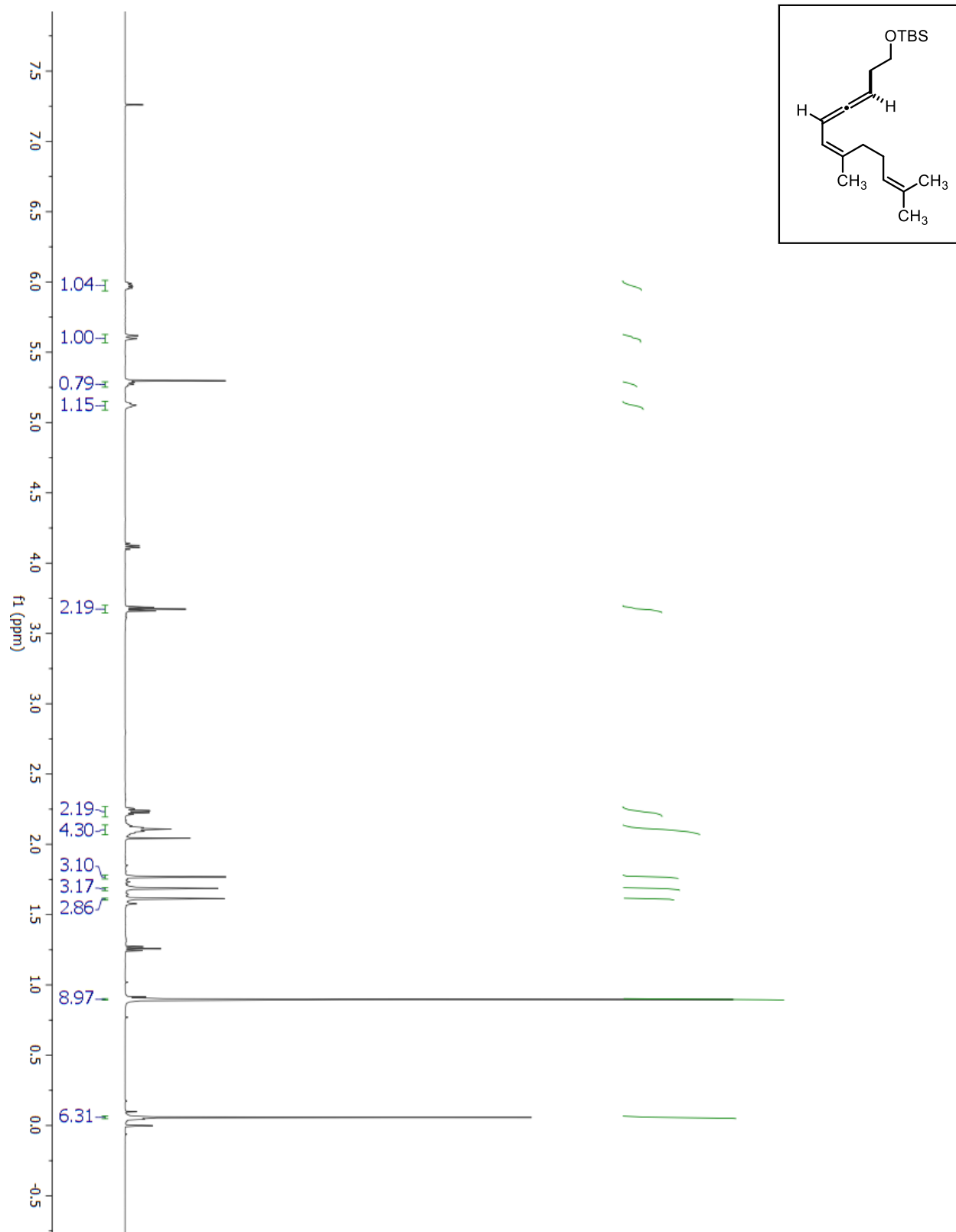
^{13}C -NMR for OTBS Precursor to 5.14

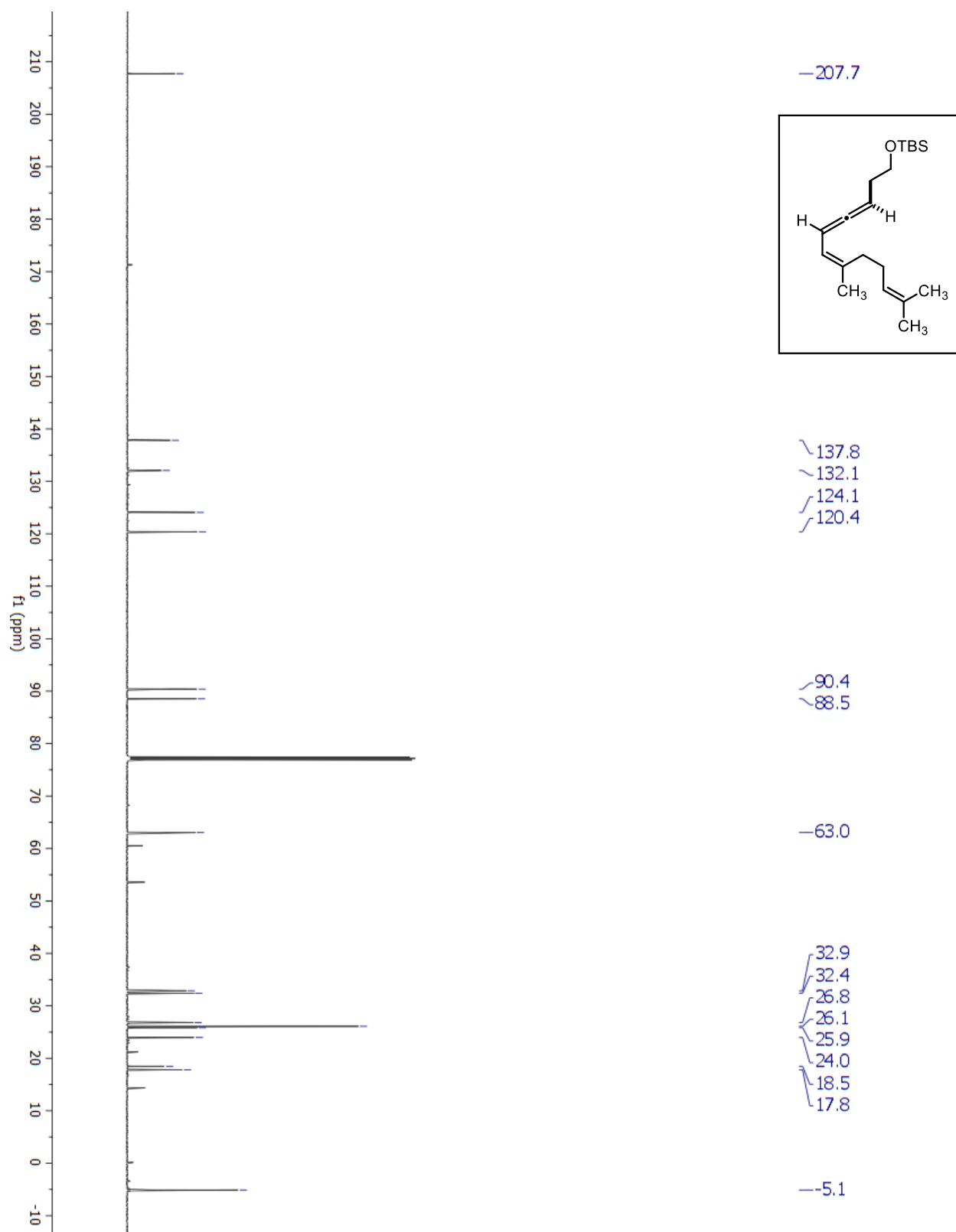
¹H-NMR for OTBS Precursor to 5.15

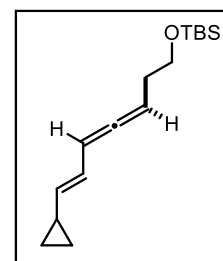
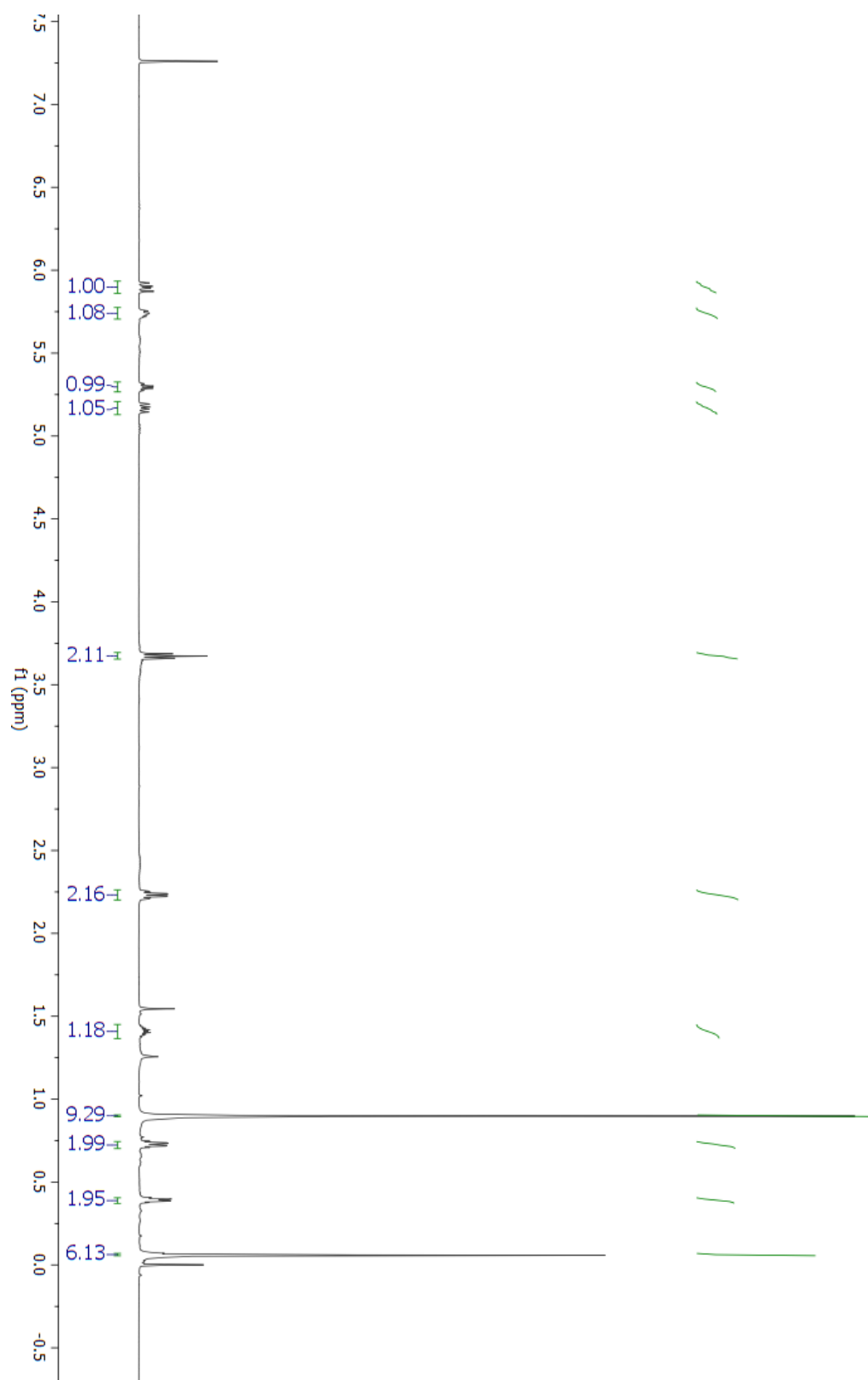
^{13}C -NMR for OTBS Precursor to 5.15

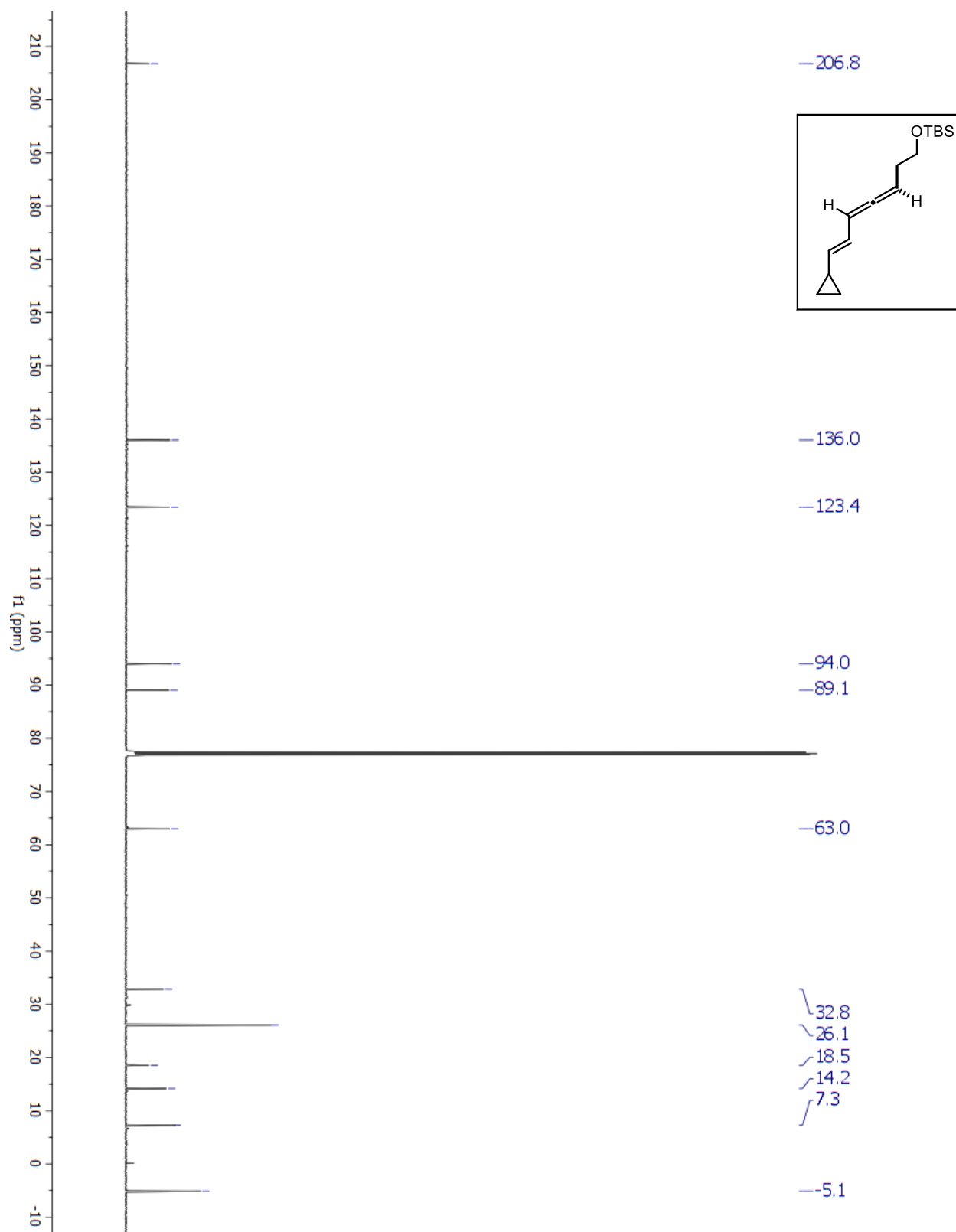
¹H-NMR for OTBS Precursor to 5.16

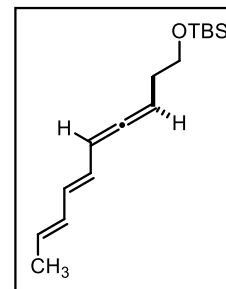
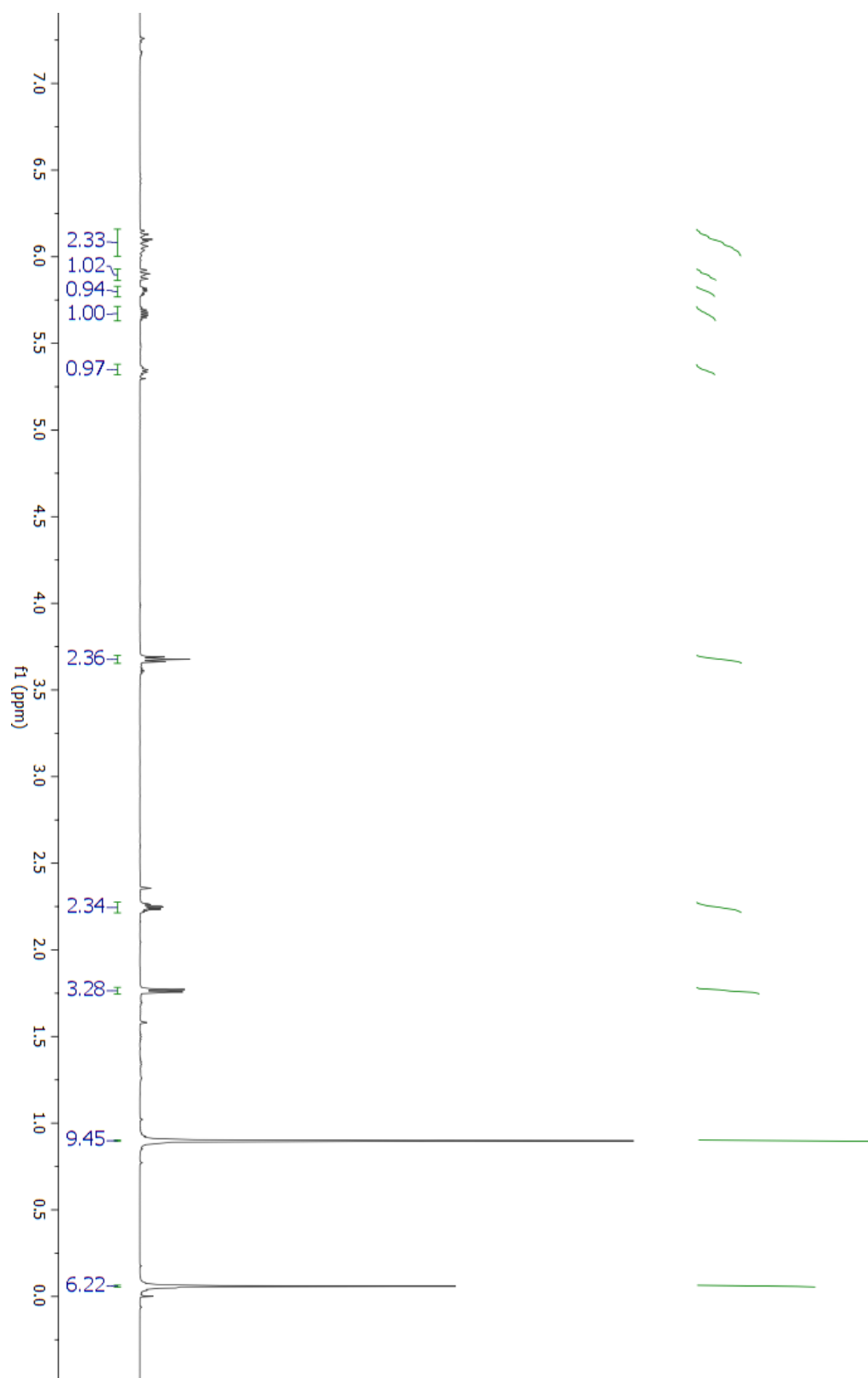
^{13}C -NMR for OTBS Precursor to 5.16

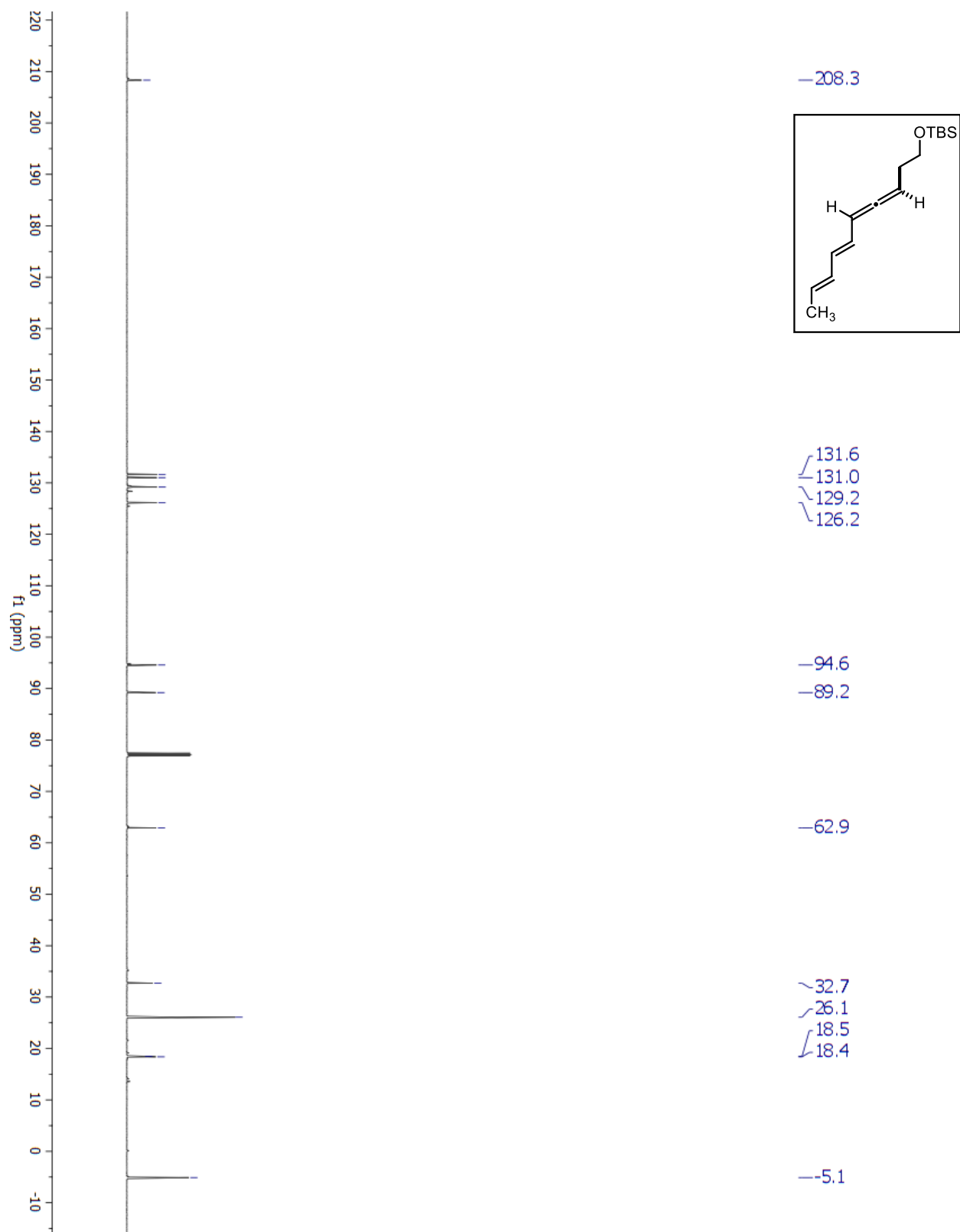


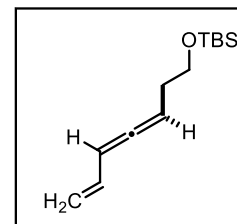
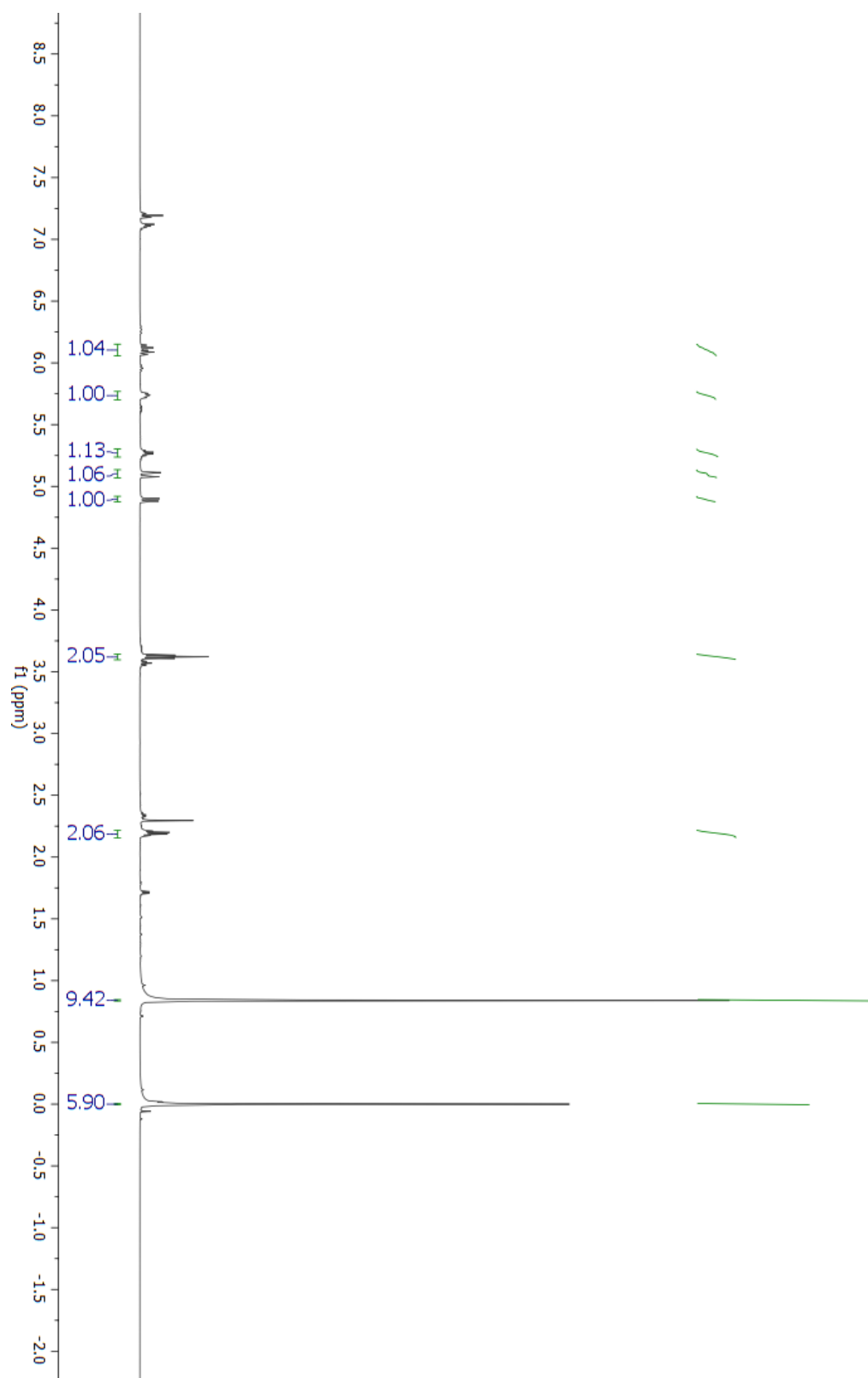
^{13}C -NMR for OTBS Precursor to 5.17

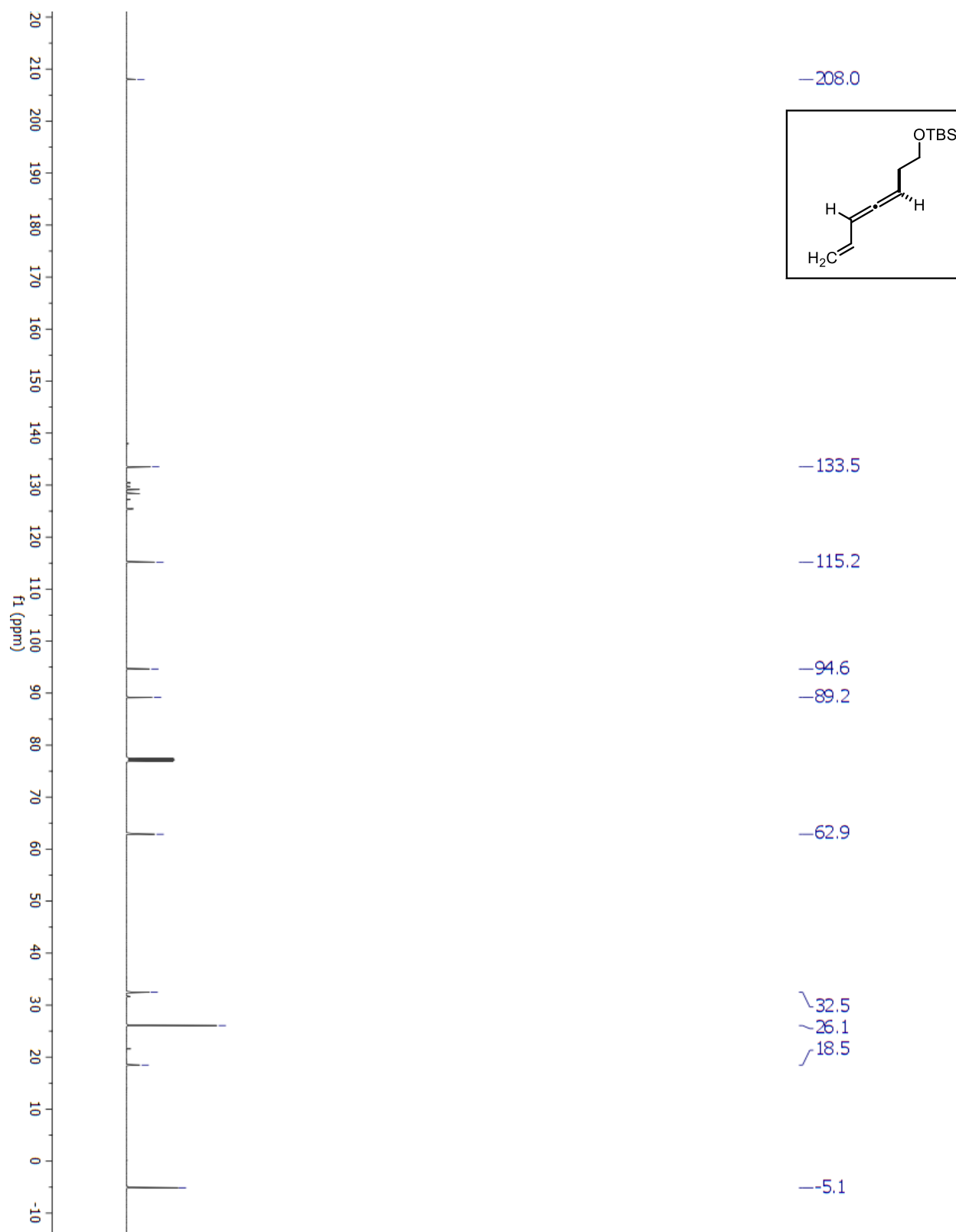
¹H-NMR for OTBS Precursor to 5.18

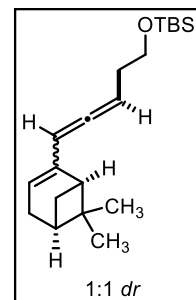
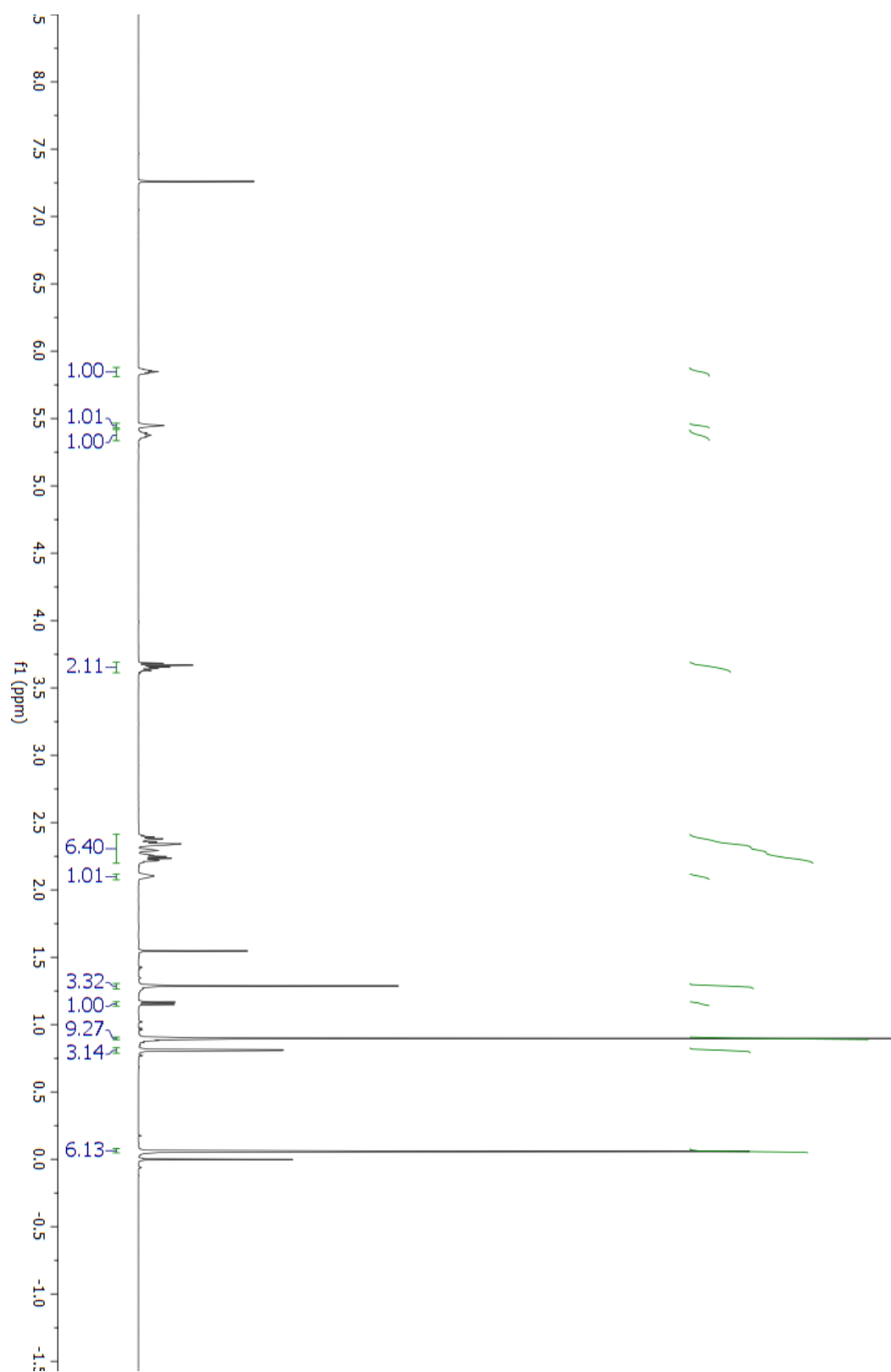
^{13}C -NMR for OTBS Precursor to 5.18

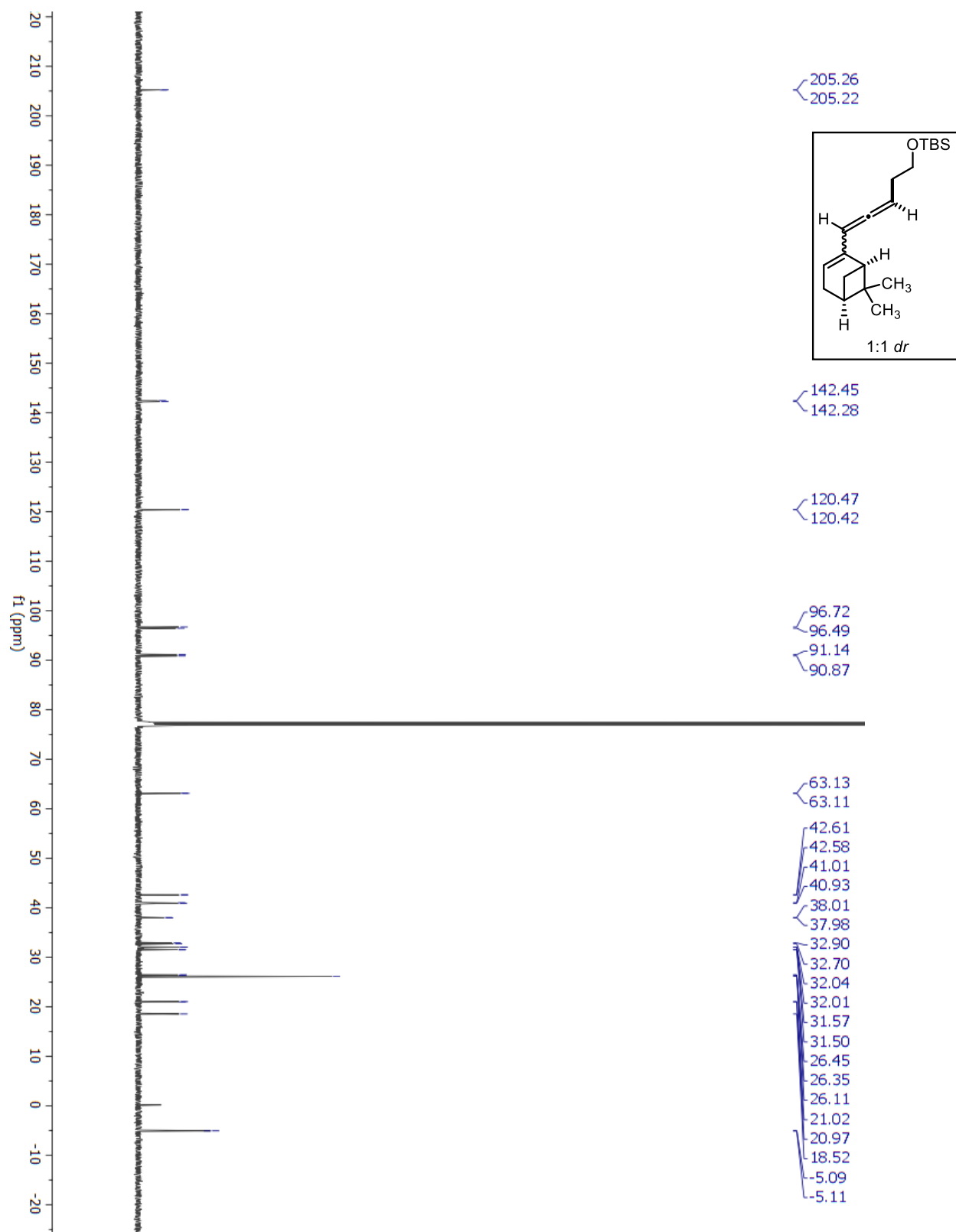
¹H-NMR for OTBS Precursor to 5.19

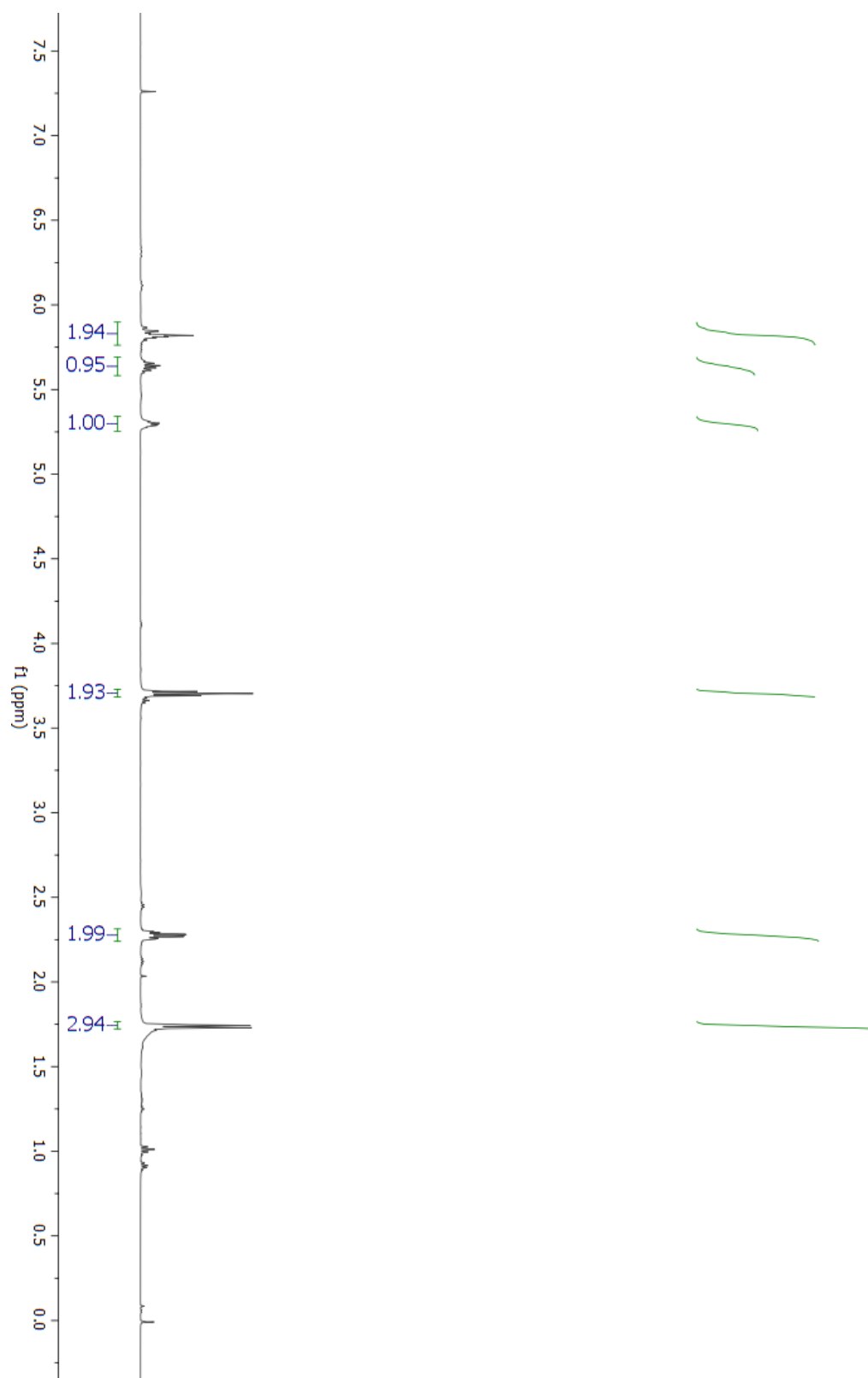
^{13}C -NMR for OTBS Precursor to 5.19

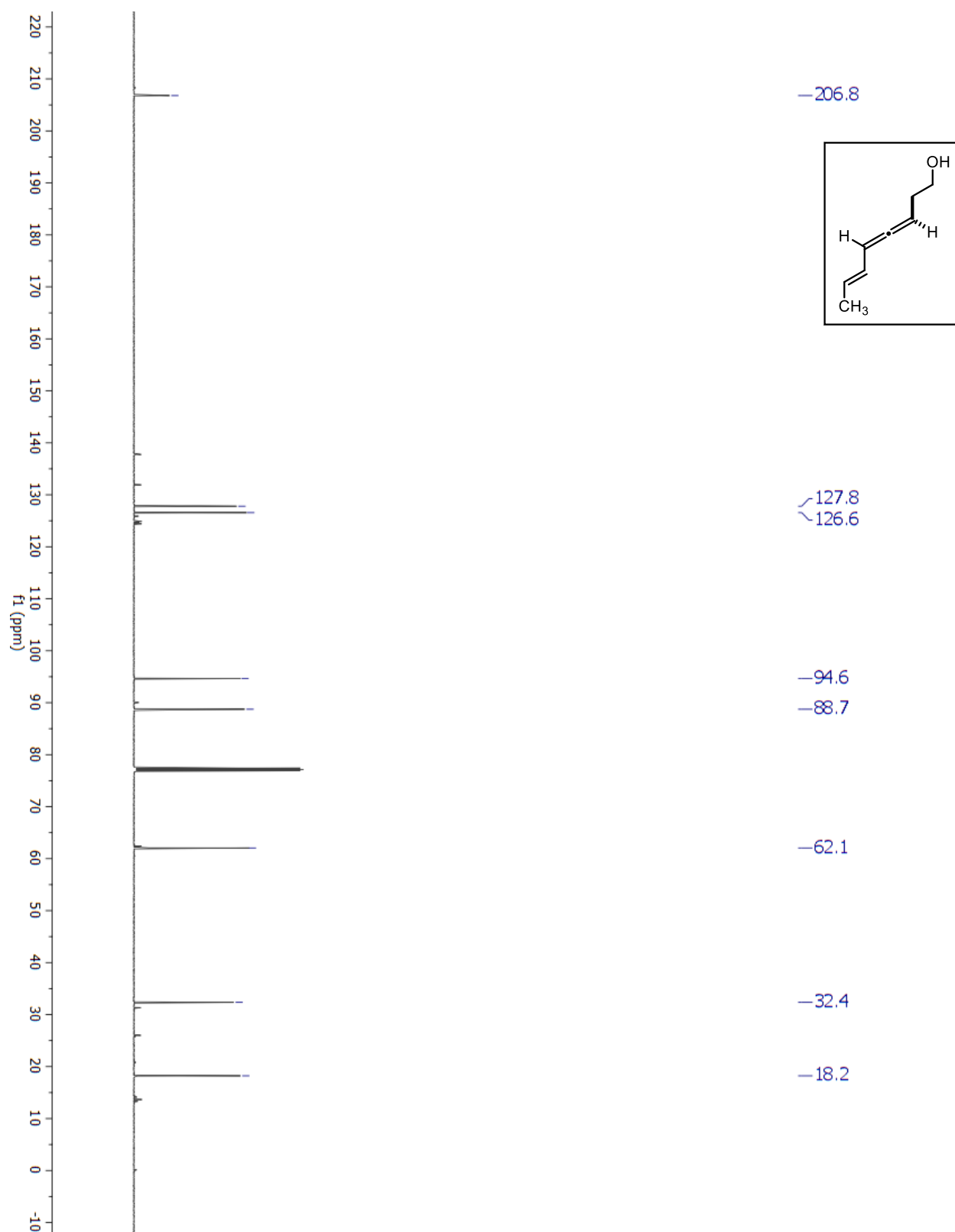
^1H -NMR for OTBS Precursor to 5.20

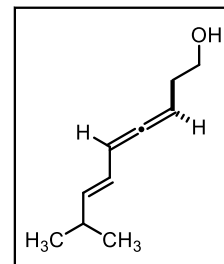
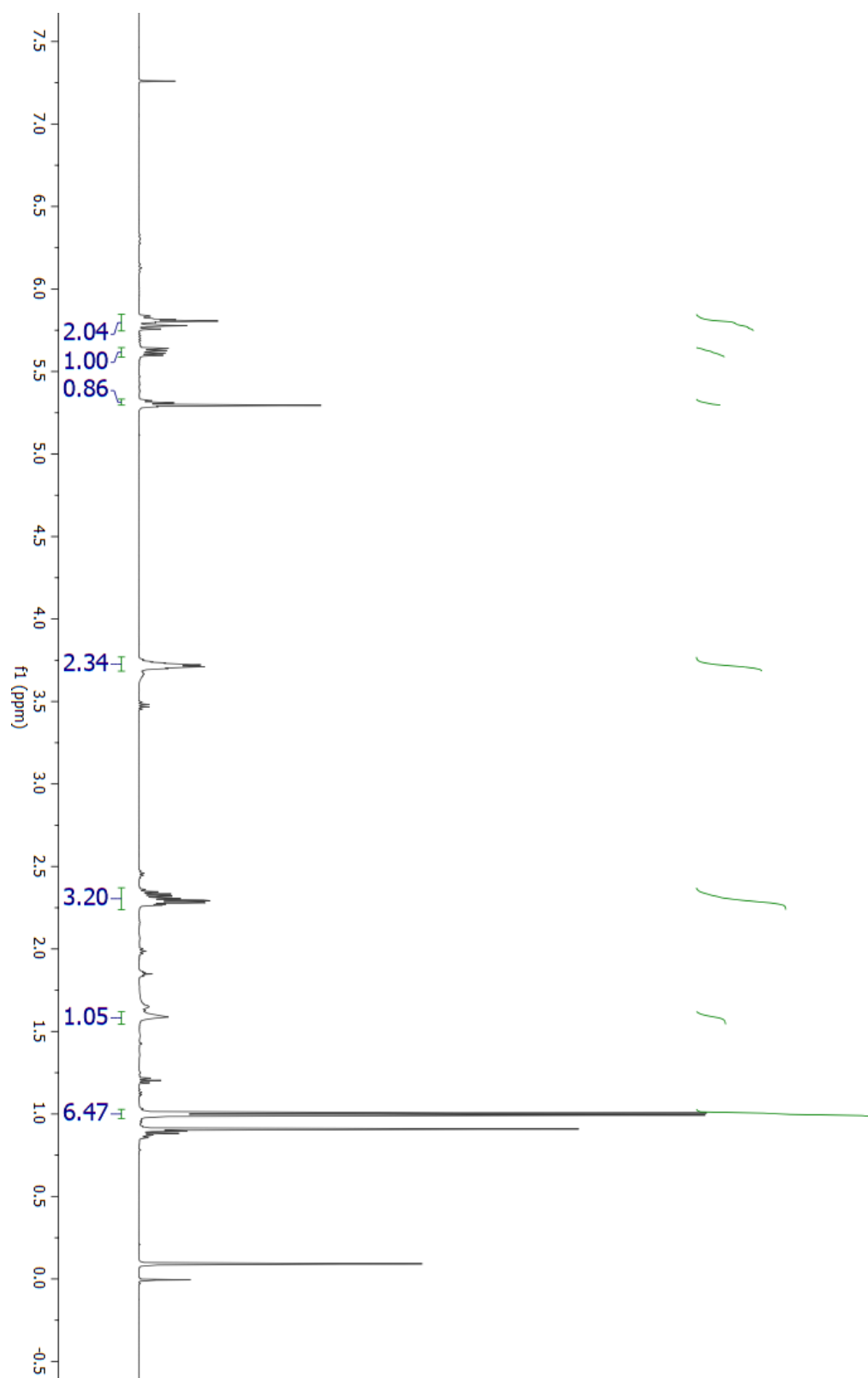
^{13}C -NMR for OTBS Precursor to 5.20

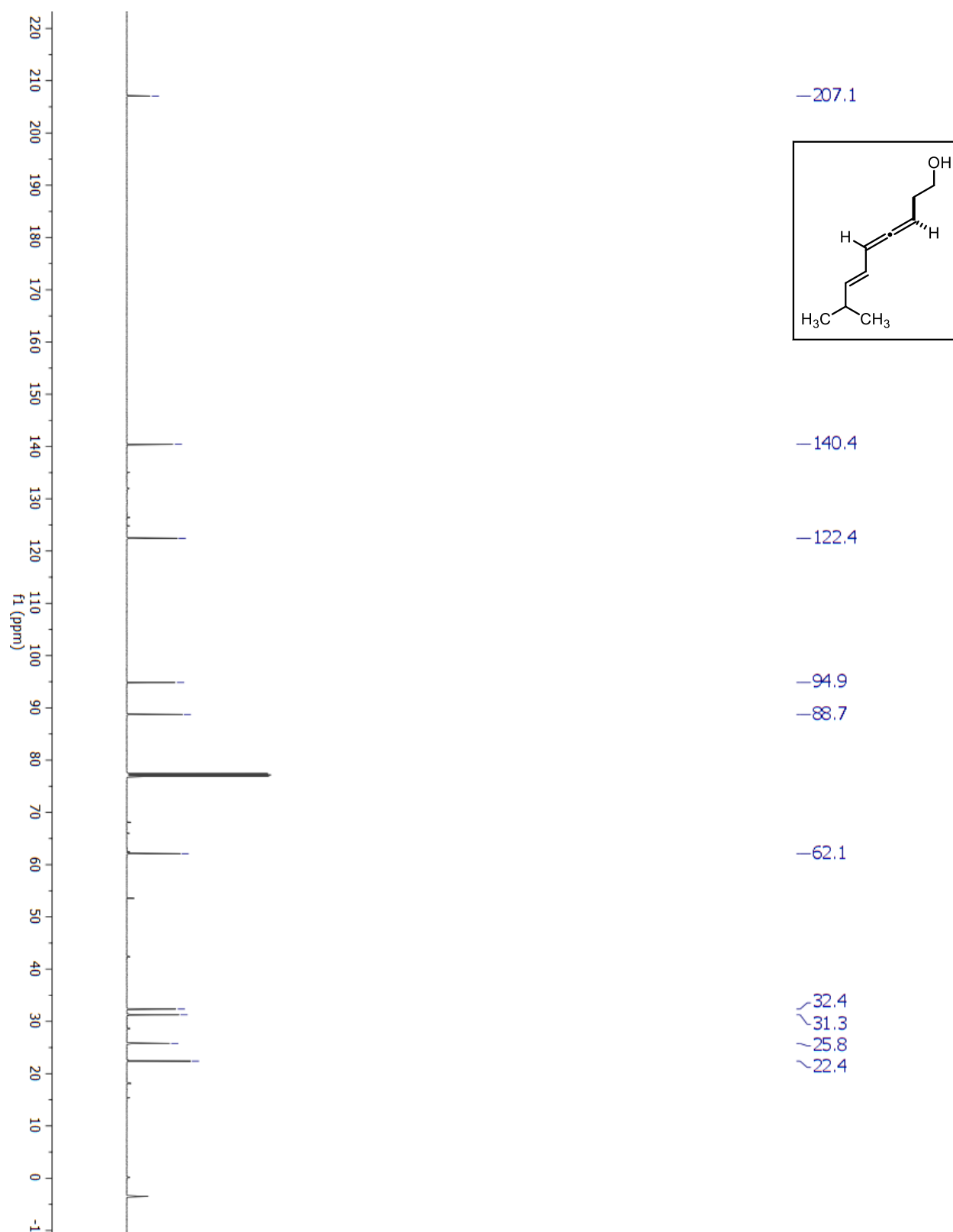
¹H-NMR for OTBS Precursor to 5.21

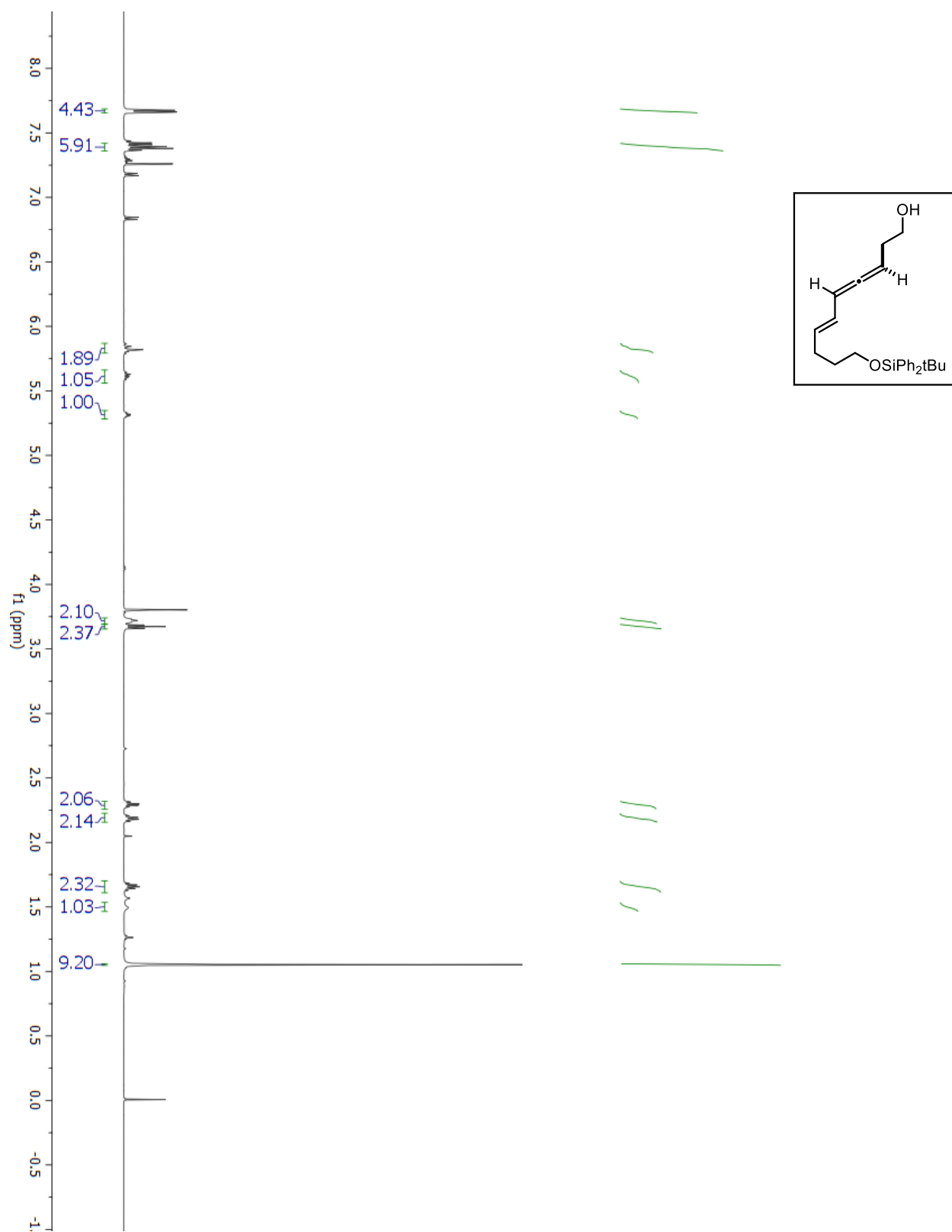
^{13}C -NMR for OTBS Precursor to 5.21

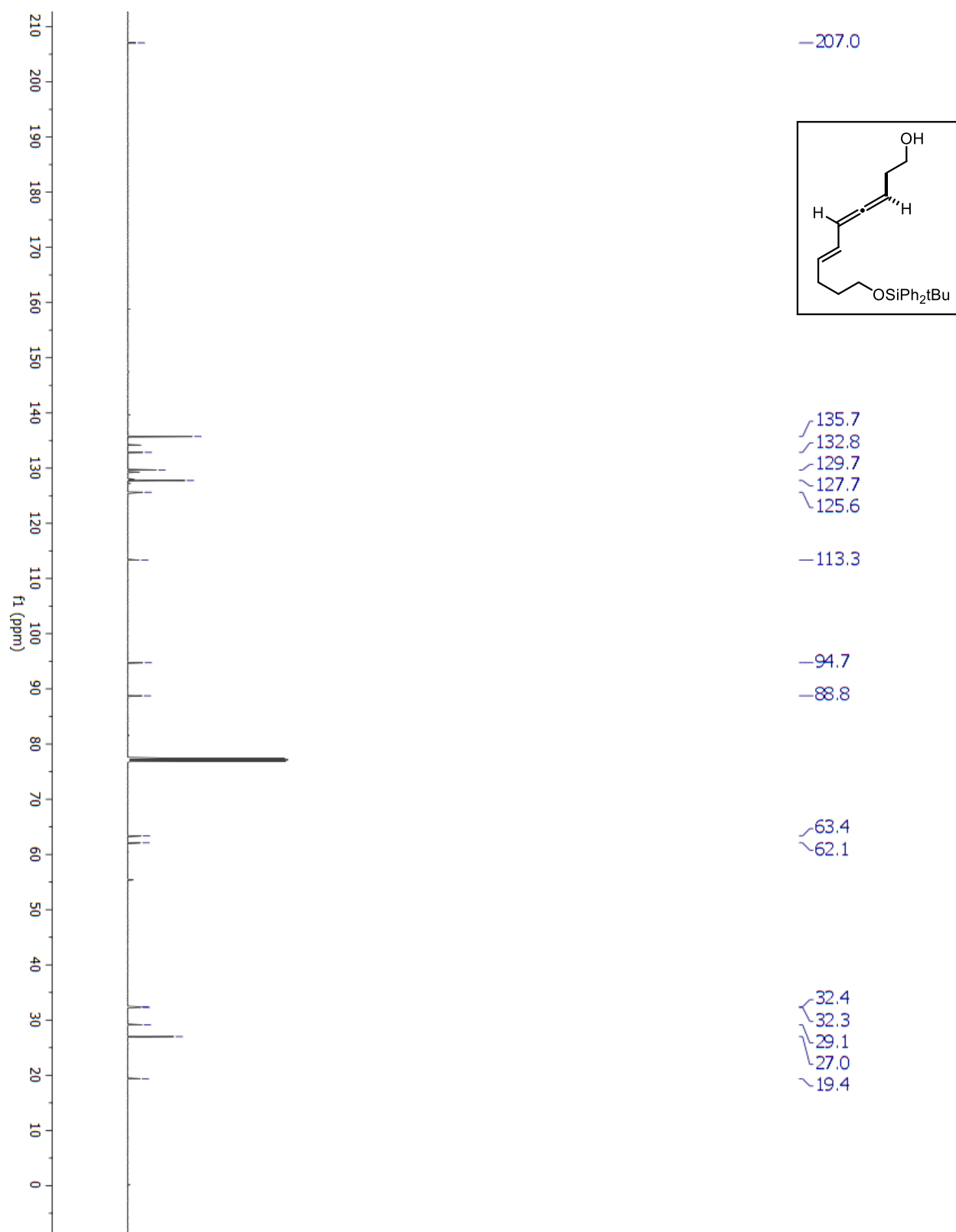
¹H-NMR for ROH Precursor to 5.4

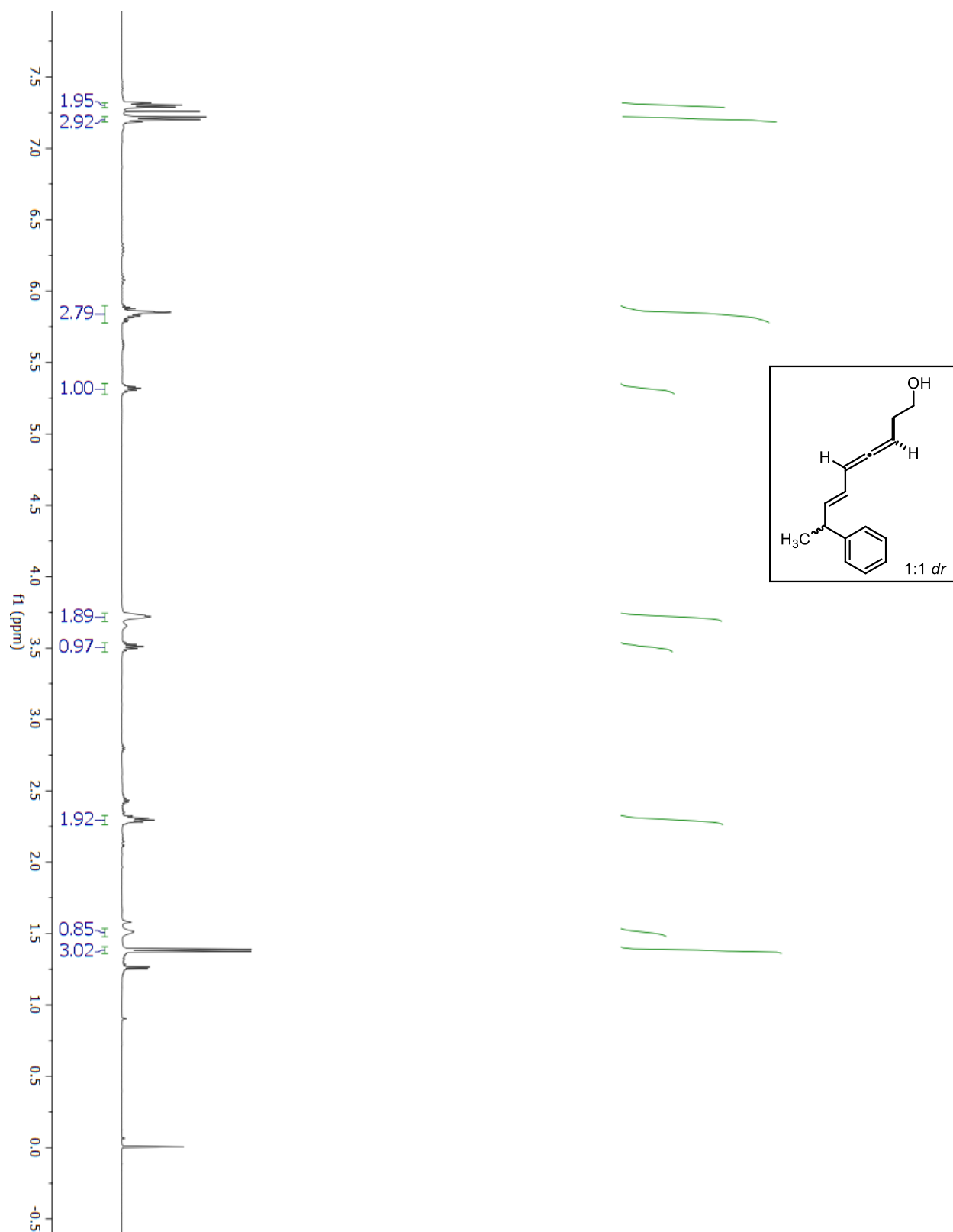
^{13}C -NMR for ROH Precursor to 5.4

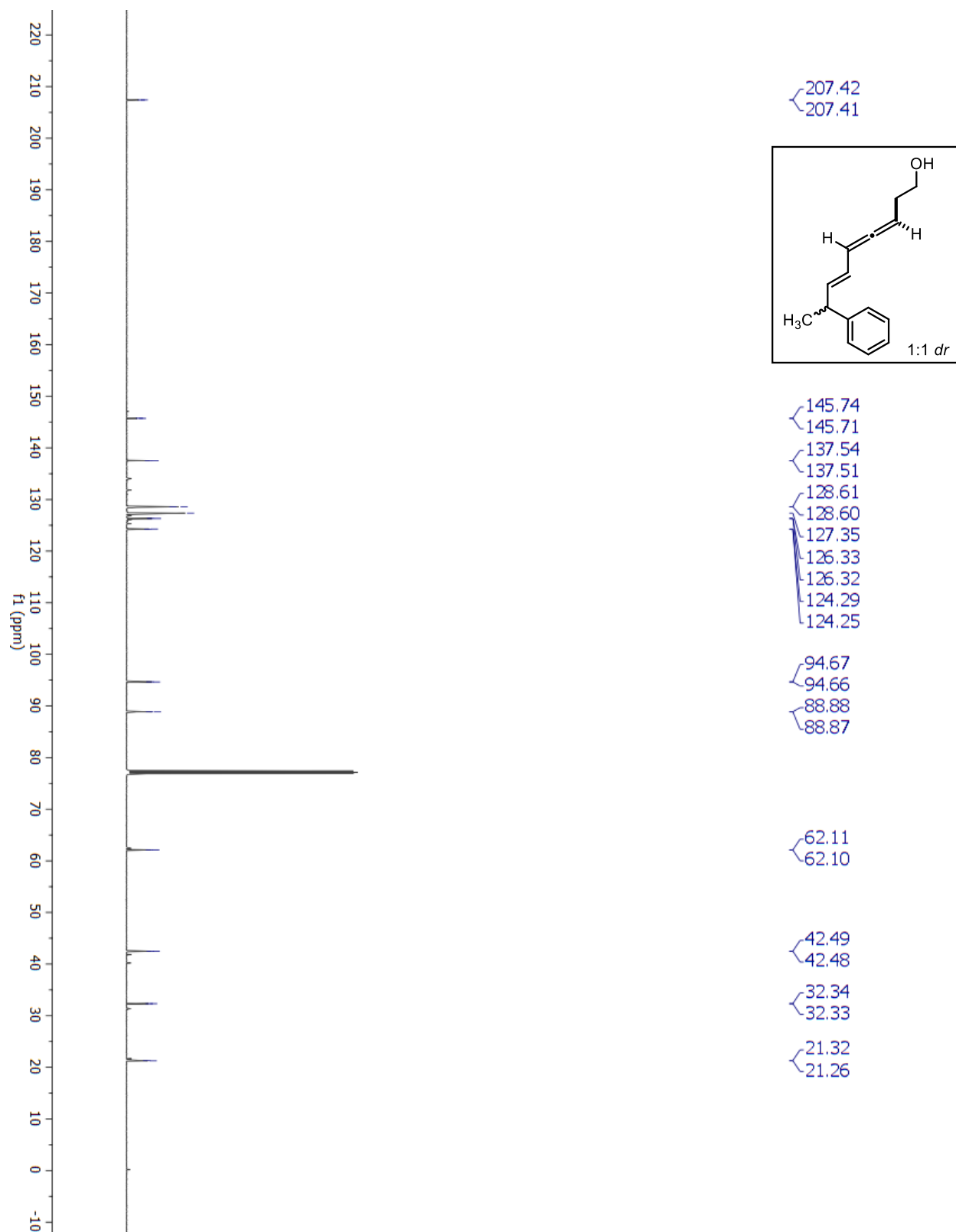
^1H -NMR for ROH Precursor to 5.6

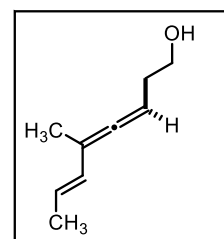
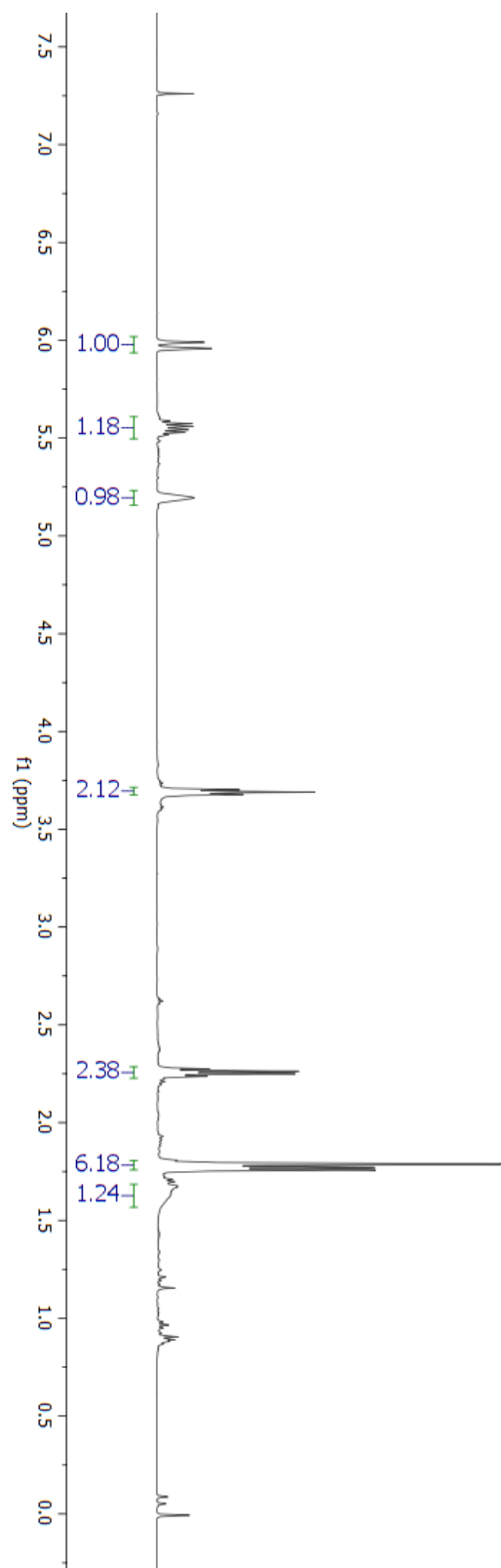
^{13}C -NMR for ROH Precursor to 5.6

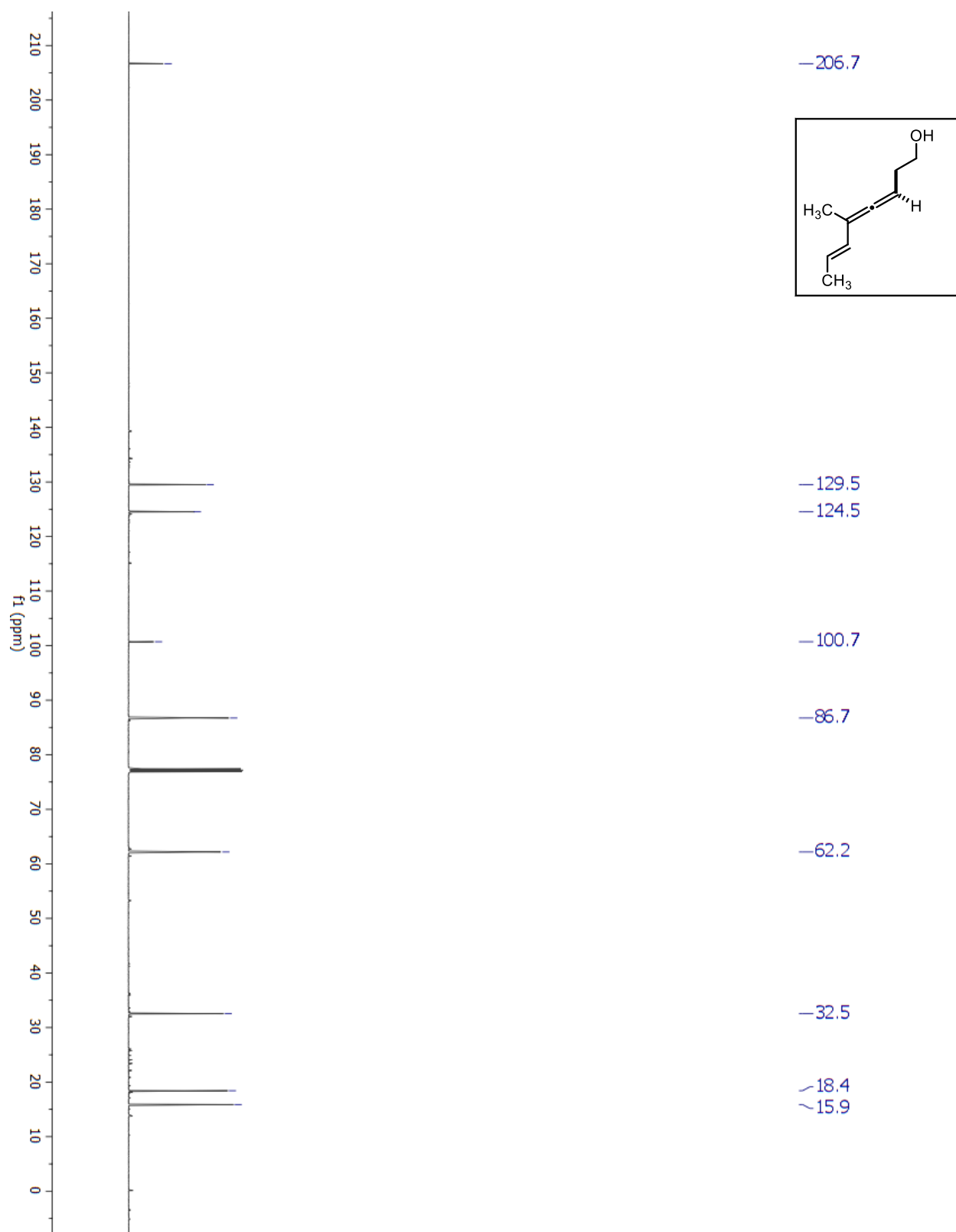
¹H-NMR for ROH Precursor to 5.7

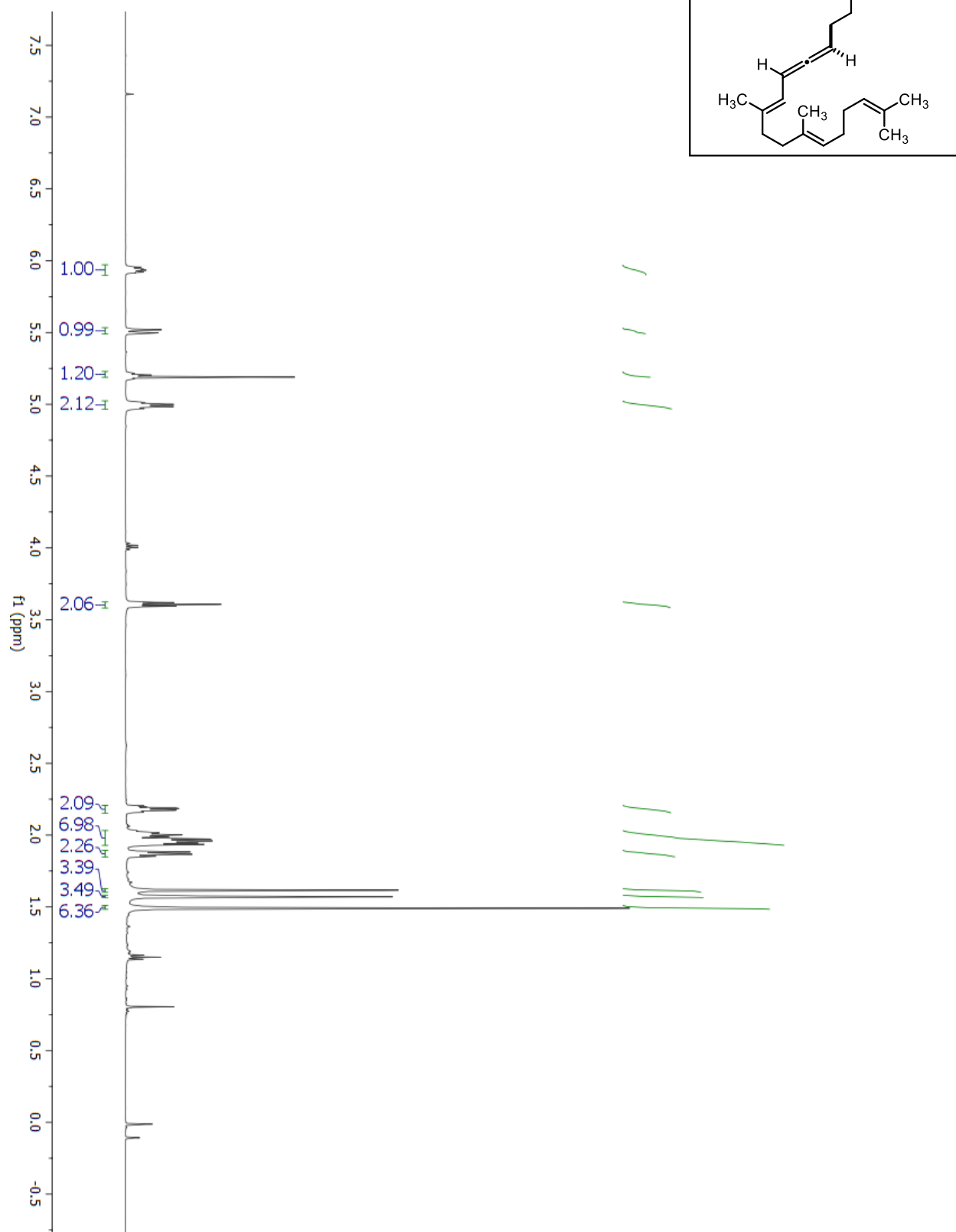
^{13}C -NMR for ROH Precursor to 5.7

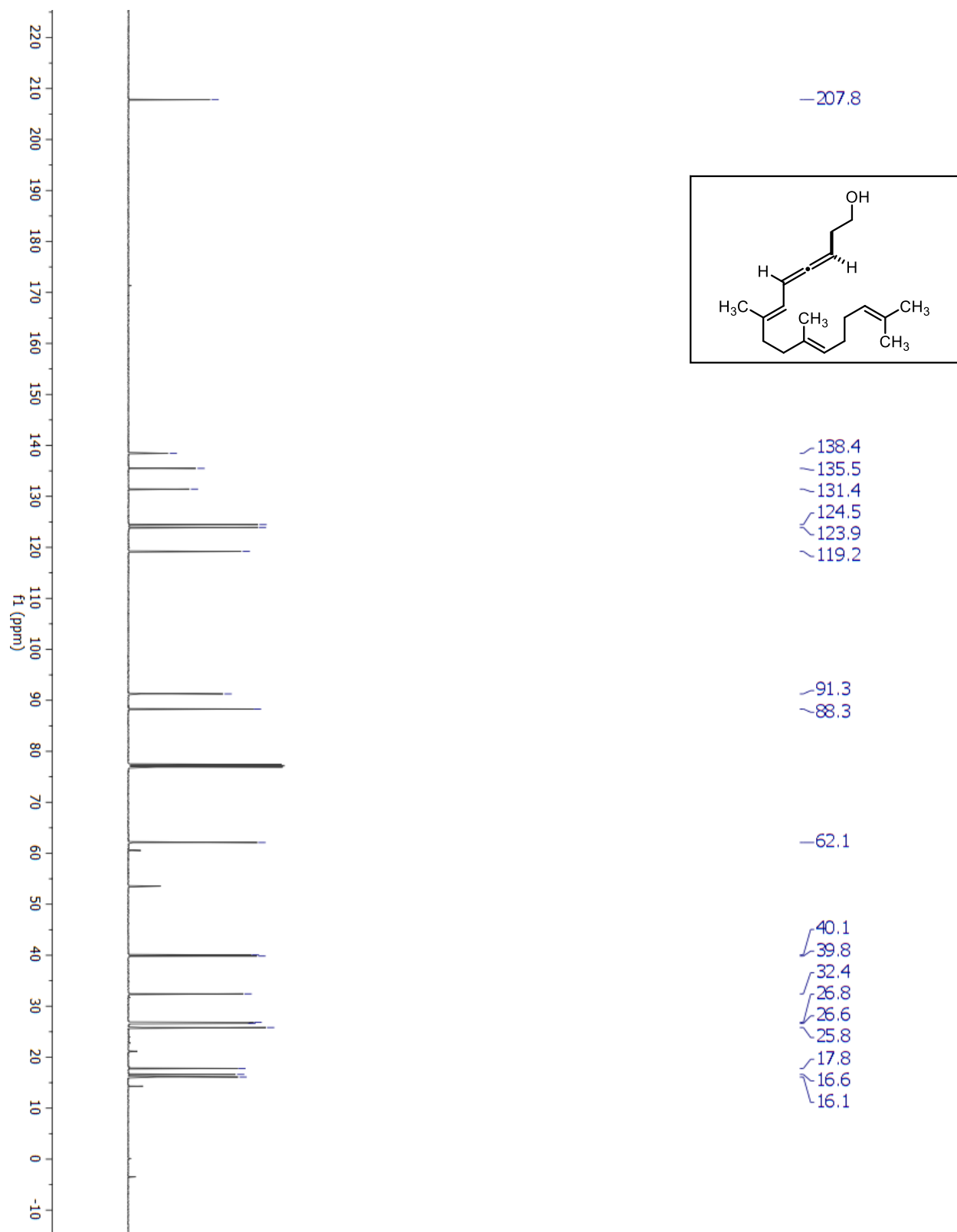
¹H-NMR for ROH Precursor to 5.8

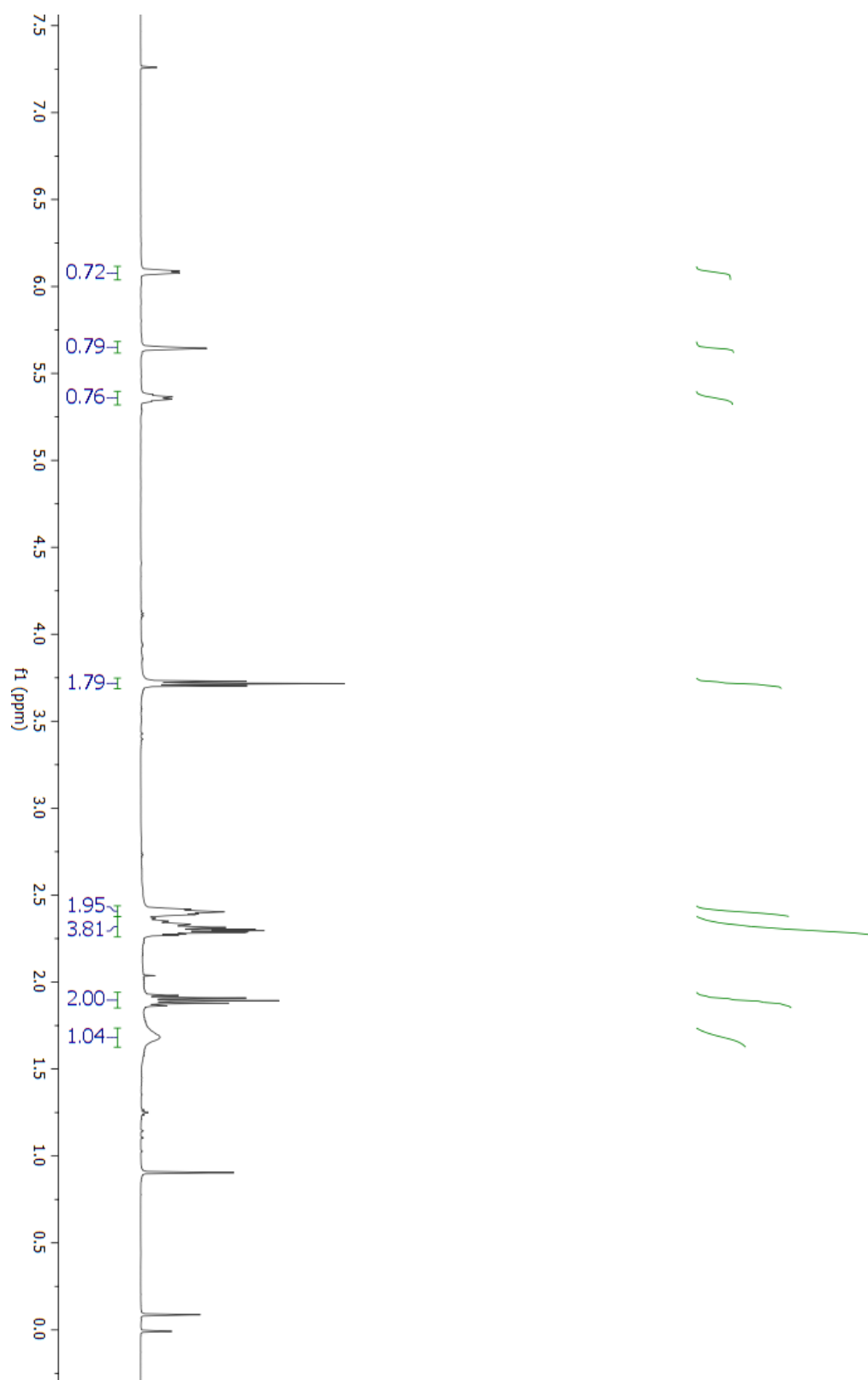
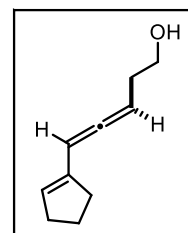
^{13}C -NMR for ROH Precursor to 5.8

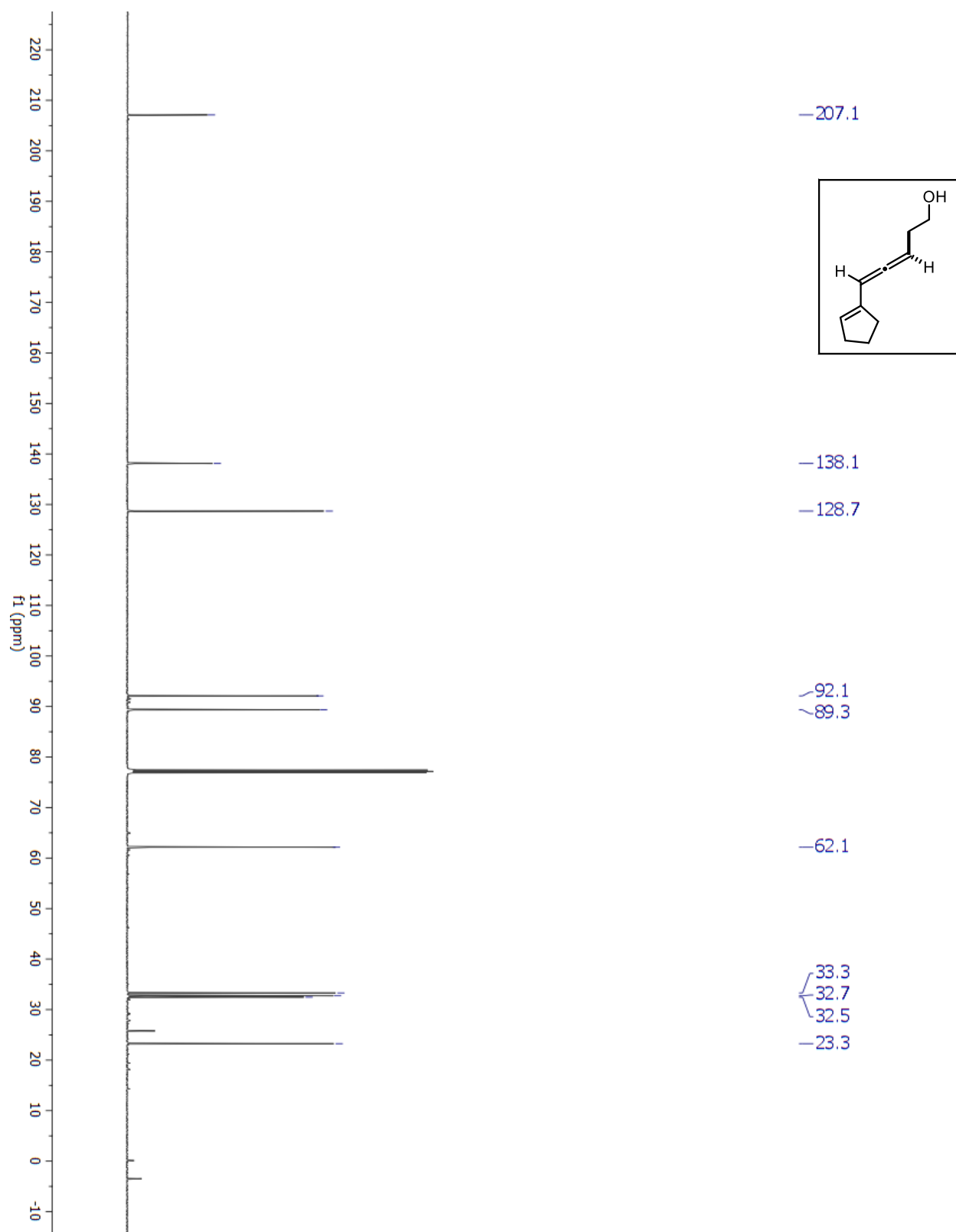
^1H -NMR for ROH Precursor to 5.9

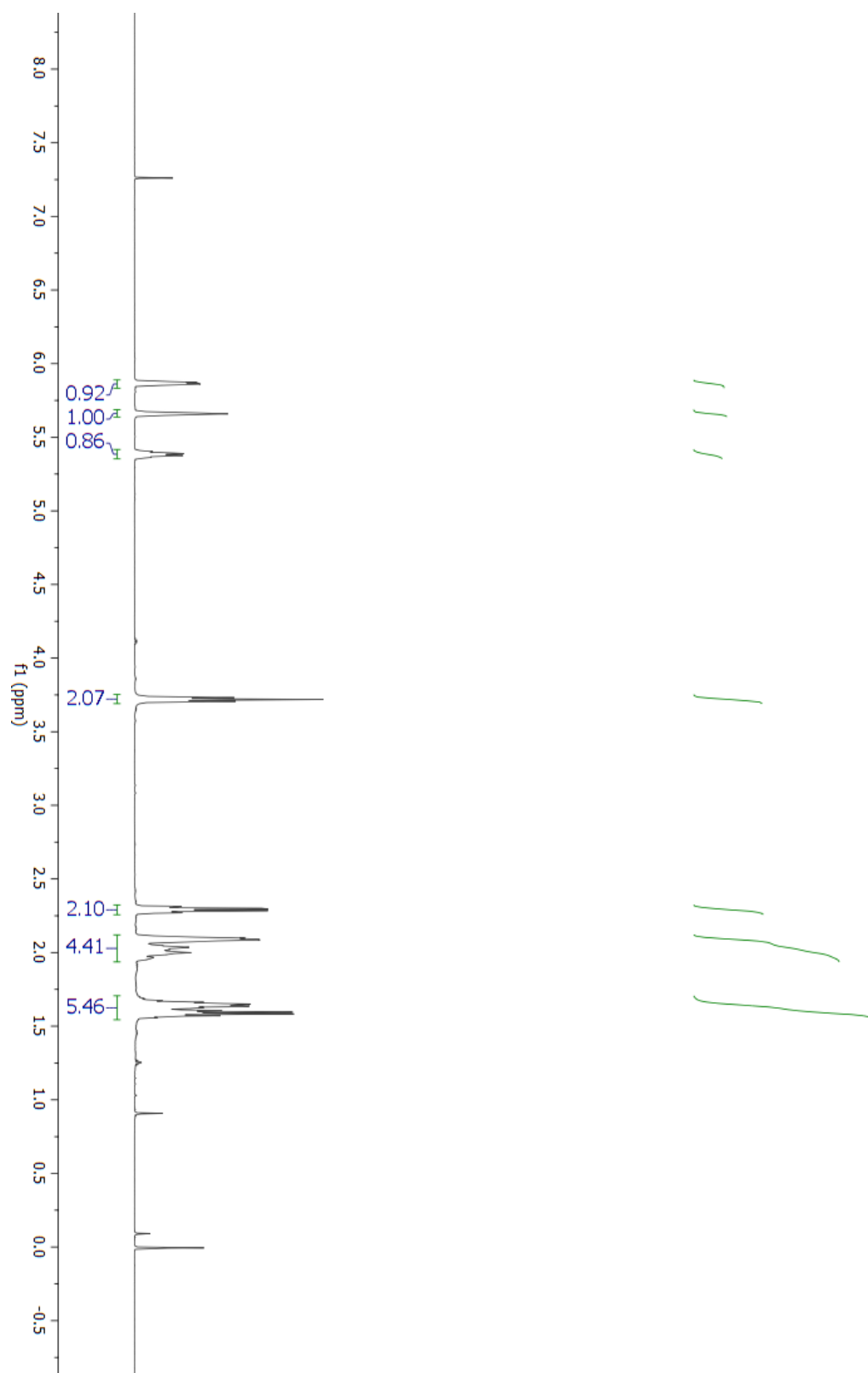
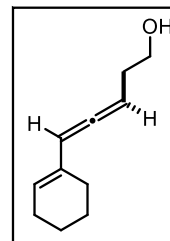
^{13}C -NMR for ROH Precursor to 5.9

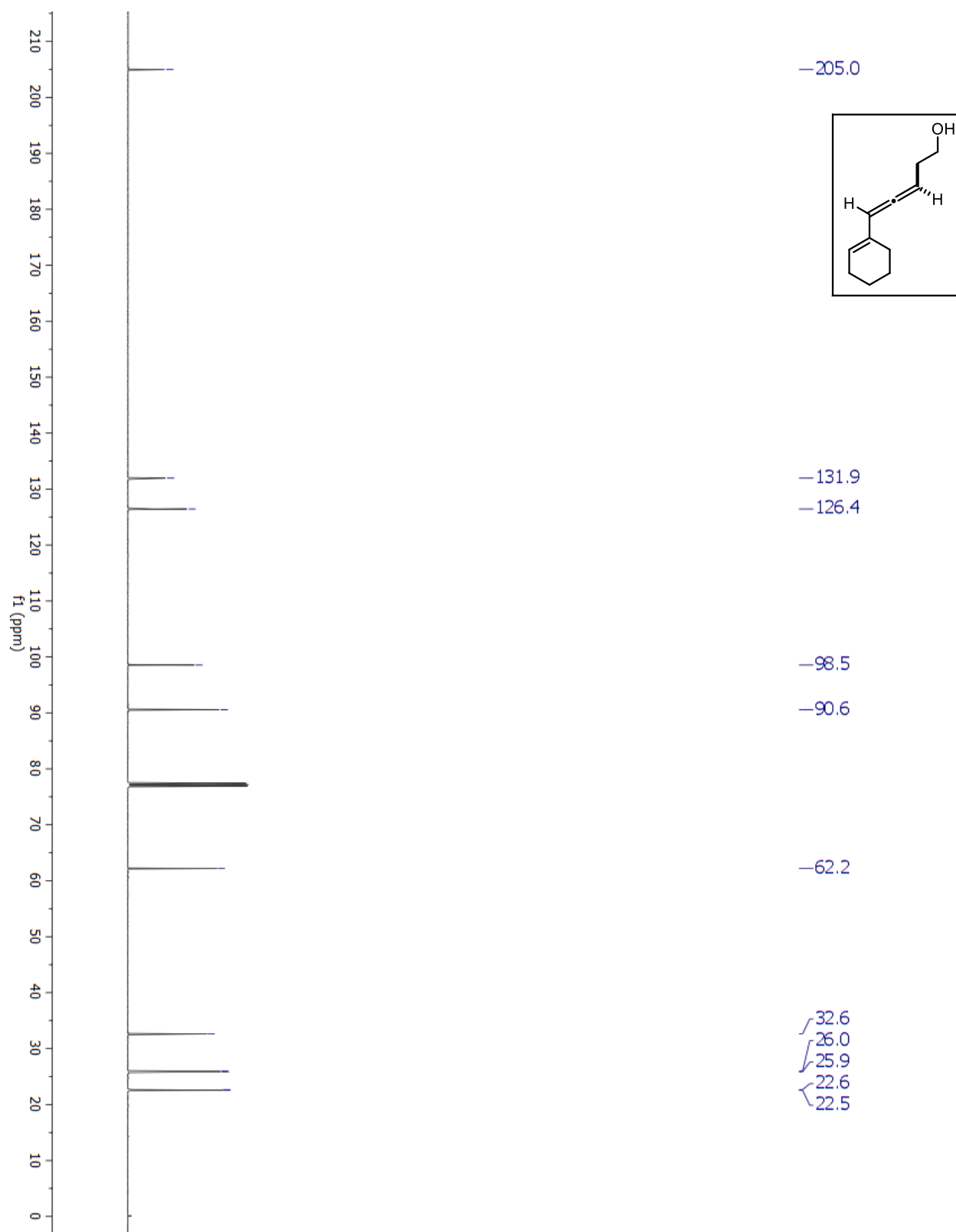
¹H-NMR for ROH Precursor to 5.12

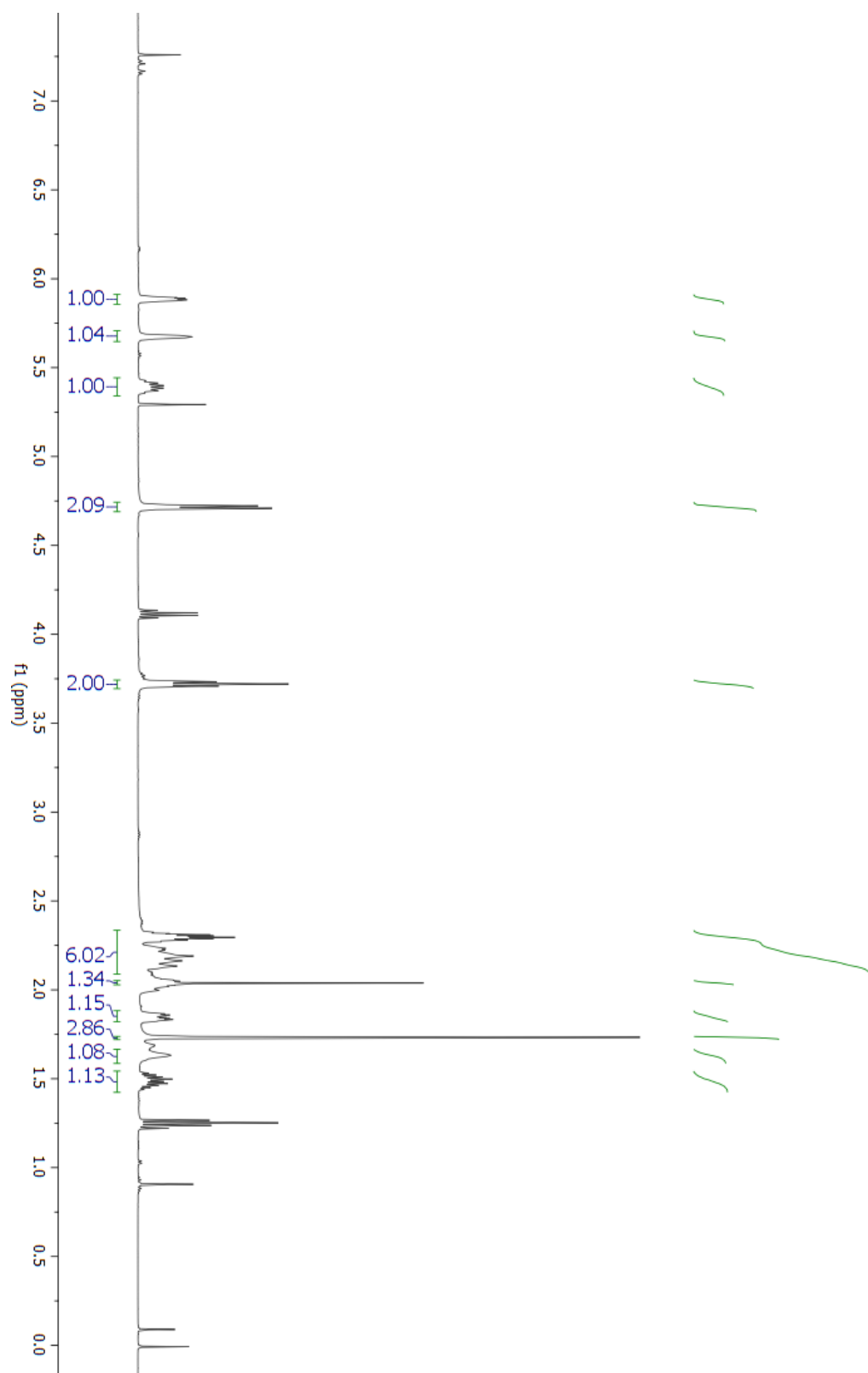
^{13}C -NMR for ROH Precursor to 5.12

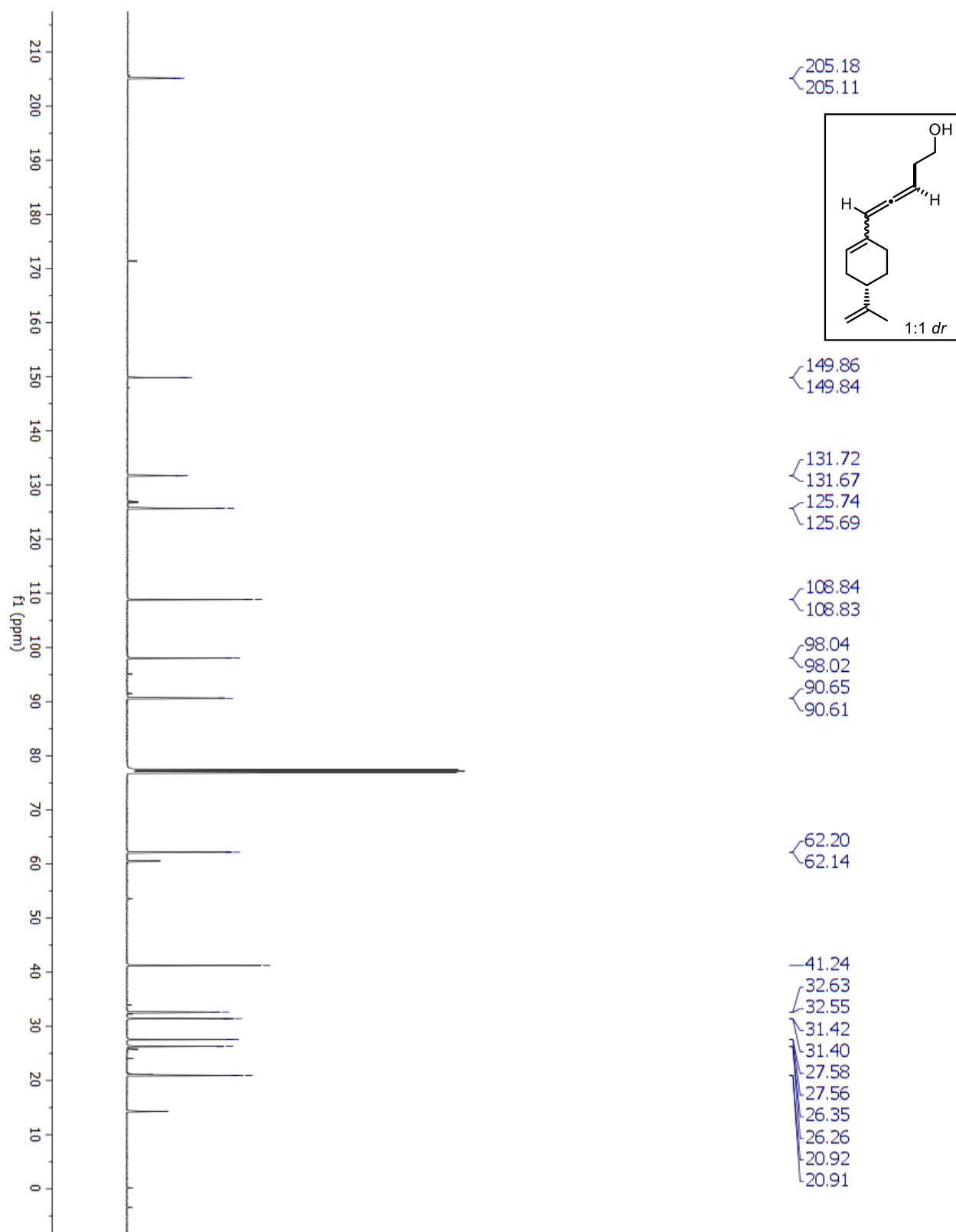
¹H-NMR for ROH Precursor to 5.13

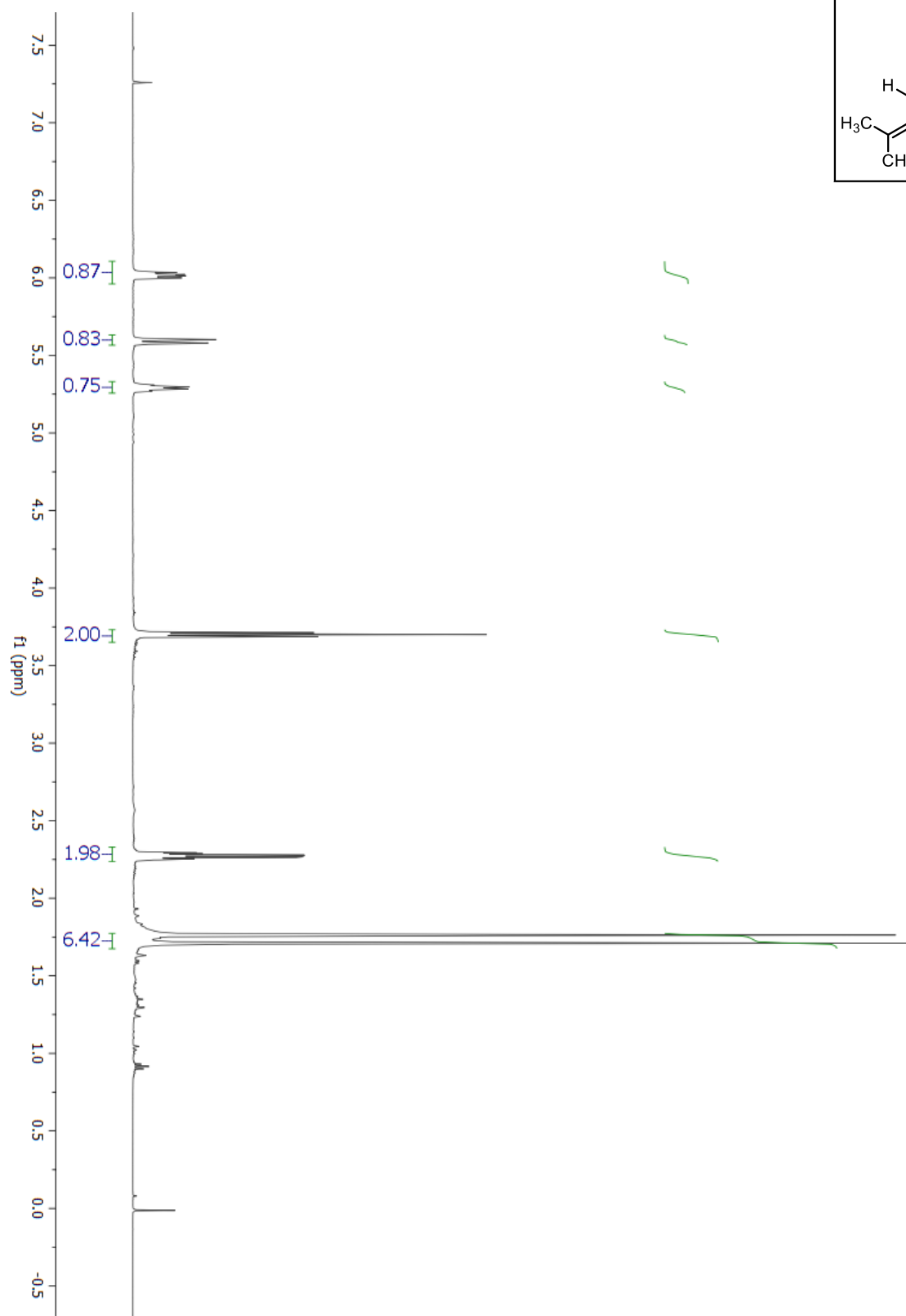
^{13}C -NMR for ROH Precursor to 5.13

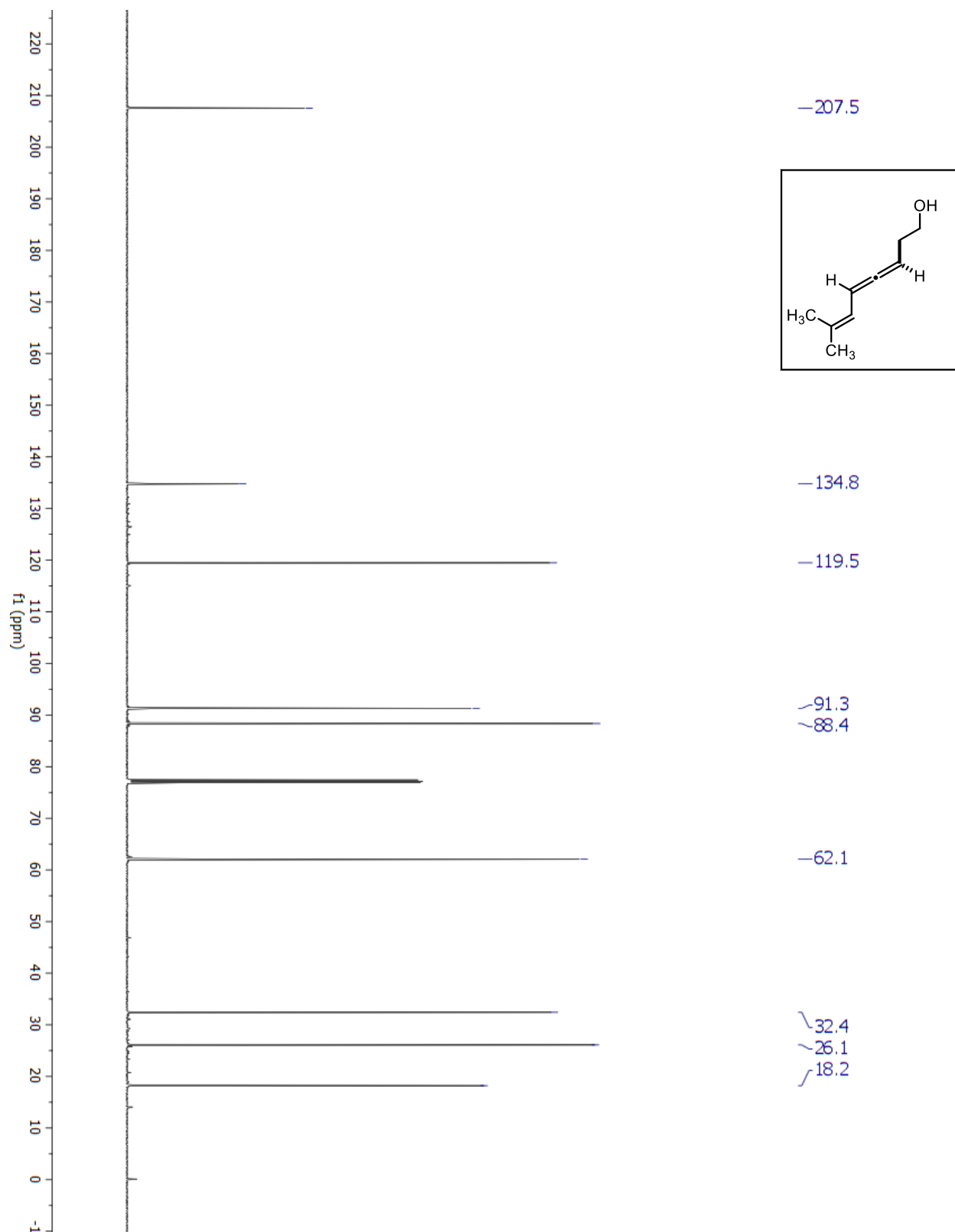
¹H-NMR for ROH Precursor to 5.14

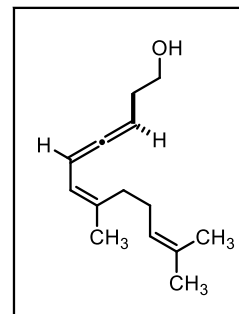
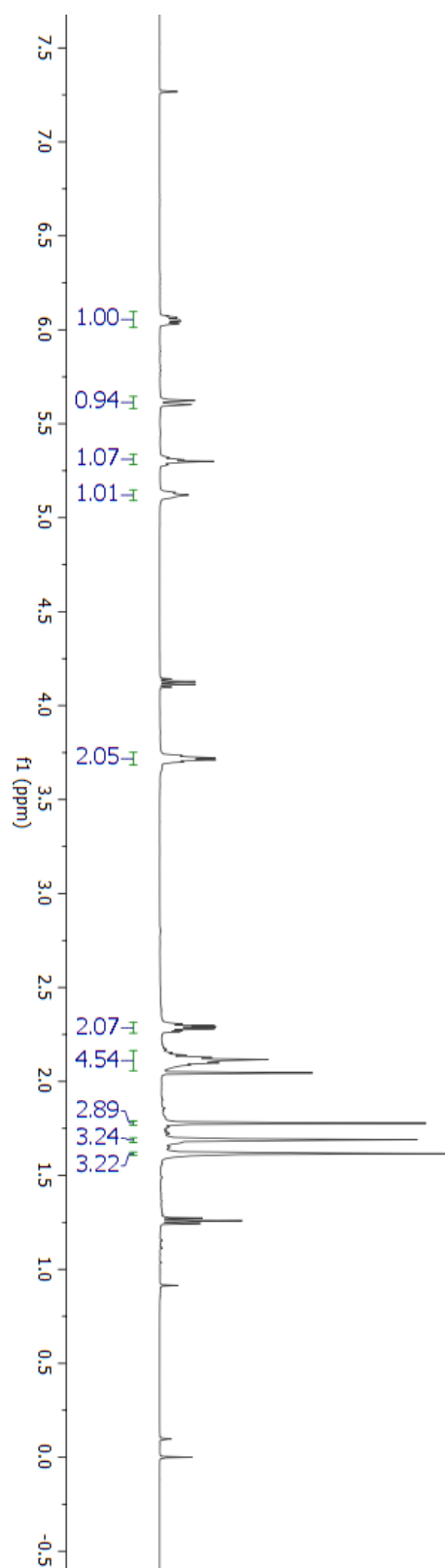
^{13}C -NMR for ROH Precursor to 5.14

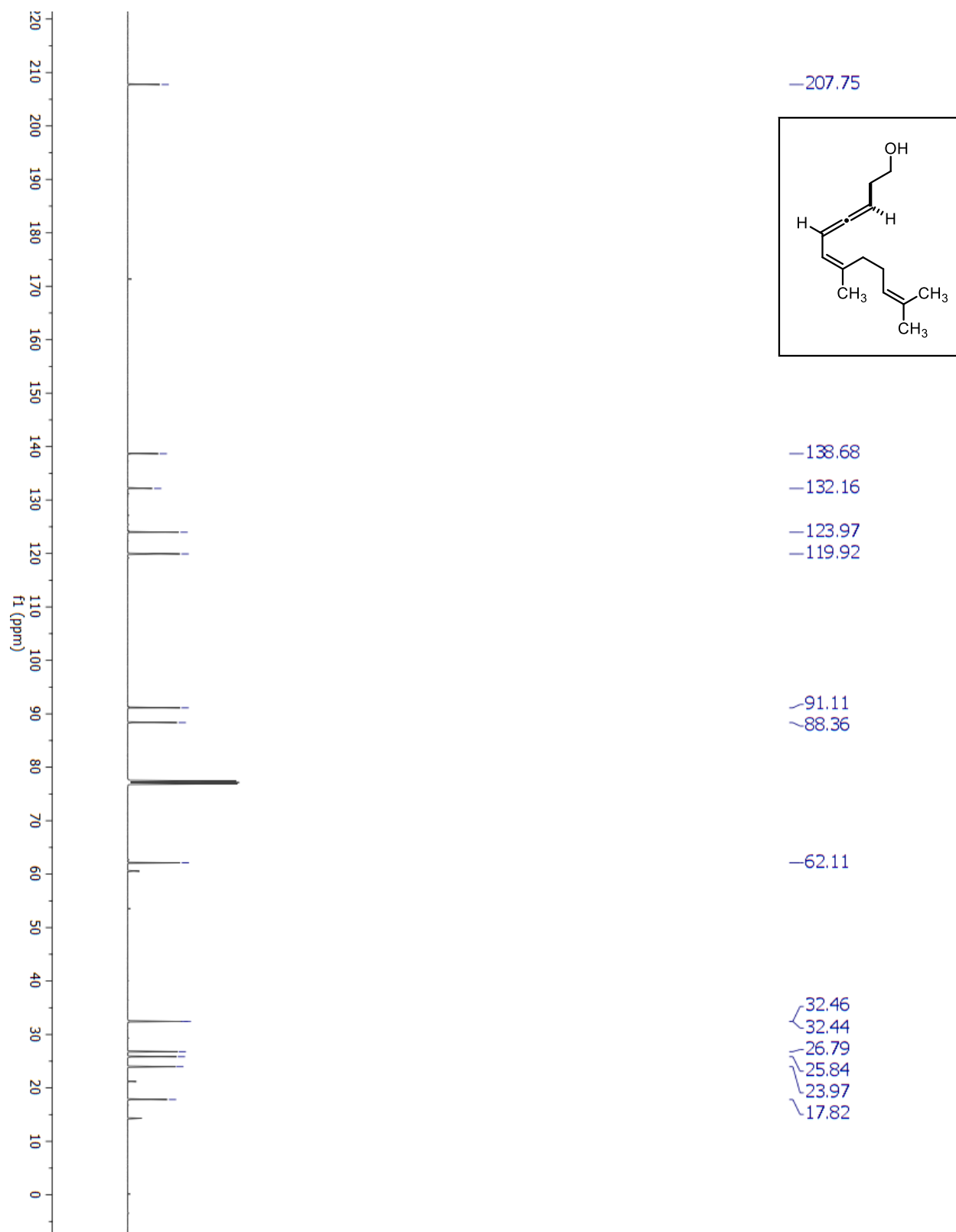
¹H-NMR for ROH Precursor to 5.15

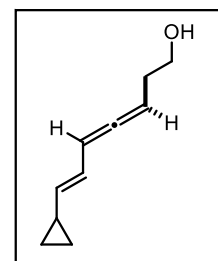
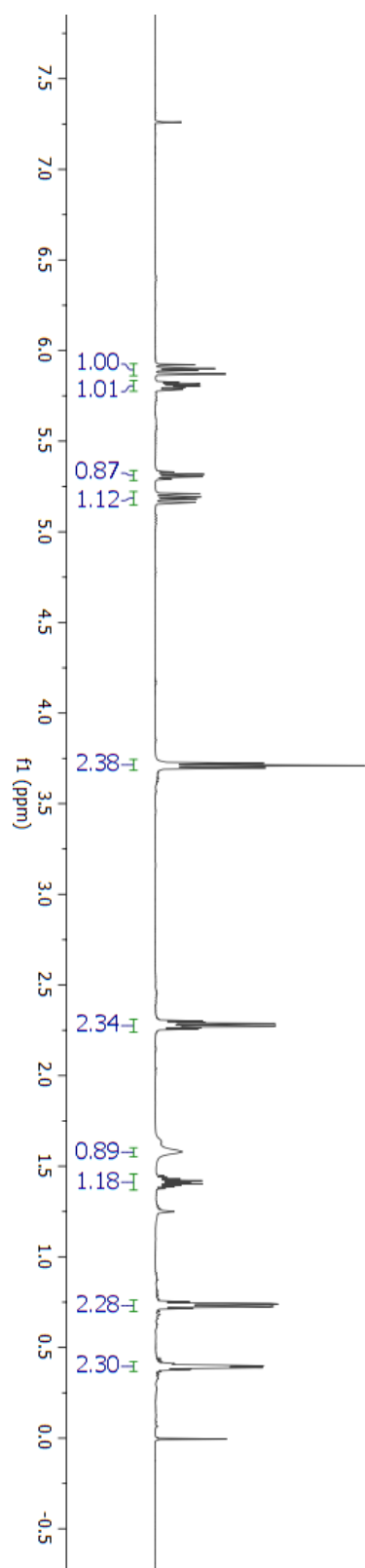
^{13}C -NMR for ROH Precursor to 5.15

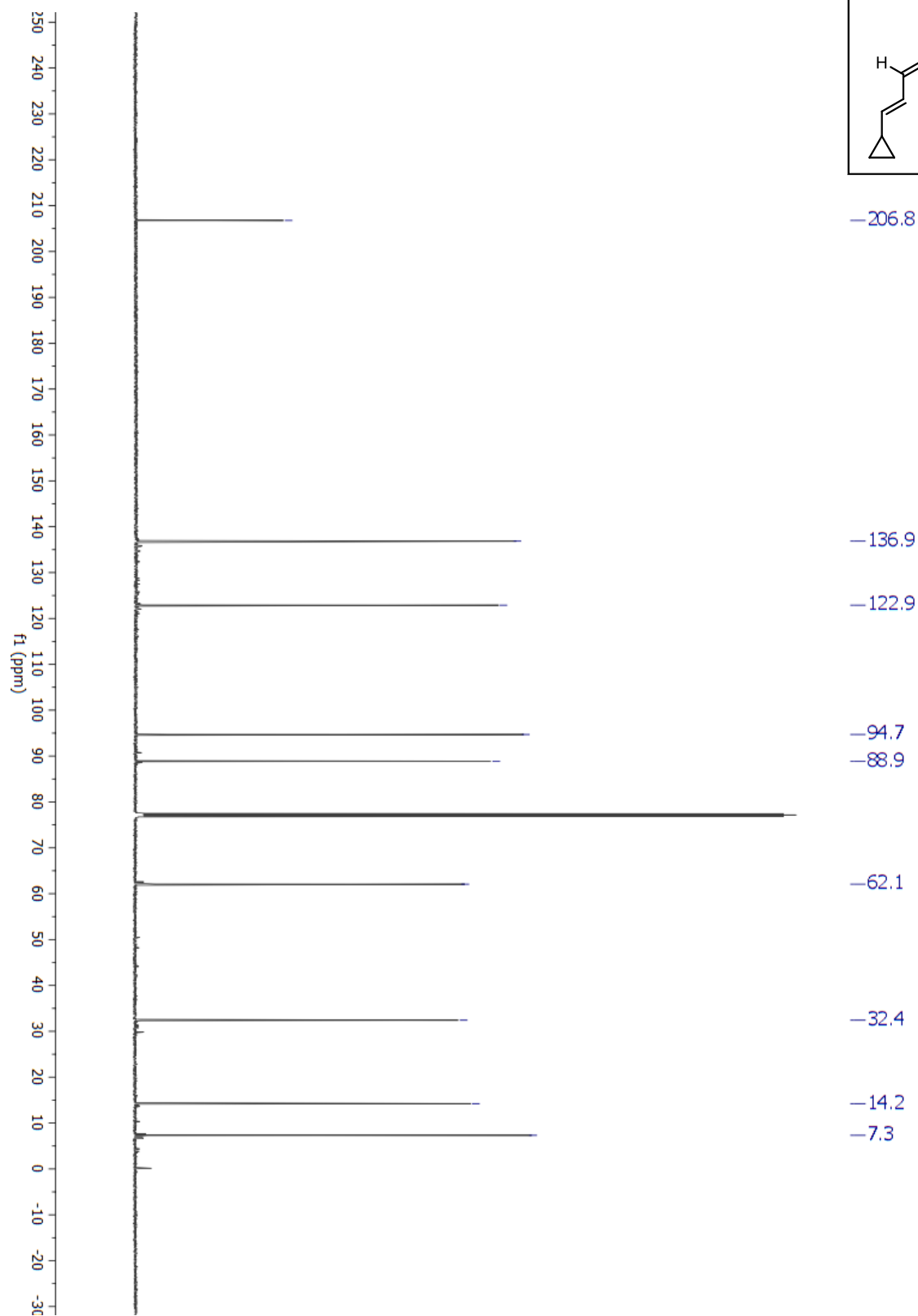
^1H -NMR for ROH Precursor to 5.16

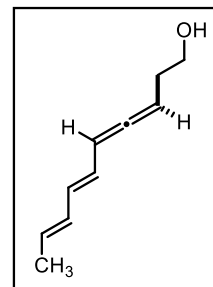
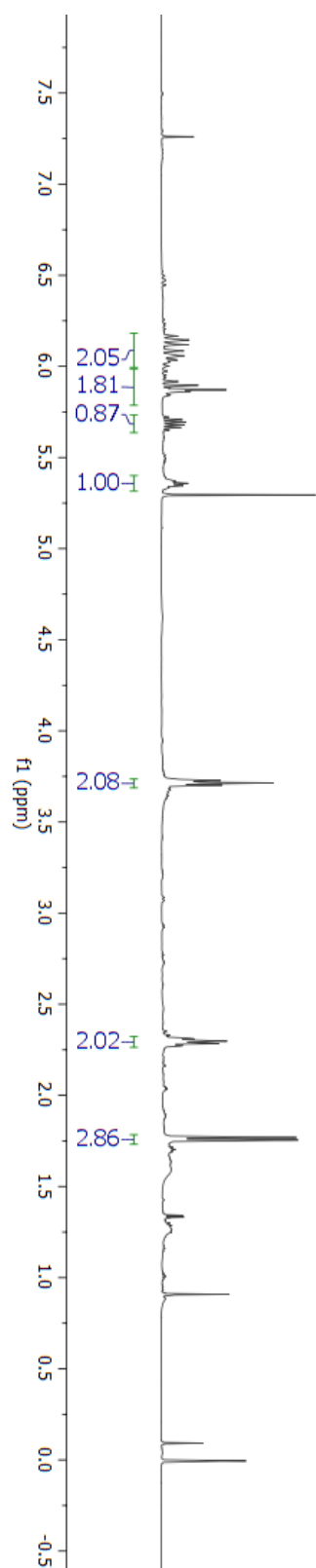
^{13}C -NMR for ROH Precursor to 5.16

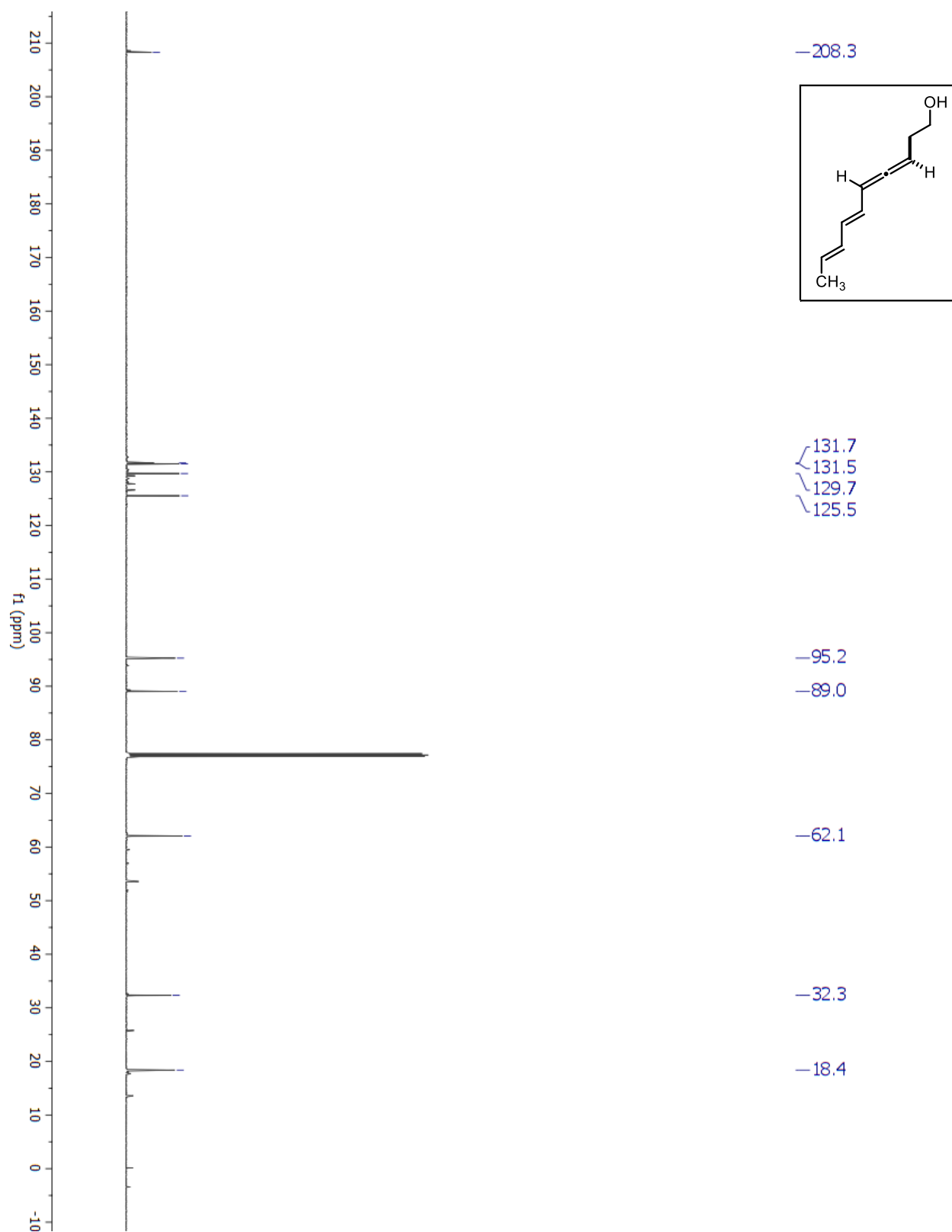
^1H -NMR for ROH Precursor to 5.17

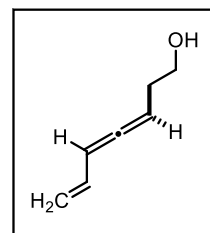
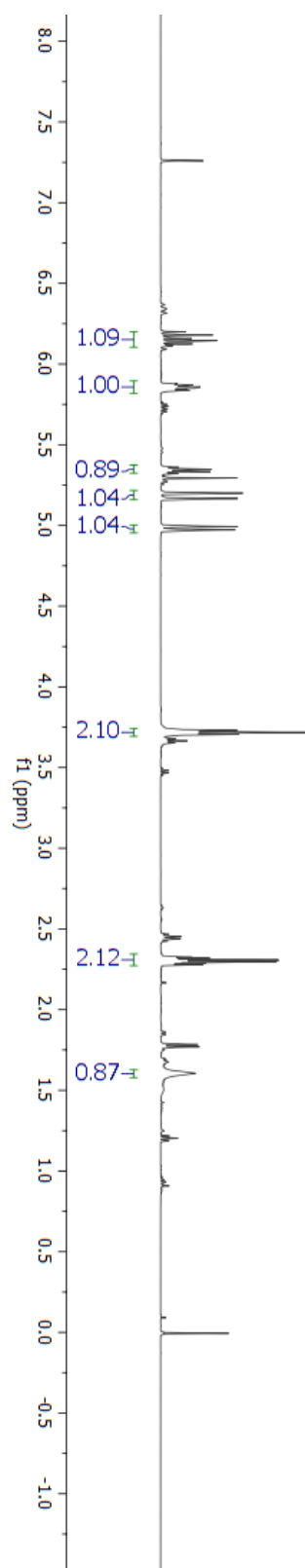
^{13}C -NMR for ROH Precursor to 5.17

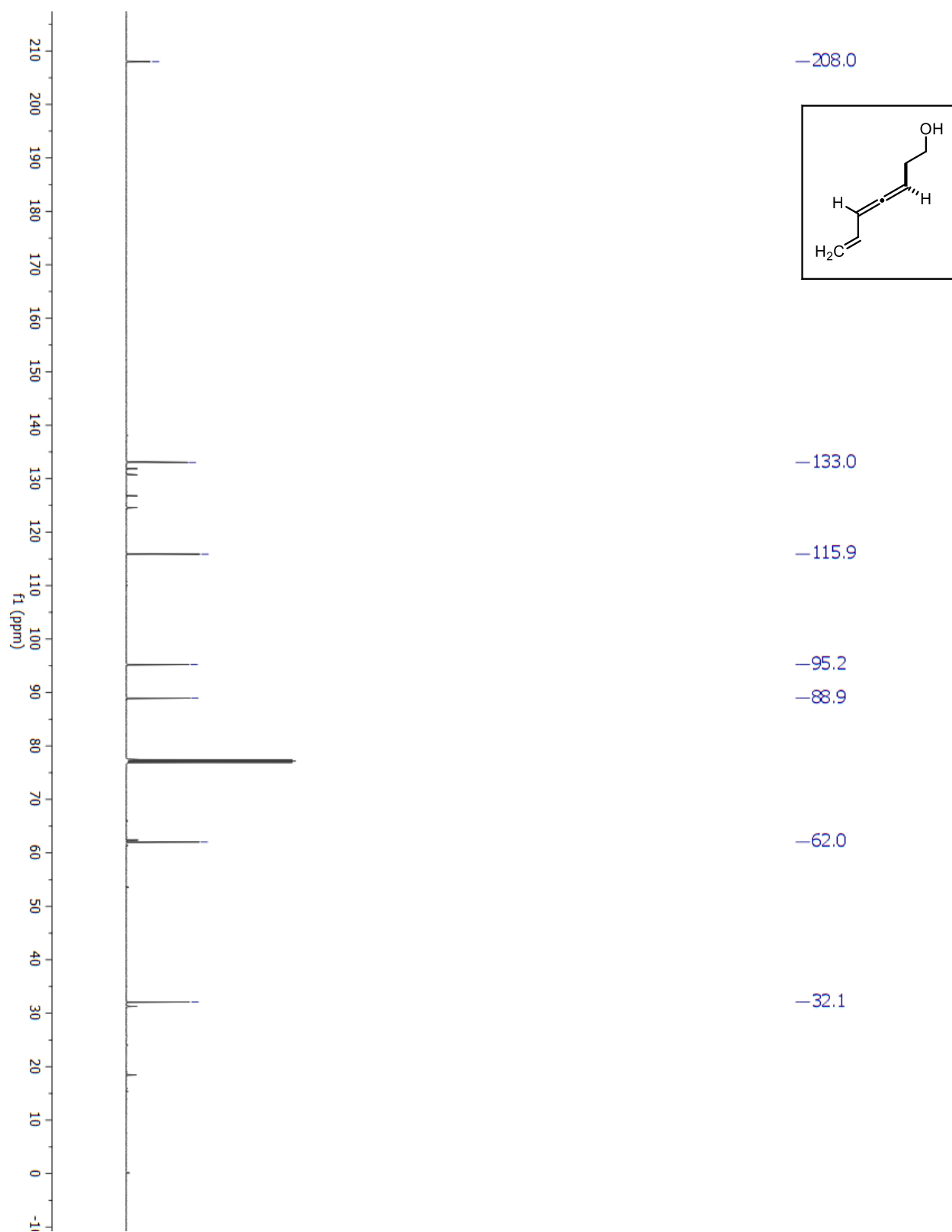
¹H-NMR for ROH Precursor to 5.18

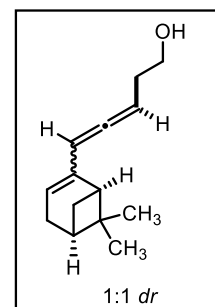
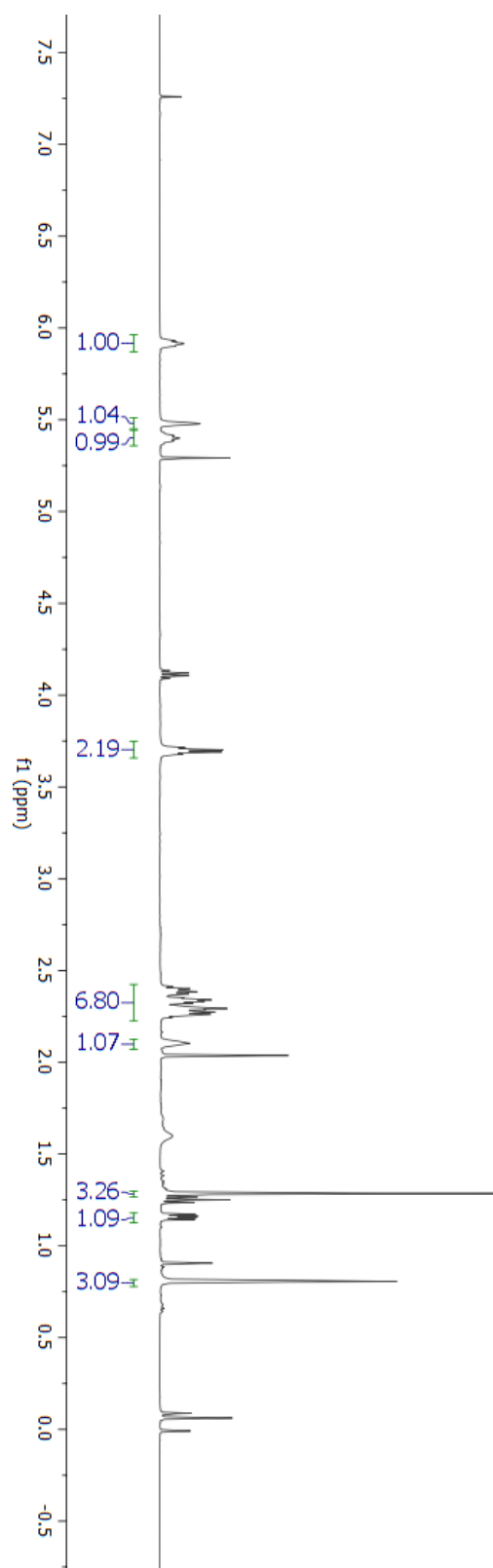
^{13}C -NMR for ROH Precursor to 5.18

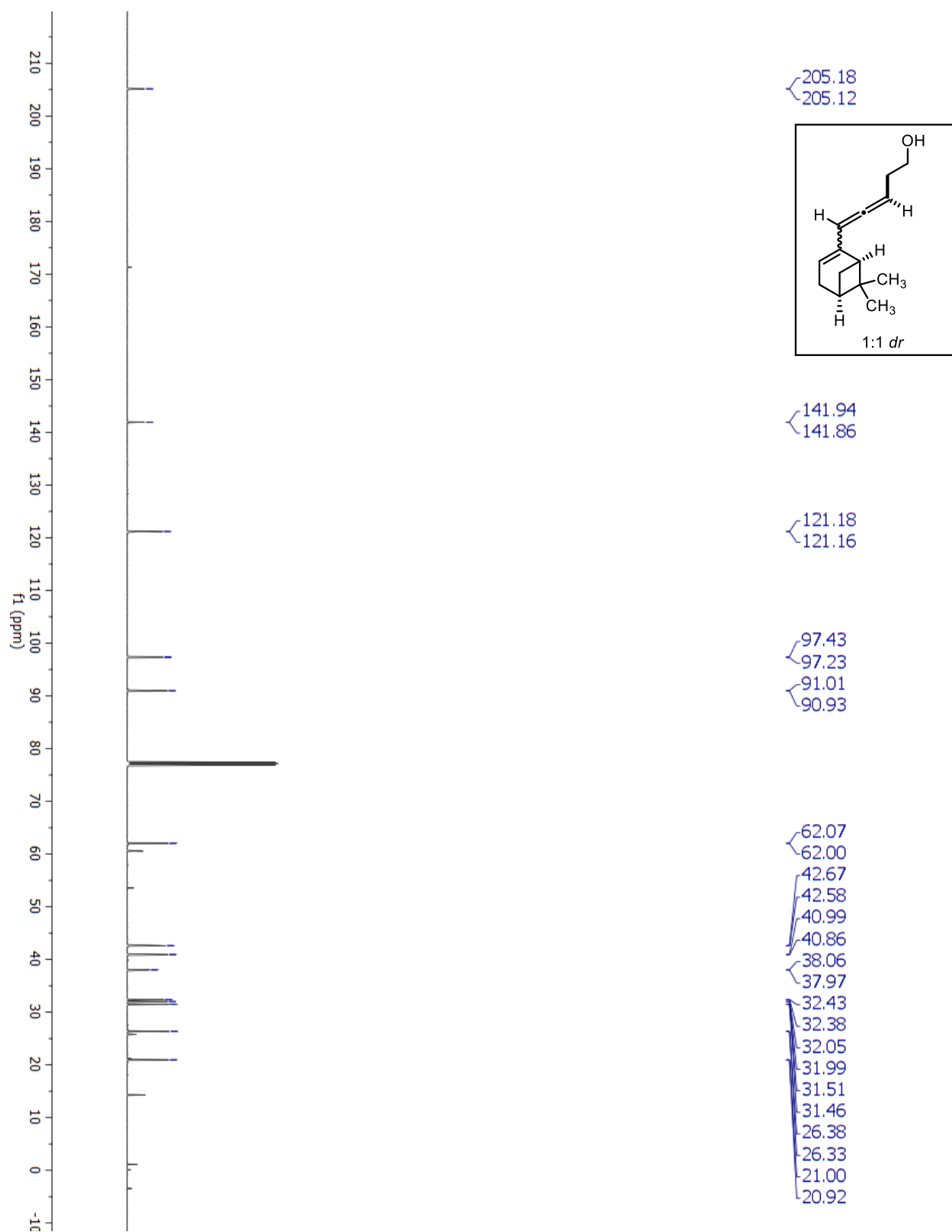
¹H-NMR for ROH Precursor to 5.19

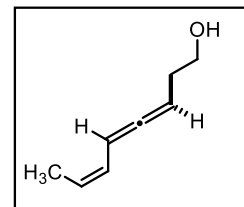
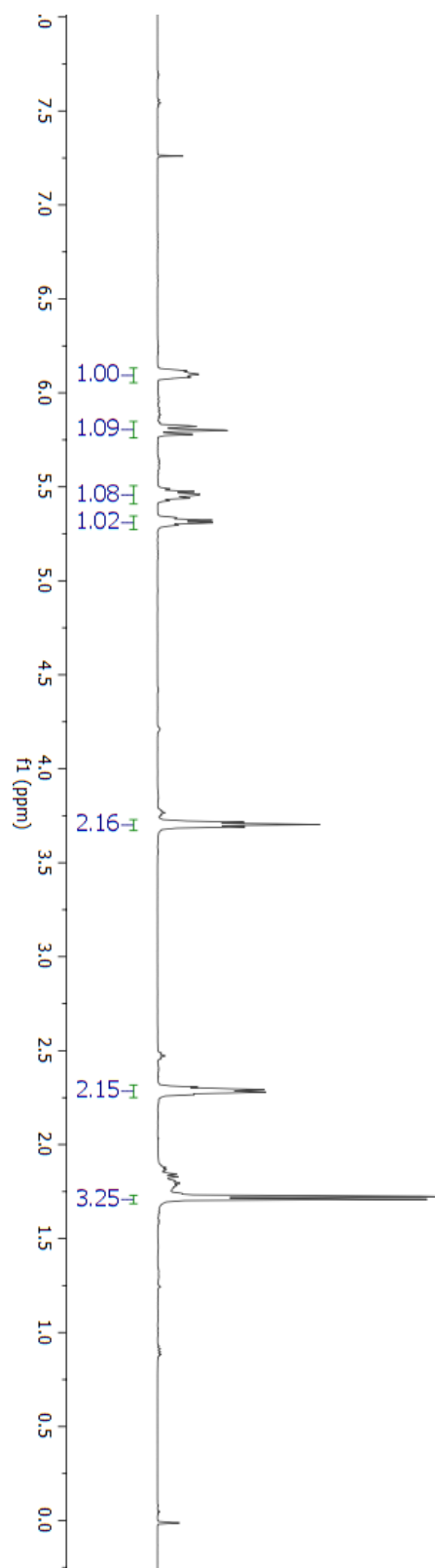
^{13}C -NMR for ROH Precursor to 5.19

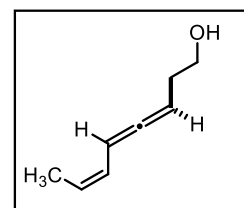
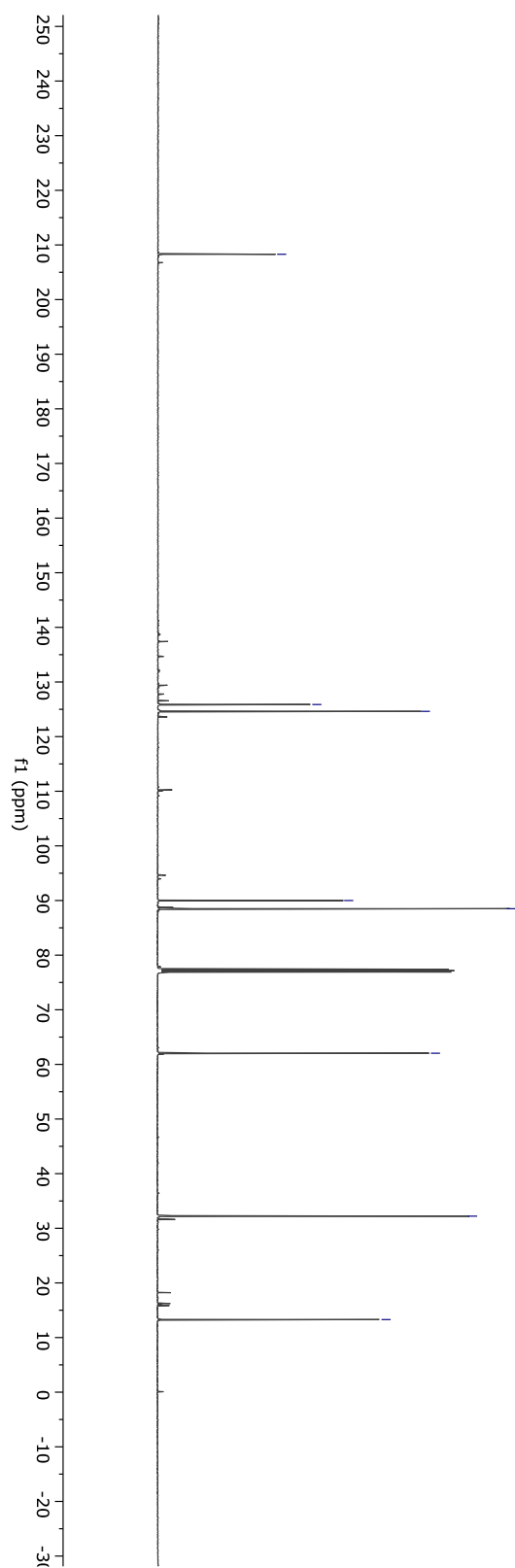
^1H -NMR for ROH Precursor to 5.20

^{13}C -NMR for ROH Precursor to 5.20

¹H-NMR for ROH Precursor to 5.21

^{13}C -NMR for ROH Precursor to 5.21

¹H-NMR for ROH Precursor to 5.5

^{13}C -NMR for ROH Precursor to 5.5

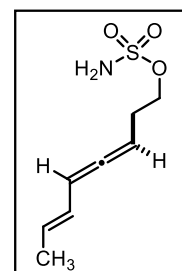
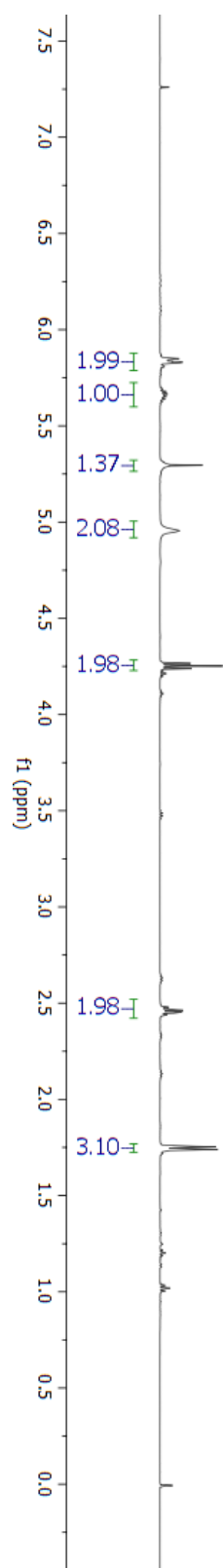
— 208.3

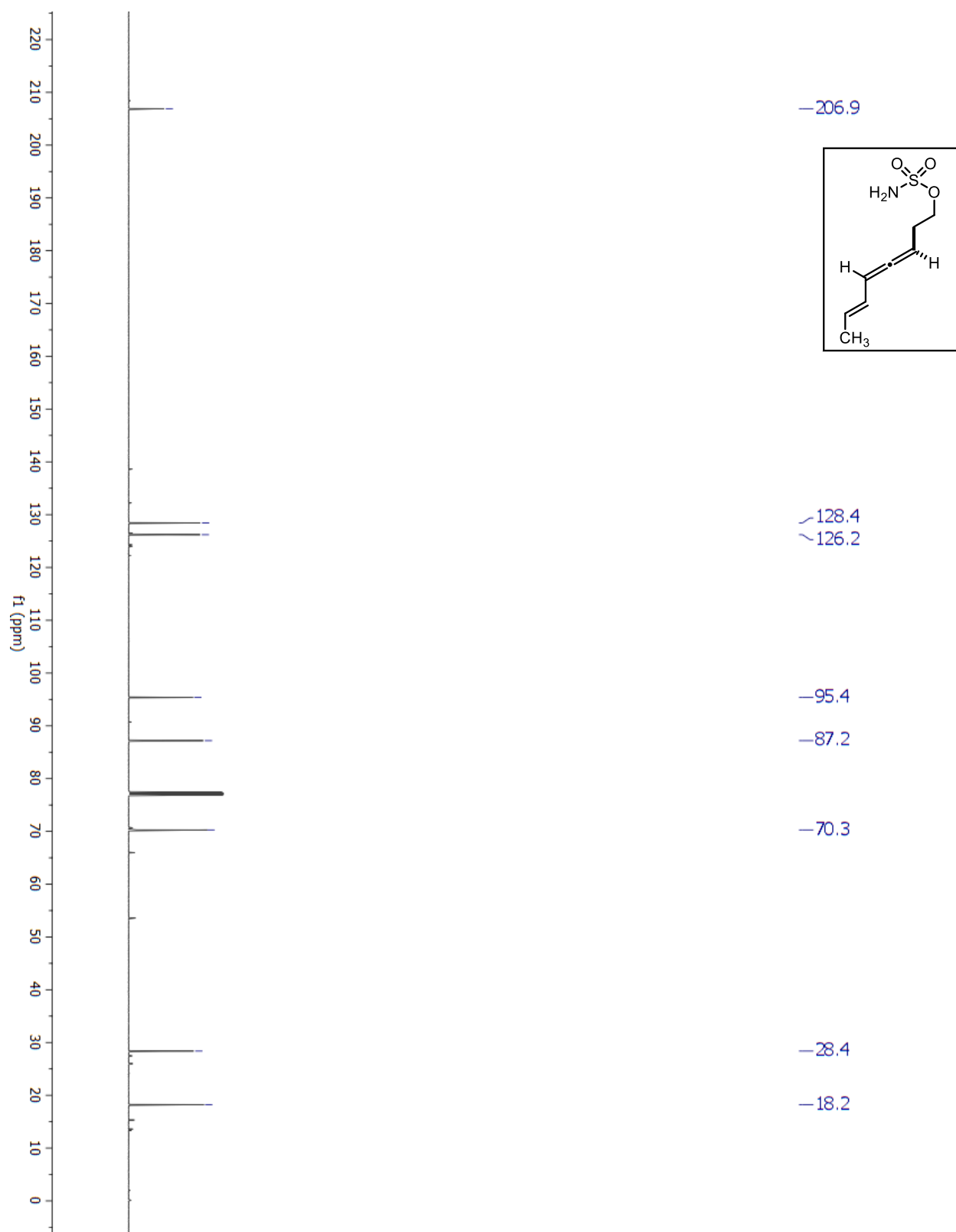
~ 125.9
~ 124.6~ 90.0
~ 88.5

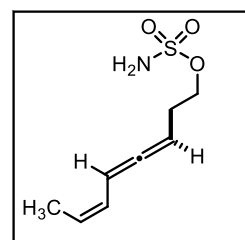
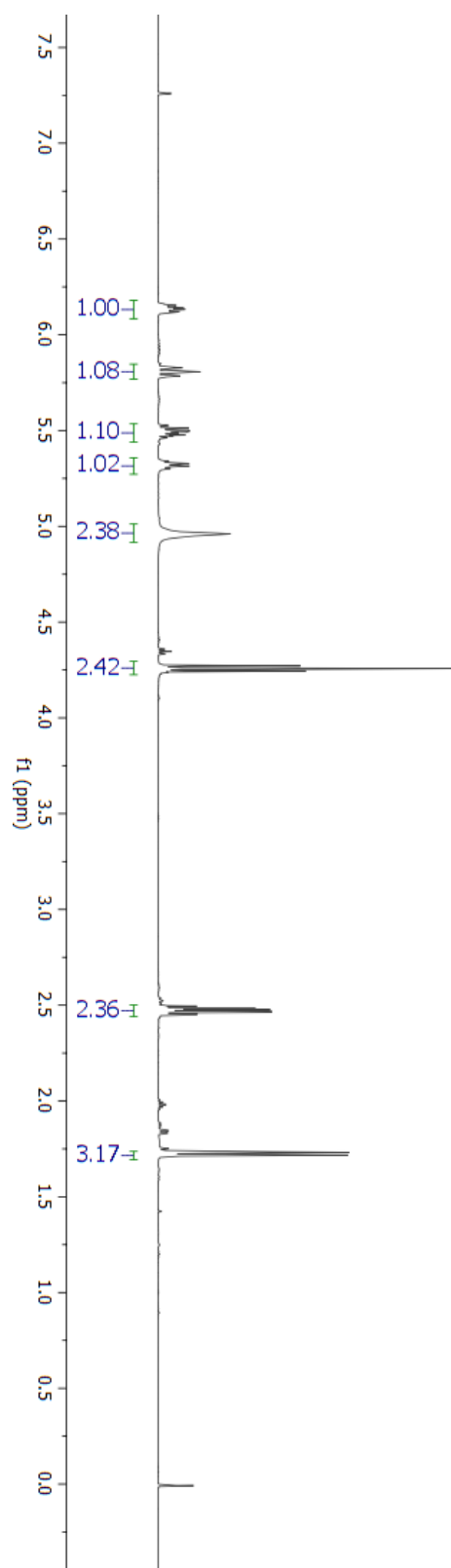
— 62.0

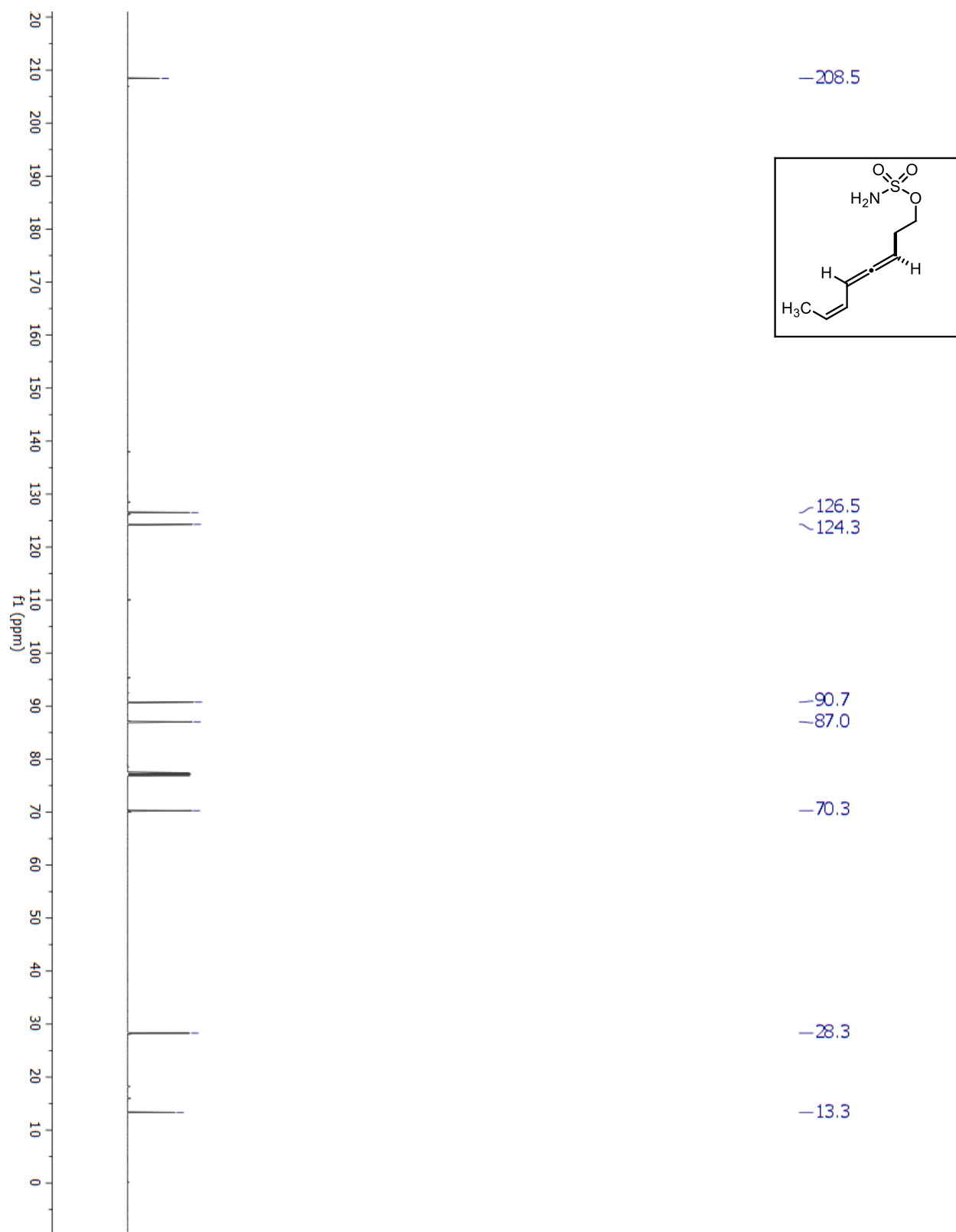
— 32.2

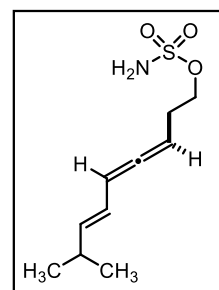
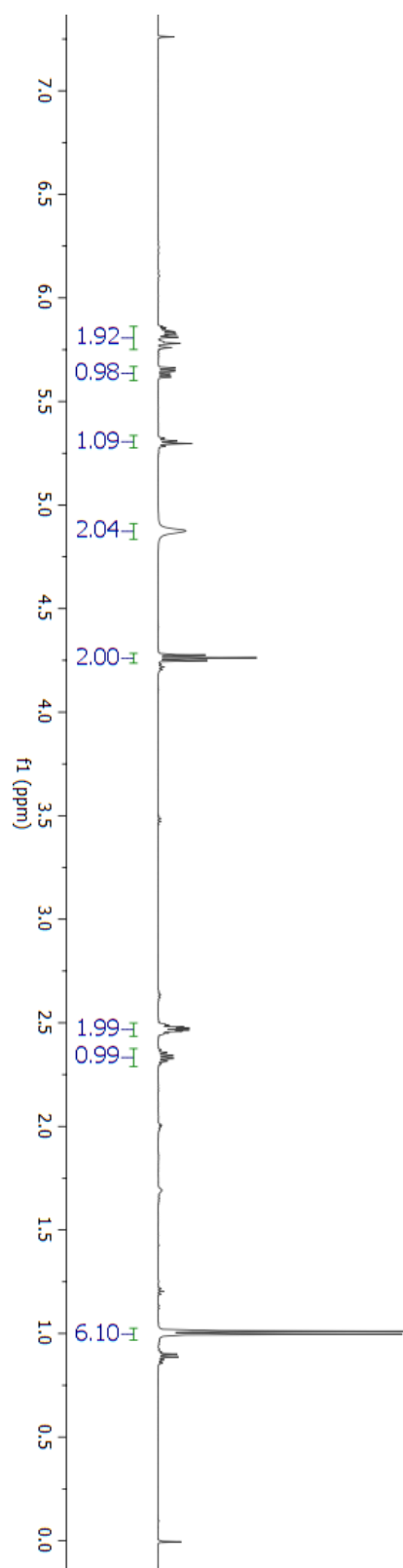
— 13.3

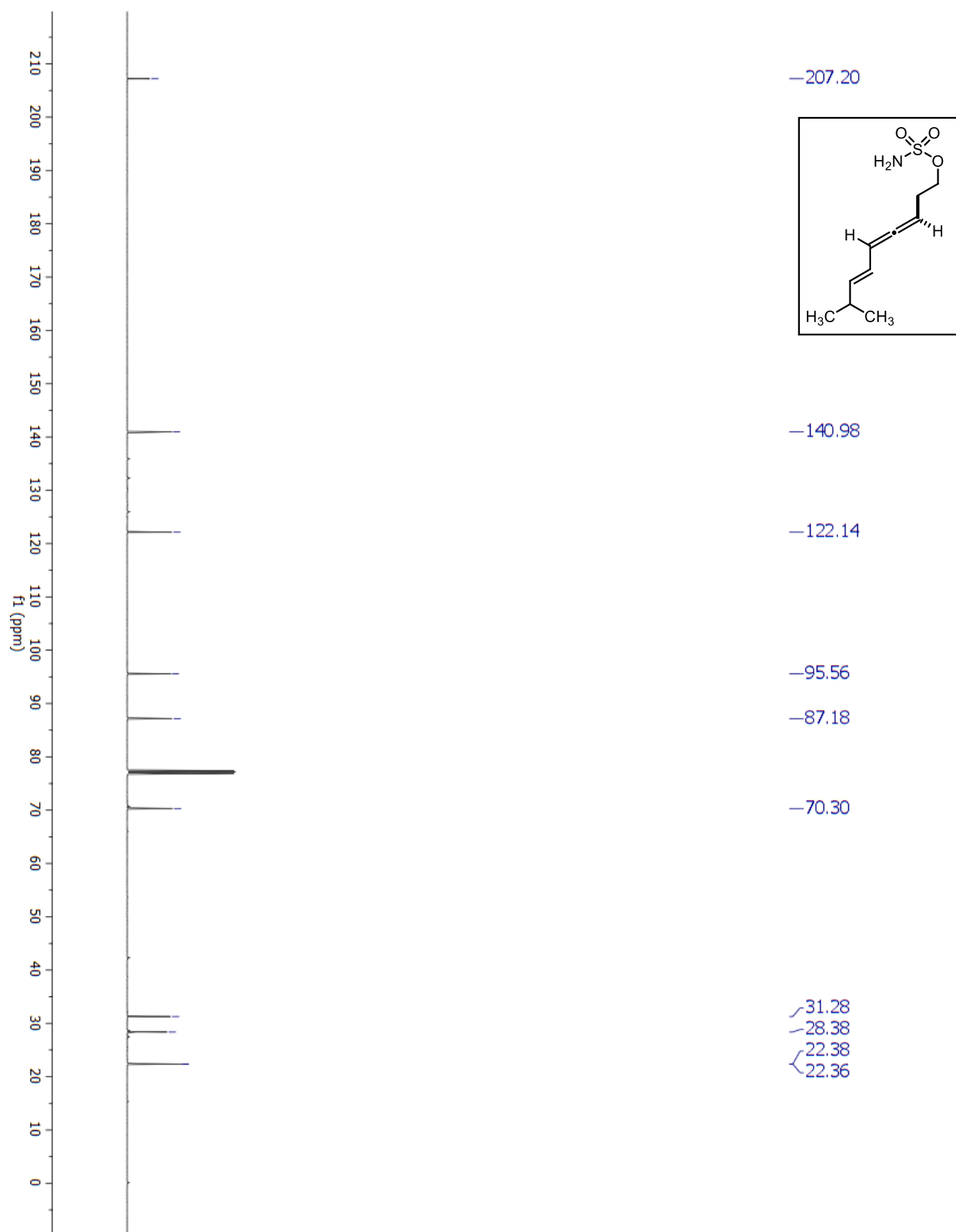
^1H -NMR for Compound 5.4

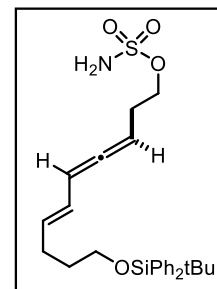
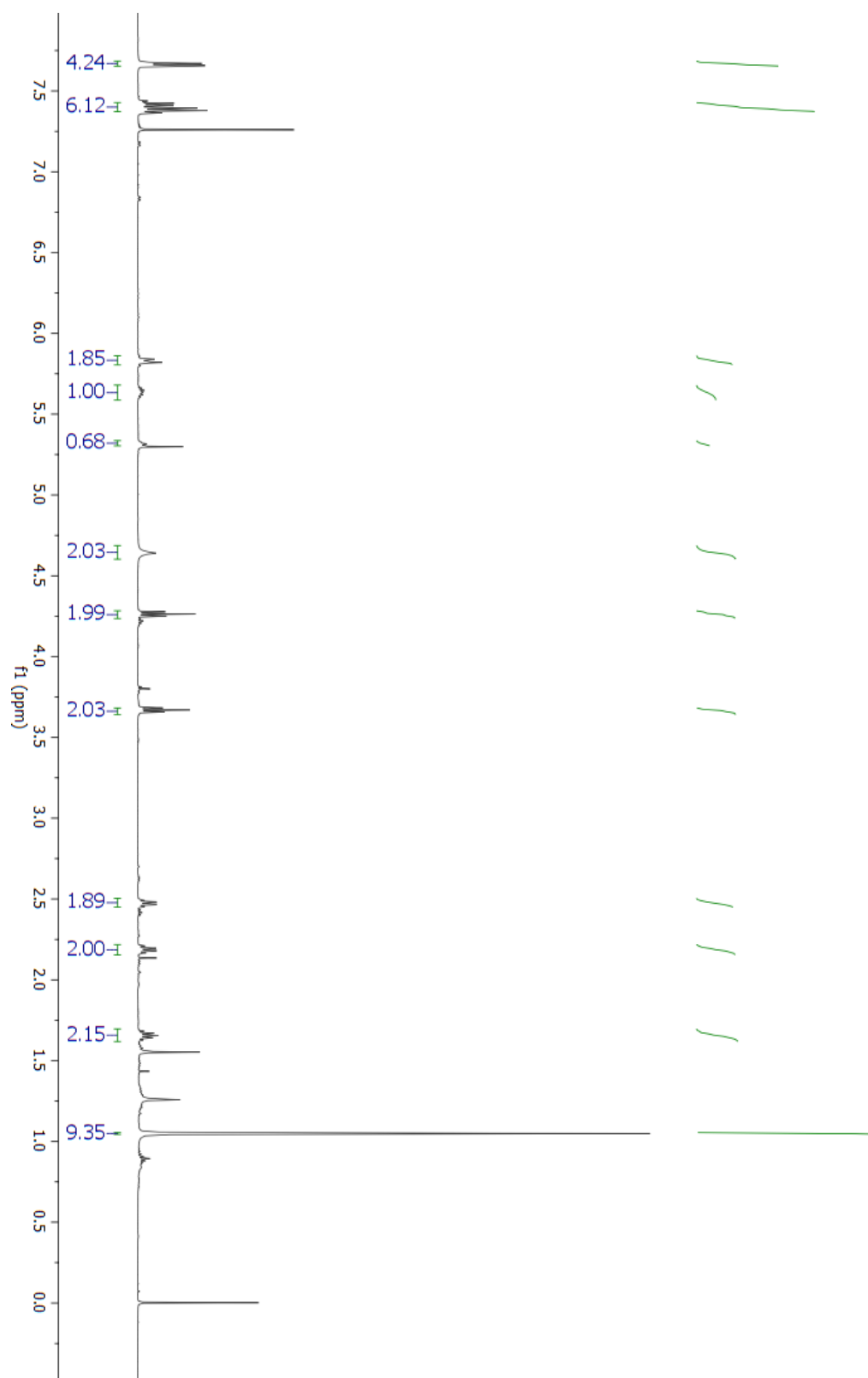
^{13}C -NMR for Compound 5.4

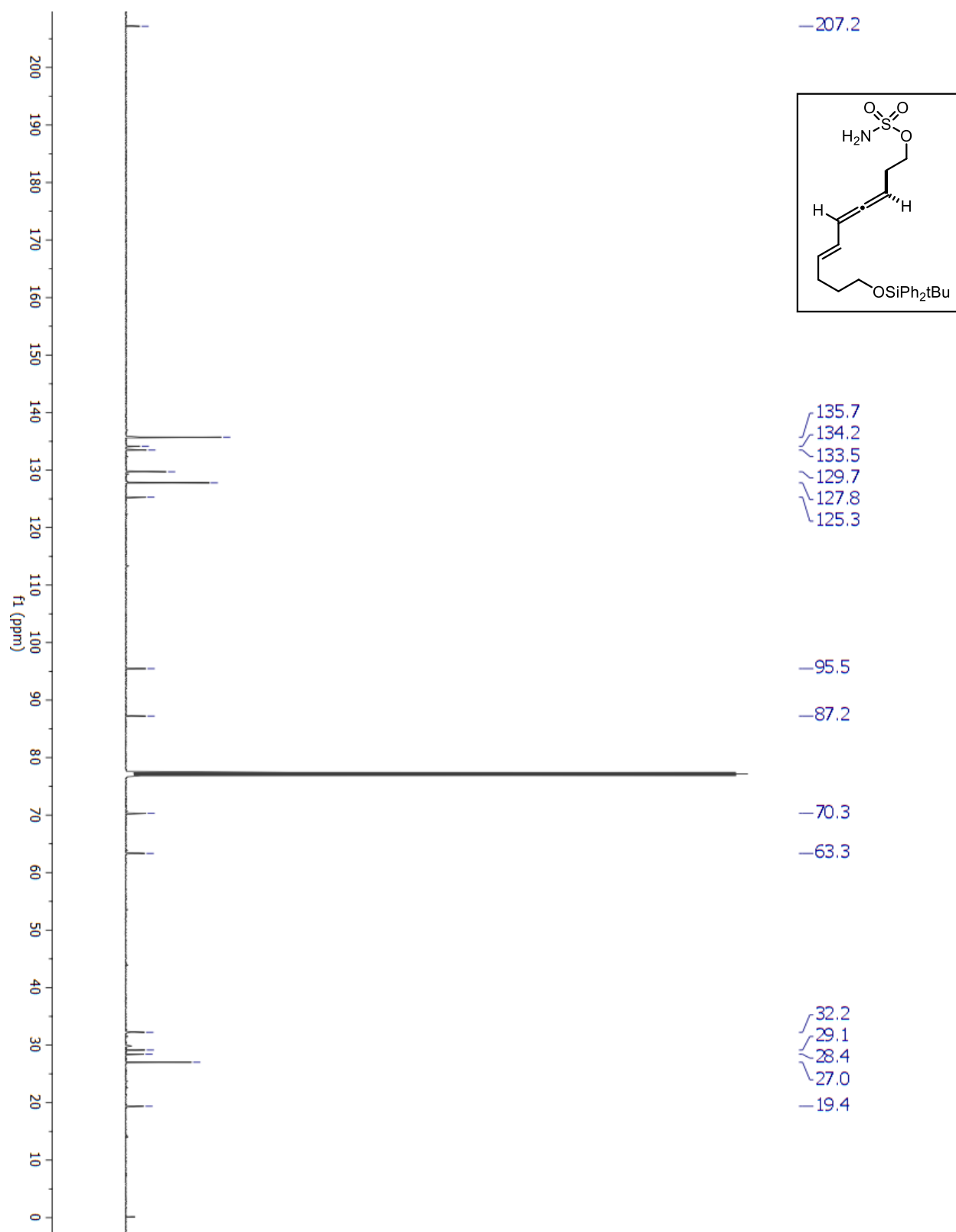
¹H-NMR for Compound 5.5

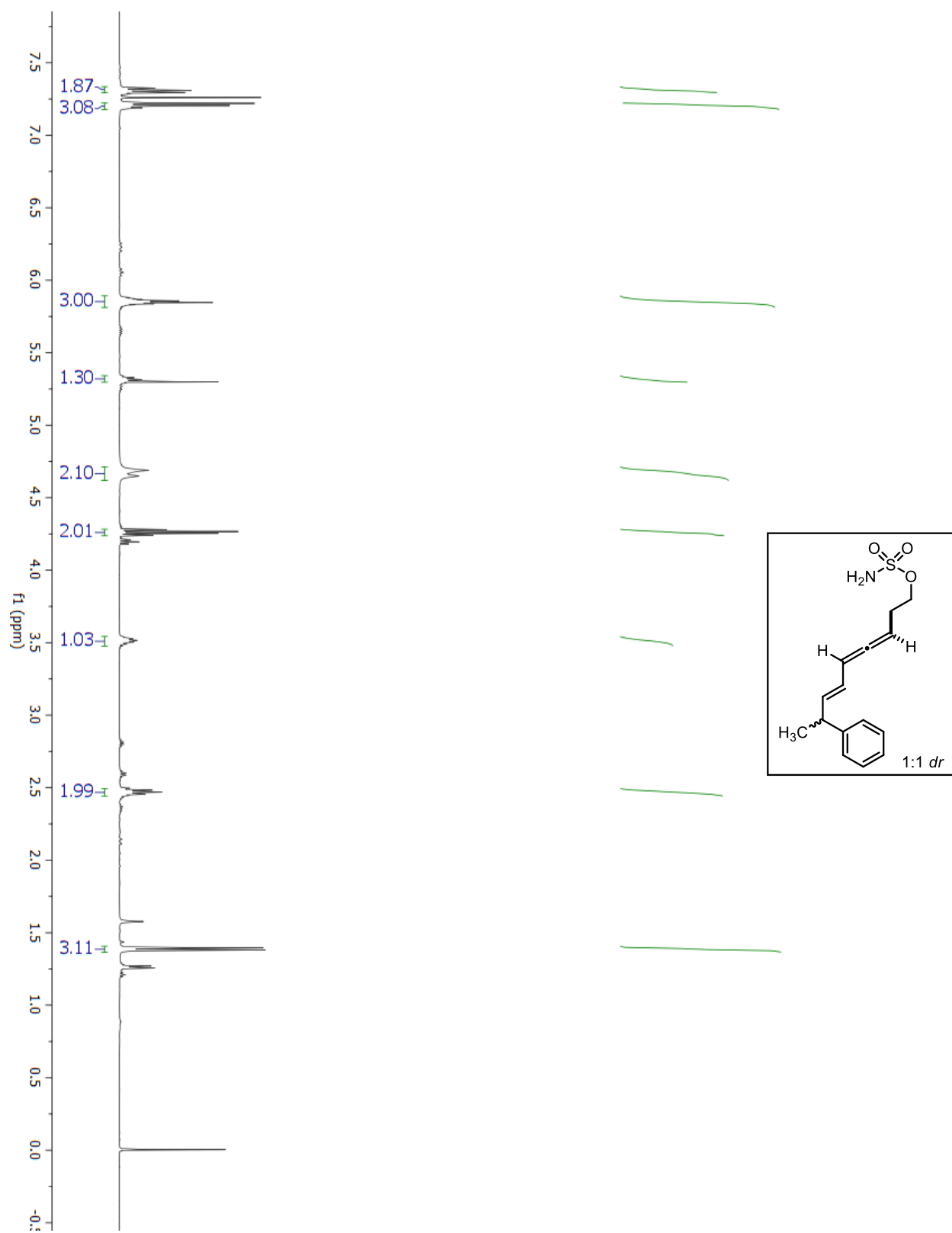
^{13}C -NMR for Compound 5.5

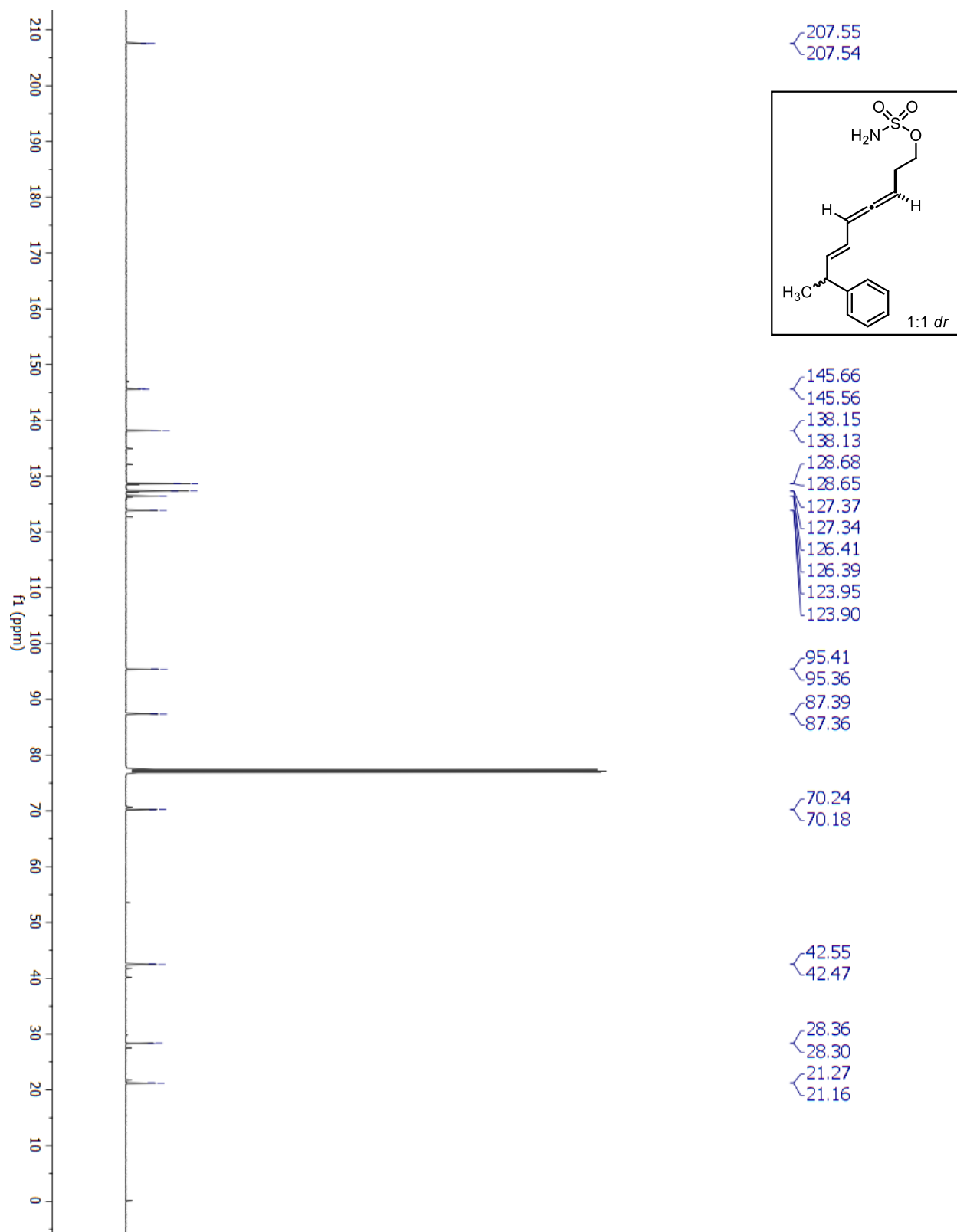
¹H-NMR for Compound 5.6

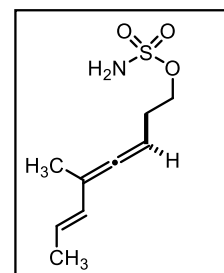
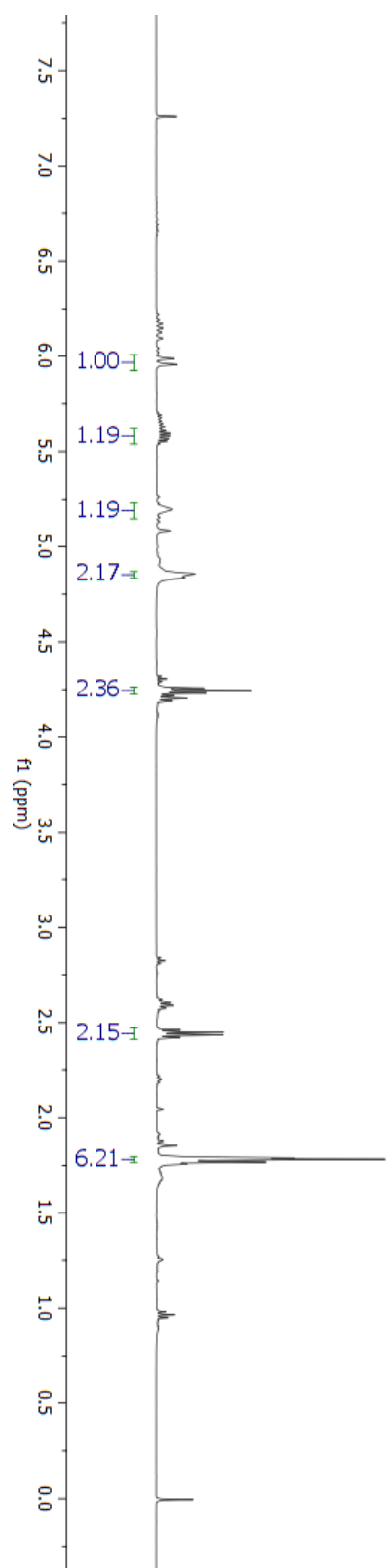
^{13}C -NMR for Compound 5.6

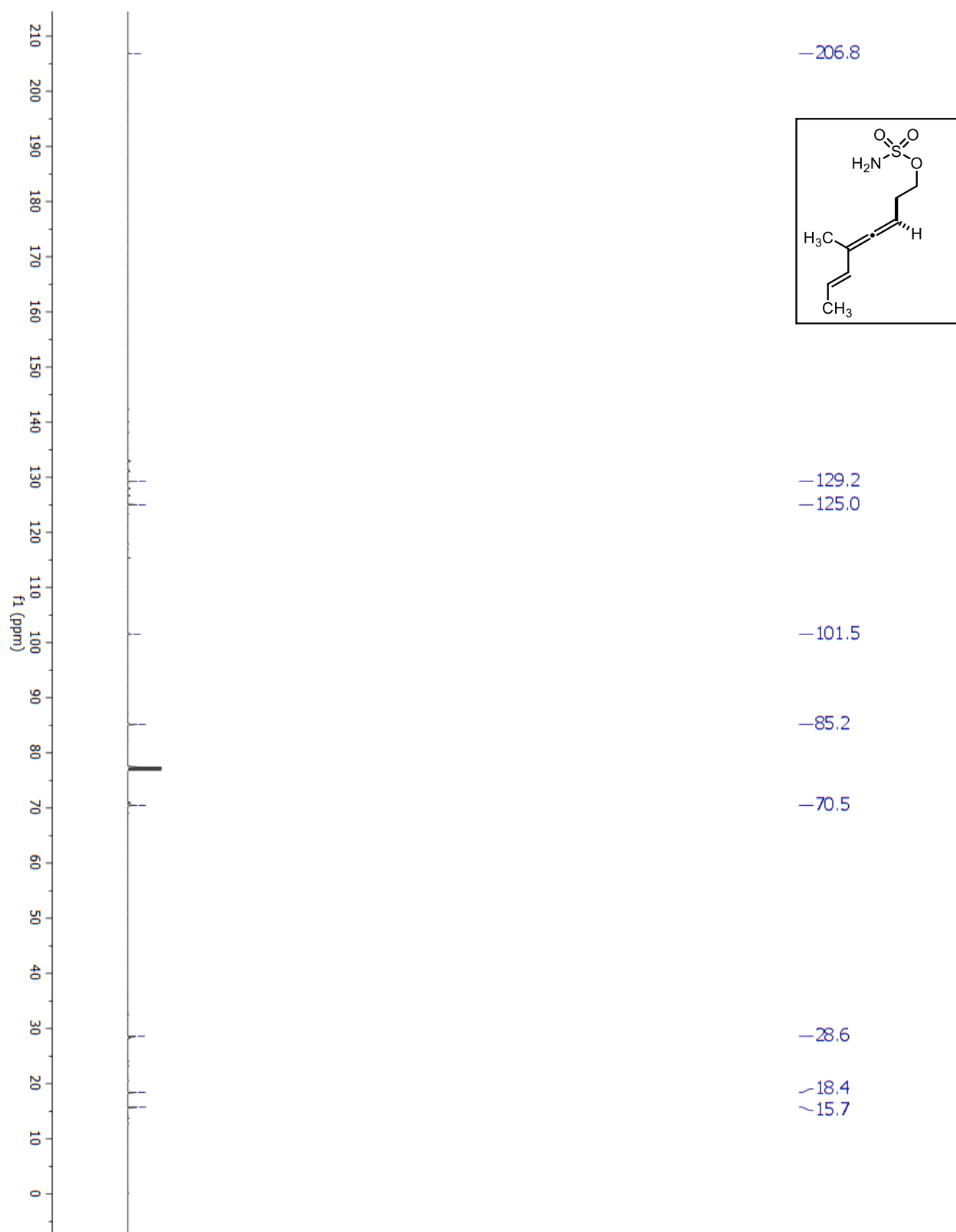
¹H-NMR for Compound 5.7

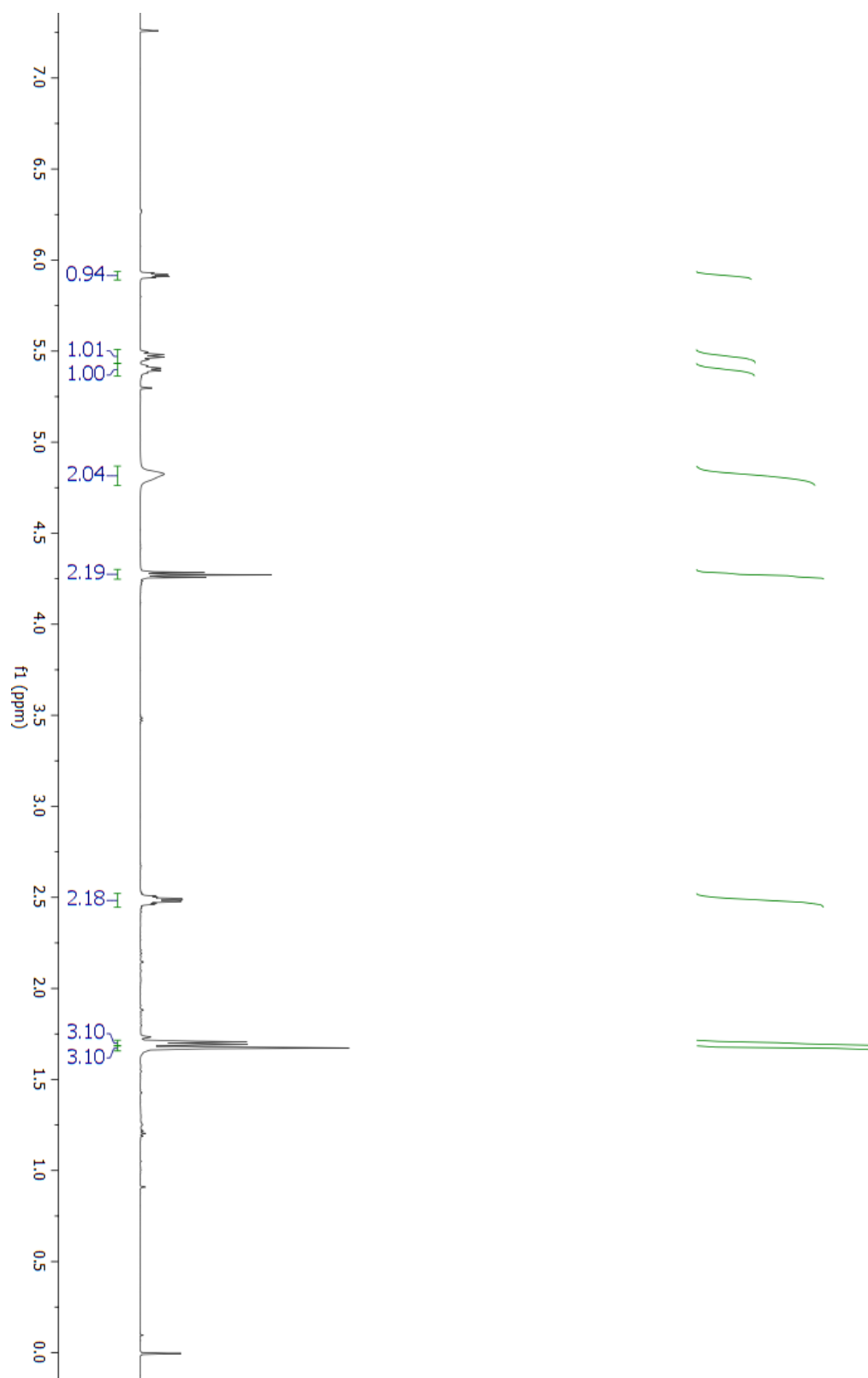
^{13}C -NMR for Compound 5.7

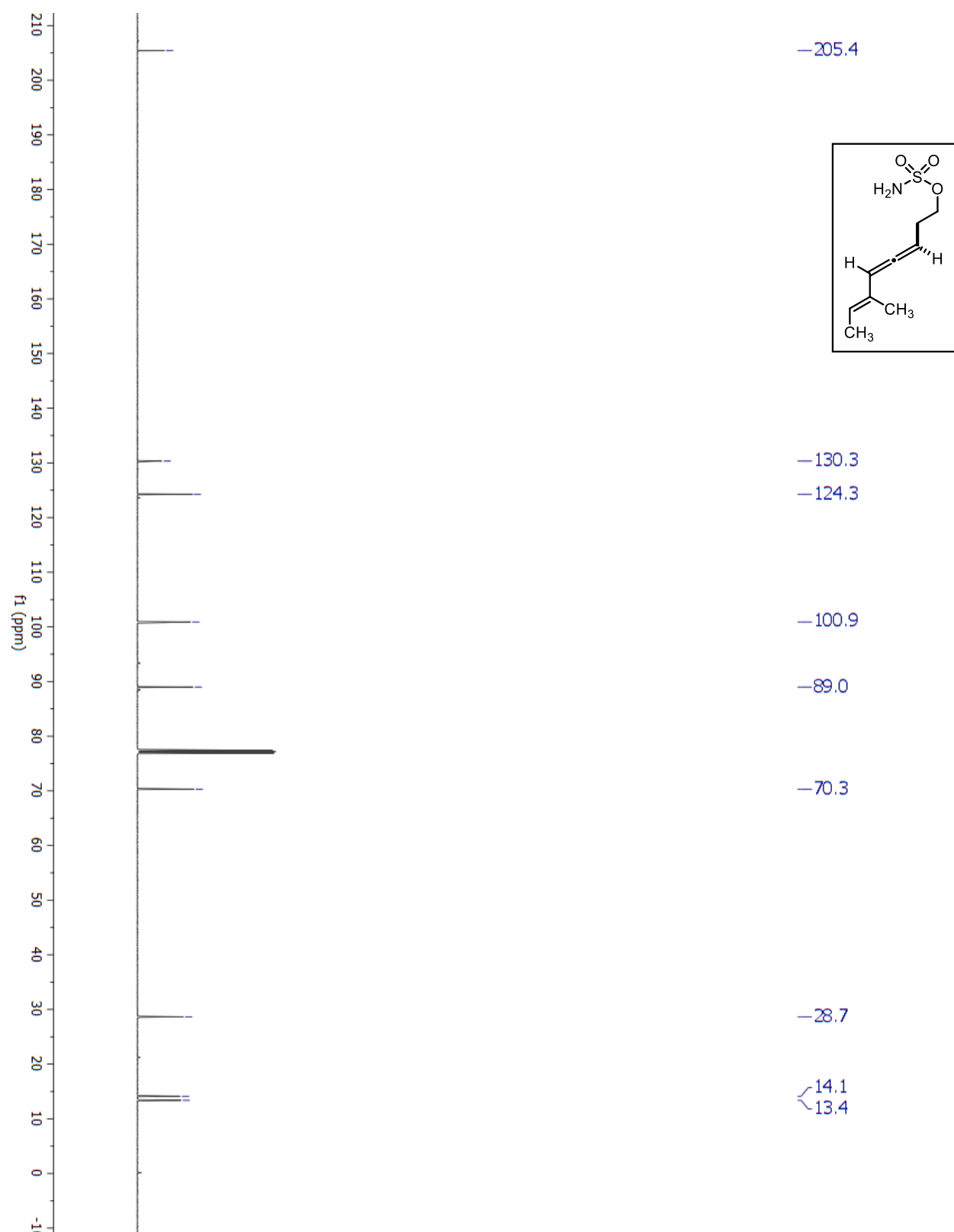
¹H-NMR for Compound 5.8

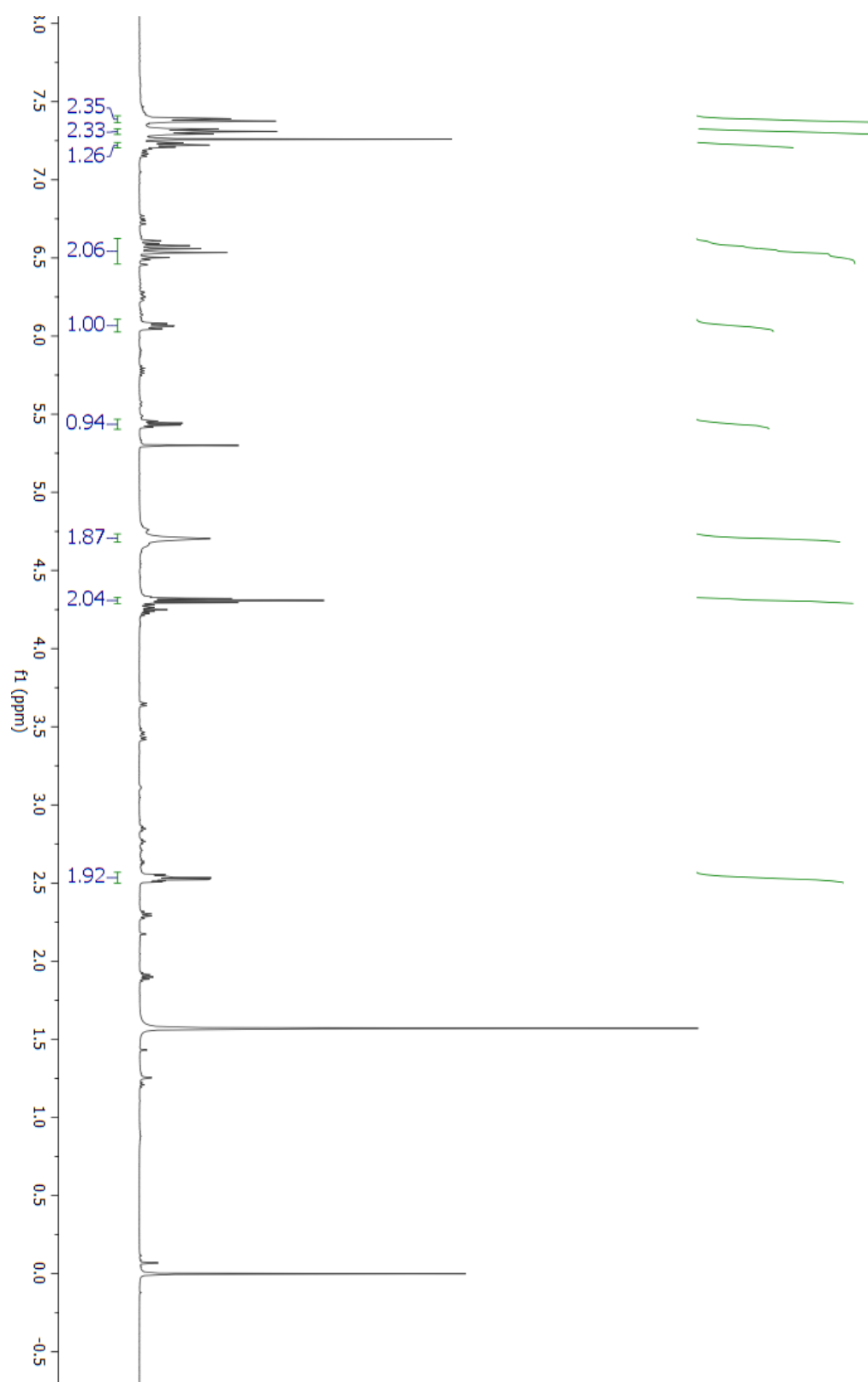
^{13}C -NMR for Compound 5.8

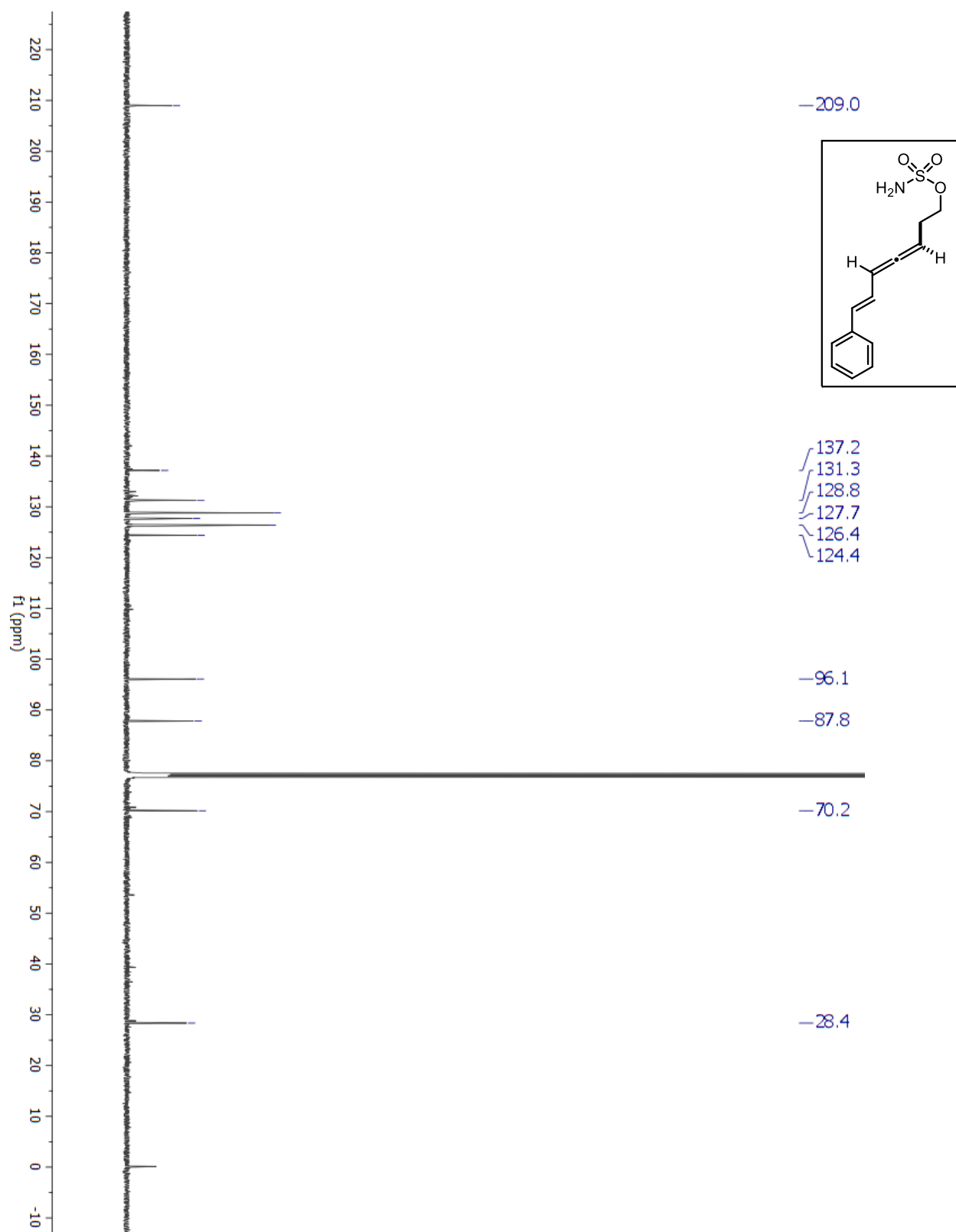
¹H-NMR for Compound 5.9

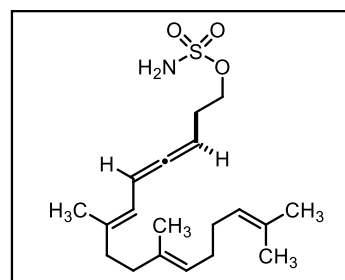
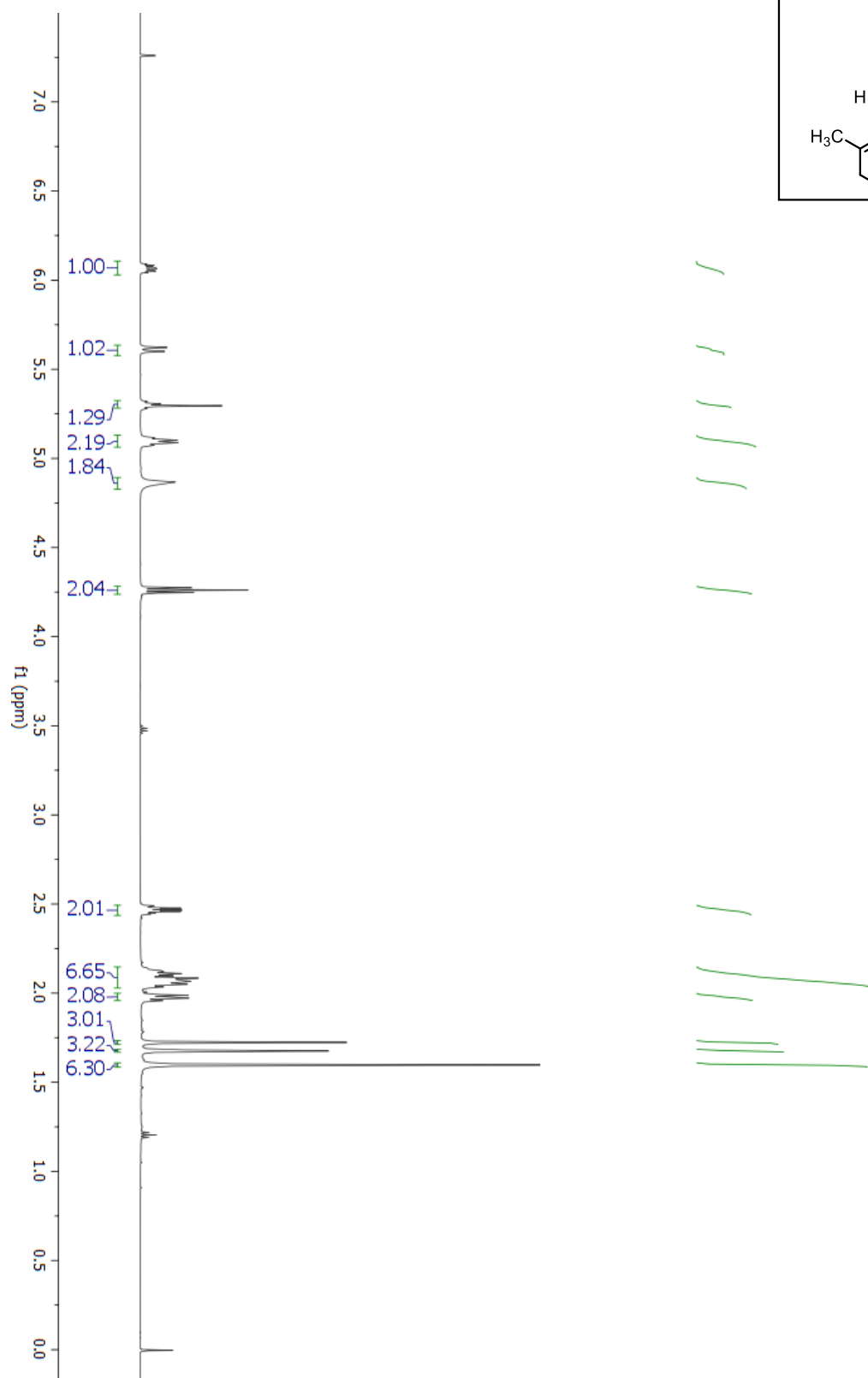
^{13}C -NMR for Compound 5.9

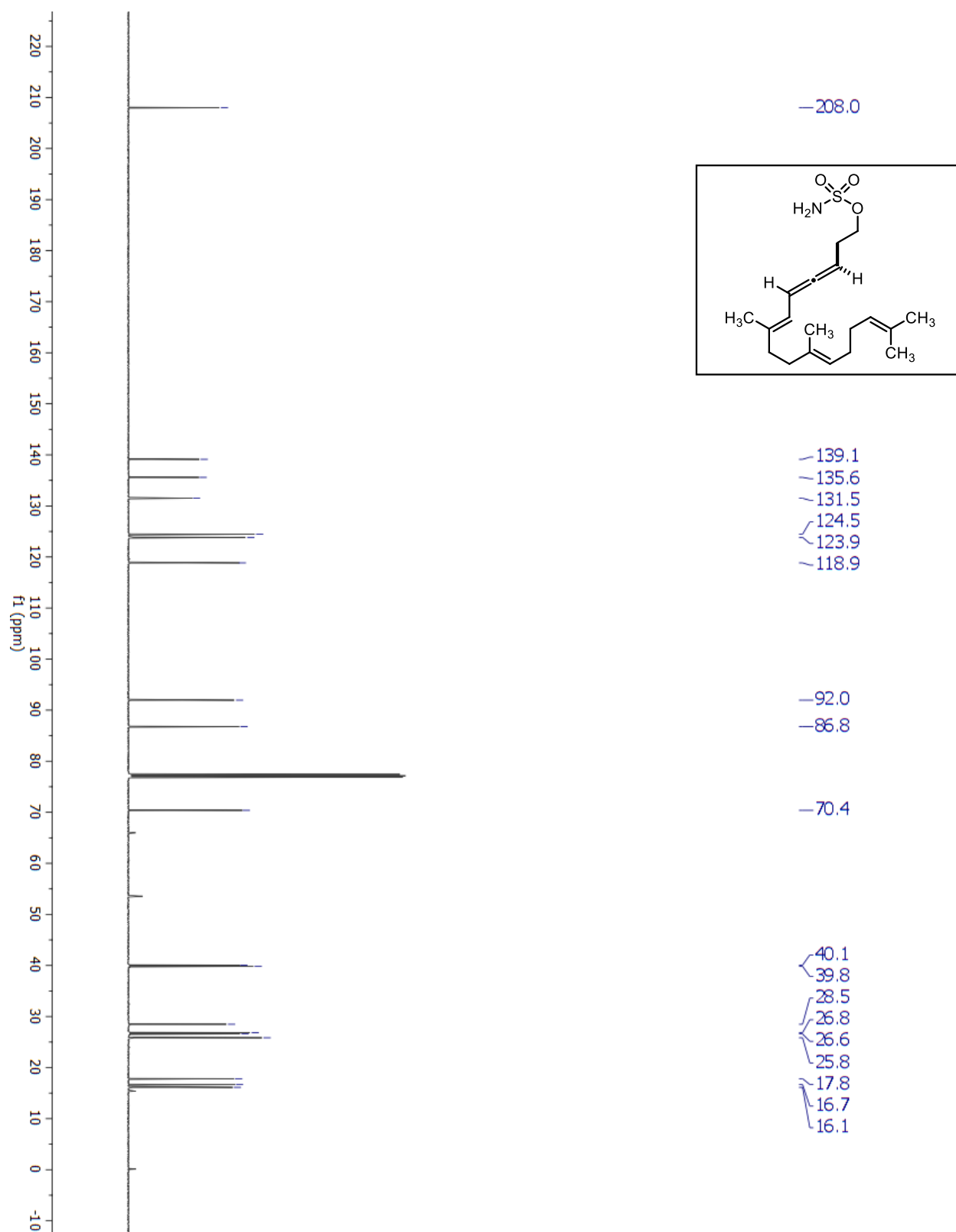
¹H-NMR for Compound 5.10

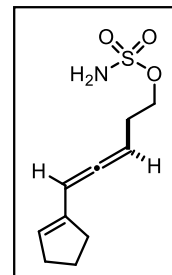
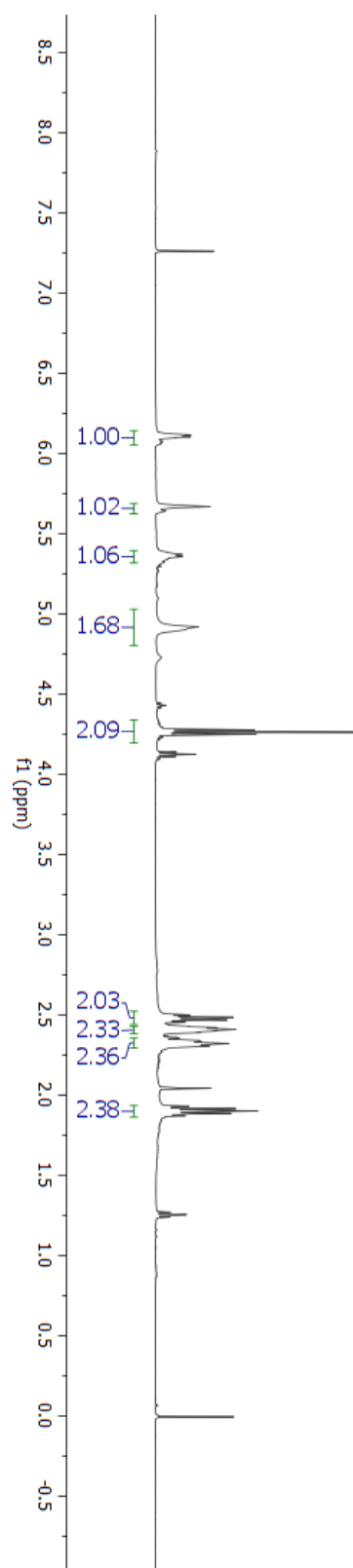
^{13}C -NMR for Compound 5.10

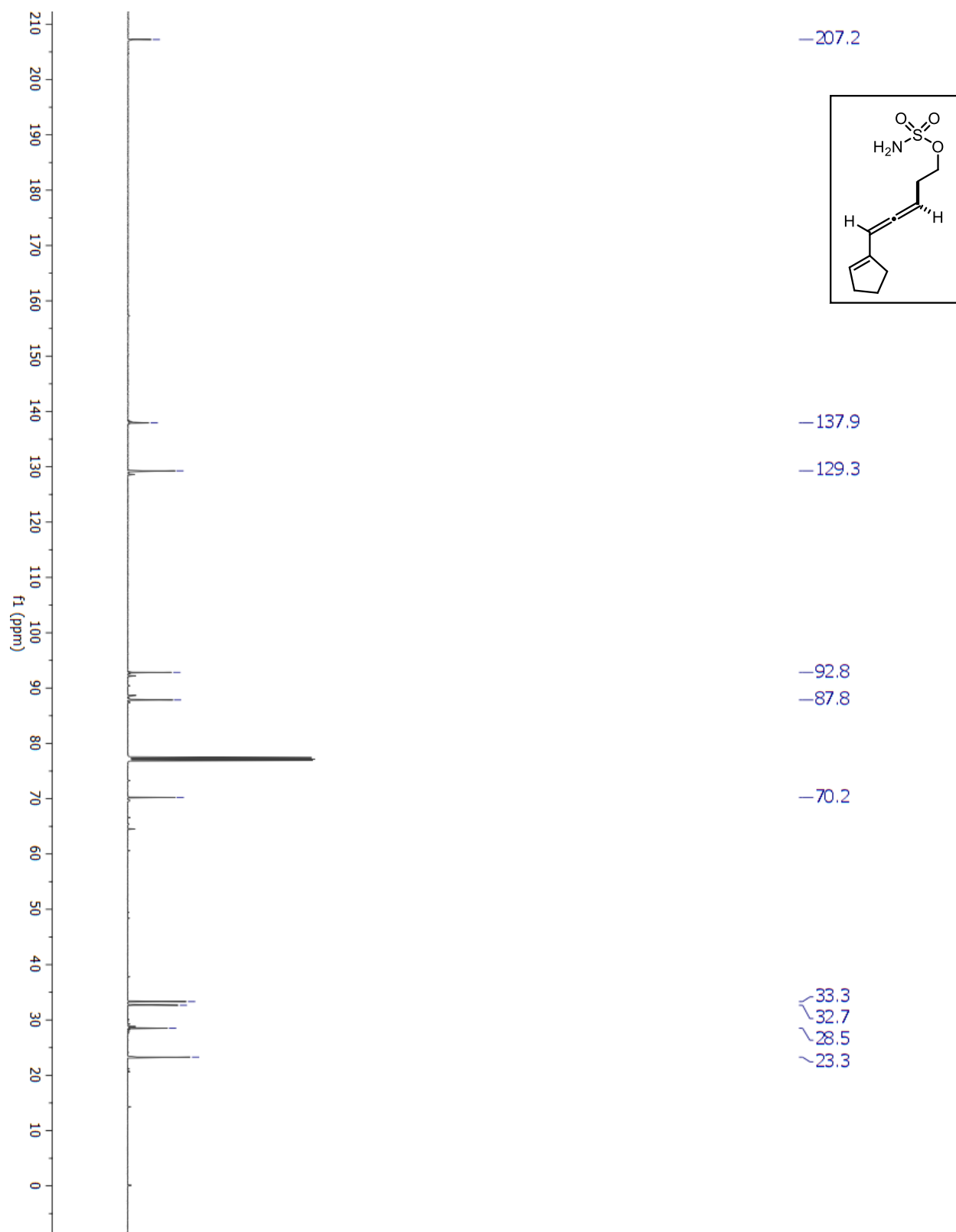
¹H-NMR for Compound 5.11

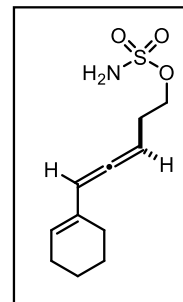
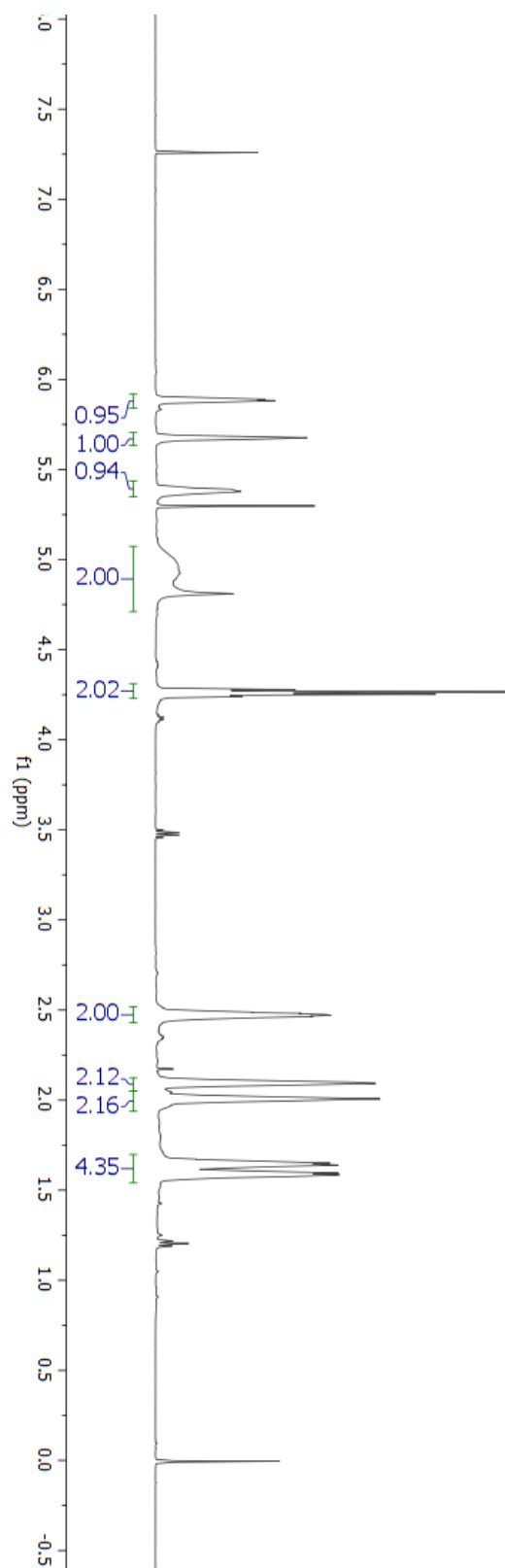
^{13}C -NMR for Compound 5.11

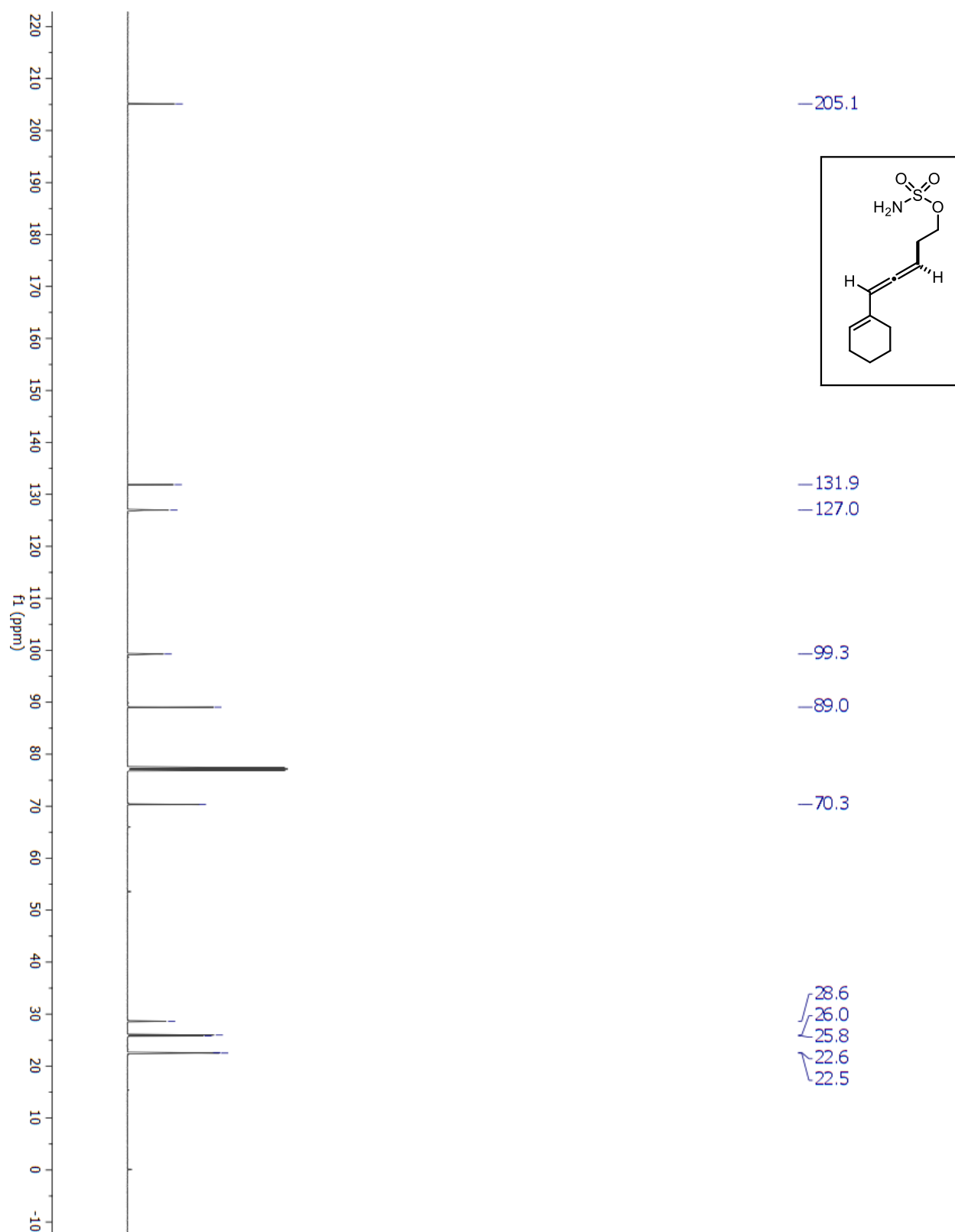


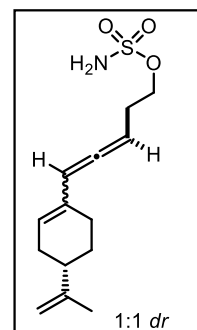
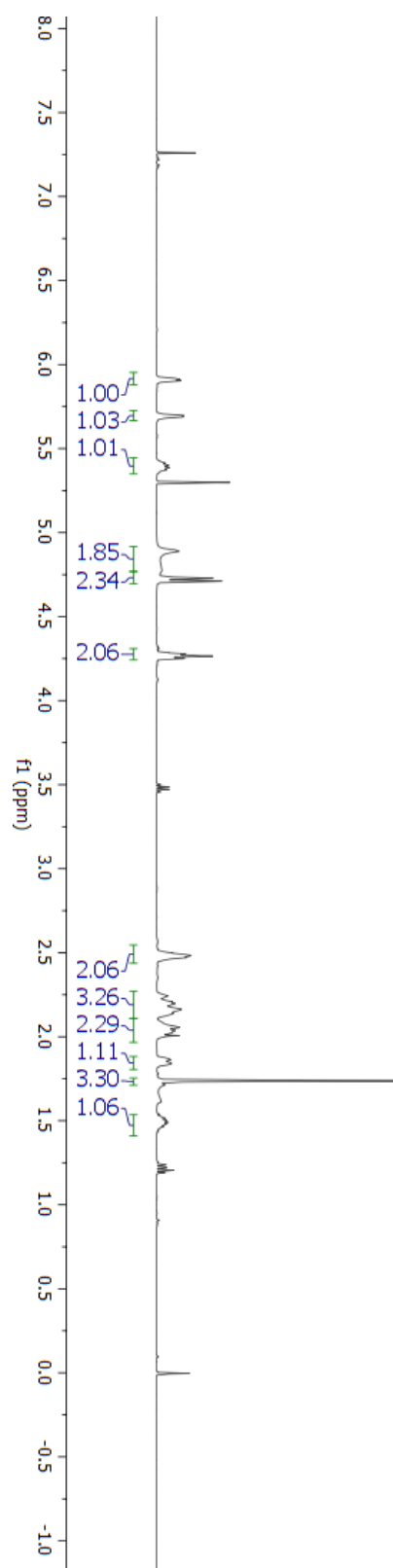
^{13}C -NMR for Compound 5.12

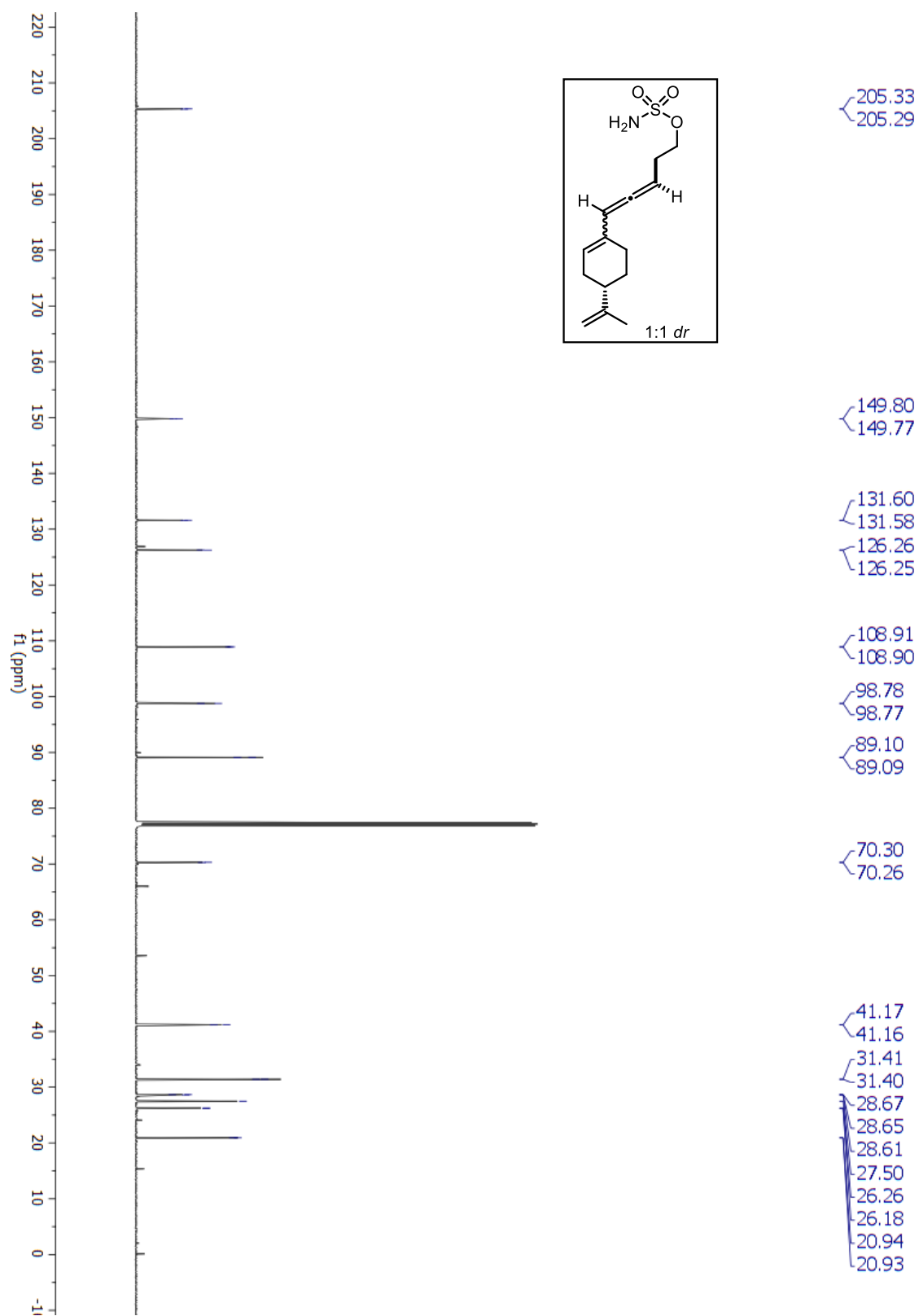
¹H-NMR for Compound 5.13

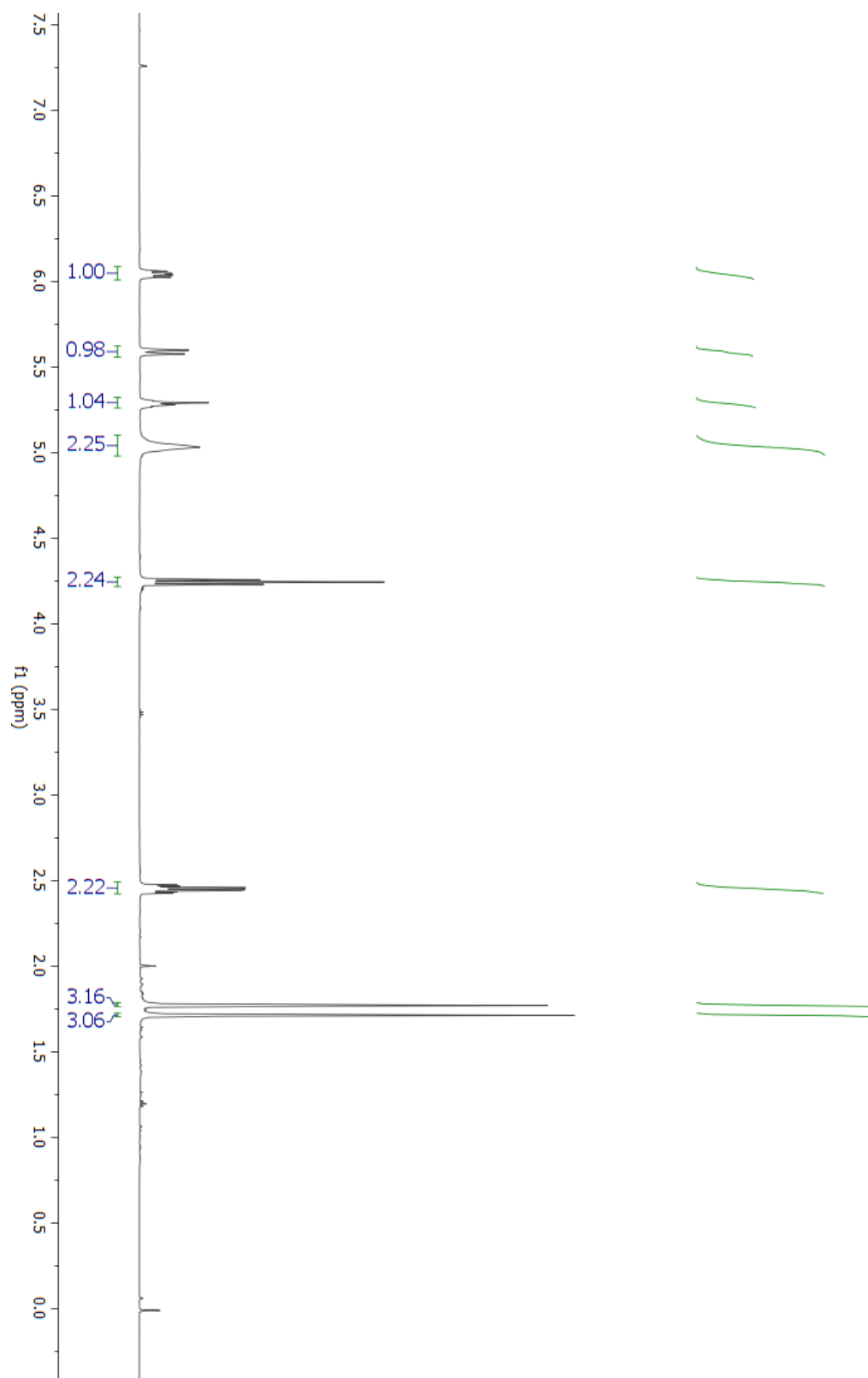
^{13}C -NMR for Compound 5.13

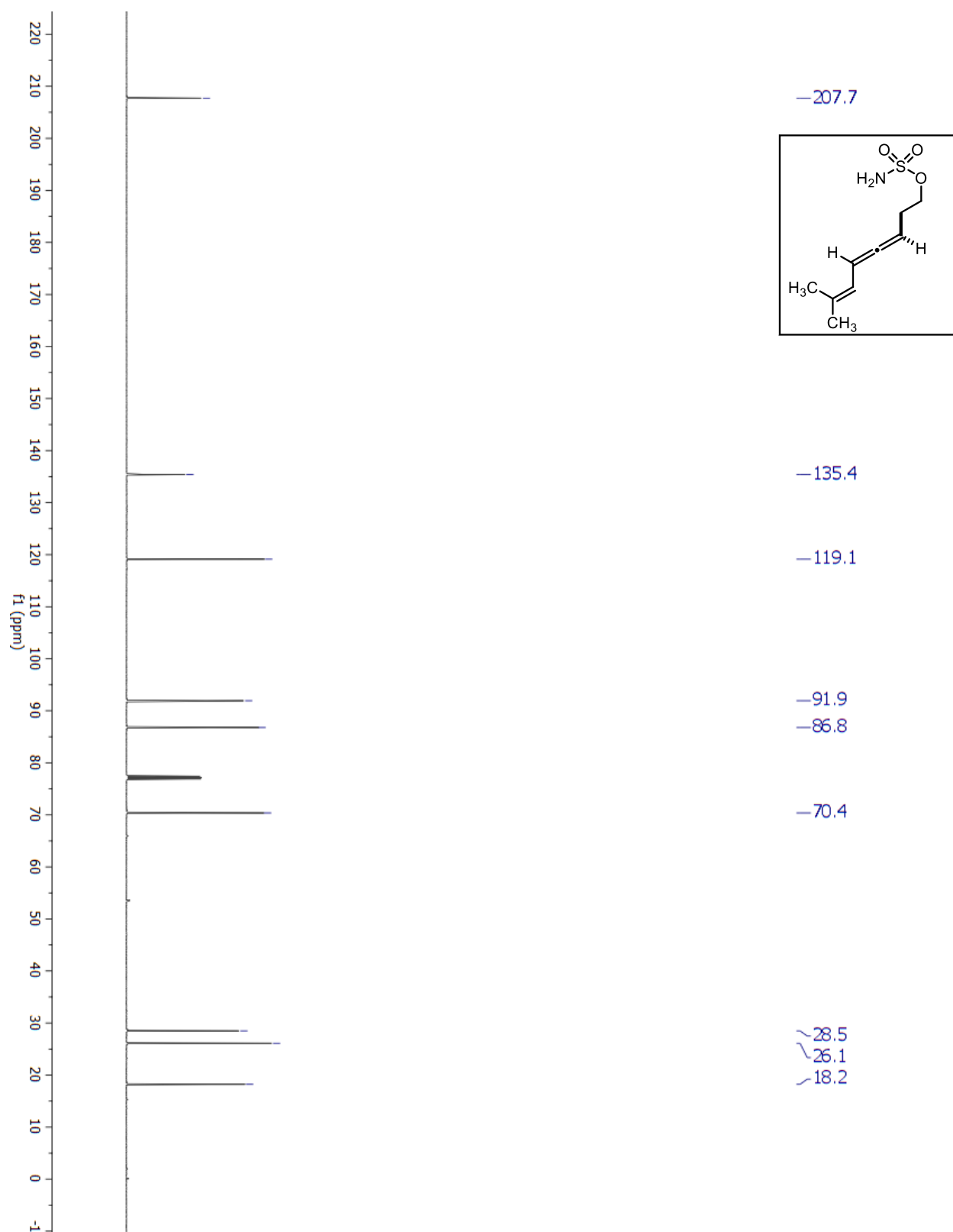
¹H-NMR for Compound 5.14

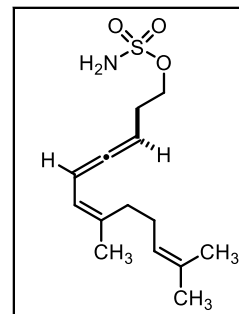
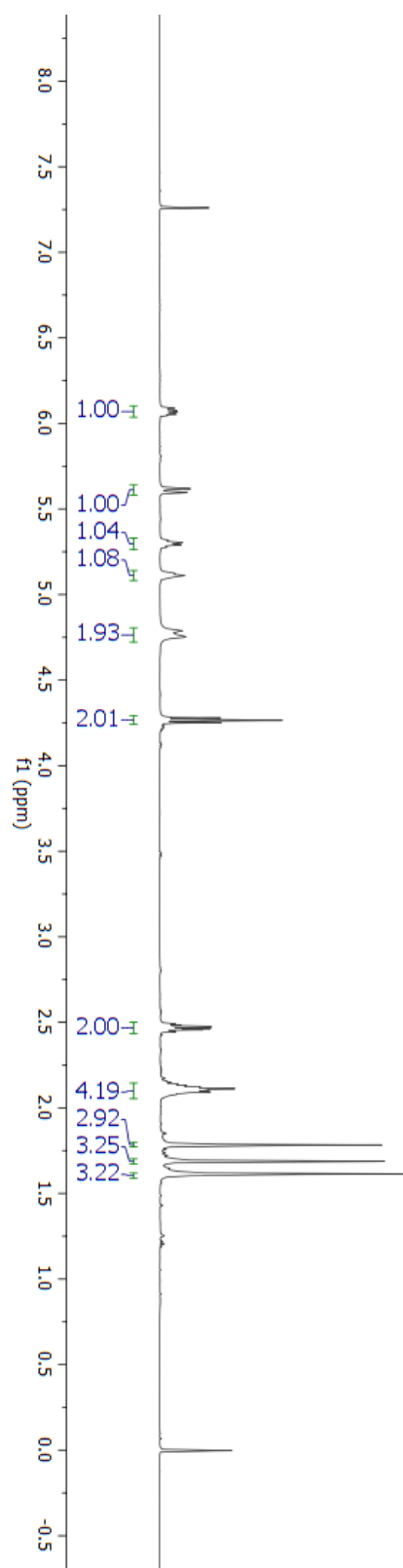
^{13}C -NMR for Compound 5.14

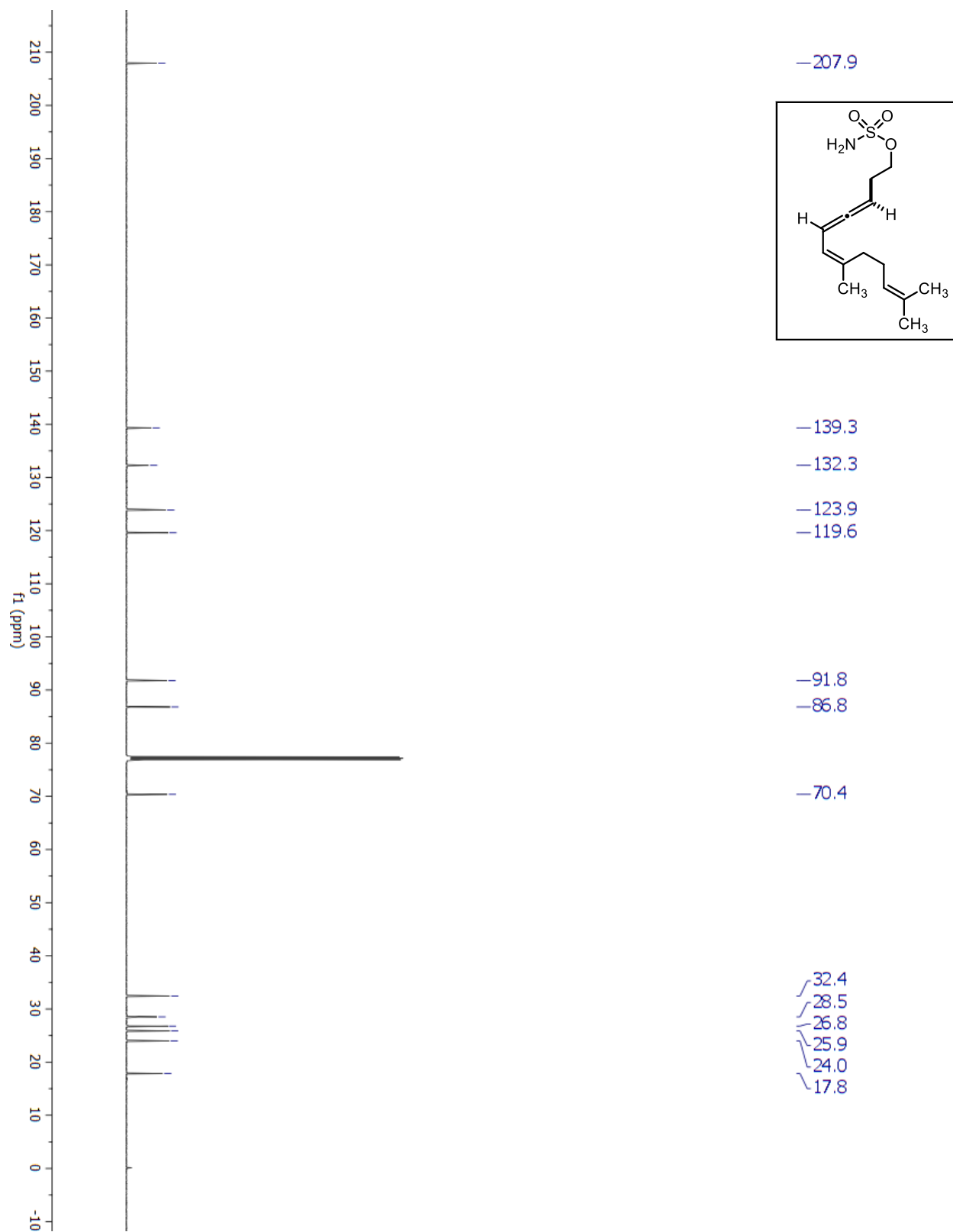
¹H-NMR for Compound 5.15

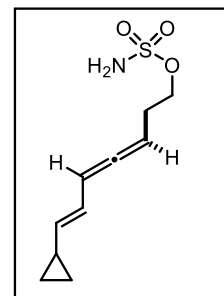
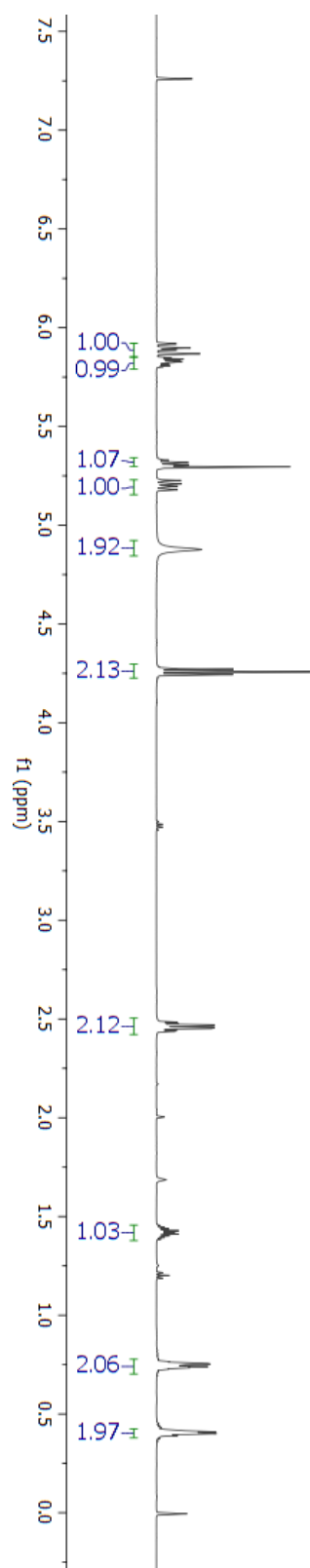
^{13}C -NMR for Compound 5.15

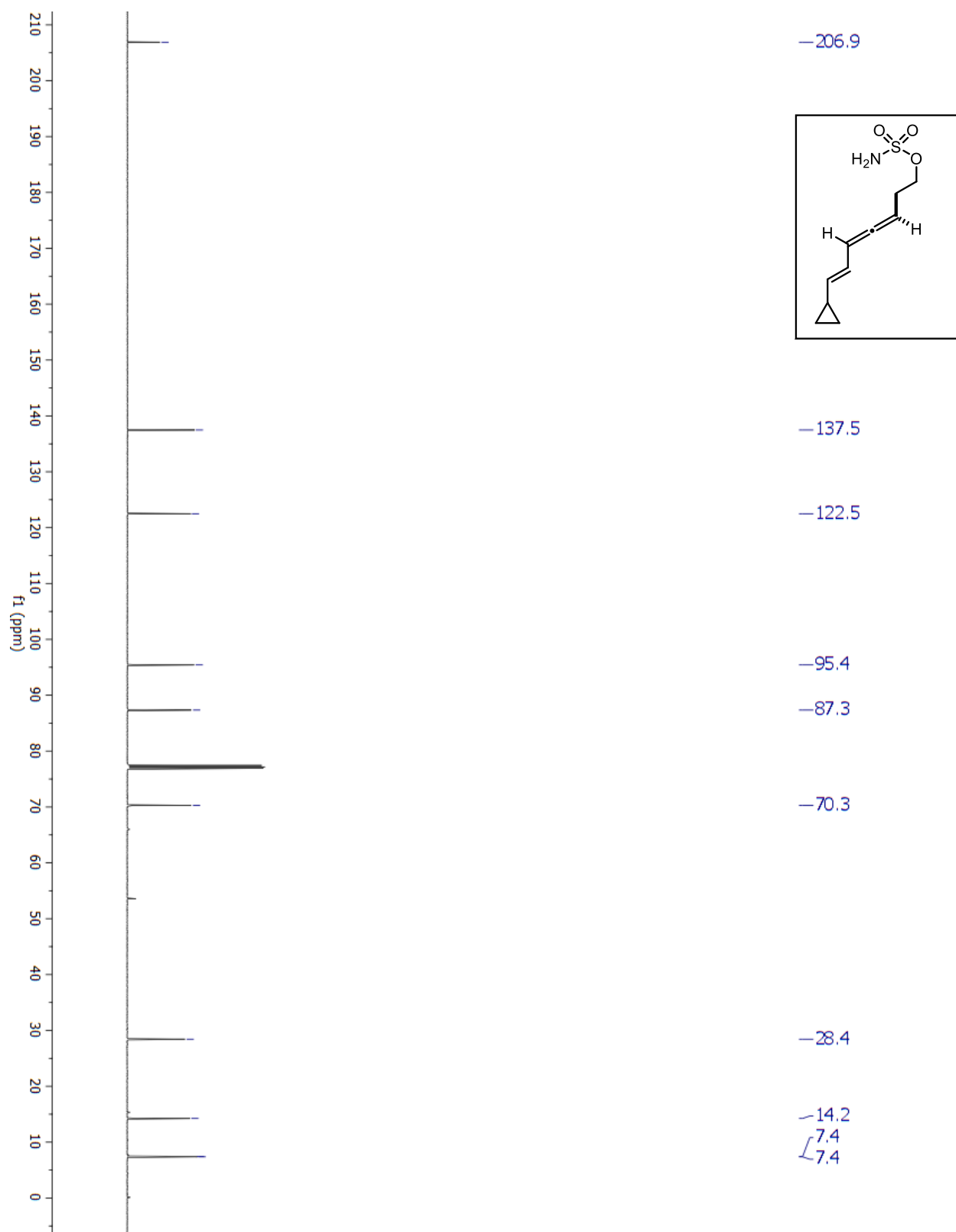
¹H-NMR for Compound 5.16

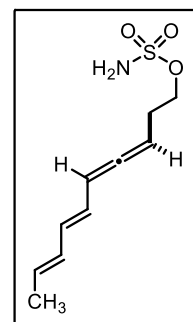
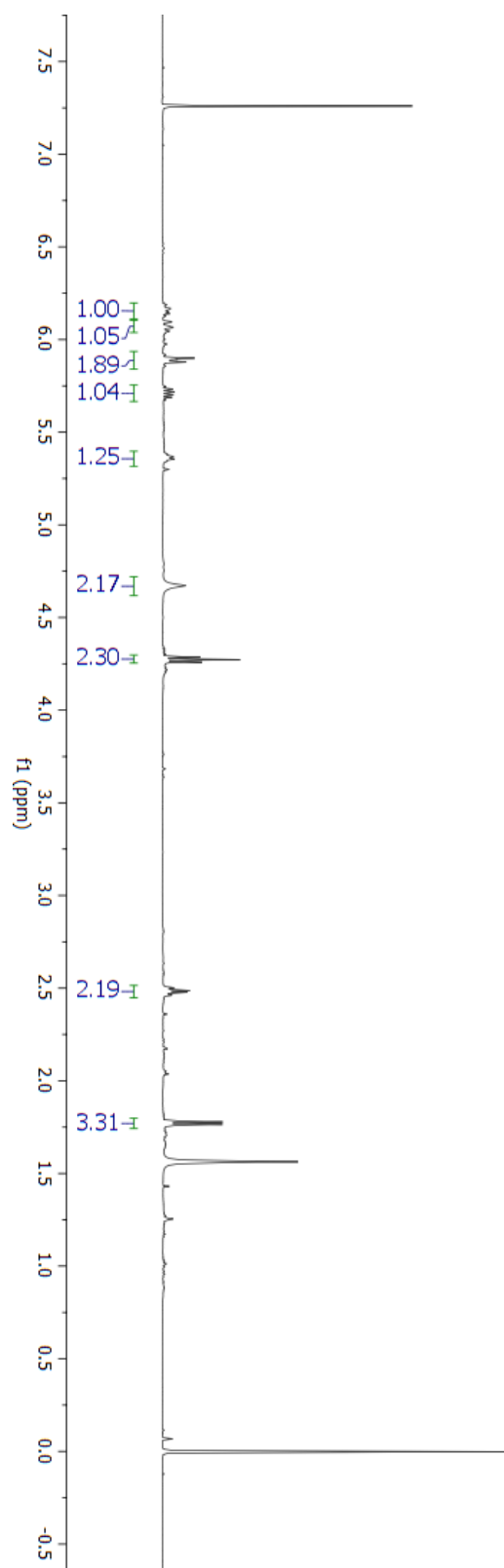
^{13}C -NMR for Compound 5.16

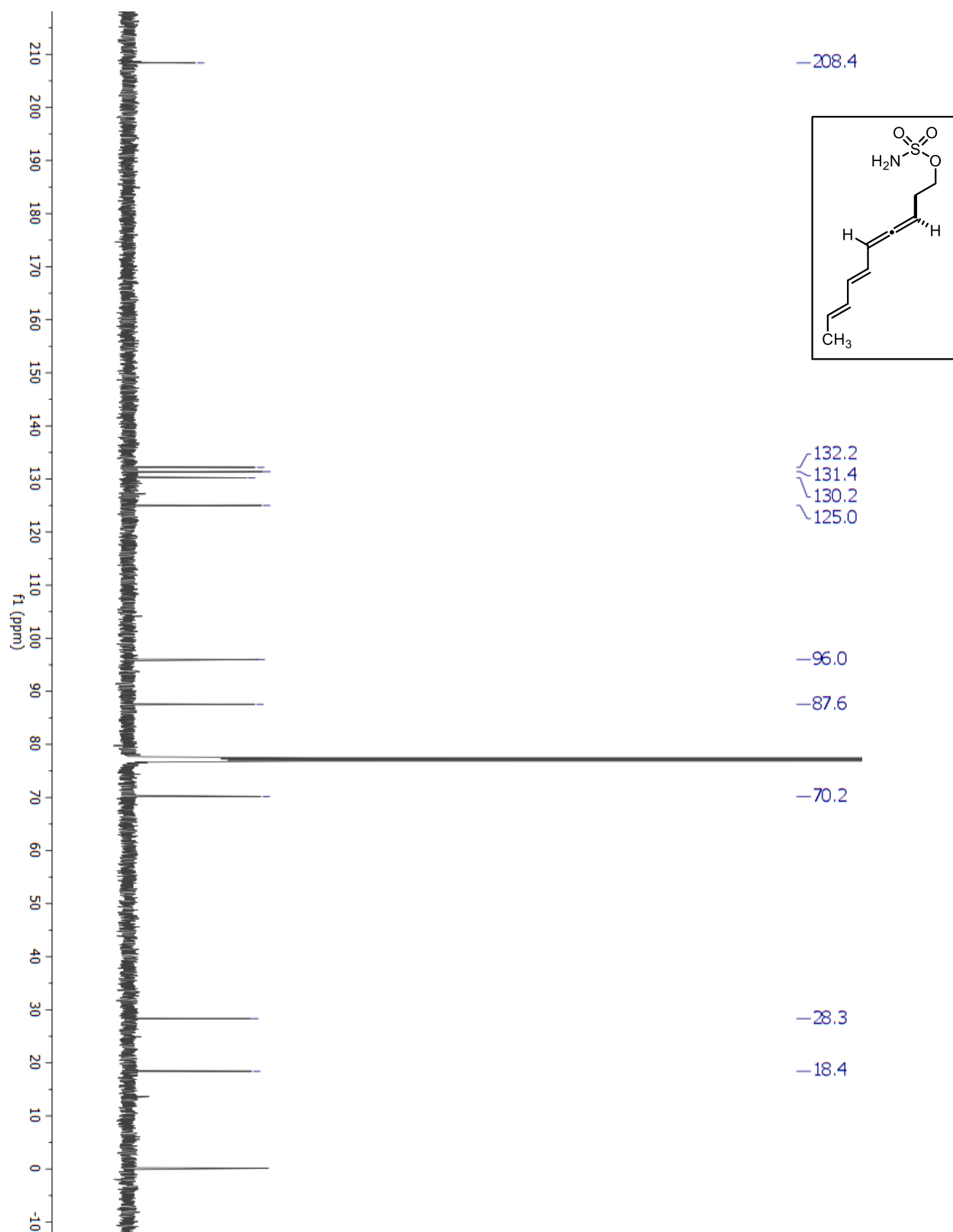
¹H-NMR for Compound 5.17

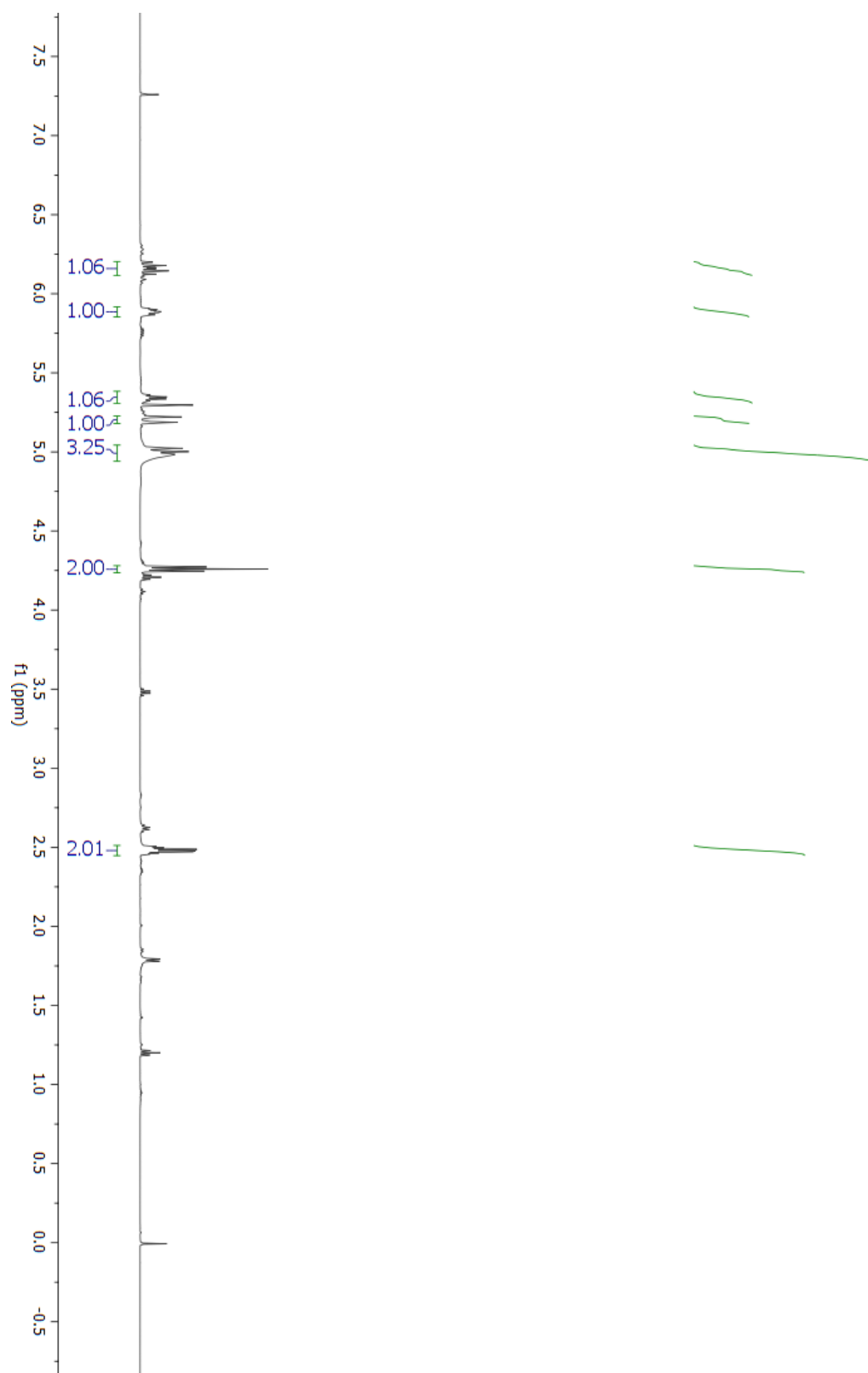
^{13}C -NMR for Compound 5.17

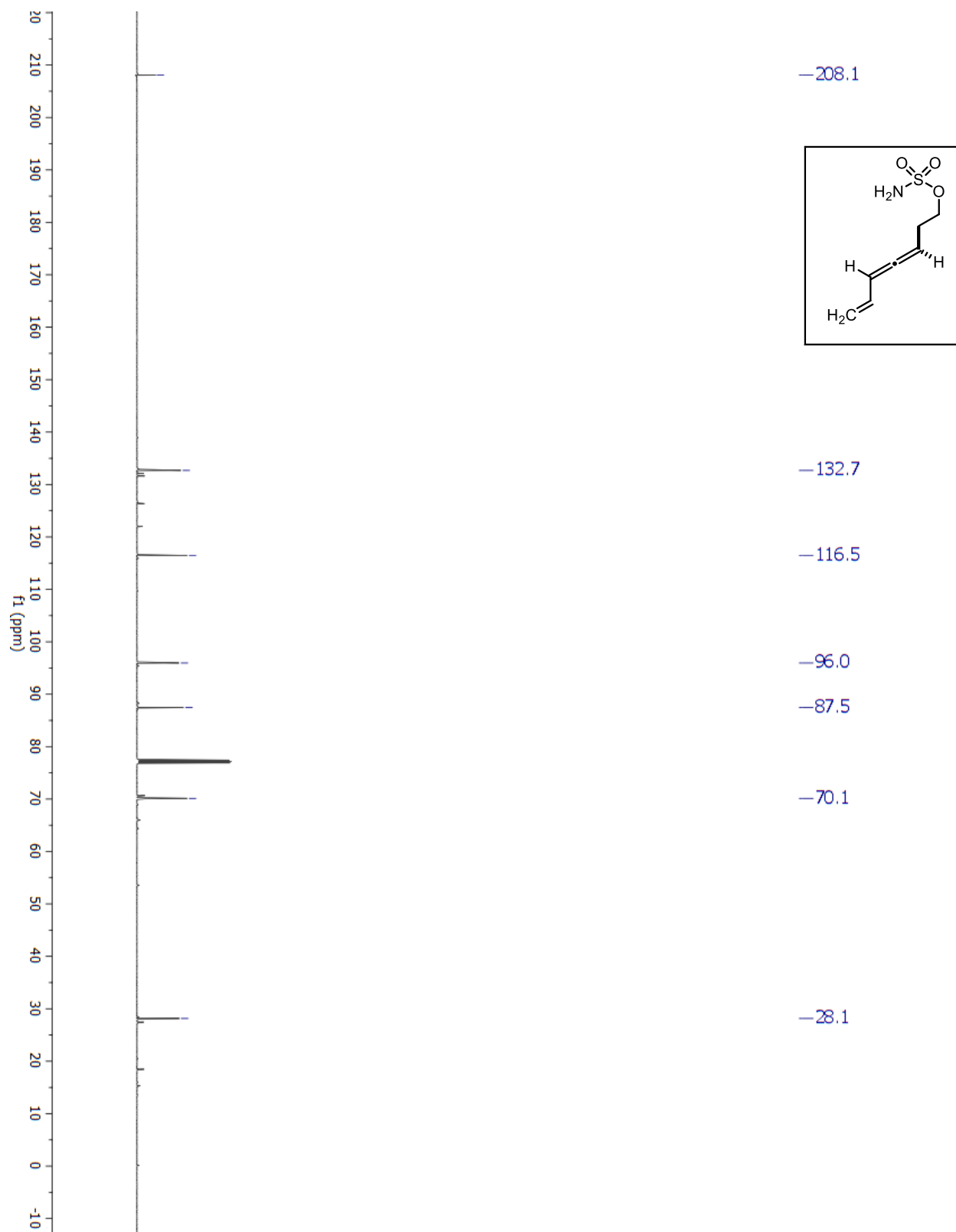
¹H-NMR for Compound 5.18

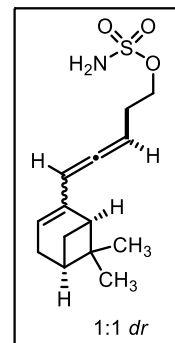
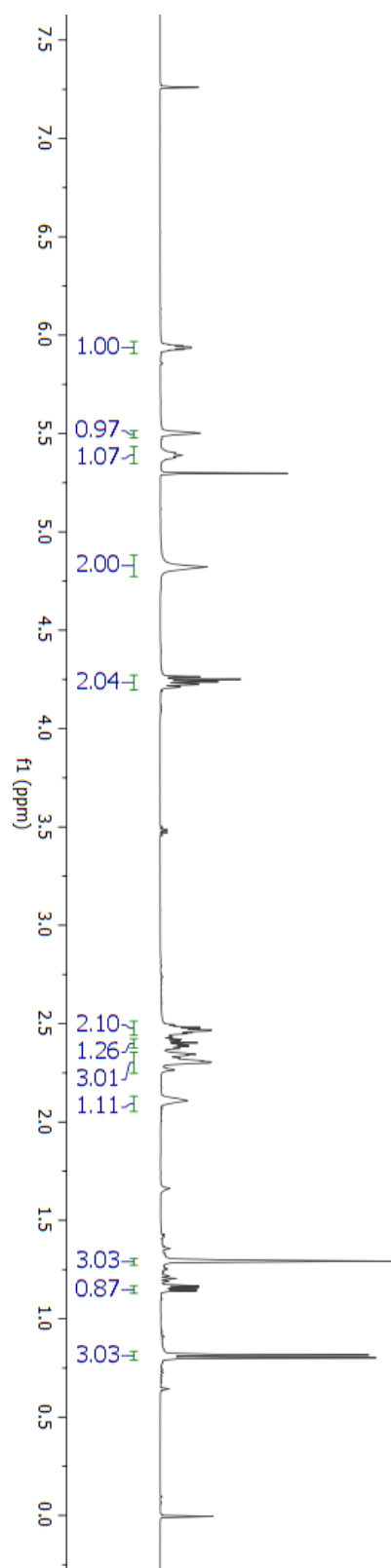
^{13}C -NMR for Compound 5.18

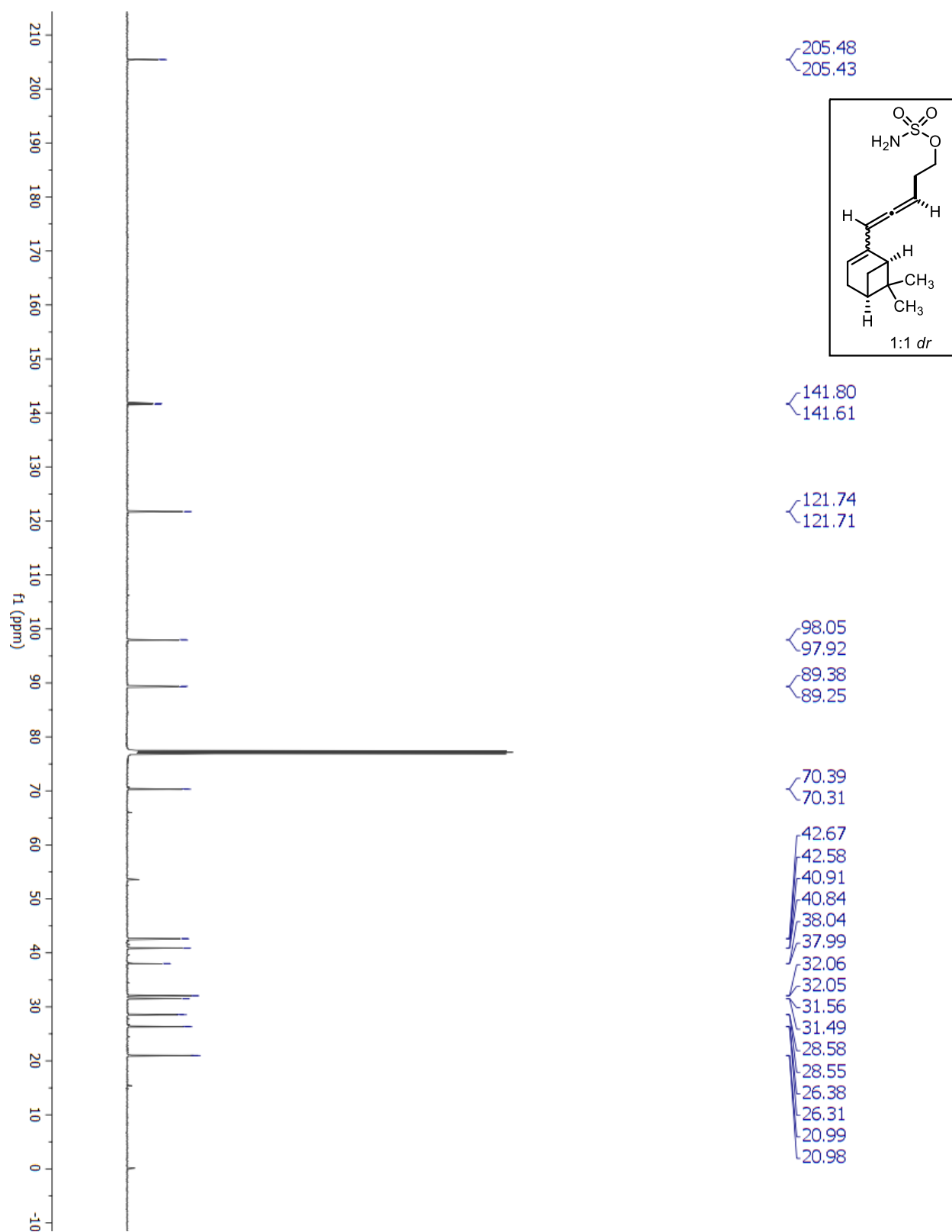
¹H-NMR for Compound 5.19

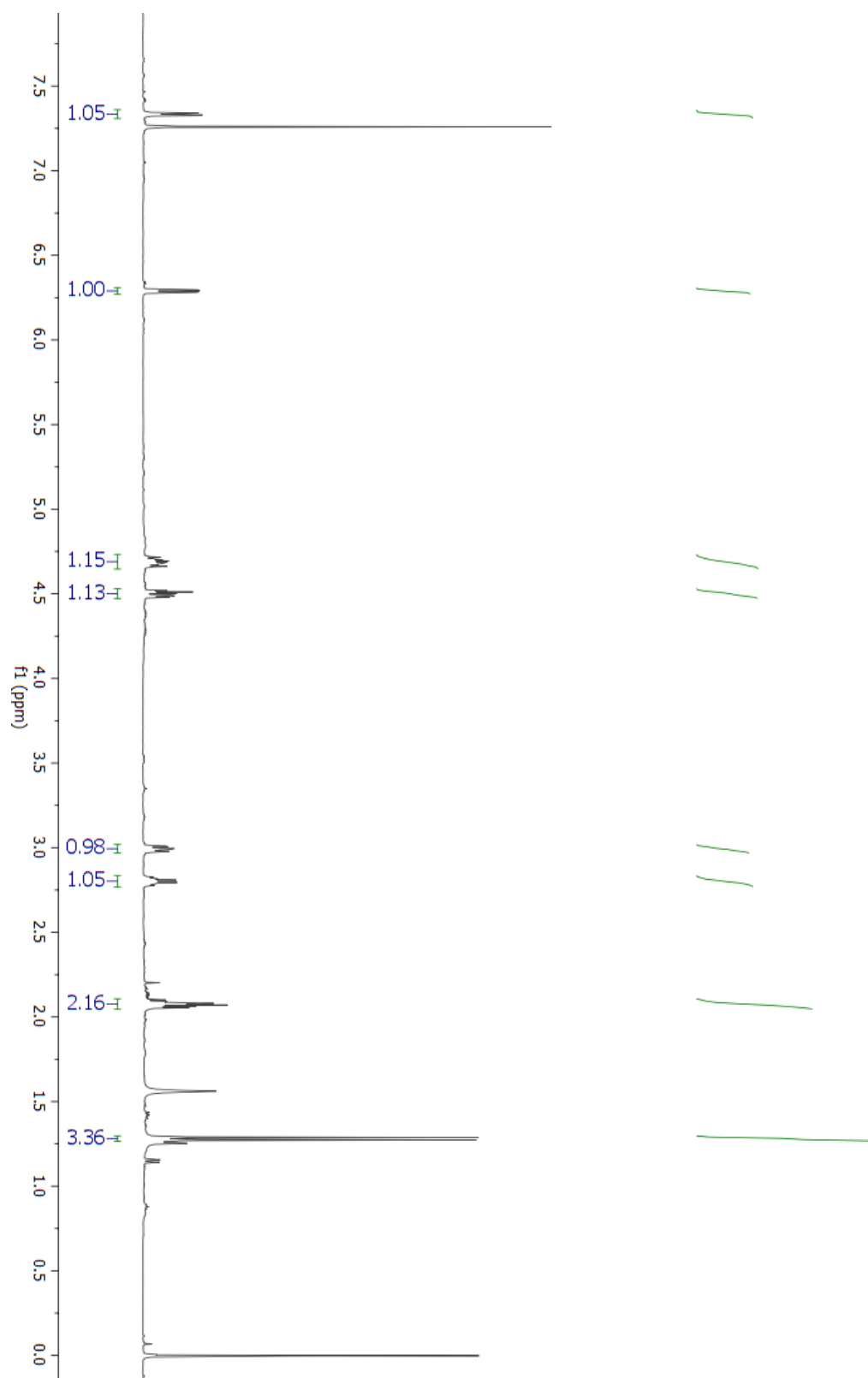
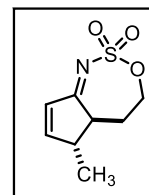
^{13}C -NMR for Compound 5.19

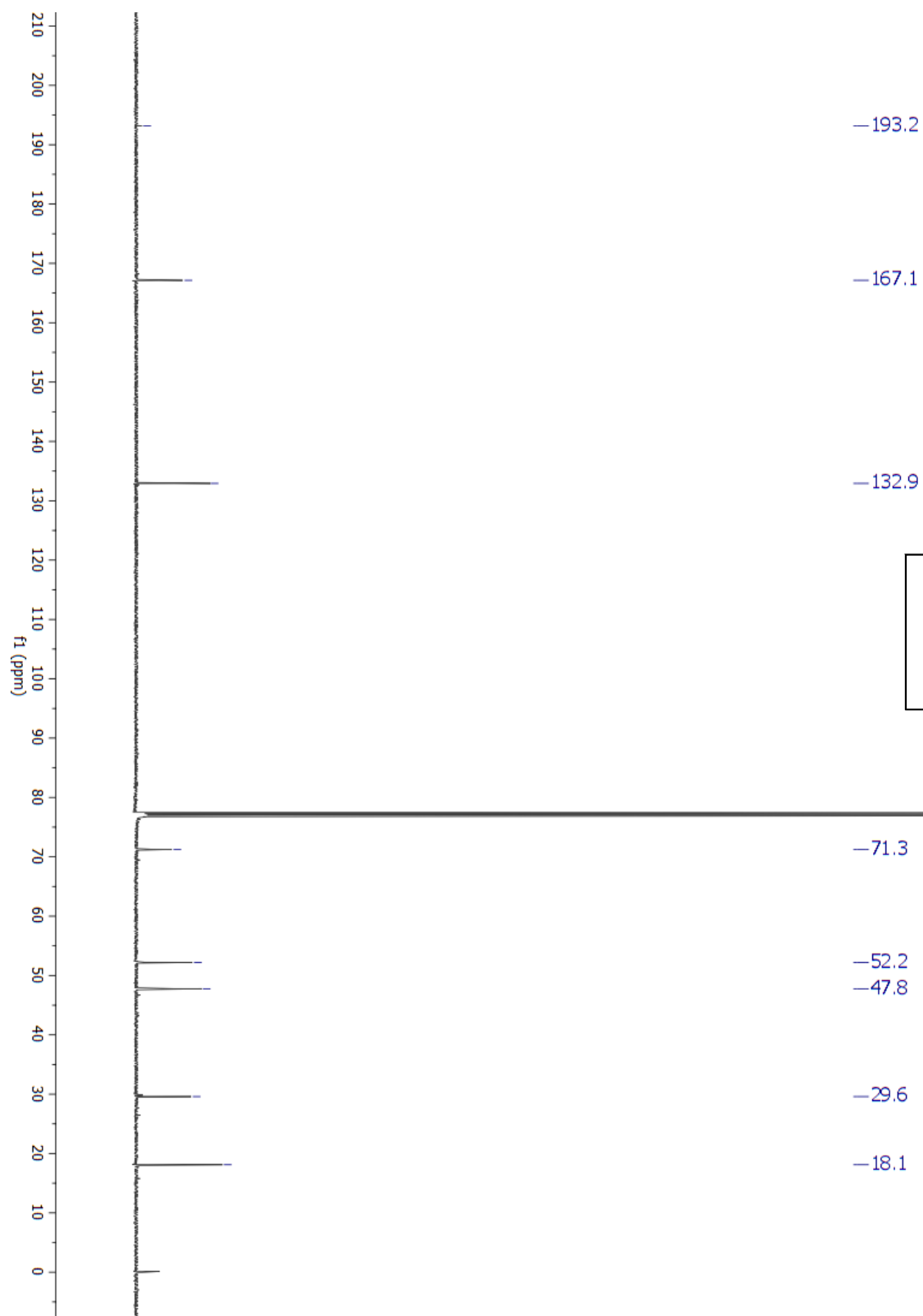
¹H-NMR for Compound 5.20

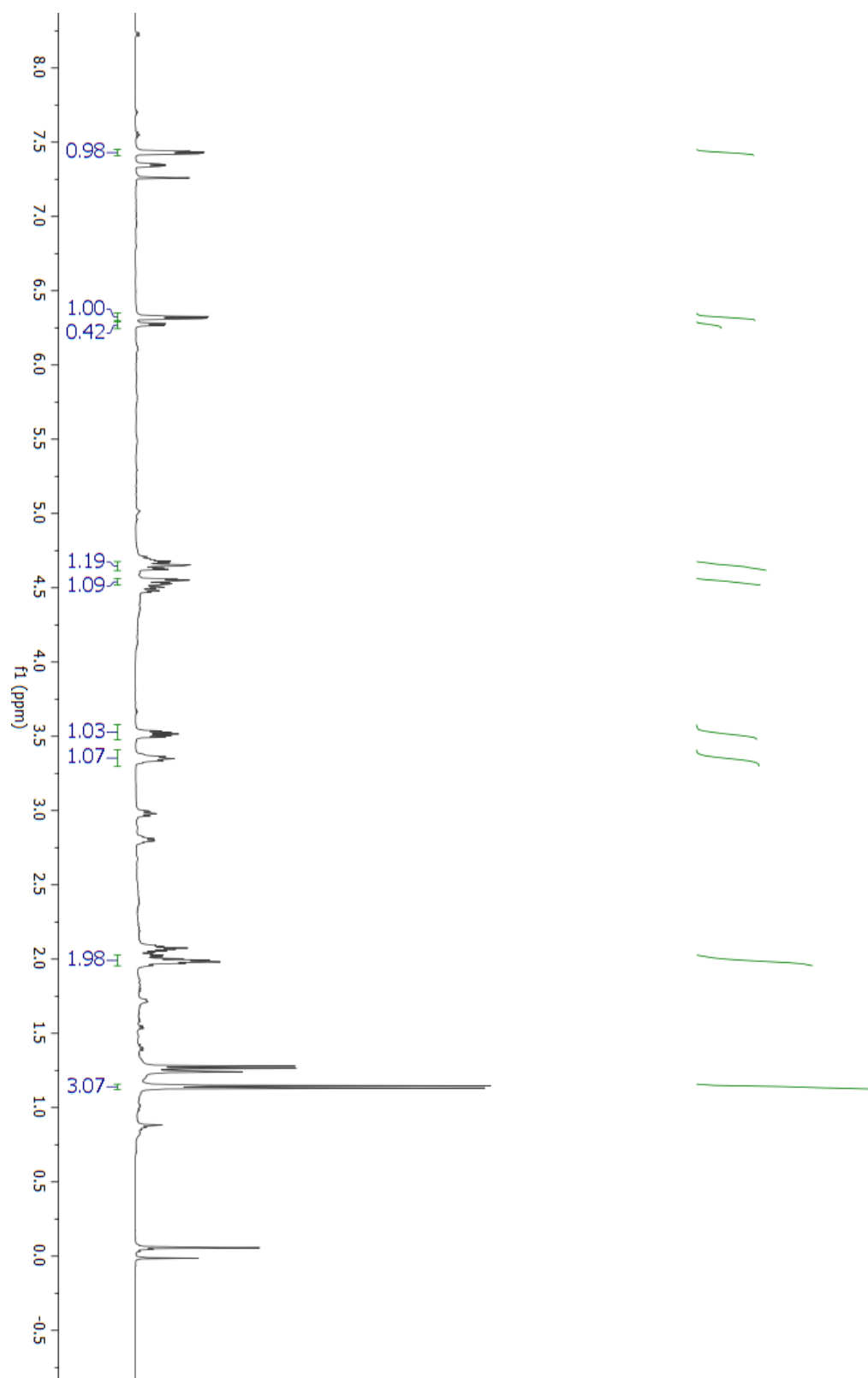
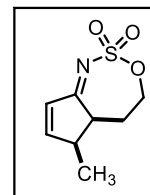
^{13}C -NMR for Compound 5.20

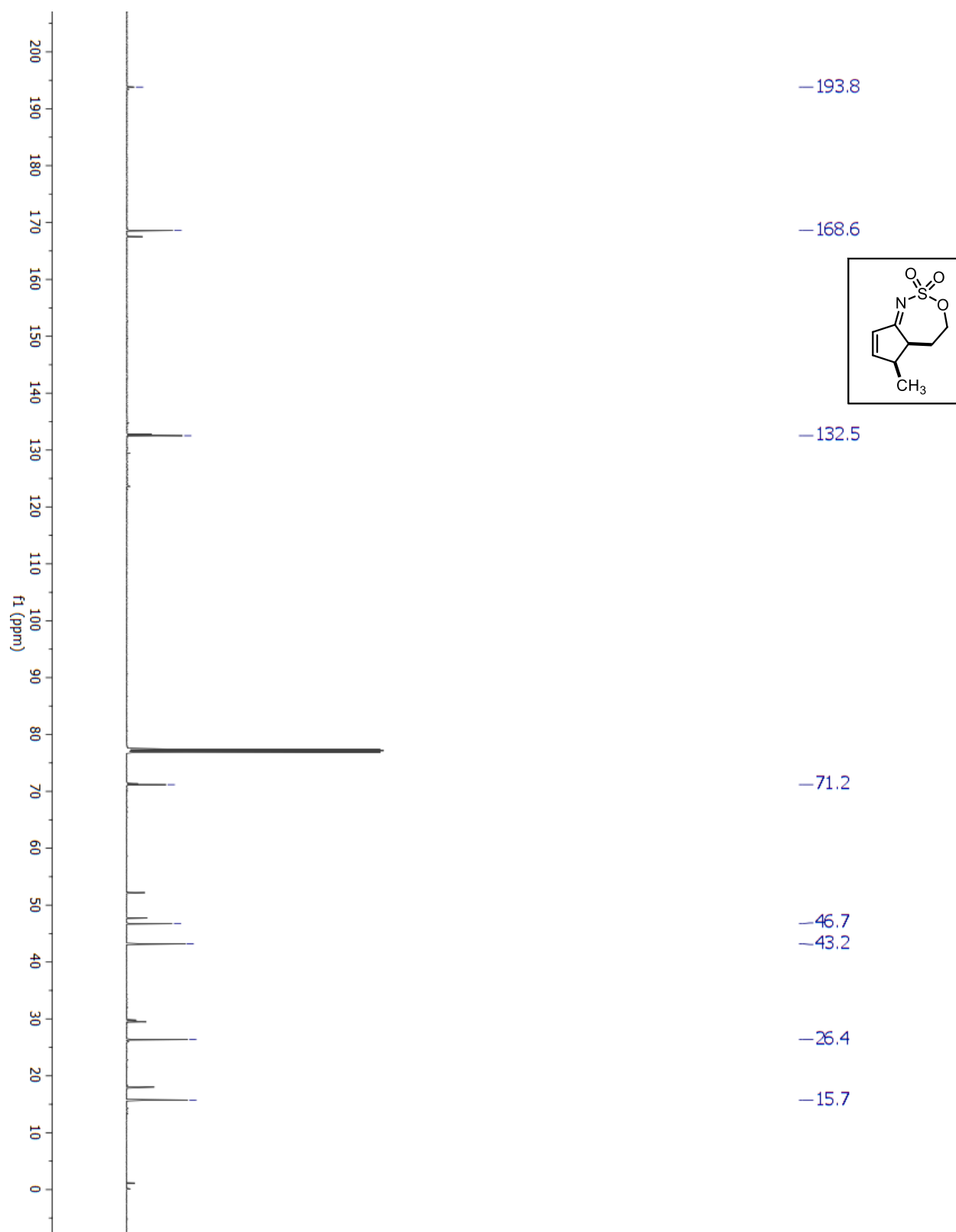
¹H-NMR for Compound 5.21

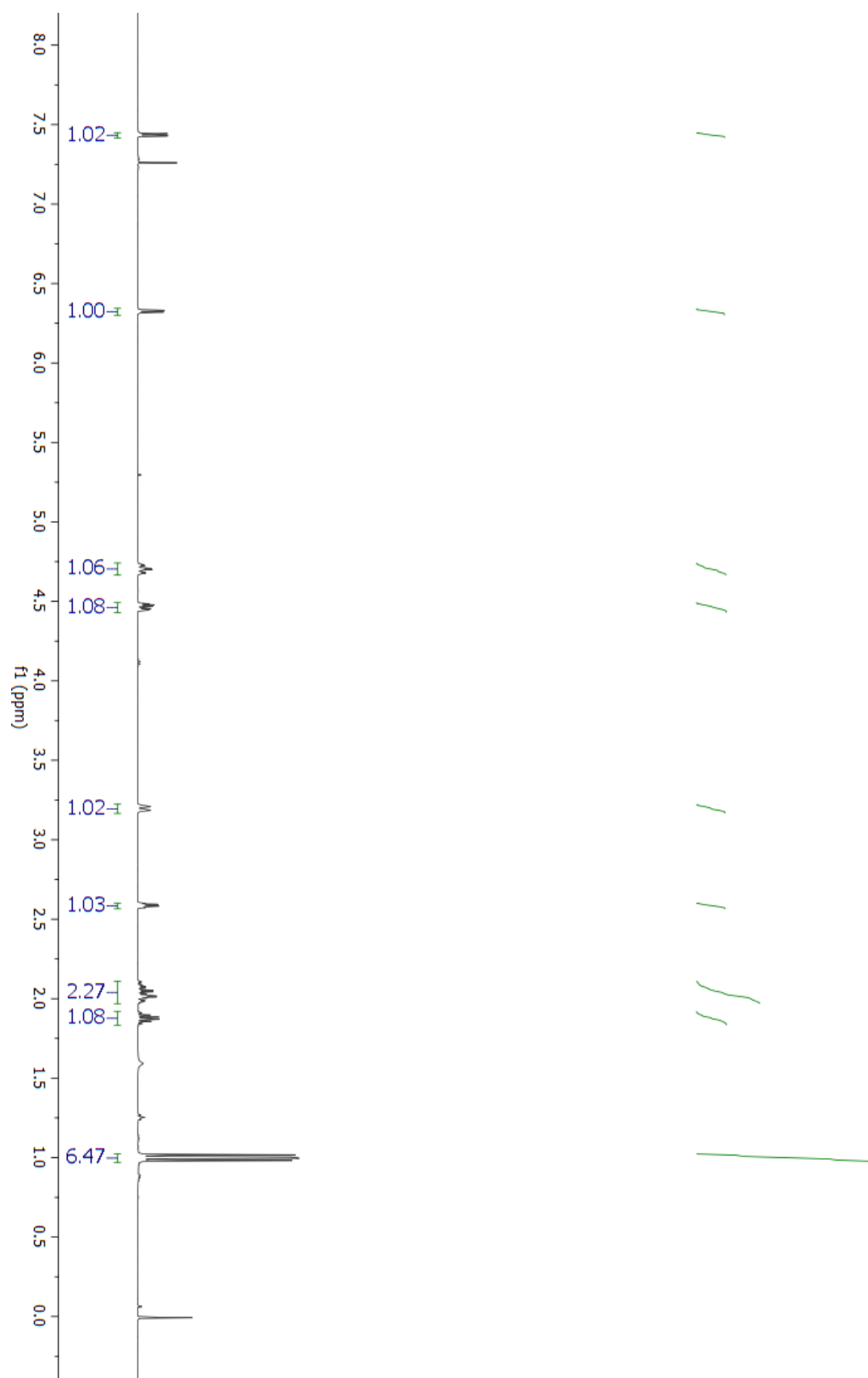
^{13}C -NMR for Compound 5.21

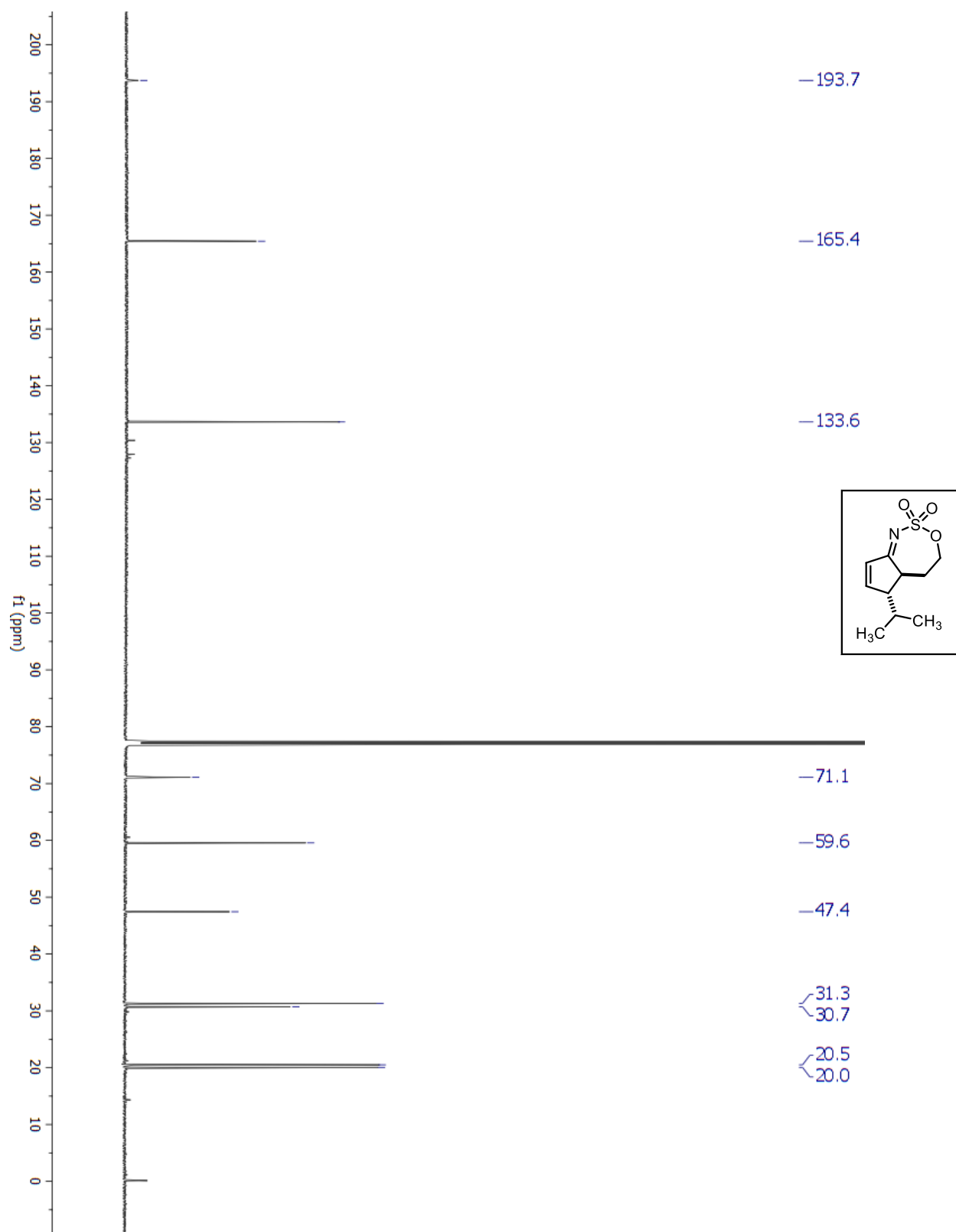
¹H-NMR for Compound 5.4a

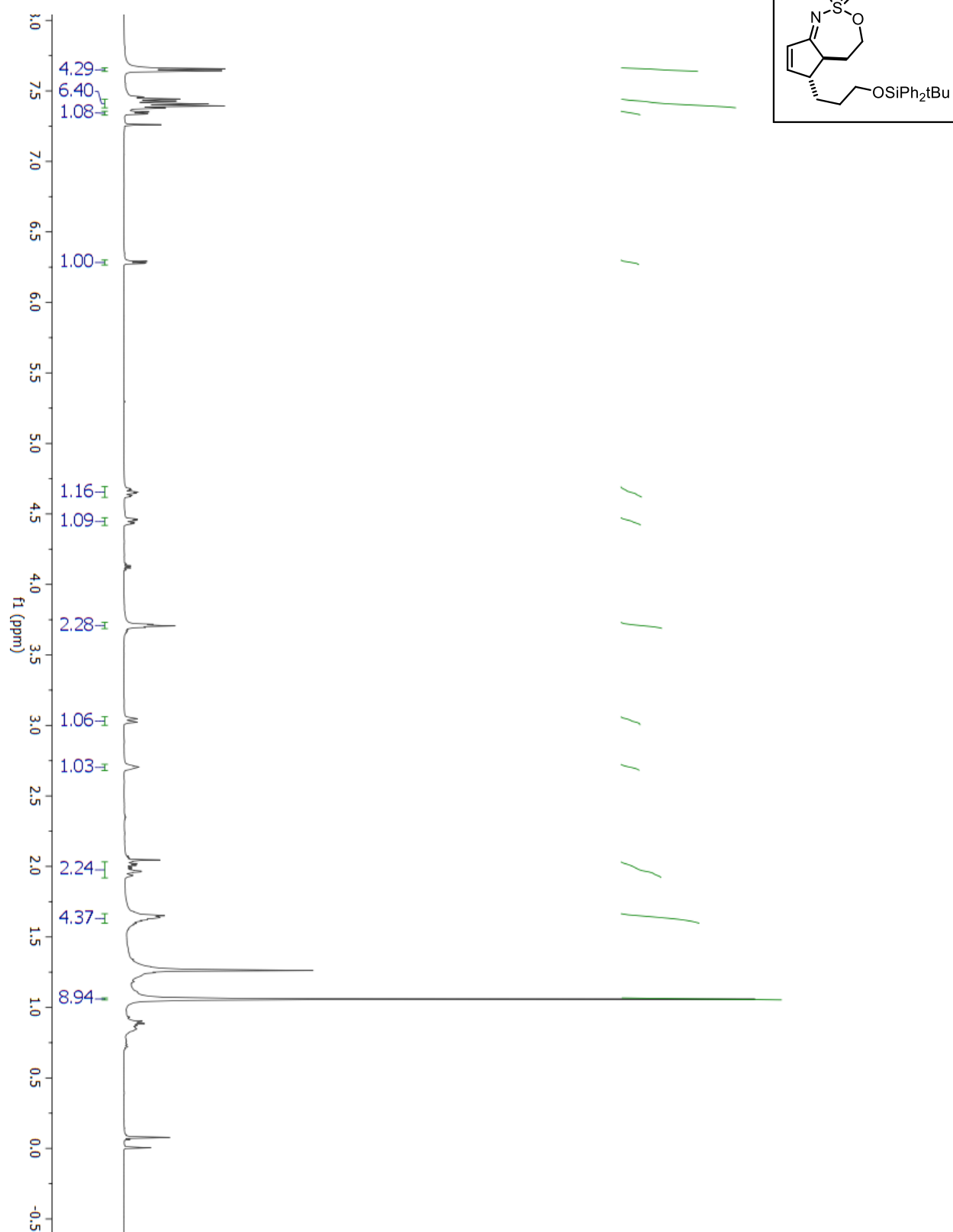
^{13}C -NMR for Compound 5.4a

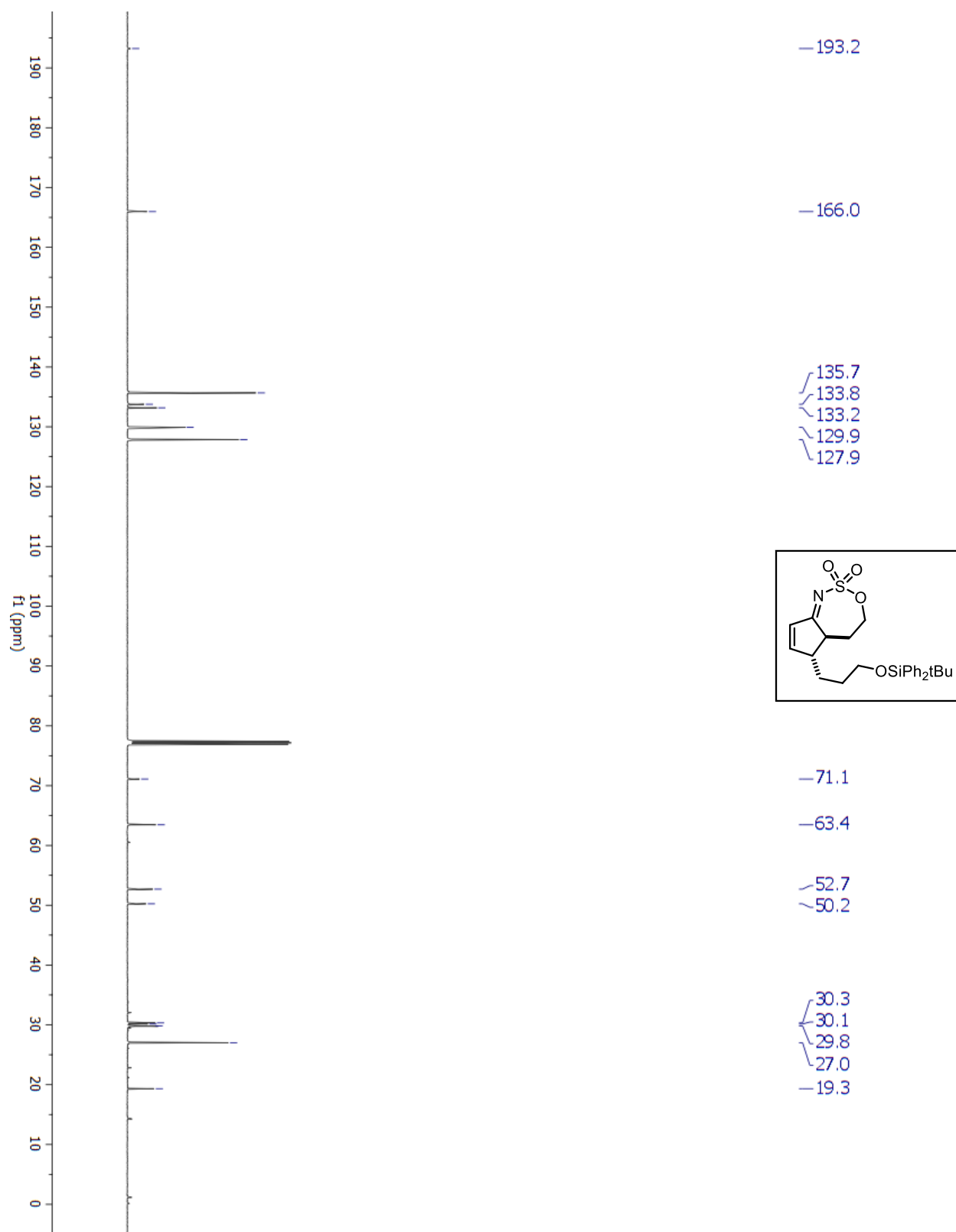
¹H-NMR for Compound 5.5a

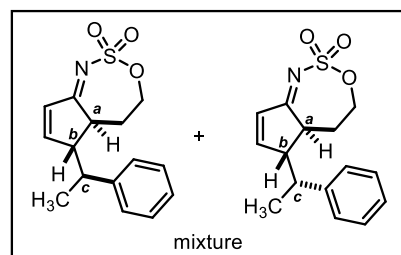
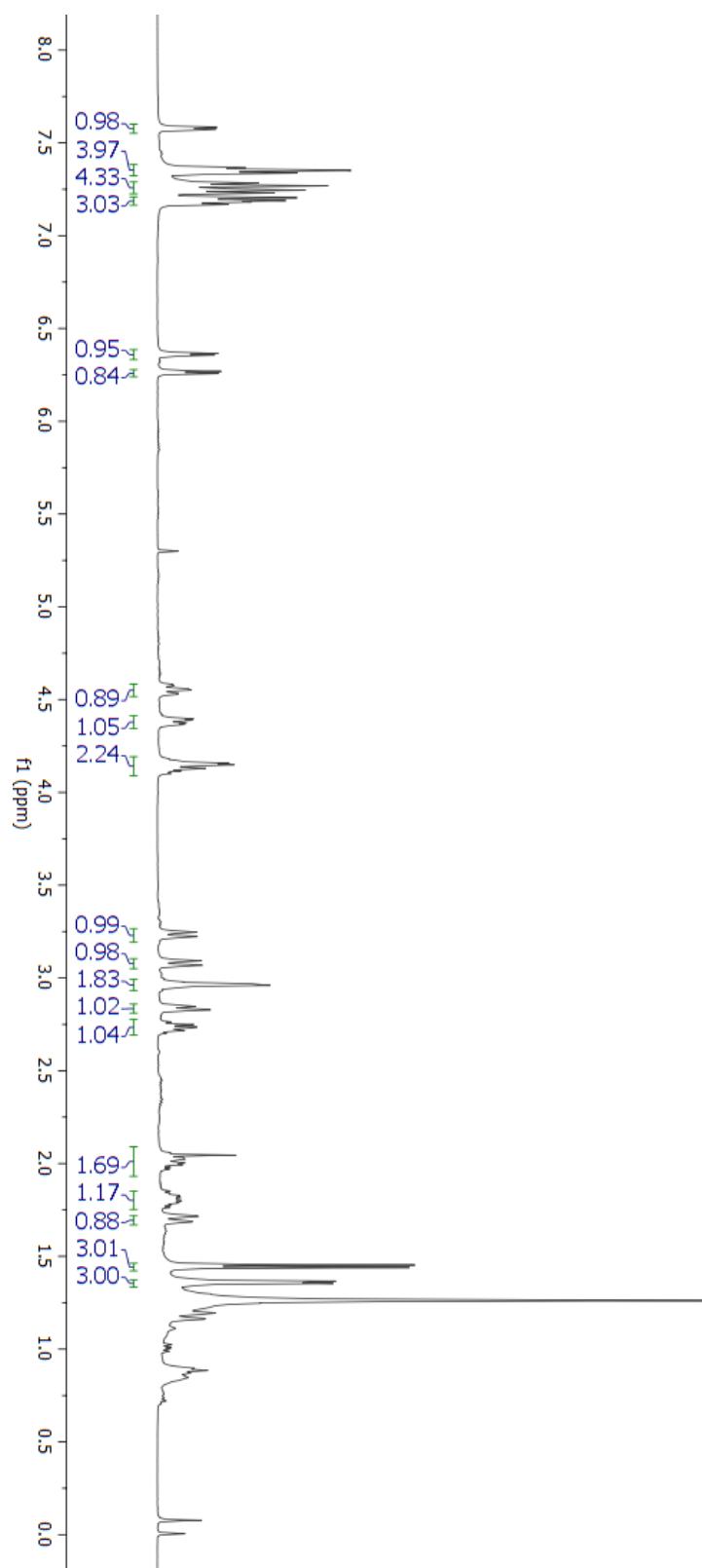
^{13}C -NMR for Compound 5.5a

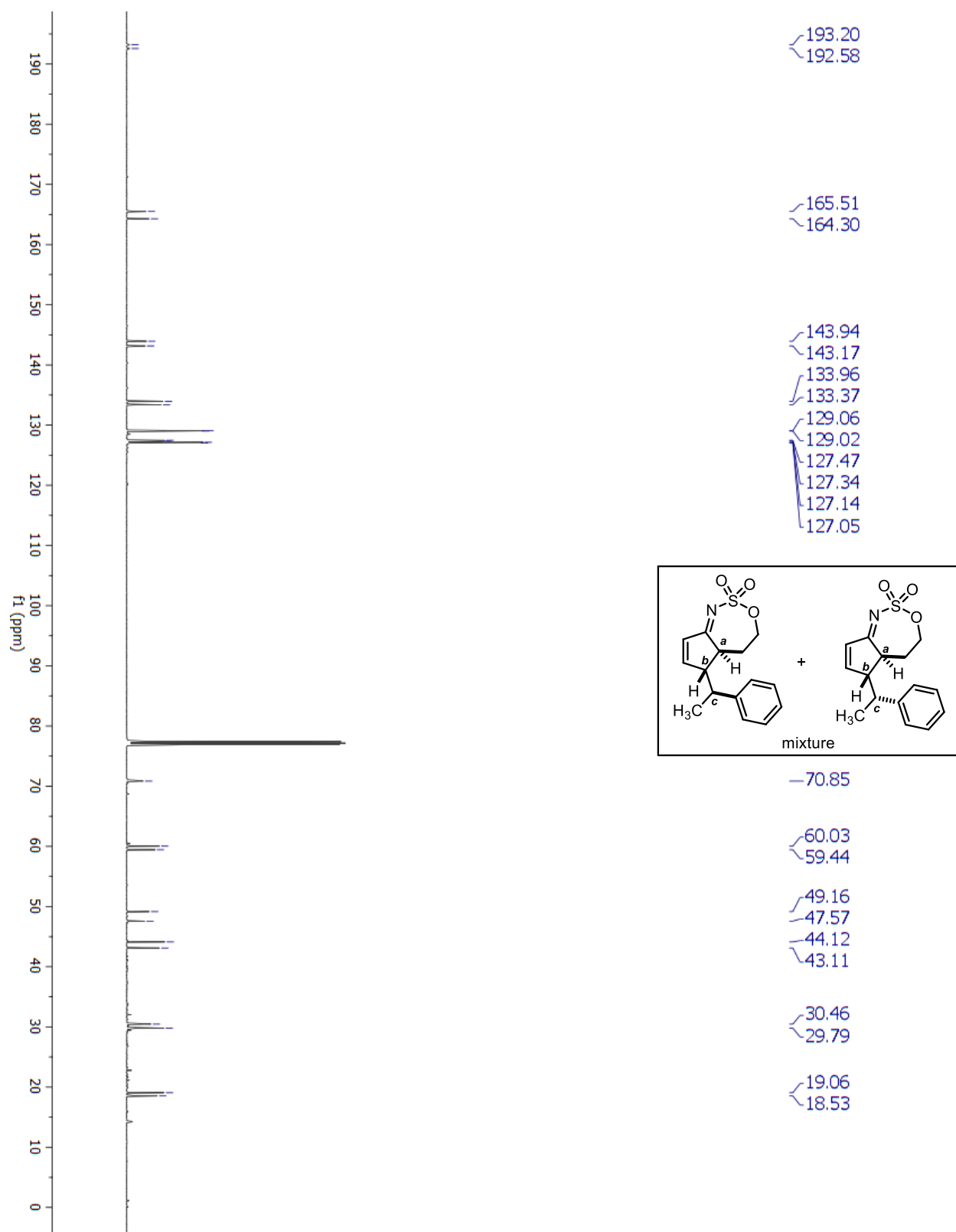
¹H-NMR for Compound 5.6a

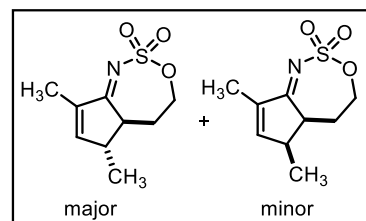
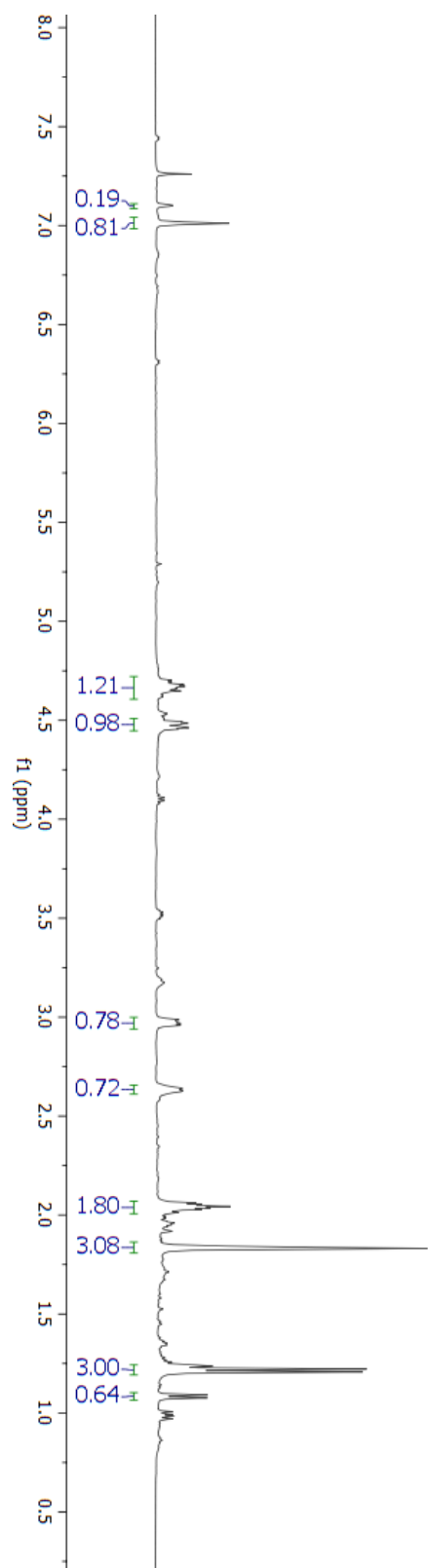
^{13}C -NMR for Compound 5.6a

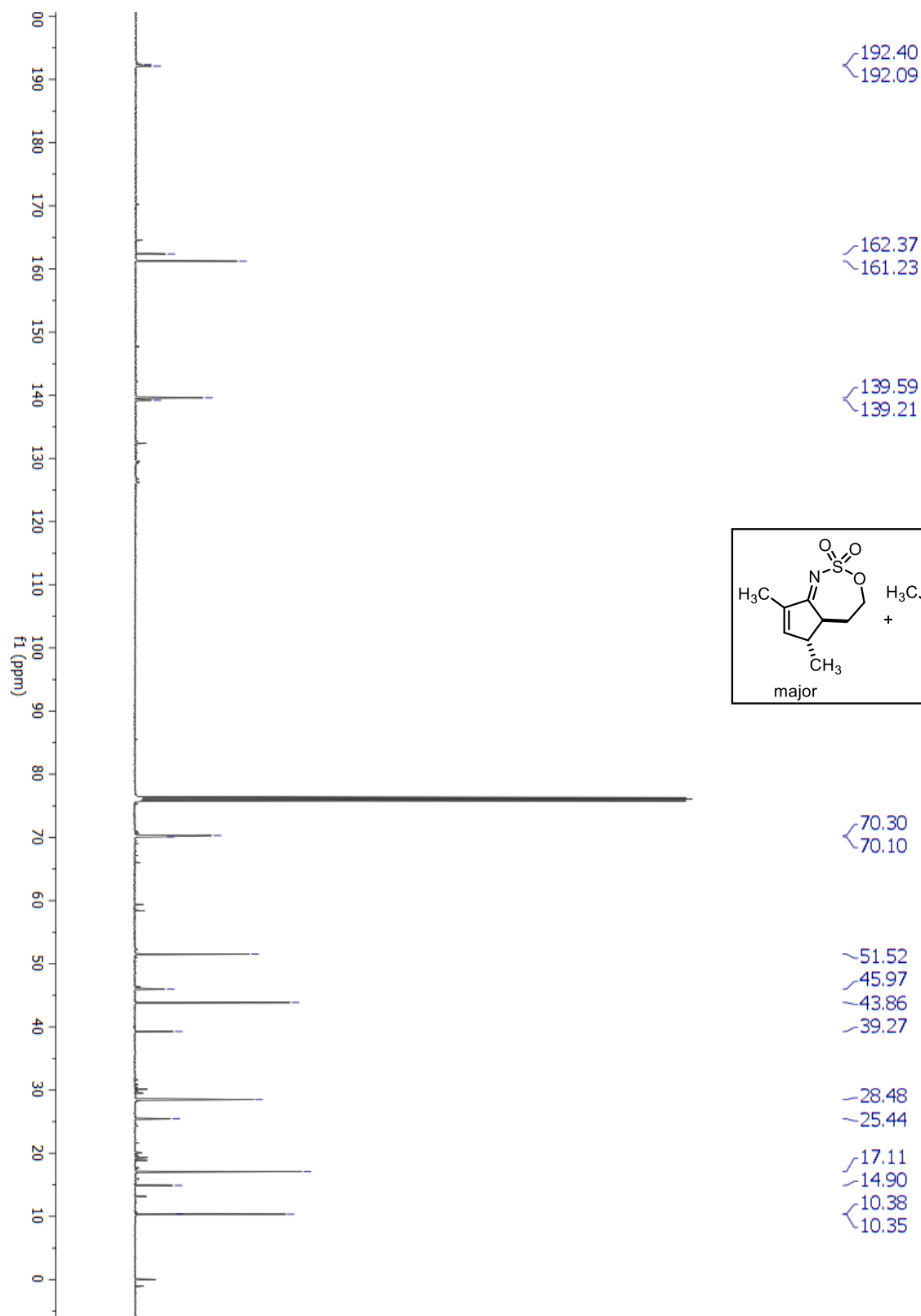
¹H-NMR for Compound 5.7a

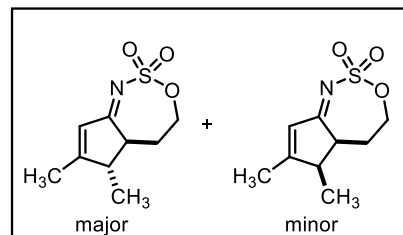
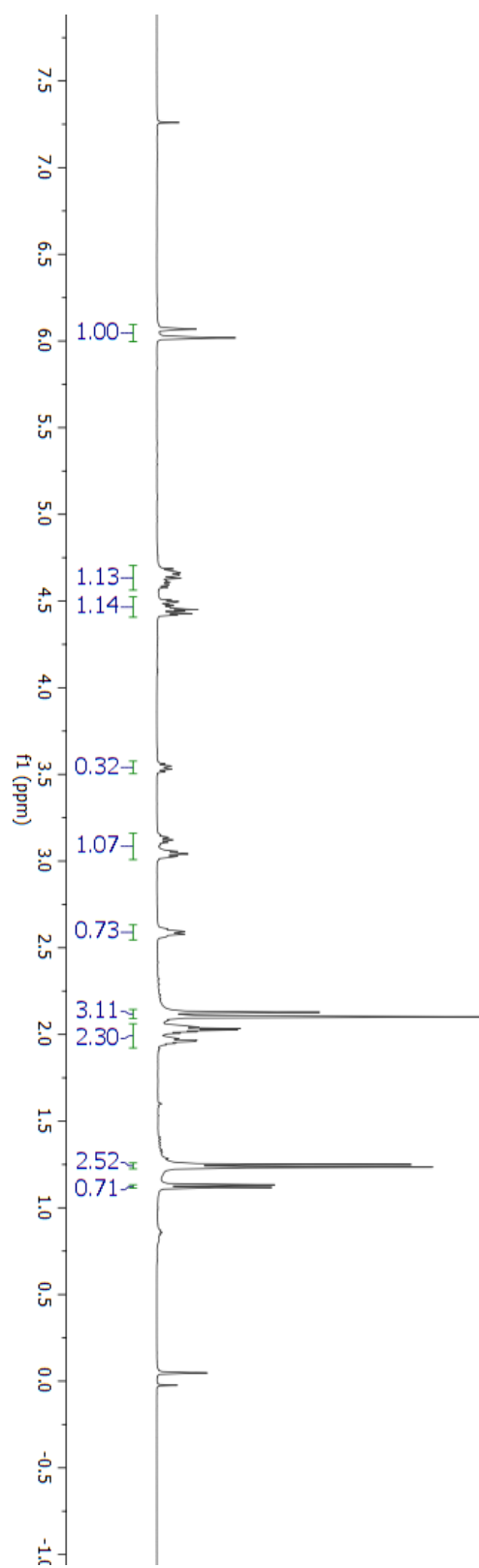
^{13}C -NMR for Compound 5.7a

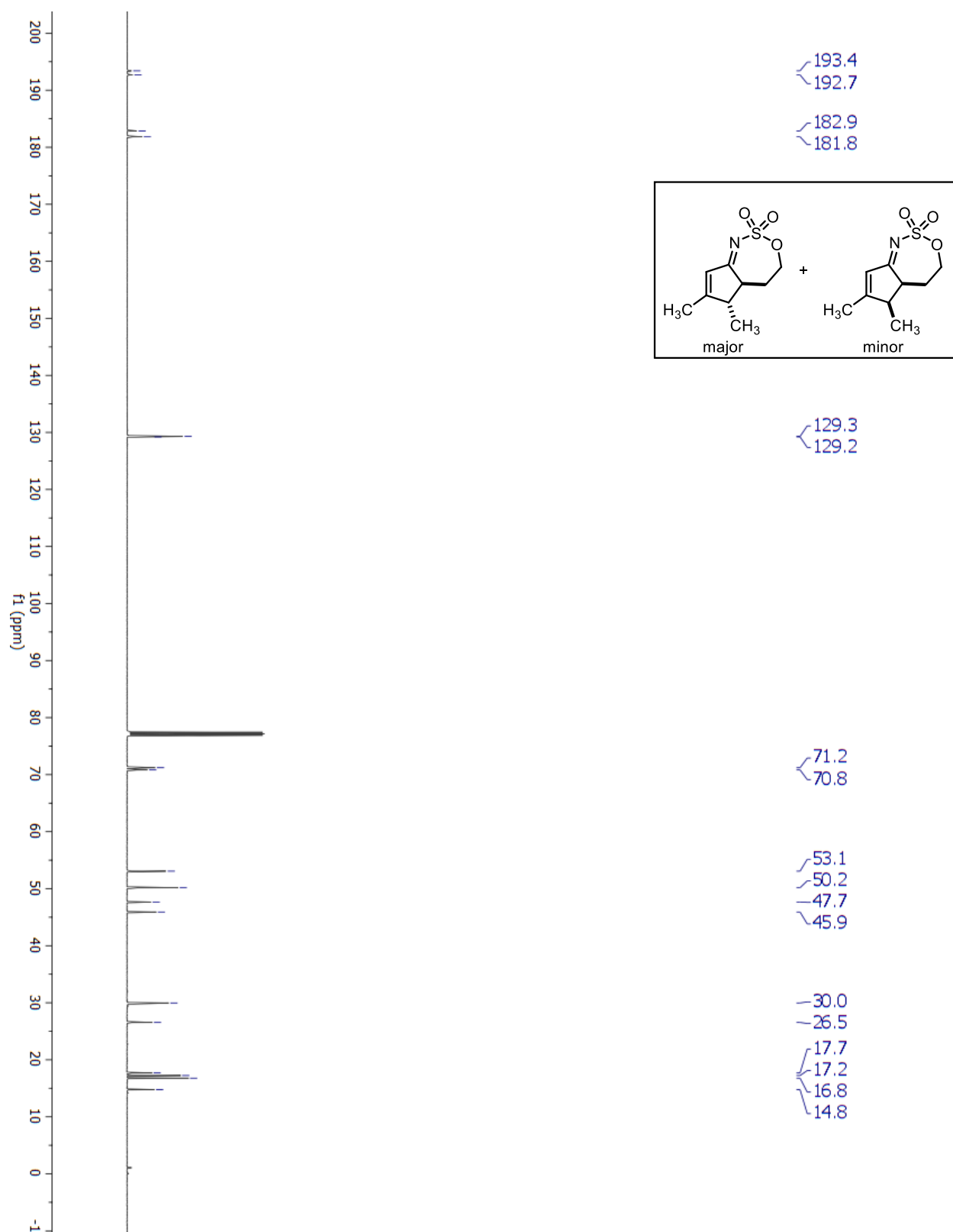
¹H-NMR for Compound 5.8a

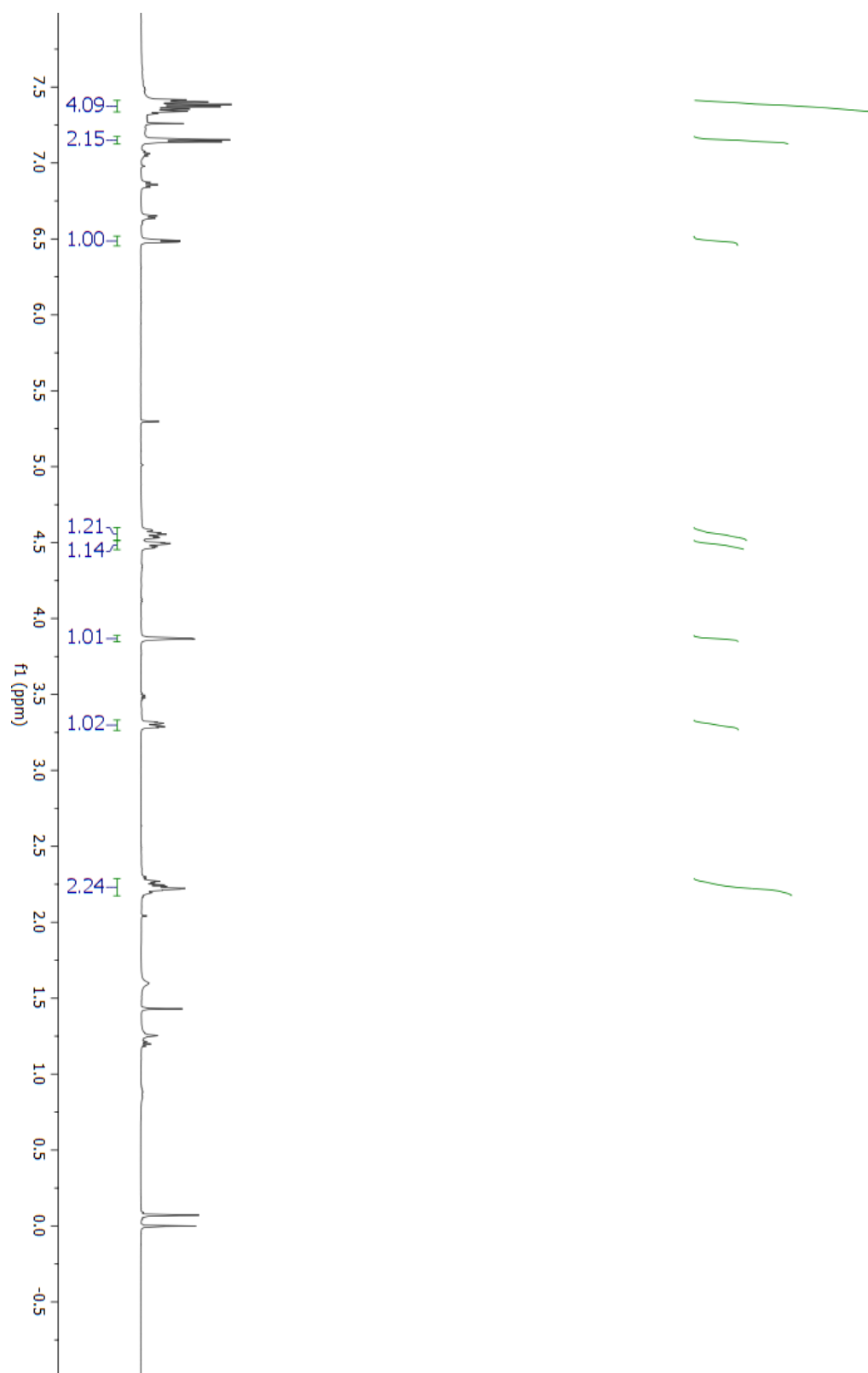
^{13}C -NMR for Compound 5.8a

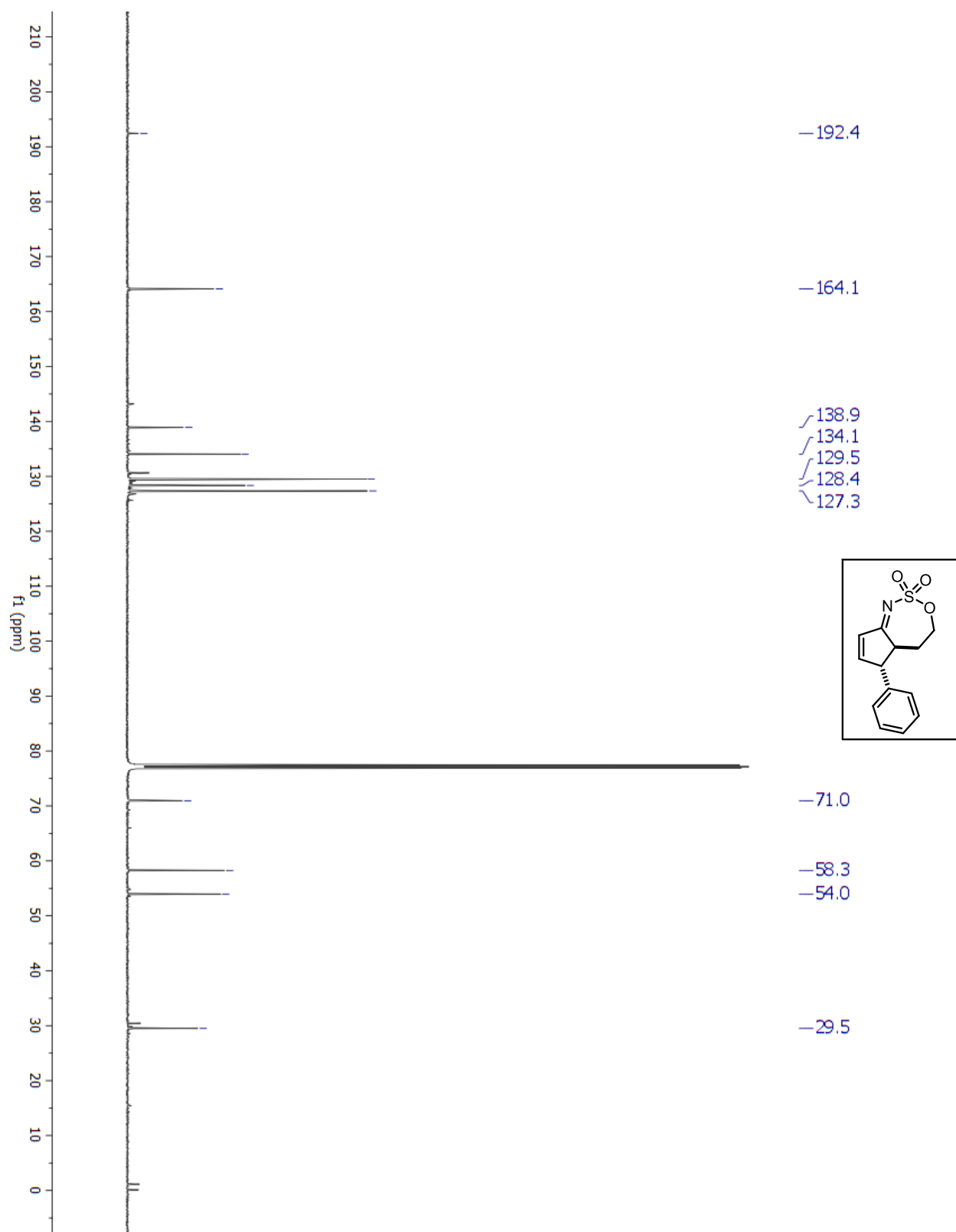
¹H-NMR for Compound 5.9a

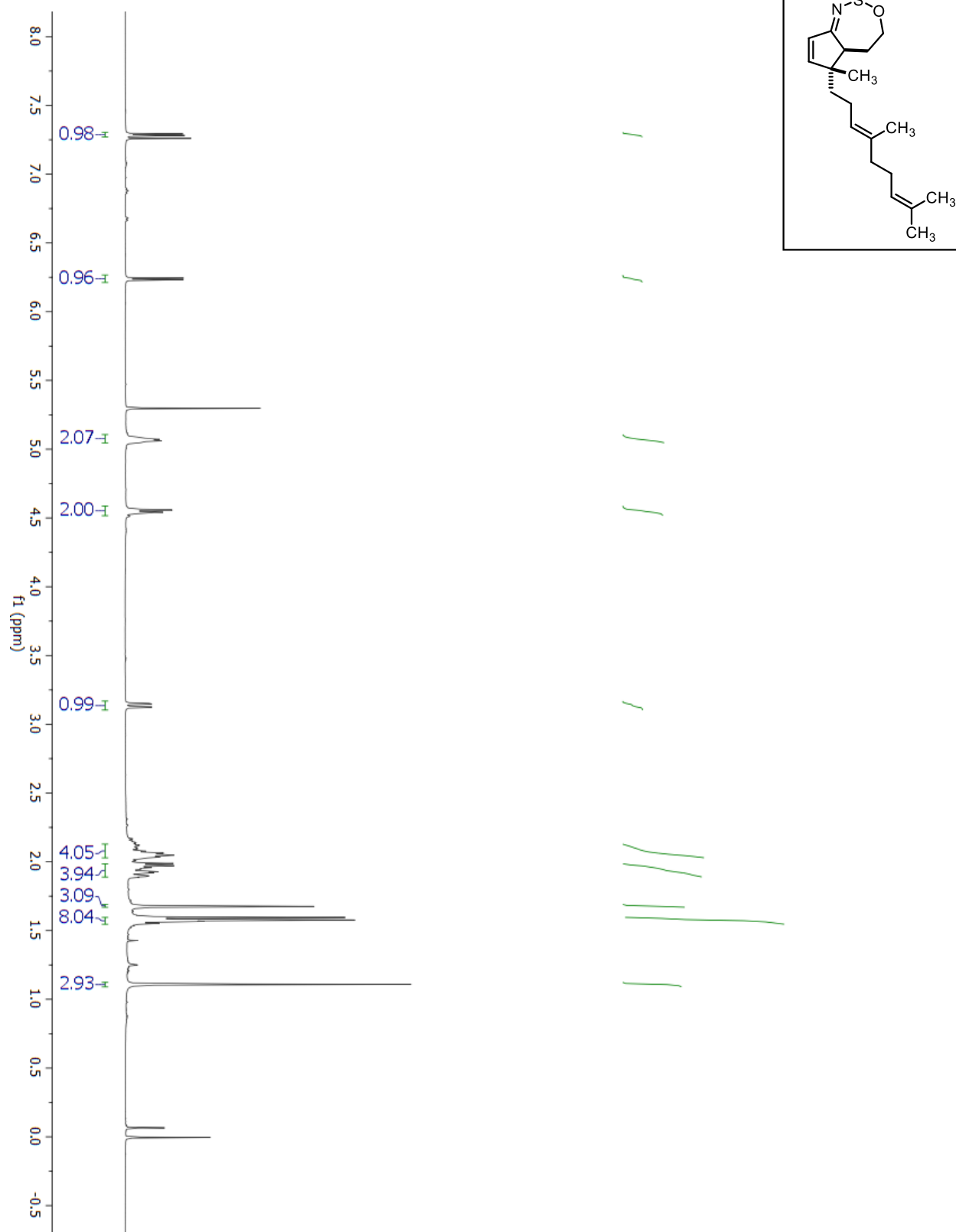
^{13}C -NMR for Compound 5.9a

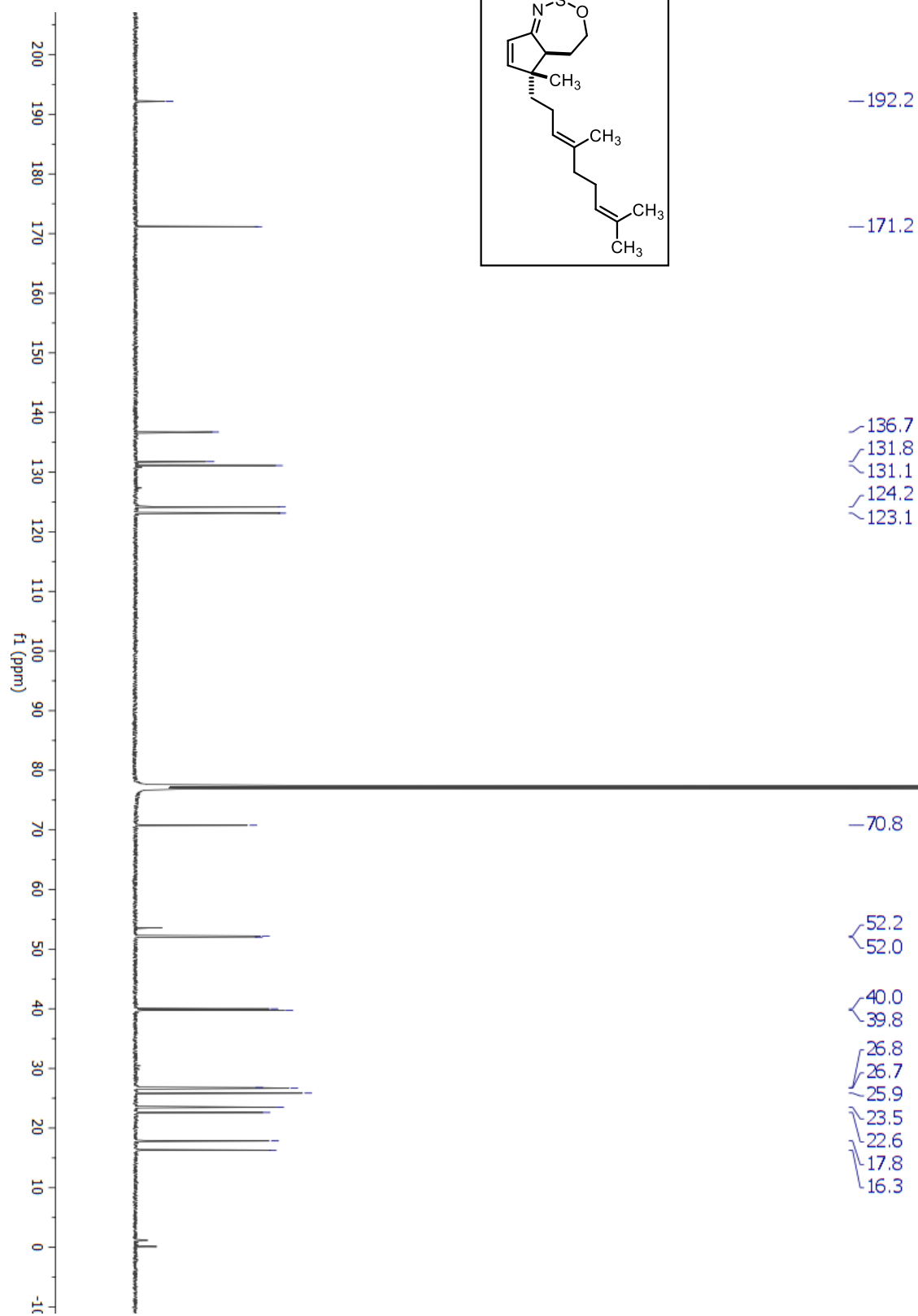
¹H-NMR for Compound 5.10a

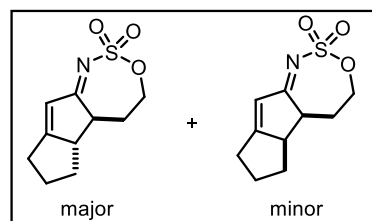
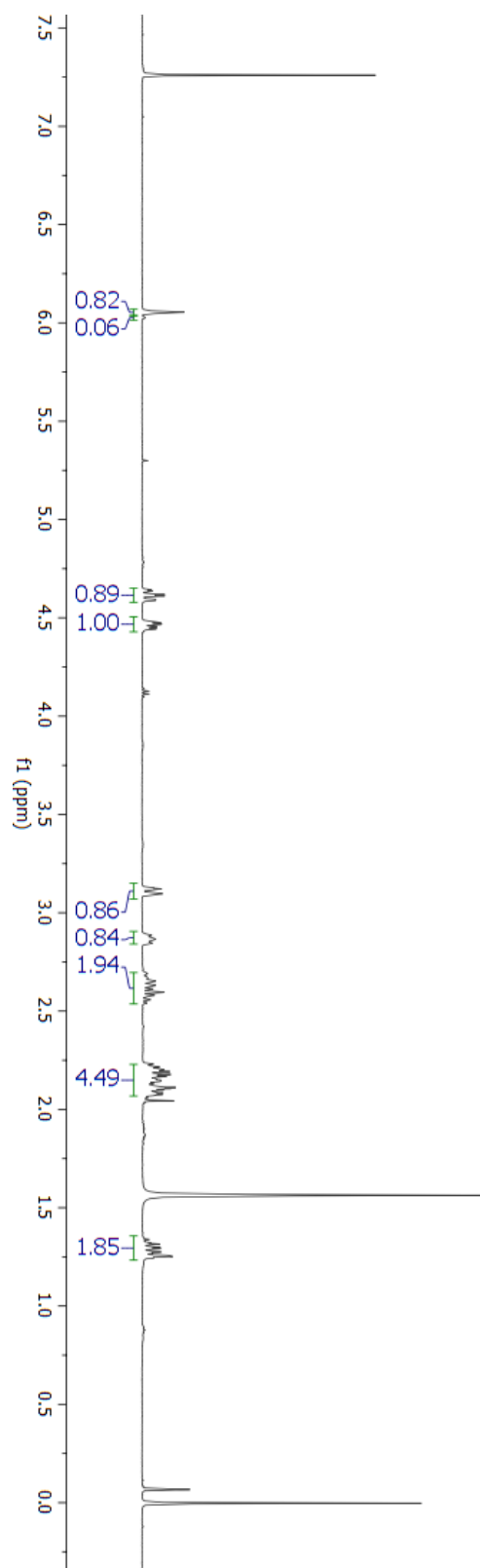
^{13}C -NMR for Compound 5.10a

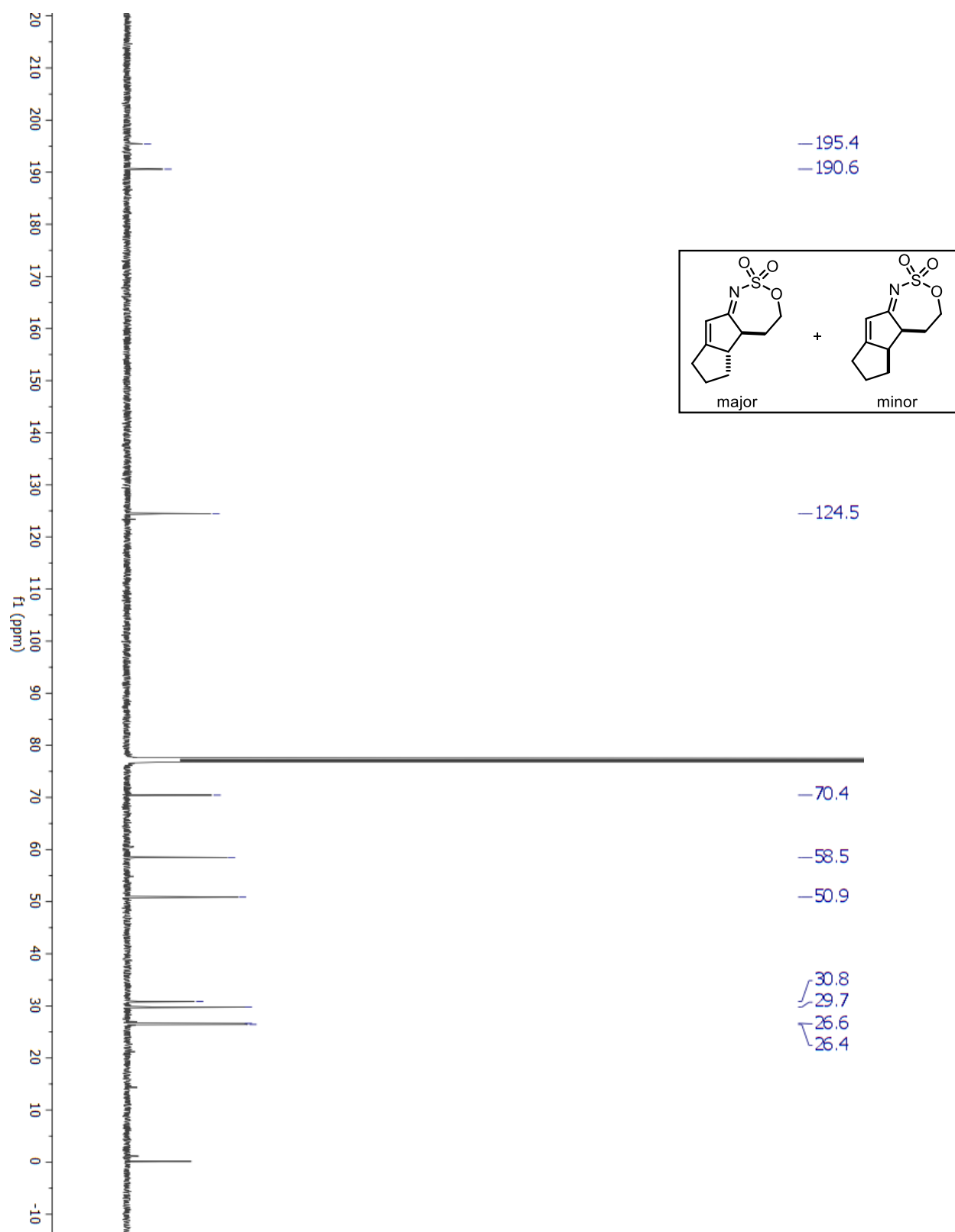
¹H-NMR for Compound 5.11a

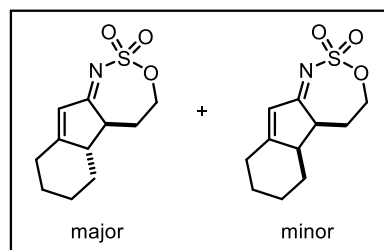
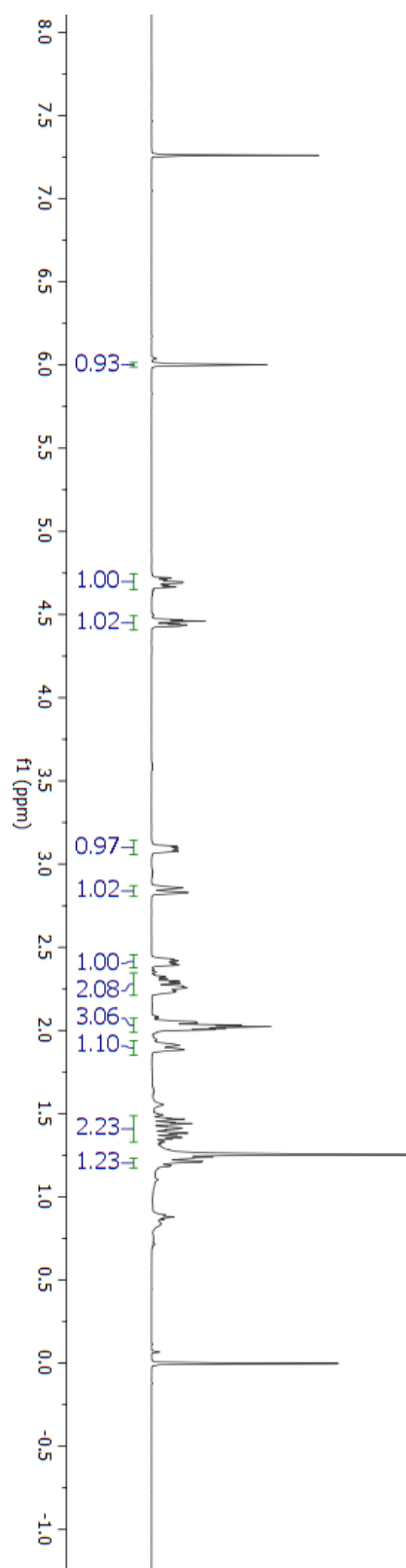
^{13}C -NMR for Compound 5.11a

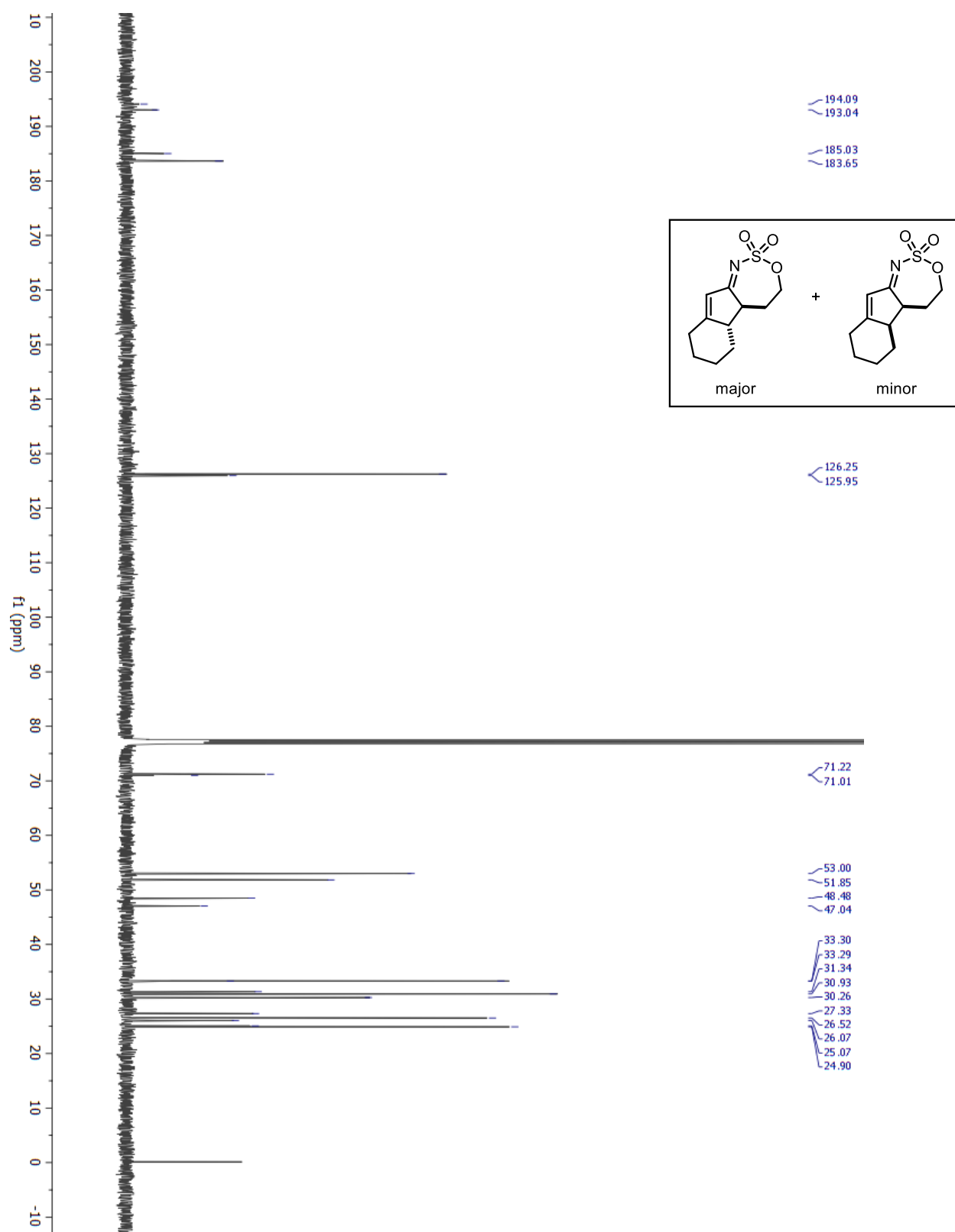
¹H-NMR for Compound 5.12a

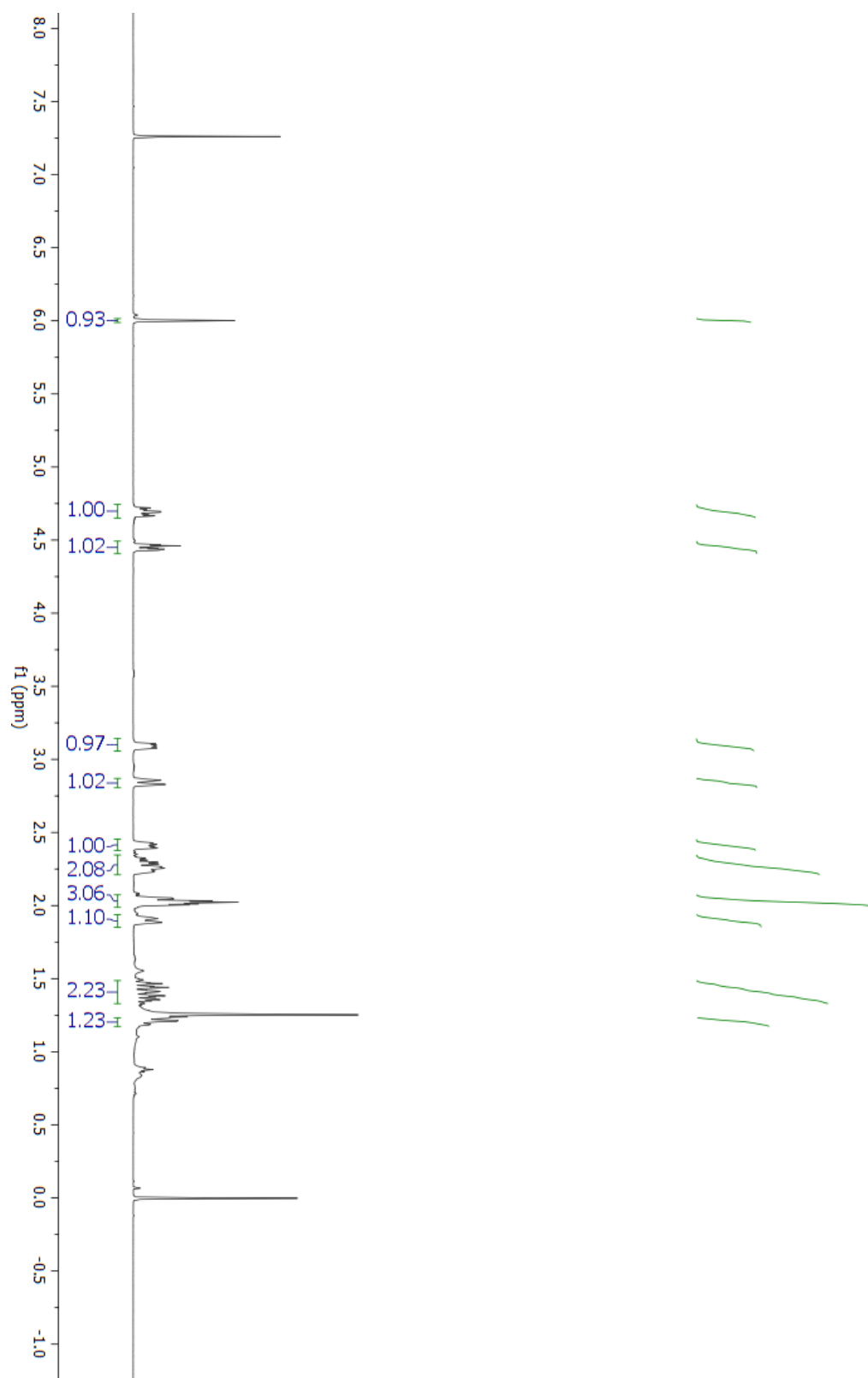
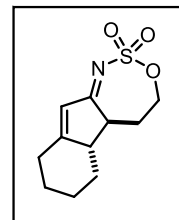
^{13}C -NMR for Compound 5.12a

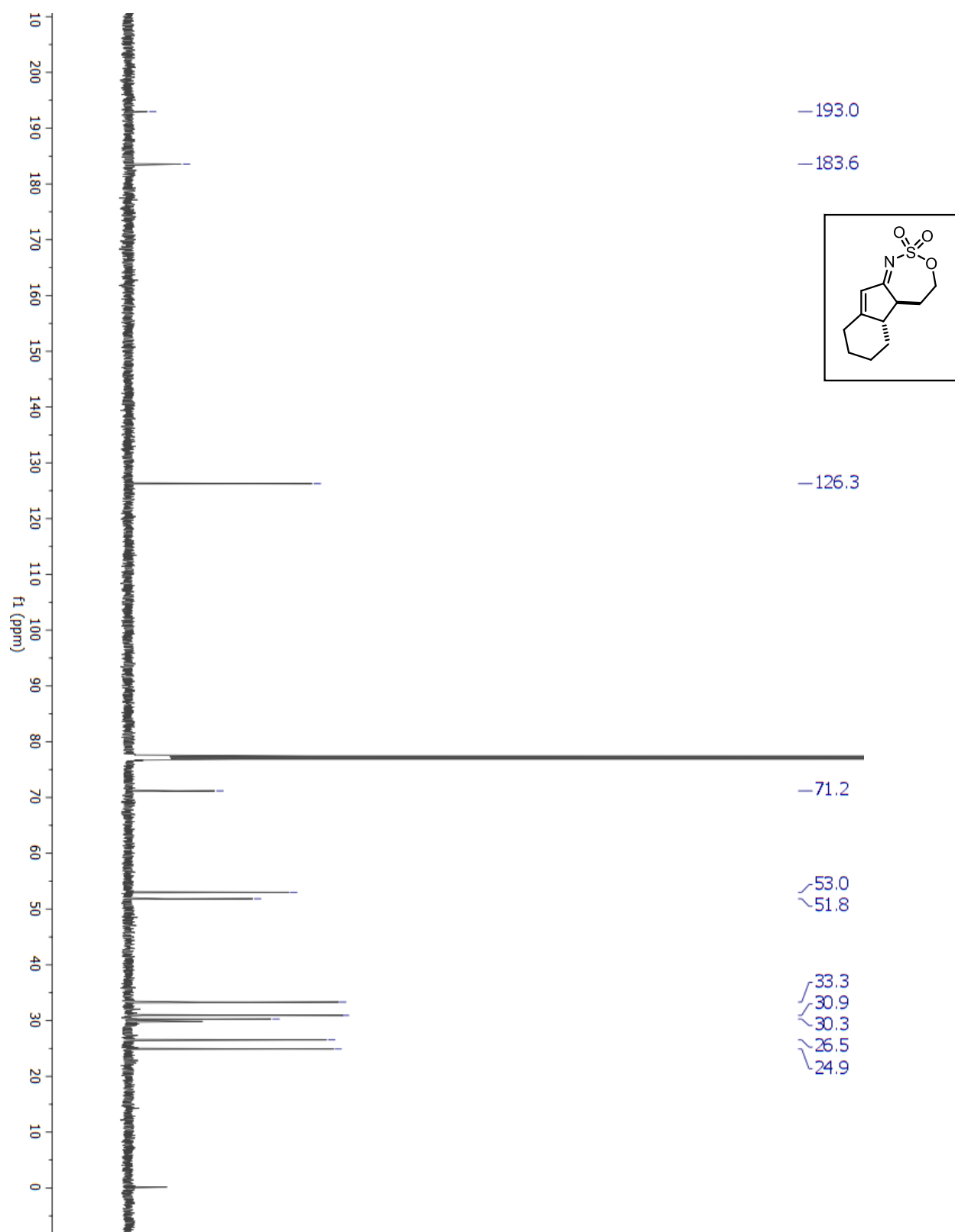
¹H-NMR for Compound 5.13a

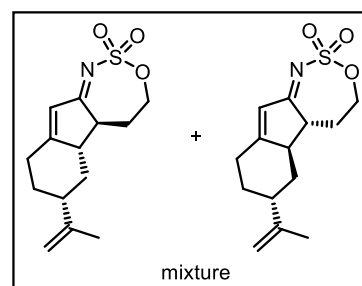
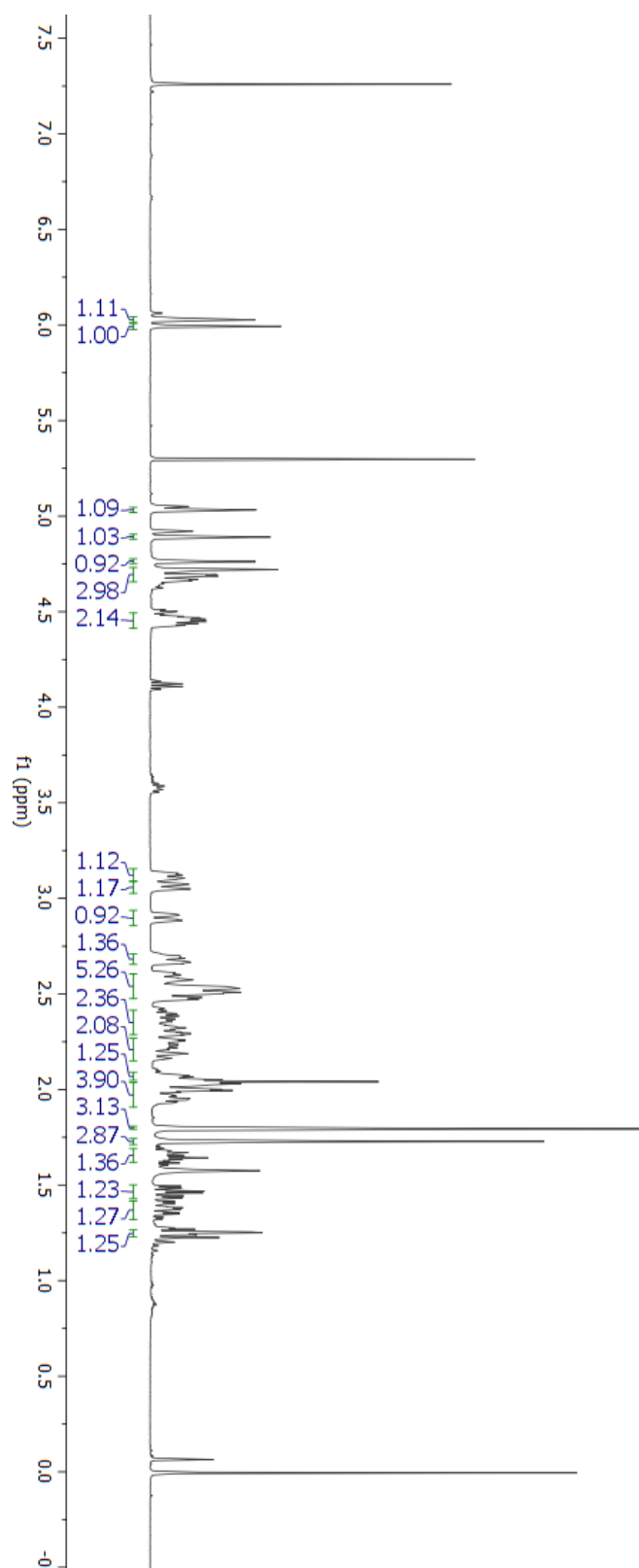
^{13}C -NMR for Compound 5.13a

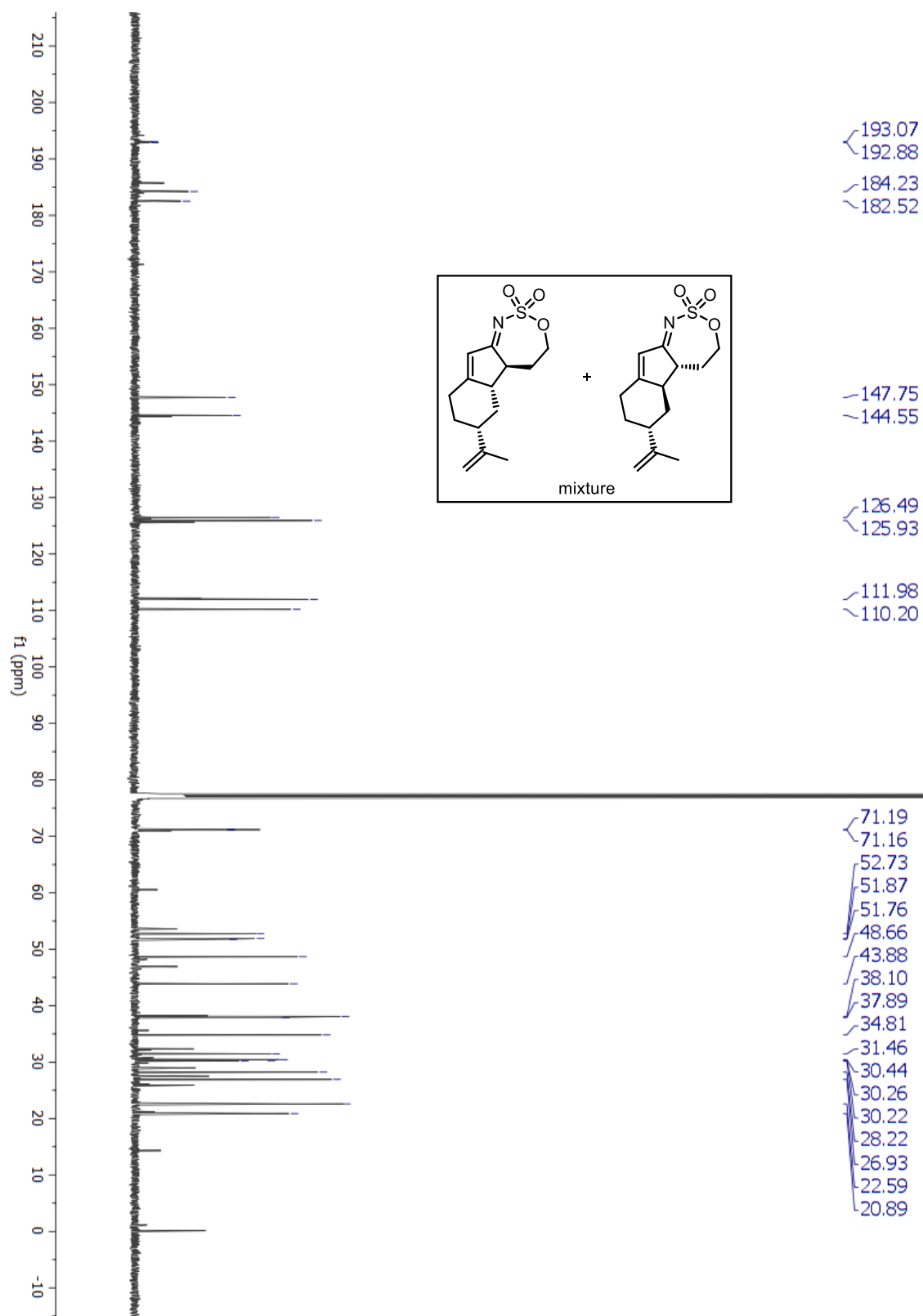
¹H-NMR for Compound 5.14a (mix of diastereomers)

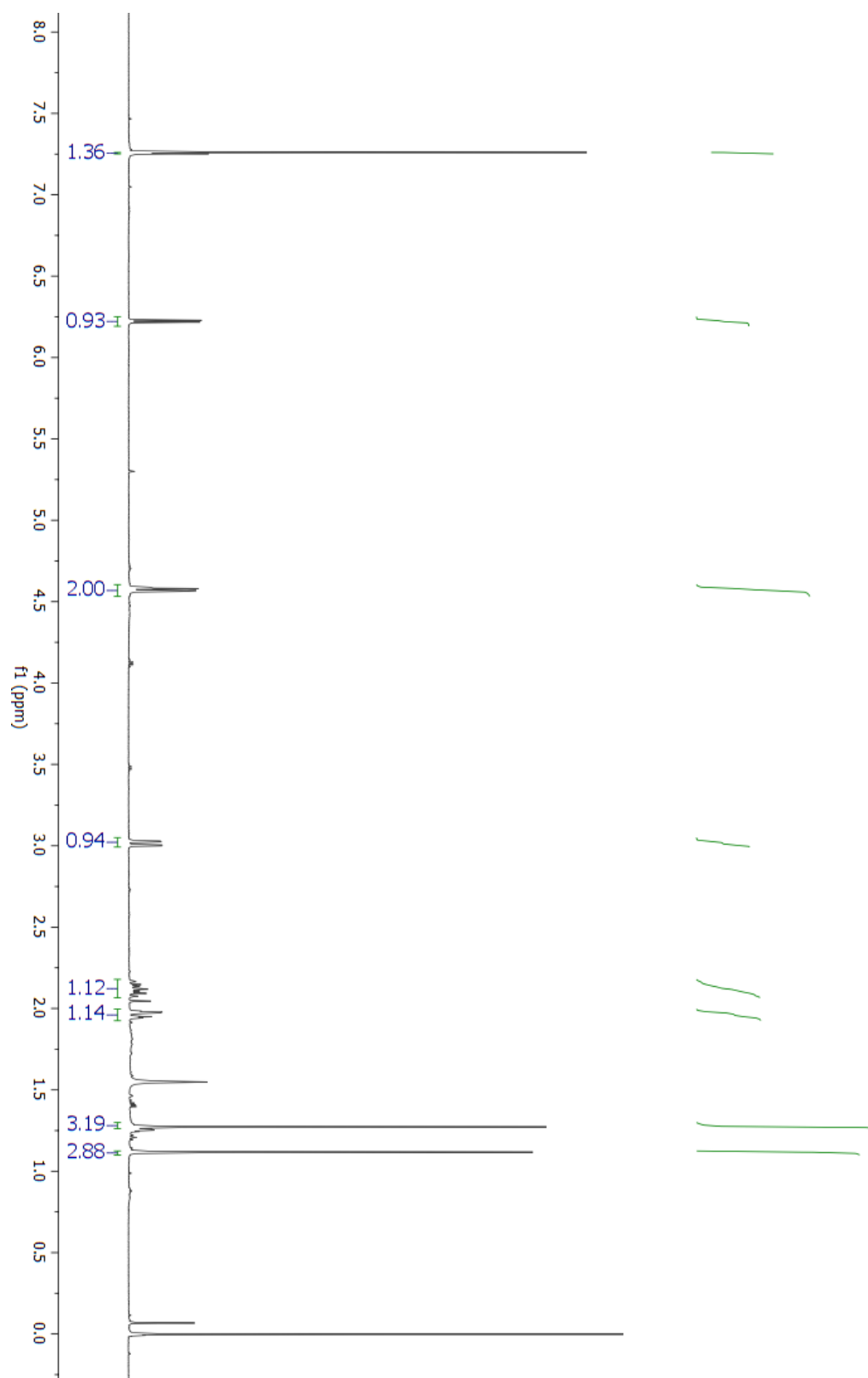
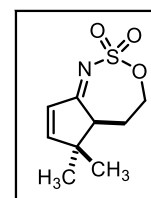
^{13}C -NMR for Compound 5.14a (mix of diastereomers)

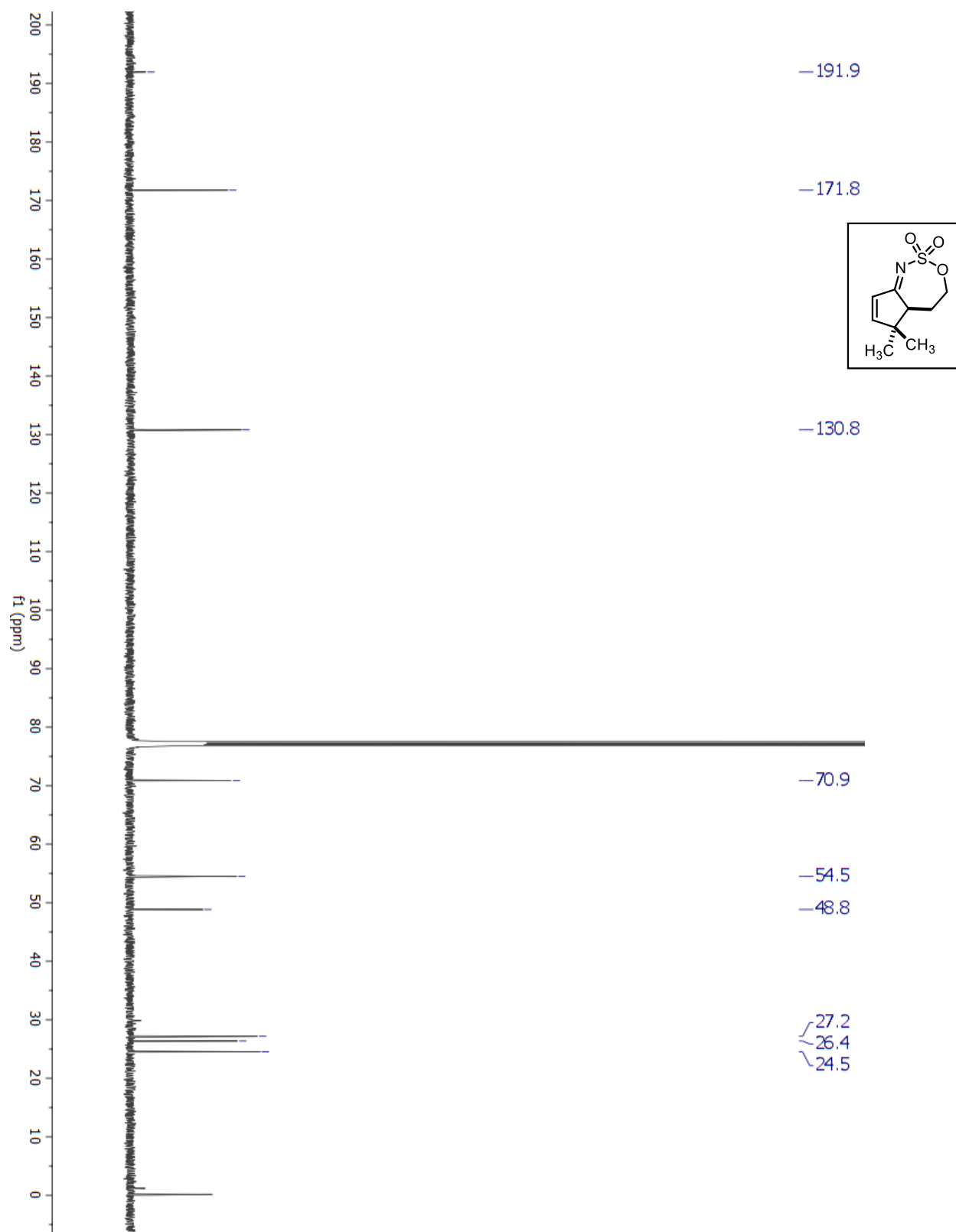
¹H-NMR for Compound *anti*-5.14a

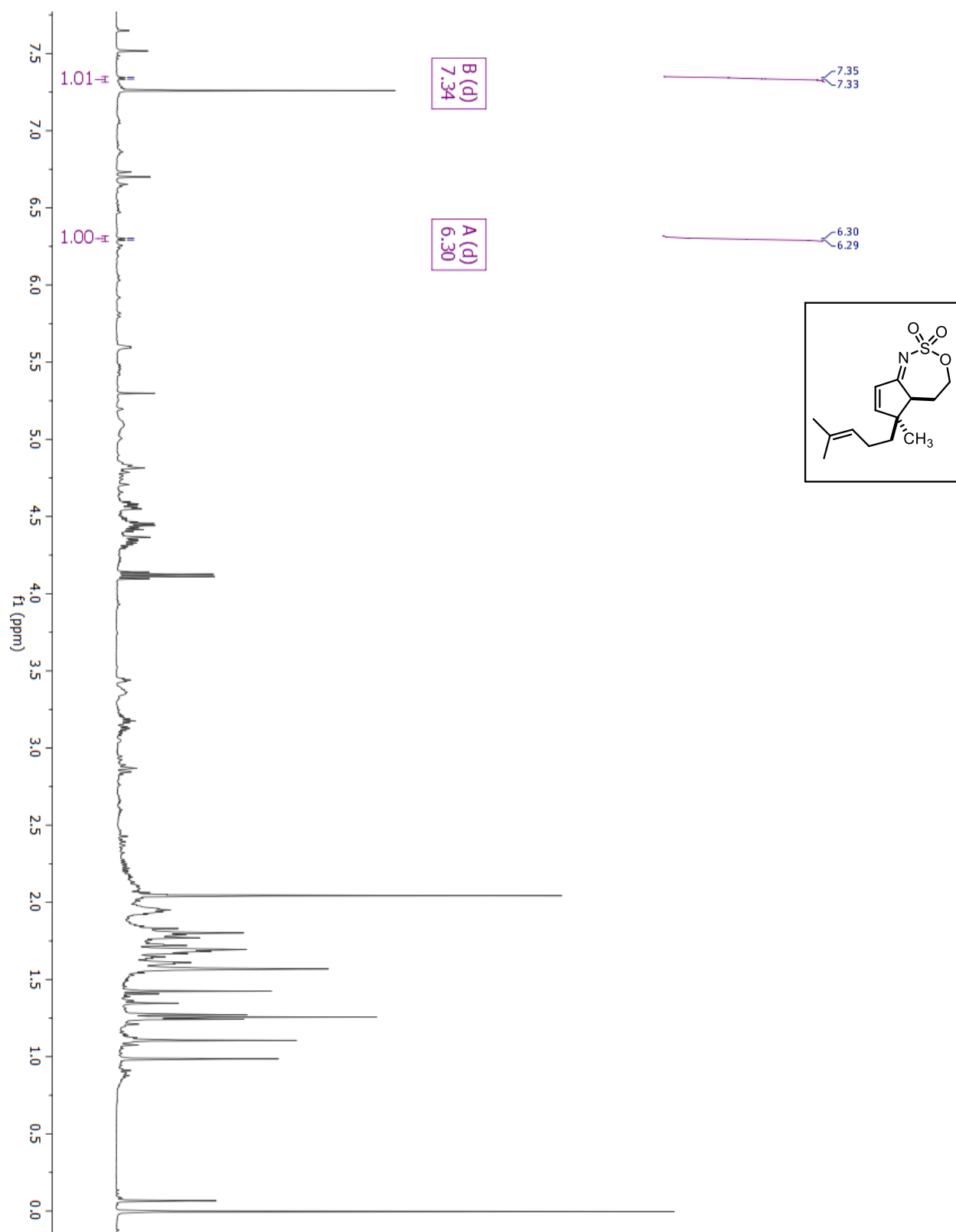
^{13}C -NMR for Compound *anti*-5.14a

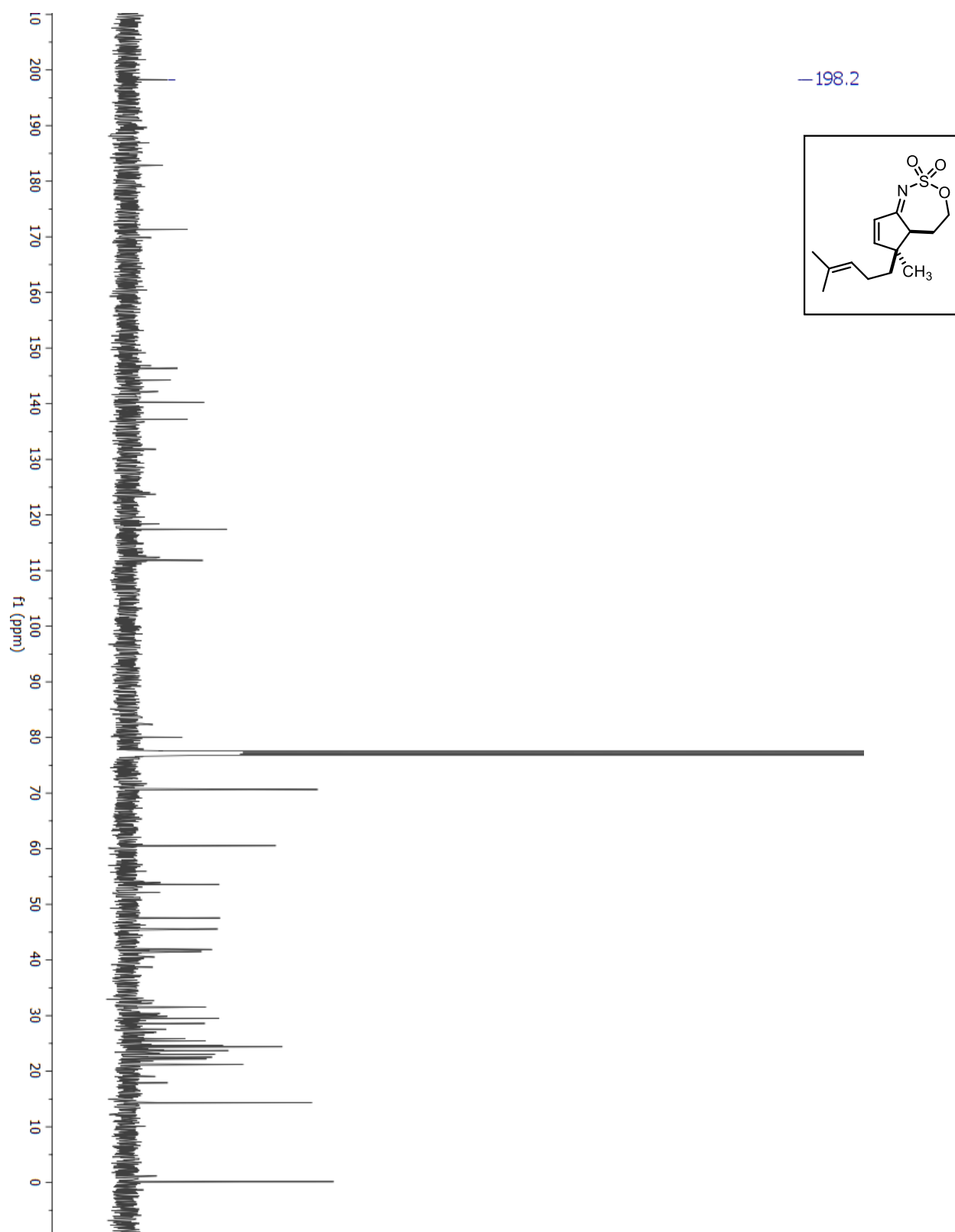
¹H-NMR for Compound 5.15a

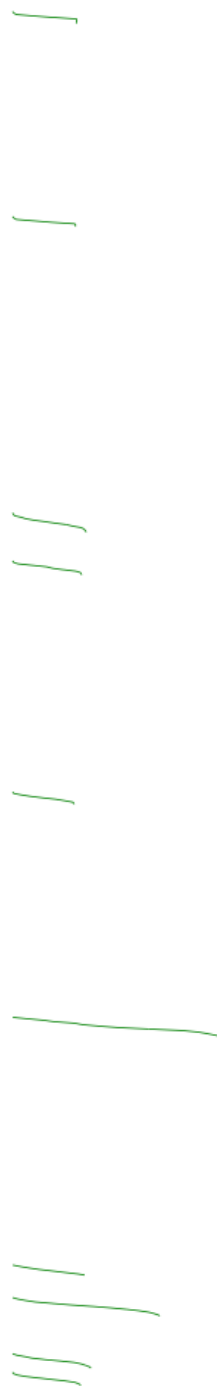
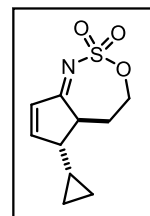
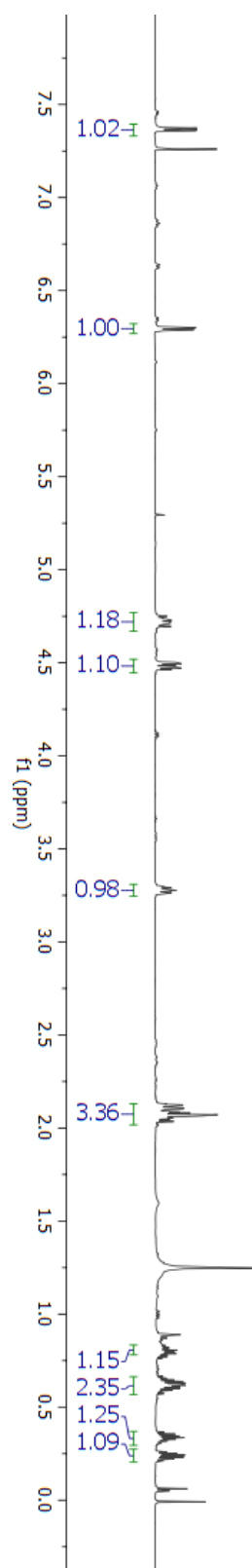
^{13}C -NMR for Compound 5.15a

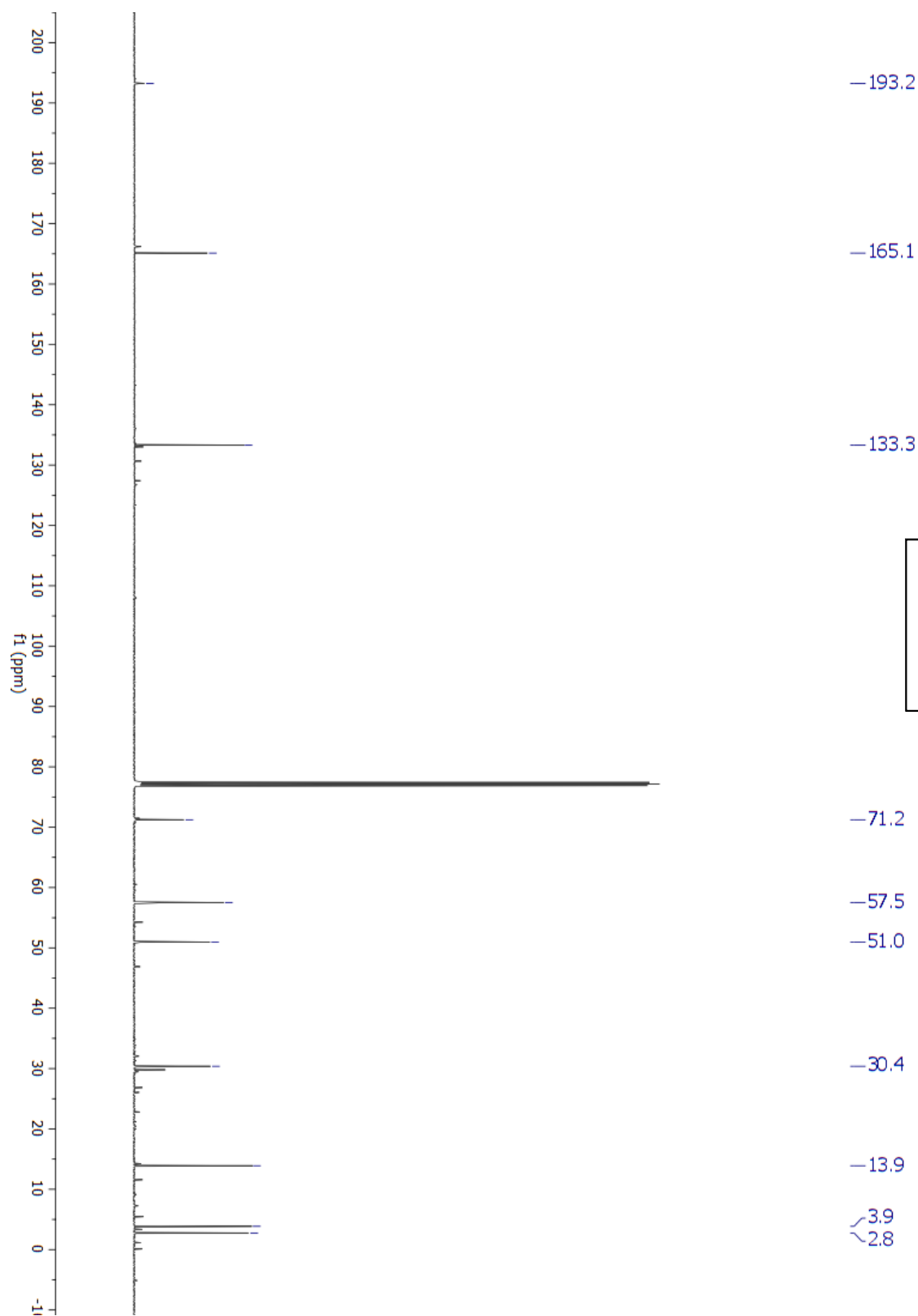
¹H-NMR for Compound 5.16a

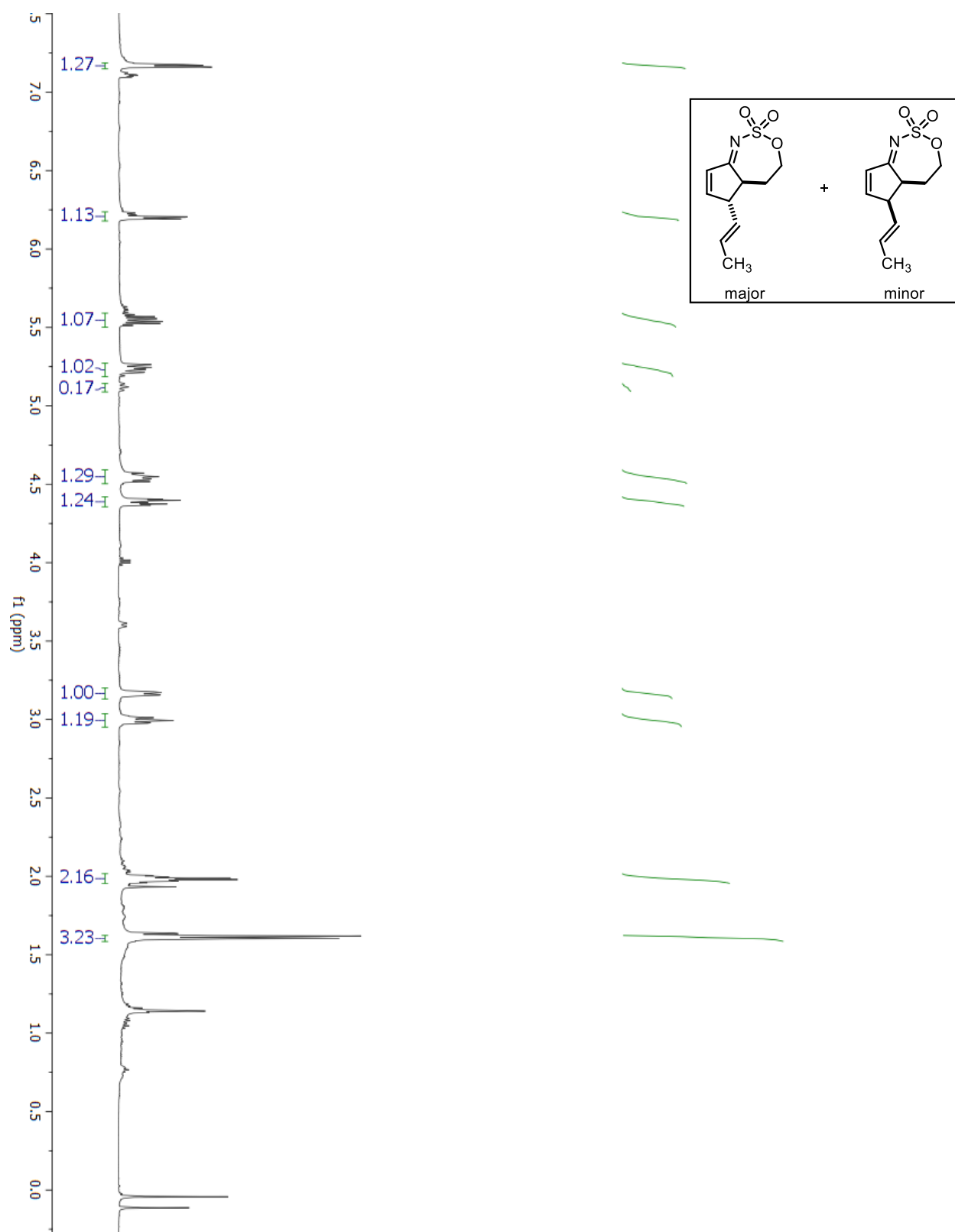
^{13}C -NMR for Compound 5.16a

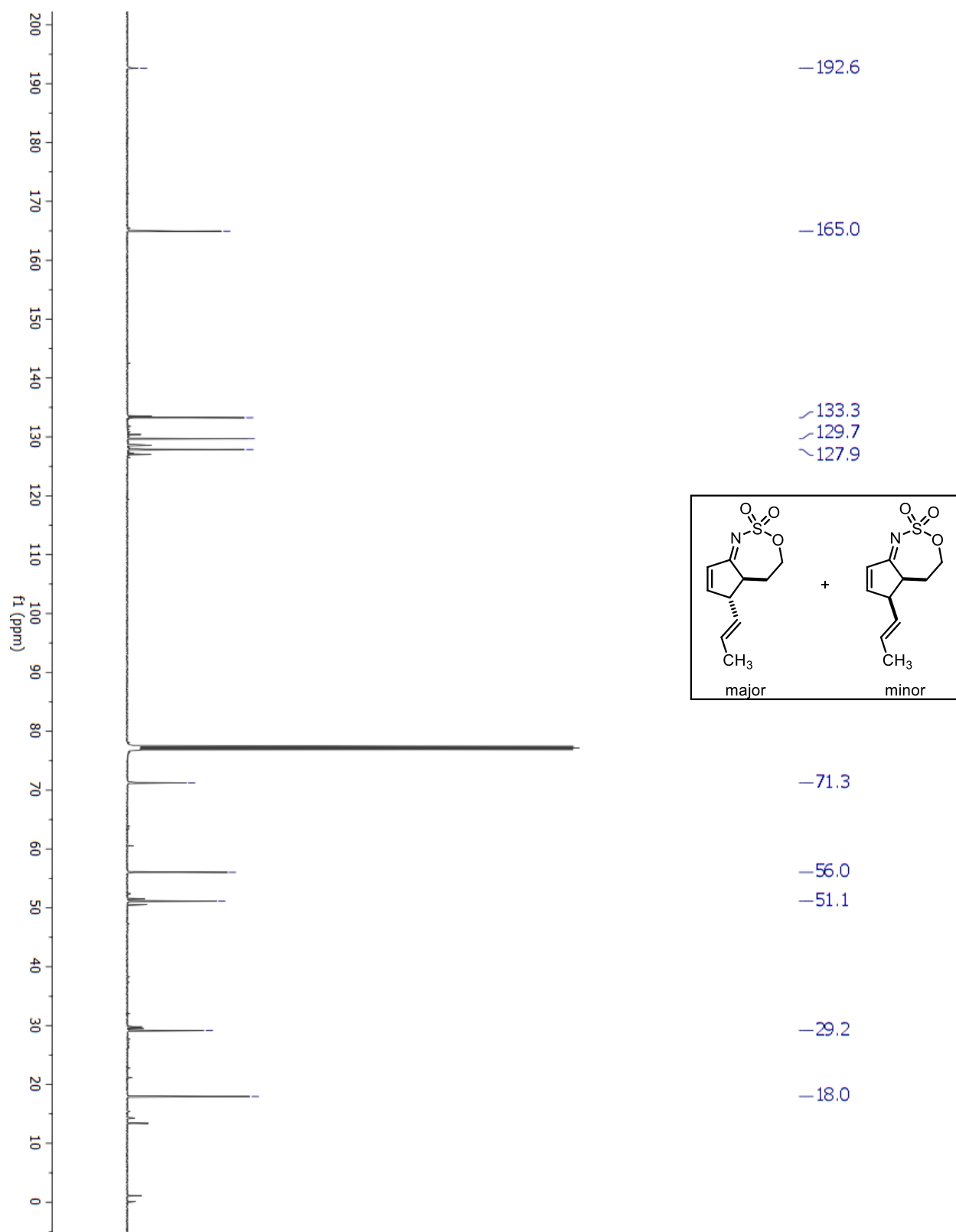
¹H-NMR for Compound 5.17a

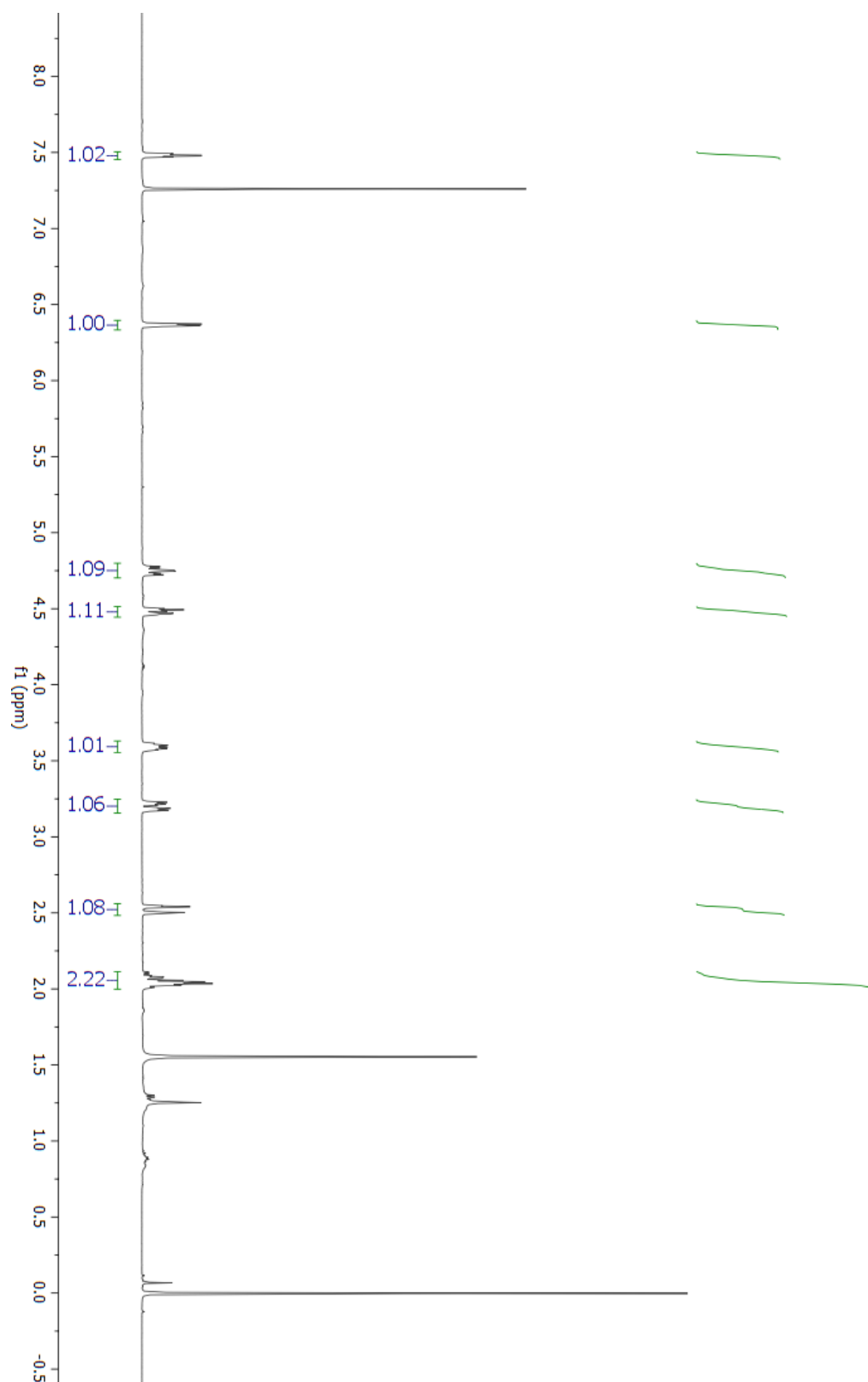
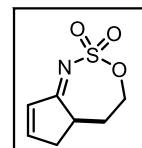
^{13}C -NMR for Compound 5.17a

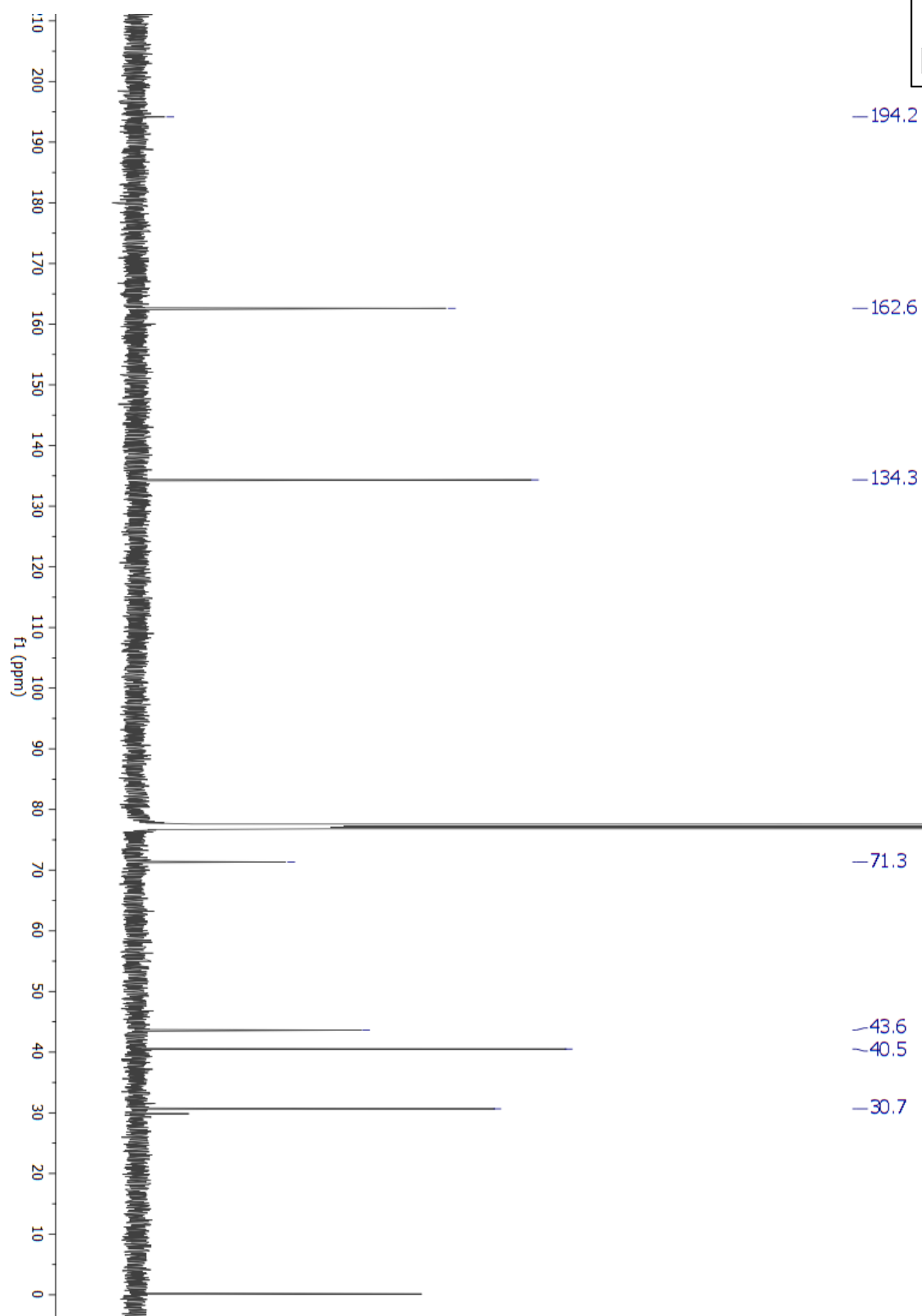
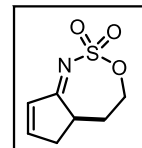
¹H-NMR for Compound 5.18a

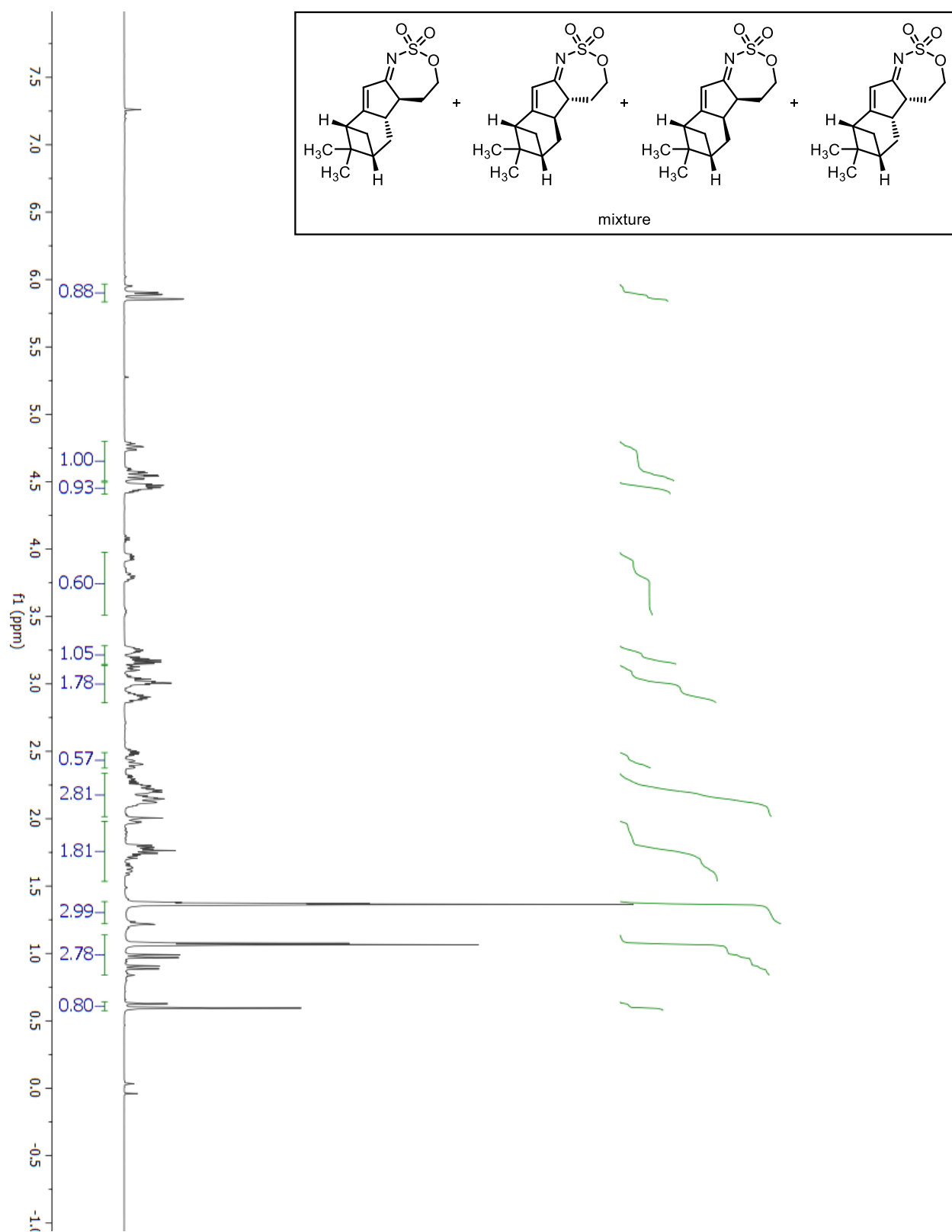
^{13}C -NMR for Compound 5.18a

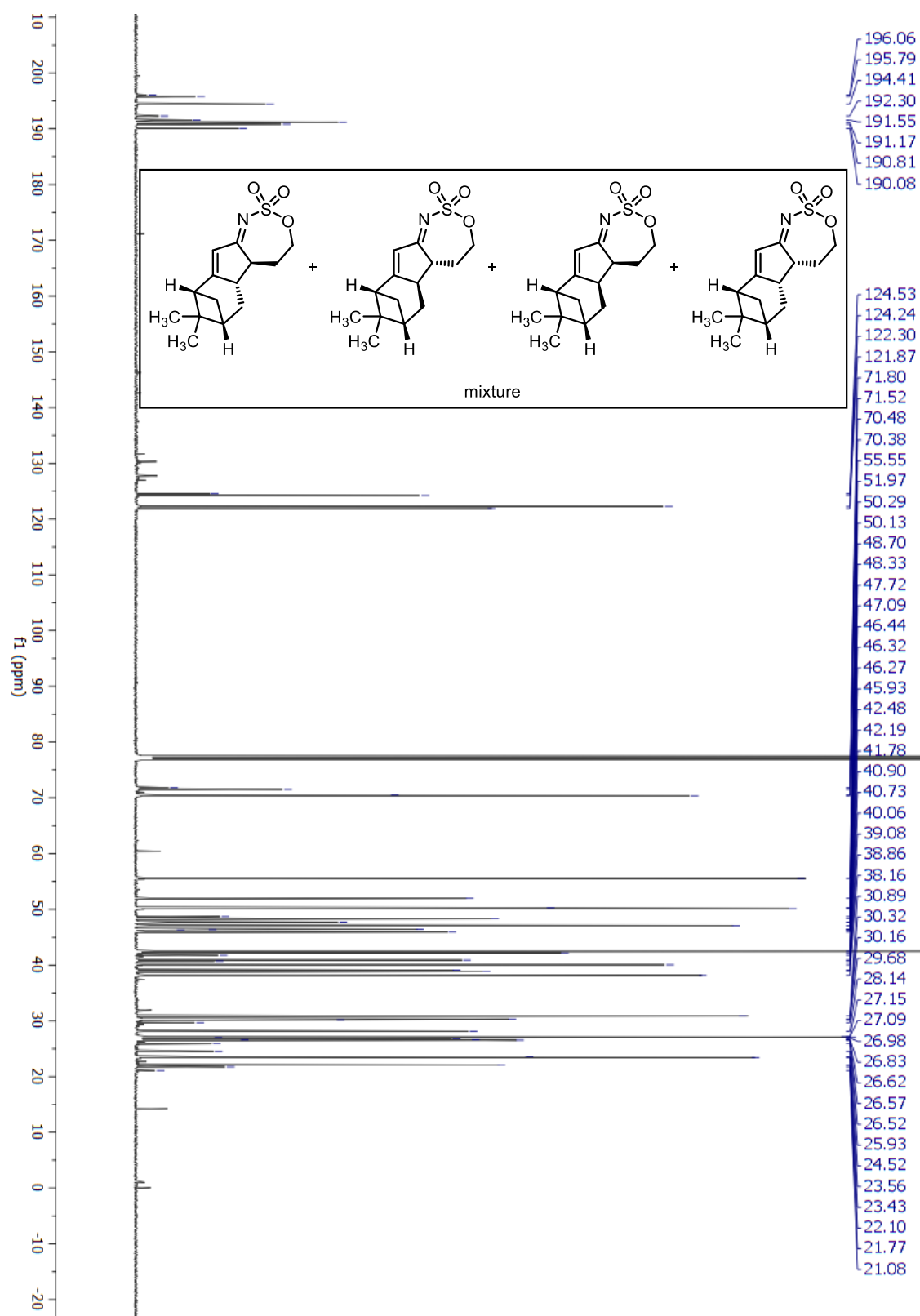
¹H-NMR for Compound 5.19a

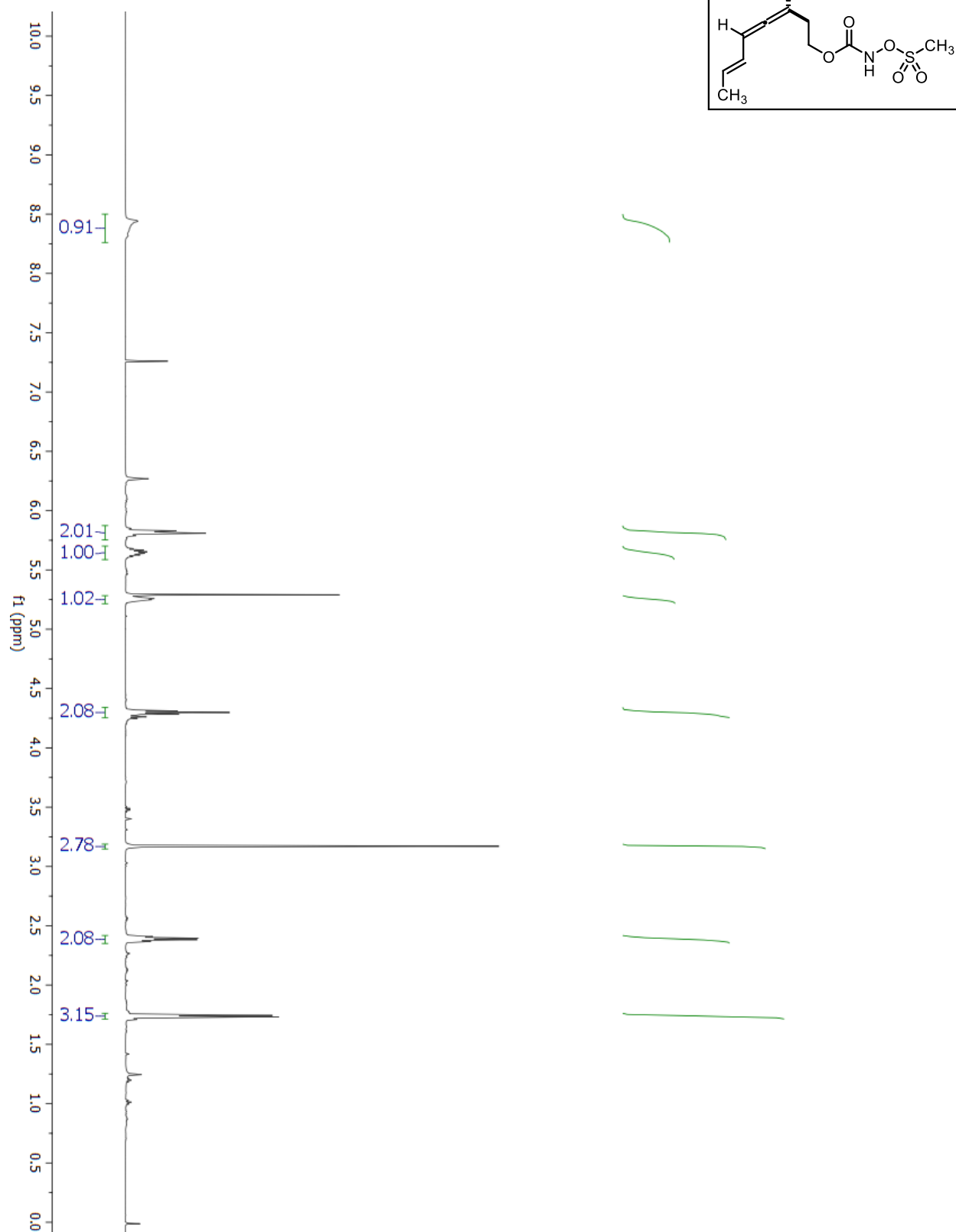
^{13}C -NMR for Compound 5.19a

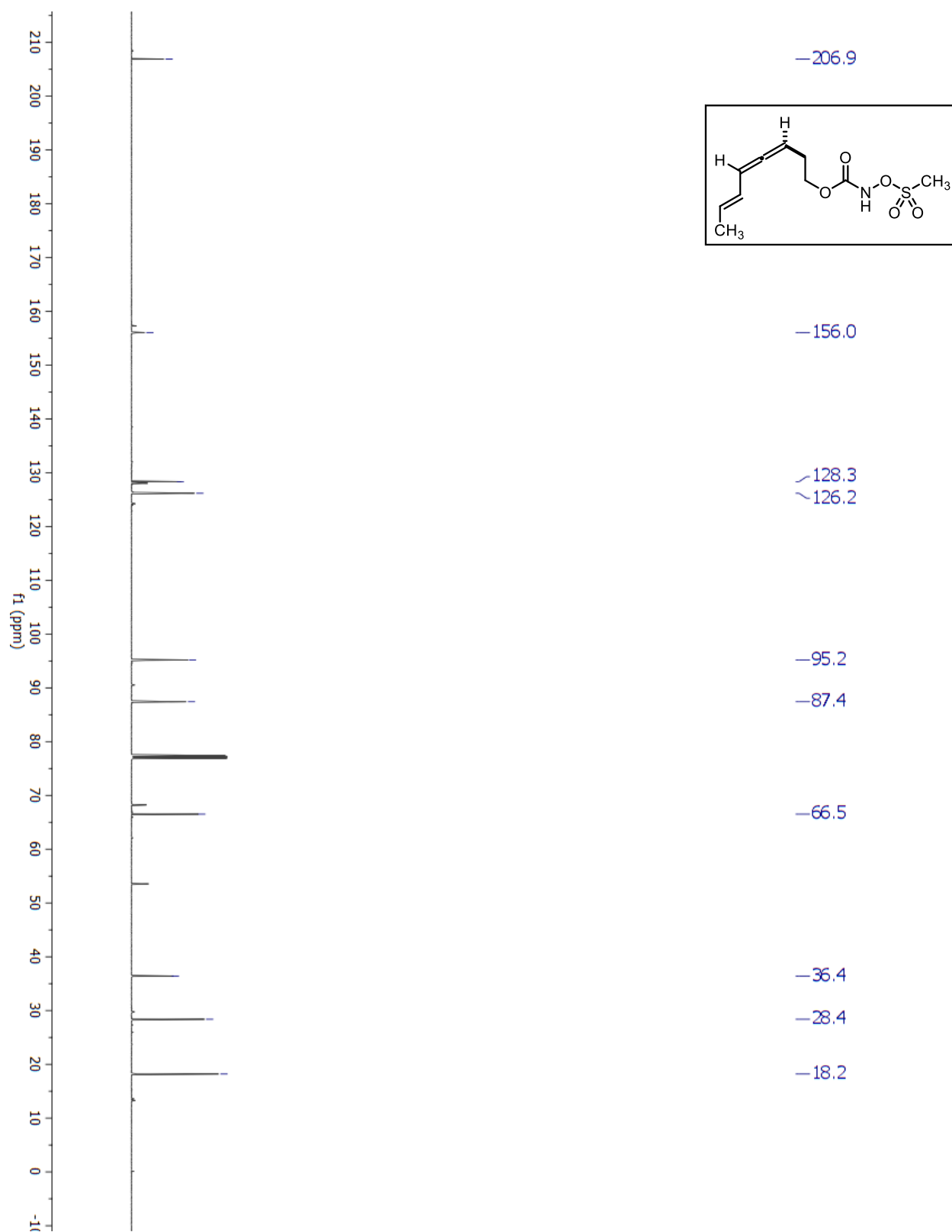
¹H-NMR for Compound 5.20a

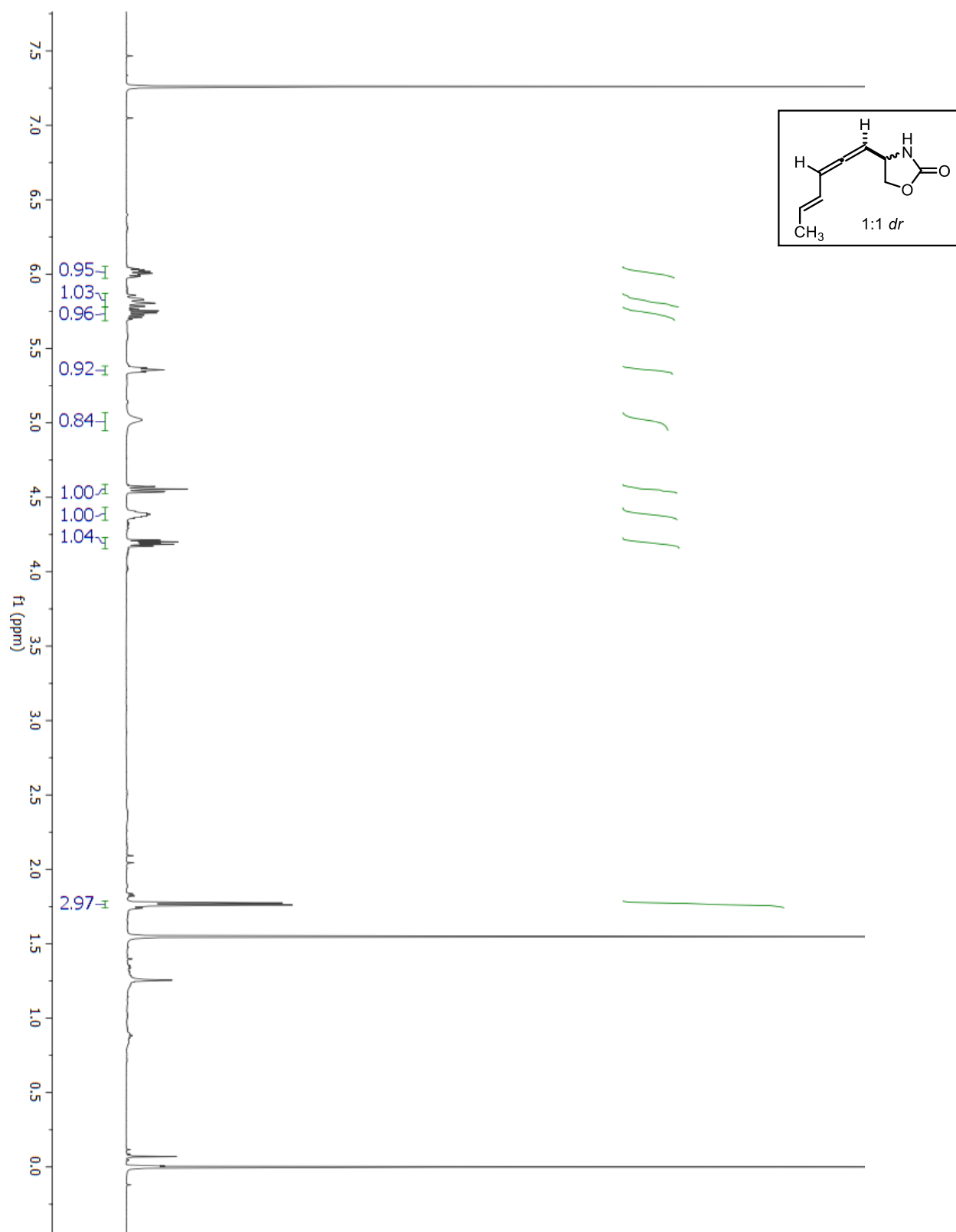
^{13}C -NMR for Compound 5.20a

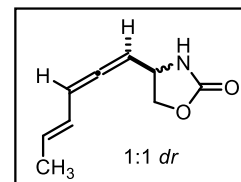
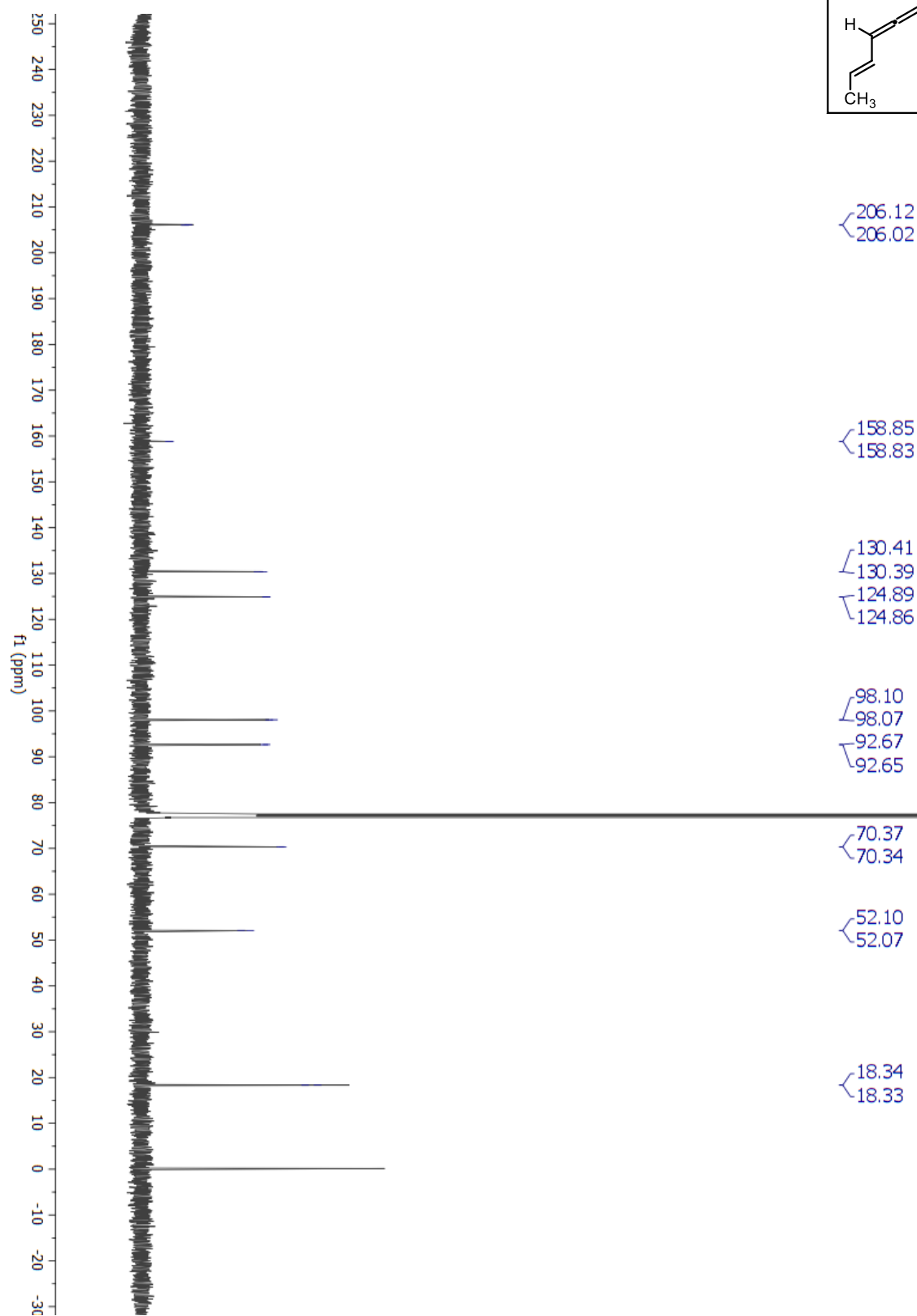
¹H-NMR for Compound 5.21a

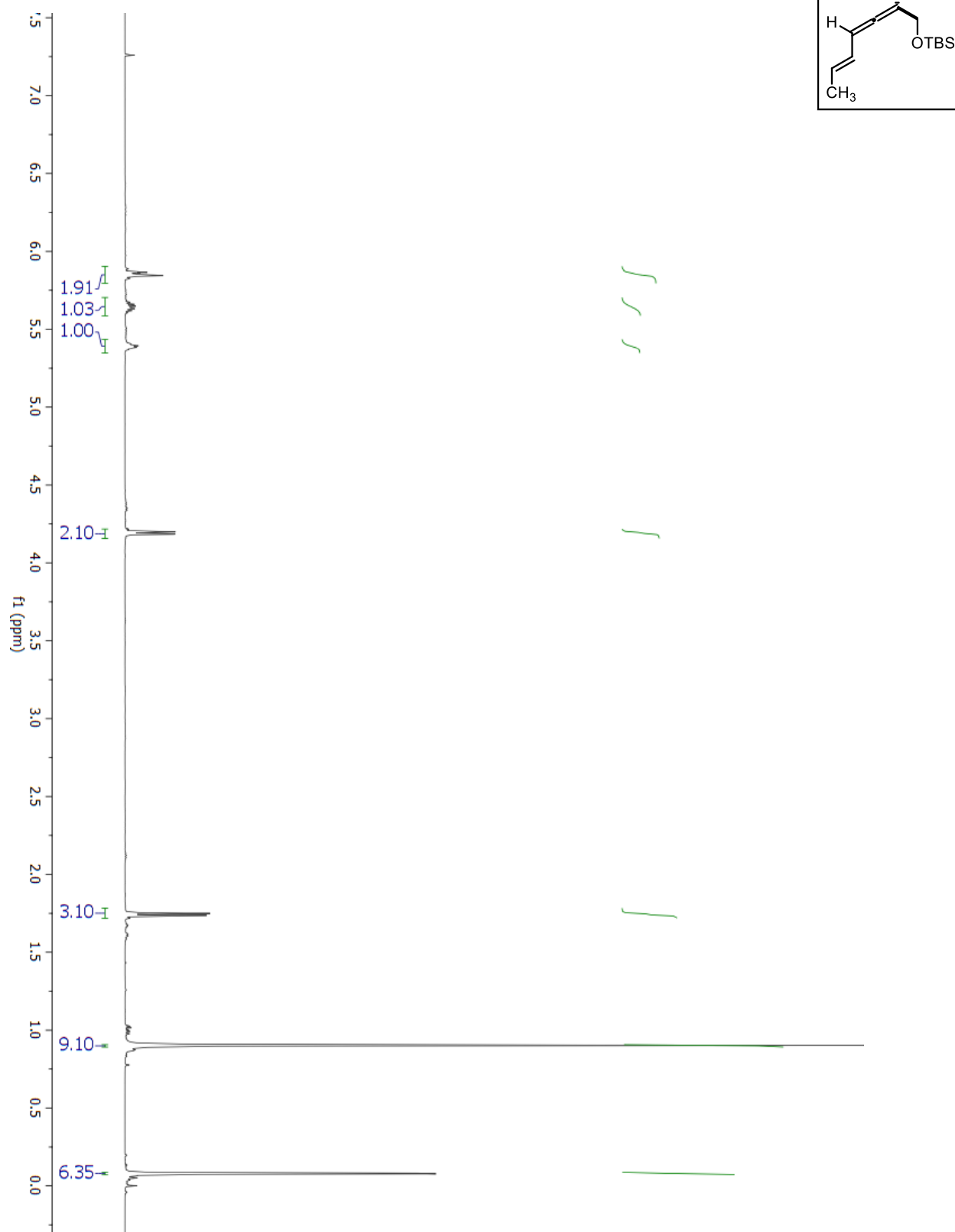
^{13}C -NMR for Compound 5.21a

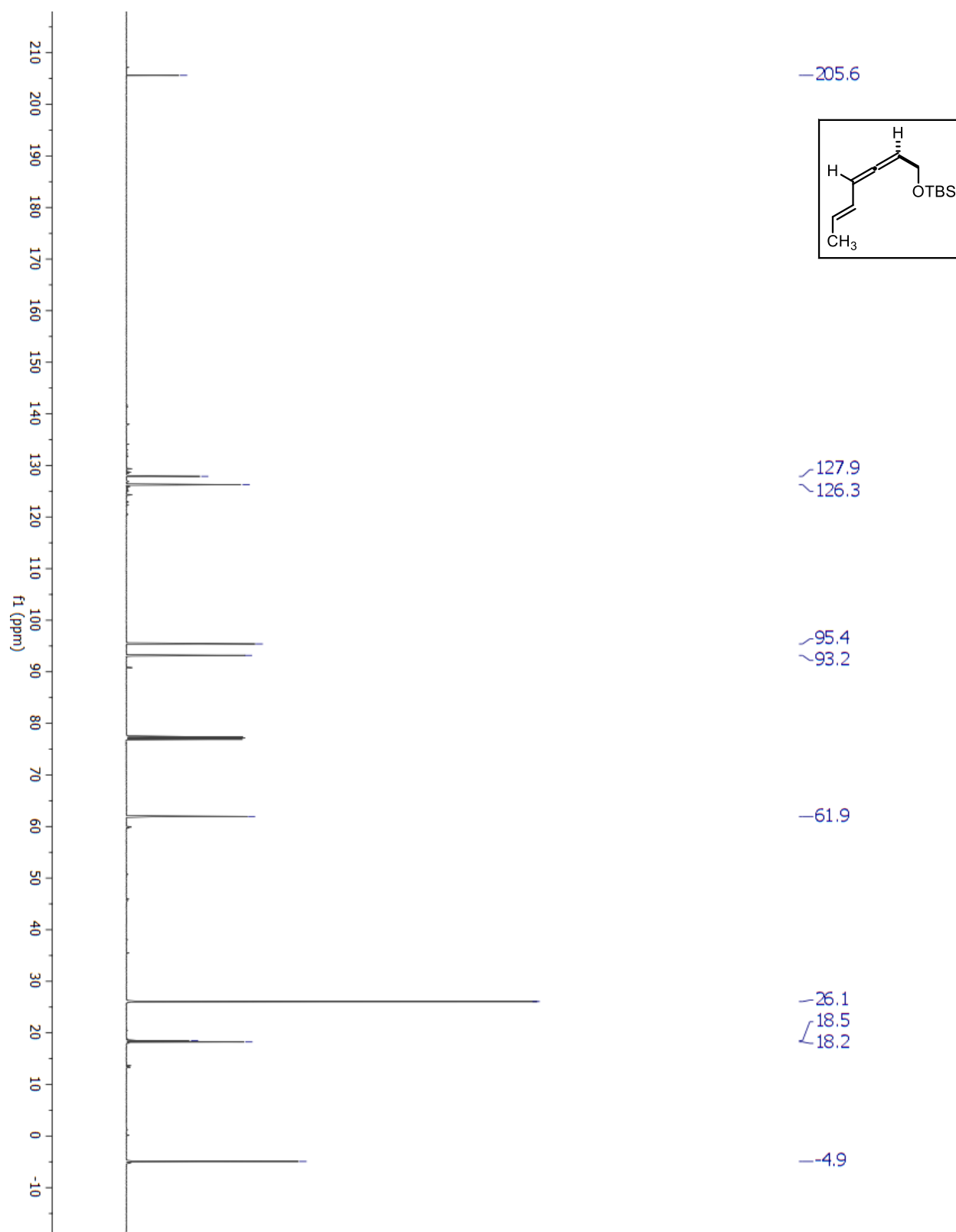
¹H-NMR for Compound S5.1

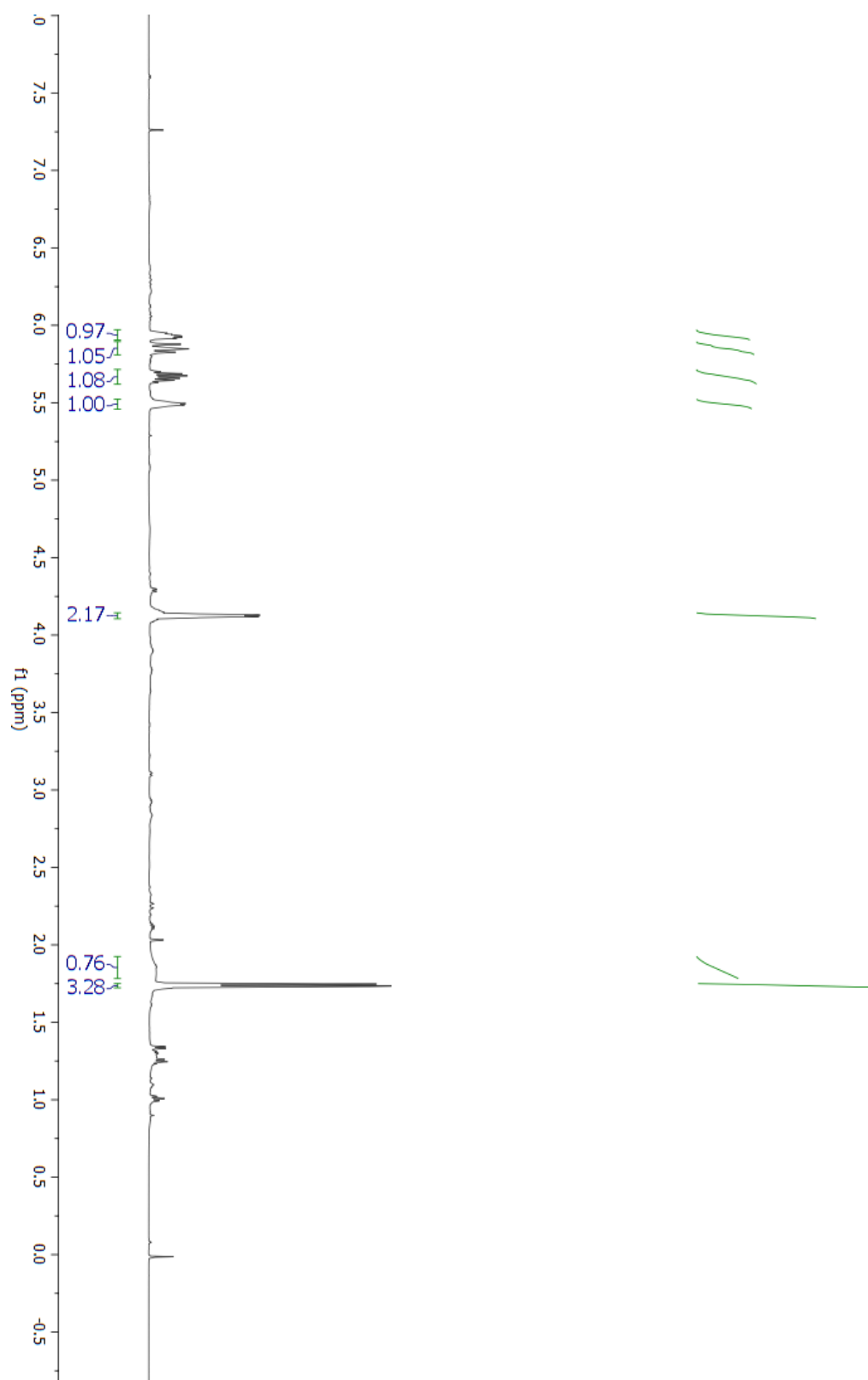
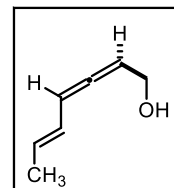
^{13}C -NMR for Compound S5.1

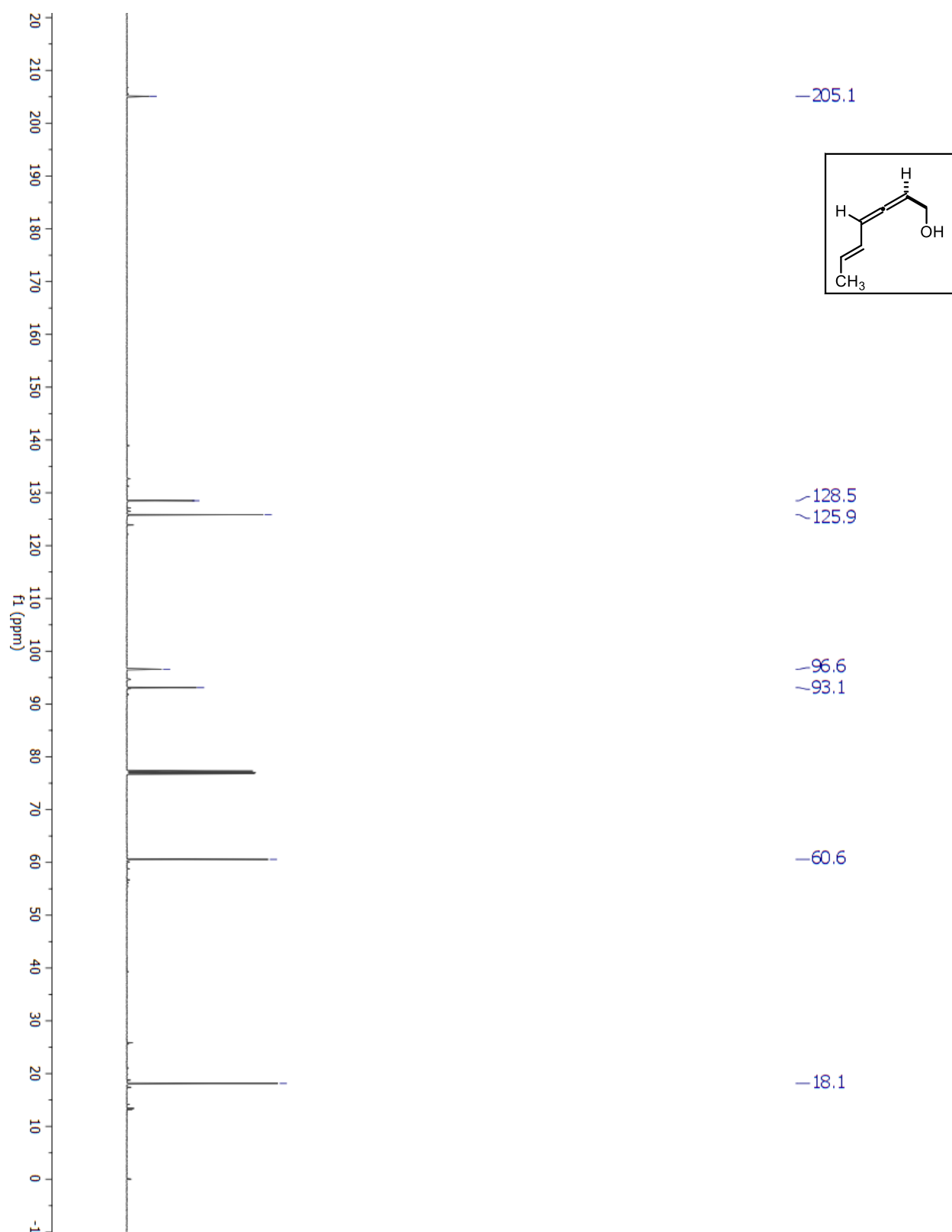
¹H-NMR for Compound S5.2

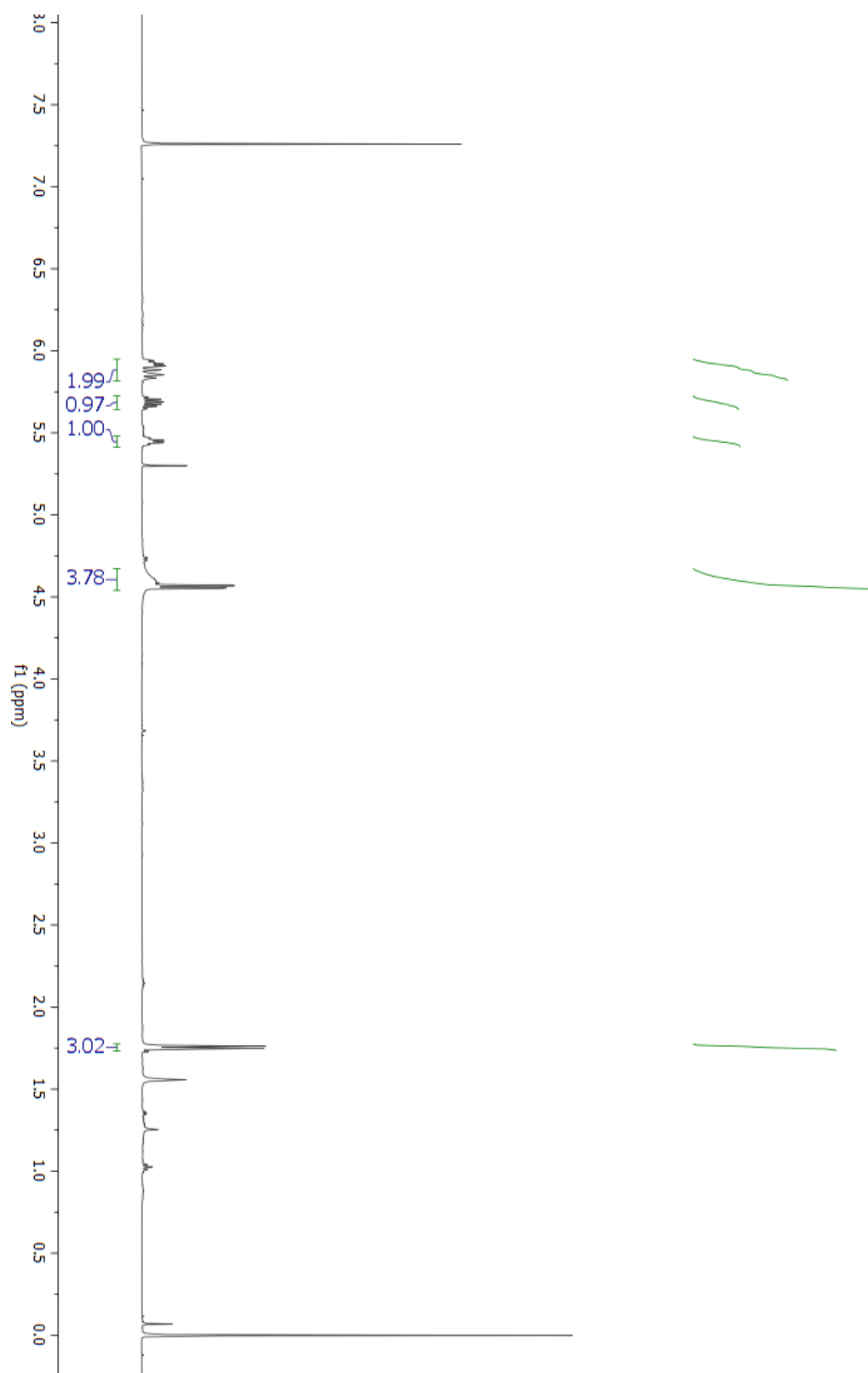
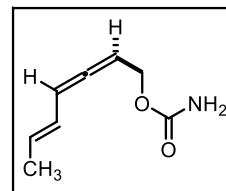
^{13}C -NMR for Compound S5.2

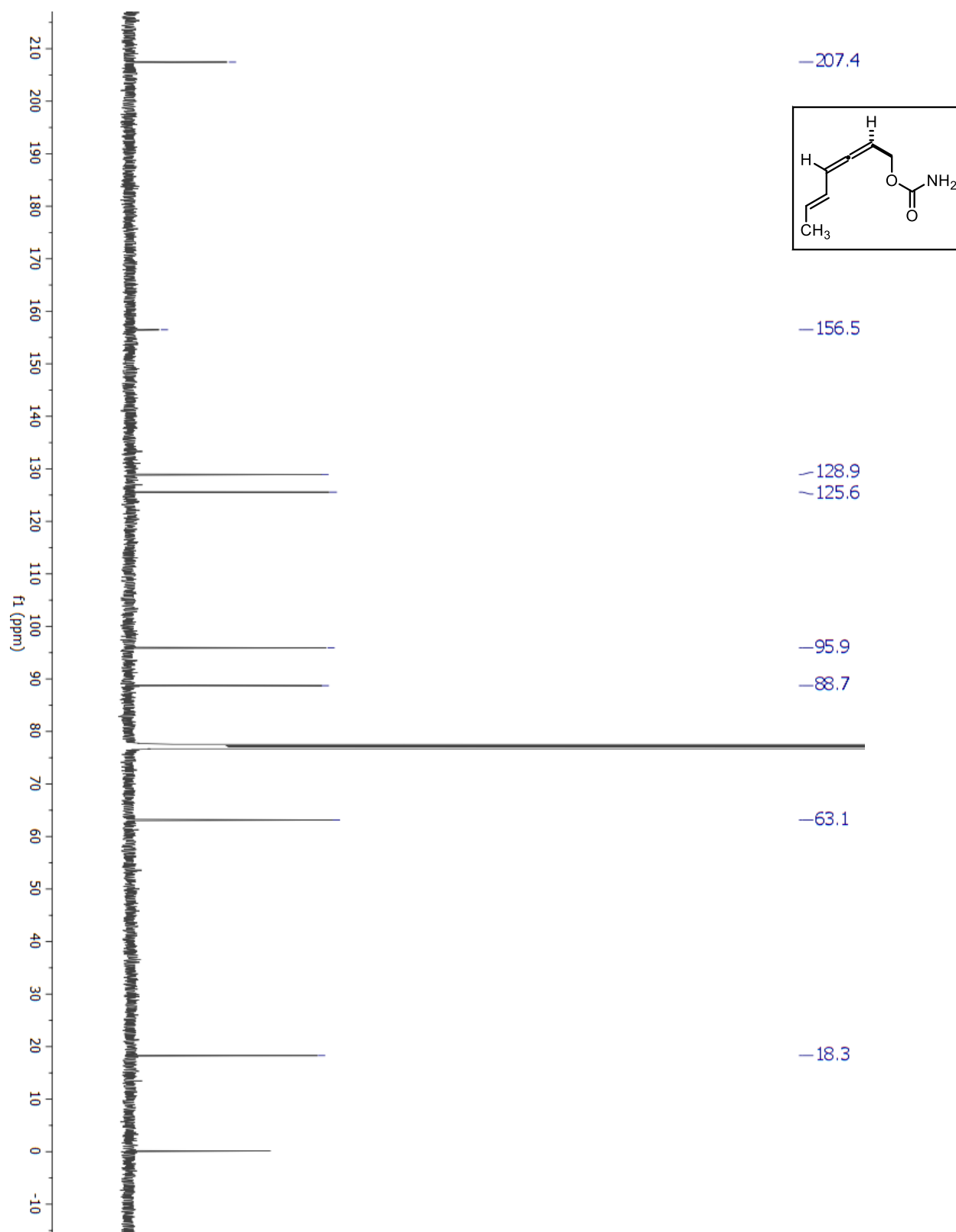
¹H-NMR for Compound S5.3

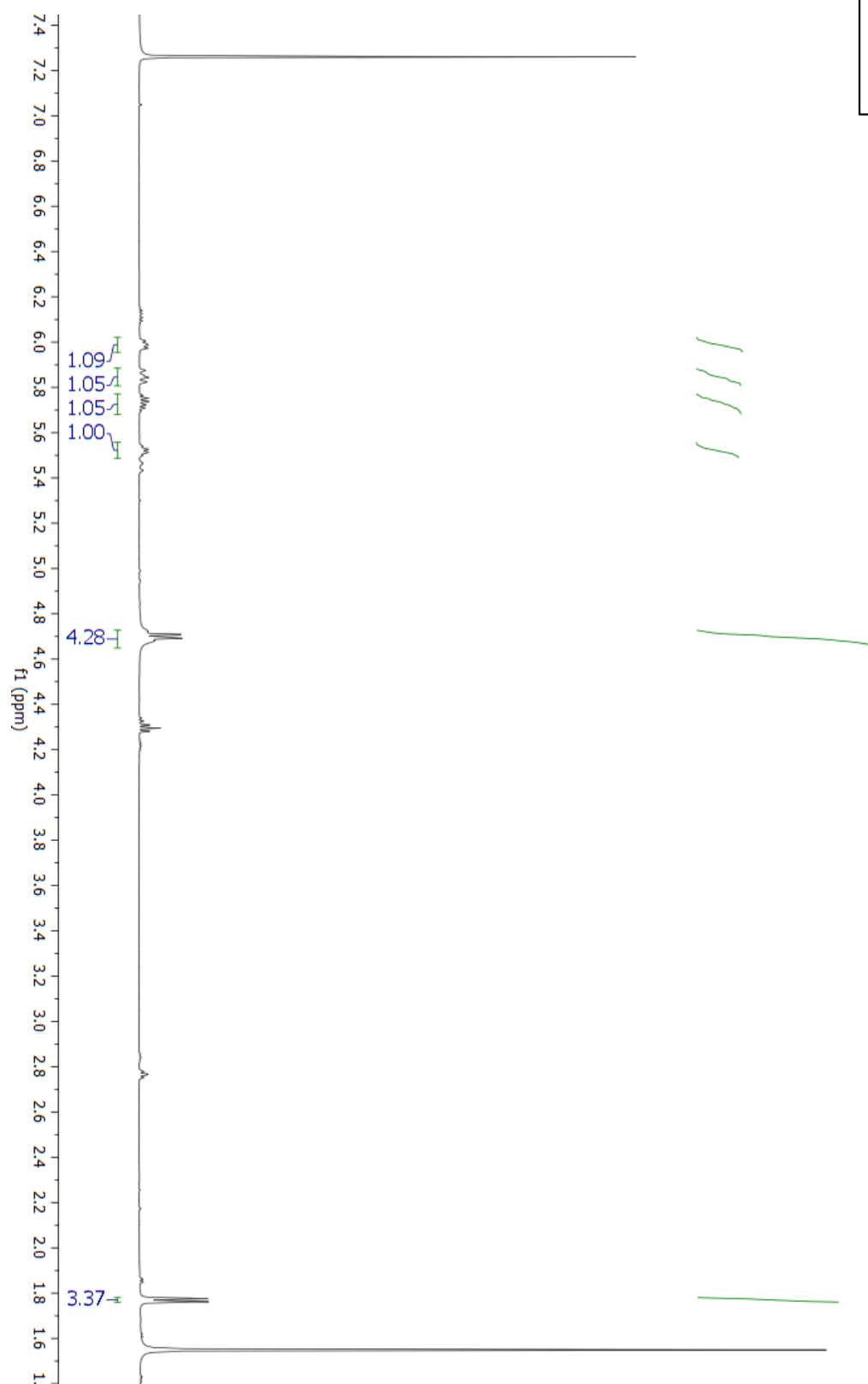
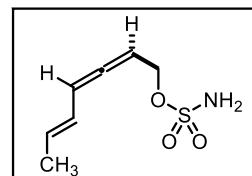
^{13}C -NMR for Compound S5.3

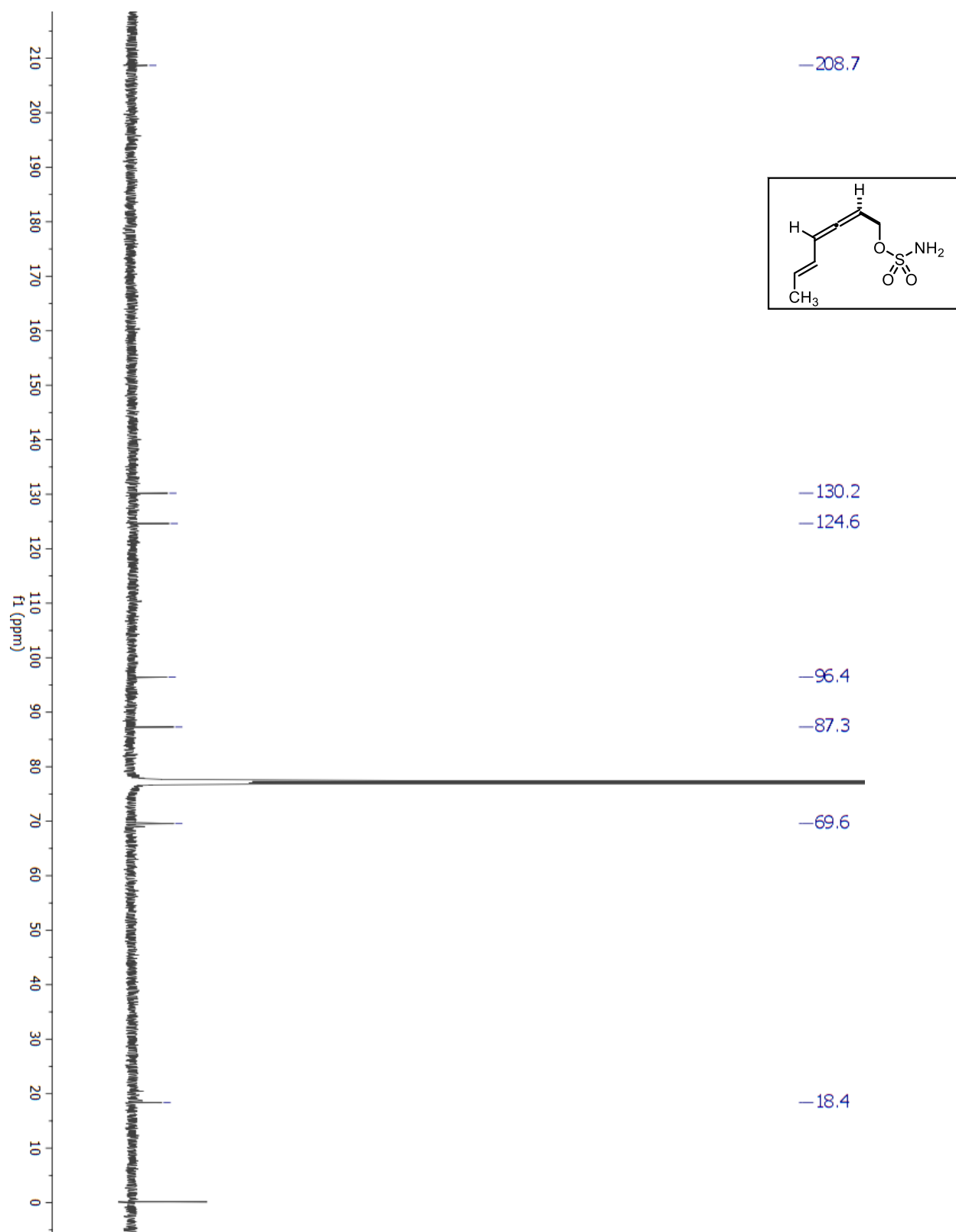
¹H-NMR for Compound S5.4

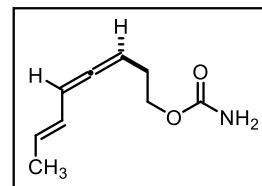
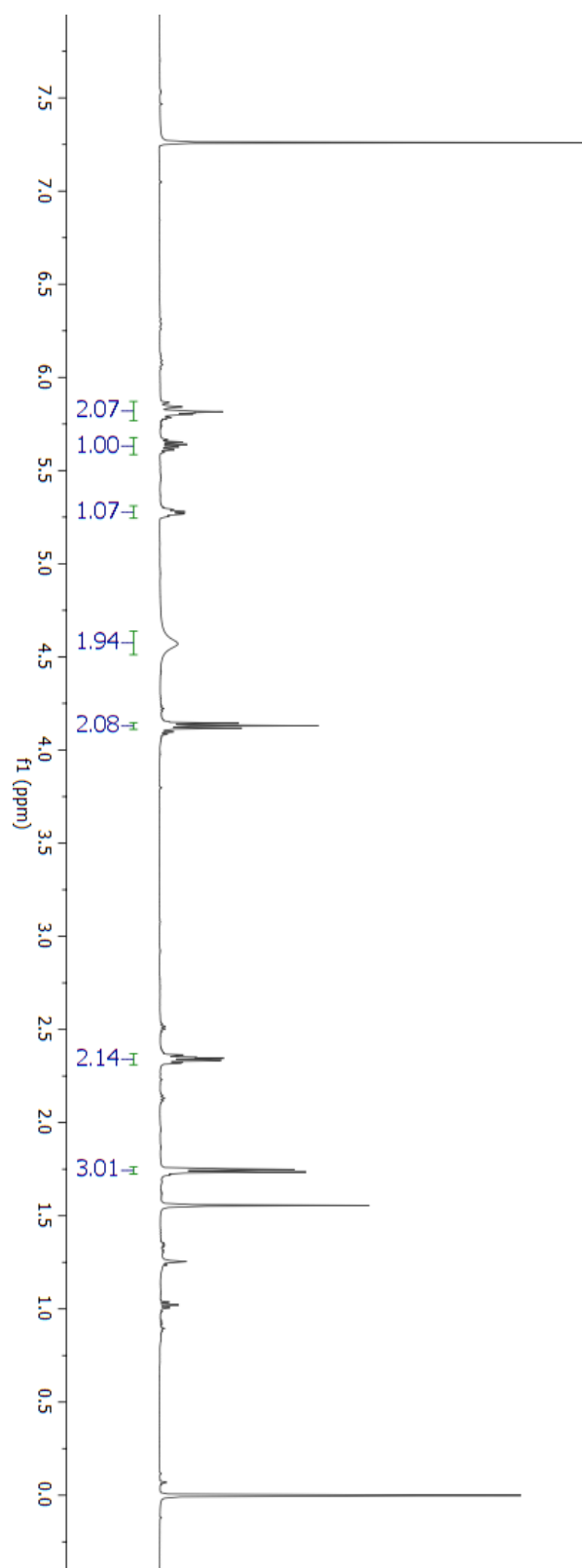
^{13}C -NMR for Compound S5.4

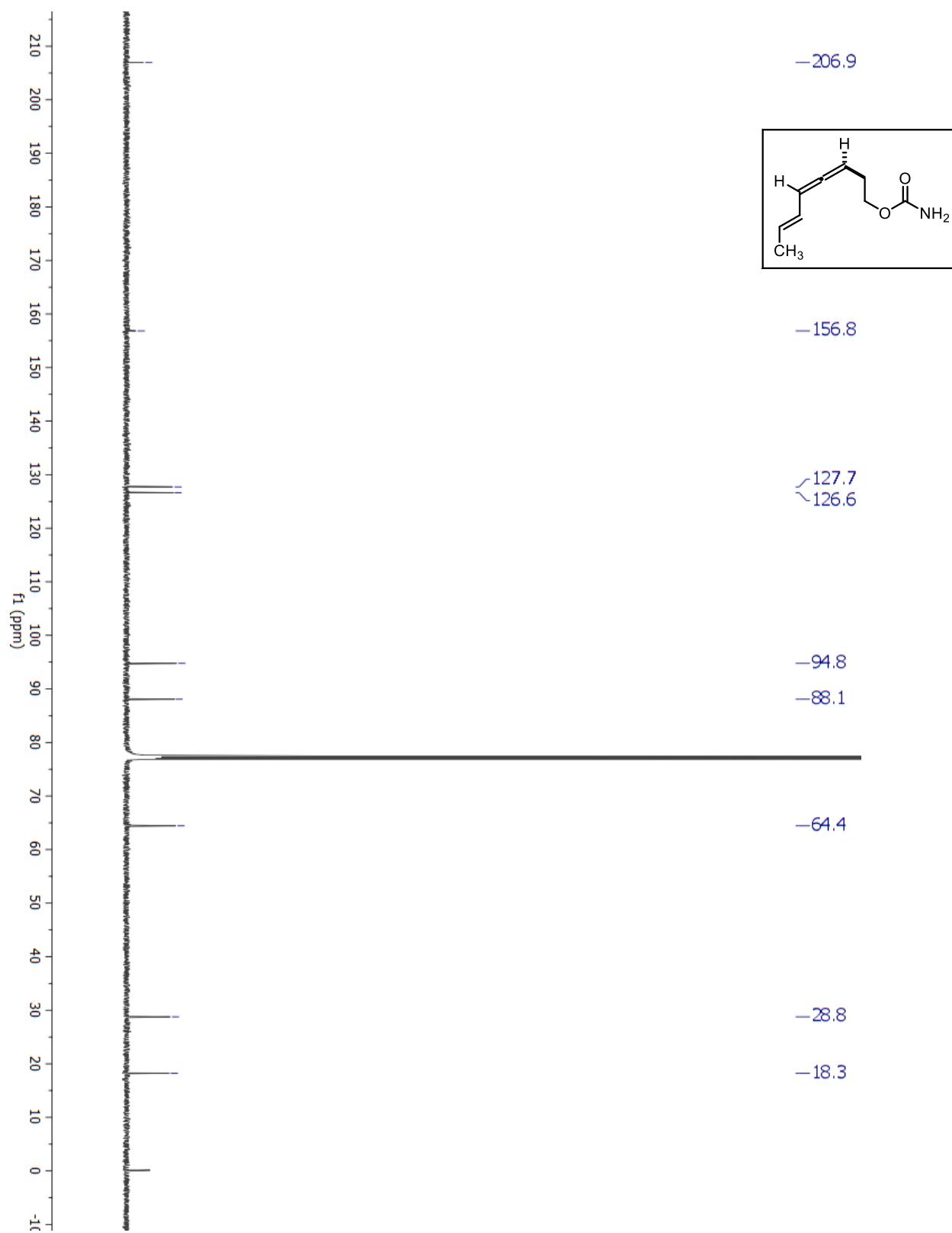
¹H-NMR for Compound S5.5

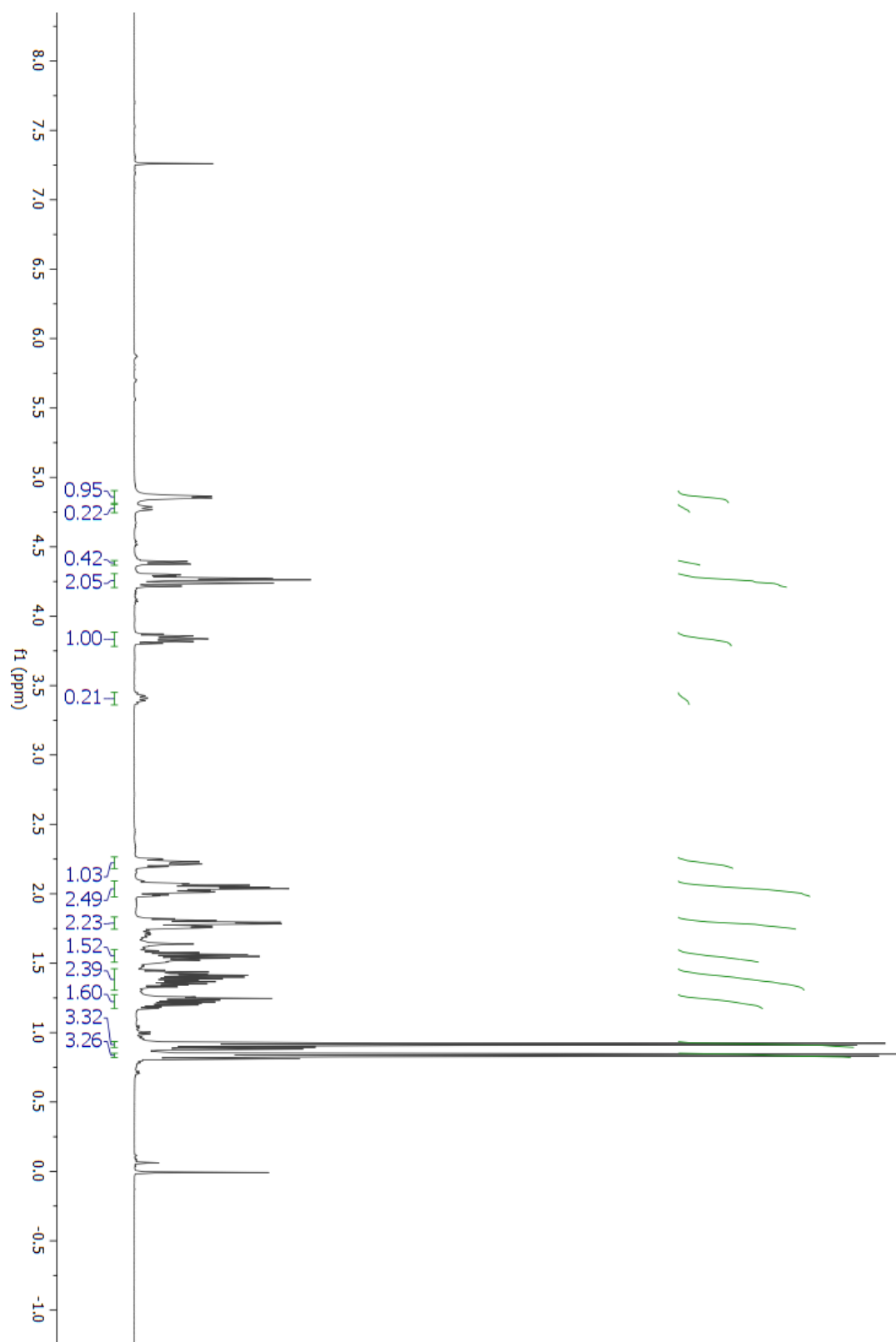
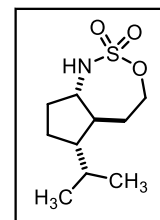
^{13}C -NMR for Compound S5.5

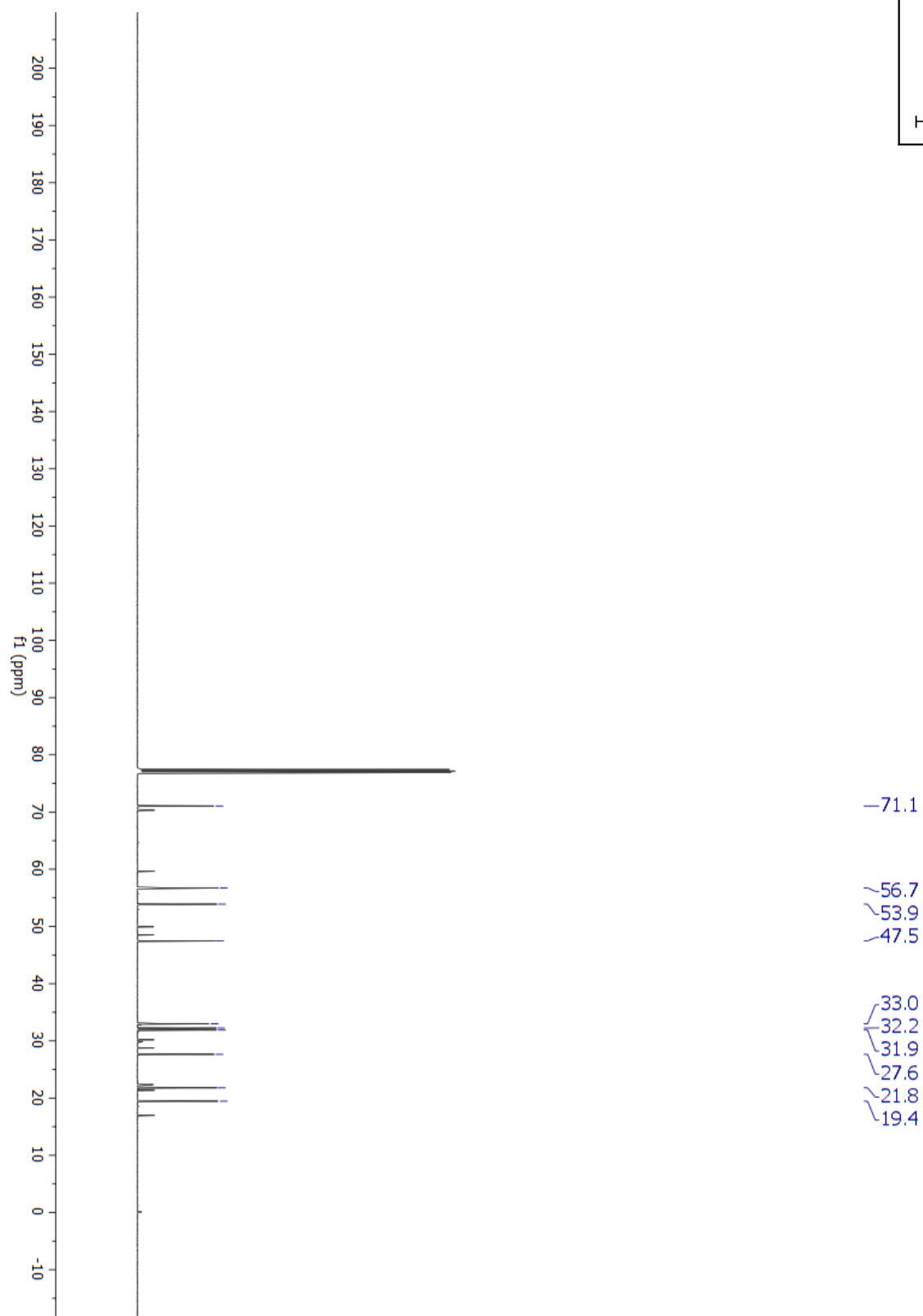
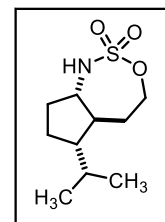
¹H-NMR for Compound S5.6

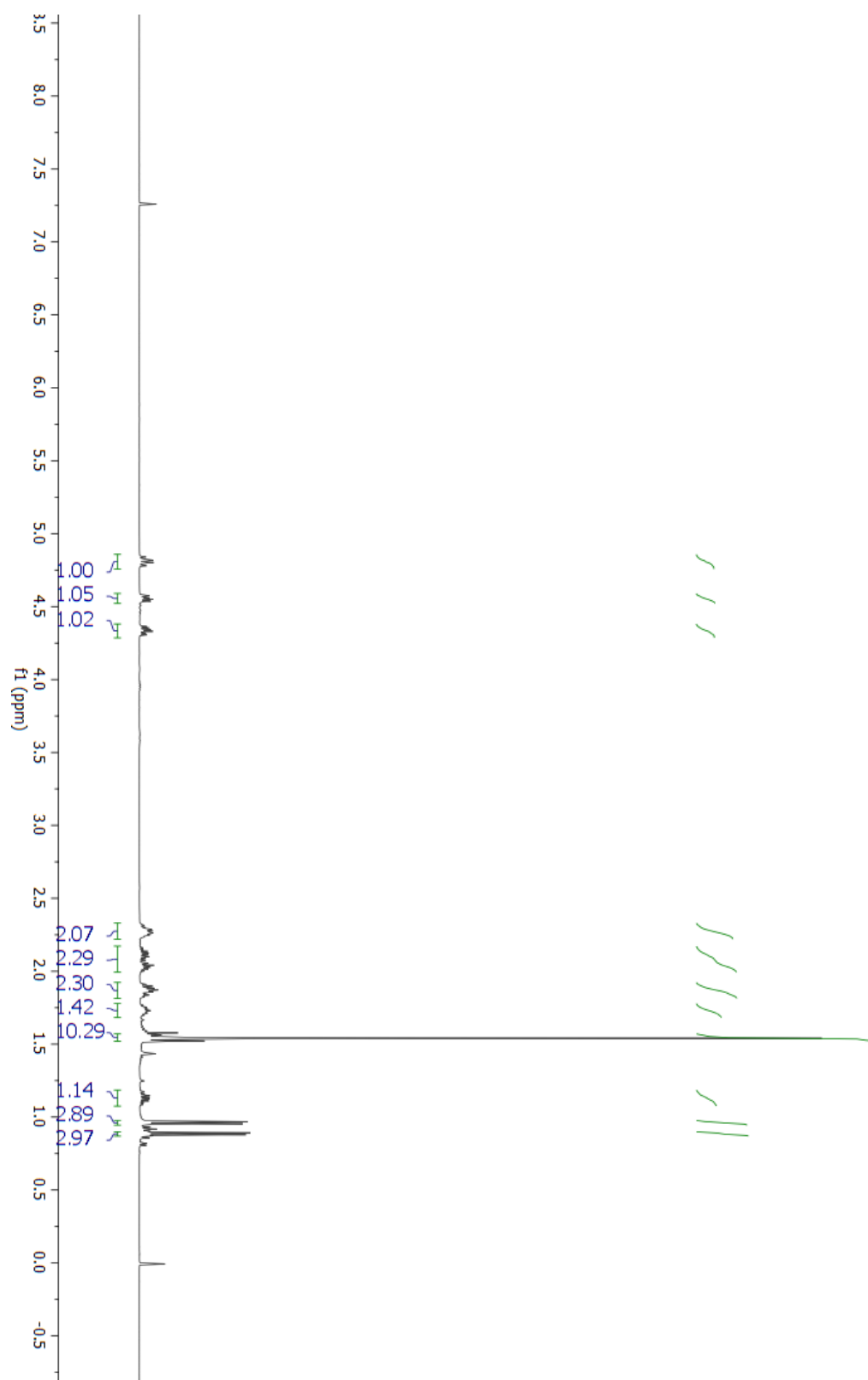
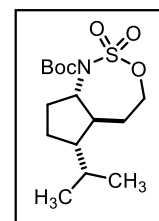
^{13}C -NMR for Compound S5.6

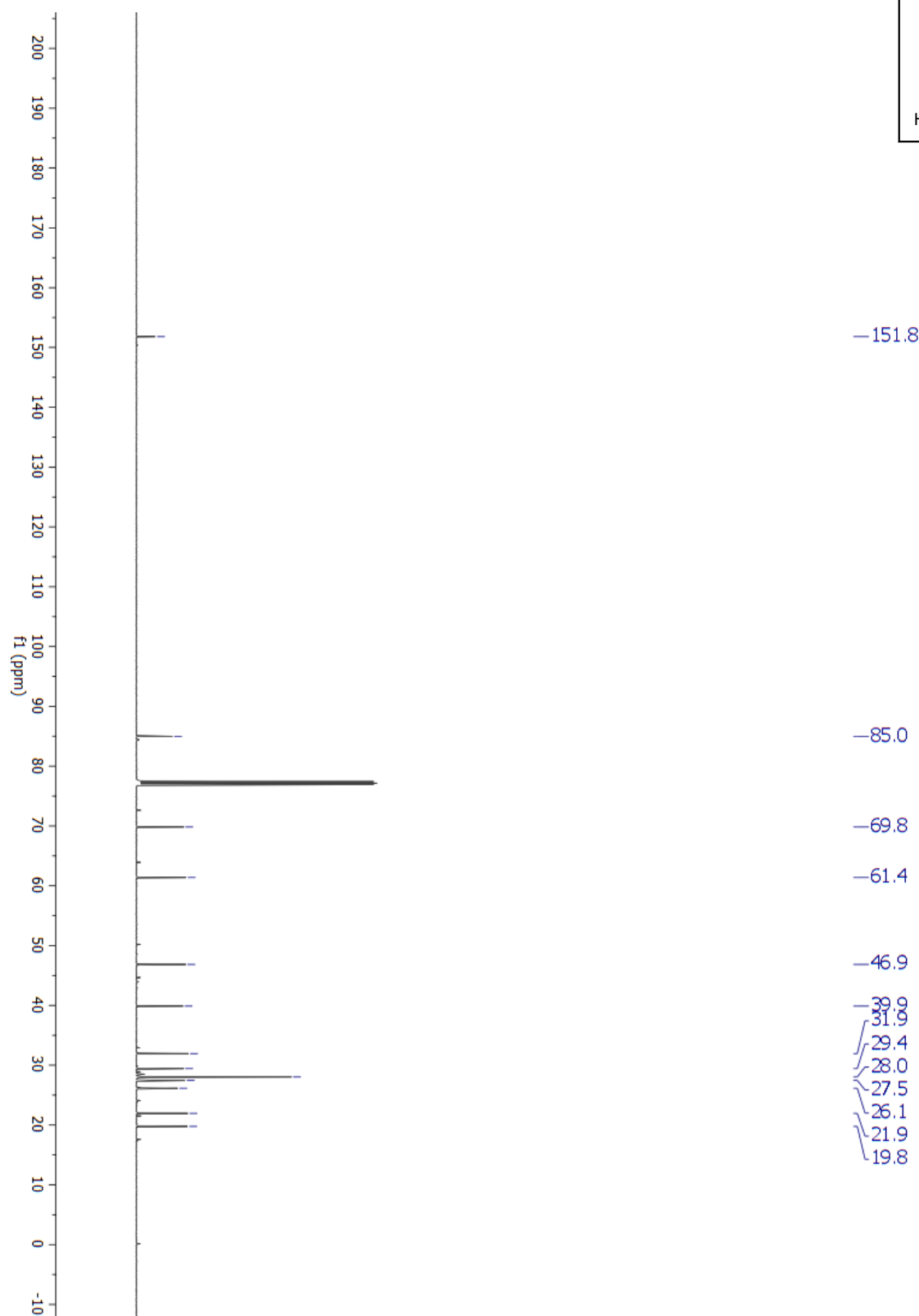
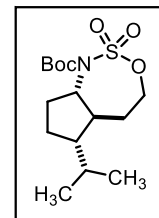
¹H-NMR for Compound S5.7

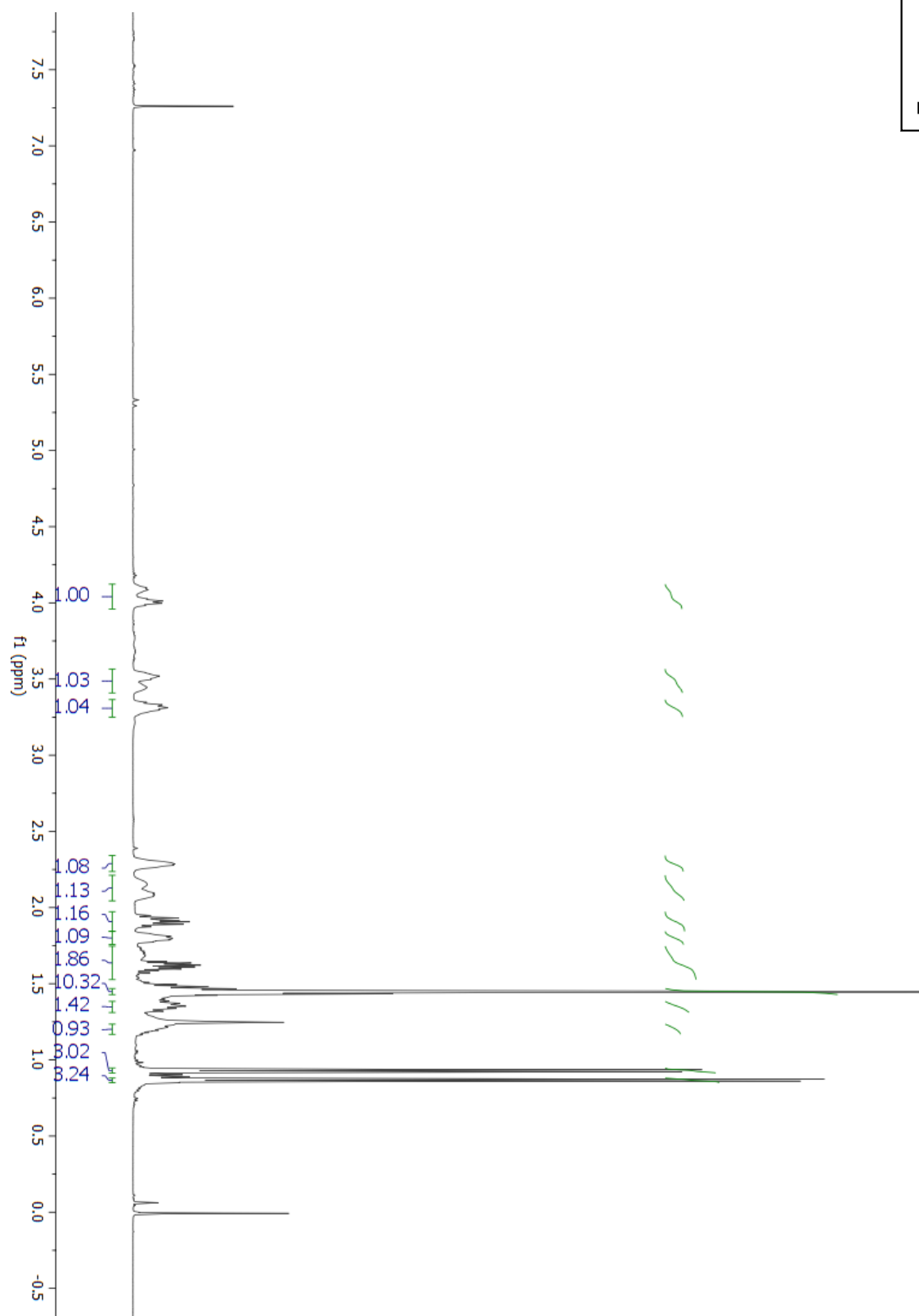
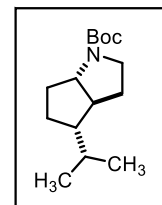
^{13}C -NMR for Compound S5.7

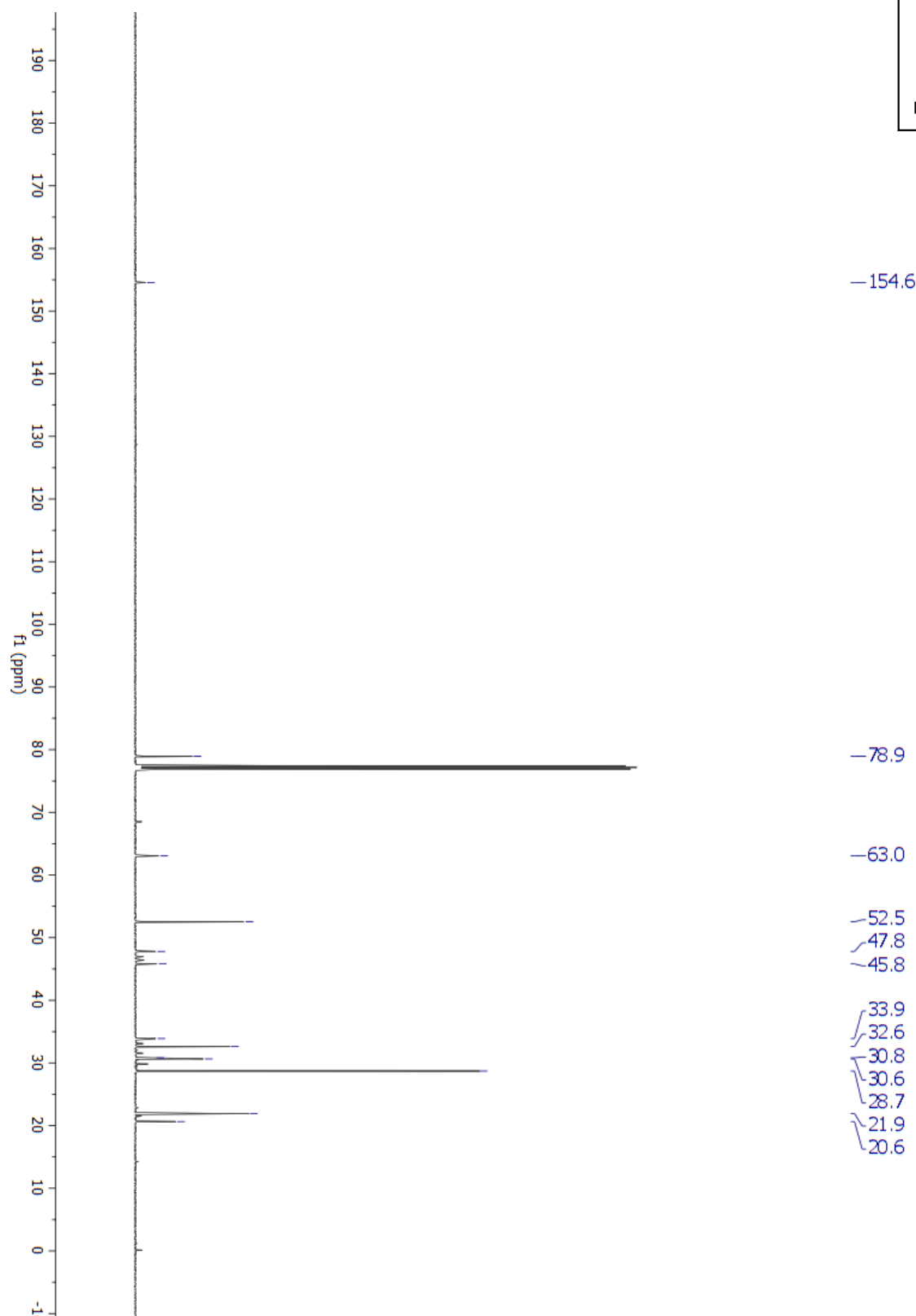
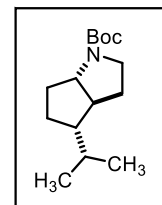
¹H-NMR for Compound 5.23

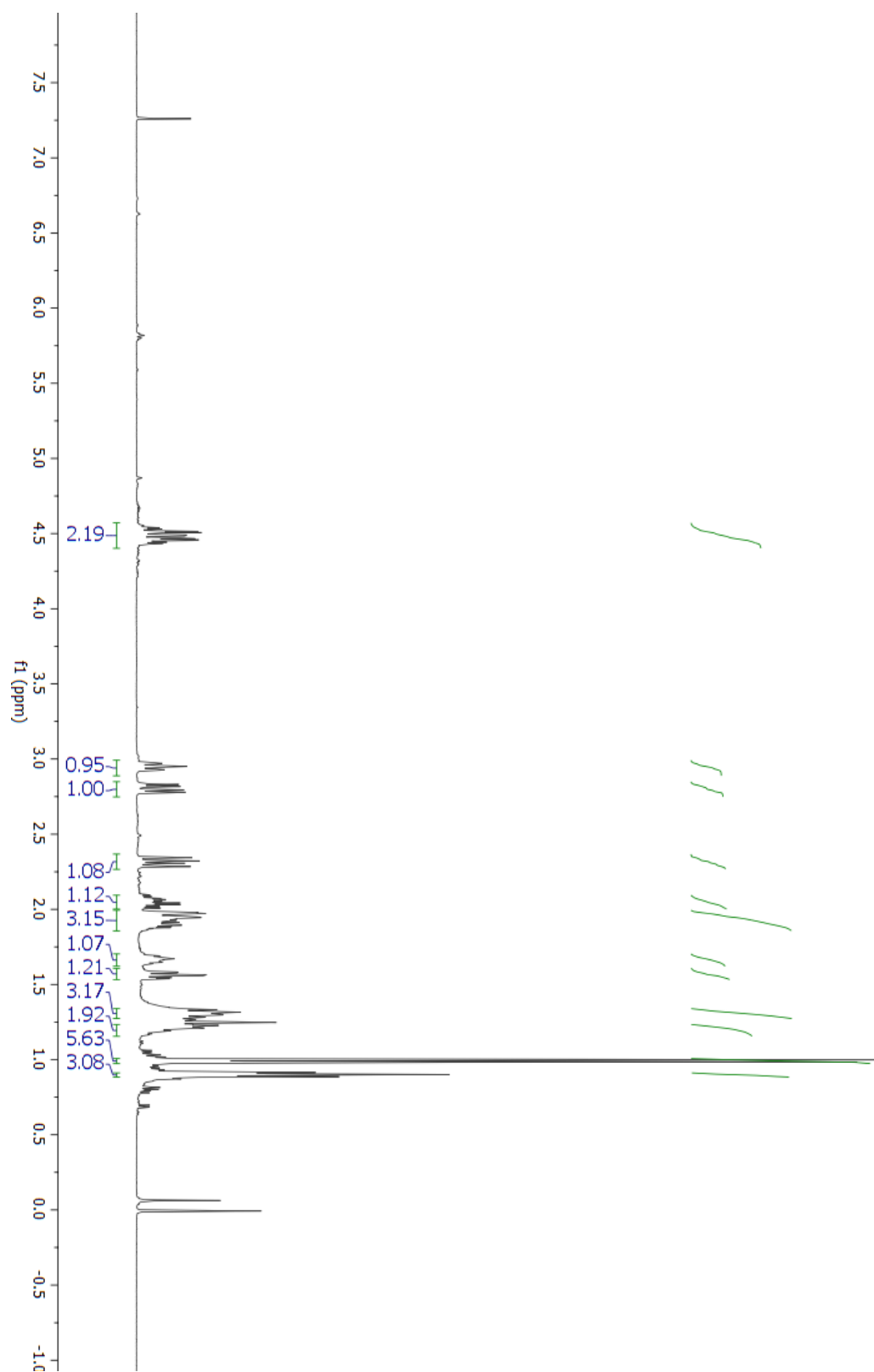
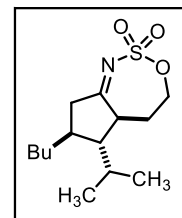
^{13}C -NMR for Compound 5.23

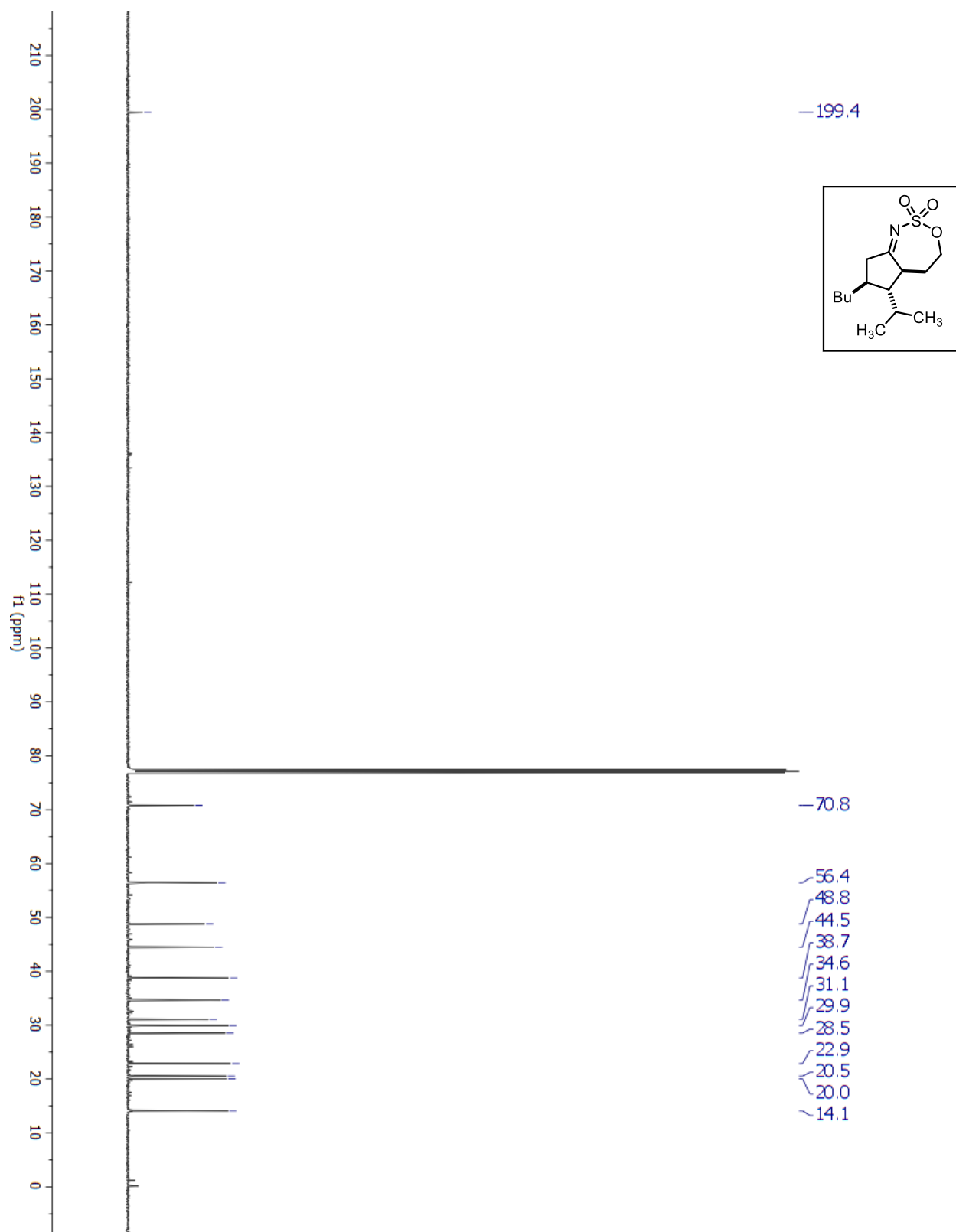
¹H-NMR for Precursor to Compound 5.24

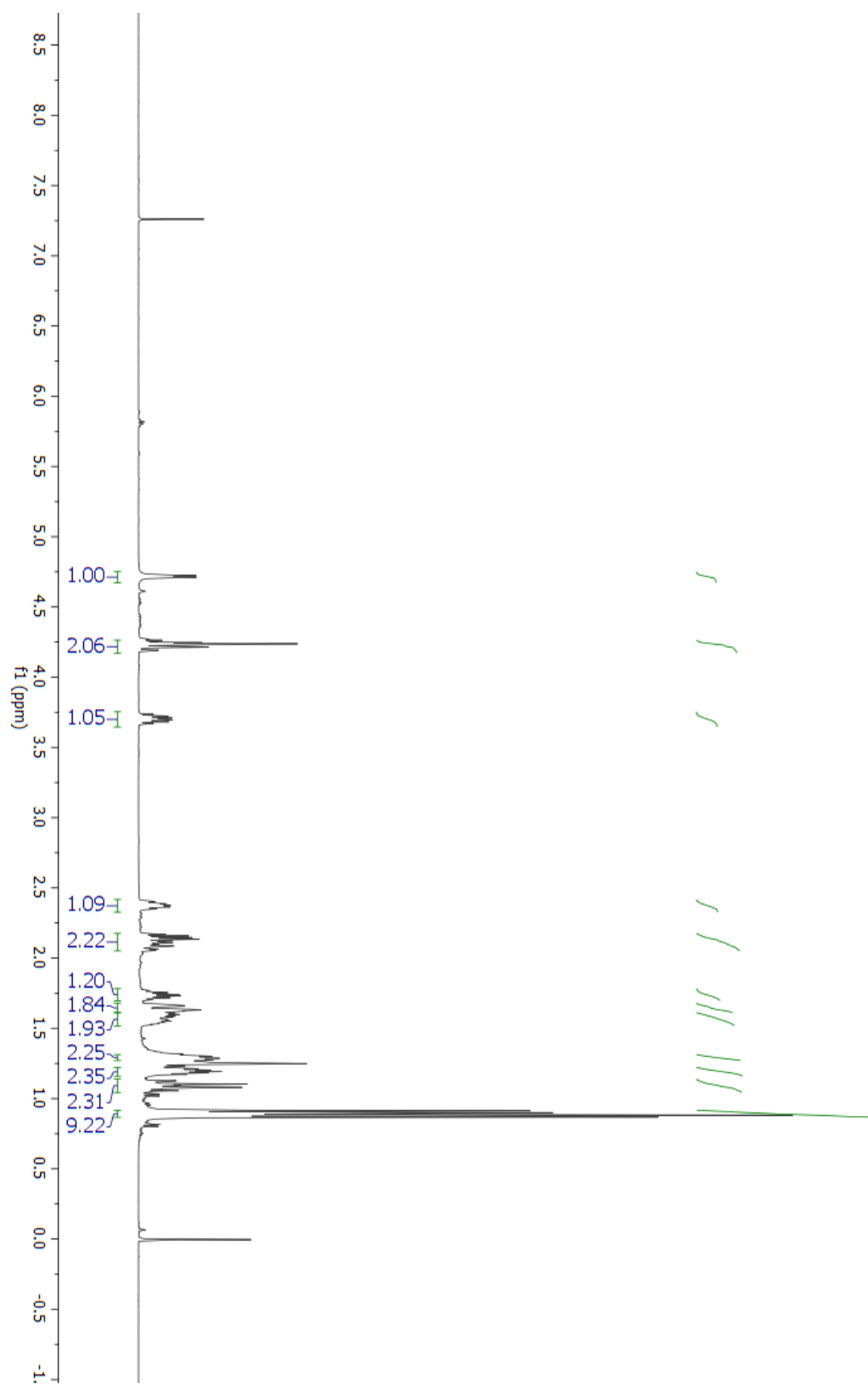
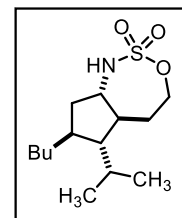
^{13}C -NMR for Precursor to Compound 5.24

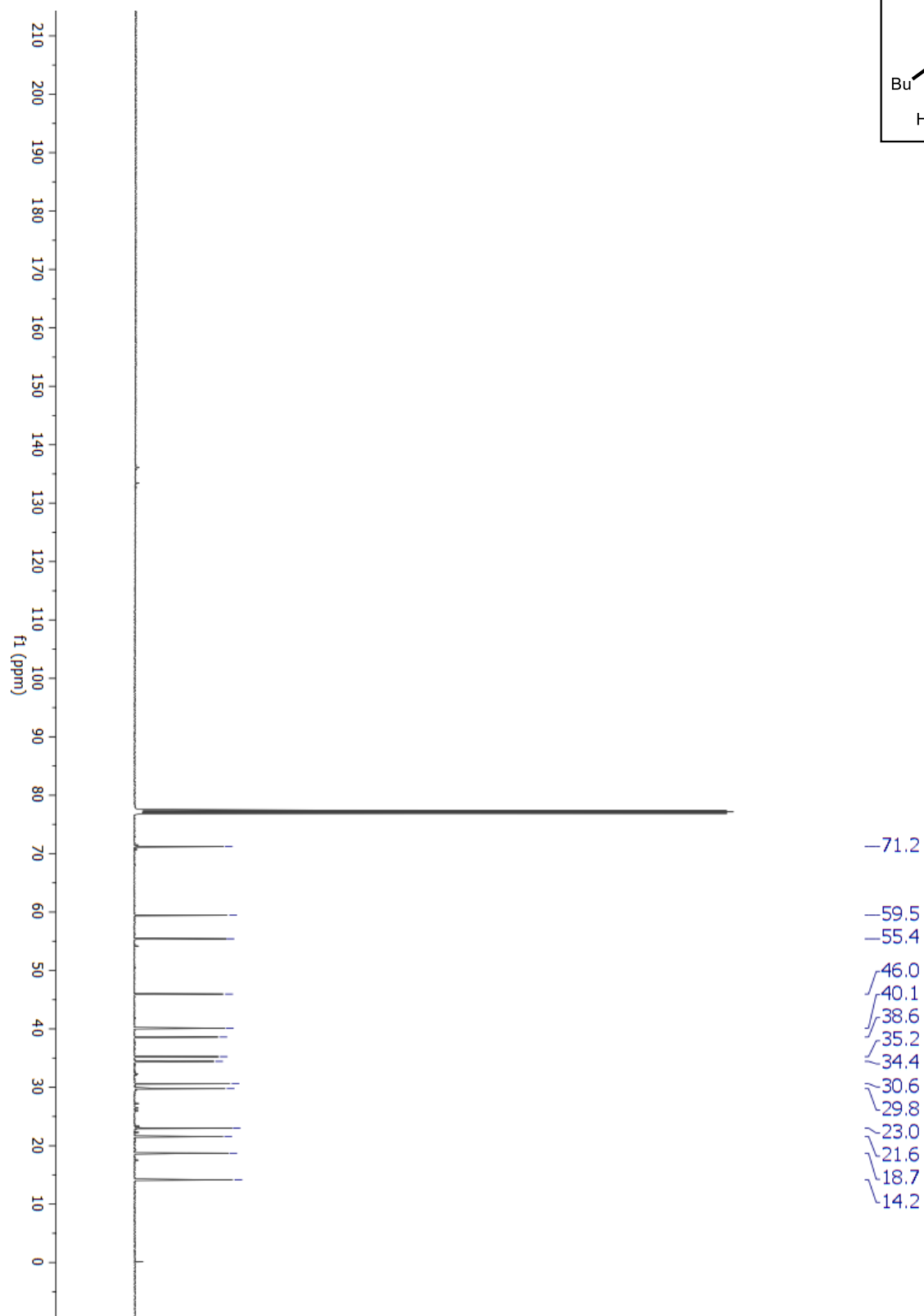
¹H-NMR for Compound 5.24

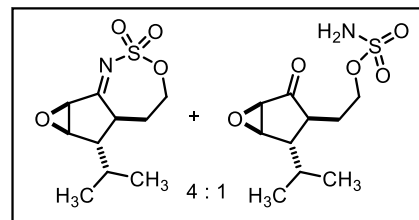
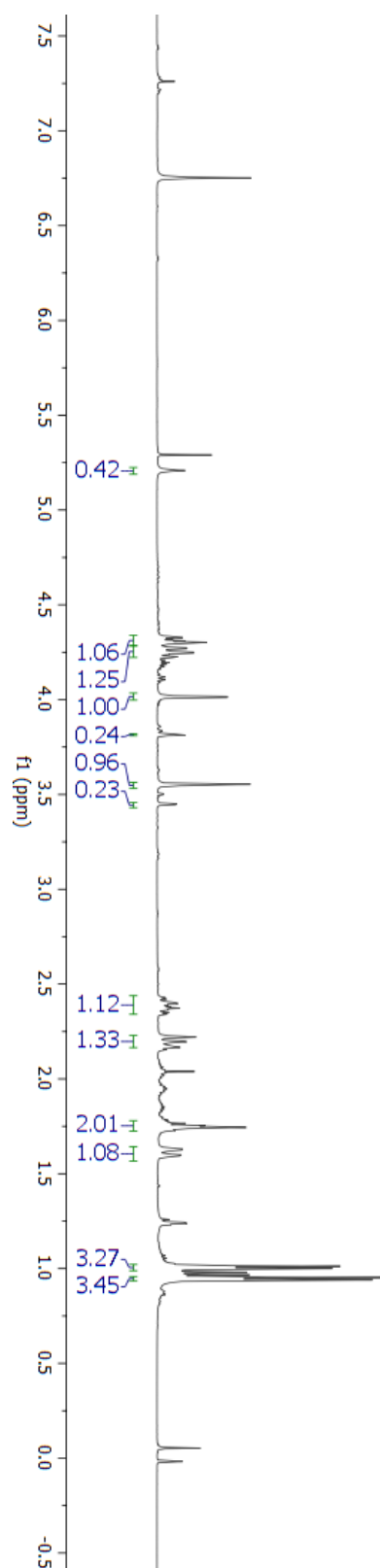
^{13}C -NMR for Compound 5.24

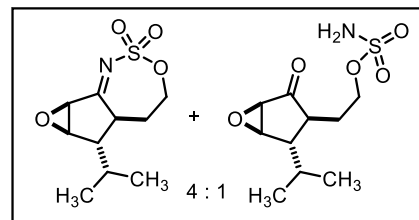
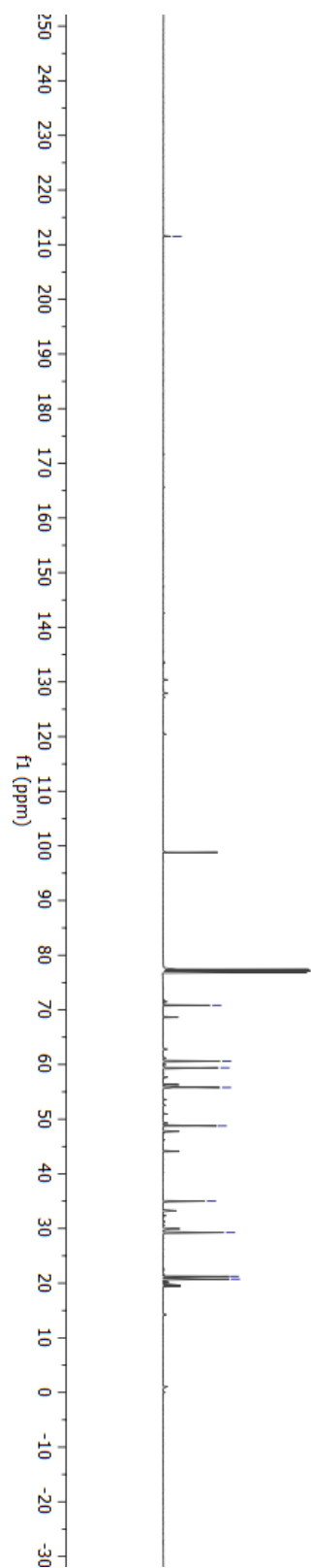
¹H-NMR for Precursor to Compound 5.25

^{13}C -NMR for Precursor to Compound 5.25

¹H-NMR for Compound 5.25

^{13}C -NMR for Compound 5.25

¹H-NMR for Compound 5.26

^{13}C -NMR for Compound 5.26

—211.5

—70.8

—60.6

—59.4

—55.8

—48.8

—35.0

—29.2

—21.2

—20.7

Chapter 5 Computational Details

Computational studies

All the calculations reported in this paper were performed with the Gaussian 09 suite of programs.¹ Electron correlation was partially taken into account using the hybrid functional usually denoted as B3LYP² in conjunction with the D3 dispersion correction suggested by Grimme et al.³ using the standard double- ζ quality def2-SVP⁴ basis set for all atoms. The SMD continuum model was used to model the effects of the solvent (CH_2Cl_2). This level is denoted SMD(CH_2Cl_2)-B3LYP-D3/def2-SVP. Geometries were fully optimized in solution without any geometry or symmetry constraints. Reactants, intermediates, and products were characterized by frequency calculations,⁵ and have positive definite Hessian matrices. Transition structures (TS's) show only one negative eigenvalue in their diagonalized force constant matrices, and their associated eigenvectors were confirmed to correspond to the motion along the reaction coordinate under consideration using the Intrinsic Reaction Coordinate (IRC) method.⁶ Potential energies were refined by means of single point calculations at the same level with a larger basis set, def2-TZVPP,⁴ where all elements were described with a triple- ζ plus polarization quality basis set. This level is denoted SMD(CH_2Cl_2)-B3LYP-D3/def2-TZVPP//SMD(CH_2Cl_2)-B3LYP-D3/def2-SVP.

¹ Gaussian 09, Revision D.01, Frisch, M. J.; Trucks, G. W.; Schlegel, H. B.; Scuseria, G. E.; Robb, M. A.; Cheeseman, J. R.; Scalmani, G.; Barone, V.; Mennucci, B.; Petersson, G. A.; Nakatsuji, H.; Caricato, M.; Li, X.; Hratchian, H. P.; Izmaylov, A. F.; Bloino, J.; Zheng, G.; Sonnenberg, J. L.; Hada, M.; Ehara, M.; Toyota, K.; Fukuda, R.; Hasegawa, J.; Ishida, M.; Nakajima, T.; Honda, Y.; Kitao, O.; Nakai, H.; Vreven, T.; Montgomery, J. A., Jr.; Peralta, J. E.; Ogliaro, F.; Bearpark, M.; Heyd, J. J.; Brothers, E.; Kudin, K. N.; Staroverov, V. N.; Kobayashi, R.; Normand, J.; Raghavachari, K.; Rendell, A.; Burant, J. C.; Iyengar, S. S.; Tomasi, J.; Cossi, M.; Rega, N.; Millam, J. M.; Klene, M.; Knox, J. E.; Cross, J. B.; Bakken, V.; Adamo, C.; Jaramillo, J.; Gomperts, R.; Stratmann, R. E.; Yazyev, O.; Austin, A. J.; Cammi, R.; Pomelli, C.; Ochterski, J. W.; Martin, R. L.; Morokuma, K.; Zakrzewski, V. G.; Voth, G. A.; Salvador, P.; Dannenberg, J. J.; Dapprich, S.; Daniels, A. D.; Farkas, Ö.; Foresman, J. B.; Ortiz, J. V.; Cioslowski, J.; Fox, D. J. Gaussian, Inc., Wallingford CT, 2009.

² a) Becke, A. D. *J. Chem. Phys.* **1993**, 98, 5648; b) Lee, C.; Yang, W.; Parr, R. G. *Phys. Rev. B* **1998**, 37, 785; c) Vosko, S. H.; Wilk, L.; Nusair, M. *Can. J. Phys.* **1980**, 58, 1200.

³ Grimme, S.; Antony, J.; Ehrlich, S.; Krieg, H. *J. Chem. Phys.* **2010**, 132, 154104.

⁴ Weigend, F.; Ahlrichs, R. *Phys. Chem. Chem. Phys.* **2005**, 7, 3297

⁵ McIver, J. W.; Komornicki, A. K. *J. Am. Chem. Soc.* **1972**, 94, 2625.

⁶ González, C.; Schlegel, H. B. *J. Phys. Chem.* **1990**, 94, 5523.

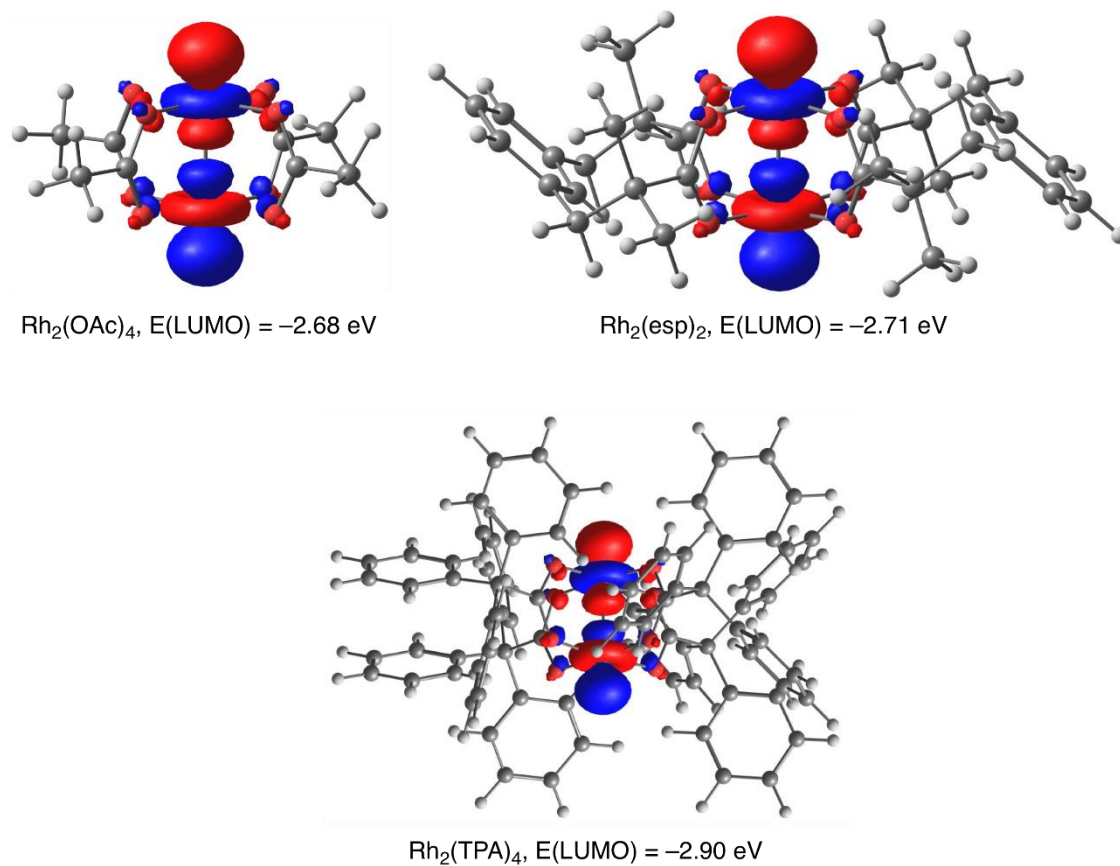


Figure S5-1. Computed LUMO (in eV, at the SMD-B3LYP-D3/def2-SVP level) for the dirhodium catalysts used in this study.

Table S5-1. Cartesian coordinates (in Å) and energies (in a.u.) of all the stationary points discussed in the text. All calculations have been performed at the SCM(dichloromethane)-B3LYP-D3/def2-SVP level.

Aziridine-4, E = -990.287459

N	0.833266000	-0.396882000	1.085216000
C	-0.115425000	0.796220000	1.214412000
C	-0.511061000	-0.503519000	0.697574000
C	-1.347904000	-1.348680000	0.089820000
H	-0.924620000	-2.306373000	-0.227092000
H	-0.310838000	1.046720000	2.263694000
C	0.051783000	1.980204000	0.279420000

C	0.749545000	1.604228000	-1.018185000
O	2.063432000	1.057036000	-0.710458000
S	2.086923000	-0.445847000	-0.081206000
H	0.176586000	0.876109000	-1.615468000
H	0.946539000	2.485633000	-1.641288000
H	-0.944442000	2.393778000	0.051941000
H	0.631686000	2.765620000	0.788530000
C	-2.762583000	-1.105381000	-0.201373000
H	-3.288224000	-1.948924000	-0.663950000
C	-3.453395000	0.027799000	0.034809000
H	-2.935634000	0.881090000	0.491967000
C	-4.902263000	0.229410000	-0.277186000
H	-5.474192000	0.476371000	0.635947000
H	-5.046103000	1.082414000	-0.965256000
H	-5.355386000	-0.663786000	-0.735888000
O	3.355883000	-0.546077000	0.612022000
O	1.711787000	-1.418284000	-1.101076000

Rh₂(OAc)₄, E = -1135.797077

Rh	-0.002728000	0.001161000	-1.194894000
Rh	-0.006234000	-0.001684000	1.196216000
O	-1.505171000	1.400991000	1.127942000
C	-1.890482000	1.846876000	0.003283000
O	-1.437624000	1.469818000	-1.121637000
O	1.396905000	1.497760000	1.130344000

C	1.846962000	1.881999000	0.007279000
O	1.472811000	1.429321000	-1.118930000
O	-1.412425000	-1.497585000	1.121268000
C	-1.856661000	-1.881285000	-0.004887000
O	-1.479604000	-1.425127000	-1.128161000
O	1.490034000	-1.408709000	1.122521000
C	1.879204000	-1.850458000	-0.002762000
O	1.428469000	-1.470841000	-1.127380000
C	-2.882677000	-2.981581000	-0.005554000
H	-2.355430000	-3.946900000	0.076300000
H	-3.548459000	-2.884220000	0.863183000
H	-3.459561000	-2.975485000	-0.939663000
C	2.979643000	-2.876442000	0.000418000
H	2.992008000	-3.437767000	-0.942946000
H	3.943340000	-2.351707000	0.111914000
H	2.864359000	-3.556717000	0.855758000
C	2.917845000	2.938886000	-0.000377000
H	3.056960000	3.366472000	1.000512000
H	3.862427000	2.482752000	-0.338643000
H	2.654563000	3.727820000	-0.720601000
C	-2.939840000	2.924930000	-0.002474000
H	-3.644148000	2.762823000	-0.830751000
H	-3.472069000	2.959122000	0.956846000
H	-2.441845000	3.894767000	-0.168666000

INT1, E = -2126.104515

Rh	-0.449383000	-0.115453000	0.053644000
N	1.723484000	-0.845486000	0.149064000
C	2.634948000	-0.277309000	1.267798000
C	2.672667000	0.180231000	-0.103020000
C	3.120389000	0.908620000	-1.125756000
H	2.677910000	0.693175000	-2.100608000
H	2.037595000	0.286625000	1.992525000
C	3.742927000	-1.138263000	1.835589000
C	4.285243000	-2.134222000	0.827784000
O	3.205968000	-3.026295000	0.432923000
S	2.030738000	-2.444039000	-0.523645000
H	4.716200000	-1.651834000	-0.064335000
H	5.043746000	-2.791363000	1.271151000
H	4.554362000	-0.467358000	2.162233000
H	3.374862000	-1.675798000	2.722900000
Rh	-2.684023000	0.790470000	-0.004961000
O	-3.101067000	-0.524559000	-1.524903000
C	-2.194099000	-1.315580000	-1.928851000
O	-1.010292000	-1.364052000	-1.476823000
O	-2.005082000	2.161798000	-1.383317000
C	-0.799781000	2.113148000	-1.771259000
O	0.068267000	1.281884000	-1.361173000
O	-3.216818000	-0.642767000	1.372323000
C	-2.335412000	-1.442677000	1.812017000
O	-1.113063000	-1.447707000	1.470736000

O	-2.122727000	2.057547000	1.526510000
C	-0.942661000	2.006333000	1.980441000
O	-0.034223000	1.216255000	1.568194000
C	-0.340075000	3.140663000	-2.771738000
H	0.385505000	2.695900000	-3.467089000
H	-1.193266000	3.561411000	-3.319758000
H	0.167878000	3.954194000	-2.227144000
C	-2.565333000	-2.305521000	-3.000902000
H	-1.673446000	-2.643156000	-3.544915000
H	-3.029637000	-3.180193000	-2.514832000
H	-3.300579000	-1.868409000	-3.690574000
C	-0.559124000	2.958493000	3.082374000
H	-1.436915000	3.495734000	3.462863000
H	-0.069619000	2.403465000	3.896745000
H	0.172279000	3.682555000	2.687914000
C	-2.775210000	-2.499780000	2.790757000
H	-3.685593000	-2.188390000	3.319759000
H	-2.994117000	-3.422113000	2.226692000
H	-1.968840000	-2.722821000	3.503068000
C	4.126685000	1.967774000	-1.054915000
H	4.297464000	2.505230000	-1.994766000
C	4.837811000	2.329845000	0.032113000
H	4.680810000	1.790520000	0.975469000
C	5.844431000	3.434315000	0.068044000
H	5.554933000	4.205320000	0.805270000
H	6.832868000	3.060683000	0.391566000

H	5.961518000	3.921662000	-0.912708000
O	0.893838000	-3.298551000	-0.262267000
O	2.537792000	-2.232829000	-1.872219000

TS1, E = -2126.082773

Rh	-0.441043000	-0.136751000	-0.069892000
N	1.635677000	-0.863220000	-0.295911000
C	2.869792000	0.117234000	1.068287000
C	2.667794000	0.096180000	-0.351350000
C	3.056948000	0.920045000	-1.347946000
H	2.597268000	0.778169000	-2.328572000
H	2.480255000	0.977767000	1.628597000
C	3.459877000	-0.973983000	1.877057000
C	3.875796000	-2.251693000	1.158441000
O	2.743873000	-2.992131000	0.662200000
S	2.057205000	-2.430797000	-0.723936000
H	4.576015000	-2.041985000	0.332987000
H	4.369181000	-2.929838000	1.866952000
H	4.364153000	-0.524964000	2.338046000
H	2.792504000	-1.193995000	2.729693000
Rh	-2.649376000	0.815042000	0.233019000
O	-3.151389000	-0.883811000	1.278410000
C	-2.277869000	-1.785742000	1.459672000
O	-1.079303000	-1.741882000	1.047112000
O	-3.197213000	-0.107826000	-1.521239000

C	-2.347655000	-0.808443000	-2.151281000
O	-1.143169000	-0.994043000	-1.800481000
O	-1.939824000	1.670236000	1.976808000
C	-0.733094000	1.502532000	2.313387000
O	0.116720000	0.809576000	1.667104000
O	-1.992563000	2.455057000	-0.832566000
C	-0.814978000	2.469917000	-1.298138000
O	0.045692000	1.548470000	-1.145526000
C	-2.807991000	-1.511458000	-3.401834000
H	-2.005548000	-1.516664000	-4.152915000
H	-3.036718000	-2.559622000	-3.146137000
H	-3.713676000	-1.040657000	-3.806028000
C	-2.694061000	-3.031462000	2.198659000
H	-3.653860000	-2.885344000	2.710661000
H	-2.793314000	-3.852554000	1.469732000
H	-1.913982000	-3.320185000	2.918222000
C	-0.393176000	3.656918000	-2.124875000
H	-0.427573000	3.370728000	-3.189324000
H	-1.066400000	4.508681000	-1.963201000
H	0.644016000	3.932919000	-1.886101000
C	-0.235726000	2.191240000	3.557169000
H	0.361760000	1.491925000	4.160520000
H	0.424263000	3.022389000	3.258113000
H	-1.070228000	2.589767000	4.147868000
C	3.979563000	2.019142000	-1.145368000
H	3.888170000	2.856519000	-1.848081000

C	4.910752000	2.094670000	-0.164169000
O	3.098477000	-2.405080000	-1.754942000
O	0.874934000	-3.252369000	-0.891521000
H	5.094041000	1.212172000	0.461776000
C	5.775072000	3.281043000	0.108082000
H	5.635320000	3.631443000	1.146860000
H	6.844653000	3.019353000	0.017335000
H	5.557373000	4.119774000	-0.570984000

INT2, E = -2126.11012

Rh	-0.425478000	-0.044742000	-0.203506000
N	1.665735000	-0.595343000	-0.697961000
C	3.160948000	-0.053962000	1.173330000
C	2.624662000	0.226322000	-0.073218000
C	2.869486000	1.480765000	-0.692670000
H	2.051951000	1.838335000	-1.329691000
H	3.832981000	0.677404000	1.626463000
C	2.766715000	-1.239723000	1.979230000
C	3.045641000	-2.625233000	1.359580000
O	2.120730000	-2.984361000	0.339521000
S	2.165602000	-2.085345000	-1.067322000
H	4.080198000	-2.692182000	0.983081000
H	2.911468000	-3.385551000	2.142505000
H	3.249333000	-1.195602000	2.966008000
H	1.671336000	-1.172273000	2.125821000

Rh	-2.662530000	0.662200000	0.420944000
O	-2.923350000	-1.193891000	1.271048000
C	-1.974842000	-2.035322000	1.228047000
O	-0.838710000	-1.838315000	0.700107000
O	-3.318968000	-0.073303000	-1.383348000
C	-2.479021000	-0.584908000	-2.185828000
O	-1.233072000	-0.694811000	-1.978796000
O	-1.865198000	1.344411000	2.197789000
C	-0.627334000	1.210148000	2.420343000
O	0.210993000	0.689299000	1.618934000
O	-2.243581000	2.478124000	-0.471109000
C	-1.116019000	2.670432000	-1.010310000
O	-0.168249000	1.823032000	-1.052040000
C	-2.999991000	-1.138833000	-3.487451000
H	-2.329540000	-0.856874000	-4.312241000
H	-3.001858000	-2.239585000	-3.423199000
H	-4.021249000	-0.788021000	-3.684533000
C	-2.222960000	-3.400550000	1.815645000
H	-2.993379000	-3.356015000	2.597128000
H	-2.581006000	-4.063214000	1.009757000
H	-1.288989000	-3.822929000	2.211020000
C	-0.862243000	3.999091000	-1.674851000
H	-0.795471000	3.843725000	-2.763900000
H	-1.669956000	4.709237000	-1.456988000
H	0.103452000	4.404987000	-1.337866000
C	-0.079055000	1.728128000	3.725382000

H	0.622155000	0.997264000	4.154283000
H	0.484422000	2.655301000	3.529018000
H	-0.888213000	1.943889000	4.434748000
C	4.017096000	2.295735000	-0.575241000
H	3.909305000	3.352171000	-0.844928000
C	5.269124000	1.813543000	-0.289341000
O	3.585298000	-2.067352000	-1.466695000
O	1.192260000	-2.764302000	-1.908520000
H	5.401720000	0.729077000	-0.198518000
C	6.486351000	2.642236000	-0.175986000
H	6.958911000	2.459921000	0.807771000
H	7.236282000	2.315398000	-0.919689000
H	6.290149000	3.717362000	-0.292969000

TS2, E = -2126.102281

Rh	-0.449985000	-0.097812000	-0.184462000
N	1.622118000	-0.600091000	-0.780522000
C	3.101269000	0.575501000	0.804884000
C	2.500984000	0.436452000	-0.469368000
C	2.820582000	1.429498000	-1.426187000
H	2.151294000	1.628823000	-2.264496000
H	3.250119000	1.590566000	1.177014000
C	3.145779000	-0.495799000	1.842274000
C	3.530609000	-1.916344000	1.425665000
O	2.522497000	-2.597324000	0.672801000

S	2.274180000	-2.066998000	-0.889132000
H	4.485244000	-1.925004000	0.872749000
H	3.657915000	-2.524994000	2.332411000
H	3.817613000	-0.174840000	2.653816000
H	2.124817000	-0.514685000	2.273148000
Rh	-2.689994000	0.604518000	0.427685000
O	-2.892973000	-1.179707000	1.433188000
C	-1.925818000	-2.001351000	1.438045000
O	-0.806948000	-1.825472000	0.868526000
O	-3.358019000	-0.299589000	-1.293351000
C	-2.523400000	-0.863963000	-2.064710000
O	-1.269932000	-0.918243000	-1.880157000
O	-1.870537000	1.459712000	2.119546000
C	-0.624250000	1.379350000	2.320664000
O	0.207690000	0.795986000	1.555734000
O	-2.331897000	2.346560000	-0.625094000
C	-1.218226000	2.516963000	-1.202420000
O	-0.246512000	1.698745000	-1.181285000
C	-3.059995000	-1.558855000	-3.289668000
H	-2.405484000	-1.366643000	-4.151951000
H	-3.054650000	-2.645602000	-3.102953000
H	-4.087320000	-1.238209000	-3.505906000
C	-2.131457000	-3.316639000	2.144645000
H	-2.885118000	-3.220345000	2.937751000
H	-2.493868000	-4.051685000	1.406302000
H	-1.180751000	-3.686072000	2.552828000

C	-1.035350000	3.773497000	-2.014362000
H	-1.270175000	3.541784000	-3.066912000
H	-1.716711000	4.562731000	-1.670159000
H	0.008218000	4.114816000	-1.967441000
C	-0.056705000	2.048108000	3.546548000
H	0.673755000	1.385168000	4.033057000
H	0.477183000	2.960614000	3.233486000
H	-0.852462000	2.321797000	4.251018000
C	4.021157000	2.092550000	-1.208455000
H	4.228864000	3.072100000	-1.654591000
C	4.964691000	1.505298000	-0.347615000
O	3.622095000	-1.970694000	-1.483735000
O	1.320489000	-3.031096000	-1.414277000
H	5.074362000	0.416796000	-0.389613000
C	6.046396000	2.251102000	0.342283000
H	6.194836000	1.850259000	1.358522000
H	7.000819000	2.078745000	-0.190363000
H	5.853643000	3.331505000	0.398513000

INT3, E = -2126.173671

Rh	-0.453987000	-0.063972000	-0.088683000
N	1.812670000	-0.432686000	-0.111556000
C	4.225377000	0.383700000	-0.111904000
C	2.709202000	0.511448000	-0.207813000
C	2.383538000	1.907852000	-0.450854000

H	1.373264000	2.263575000	-0.626645000
H	4.475114000	-0.141392000	0.821681000
C	4.813980000	-0.425266000	-1.290864000
C	4.127713000	-1.778121000	-1.453278000
O	3.769885000	-2.273644000	-0.138458000
S	2.240705000	-2.025886000	0.381474000
H	3.227459000	-1.718267000	-2.084835000
H	4.792653000	-2.534698000	-1.891522000
H	4.715574000	0.143272000	-2.229281000
H	5.888499000	-0.559501000	-1.093931000
Rh	-2.807131000	0.442607000	0.136463000
O	-3.190155000	-1.048428000	-1.221714000
C	-2.217295000	-1.680511000	-1.737936000
O	-0.992422000	-1.477867000	-1.483578000
O	-2.588329000	1.788614000	-1.411839000
C	-1.458293000	1.926270000	-1.965312000
O	-0.397978000	1.310633000	-1.628117000
O	-2.872997000	-0.936906000	1.664054000
C	-1.817921000	-1.565301000	1.981421000
O	-0.682839000	-1.406848000	1.439546000
O	-2.272575000	1.911554000	1.479516000
C	-1.052291000	2.085587000	1.770219000
O	-0.084228000	1.415850000	1.291938000
C	-1.358133000	2.863384000	-3.140126000
H	-2.151600000	3.621408000	-3.103119000
H	-0.367762000	3.338332000	-3.171144000

H	-1.481144000	2.272883000	-4.063808000
C	-2.548874000	-2.789192000	-2.702463000
H	-1.702038000	-2.989437000	-3.372107000
H	-2.755301000	-3.702341000	-2.119163000
H	-3.450827000	-2.541458000	-3.279153000
C	-0.715772000	3.145910000	2.785059000
H	-1.485714000	3.928909000	2.796515000
H	-0.682048000	2.675241000	3.781921000
H	0.273607000	3.575733000	2.576611000
C	-1.926700000	-2.599711000	3.070047000
H	-2.441105000	-3.484786000	2.660480000
H	-0.931926000	-2.896468000	3.426072000
H	-2.536595000	-2.211935000	3.898881000
C	3.509485000	2.649904000	-0.380378000
H	3.539526000	3.736907000	-0.494466000
C	4.737224000	1.846354000	-0.070428000
H	5.493585000	2.014485000	-0.857351000
C	5.361697000	2.237550000	1.278628000
H	4.646093000	2.079272000	2.101713000
H	6.257740000	1.629390000	1.479066000
H	5.660917000	3.297715000	1.282831000
O	1.367222000	-2.932262000	-0.341685000
O	2.346263000	-2.064640000	1.830821000

4a, E = -990.357644

N	0.704486000	-1.227671000	-0.364135000
C	-1.134585000	0.490462000	0.111293000
C	-0.526846000	-0.829536000	-0.358368000
C	-1.604343000	-1.694686000	-0.819417000
H	-1.427731000	-2.690468000	-1.228042000
H	-0.851651000	0.613736000	1.168848000
C	-0.634753000	1.731459000	-0.657647000
C	0.890426000	1.824532000	-0.724615000
O	1.480603000	1.204265000	0.444611000
S	1.983004000	-0.348540000	0.246995000
H	1.292162000	1.341965000	-1.629295000
H	1.239656000	2.866262000	-0.723606000
H	-1.032176000	1.721335000	-1.685148000
H	-1.053596000	2.617332000	-0.155682000
C	-2.792687000	-1.086214000	-0.629836000
H	-3.764077000	-1.527474000	-0.869464000
C	-2.668420000	0.279090000	-0.013629000
H	-3.097866000	1.020664000	-0.711324000
C	-3.422143000	0.396673000	1.318776000
H	-3.038729000	-0.330309000	2.053194000
H	-3.304462000	1.407159000	1.741333000
H	-4.499162000	0.209426000	1.181199000
O	3.020640000	-0.366830000	-0.778812000
O	2.278541000	-0.806180000	1.596159000

Aziridine-4(cis), E = -990.286054

N	-0.548692000	-0.228985000	-1.058541000
C	0.395842000	0.952282000	-0.840828000
C	0.716442000	-0.418499000	-0.478585000
C	1.422473000	-1.363745000	0.150756000
H	0.912784000	-2.322099000	0.295579000
H	0.760817000	1.362794000	-1.788757000
C	0.065846000	1.973741000	0.232517000
C	-0.832879000	1.405268000	1.319566000
O	-2.072885000	0.937994000	0.715359000
S	-1.978563000	-0.442888000	-0.144154000
H	-0.359009000	0.580212000	1.875731000
H	-1.138669000	2.176977000	2.036857000
H	1.007688000	2.326700000	0.682854000
H	-0.430004000	2.840706000	-0.231208000
C	2.764617000	-1.224407000	0.716032000
H	2.991278000	-1.936663000	1.517405000
C	3.738483000	-0.361022000	0.354691000
H	4.674661000	-0.408157000	0.923059000
O	-3.113170000	-0.405680000	-1.045110000
O	-1.769840000	-1.575361000	0.750672000
C	3.682918000	0.644349000	-0.756154000
H	4.692638000	0.880137000	-1.126799000
H	3.075055000	0.286241000	-1.602476000
H	3.235327000	1.598809000	-0.421336000

INT1-Z, E = -2126.101148

Rh	-0.419811000	-0.067447000	0.051480000
N	1.814187000	-0.561657000	0.092852000
C	2.657273000	0.018445000	1.254432000
C	2.676071000	0.559990000	-0.090413000
C	2.905375000	1.426985000	-1.077836000
H	2.366073000	1.209171000	-2.004463000
H	2.001229000	0.503729000	1.986108000
C	3.778637000	-0.811060000	1.842213000
C	4.417271000	-1.744705000	0.831733000
O	3.401029000	-2.667863000	0.353324000
S	2.279669000	-2.089293000	-0.666187000
H	4.864788000	-1.215101000	-0.024774000
H	5.184809000	-2.380734000	1.289965000
H	4.536823000	-0.125016000	2.250415000
H	3.381446000	-1.402448000	2.681455000
Rh	-2.774133000	0.466462000	0.050206000
O	-3.054031000	-1.193832000	1.237775000
C	-2.057223000	-1.895956000	1.586341000
O	-0.852786000	-1.670398000	1.258568000
O	-2.957339000	-0.711692000	-1.632470000
C	-1.919490000	-1.239529000	-2.135411000
O	-0.745691000	-1.137508000	-1.665335000
O	-2.426782000	1.612144000	1.729458000
C	-1.259106000	1.684261000	2.213178000

O	-0.235658000	1.088855000	1.747283000
O	-2.334775000	2.092964000	-1.136639000
C	-1.130951000	2.309370000	-1.468204000
O	-0.136345000	1.598236000	-1.123765000
C	-2.077030000	-2.023333000	-3.411509000
H	-3.104911000	-2.395580000	-3.515190000
H	-1.858980000	-1.354065000	-4.260679000
H	-1.357425000	-2.853168000	-3.438792000
C	-2.324296000	-3.116215000	2.428255000
H	-3.242075000	-2.986729000	3.017518000
H	-2.462159000	-3.978110000	1.753917000
H	-1.468378000	-3.328892000	3.083221000
C	-0.838408000	3.491382000	-2.355287000
H	-0.501972000	3.122520000	-3.337827000
H	-1.729381000	4.118412000	-2.485255000
H	-0.015472000	4.081415000	-1.924410000
C	-1.041975000	2.558915000	3.419511000
H	-0.436258000	2.023209000	4.165301000
H	-0.474807000	3.451895000	3.109308000
H	-1.998481000	2.871522000	3.857040000
C	3.683286000	2.664894000	-1.049692000
H	3.291326000	3.437860000	-1.721323000
C	4.800503000	2.958101000	-0.352690000
H	5.202774000	3.970837000	-0.475070000
O	2.890732000	-1.747074000	-1.943479000
O	1.188802000	-3.033036000	-0.576651000

C	5.579498000	2.048633000	0.543952000
H	5.388188000	0.990130000	0.320615000
H	6.661064000	2.236148000	0.442699000
H	5.331372000	2.220182000	1.607405000

TS1-Z, E = -2126.078892

Rh	-0.425455000	-0.102557000	-0.099014000
N	1.701012000	-0.573517000	-0.391329000
C	2.832536000	0.451850000	1.063903000
C	2.646924000	0.474580000	-0.359609000
C	2.924389000	1.403327000	-1.298795000
H	2.448011000	1.275983000	-2.275131000
H	2.391276000	1.272411000	1.644007000
C	3.454852000	-0.623616000	1.862249000
C	3.975374000	-1.861745000	1.144012000
O	2.915604000	-2.647864000	0.567715000
S	2.280214000	-2.080211000	-0.840559000
H	4.709617000	-1.599563000	0.365090000
H	4.461885000	-2.528663000	1.867659000
H	4.310762000	-0.130291000	2.369304000
H	2.769434000	-0.895239000	2.685430000
Rh	-2.728240000	0.534664000	0.301779000
O	-2.966398000	-1.260643000	1.279351000
C	-1.981121000	-2.054052000	1.378242000
O	-0.815085000	-1.837990000	0.929158000

O	-3.204444000	-0.381187000	-1.476930000
C	-2.281359000	-0.891324000	-2.182619000
O	-1.052465000	-0.926147000	-1.871963000
O	-2.080590000	1.403937000	2.062549000
C	-0.857511000	1.355858000	2.376893000
O	0.052831000	0.794907000	1.686180000
O	-2.331335000	2.294013000	-0.704962000
C	-1.168451000	2.500685000	-1.162302000
O	-0.187703000	1.698216000	-1.067279000
C	-2.667241000	-1.472041000	-3.518393000
H	-3.703880000	-1.834567000	-3.497422000
H	-2.595560000	-0.674941000	-4.277757000
H	-1.979072000	-2.280041000	-3.801063000
C	-2.224634000	-3.380094000	2.050664000
H	-3.003091000	-3.286595000	2.820255000
H	-2.579628000	-4.092884000	1.287296000
H	-1.294935000	-3.773613000	2.482997000
C	-0.906808000	3.794146000	-1.890064000
H	-0.666127000	3.570085000	-2.941616000
H	-1.778739000	4.458820000	-1.845344000
H	-0.028268000	4.290729000	-1.450228000
C	-0.418948000	2.032641000	3.648968000
H	0.278008000	1.383019000	4.198609000
H	0.120962000	2.957635000	3.386799000
H	-1.281881000	2.286386000	4.277667000
C	3.711033000	2.601013000	-1.052950000

H	3.335103000	3.501454000	-1.554490000
C	4.843932000	2.726311000	-0.320618000
H	5.251775000	3.740747000	-0.231619000
O	3.386437000	-1.923143000	-1.789839000
O	1.185646000	-2.985793000	-1.127812000
C	5.680243000	1.650792000	0.301013000
H	5.386393000	0.641197000	-0.019780000
H	6.740173000	1.806692000	0.036487000
H	5.634319000	1.687963000	1.403766000

INT2-Z, E = -2126.0918689

Rh	-0.403920000	-0.027148000	-0.198569000
N	1.744953000	-0.312336000	-0.664340000
C	3.145488000	0.312123000	1.248697000
C	2.593274000	0.585113000	0.009230000
C	2.686926000	1.892836000	-0.526773000
H	1.812177000	2.195564000	-1.118209000
H	3.803895000	1.056477000	1.701503000
C	2.812936000	-0.911474000	2.022670000
C	3.259221000	-2.251417000	1.392428000
O	2.433304000	-2.671243000	0.313711000
S	2.433889000	-1.721500000	-1.058350000
H	4.315224000	-2.211030000	1.077168000
H	3.152458000	-3.038814000	2.152345000
H	3.243930000	-0.844451000	3.031513000

H	1.710843000	-0.957827000	2.110927000
Rh	-2.724798000	0.377693000	0.388004000
O	-2.710815000	-1.450245000	1.337864000
C	-1.647949000	-2.141127000	1.346255000
O	-0.547828000	-1.804142000	0.811759000
O	-3.247205000	-0.546083000	-1.372741000
C	-2.335465000	-0.960499000	-2.152378000
O	-1.089351000	-0.888146000	-1.932575000
O	-2.049402000	1.261069000	2.126277000
C	-0.806860000	1.321440000	2.355104000
O	0.105093000	0.894991000	1.578400000
O	-2.564740000	2.183183000	-0.603387000
C	-1.469818000	2.513295000	-1.143650000
O	-0.410042000	1.809257000	-1.144581000
C	-2.765060000	-1.555480000	-3.468930000
H	-3.774188000	-1.982065000	-3.390684000
H	-2.785250000	-0.750735000	-4.223294000
H	-2.045587000	-2.316490000	-3.800235000
C	-1.699646000	-3.492237000	2.010816000
H	-2.409707000	-3.484701000	2.849175000
H	-2.053120000	-4.227030000	1.267903000
H	-0.699796000	-3.797115000	2.347600000
C	-1.395680000	3.842223000	-1.851054000
H	-1.148658000	3.674143000	-2.911112000
H	-2.345573000	4.385675000	-1.771623000
H	-0.582649000	4.442796000	-1.413929000

C	-0.347113000	1.941877000	3.649523000
H	0.209414000	1.188897000	4.229939000
H	0.346011000	2.769547000	3.432823000
H	-1.197151000	2.309838000	4.237757000
C	3.729052000	2.841867000	-0.380482000
H	3.434739000	3.890015000	-0.502747000
C	5.075253000	2.586520000	-0.290808000
H	5.714038000	3.477373000	-0.245136000
O	3.859494000	-1.524231000	-1.388260000
O	1.589990000	-2.477981000	-1.969326000
C	5.809620000	1.299301000	-0.372645000
H	5.185669000	0.434708000	-0.637210000
H	6.629271000	1.406984000	-1.104390000
H	6.306345000	1.096469000	0.594147000

TS2-Z, E = -2126.091869

Rh	-0.412618000	-0.044288000	-0.194576000
N	1.713094000	-0.311164000	-0.777387000
C	3.019956000	0.809524000	0.990979000
C	2.489811000	0.750348000	-0.316368000
C	2.686536000	1.901108000	-1.126702000
H	1.980157000	2.136461000	-1.924902000
H	3.056026000	1.787330000	1.473001000
C	3.143503000	-0.351882000	1.918095000
C	3.627086000	-1.698492000	1.378233000

O	2.670503000	-2.370794000	0.553305000
S	2.424983000	-1.741774000	-0.968233000
H	4.583315000	-1.595990000	0.840342000
H	3.787447000	-2.378521000	2.227120000
H	3.791717000	-0.061327000	2.760400000
H	2.128255000	-0.479082000	2.346372000
Rh	-2.724809000	0.344412000	0.425249000
O	-2.708145000	-1.501988000	1.335727000
C	-1.646281000	-2.196254000	1.309721000
O	-0.553532000	-1.848867000	0.770060000
O	-3.261942000	-0.544187000	-1.350373000
C	-2.358536000	-0.940755000	-2.148706000
O	-1.109933000	-0.866111000	-1.942826000
O	-2.027995000	1.192389000	2.174343000
C	-0.783263000	1.232418000	2.397849000
O	0.119647000	0.824795000	1.600705000
O	-2.575197000	2.169872000	-0.531084000
C	-1.485671000	2.508955000	-1.079593000
O	-0.422978000	1.812449000	-1.096027000
C	-2.801308000	-1.515003000	-3.470105000
H	-2.098885000	-2.289874000	-3.806411000
H	-3.819628000	-1.919637000	-3.396115000
H	-2.801017000	-0.705021000	-4.219097000
C	-1.694138000	-3.565495000	1.937393000
H	-2.028917000	-4.284154000	1.170421000
H	-0.695542000	-3.869711000	2.278992000

H	-2.414325000	-3.587873000	2.766714000
C	-1.446733000	3.828388000	-1.807571000
H	-1.646411000	3.641207000	-2.876039000
H	-2.217214000	4.509705000	-1.422750000
H	-0.450481000	4.284624000	-1.723371000
C	-0.319943000	1.767259000	3.728460000
H	-0.144481000	0.910812000	4.401323000
H	0.630324000	2.307783000	3.614954000
H	-1.082499000	2.416287000	4.178733000
C	3.757985000	2.699789000	-0.769941000
H	3.763831000	3.771454000	-1.006055000
C	4.808947000	2.175675000	0.013527000
O	3.774882000	-1.561921000	-1.538622000
O	1.516035000	-2.697249000	-1.579013000
H	5.318820000	2.900097000	0.664876000
C	5.626779000	0.955502000	-0.274593000
H	5.977281000	0.476287000	0.652116000
H	5.118586000	0.219525000	-0.909530000
H	6.537347000	1.316995000	-0.791558000

INT3-Z, E = -2126.170717

Rh	0.461142000	-0.030913000	0.038893000
N	-1.789215000	-0.443065000	-0.080509000
C	-4.220170000	0.299323000	-0.279861000
C	-2.711295000	0.480050000	-0.146310000

C	-2.423025000	1.902866000	-0.084133000
H	-1.429356000	2.303883000	0.089597000
H	-4.423267000	-0.376673000	-1.122730000
C	-4.822244000	-0.346380000	0.991267000
C	-4.106096000	-1.642495000	1.360076000
O	-3.701062000	-2.313822000	0.139837000
S	-2.162028000	-2.100923000	-0.366729000
H	-3.224977000	-1.468479000	1.997425000
H	-4.764727000	-2.345338000	1.888067000
H	-4.763229000	0.344287000	1.845338000
H	-5.886043000	-0.542766000	0.795956000
Rh	2.832378000	0.437517000	0.002406000
O	3.031723000	-0.808088000	1.627810000
C	1.998507000	-1.365706000	2.110804000
O	0.816915000	-1.223873000	1.675874000
O	2.463540000	2.027861000	1.261667000
C	1.284340000	2.241361000	1.668845000
O	0.262333000	1.558211000	1.343797000
O	3.045310000	-1.180589000	-1.256162000
C	2.016618000	-1.829183000	-1.616271000
O	0.828632000	-1.571244000	-1.257232000
O	2.479731000	1.655226000	-1.624913000
C	1.297724000	1.797522000	-2.057836000
O	0.266258000	1.237221000	-1.570157000
C	1.065537000	3.372154000	2.639378000
H	1.898390000	4.086449000	2.603188000

H	0.112753000	3.878023000	2.427739000
H	1.004084000	2.950501000	3.656670000
C	2.199959000	-2.302582000	3.273265000
H	1.269551000	-2.421327000	3.843869000
H	2.494941000	-3.288081000	2.875230000
H	3.010552000	-1.941677000	3.921593000
C	1.087838000	2.673193000	-3.264984000
H	1.927672000	3.367879000	-3.396735000
H	1.019243000	2.027174000	-4.156286000
H	0.140091000	3.222519000	-3.174228000
C	2.224444000	-3.009190000	-2.528338000
H	2.735594000	-3.805986000	-1.963714000
H	1.264253000	-3.386962000	-2.901893000
H	2.878220000	-2.723552000	-3.365907000
C	-3.553304000	2.599959000	-0.328253000
H	-3.608050000	3.691314000	-0.369968000
C	-4.747375000	1.732598000	-0.592593000
H	-4.946111000	1.786784000	-1.679599000
O	-1.296402000	-2.885156000	0.494425000
O	-2.217230000	-2.332973000	-1.801134000
C	-6.021835000	2.195189000	0.121486000
H	-6.864513000	1.521770000	-0.096807000
H	-5.892030000	2.242553000	1.212961000
H	-6.300191000	3.202487000	-0.226782000

12a, E = -990.354907

N	0.802716000	-1.204000000	-0.394309000
C	-1.102167000	0.285245000	0.447572000
C	-0.449082000	-0.930557000	-0.207445000
C	-1.496101000	-1.852532000	-0.622268000
H	-1.290008000	-2.773827000	-1.168447000
H	-0.648356000	0.406852000	1.442617000
C	-0.847266000	1.597619000	-0.328250000
C	0.634937000	1.823090000	-0.629303000
O	1.452374000	1.258611000	0.425852000
S	2.060643000	-0.239698000	0.127021000
H	0.930813000	1.379138000	-1.592881000
H	0.885165000	2.892353000	-0.669092000
H	-1.396078000	1.599518000	-1.281512000
H	-1.242097000	2.425614000	0.278058000
C	-2.692729000	-1.407867000	-0.187864000
H	-3.644088000	-1.923923000	-0.343954000
C	-2.604591000	-0.121424000	0.584927000
H	-2.792454000	-0.370367000	1.646166000
O	2.986808000	-0.139285000	-0.995709000
O	2.529476000	-0.705169000	1.423814000
C	-3.662054000	0.908306000	0.171410000
H	-3.562628000	1.836271000	0.754239000
H	-3.594423000	1.163369000	-0.896838000
H	-4.670095000	0.503632000	0.355134000

Figure S5-2. Computed *Z*- to *E*- isomerization barriers of **INT1** and **INT2** exceed >20 kcal/mol.

